The Norris Survey of the Corona Borealis Supercluster

Thesis by

Todd A. Small

In Partial Fulfillment of the Requirements
for the Degree of
Doctor of Philosophy

California Institute of Technology
Pasadena, California

1996
(Submitted December 6, 1995)

Acknowledgements

First and foremost, I am grateful to my advisor, Wal Sargent. I've been very fortunate to work with and learn from him. I will always appreciate his deep understanding of astronomy, his concern and enthusiasm for his students, and his great interest in the so many things beyond astronomy that are important, enjoyable, and fulfilling.

Don Hamilton's endless assistance has been invaluable. The success of the Norris Spectrograph is largely due to Don's perseverance. Don, like Wal, has spent many hours with me in front of Elgar the SPARCstation instructing me in the nuances of spectroscopy.

Keeping the Norris Spectrograph in working order has often required herculean efforts from the staff of the Palomar Observatory. In particular, Mike Doyle and James Hickey have poured their hearts and souls into Norris. As with so many students, I have benefited from the expert assistance of the telescope night assistants, Juan Carrasco and Skip Staples. They managed to prevent me from making innumerable mistakes, and, when they could not, they regaled me with tales of fried CCD's and observing with the mirror half covered and otherwise lent the proper perspective to a botched arc.

I am also fortunate to have had opportunities to work with Roger Blandford and Jeremy Mould. Roger has been a source of wisdom and advice since the very beginning of my graduate school career. I thank Jeremy for his many early contributions to what developed into my thesis. He is sorely missed in Robinson.

I am grateful to my friends in the astronomy department for sharing my enthusiasms for soccer, mountain biking, rock climbing, snowboarding, and tacos; for introducing me to AWK and explaining to me that my programming "*defied* optimization;" for lending me distinguished clothes from their own closets when mine was populated with t-shirts and Levi's; and for many enlightening scientific discussions.

My family has encouraged and supported me at every obstacle, even though I

have strayed so far from the beaten path, all the way to the physical sciences. I am very glad that they have been able to see the "Big Eye" in action and to understand the work that I have been doing.

It is impossible to say enough about Rebecca. However, since she has red-lined my last four attempts, I leave it at that.

Abstract

We describe the design, construction, and first results of the Norris Survey of the Corona Borealis Supercluster, a redshift survey of a $6° \times 6°$ region in the core of the Corona Borealis supercluster.

The redshift survey has been conducted with the 176-fiber Norris Spectrograph on the Hale 5m telescope. The input catalog is based on machine scans of Schmidt plates and consists of over 5×10^5 objects calibrated in the Gunn g and r bands. We chose to observe 36 $20'$ diameter fields arranged in a 6×6 grid across the core of the supercluster. We have completed observations of 23 of these fields, plus an additional 9 fields which were closely spaced along the ridge of galaxies between Abell 2061 and Abell 2067. We have measured redshifts for 1491 extragalactic objects, 420 with ~ 8Å resolution and the remainder with ~ 4Å resolution. Our newly measured redshifts were augmented with 163 from the literature, yielding 1654 redshifts for the entire survey. The faintest galaxies in the survey have magnitudes of $g \sim 22.5^m$, and the most distant galaxies have redshifts of $z \sim 0.7$.

We have measured an unexpectedly small number of redshifts (528) in the Corona Borealis supercluster since the supercluster is not as dense as originally believed and since a background supercluster at $z \approx 0.11$ makes a substantial contribution to the projected surface density of galaxies. Despite the small number of redshifts for galaxies in the supercluster, we are able to draw the following conclusions about the dynamics and structure of the Corona Borealis supercluster. (1) The galaxy distribution within the supercluster is far from smooth. The galaxy density falls rapidly away from the Abell cluster cores. (2) The virial mass of the supercluster is $(1.7 \pm 0.2) \times 10^{16} h^{-1}$ $M_\odot$, which yields a B band mass-to-light ratio of $224 \pm 121 h \left(\frac{M}{L}\right)_\odot$. (3) The dynamics of the supercluster, as revealed through an analysis of the two-point correlation function, suggest that the supercluster has not yet generated large mean flows towards itself and that, therefore, the supercluster has only recently begun to

break away from the Hubble expansion.

Since the sample of redshifts extends to $z = 0.5$, we have been able to investigate the evolution of large-scale structure and of the galaxy population. By computing the projected two-point spatial correlation function $w_p(r_p)$, we have measured the correlation length $r_0(z)$ and the power-law index γ of the real space correlation function $\xi(r)$ as a function of redshift. We find that the correlation length declines dramatically with increasing redshift. Incorporating measurements of $r_0(z)$ from other surveys, we measure the evolutionary parameter ϵ to be 2.25 ± 0.1 for $\gamma = 1.7$, well in excess of the linear theory prediction $\epsilon = \gamma - 1$. We do not see evolution in the clustering of red galaxies; the clustering evolution is limited to the blue galaxies.

We have also measured the pairwise velocity dispersion σ_{12} on a scale of $\sim 1h^{-1}$ Mpc through an analysis of the two-point spatial correlation function computed as a function of pair separations along and perpendicular to the line-of-sight. Although σ_{12} is quite sensitive to the treatment of rich clusters in the survey, we conclude that σ_{12} is significantly larger than the canonical value of 340 ± 40 km s^{-1} computed by Davis and Peebles (1983). This result is in accord with other recent estimates of σ_{12}.

We have characterized structure on scales of $\sim 100h^{-1}$ Mpc by measuring the one-dimensional power spectrum of our survey. We measure a significant peak on scales of $\sim 100h^{-1}$ Mpc. The structures responsible for the peak are readily identifiable in redshift-right- ascension cone diagrams: superclusters are separated by large underdense regions.

Using 598 field galaxies with $0 < z < 0.5$ from our survey, we have computed the field galaxy luminosity function as a function of color and redshift. We find compelling evidence that the B band field galaxy luminosity function evolves with redshift. The evolution is limited to blue galaxies; the red galaxies show no sign of change to $z = 0.5$. The evolution of the luminosity function of blue galaxies, which is corroborated by a $\langle V/V_{max} \rangle$ test, is reflected in the blueward shift of the median galaxy color with redshift and in the increasing fraction of galaxies displaying the star-formation indicators [O II] and Hδ with redshift.

Contents

List of Figures

List of Tables

Chapter 1 Introduction

As the largest identified structures in the universe, superclusters are of fundamental interest. The superclusters are only $\lesssim 10$ times more dense than the field, and thus the superclusters are still expanding with the Hubble flow, albeit at a decelerated rate. In contrast, the overdensity of an object that has just become virialized is ~ 200, and the overdensity of an Abell cluster is ~ 1000. Since the dynamical times of superclusters are comparable to the Hubble time, superclusters are unlikely to be relaxed and should therefore bear imprints of the physical processes that were dominant during the epoch of supercluster formation. For example, Zeldovich (1970) has predicted that superclusters should be flattened along one axis (shaped like a "pancake") in a universe in which the largest structures form first. Redshift surveys of superclusters also offer the possibility of measuring the distribution of dark matter on scales far larger than hitherto possible. Understanding the distribution of dark matter on large scales is crucial for estimating the mean density of the universe, Ω_0. In addition, a measurement of the peculiar velocites generated by the supercluster, either directly using an independent distance indicator or statistically from the anisotropy of the galaxy distribution of the supercluster in redshift-space, can provide a complementary estimate of Ω_0.

The Corona Borealis Supercluster is the most prominent example of superclustering in the northern sky. Using the "Lick Counts," Shane and Wirtanen (1954) were the first to remark on the extraordinary cloud of galaxies that constitute the supercluster. Abell also noted the Corona Borealis Supercluster and included it in his catalog of "second-order clusters," or clusters of clusters of galaxies. In fact, the Corona Borealis Supercluster includes 7 Abell clusters at $z \approx 0.07$ in a 36 deg^2 region on the sky and contributes significant power to the two-point correlation function of nearby Abell clusters. In the same region, there are five background Abell clusters, three of which are at $z \approx 0.11$. Counts of galaxies in the field of the supercluster,

which include the background clusters, show a factor of 3 excess over counts in similarly high galactic fields. Picard (1991a) speculated that the supercluster may be responsible for the excess counts, although he realized that if the supercluster were entirely responsible for the excess, it would generate fluctuations in the microwave background of the order $\delta T/T \approx 2 \times 10^{-4}$, far in excess of what is observed (Smoot *et al.* 1992).

The only previous observational investigation of the dynamics of a supercluster was the study by Postman, Geller, and Huchra (1988) of the Corona Borealis supercluster. They collected 182 redshifts for galaxies mainly near the cores of the Abell clusters contained within supercluster. By adding up the virial masses of the Abell clusters, they concluded that the lower limit to the mass of the supercluster is 2.4×10^{15} $M_{\odot}$. They also computed that if the mass-to-light ratio on supercluster scales is comparable to that on cluster scales, then the supercluster mass is 8.2×10^{15} $M_{\odot}$, or about the mass required to bind the system (assuming a supercluster radius of 10-15 Mpc). Their analysis was limited by the fact that they had to make assumptions about the shape of the supercluster. In order to overcome this limitation, a new study of the dynamics of the supercluster would require several thousand redshifts, a number sufficient to measure the mean density of the supercluster to 5%. The only feasible way to obtain such a large number of redshifts, many of which would necessarily be for intrinsically faint galaxies, would be to use an efficient multiobject spectrograph on a 4-m class telescope.

The Norris Spectrograph, which mounts at the Cassegrain focus of the Palomar 200-inch telescope, is just such an instrument. Norris uses 176 fibers which can be independently positioned across the 400 arcmin^2 field-of-view. Norris was originally designed to conduct a survey of faint field galaxies. However, the commissioning of Norris was such a struggle that it seemed wise to pursue a more modest goal in order to gain experience with the spectrograph before embarking on a very challenging survey of faint field galaxies. With the results of Picard's (1992) analysis of galaxy counts in the Corona Borealis region fresh in our minds, and with Picard's catalogs from which to select objects to observe, we decide to do an extensive redshift survey

of the Corona Borealis Supercluster.

The core of the Corona Borealis Supercluster covers a $6° \times 6°$ region on the sky, centered at right ascencion 15^h20^m, declination $+30°$. Since it is infeasible to survey 36 deg^2 with an instrument with a field-of-view of 400 arcmin^2, we decided to observe 36 fields arranged in a regular grid with a grid spacing of 1 deg. We chose to avoid the cores of the Abell clusters since redshifts for many galaxies in the cluster cores are available from Postman, Geller, and Huchra (1988). Our observing strategy was strongly influenced by the long time ($\sim$ 1 hour) required to retrieve and redeploy the fibers. It is clearly very inefficient to change setups frequently during the night. We thus observed at most three fields a night, with total exposures of 2-3 hours per field. Our principal goals at the outset were to delineate the structure of the supercluster, to study the dynamics of the supercluster, and to investigate the relationship between the spectral properties of galaxies and the environment in which they are embedded.

In short, we find that the supercluster is clumpy, far from relaxed, and that the density falls rapidly away from the Abell clusters. Since the virial theorem yields reasonable estimates of the masses of unrelaxed systems (Carlberg 1994), we have computed the virial mass of the supercluster, $M_V = (1.7 \pm 0.2) \times 10^{16} h^{-1}$ M$_\odot$. The mass-to-light ratio of the supercluster is $224 \pm 121 h \left(\frac{M}{L}\right)_\odot$, comparable to that of rich clusters of galaxies (Faber and Gallagher 1979). By modeling the two-point correlation function, we conclude that the supercluster has not yet generated large mean flows towards itself and that, therefore, the supercluster has only recently begun to break away from the Hubble expansion. Although the mean overdensity of the supercluster is approximately 10, many of the galaxies that appear in images to be part of the supercluster are actually in the background. These background objects constitute a faint galaxy sample, which consists of roughly 1000 objects and reaches redshifts of $z \sim 0.7$ and magnitudes as faint as $r \sim 22^m$. We have thus collected a sample of galaxies well-suited for studying the evolution of galaxies and large-scale structure to a look-back time of roughly half the Hubble time ($z \approx 0.5$).

In order to observe directly the evolution of field galaxies, one needs large samples of galaxies with measured redshifts from which to construct the luminosity function

as function of redshift. Construction of such a sample has only recently become possible with the introduction of efficient multiobject spectrographs on 4-m class telescopes (*e.g.,* Ellis *et al.* 1995, Lilly *et al.* 1995). We, and many others, have been motivated to search for evolution in the galaxy population by the suggestive results of faint galaxy counts and of redshift surveys of small numbers of faint galaxies. Estimates of galaxy counts based on replicating the properties of the local galaxy population at higher redshifts fall short of the observed counts for $B \gtrsim 20^m$ (Tyson 1988, Maddox *et al.* 1990b, Metcalfe *et al.* 1995), a discrepancy which requires rapid galaxy evolution in the last billion years ($z \sim 0.1$). In addition, the redshift distribution observed in surveys of faint galaxies, while having roughly the range in redshift expected from the local population, has far more galaxies at intermediate redshifts than predicted (Glazebrook *et al.* 1995a). A natural interpretation of such observations is that the number density of galaxies has evolved strongly since $z \sim 0.5$.

Indeed, the existence of such evolution is revealed in our survey. Galaxies as blue or bluer than a Coleman, Wu, and Weedman (1980) Sbc galaxy show convincing signs of evolution. The luminosity function of blue galaxies at $0.2 < z \leq 0.5$ has a higher normalization and possibly a steeper power-law slope at faint absolute magnitudes. There is no sign that red galaxies evolve, which suggests that we may be observing two different galaxy populations. The change in the nature of the galaxy population with redshift is also revealed in the spectra of individual galaxies. Galaxies show more signs of star formation with increasing redshift, although galaxies with spectra typical of old stellar populations certainly continue to appear.

The evolution we observe is not, however, as rapid as expected from the galaxy counts. This is due to the fact that the normalization of our local luminosity function is at least a factor of 2 higher than that found by Loveday *et al.* (1992) in the Stromlo/APM survey. The higher normalization removes the need for rapid evolution since $z \sim 0.1$. Although the APM survey is based on photographic plates which are difficult to calibrate, it is unlikely that there are large enough systematic errors to account for the discrepancy in the normalization (Metcalfe, Fong, and Shanks 1995). We conclude that the most plausible explanation is that our Galaxy resides in an

underdense region with a diameter of $\sim 100h^{-1}$ Mpc.

We have also studied the large-scale structure in our survey. Our most striking observation is that immediately beyond the Corona Borealis Superclusters, there is a void with a diameter of $100h^{-1}$ Mpc (h is the Hubble constant H_0 in units of 100 km s^{-1} Mpc^{-1}) which is bordered on its far side by another supercluster. This background supercluster, which we have dubbed the "Abell 2069 Supercluster," contains three Abell clusters and is roughly half as dense as the Corona Borealis Supercluster. By measuring the two-point spatial correlation $\xi(r)$ as a function of redshift, we have studied the evolution of clustering. One of the fundamental postulates of cosmology is that structure grows from tiny fluctuations in the early universe under the action of gravity (Peebles 1994). Observing the evolution of clustering is therefore of crucial importance for constraining models of the growth of structure. We find that the correlation length declines rapidly beyond $z \approx 0.3$. The interpretation of this observation is complicated by the fact that we may not be observing the same galaxy population at high redshift as at low redshift, and we know that the correlation lengths of different galaxy types vary in local samples. The population at high redshift is bluer than the local population and since local blue galaxies have a smaller correlation length than the red galaxies (Loveday *et al.* 1995), the inferred evolution is much more modest.

We have also measured the pairwise peculiar velocities of the galaxies in our sample. The canonical value of the pairwise peculiar velocity is $\sigma_{12} = 350 \pm 50$ km s^{-1} (Davis and Peebles 1983). This is much lower than predicted in the cold dark matter model. Recently, however, Marzke *et al.* (1995) have measured $\sigma_{12} \sim 540 \pm 180$ km s^{-1}, a value which is much easier to reconcile with the CDM model. We, too, measure a high value of σ_{12}. The volume of our survey is sufficiently large that we should be measuring a fair value of σ_{12}; however, the presence of the Corona Borealis supercluster could certainly be biasing our result high.

This thesis has by no means tapped all of the scientific potential of our vast data set. In particular, many of the individual objects have very interesting spectra which warrant detailed studies. We have discovered six quasars, including one at

$z = 3.88$. We have also found many active galaxies and many starburst galaxies. Most interestingly, perhaps, galaxies with E+A spectra, that is, an A-star spectrum superposed on the spectrum of an old stellar population, are quite common in our survey.

Although we originally intended for this thesis to be a detailed study of the dynamics of the Corona Borealis Supercluster, our most compelling results come from the analysis of the faint, intermediate redshift galaxies in our sample. The fact that there is marked evolution of both galaxies and large scale structure at intermediate redshifts suggests where the future of the Norris Spectrograph lies. Norris is ideally suited to carry out an extensive redshift survey of galaxies at $z \sim 0.5$. Such a redshift survey would complement the extremely large local redshift surveys which will soon be underway (*e.g.*, the 2dF survey, the Sloan survey) and the faint galaxy redshift surveys which have already begun at the Keck Telescope.

Chapter 2 Observations and Catalog Construction

2.1 Introduction

Abell, from his survey of galaxy clusters on the Palomar Observatory Sky Survey plates (Abell 1958), was the first to observe and note the existence of clusters of clusters of galaxies. These clusters of clusters of galaxies, which he called "second-order clusters" and which have since dubbed "superclusters," are the largest identified structures in the Universe. The dynamical timescale of superclusters is comparable to the Hubble time, which implies that dynamical processes have not yet erased imprints of the principal processes at work during the formation of the supercluster. One hopes, therefore, that studies of superclusters will ultimately yield information on the nature of density fluctuations in the early Universe and may offer clues about the epoch of galaxy formation. In addition, by studying the peculiar velocities of galaxies generated by the supercluster, one may be able to estimate Ω_0.

The Corona Borealis supercluster was first noted as an extraordinary "cloud" of galaxies by Shane and Wirtanen (1954). In the $6^\circ \times 6^\circ$ region centered on right ascension 15^h20^m, declination $+30^\circ$, there are 12 rich Abell clusters, seven of which have redshifts near $z \approx 0.07$. These seven (Abell 2056, 2061, 2065, 2067, 2079, 2089, and 2092) define the core of the Corona Borealis supercluster. Three of the remaining clusters (Abell 2062, 2069, 2083) have redshifts near $z \approx 0.11$, and two (Abell 2059, 2073) are even more distant. Using the magnitudes of the brightest galaxies in the individual clusters as rough distance indicators, Shane and Wirtanen (1967) were able to deduce that the supercluster consisted of two separate components seen in projection, with the more distant component roughly twice as distant as the nearer one. In Figure 2.1, we show a combined contour/greyscale plot of the galaxy surface

density in the core of the supercluster. The Abell clusters are the prominent regions of enhanced galaxy surface density (the precise location of the Abell clusters is show in Figure 2.10). One can also discern an overall density enhancement between the Abell clusters. Galaxy counts in Corona Borealis confirm the presence of the supercluster, as noted by Picard (1991a). In Figure 2.2, we plot the galaxy number counts in the g and r bands and compare the counts to a fit to the counts of Weir, Djorgovski, and Fayyad (1995) in a high Galactic latitude field. Over the range $16.0 \lesssim g \lesssim 19.0$ (correspondingly, $16.5 \lesssim r \lesssim 19.5$), the Corona Borealis counts are roughly a factor of three higher than those in the field of Weir, Djorgovski, and Fayyad (1995).

The true extent of the Corona Borealis supercluster on the sky is unknown. Bahcall (1992) has marshalled circumstantial evidence to argue that while the region containing the 7 Abell clusters is only $\sim 20h^{-1}$ Mpc (h is the Hubble constant H_0 divided by 100 km s^{-1} Mpc^{-1}) on a side, the entire supercluster extends for at least $\sim 100h^{-1}$ Mpc on the sky. First, one of the peaks in the redshift distibution of the Broadhurst *et al.* (1990) pencil-beam survey is at the redshift of Corona Borealis, even though the survey was aimed 45° away from the core of the supercluster. Second, the far side of the Boötes void, at right ascension 14^h30^m, declination +50°, (Kirshner *et al.* 1987) is also at a redshift of $z \approx 0.07$. As our data show, the depth of Corona Borealis on the sky is only $\sim 40h^{-1}$ Mpc. Corona Borealis thus appears to be a flattened pancake similar to the structures originally hypothesized by Zeldovich (1970).

Although it was certainly not practical to survey the whole $100h^{-1}$ Mpc $\times$ $100h^{-1}$ Mpc region (which corresponds to 730 square degrees), our aim was to delineate accurately the structure of Corona Borealis out to a radius of $\sim 20h^{-1}$ Mpc. Since there are far too many galaxies even within the core of the supercluster to hope to obtain spectroscopy for each one, we have chosen a sparse-sampling strategy of observing 36 fields distributed in a regular 6 $\times$ 6 grid across the core of the supercluster. The grid spacing is 1°. Each of the fields was to be observed once with the 176-fiber Norris Spectrograph mounted at the Cassegrain focus of the Palomar 5m telescope. Since retrieving and redeploying the fibers, which is done by a robot, takes nearly an hour,

we decided to observe only two fields a night, with one field change in the middle of the night. The total exposure times on each field were thus typically 2-3 hours, yielding redshifts for galaxies as faint at $g \sim 22^m$. We have obtained 1491 redshifts for extragalactic objects, 469 of which lie within the core of the supercluster.

With this sample, we intend to examine the structure and dynamics of the core of the supercluster and to investigate the relationship between the spectral properties of galaxies and the large-scale structure in which the galaxies are embedded. The dynamics of the core of Corona Borealis were previously studied by Postman, Geller, and Huchra (1988), who measured 182 velocities for galaxies in the vicinities of the clusters A2061, A2065, A2067, A2079, A2089, and A2092. With this small number of redshifts, they were limited to calculating the virial masses of the Abell clusters and could say little about the structure of the supercluster as a whole. With over 2.5 times as many galaxies, we hope to be able to perform a more detailed examination of the supercluster.

Roughly two-thirds of the galaxies for which we have obtained redshifts are more distant than Corona Borealis. This large sample provides an excellent basis for studies of large-scale structure and galaxy evolution to redshifts of $z \sim 0.5$. In future papers in this series, we will present measurements of the evolution of both the two-point spatial correlation function and the luminosity function. In addition, we will constrain the star-formation history of galaxies by investigating the change in the equivalent widths of diagnostic spectral lines (*e.g.*, [O II] λ3727, Hδ, and Hβ) with redshift.

The paper, the first in the series presenting results from the Norris Survey of the Corona Borealis Supercluster, is organized as follows. We describe the construction of the input catalog and the selection of objects to observe in §2 and the details of the observations and data reduction in §3. We present the redshift catalog in §4, along with an analysis of potential selection effects within the catalog. In §5, we briefly discuss the six quasars discovered in our survey. We will generally use $H_0 = 75$ km s^{-1} Mpc^{-1}, although we will when appropriate parameterize it as $H_0 = 100h$ km s^{-1} Mpc^{-1}, and $q_0 = 0.5$.

2.2 Description of the Survey

2.2.1 Construction of the Input Catalog

All of the spectroscopic targets have been selected from catalogs based on Second Palomar Observatory Sky Survey (POSS-II, Reid *et al.* 1991) plates. The 14 inch square glass plates are taken with the Oschin Schmidt 48-inch telescope at Palomar and cover $6.6° \times 6.6°$ on the sky. The unvignetted portion of the plate extends to a radius of 3° from the plate center. We have used plates taken in two colors: blue (IIIa-J emulsion and a GG395 filter, $\lambda_{\rm central} \sim 4800$Å) and red (IIIa-F emulsion and a RG610 filter, $\lambda_{\rm central} \sim 6500$Å). We refer to the blue plates as J plates and the red plates as F plates. The plates are graded by the POSS-II staff according to image quality, number and type of cosmetic defects, uniformity of response, and blank sky photographic density. The two plates we have used in the survey were both graded C1, primarily because of noticeable but generally unimportant cosmetic blemishes. The field number, plate number, center location, approximate photographic sky density, exposure time, sky transmission quality, grade, and calibrated limiting magnitude are summarized in Table 2.1.

The principal requirements for the catalogs derived from the plates are that the positions be accurate to 0.3″ RMS in order to place accurately the fiber probes, that the object magnitudes be well calibrated ($\sigma_{\rm mag} \lesssim 0.3^m$), and that the star-galaxy separation be reliable to as faint a magnitude as possible. The original catalog was constructed by A. Picard from a COSMOS scan of an F plate of POSS-II field 449. Since a comprehensive description of the construction of the catalog has already been given by Picard (1991b) (see also Picard 1991a), we will only briefly describe the salient points. The COSMOS machine of the Royal Observatory of Edinburgh generates, for every object detected, a long list of parameters, the most important of which for us are right ascension, declination, instrumental magnitude, area, and peak intensities. The procedure for separating stars from galaxies is based on the simple observation that stars, being unresolved, occupy a well defined locus on a plot of area versus magnitude for all objects. In contrast, galaxies have a larger area than

stars at a given magnitude, allowing galaxies and stars to be objectively separated. In fact, Picard uses a more complex statistic incorporating area, peak intensity, and local sky brightness which allows for a cleaner separation of stars from galaxies. He estimates that for $r \leq 19.0$ the completeness in the catalog is greater than 90% and the stellar contamination is less than 10%. The catalog was magnitude calibrated using CCD images of clusters of galaxies in the g and r bands of the Thuan-Gunn (1976) photometric system. For objects in the magnitude range $16.5^m \leq r \leq 19.0^m$, the accuracy of the COSMOS magnitudes is 0.18^m. Fainter than $r = 19.0^m$, the COSMOS magnitudes become increasingly more unreliable with an RMS error of $\sim 1^m$ at $r \sim 21^m$.

In 1995, we switched from the COSMOS-based catalog of the F plate to J and F catalogs generated with the Sky Image Cataloging and Analysis Tool (SKICAT, Weir, Djorgovski, and Fayyad 1995; Weir, Fayyad, and Djorgovski 1995; Weir 1995). SKICAT processes digitized versions of the plates and uses sophisticated machine-learning techniques to perform star-galaxy separation, thereby pushing the limit of accurate star-galaxy separation to $g \sim 20.5^m$ and $r \sim 19.6^m$, over half a magnitude fainter than the COSMOS scan. The evaluation of object parameters (*e.g.*, magnitudes, second moments, etc.) is carried out using the Faint Object Classification and Analysis System (FOCAS, Jarvis and Tyson 1979; Valdes 1982. The principal advantage of the SKICAT catalog was the substantial decrease in the number of observed objects which turned out to be stars.

One difficulty with the SKICAT system, however, is that the errors in the celestial coordinates are $\sim 1''$. These errors are far too large for use with the Norris Spectrograph. Therefore, we have matched several thousand objects in the SKICAT J catalog with objects in the original COSMOS catalog and used these objects as reference objects to determine the transformation between SKICAT (x, y) coordinates and celestial coordinates, thus reducing the RMS errors to $\sim 0.3''$.

We have magnitude-calibrated both plates using g, r, and i CCD images of galaxies in Abell 2069. The fitted linear relations between the CCD magnitudes and the plate instrumental magnitudes are shown in Figure 2.3 (J) and Figure 2.4 (F). We only

fit the data in the regions $16.0^m < g < 20.5^m$ and $16.5^m < r < 19.6^m$ where the plate instrumental magnitude response is linear (Weir, Djorgovski, and Fayyad 1995). In these regions, the RMS error was $g \sim 0.3^m$ and $r \sim 0.2^m$. Beyond $g = 20.5^m$ and $r = 19.6^m$, the scatter is markedly larger, reaching $\sim 1^m$ for the faintest galaxies. The g band fit is noticeably biased for objects with magnitudes greater than $g = 20.5^m$. The r band fit shows no apparent bias.

From the SKICAT catalogs, we were able to record a large number of features for each object. These included the objects' total magnitudes, aperture magnitudes, core magnitudes, detection areas, total areas, ellipticities, positions angles on the sky, and intensity-weighted first moment radii. Weir, Djorgovski, and Fayyad (1995) have shown that the FOCAS total magnitude, measured by integrating the sky-subtracted light of the object across an area determined by growing the detection area out until the total area is twice the detection area, provides an unbiased estimate of the true magnitude of an object to at least $g = 22^m$. Due to the bright isophotal limits for photographic plates, isophotal magnitudes consistently underestimate the total light in an object. We have also measured aperture magnitudes in a circular aperture with a $5''$ radius, which is 2.5 times the typical full-width at half-maximum (FWHM) of the seeing disk. Aperture magnitudes substantially underestimate the total luminosity of large objects but provide accurate and unbiased estimates for faint objects. The core magnitude is the integrated luminosity of the center 9 arcsec^2 of the object and is thus closely related to the object's central surface brightness. The intensity-weighted first moment radius, obtained by evaluating

$$\sum_{area} rI(x,y) / \sum_{area} I(x,y), \tag{2.1}$$

characterizes the size of an object on the sky and is equal to twice the scale-length for a galaxy with an exponential profile and to twice the half-light radius for a galaxy with an $r^{1/4}$ profile.

2.2.2 Selection of Norris Fields

During the early, exploratory phase of the project, we observed 9 fields along the ridge of galaxies between Abell 2061 and Abell 2067. These 9 fields are called "corbor1" through "corbor9." After the exploratory observations proved successful, we chose to observe 36 fields, "cb1" throught "cb36," arranged in a 6 $\times$ 6 rectangular grid over the 6° $\times$ 6° field centered on the Corona Borealis supercluster. We have mainly avoided fields which contain an Abell cluster within them since redshifts for galaxies within the Abell clusters can be obtained from the literature. Within each field, we would fine tune the placement of the spectrograph on the sky, typically by 15′ and occasionally by nearly half a degree, in order to maximize the number of fibers on bright galaxies. Occasionally, for example, a bright star would saturate a significant portion of the field on the original plates, making galaxy detection impossible in the saturated region, and we would move from the nominal center in order to avoid the blank zone. The observed field centers are listed in Table 2.2.

2.2.3 Selection of Objects

Objects are selected from the input catalogs by an interactive computer program called AUTOFID2. Every object in a field is assigned a priority based on its magnitude and its star-galaxy classification. The scheme for assigning priorities is summarized in Table 2.3. AUTOFID2 attempts to assign fibers to as many high priority objects as possible subject to the simple rules designed to protect the fibers. The fibers are not allowed to cross, are not allowed to bend more than 5°, and are not allowed to come within 16″ of each other. These rules combine to virtually eliminate pairs of objects with separations less than 30″ on the sky. Sky fibers were placed interactively by the observer. We attempted to use fibers not assigned to objects as the sky fibers, but we were often forced to remove fibers from extremely faint objects in order to have sky fibers well distributed across the field. We generally placed 8 to 18 sky fibers, as recommended by Wyse and Gilmore (1992) for adequate sampling of the sky.

2.3 Observations and Data Reduction

2.3.1 Observations with the Norris Spectrograph

All of the spectra were obtained with the Norris Spectrograph mounted at the Cassegrain focus ($f/16$) of the Hale 5m telescope. The Norris Spectrograph has been extensively described by Hamilton *et al.* (1993). The spectrograph has 176 fibers, each of which covers 1.6″ (FWHM) on the sky. The fibers are positioned individually by a robot and are held to the focal plane by magnets. The field-of-view of the spectrograph is nearly 400 arcmin^2, although edges of the field are severely vignetted. We have used two detectors in the course of the survey. In 1992 and 1993, we used a Tektronix 1024^2 thinned, back-side illuminated CCD with 24μm pixels, which was the largest CCD then available at Palomar. Since the spectrograph was designed to be used with 2048^2 CCD with 27μm pixels, we were only able to image half of the fibers during the 1992 and 1993 runs. Starting in 1994, we used a Tektronix/SITe 2048^2 thinned, back-side illuminated CCD with 24μm pixels, enabling $\sim$ 150 fibers to be imaged. The large CCD has excellent blue response, which substantially improved the quality of the spectra obtained.

The wavelength range for all observations was $\sim$3900 Å to $\sim$6500 Å. The lower edge of the range was determined by the requirement that [O II]3727 Å be observable for galaxies in the supercluster ($z \sim 0.07$). The upper edge of the range was limited by the bright sky at Palomar which makes sky subtraction with fibers infeasible beyond $\sim$6500 Å. With the small CCD, the required spectral coverage was obtained using a 300 lines mm^{-1} grating, yielding a resolution of $\sim$8 Å. With the large CCD, we were able to cover the same range with a 600 lines mm^{-1} grating, yielding a resolution of $\sim$4 Å.

We have experimented with various schemes for flatfielding the spectra and determining the relative throughput of the fibers. The Norris Spectrograph was designed with a moveable collimator that can be "dithered" perpendicular to the dispersion so that each fiber illuminates a swath which is 2-3 times the width of the undithered spectrum. With a dithered flatfield, the data could still be flatfielded even if the

position of the spectra on the chip had changed due to spectrograph flexure. Unfortunately, the profiles of the dithered flatfield spectra were not rectangular. Rather, the profiles have sharp horns at each end where the chip was exposed for a greater length of time as the collimator slowed and reversed its direction of motion at the ends of each cycle. We eventually decided that since modern Tektronix chips are so flat, we would use traditional undithered dome flats and hope that the minor shifts in the position of the spectra on the chip would cause negligible errors.

The total exposure time varied from field to field and ranged from 5000 seconds to nearly 12000 seconds. The total exposure time was made up of individual short exposures, ranging in length from 1500 seconds to 4000 seconds, to facilitate cosmic-ray removal and to pause for reference arc exposures. No attempt was made to obtain spectra of flux standard stars. Two velocity standard stars, HD 132737 (spectral type K0 III) and HD 171232 (spectral type G8 III), were observed for use as cross-correlation templates. See Table 2.4 for a summary of the dates of the observations, the exposure times, the seeing, the sky transparency, the spectral resolution, and the number of extragalactic objects successfully identified.

The data were reduced using standard IRAF [1] routines. As described in detail by Wyse and Gilmore (1992), it is crucial to account for the scattered light in the spectrograph. Although most of the light from a fiber is emitted in a narrow cone, a small but nevertheless significant amount (a few percent) is emitted into 2π radians. The scattered light was successfully removed using the IRAF task APSCATTER which makes a two-dimensional fit to the regions in between the spectra where, after bias-subtraction, all the counts are due to scattered light. After the scattered light was subtracted, the apertures were extracted from the object, arc, and flatfield frames. The fiber-to-fiber throughput variations, including the effect of the vignetting of the field, were removed with dome flatfield frames. The fibers in the center of the field have throughput variations of $\pm 30\%$, while the fibers on the vignetted portions of

[1] IRAF is distributed by the National Optical Astronomy Observatories, which are operated by the Association of Universities for Research in Astronomy, Inc. (AURA) under cooperative agreement with the National Science Foundation.

the field have overall throughputs as much as 20 times less than the fibers in the center of the field. A mean flatfield spectrum was formed by averaging together all of the extracted flatfield spectra and was then divided back into the extracted flatfield spectra in order to create normalized flatfield spectra. A 20-piece third-order spline was fit to the normalized flatfield spectra in order to remove pixel-to-pixel variations. The correction for the fiber-to-fiber wavelength-dependent throughput differences was completed by dividing these smooth fits into the object spectra. Note that this process leaves pixel-to-pixel sensitivity variations uncorrected, but we believe that the CCD's we used are sufficiently flat that this is not a significant problem. We also verified that the dome flatfields were exposing the instrument similarly to the night sky by computing the overall throughput of the fibers by measuring the flux in the [O I] λ5577 night sky line. The throughputs computed in these two manners agreed very well. The object and sky spectra were wavelength calibrated using the comparison arc spectra to an accuracy of better than 0.2 Å RMS. The sky spectra were averaged with 3σ rejection to form a master sky spectrum. Since the fiber-to-fiber throughput variations had already been corrected with the dome flatfieds, the master sky spectrum could be directly subtracted from the object spectra without any rescaling. The accuracy of the sky subtraction ranged from 1-4% RMS, with the quality of the sky subtraction strongly dependent on the brightness of the night sky. Finally, the reduced object spectra from each individual exposure were median-combined in order to reject cosmic rays. In a number of cases, however, there were only two individual exposures, in which case the spectra were simply added together without applying any sort of cosmic ray rejection scheme.

A random sample of 24 spectra is shown in Figures 2.6 - 2.8. The spectra have been smoothed with a 4 pixel boxcar to the resolution of the spectrograph. Since the continua have not been flux-calibrated, the shape of the spectra reflects both the intrinsic continuum of the object and the spectral response of the spectrograph. We have marked the spectral features used in the identifications with dotted lines. There are four stars in the 24 spectra (Figure 2.6a, 2.6b, 2.7g, and 2.7h), with the star in Figure 2.6 showing the deep TiO absorption bands of a late-type star. The objects

in Figure 2.6d and Figure 2.8a exhibit the strong nebular emission lines of galaxies undergoing starbursts. Many of the other galaxies have [O II] λ3727 emission, which is indicative of modest continuing star formation. Two of the objects (Figure 2.6h and 2.8h) have strong Balmer series absorption lines, a signature of the presence of an A-star population in the galaxy.

2.3.2 Redshift Identification

All redshift identifications were made by TAS. The vast majority of identifications were straightforward as the blue-sensitive CCD's we used ensured that we generally had a strong signal in the region of Ca K λ3934, Ca H λ3968, and the 4000Å break, features which are visible in our spectra from $z = 0$ to $z \sim 0.6$. We also frequently identified [O II] λ3727, G band λ4304, Hβ λ4861, [O III] $\lambda\lambda$4959, 5007, Mg b band λ5175, and Na D λ5893. For a small number of spectra, the redshift is based solely on the identification of a single emission line as [O II] λ3727. There are no other "single-line" redshifts included in the sample.

WLWS and DH independently reviewed a random sample of 100 objects identified by TAS. There were only five disagreements, four which we judged unclassifiable on the second inspection and one which TAS incorrectly identified. We therefore believe that our redshift identifications are 95% accurate.

2.3.3 Automatic Measurement of Lines

With 1485 galaxies (the remaining extragalactic objects are quasars) in the catalog, it is clearly impractical to measure the equivalent widths of lines by hand. We have, therefore, chosen to develop an entirely automated program to detect and measure lines. Automated detection and measurement of spectra lines was first successfully employed by Young *et al.* (1979) (YSBCW), and the state-of-the-art is the program developed by Schneider *et al.* (1993) for the *Hubble Space Telescope* Quasar Absorption Line Key Project. Not surprisingly, all of these programs are bedevilled by the difficulty of automatically finding the level of the continuum. The Key Project team

resorted to modifying interactively the level found by the software. Determining the continuum level for galaxies is even more difficult than for quasars. Galaxies have not only the problem of crowding of lines, notably in the Balmer series of galaxies with prominent A-star features, but also have both sharp absorption lines and sharp emission lines. We were unable to develop an algorithm that could cope simultaneously with the crowded Balmer series and with emission lines. YSBCW employed a scheme in which the standard deviation of a segment of the spectrum is compared with the "theoretical" standard deviation based on the counting statistics and points in deep absorption lines are rejected until the two standard deviations agree. We found that this scheme biased the continuum level unacceptably high.

Since, however, the important lines for the study of the spectral evolution of galaxies (*e.g.*, [O II], Hδ, Hβ, etc.) occur in relatively uncrowded regions of the spectrum, we decided to fit the continuum with a 20-piece third-order spline and to accept that the fit would be poor in crowded regions. Tests of our software, which are described below, demonstrate that our equivalent width estimates are not biased. We only report equivalent widths for the following four lines: [O II] λ 3727, Hδ, Hβ, and [O III] λ 5007.

We searched for lines using the technique described by Schneider *et al.* (1993). First, the error array for the continuum-normalized spectrum was computed. At each pixel, the standard deviation in a 10 pixel segment centered on the pixel was calculated. The array of such points was fitted with a one-piece third-order spline in order to interpolate over sharp features due to spectral lines, and this fit was used as our error array. We next formed an equivalent width array by computing at each pixel the equivalent width of a marginally resolved Gaussian line. (Note that we define an emission line to have a positive equivalent width and an absorption line to have a negative equivalent width.) The error in the equivalent width at each pixel is computed by summing the error array weighted by the same Gaussian profile. The local extrema of the equivalent width array are candidate lines. If the equivalent width at a local extremum point was less than 4 times the error in the equivalent width, we rejected the line. The accepted lines were passed on to a Gaussian deblending

routine, and the equivalent widths W and centroids Λ of the deblended lines were remeasured using the expressions derived by YSBCW:

$$W = \sum_i (1 - N_i), \tag{2.2}$$

$$\Lambda = \sum_i \lambda_i (1 - N_i) / \sum_i (1 - N_i), \tag{2.3}$$

where the sum extends from Λ - 1.5FWHM$_{\rm Gaussian}$ to Λ + 1.5FWHM$_{\rm Gaussian}$, N_i is the number of counts in pixel i, and λ_i is the wavelength of the center of pixel i. In order to be finally accepted as a real line, the putative line had to pass five tests:

1. The difference between the Gaussian centroid and the YSBCW centroid must be less than 10Å.

2. The Gaussian FWHM must be greater than 3.5Å and less than 50Å.

3. The Gaussian equivalent width must be 4 times the YSBCW error in the equivalent width.

4. The difference between the Gaussian equivalent width and the YSBCW equivalent width must be less than 5Å.

5. The RMS error of the Gaussian fit must be less than 1.0.

Once a line was judged real, its features were recorded in a database file. The FWHM, amplitude, centroid, and equivalent width all came from the Gaussian fit. The error in the equivalent width was estimated by summing in quadrature the error in each pixel involved in the equivalent width computation. The error in the centroid was calculated with the following expression from Schneider *et al.* (1993):

$$\sigma(\Lambda) = \sqrt{2}\sigma_{\rm line} \left| \frac{\sigma(W)}{W} \right|, \tag{2.4}$$

where $\sigma_{\rm line} = 0.4247$FWHM. From tests with mock spectra (described below), we determined that the estimated errors were accurate for spectra in which the wavelength

scale was known exactly. For the real spectra, however, the wavelength scale is not known exactly, resulting in an often dramatic underestimate of the error in the line centroid. In order to calibrate the line centroid error due to errors in the wavelength scale, we measured the positions of the bright sky lines in our 32 master sky spectra. The sky lines are sufficiently strong that the purely statistical errors in the line centroids are negligible. The standard deviation of the measurements of the lines's centroids about their published central wavelengths was then taken as an estimate of the wavelength scale-induced errors. For the data taken with the lower resolution 300 l/mm grating, we added a wavelength scale error of 0.6Å in quadrature with the statistical estimate. For the 600 l/mm grating, we added 0.2Å in quadrature. The mean wavelength errors of the sky lines were 0.09Å and 0.12Å for the 300 l/mm grating and the 600 l/mm grating, respectively.

In order to test our line finding and measuring program, we ran the program on simulated spectra created using the MK1DSPEC task in IRAF. We attempted to recover lines of equivalent width 1.3Å and FWHM 6Å in spectra with signal-to-noise ratios in the continua ranging from 10 to 100 per pixel. The trials verified that the program was correctly estimating the equivalent widths and centroids and their errors. Figure 2.5 illustrates the results for 1825 trials with a signal-to-noise ratio of 17.3.

The positions of features found by our automatic program were compared with the expected positions of the prominent lines based on our estimate of the redshift of the object. If the centroid was within 5Å, we considered the line matched. The redshift of the object was then computed from the weighted mean of the redshifts of the identified lines. Only 5% of the 1493 non-stellar objects were not successfully matched by the program.

2.3.4 Automatic Measurement of Velocities

We attempted to measure the recession velocities of every object using cross-correlation techniques as described by Tonry and Davis (1979) and implemented in the IRAF

external package XCSAO. As note above (§3.1), we used HD 132737 (spectral type K0 III) and HD 171232 (spectral type G8 III) as our cross-correlation templates. The spectra were cleaned of emission lines (and prominent sky line residuals) and continuum-subtracted by fitting with a 20-piece third-order spline with rejection of points more than 3σ above the continuum. Before performing the cross-correlation, the template was redshifted to the estimated redshift. We found that this procedure greatly increased the reliability of the cross-correlation redshift determinations.

For objects for which we successfully estimated redshifts with both the line measurement program and the cross-correlation program, the final estimate of the velocity of the object was formed by computing the weighted mean of the two velocity determinations. If only one of the methods yielded a velocity, then we simply used that one estimate as our final estimate. There were 70 objects for which the redshift could not be estimate by either the line measuring program or the cross-correlation program. For these 70 objects, we simply recorded our visual estimate of the redshift and assigned a velocity error of 300 km s^{-1} (0.001 in redshift). All velocites were corrected for heliocentric motion.

We determined the typical errors of the velocities by comparing velocities determined for the 25 objects which we successfully observed twice and by comparing velocities for the 31 objects we observed for which velocities are listed in ZCAT (Huchra *et al.* 1992). The distributions of velocity differences for the objects observed twice and for the objects with matches in ZCAT are shown in panels (*a*) and (*b*), respectively, of Figure 2.9. For the 25 objects with two observations, the average velocity difference was 6 km s^{-1} and the standard deviation was 115 km s^{-1}. For the 31 objects with velocities listed in ZCAT (Huchra *et al.* 1992), the average velocity difference was 35 km s^{-1} and the standard deviation was 108 km s^{-1}. A further check on the accuracy of our velocity estimates is provided by comparing the velocities of the 1014 objects for which we were able to measure velocities with both the line measuring routine and the cross-correlation routine. The velocity differences, which are shown in panel (*c*) of Figure 2.9, are Gaussian-distributed with a mean error of 48 km s^{-1} and a standard deviation of 105 km s^{-1}. We therefore set the velocity error for

all the objects with automatic velocity measurements at 100 km s^{-1} unless the error estimates from the automatic measurements were larger than 100 km s^{-1}, in which case we used the larger error estimate.

2.3.5 Objects Culled from the Literature

We have added 163 objects from ZCAT (Huchra *et al.* 1992) and from the Postman, Geller, and Huchra (1988) redshift survey of Corona Borealis. The velocites and velocity errors were taken from the published catalogs. All other object features were taken from our SKICAT catalogs. The objects taken from the literature may be identified in the redshift catalog by having names that do not have the "CB" prefix.

2.4 The Redshift Catalog

The redshift catalog is summarized in Tables 2.5 and 2.6, which list the data for identified objects and unidentified objects, respectively. The columns listed in Table 2.5 are the following: (1) object name; (2) and (3), 1950.0 equinox right ascension and declination; (4) and (5), total and core magnitude in the g band; (6) and (7), total and core magnitude in the r band; (8) the total area; (9) the intensity-weighted first radial moment; (10) the redshift; and (11) - (14), the rest equivalent widths of [O II] λ3727, Hδ, Hβ, and [O III] λ5007. The total area and intensity-weighted first radial moment are taken from the J plate, unless the object was only detected on the F plate, in which case the measurements from that plate were used. Objects that were only identified on the F plate are identifed by having a name beginning with "CB-99." Stars were recorded as "star" in the redshift column. As noted above (§3.2), only equivalent widths for spectral lines in uncrowded regions of the spectrum are reported in Table 2.5. For the table of unidentified objects, Table 2.6, the listed columns record the information that can be gleaned from the plates only: (1) object name; (2) and (3), 1950.0 equinox right ascension and declination; (4) and (5), total and core magnitude in the g band; (6) and (7), total and core magnitude in the r band; (8) total area; and (9) the intensity-weighted first radial moment. Unidentified

objects only detected on the F plate have names beginning with "CB-00."

The distribution of the identified galaxies on the sky is given in Figure 2.10. The positions of the 12 Abell clusters in the field are marked with large circles. The objects without many close neighbors were taken from the literature. The largest concentration of identified objects is along the ridge of galaxies between Abell 2061 and Abell 2067. The distibution of the galaxies in redshift is given in Figure 2.11. There are two prominent peaks in the figure: the Corona Borealis supercluster at $z \approx 0.07$ and the more distant supercluster at $z \approx 0.11$.

We present two redshift-right-ascension "pie" diagrams in Figures 2.12 and 2.13. In Figure 2.12, we plot all of the galaxies in our survey, whereas in Figure 2.13 we plot an expanded view of galaxies with redshifts less that $z = 0.15$. The pie diagrams have been plotted with enlarged opening angles of 90°, which, since the survey only covers 6°, stretches structures along the dotted lines. The most striking feature of the pie diagrams is the sharply delineated void of $\sim 75h^{-1}$ Mpc diameter centered at right ascension 15^h22^m, $z \approx 0.09$ and bounded by the two superclusters. There are no prominent "fingers-of-God" in these diagrams because we have measured velocities for comparatively few galaxies in the cores of the Abell clusters.

Redshift-magnitude diagrams for the g and r bands are shown in Figure 2.14. We have also plotted for reference the tracks of non-evolving, k-corrected L^* galaxies with spectra typical of E, Sbc, Scd, and Im type galaxies. The spectral energy distributions for the different morphological types were taken from Coleman, Wu, and Weedman (1980). The most luminous galaxies in our survey are roughly 2.5 times (1^m) brighter than L^*. The prominent horizontal strips at $z \approx 0.07$ and $z \approx 0.11$ are the two superclusters.

2.4.1 Completeness in Magnitude

The distribution of galaxies with measured redshifts is shown in Figure 2.15. We also plot, with the right-hand ordinate, the galaxy counts in the field. By a comparison of the *shapes* of the two distributions, we deduce that the redshift catalog is complete

only to $g = 19.0^m$ and $r = 18.5^m$ magnitude. However, we have measured a substantial number of redshifts for galaxies out to $g = 22.5^m$ and $r = 22.0^m$. We utilize the entire incomplete catalog for statistical studies by averaging over a large number of randomly-selected magnitude-limited sub-samples, each of which can be analyzed using standard techniques.

The spectroscopic identification rate, the ratio number of objects (stars, galaxies, and quasars) successfully identified to the number of objects observed, is shown in Figure 2.16. The rate remains above 80% to $g = 19.5^m$ and $r = 19.0^m$ and then falls to fainter magnitudes.

2.4.2 Completeness in Surface Brightness

The discovery of large numbers of low surface brightness galaxies (*e.g.*, Sprayberry *et al.* 1995) has raised the issue of how surface brightness effects may be biasing the results of galaxy surveys, especially those, such as this one, which are based on catalogs originally derived from photographic plates. In particular, surface brightness selection effects may be an important element in the explanation for the excess counts of blue galaxies relative to observations of local galaxies. McGaugh (1994) has demonstrated that the deep surveys, such as those by Tyson (1988) and, more recently, Metcalfe *et al.* (1995), are sufficiently sensitive to detect low surface brightness galaxies to intermediate redshifts ($z \sim 0.5$), whereas the Schmidt-plate based surveys used to define the properties of the local galaxy distribution (*e.g.*, Maddox *et al.* 1990b) will miss most low surface brightness galaxies.

As our survey is based on plates from POSS-II, which are taken at a location with a bright night sky, we do not expect to be sensitive to low surface brightness galaxies. In Figure 2.17 (g) and Figure 2.18 (r), we plot the objects' core magnitudes against their total magnitudes. Since objects are detected by the presence of contiguous pixels 2.5σ above the sky background, whether or not an object is detected depends directly on the core magnitude. In Figures 2.17 and 2.18, the stars form a narrow sequence, and the galaxies are broadly distributed above the stars (*i.e.*, with lower

surface brightness). The distribution of the galaxies in $g_{\rm core}$ does not appear to be restricted in surface brightness until $g_{\rm core} \approx 22.0^m$, which corresponds to a central surface brightness of $g \approx 24.4$ mag arcsec^{-2}. We have also plotted the tracks, as a function of redshift, of three illustrative model galaxies as observed in 2″ seeing. The locus of galaxies is bounded by an L^* disk with an exponential scale-length of $3.5h^{-1}$ kpc and an absolute magnitude of $\mathrm{M}_g = -20.0 + 5\log_{10} h$ and an L^* spheroid with a half-light radius of $3.0h^{-1}$ kpc and absolute magnitude of $\mathrm{M}_g = -20.2 + 5\log_{10} h$. A low surface brightness L^* disk with an exponential scale-length of $10h^{-1}$ kpc would only be detectable to $z \approx 0.13$. The bulges of low surface brightness spiral galaxies, with half-light radii of $\sim 4h^{-1}$ kpc and luminosities of approximately one half the disk luminosities (Sprayberry *et al.* 1995), would be readily detectable in our survey to high redshifts; however, it is unlikely that all of the light of the low surface brightness disks would be recovered.

Statistical analyses of the data will be based on samples with $g_{\rm core} \leq 22.0^m$ or with $r_{\rm core} \leq 21.7^m$ and should be free from surface brightness selection effects.

2.4.3 Completeness in Color

In Figure 2.19 we plot the $g - r$ color of every galaxy as a function of redshift. Lower and upper limits on the colors of galaxies which were only detected on one plate are also shown. The typical error in the color is 0.4^m. We also plot the tracks of non-evolving, k-corrected galaxies with spectral energy distributions from Coleman, Wu, and Weedman (1980). The galaxy population appears to become slightly redder with increasing redshift, although there is a substantial number of galaxies at all redshifts bluer than a flat-spectrum object ($f_\nu = 0$).

The $g - r$ color distributions as function of total magnitude of the galaxies and unidentified objects and of the stars and unidentified objects are shown in Figure 2.20 and Figure 2.21, respectively. The galaxies and the unidentified objects cover the same parts of the diagram except for the region with $g - r > 1^m$ and $g < 20^m$, which is exclusively populated by stars. Taking the galaxies and stars together, it is

clear that the color distibution of the identified objects covers the same range as that of the unidentified objects. This fact indicates that the survey does not suffer from significant color biases.

2.4.4 Completeness in Angular Separation on the Sky

The fiber assignment program AUTOFID2 introduces spatial selection biases on a range of angular scales. In panel (*a*) of Figure 2.22, we plot the ratios of the number pairs of attempted objects and the number of pairs of identified objects to the number of pairs in the input catalog as a function of angular separation on the sky. The restrictions on the proximity and bending angles of fibers combine to eliminate pairs with angular separations of $\lesssim 30''$. There is also a gradual bias against pairs with separations $\gtrsim 10'$. The maximum possible angular separation of a pair, given the field-of-view of the Norris Spectrograph, is $26'$.

In panel (*b*) of Figure 2.22, we plot the ratio of the number of identified objects to the number of attempted objects as a function of angular separation. The ratio remains constant to $\sim 10'$, falls gradually to $\sim 17'$, and falls steeply thereafter. The decline to large angular separation reflects the vignetting of the edges of the field of the Norris Spectrograph.

2.5 Quasars

We have discovered six quasars in the course of our survey. The redshifts range from $z = 1.04$ to $z = 3.88$. The basic data for the quasars are given in Table 2.7, and the spectra are shown in Figure 2.23. All of the quasars were discovered when we were selecting objects from the COSMOS scan of the F plate. It is curious that no quasars were discovered when the object selection was based on detection on the J plate. Quasar CB-26.2177 (Figure 2.23e) is the only quasar for which we have detected intervening absorption systems. The quasar has four Mg II systems at $z = 0.742$, 0.903, 1.102, and 1.160. The strongest system at $z = 0.903$ has associated Fe II $\lambda 2585$, $\lambda 2600$ absorption at the observed wavelengths of 4919.3Å and 4947.8Å. The

faintness of CB-26.2177 ($g = 20.6^m$) ought to facilitate the detection in deep images of the objects responsible for the Mg II absorption systems.

2.6 Summary

We have presented the 1485 galaxies, 6 quasars, and 395 stars which comprise the Norris Survey of the Corona Borealis Supercluster. We have augmented these data with an additional 163 galaxies taken from the literature. Although not magnitude-limited, the survey includes galaxies as faint as $g = 22.5^m$ and $r = 22.0^m$. We have quantified and understood the selection biases in magnitude, surface brightness, color, and angular separation on the sky. Our survey not only provides the largest dataset ever assembled for the study of the dynamics and structure of a supercluster, but also provides a large sample useful for studies of large-scale structure and of galaxy evolution to $z \sim 0.5$. Subsequent papers in the series will present studies of the evolution of the two-point spatial correlation function and of the luminosity function as a function of redshift. We will also discuss in a future paper objects of individual interest, such as E+A galaxies, Seyfert galaxies, and quasars, and include Palomar 60-inch images of many of the objects.

All of the data which we have collected for this survey and which we have not presented here (*e.g.*, the entire plate catalogs, spectra for individual objects, etc.) may be obtained from TAS.

TABLE 2.1

POSS-II PLATES IN CORONA BOREALIS

Field	Plate	RA (1950.0)	Dec (1950.0)	Density	Exp (min)	Trans	Grade	m_{lim}
$J449$	3091	15^h20^m	30°	1.46	70	Hazy	C1	$g \approx 21.6$
$F449$	1165	15^h20^m	30°	0.99	60	Clear	C1	$r \approx 21.1$

TABLE 2.2

Survey Fields in Corona Borealis

Field	RA (1950)	Dec (1950)	Observed?
corbor1	15:22:38	31:24:24	Yes
corbor2	15:22:00	31:17:02	Yes
corbor3	15:21:16	31:09:39	Yes
corbor4	15:20:41	31:02:42	Yes
corbor5	15:20:06	30:56:13	Yes
corbor6	15:19:33	30:52:04	Yes
corbor7	15:19:02	30:46:29	Yes
corbor8	15:18:34	30:41:22	Yes
corbor9	15:17:59	30:34:23	Yes
cb1	15:11:26	28:09:20	Yes
cb2	15:11:28	28:34:45	Yes
cb3	15:12:01	29:35:31	Yes
cb4	15:13:01	30:37:20	Yes
cb5	15:13:14	31:25:46	Yes
cb6	15:13:05	32:04:26	Yes
cb7	15:17:09	27:52:06	Yes
cb8	15:17:04	28:30:37	Yes
cb9	15:16:02	29:39:17	No
cb10	15:16:02	30:27:17	No
cb11	15:16:12	31:24:36	Yes
cb12	15:16:02	32:03:17	No
cb13	15:19:18	28:15:30	Yes
cb14	15:19:34	28:45:10	Yes
cb15	15:19:20	29:39:07	Yes
cb16	15:20:02	30:27:17	No
cb17	15:20:02	31:15:17	No

TABLE 2.2—*Continued*

Field	RA (1950)	Dec (1950)	Observed?
cb18	15:20:02	32:03:17	No
cb19	15:24:37	28:02:45	Yes
cb20	15:23:49	28:36:17	Yes
cb21	15:24:09	29:52:30	Yes
cb22	15:22:53	30:29:35	Yes
cb23	15:24:50	31:19:36	Yes
cb24	15:24:23	32:14:56	Yes
cb25	15:28:44	28:03:18	Yes
cb26	15:29:12	29:07:46	Yes
cb27	15:28:37	29:38:37	Yes
cb28	15:28:02	30:27:17	No
cb29	15:27:50	31:05:09	Yes
cb30	15:28:02	32:03:17	No
cb31	15:32:02	28:03:17	No
cb32	15:32:02	28:51:17	No
cb33	15:32:02	29:39:17	No
cb34	15:32:02	30:27:17	No
cb35	15:31:31	31:13:53	Yes
cb36	15:32:02	32:03:17	No

TABLE 2.3

PRIORITY SCHEME FOR AUTOFID2

Magnitude Range	Classification	Priority
$14.0 \leq g \leq 19.0$	galaxy	900
$19.0 \leq g \leq 20.0$	galaxy	800
$20.0 \leq g \leq 22.0$	galaxy	600
$14.0 \leq g \leq 20.0$	star	200
$20.0 \leq g \leq 22.0$	star	100

TABLE 2.4

Summary of Observations

Field	UT Date	Exp (sec)	Seeing (″)	Trans	Spec. Res. (Å)	N(z)
corbor1	26 Apr 1992	7200	1.0	Cirrus	8	24
corbor2	27 Apr 1992	7200	1.0	Clear	8	23
corbor3	27 Apr 1992	7200	1.0	Clear	8	37
corbor4	27 May 1992	9800	1.5	Clear	8	31
corbor5	30 May 1992	9000	1.5	Cirrus	8	28
corbor6	28 May 1992	10934	2.0	Clouds	8	26
corbor7	29 May 1992	8714	2.0	Cirrus	8	42
corbor8	29 May 1992	6600	1.5	Cirrus	8	38
corbor9	30 May 1992	9000	1.5	Clear	8	20
cb1	17 Mar 1993	8000	1.8	Cirrus	8	30
cb2	18 Mar 1993	8000	2.2	Clear	8	11
cb3	20 Apr 1993	8000	1.0	Clouds	8	10
cb4	20 Apr 1993	5800	1.0	Clouds	8	32
cb5	19 May 1993	8000	1.0	Clear	8	21
cb6	19 May 1993	6700	1.0	Clear	8	26
cb7	20 May 1993	7200	2.5	Fog	8	24
cb8	20 May 1993	6800	2.5	Fog	8	30
cb11	30 May 1995	7500	1.0	Clear	4	65
cb13	4 May 1994	5000	1.0	Cirrus	4	82
cb14	3 May 1994	9000	1.0	Clear	4	70
cb15	8 Apr 1994	7200	1.5	Clouds	4	69
cb19	29 May 1995	7500	< 1.0	Clear	4	59
cb20	2 May 1994	6000	1.0	Cirrus	4	87
cb21	2 May 1994	7000	1.0	Cirrus	4	81
cb22	3 May 1994	9000	1.5	Clear	4	79
cb23	28 May 1995	12000	1.0	Clouds	4	70

TABLE 2.4—*Continued*

Field	UT Date	Exp (sec)	Seeing (″)	Trans	Spec. Res. (Å)	N(z)
cb24	30 May 1995	7500	1.0	Clear	4	59
cb25	29 May 1995	7500	1.0	Clear	4	72
cb26	4 May 1994	8000	< 1.0	Cirrus	4	76
cb27	4 May 1995	12000	1.5	Clear	4	69
cb29	5 May 1994	5000	< 1.0	Clouds	4	68
cb35	5 May 1994	6000	< 1.0	Clouds	4	65

TABLE 2.5

THE REDSHIFT CATALOG

Object	RA (1950)	Dec. (1950)	g_{tot}	g_{core}	r_{tot}	r_{core}	Area (□″)	irl (″)	z	W_λ([O II]) (Å)	W_λ(Hδ) (Å)	W_λ(Hβ) (Å)	W_λ([O III]5007) (Å)
1510+2810B	15:10:04.2	28:10:53.0	16.65	18.41	16.38	17.97	431	3.75	0.0575 ± 0.0002	···	···	···	···
CB-1.7694	15:11:03.4	28:10:55.7	19.83	20.73	18.36	19.70	110	1.94	0.2343 ± 0.0003	···	···	···	···
CB-2.7826	15:11:05.4	28:35:14.5	17.43	18.38	16.09	17.07	208	2.07	star	···	···	···	···
CB-1.7624	15:11:05.5	28:16:54.8	19.19	20.56	18.62	20.13	75	1.73	0.1243 ± 0.0003	22.1 ± 1.6	···	···	···
CB-1.7615	15:11:06.3	28:13:01.9	20.38	20.99	20.29	20.92	66	1.51	0.2346 ± 0.0003	16.5 ± 1.2	···	6.1 ± 0.7	···
CB-1.7601	15:11:07.3	28:07:04.4	18.00	18.79	16.91	17.85	211	1.91	star	···	···	···	···
CB-2.7718	15:11:08.0	28:41:46.1	20.85	21.55	20.55	21.46	37	1.35	0.3166 ± 0.0003	9.7 ± 1.4	···	···	···
CB-1.7485	15:11:10.4	28:14:47.3	21.89	22.61	21.54	22.12	29	1.17	0.4451 ± 0.0003	24.1 ± 1.5	···	···	···
CB-1.7456	15:11:11.2	28:13:58.7	18.55	19.58	18.64	19.72	128	2.12	0.1137 ± 0.0003	64.8 ± 0.7	···	24.8 ± 0.3	88.9 ± 0.3
CB-1.7476	15:11:11.2	28:05:21.1	21.14	22.00	19.91	20.96	67	1.49	0.3719 ± 0.0003	···	···	···	···
CB-1.7415	15:11:12.8	28:10:08.2	18.21	19.55	18.28	19.63	123	2.21	0.1301 ± 0.0003	23.7 ± 1.3	-5.2 ± 1.0	5.3 ± 0.4	3.4 ± 0.5
CB-2.7516	15:11:12.9	28:43:49.7	18.63	19.95	18.76	19.88	221	2.57	0.1148 ± 0.0003	···	···	···	···
CB-2.7482	15:11:14.0	28:43:27.3	19.72	20.90	20.14	21.29	126	2.27	0.1131 ± 0.0003	···	···	13.7 ± 1.4	···
CB-1.7325	15:11:14.4	28:26:11.3	18.66	19.71	17.82	18.80	204	2.20	0.1116 ± 0.0003	···	···	-3.3 ± 0.5	···
CB-1.7331	15:11:15.1	28:13:33.4	18.65	19.98	18.31	19.60	226	2.47	0.1129 ± 0.0003	···	···	···	···
CB-1.7310	15:11:16.3	28:12:39.0	19.29	20.49	18.35	19.51	204	2.29	0.2343 ± 0.0003	···	···	···	···
CB-1.7293	15:11:17.4	28:04:54.1	17.17	18.59	17.03	18.55	430	2.88	0.0909 ± 0.0003	34.9 ± 0.8	···	11.5 ± 0.2	10.4 ± 0.2
15113+3108	15:11:18.0	31:07:60.0	16.35	18.07	15.61	17.29	166	2.30	0.0717 ± 0.0003	···	···	···	···
CB-1.7211	15:11:18.3	28:29:01.3	19.91	20.53	18.43	19.20	73	1.38	star	···	···	···	···
CB-1.7214	15:11:19.6	28:09:02.9	18.56	19.81	17.84	19.16	254	2.52	0.1141 ± 0.0003	···	···	···	7.3 ± 0.3
CB-1.7157	15:11:21.0	28:13:54.9	20.27	21.40	21.16	21.88	89	1.81	0.1140 ± 0.0003	41.7 ± 2.8	···	···	29.6 ± 1.2
CB-1.7084	15:11:21.7	28:31:29.5	18.95	19.59	17.77	18.57	123	1.66	star	···	···	···	···
CB-2.7169	15:11:22.2	28:37:42.3	17.91	19.67	17.85	19.45	295	3.31	0.0587 ± 0.0003	···	···	···	···
CB-1.7092	15:11:22.4	28:18:26.0	20.60	21.96	19.86	20.91	71	1.72	0.3729 ± 0.0003	···	···	···	···
CB-99.1	15:11:23.3	28:03:56.6	···	···	20.78	21.92	66	1.82	0.4222 ± 0.0004	···	···	···	···
CB-1.7024	15:11:24.4	28:15:09.5	18.80	19.92	18.04	19.01	195	2.21	0.1166 ± 0.0003	9.2 ± 1.6	···	···	···
CB-2.7067	15:11:24.6	28:40:25.1	19.14	20.19	18.34	19.36	186	2.16	0.1793 ± 0.0003	···	···	···	···
CB-1.6990	15:11:25.3	28:11:15.2	18.08	19.41	17.20	18.60	267	2.66	0.1165 ± 0.0003	···	···	···	···
CB-2.7050	15:11:25.5	28:33:49.0	19.98	20.62	18.41	19.33	116	1.78	star	···	···	···	···
CB-2.7003	15:11:26.6	28:35:44.7	17.32	18.77	16.48	17.91	480	3.19	0.0594 ± 0.0003	···	···	···	···
CB-1.6935	15:11:26.8	28:11:57.2	19.09	20.18	18.57	19.78	183	2.10	0.1168 ± 0.0003	···	···	···	···
CB-1.6939	15:11:27.2	28:06:02.9	19.56	20.32	18.19	18.82	108	1.66	star	···	···	···	···
CB-1.6913	15:11:27.9	28:04:41.1	20.53	21.98	19.83	21.09	109	2.42	1.0360 ± 0.0010	···	···	···	···
CB-1.6863	15:11:28.7	28:08:33.4	16.91	18.00	15.78	16.66	107	1.87	star	···	···	···	···
CB-2.6911	15:11:28.8	28:36:54.4	16.91	18.64	16.19	17.88	667	3.95	0.0792 ± 0.0003	···	···	-2.1 ± 0.3	···
CB-1.6808	15:11:29.5	28:12:30.4	19.58	21.43	18.37	20.28	233	3.51	0.3724 ± 0.0003	···	···	···	···
CB-1.6793	15:11:30.2	28:10:31.6	21.99	22.43	20.40	21.46	58	1.39	0.3679 ± 0.0003	···	···	···	···
CB-2.6792	15:11:31.7	28:40:05.6	18.14	19.68	17.52	19.09	386	3.08	0.1796 ± 0.0003	8.3 ± 1.2	-4.5 ± 0.8	···	···
CB-1.6707	15:11:32.5	28:10:04.1	21.86	22.42	20.10	21.34	57	1.52	0.3730 ± 0.0003	···	···	···	···
CB-1.6664	15:11:33.4	28:10:55.9	17.49	19.21	16.72	18.29	410	3.43	0.1143 ± 0.0003	···	3.1 ± 0.4	-1.5 ± 0.2	···
CB-1.6650	15:11:34.4	28:02:35.1	18.66	20.00	17.89	19.31	251	2.55	0.1146 ± 0.0003	···	···	···	···
CB-2.6651	15:11:35.8	28:40:50.3	15.73	17.89	15.63	17.83	1086	4.46	0.0455 ± 0.0003	···	-4.5 ± 0.5	2.8 ± 0.1	···
CB-2.6637	15:11:36.8	28:33:33.3	18.08	18.92	···	···	216	1.92	star	···	···	···	···
CB-1.6415	15:11:38.5	28:14:21.0	17.76	19.64	17.46	19.37	381	3.31	0.1119 ± 0.0003	···	···	···	···
CB-1.6352	15:11:40.5	28:05:48.2	16.80	18.79	16.65	18.60	616	3.77	0.0903 ± 0.0003	···	-3.1 ± 0.6	···	···

TABLE 2.5—*Continued*

Object	RA (1950)	Dec.	g_{tot}	g_{core}	r_{tot}	r_{core}	Area (□″)	irl (″)	z	W_λ([O II]) (Å)	W_λ(Hδ) (Å)	W_λ(Hβ) (Å)	W_λ([O III]5007) (Å)
CB-1.6327	15:11:40.5	28:14:48.7	18.36	19.91	18.01	19.44	279	2.87	0.1143 ± 0.0003	···	···	···	8.1 ± 0.2
CB-2.6461	15:11:41.0	28:33:36.3	17.96	19.47	17.37	18.85	367	2.96	0.0808 ± 0.0003	···	···	-3.9 ± 0.7	···
CB-3.6428	15:11:41.1	29:35:38.9	19.16	19.90	18.18	19.04	66	1.38	star	···	···	···	···
CB-3.6390	15:11:42.1	29:39:09.4	15.85	17.48	13.97	15.35	719	3.16	star	···	···	···	···
CB-2.6371	15:11:43.0	28:42:15.6	19.48	20.08	17.60	18.69	20	0.88	star	···	···	···	···
CB-1.6223	15:11:43.1	28:09:44.5	17.71	19.34	17.28	18.92	332	3.09	0.1134 ± 0.0003	5.9 ± 1.2	···	···	6.4 ± 0.3
CB-1.6123	15:11:43.8	28:33:04.4	18.58	19.29	17.58	18.34	181	1.76	star	···	···	···	···
CB-1.6188	15:11:43.9	28:09:00.8	18.13	19.58	17.79	19.15	259	2.78	0.1173 ± 0.0003	13.8 ± 1.0	-4.3 ± 0.6	···	···
CB-1.6186	15:11:44.1	28:07:08.6	17.75	19.13	17.01	18.30	353	2.86	0.0901 ± 0.0003	···	···	···	···
CB-1.6134	15:11:45.2	28:07:43.5	17.74	19.60	17.40	19.09	212	2.85	0.1143 ± 0.0003	···	···	···	7.0 ± 0.6
CB-3.6246	15:11:45.6	29:41:32.9	18.76	19.84	18.59	19.81	195	2.13	0.1127 ± 0.0003	26.2 ± 3.0	···	5.9 ± 0.6	···
CB-3.6070	15:11:50.6	29:43:32.6	17.57	18.48	16.06	16.85	249	2.06	star	···	···	···	···
CB-3.5954	15:11:54.2	29:43:08.2	20.49	20.94	19.34	20.12	93	1.51	star	···	···	···	···
CB-3.5946	15:11:55.0	29:36:30.6	21.05	21.59	20.57	20.90	68	1.48	star	···	···	···	···
CB-3.5878	15:11:57.2	29:27:44.9	18.83	19.57	17.73	18.47	186	1.90	star	···	···	···	···
1511+3019	15:11:59.0	30:19:54.0	15.82	18.12	15.23	17.39	919	5.28	0.0927 ± 0.0008	···	···	···	···
CB-3.5768	15:11:59.4	29:37:48.3	18.69	19.49	18.14	18.90	180	1.78	star	···	···	···	···
CB-3.5766	15:11:60.0	29:29:33.2	18.75	19.91	18.50	19.73	190	2.27	star	···	···	···	···
CB-3.5606	15:12:03.4	29:40:38.8	16.93	18.02	15.33	16.46	382	2.38	star	···	···	···	···
CB-3.5544	15:12:05.3	29:42:02.3	19.16	19.91	18.48	19.35	126	1.79	0.1307 ± 0.0003	19.8 ± 2.0	···	6.2 ± 0.6	···
CB-3.5531	15:12:06.9	29:26:11.4	18.89	19.82	18.76	19.78	90	1.74	star	···	···	···	···
CB-3.5496	15:12:07.1	29:36:56.8	16.94	18.06	15.23	16.03	222	2.26	star	···	···	···	···
CB-3.5444	15:12:08.6	29:39:04.9	19.78	20.99	18.99	20.02	117	2.15	0.2899 ± 0.0003	···	···	···	···
CB-3.5394	15:12:09.4	29:41:59.5	22.15	22.47	20.49	21.51	28	1.07	0.2790 ± 0.0010	···	···	···	···
CB-3.5382	15:12:10.2	29:32:47.9	18.52	19.68	17.34	18.69	95	1.87	0.1317 ± 0.0003	···	···	···	···
CB-3.5311	15:12:11.7	29:43:48.3	20.08	20.75	19.09	19.97	100	1.66	0.1613 ± 0.0003	···	···	···	···
CB-3.5239	15:12:14.8	29:37:01.4	18.02	19.63	17.74	19.29	336	3.09	0.1303 ± 0.0003	···	-4.3 ± 0.9	···	···
CB-3.5104	15:12:18.4	29:43:08.3	19.72	20.83	17.91	19.65	26	1.15	0.2827 ± 0.0003	···	···	···	···
CB-4.4240	15:12:36.4	30:42:12.2	19.28	20.96	18.16	19.88	114	2.74	0.2520 ± 0.0010	···	···	···	···
CB-4.4190	15:12:38.0	30:38:03.8	19.17	19.96	18.46	19.36	132	1.84	star	···	···	···	···
CB-4.4135	15:12:39.0	30:44:55.6	19.52	20.48	18.64	19.90	116	1.95	0.2519 ± 0.0003	···	···	···	···
CB-4.4106	15:12:40.2	30:40:09.2	17.72	19.30	16.91	18.49	423	3.26	0.1101 ± 0.0003	···	···	···	···
CB-4.4051	15:12:41.4	30:42:17.5	18.68	19.90	18.71	19.74	213	2.37	0.0830 ± 0.0003	···	···	···	2.1 ± 0.4
CB-4.4014	15:12:42.5	30:41:55.5	19.95	21.09	19.66	21.05	113	2.00	0.2550 ± 0.0010	···	···	···	···
CB-4.3985	15:12:43.1	30:44:47.0	19.54	21.03	18.61	19.97	90	2.36	0.2540 ± 0.0003	···	···	···	···
CB-4.3938	15:12:44.2	30:44:08.5	18.52	20.10	18.73	20.31	257	2.86	0.1088 ± 0.0003	···	···	···	···
CB-6.4055	15:12:44.2	32:00:41.0	17.94	19.37	17.10	18.48	316	2.96	0.1200 ± 0.0010	···	···	-3.6 ± 0.2	···
CB-4.3903	15:12:45.2	30:43:22.9	19.85	20.80	18.61	19.86	96	1.89	0.2596 ± 0.0003	···	···	-3.8 ± 0.6	···
CB-6.3995	15:12:45.9	31:59:57.4	18.49	19.61	17.61	18.77	256	2.36	0.1177 ± 0.0003	···	···	···	···
CB-6.3922	15:12:47.4	32:00:45.7	19.65	20.68	18.76	19.90	179	2.39	0.1194 ± 0.0003	···	···	···	···
CB-4.3854	15:12:47.4	30:33:12.9	19.94	20.96	19.66	20.68	134	2.32	0.2298 ± 0.0003	···	···	···	11.0 ± 1.1
CB-6.3909	15:12:48.1	31:55:00.6	18.82	20.11	18.58	20.05	209	2.40	0.1358 ± 0.0003	···	-9.6 ± 1.3	4.2 ± 0.6	···
CB-6.3890	15:12:48.3	31:59:59.8	18.45	19.72	17.55	18.85	252	2.56	0.1169 ± 0.0003	···	···	-3.4 ± 0.4	···
CB-6.3876	15:12:48.4	32:04:59.1	20.13	20.97	20.13	20.96	97	1.59	0.3074 ± 0.0003	8.0 ± 0.7	···	···	···
CB-4.3775	15:12:49.0	30:39:49.6	19.44	20.58	18.19	19.46	126	2.14	0.2547 ± 0.0003	···	···	···	···

TABLE 2.5—*Continued*

Object	RA (1950)	Dec. (1950)	g_{tot}	g_{core}	r_{tot}	r_{core}	Area (□″)	irl (″)	z	W_λ([O II]) (Å)	W_λ(Hδ) (Å)	W_λ(Hβ) (Å)	W_λ([O III]5007) (Å)
CB-6.3814	15:12:49.4	32:10:03.8	17.82	19.28	17.63	19.03	288	2.84	0.0902 ± 0.0003	···	···	7.7 ± 0.5	24.0 ± 0.7
CB-6.3804	15:12:50.3	32:01:01.1	18.45	19.84	17.97	19.15	298	2.76	0.1372 ± 0.0003	···	···	···	···
CB-4.3705	15:12:51.0	30:41:09.8	20.29	21.15	19.65	20.38	93	1.72	0.2522 ± 0.0003	···	···	···	···
CB-4.3688	15:12:52.3	30:29:53.5	19.24	20.33	18.59	19.74	210	2.51	0.1997 ± 0.0004	···	···	···	···
CB-5.3501	15:12:52.6	31:31:19.8	18.58	20.22	18.68	20.28	243	3.11	0.1016 ± 0.0003	···	···	···	6.3 ± 0.8
CB-6.3715	15:12:52.6	31:57:49.8	18.45	19.63	18.24	19.55	190	2.24	0.1157 ± 0.0003	10.5 ± 1.9	-4.1 ± 0.9	···	···
CB-6.3675	15:12:53.5	31:59:29.4	18.55	19.91	18.26	19.57	239	2.60	0.1362 ± 0.0003	···	···	1.8 ± 0.3	···
CB-4.3579	15:12:53.8	30:43:48.7	19.74	20.81	18.83	19.97	110	2.01	0.2542 ± 0.0003	···	···	···	···
CB-4.3524	15:12:55.2	30:41:22.3	19.62	20.61	18.39	19.44	152	2.21	0.2540 ± 0.0003	···	···	···	···
CB-6.3584	15:12:55.7	31:56:15.2	18.63	19.69	18.11	19.24	227	2.25	0.1362 ± 0.0003	13.4 ± 0.9	···	4.3 ± 0.4	···
CB-4.3456	15:12:56.6	30:40:15.5	19.62	20.71	18.57	19.73	170	2.07	0.2550 ± 0.0003	···	···	···	···
CB-6.3513	15:12:56.8	32:02:48.1	19.91	20.82	19.27	20.29	109	1.91	0.1148 ± 0.0003	···	-3.9 ± 0.6	···	···
CB-4.3417	15:12:57.7	30:35:31.4	19.37	20.10	17.98	18.77	114	1.71	star	···	···	···	···
CB-5.3250	15:12:58.6	31:31:24.4	18.71	19.77	18.24	19.36	159	2.21	0.0939 ± 0.0003	9.0 ± 1.1	···	···	···
CB-4.3335	15:12:59.1	30:41:25.2	20.06	21.16	19.45	20.79	109	2.01	0.2550 ± 0.0003	21.8 ± 1.5	···	4.5 ± 0.7	···
CB-6.3421	15:12:59.3	31:58:46.1	19.17	20.41	18.88	20.13	96	2.01	0.1170 ± 0.0003	···	···	···	···
CB-5.3226	15:13:00.1	31:18:23.3	20.20	21.05	19.13	20.16	94	1.72	0.2659 ± 0.0003	···	···	···	14.1 ± 0.5
CB-4.3295	15:13:00.3	30:34:42.6	19.66	21.05	18.87	20.10	149	2.55	0.1992 ± 0.0003	···	···	···	···
CB-5.3191	15:13:00.4	31:27:11.2	19.97	21.19	19.94	21.20	110	2.15	0.0966 ± 0.0003	28.9 ± 2.0	···	4.7 ± 0.8	16.3 ± 1.0
CB-5.3172	15:13:01.0	31:23:55.1	18.61	19.44	17.83	18.65	76	1.52	star	···	···	···	···
CB-6.3329	15:13:01.2	31:59:28.5	17.74	19.55	17.41	18.96	212	3.01	0.1153 ± 0.0003	···	···	-2.2 ± 0.4	···
CB-5.3128	15:13:01.5	31:33:37.8	20.85	21.18	20.30	21.54	72	1.22	star	···	···	···	···
CB-4.3246	15:13:01.7	30:30:57.6	18.87	19.79	17.92	18.83	204	2.32	star	···	···	···	···
CB-6.3295	15:13:02.2	31:59:55.6	17.72	19.78	18.21	20.10	120	2.57	0.0772 ± 0.0003	24.8 ± 1.3	···	5.2 ± 0.5	9.0 ± 0.5
CB-4.3112	15:13:03.9	30:46:32.5	18.72	19.92	18.69	19.68	141	2.21	0.0888 ± 0.0003	23.0 ± 3.4	···	···	···
CB-5.3072	15:13:04.1	31:18:11.5	17.96	19.37	17.19	18.48	350	2.96	0.1089 ± 0.0003	···	···	-3.1 ± 0.6	···
CB-6.3204	15:13:04.2	32:00:26.0	17.19	19.76	17.14	19.17	802	5.12	0.1357 ± 0.0003	···	···	-2.5 ± 0.4	···
CB-4.3127	15:13:04.6	30:29:43.7	17.51	18.57	16.27	17.34	261	2.24	star	···	···	···	···
CB-4.3092	15:13:04.7	30:43:13.9	20.42	21.63	20.18	21.25	92	1.95	0.2656 ± 0.0003	···	5.4 ± 0.2	···	···
CB-5.3033	15:13:04.7	31:27:51.1	16.39	18.57	15.69	17.73	883	4.90	0.0946 ± 0.0003	···	···	···	···
CB-5.3014	15:13:04.9	31:32:44.4	18.16	19.62	17.64	18.94	366	2.96	0.0940 ± 0.0003	···	···	-3.0 ± 0.5	···
CB-4.3065	15:13:05.5	30:38:26.0	19.43	20.54	18.19	19.49	131	2.19	0.2473 ± 0.0003	···	···	-1.9 ± 0.4	···
CB-6.3135	15:13:05.9	31:56:32.5	19.54	19.95	18.83	19.21	28	1.14	0.1148 ± 0.0003	···	···	···	···
CB-4.3010	15:13:07.3	30:36:29.4	16.86	18.46	16.39	17.82	588	3.61	0.0841 ± 0.0003	···	-2.7 ± 0.4	-2.6 ± 0.4	···
CB-6.3069	15:13:07.5	31:59:26.7	18.01	20.05	18.35	20.24	446	4.03	0.0774 ± 0.0003	36.9 ± 1.5	···	9.9 ± 0.4	11.7 ± 0.5
CB-5.2908	15:13:07.5	31:29:58.7	17.55	20.13	17.54	19.94	688	4.86	0.0943 ± 0.0003	···	···	···	···
CB-4.2985	15:13:08.2	30:32:01.8	19.15	20.18	19.50	20.68	136	2.13	0.1629 ± 0.0003	···	···	···	23.1 ± 1.8
CB-4.2926	15:13:09.0	30:42:56.7	20.30	21.29	19.16	20.37	115	2.18	0.2632 ± 0.0003	···	···	···	···
CB-5.2833	15:13:09.2	31:35:11.4	18.39	19.22	17.00	17.90	225	1.95	star	···	···	···	···
CB-4.2934	15:13:09.2	30:35:42.4	19.18	20.08	18.86	19.94	98	1.77	0.1284 ± 0.0003	14.3 ± 1.3	···	···	3.8 ± 0.6
CB-5.2856	15:13:09.4	31:24:58.7	20.57	21.35	18.99	20.15	82	1.72	0.3572 ± 0.0003	···	···	···	···
CB-6.2958	15:13:09.7	32:03:52.8	18.64	19.97	18.61	19.75	230	2.50	0.2172 ± 0.0003	6.8 ± 0.5	-2.4 ± 0.4	···	···
CB-5.2798	15:13:10.6	31:27:52.7	19.58	20.62	18.48	19.63	124	1.93	0.2409 ± 0.0003	···	···	-3.5 ± 0.5	···
CB-6.2933	15:13:10.7	31:59:18.5	19.54	20.37	18.59	19.58	118	1.91	0.1378 ± 0.0003	···	···	···	···
CB-5.2761	15:13:11.2	31:35:32.3	18.68	19.88	18.20	19.44	220	2.37	0.0671 ± 0.0003	···	···	···	···

TABLE 2.5—*Continued*

Object	RA (1950)	Dec.	g_{tot}	g_{core}	r_{tot}	r_{core}	Area (□″)	irl (″)	z	W_λ([O II]) (Å)	W_λ(Hδ) (Å)	W_λ(Hβ) (Å)	W_λ([O III]5007) (Å)
CB-4.2867	15:13:11.4	30:29:24.1	19.15	20.40	19.20	20.31	211	2.41	0.2461 ± 0.0003	30.5 ± 2.6	···	3.7 ± 0.7	···
CB-5.2738	15:13:12.4	31:29:04.3	17.64	19.59	17.41	19.33	407	4.09	0.0903 ± 0.0003	···	···	···	···
CB-4.2811	15:13:12.6	30:38:14.9	18.28	19.90	18.19	19.77	254	2.98	0.1300 ± 0.0010	···	···	···	···
CB-4.2794	15:13:13.1	30:36:12.0	18.03	19.37	17.42	18.89	265	2.61	0.1301 ± 0.0003	8.0 ± 0.9	···	···	···
CB-4.2767	15:13:13.7	30:39:18.4	17.94	19.45	17.27	18.62	402	3.08	0.1276 ± 0.0003	···	···	···	···
CB-6.2785	15:13:13.9	32:02:58.9	21.77	22.42	21.50	22.14	23	1.23	0.3488 ± 0.0003	···	···	···	···
CB-5.2673	15:13:14.3	31:26:00.8	17.97	19.56	17.99	19.46	277	2.98	0.1009 ± 0.0003	8.0 ± 0.9	-4.2 ± 0.6	···	···
CB-6.2742	15:13:14.7	32:06:05.4	20.67	21.89	19.63	21.21	86	1.84	0.4111 ± 0.0003	···	···	···	···
CB-6.2726	15:13:15.3	31:59:19.0	18.19	19.76	17.55	18.75	397	3.28	0.1363 ± 0.0003	···	···	···	···
CB-4.2680	15:13:15.5	30:43:42.0	18.76	20.62	18.38	20.19	249	3.06	0.2813 ± 0.0003	···	···	···	···
CB-00.40	15:13:15.9	30:31:27.0	···	···	21.03	21.49	37	1.77	star	···	···	···	···
CB-6.2628	15:13:17.7	31:55:20.2	18.38	19.69	17.75	18.90	198	2.63	0.1155 ± 0.0003	···	···	···	···
CB-5.2477	15:13:18.2	31:32:30.1	18.39	19.23	17.50	18.34	198	1.94	star	···	···	···	···
CB-4.2563	15:13:18.4	30:37:41.0	18.27	19.63	18.40	19.71	137	2.26	0.1296 ± 0.0003	36.0 ± 1.5	···	13.8 ± 0.4	13.0 ± 0.5
CB-5.2487	15:13:18.6	31:24:50.3	18.37	19.69	18.27	19.50	304	3.01	0.1010 ± 0.0003	26.8 ± 1.1	···	5.4 ± 0.3	10.0 ± 0.3
CB-4.2502	15:13:19.4	30:43:37.7	21.18	21.68	20.49	21.61	69	1.45	0.2466 ± 0.0003	57.4 ± 8.8	-9.2 ± 0.1	···	···
CB-6.2536	15:13:19.5	32:03:24.8	21.20	21.83	19.97	20.99	80	1.63	0.4196 ± 0.0003	14.2 ± 1.0	···	···	···
CB-4.2522	15:13:19.6	30:31:03.0	19.40	19.96	18.64	19.31	122	1.64	star	···	···	···	···
CB-5.2420	15:13:19.9	31:27:27.4	18.87	19.95	18.34	19.46	197	2.21	0.1169 ± 0.0003	8.7 ± 0.9	···	···	···
CB-4.2442	15:13:20.5	30:42:07.0	19.57	20.61	18.35	19.44	143	2.05	0.2473 ± 0.0003	···	···	-3.8 ± 0.5	···
CB-5.2396	15:13:20.6	31:26:08.7	17.92	18.86	15.95	17.03	220	2.04	star	···	···	···	···
CB-5.2371	15:13:21.3	31:24:02.2	16.57	18.78	16.37	18.36	708	4.39	0.1060 ± 0.0003	···	-2.4 ± 0.4	-3.3 ± 0.4	···
CB-6.2442	15:13:22.6	31:55:53.8	18.18	19.00	17.15	18.03	131	1.82	star	···	···	···	···
CB-6.2371	15:13:23.7	32:04:25.1	17.80	19.15	16.94	18.27	327	2.99	0.0914 ± 0.0003	···	···	···	···
CB-5.2243	15:13:24.6	31:25:21.7	19.72	20.84	19.94	20.83	67	1.49	0.1331 ± 0.0003	17.2 ± 3.0	···	···	7.7 ± 1.3
CB-5.2174	15:13:25.6	31:32:35.5	15.99	17.98	15.28	16.80	1025	4.58	0.0714 ± 0.0003	···	···	···	···
CB-5.2089	15:13:27.2	31:35:07.8	18.43	19.23	17.38	18.25	196	1.85	star	···	···	···	···
CB-5.2091	15:13:27.8	31:23:46.9	18.75	19.58	17.92	18.66	204	2.03	star	···	···	···	···
CB-5.1998	15:13:29.5	31:29:25.8	17.62	19.19	17.27	18.64	432	3.19	0.1006 ± 0.0003	9.4 ± 0.5	-1.4 ± 0.3	3.1 ± 0.2	2.1 ± 0.2
CB-5.1879	15:13:32.2	31:29:45.0	18.59	19.58	18.04	18.94	196	2.05	0.1008 ± 0.0003	28.1 ± 0.7	···	5.3 ± 0.2	91.5 ± 0.2
CB-5.1773	15:13:34.6	31:33:47.5	18.57	20.09	18.08	19.33	301	3.46	0.1368 ± 0.0003	9.0 ± 1.2	···	···	···
1514+2815	15:14:03.5	28:15:14.0	18.55	19.61	17.79	18.76	79	1.69	0.1206 ± 0.0007	···	···	···	···
CB-11.6857	15:15:31.5	31:30:54.8	18.12	19.38	···	···	217	2.41	star	···	···	···	···
CB-11.6784	15:15:33.8	31:25:10.3	18.15	19.62	17.51	18.95	297	3.04	0.1283 ± 0.0003	···	···	-2.7 ± 0.4	···
CB-11.6722	15:15:35.2	31:24:06.8	19.70	20.71	19.12	19.97	115	1.91	star	···	···	···	···
CB-11.6708	15:15:35.4	31:26:57.5	18.36	20.54	18.45	20.47	346	4.68	0.0592 ± 0.0003	···	···	···	···
CB-11.6664	15:15:37.1	31:16:53.4	20.16	20.97	19.99	21.20	106	1.83	0.1842 ± 0.0003	48.9 ± 1.4	···	9.6 ± 0.6	17.7 ± 0.7
CB-11.6614	15:15:38.2	31:19:03.9	20.43	21.25	19.51	20.40	100	1.74	star	···	···	···	···
CB-11.6549	15:15:39.4	31:25:00.2	20.47	21.52	20.50	21.76	88	1.84	0.1601 ± 0.0003	12.2 ± 1.4	···	···	5.2 ± 0.9
CB-11.6494	15:15:40.6	31:23:28.7	22.21	22.47	···	···	23	1.00	0.4065 ± 0.0003	47.8 ± 1.0	···	···	···
CB-11.6487	15:15:40.7	31:28:13.8	19.78	21.02	19.80	20.84	115	2.01	0.3131 ± 0.0003	9.2 ± 0.7	···	3.7 ± 0.5	···
CB-11.6481	15:15:41.2	31:19:05.2	19.82	20.67	18.34	19.33	111	1.90	star	···	···	···	···
CB-11.6427	15:15:41.9	31:30:01.9	20.44	21.45	21.40	21.72	95	1.84	0.2934 ± 0.0003	43.2 ± 0.7	···	···	21.3 ± 0.5
CB-11.6392	15:15:43.0	31:26:10.6	18.55	19.75	18.10	19.47	225	2.33	0.1282 ± 0.0003	3.4 ± 0.6	-2.8 ± 0.6	···	···
CB-11.6376	15:15:43.7	31:17:18.6	20.87	21.66	21.60	21.64	87	1.80	0.1847 ± 0.0003	25.5 ± 1.8	···	···	5.5 ± 0.7

TABLE 2.5—*Continued*

Object	RA (1950)	Dec.	g_{tot}	g_{core}	r_{tot}	r_{core}	Area (□″)	irl (″)	z	W_λ([O II]) (Å)	W_λ(Hδ) (Å)	W_λ(Hβ) (Å)	W_λ([O III]5007) (Å)
CB-11.6285	15:15:45.9	31:28:04.1	21.03	21.75	20.55	21.64	77	1.62	0.3127 ± 0.0003	32.9 ± 1.4	···	5.6 ± 0.7	···
CB-11.6222	15:15:47.4	31:29:08.4	20.48	21.03	19.06	19.82	29	1.22	star	···	···	···	···
CB-11.6218	15:15:47.8	31:17:22.5	20.13	21.54	21.85	22.06	104	2.12	0.1483 ± 0.0003	30.3 ± 1.8	···	···	22.6 ± 0.7
CB-11.6202	15:15:48.1	31:23:24.7	20.36	21.14	20.08	20.76	99	1.79	0.1279 ± 0.0003	···	···	···	···
CB-11.6133	15:15:49.9	31:22:24.4	21.81	22.28	20.52	21.32	30	1.25	star	···	···	···	···
CB-11.6059	15:15:51.8	31:26:17.8	18.19	19.52	17.95	19.36	292	2.69	0.1103 ± 0.0003	6.9 ± 0.7	···	6.2 ± 0.2	0.9 ± 0.2
CB-11.6043	15:15:52.4	31:19:12.9	19.76	20.92	19.57	21.20	123	2.19	0.0789 ± 0.0003	···	···	3.7 ± 0.5	13.8 ± 0.6
CB-11.5982	15:15:53.6	31:22:04.8	17.41	19.17	16.59	18.29	469	3.57	0.1288 ± 0.0003	···	···	-1.5 ± 0.3	···
CB-11.5942	15:15:54.1	31:28:47.0	18.85	20.02	18.89	20.20	193	2.19	0.1082 ± 0.0003	13.2 ± 1.6	-3.6 ± 0.9	2.9 ± 0.5	2.9 ± 0.5
CB-11.5932	15:15:54.8	31:16:14.0	19.58	20.48	19.91	20.91	117	1.90	0.0667 ± 0.0003	54.0 ± 2.0	···	8.0 ± 0.5	27.4 ± 0.4
CB-11.5857	15:15:56.0	31:29:42.0	19.17	20.58	18.54	19.72	243	2.71	0.2396 ± 0.0003	4.6 ± 1.0	···	···	···
CB-11.5808	15:15:56.9	31:25:46.8	21.45	22.06	21.61	22.15	60	1.35	0.5572 ± 0.0003	40.0 ± 1.3	···	···	···
CB-11.5793	15:15:57.3	31:21:21.6	22.16	22.60	···	···	20	0.94	0.2388 ± 0.0003	40.7 ± 3.9	···	16.5 ± 3.3	29.3 ± 2.2
CB-11.5729	15:15:58.3	31:24:45.6	18.45	19.67	18.07	19.50	100	1.93	0.1072 ± 0.0003	10.6 ± 0.6	···	2.5 ± 0.2	1.6 ± 0.2
CB-11.5656	15:15:59.5	31:29:18.1	17.71	19.83	17.76	19.58	448	3.75	0.1287 ± 0.0003	3.3 ± 0.8	···	···	···
CB-11.5574	15:16:01.2	31:24:44.4	18.88	20.11	18.61	20.00	162	2.31	0.2175 ± 0.0003	7.1 ± 0.7	-2.9 ± 0.5	2.2 ± 0.2	···
CB-11.5538	15:16:02.0	31:29:58.6	18.32	19.50	17.48	18.60	281	2.58	0.1073 ± 0.0003	···	···	-2.8 ± 0.3	···
CB-11.5529	15:16:02.5	31:22:51.8	21.74	22.54	21.38	22.11	80	2.02	0.1092 ± 0.0003	···	···	5.0 ± 1.0	5.6 ± 1.3
CB-11.5493	15:16:03.3	31:23:19.7	14.55	16.88	···	···	1207	4.54	star	···	···	···	···
CB-11.5429	15:16:04.7	31:28:57.7	21.03	21.97	20.57	21.71	67	1.48	0.2414 ± 0.0003	25.5 ± 1.3	···	4.8 ± 0.7	8.1 ± 0.7
CB-11.5371	15:16:05.7	31:25:19.4	18.09	19.91	18.31	20.16	325	3.42	0.1073 ± 0.0003	···	-3.9 ± 0.8	···	···
CB-11.5335	15:16:06.6	31:28:29.4	17.11	18.84	16.31	17.93	537	3.67	0.1083 ± 0.0003	···	···	-3.2 ± 0.3	···
CB-11.5313	15:16:07.2	31:24:41.5	21.87	22.56	21.38	22.17	34	1.31	0.2423 ± 0.0003	···	···	12.3 ± 2.2	36.0 ± 2.8
CB-11.5287	15:16:07.9	31:20:44.1	20.02	20.91	19.85	21.40	94	1.79	0.1280 ± 0.0003	27.5 ± 1.6	···	6.8 ± 0.6	13.3 ± 0.6
CB-11.5243	15:16:09.1	31:31:56.9	19.06	20.41	19.15	20.47	188	2.34	0.1066 ± 0.0003	18.2 ± 1.7	···	4.0 ± 0.4	2.3 ± 0.5
CB-11.5187	15:16:10.8	31:18:35.0	18.10	19.07	16.42	17.53	236	2.24	star	···	···	···	···
CB-11.5176	15:16:11.0	31:23:44.8	20.26	20.99	19.89	20.96	103	1.82	0.1069 ± 0.0003	···	-6.1 ± 1.4	3.1 ± 0.5	4.4 ± 0.6
CB-11.5171	15:16:11.1	31:25:38.3	16.57	17.88	14.73	15.86	487	2.76	star	···	···	···	···
CB-11.5155	15:16:11.7	31:16:22.9	19.47	20.46	19.55	20.48	62	1.48	star	···	···	···	···
CB-11.5131	15:16:12.0	31:29:36.6	18.45	19.91	17.82	19.27	283	2.91	0.1089 ± 0.0003	···	···	-2.4 ± 0.3	···
CB-11.5122	15:16:12.4	31:17:24.3	20.37	21.86	20.65	22.08	99	2.18	0.3781 ± 0.0003	18.8 ± 2.0	···	···	···
CB-11.5028	15:16:14.3	31:20:23.3	21.67	22.64	···	···	35	1.49	0.6722 ± 0.0003	···	···	···	···
CB-11.4982	15:16:15.3	31:22:12.7	18.00	19.28	17.89	19.35	279	2.58	0.0146 ± 0.0003	···	···	9.0 ± 0.2	32.6 ± 0.2
CB-11.4947	15:16:16.6	31:17:15.9	19.68	21.07	18.92	20.20	121	2.30	0.2945 ± 0.0003	6.6 ± 1.0	···	···	···
CB-11.4892	15:16:17.6	31:27:51.7	21.88	22.85	···	···	68	1.62	0.5680 ± 0.0010	···	···	···	···
CB-11.4837	15:16:18.5	31:29:17.3	20.50	21.32	20.24	20.60	88	1.66	star	···	···	···	···
CB-11.4807	15:16:19.3	31:33:22.1	18.87	20.05	18.39	19.45	136	2.30	0.1184 ± 0.0003	···	···	···	···
CB-11.4766	15:16:20.7	31:23:50.5	20.90	21.68	19.97	21.17	79	1.69	0.4109 ± 0.0003	8.9 ± 0.8	-2.4 ± 0.5	···	···
CB-11.4754	15:16:21.1	31:24:18.8	18.65	20.31	17.95	19.75	268	3.23	0.2391 ± 0.0003	22.5 ± 0.6	···	6.8 ± 0.3	31.5 ± 0.4
CB-11.4673	15:16:23.4	31:22:45.0	19.36	20.40	18.71	19.97	153	2.37	0.1182 ± 0.0003	9.0 ± 1.1	···	-1.6 ± 0.3	···
CB-11.4607	15:16:25.1	31:22:17.3	19.54	20.51	19.15	20.39	129	2.08	0.2374 ± 0.0003	10.2 ± 0.8	-4.4 ± 0.6	1.5 ± 0.3	···
CB-11.4547	15:16:27.0	31:16:28.7	19.87	20.76	19.66	20.60	109	1.88	0.1136 ± 0.0003	20.6 ± 2.6	···	3.1 ± 0.5	···
CB-11.4442	15:16:29.0	31:30:41.0	18.71	19.93	17.96	19.27	314	2.96	0.1084 ± 0.0003	···	···	···	···
CB-11.4365	15:16:30.6	31:30:40.1	17.76	19.30	17.13	18.61	364	3.16	0.1086 ± 0.0003	···	···	···	···
CB-11.4337	15:16:31.7	31:25:22.8	21.50	22.08	21.26	21.57	57	1.34	0.3251 ± 0.0003	13.5 ± 1.9	···	···	···

TABLE 2.5—*Continued*

Object	RA (1950)	Dec. (1950)	g_{tot}	g_{core}	r_{tot}	r_{core}	Area (□″)	irl (″)	z	W_λ([O II]) (Å)	W_λ(Hδ) (Å)	W_λ(Hβ) (Å)	W_λ([O III]5007) (Å)
CB-11.4272	15:16:32.7	31:34:01.3	19.30	20.71	19.32	20.58	196	2.45	0.2442 ± 0.0003	22.5 ± 1.7	···	···	3.5 ± 0.7
CB-11.4283	15:16:33.0	31:19:32.8	20.49	21.71	19.91	20.89	94	2.02	0.2955 ± 0.0003	···	···	···	···
CB-11.4238	15:16:34.0	31:15:57.2	17.84	18.76	16.25	17.41	198	1.98	star	···	···	···	···
CB-11.4202	15:16:34.8	31:19:12.0	20.18	21.53	19.82	21.51	107	2.14	0.3466 ± 0.0003	26.7 ± 1.4	···	···	···
CB-11.4176	15:16:35.3	31:30:38.5	20.25	21.32	20.00	21.09	115	2.24	0.2379 ± 0.0003	13.1 ± 1.0	-4.3 ± 0.8	3.6 ± 0.4	2.1 ± 0.5
CB-11.4146	15:16:36.1	31:24:18.0	22.13	22.65	20.56	21.62	28	1.25	0.4342 ± 0.0003	11.9 ± 1.5	···	···	···
CB-11.4074	15:16:38.0	31:16:57.2	21.19	21.91	21.91	22.49	38	1.39	0.1101 ± 0.0003	···	···	22.2 ± 3.1	···
CB-11.4021	15:16:39.3	31:16:30.3	19.85	20.90	18.78	20.46	132	2.59	0.0610 ± 0.0003	···	···	6.4 ± 0.3	15.0 ± 0.4
CB-11.3966	15:16:40.4	31:22:01.3	18.87	19.81	17.31	18.14	187	1.96	star	···	···	···	···
CB-8.4668	15:16:40.4	28:38:25.4	18.14	19.44	17.45	18.81	289	2.81	0.0831 ± 0.0003	···	···	···	2.1 ± 0.3
CB-7.4500	15:16:42.0	28:32:32.0	20.64	21.53	20.47	21.22	82	1.77	0.2290 ± 0.0003	15.8 ± 1.8	···	4.8 ± 0.7	···
CB-11.3894	15:16:42.3	31:28:52.3	20.42	21.50	20.86	21.69	92	1.90	0.6551 ± 0.0003	32.6 ± 0.9	···	···	···
CB-11.3820	15:16:44.0	31:31:49.3	19.84	20.76	18.78	19.91	117	1.91	0.2415 ± 0.0003	···	···	-4.0 ± 0.7	···
CB-11.3826	15:16:44.0	31:23:03.5	21.73	22.34	20.53	21.60	30	1.25	0.6102 ± 0.0003	45.6 ± 3.1	···	···	···
CB-11.3773	15:16:45.0	31:32:10.7	19.40	20.74	18.13	19.67	196	2.77	0.2382 ± 0.0003	···	···	···	···
CB-7.4365	15:16:45.7	27:55:45.7	18.09	19.44	17.55	18.86	280	2.73	0.1073 ± 0.0003	···	···	···	···
CB-11.3735	15:16:46.1	31:26:54.2	21.34	21.54	20.18	21.01	86	1.54	0.3788 ± 0.0003	31.7 ± 1.6	···	···	···
CB-8.4374	15:16:46.4	28:36:17.4	18.91	20.11	18.06	19.22	172	2.35	0.1820 ± 0.0003	···	···	-1.8 ± 0.3	···
CB-7.4321	15:16:46.6	27:54:27.3	18.65	20.07	17.59	19.14	78	1.72	0.2155 ± 0.0003	···	···	-2.3 ± 0.3	···
CB-11.3705	15:16:47.1	31:17:47.6	21.93	22.62	21.42	21.91	25	1.14	0.6435 ± 0.0007	11.0 ± 2.7	···	···	···
CB-7.4264	15:16:47.8	28:00:48.0	19.99	20.93	18.92	19.94	122	1.98	0.2291 ± 0.0003	···	···	···	···
CB-99.3	15:16:48.2	28:33:11.1	19.37	20.37	19.27	20.01	153	2.11	0.0723 ± 0.0003	···	···	···	···
CB-11.3668	15:16:48.2	31:23:11.7	18.32	19.93	17.74	19.36	317	3.59	0.0770 ± 0.0003	···	···	···	···
CB-7.4179	15:16:49.1	28:29:11.5	17.34	18.93	16.67	18.07	540	3.48	0.0733 ± 0.0003	···	···	···	···
CB-7.4200	15:16:49.3	27:53:20.9	19.23	20.18	18.45	19.48	136	1.98	0.1561 ± 0.0003	···	···	···	···
CB-11.3569	15:16:50.4	31:25:54.2	21.01	22.03	20.21	21.27	71	1.76	0.3120 ± 0.0010	···	···	···	···
CB-11.3533	15:16:51.6	31:22:06.0	20.02	20.84	19.35	20.60	115	1.90	0.3469 ± 0.0003	4.8 ± 0.4	···	···	···
CB-7.4060	15:16:51.8	28:30:31.4	20.00	21.11	18.96	20.10	116	2.09	0.2809 ± 0.0003	···	···	-2.4 ± 0.4	···
CB-7.4069	15:16:52.4	27:49:17.4	18.61	20.09	18.52	20.00	190	2.56	0.1576 ± 0.0003	20.6 ± 1.4	···	···	···
CB-7.4051	15:16:52.5	27:59:38.0	18.42	19.68	17.89	19.04	251	2.67	0.0707 ± 0.0003	···	···	···	···
CB-7.3985	15:16:53.4	28:29:30.9	18.17	19.23	17.62	18.58	89	1.76	0.0758 ± 0.0003	···	···	-3.3 ± 0.4	···
CB-7.4002	15:16:53.6	27:58:24.5	20.99	21.46	19.39	20.22	65	1.32	star	···	···	···	···
CB-7.3975	15:16:53.6	28:32:08.2	17.12	19.50	16.85	18.79	563	4.52	0.1182 ± 0.0003	···	···	···	24.2 ± 0.6
CB-11.3420	15:16:54.3	31:26:22.6	19.85	20.85	19.61	20.61	104	1.97	0.2932 ± 0.0003	23.5 ± 1.3	···	···	···
CB-7.3925	15:16:55.5	27:49:13.0	18.41	19.42	17.58	18.56	211	2.10	0.0740 ± 0.0003	···	···	···	···
CB-7.3876	15:16:55.6	28:25:42.5	19.75	20.59	18.26	19.02	75	1.49	star	···	···	···	···
CB-7.3826	15:16:56.7	28:31:23.3	16.02	18.42	15.71	17.74	113	2.45	0.0747 ± 0.0003	···	···	-1.8 ± 0.3	···
CB-7.3836	15:16:57.0	27:58:23.3	19.97	21.12	19.55	20.71	112	2.12	0.2306 ± 0.0003	13.6 ± 1.9	···	···	···
CB-7.3806	15:16:57.0	28:23:06.6	20.42	21.28	23.11	23.09	37	1.85	star	···	···	···	···
CB-8.3829	15:16:58.4	28:35:40.2	18.53	19.62	18.45	19.53	206	2.22	0.1717 ± 0.0003	45.9 ± 0.8	···	9.7 ± 0.3	8.5 ± 0.4
CB-7.3773	15:16:58.4	27:49:16.0	17.80	19.60	17.78	19.40	249	2.95	0.1199 ± 0.0003	10.3 ± 1.0	···	···	···
CB-11.3260	15:16:58.5	31:25:41.0	19.48	20.38	19.33	20.25	169	2.02	0.2913 ± 0.0003	18.8 ± 0.6	···	8.1 ± 0.3	···
CB-7.3709	15:16:59.5	27:55:16.6	18.99	20.03	18.74	19.93	98	1.89	0.1073 ± 0.0003	20.8 ± 2.4	···	4.5 ± 0.5	···
CB-7.3646	15:17:00.1	28:31:18.3	18.56	19.87	17.85	19.10	255	2.69	0.1181 ± 0.0003	···	···	-3.3 ± 0.4	···
CB-7.3668	15:17:00.3	28:01:52.5	19.85	20.96	18.56	19.96	123	2.18	0.2343 ± 0.0003	···	···	-5.0 ± 0.8	···

TABLE 2.5—*Continued*

Object	RA (1950)	Dec. (1950)	g_{tot}	g_{core}	r_{tot}	r_{core}	Area (□″)	irl (″)	z	W_λ([O II]) (Å)	W_λ(Hδ) (Å)	W_λ(Hβ) (Å)	W_λ([O III]5007) (Å)
CB-7.3617	15:17:00.7	28:29:41.9	18.80	19.62	17.72	18.67	162	2.05	star	···	···	···	···
CB-7.3571	15:17:01.6	28:32:25.8	19.33	20.21	18.60	19.51	103	1.78	0.1203 ± 0.0003	···	···	···	···
CB-7.3566	15:17:01.9	28:27:15.7	16.71	18.67	16.19	17.93	749	4.29	0.0837 ± 0.0003	6.1 ± 1.3	···	-2.6 ± 0.4	···
CB-7.3587	15:17:02.1	27:49:47.9	17.33	18.92	16.73	18.15	591	3.71	0.1208 ± 0.0003	···	-2.5 ± 0.5	-3.3 ± 0.3	···
CB-8.3610	15:17:03.2	28:33:44.1	16.61	19.35	16.47	18.73	528	4.79	0.1186 ± 0.0003	···	-2.2 ± 0.4	···	···
CB-7.3500	15:17:03.6	28:00:34.0	19.85	21.07	18.92	19.96	117	2.14	0.2354 ± 0.0003	···	···	···	···
CB-7.3443	15:17:04.3	28:30:49.7	17.79	19.23	16.96	18.33	389	2.88	0.1192 ± 0.0003	···	···	···	···
CB-7.3458	15:17:04.5	27:51:16.9	17.42	19.60	17.27	19.31	508	4.08	0.0842 ± 0.0004	···	···	···	4.8 ± 0.4
CB-7.3424	15:17:04.6	28:28:28.0	19.18	20.21	19.10	20.49	109	1.94	0.1105 ± 0.0003	46.3 ± 4.4	···	···	···
CB-00.2	15:17:05.8	28:27:27.3	16.14	17.56	14.18	15.42	96	1.96	star	···	···	···	···
CB-7.3390	15:17:06.1	27:58:36.4	20.52	21.74	20.24	21.22	83	1.95	0.3430 ± 0.0010	···	···	···	···
CB-8.3469	15:17:06.1	28:37:15.1	21.44	22.05	20.92	21.87	63	1.56	0.3093 ± 0.0003	42.8 ± 1.9	···	6.0 ± 1.0	···
CB-8.3426	15:17:07.2	28:35:00.6	18.42	19.91	17.88	19.14	273	3.05	0.1720 ± 0.0003	4.7 ± 0.5	···	···	···
CB-7.3308	15:17:08.1	27:52:19.3	16.07	17.55	14.72	15.69	570	2.98	star	···	···	···	···
CB-7.3278	15:17:08.4	28:26:17.1	20.02	20.49	19.29	19.86	92	1.39	star	···	···	···	···
CB-8.3353	15:17:08.7	28:36:07.3	15.39	17.19	13.61	15.33	816	3.54	star	···	···	···	···
1517+2815	15:17:08.7	28:15:37.0	16.58	18.87	16.71	18.73	753	4.95	0.0680 ± 0.0005	···	···	···	···
CB-7.3276	15:17:08.9	27:56:48.8	19.12	20.27	18.48	19.73	209	2.35	0.1200 ± 0.0003	···	···	-2.3 ± 0.4	···
CB-8.3317	15:17:09.7	28:34:23.8	18.55	20.06	18.42	19.76	146	2.77	0.1177 ± 0.0003	···	···	···	···
CB-7.3122	15:17:12.3	27:54:25.0	18.72	19.79	18.41	19.69	98	1.88	0.1388 ± 0.0003	···	···	···	···
CB-7.3048	15:17:13.1	28:31:26.8	19.90	21.23	19.50	20.52	127	2.64	0.1215 ± 0.0003	···	···	-3.6 ± 0.4	···
CB-8.3094	15:17:13.9	28:34:31.4	20.80	22.43	20.13	21.40	70	2.00	0.4312 ± 0.0003	···	···	···	···
CB-7.3039	15:17:14.0	27:57:50.6	17.80	19.36	17.33	18.69	499	3.47	0.0836 ± 0.0003	···	···	···	···
CB-99.4	15:17:14.9	28:33:13.4	18.62	19.80	18.64	19.85	217	2.33	0.1206 ± 0.0003	16.4 ± 0.9	-5.0 ± 0.6	2.8 ± 0.2	···
CB-8.2989	15:17:16.0	28:34:54.6	19.24	20.10	18.59	19.61	172	1.94	star	···	···	···	···
CB-8.2920	15:17:17.2	28:38:28.6	19.99	20.70	19.62	20.80	101	1.71	0.1190 ± 0.0010	···	10.9 ± 1.4	12.4 ± 0.7	···
CB-7.2883	15:17:17.3	28:29:54.9	17.15	19.06	16.44	18.15	697	4.20	0.1193 ± 0.0003	···	···	-2.3 ± 0.3	···
CB-7.2912	15:17:17.3	27:55:30.1	18.46	20.38	18.18	20.19	288	3.29	0.1372 ± 0.0003	···	···	···	···
CB-7.2833	15:17:18.1	28:32:53.2	18.65	20.11	18.25	19.80	291	2.89	0.1194 ± 0.0003	···	-4.6 ± 0.8	···	···
CB-7.2835	15:17:18.7	27:53:22.1	18.20	19.64	17.70	19.06	331	3.07	0.0845 ± 0.0003	···	···	-3.4 ± 0.5	···
CB-7.2783	15:17:19.0	28:29:21.4	18.67	19.96	18.20	19.56	206	2.35	0.1207 ± 0.0003	···	···	···	···
CB-7.2737	15:17:20.1	28:28:12.3	19.04	20.23	18.23	19.29	235	2.47	0.1472 ± 0.0003	···	···	15.1 ± 0.2	···
CB-8.2740	15:17:20.6	28:39:25.9	18.73	19.48	17.33	18.14	136	1.82	star	···	···	···	···
CB-8.2715	15:17:21.2	28:34:50.4	18.30	19.52	18.45	19.70	266	2.52	0.0746 ± 0.0003	43.2 ± 1.4	···	9.3 ± 0.2	18.2 ± 0.3
CB-7.2619	15:17:22.3	28:30:06.9	18.87	19.57	17.85	18.64	118	1.71	star	···	···	···	···
CB-7.2637	15:17:22.6	27:46:03.0	18.19	19.51	17.22	18.55	277	2.72	0.1459 ± 0.0003	···	···	···	···
CB-8.2574	15:17:24.3	28:37:39.4	19.96	21.27	19.30	20.60	126	2.38	0.3084 ± 0.0003	6.3 ± 1.0	···	···	···
CB-8.2494	15:17:25.4	28:38:27.0	17.91	19.22	17.05	18.34	101	2.03	0.0889 ± 0.0003	···	···	···	···
CB-7.2386	15:17:27.3	27:57:43.0	17.06	18.71	16.86	18.49	272	2.93	0.0708 ± 0.0003	···	···	1.5 ± 0.2	···
CB-7.2328	15:17:28.2	27:56:05.9	19.63	20.64	18.91	20.43	118	2.08	0.0840 ± 0.0003	···	···	···	···
CB-7.2287	15:17:29.0	27:55:00.6	17.37	19.11	17.25	18.64	512	3.63	0.0716 ± 0.0003	···	-3.6 ± 0.7	···	···
1517+3022A	15:17:46.0	30:22:07.0	16.44	18.54	15.82	17.68	761	5.05	0.0810 ± 0.0002	···	···	···	···
1517+3022B	15:17:48.0	30:22:02.0	16.27	18.47	15.79	17.83	688	4.91	0.0825 ± 0.0002	···	···	···	···
CB-10.1203	15:17:49.9	30:41:54.5	17.27	19.14	16.92	18.79	522	3.94	0.0816 ± 0.0003	···	···	-4.1 ± 0.4	···
CB-10.1172	15:17:50.7	30:33:41.3	17.72	19.09	16.93	18.20	226	2.50	0.0809 ± 0.0003	···	···	-1.9 ± 0.3	···

TABLE 2.5—*Continued*

Object	RA (1950)	Dec. (1950)	g_{tot}	g_{core}	r_{tot}	r_{core}	Area ($\square''$)	irl ($''$)	z	W_λ([O II]) (Å)	W_λ(Hδ) (Å)	W_λ(Hβ) (Å)	W_λ([O III]5007) (Å)
CB-10.1125	15:17:52.0	30:35:36.5	18.29	19.19	17.46	18.32	197	1.92	star	...	...	...	...
CB-10.1118	15:17:52.2	30:28:24.7	18.14	19.70	17.53	19.10	285	3.02	0.0795 ± 0.0003	...	...	-5.4 ± 0.6	...
CB-10.1034	15:17:54.6	30:37:43.1	20.78	21.46	19.78	20.95	80	1.60	0.4082 ± 0.0003	14.2 ± 1.3	...	...	...
CB-10.974	15:17:56.0	30:39:57.3	20.28	21.03	20.53	20.98	82	1.55	0.0907 ± 0.0003	...	...	12.5 ± 0.9	17.6 ± 1.0
CB-10.951	15:17:56.7	30:30:11.0	20.03	20.79	20.09	20.98	98	1.65	0.2095 ± 0.0003	26.5 ± 2.8	...	...	...
CB-10.927	15:17:57.0	30:42:33.3	17.60	18.86	16.99	18.36	141	2.18	0.0608 ± 0.0003	...	...	...	4.1 ± 0.2
CB-10.915	15:17:57.4	30:27:45.4	18.25	19.76	17.69	19.23	237	2.96	0.0779 ± 0.0003	...	...	...	...
CB-10.807	15:18:00.1	30:43:18.1	20.76	21.47	20.37	21.52	42	1.55	0.2384 ± 0.0003	...	...	17.9 ± 3.4	55.2 ± 4.5
CB-10.811	15:18:00.1	30:27:50.1	20.51	21.18	19.08	20.12	66	1.34	star	...	...	...	...
1518+3029	15:18:01.0	30:29:08.0	15.91	18.14	15.59	17.51	219	2.87	0.0664 ± 0.0001	...	...	...	...
CB-10.765	15:18:01.4	30:30:18.4	18.24	19.44	17.45	18.63	236	2.47	0.0648 ± 0.0003	...	...	-3.9 ± 0.4	...
CB-10.754	15:18:01.8	30:37:58.5	19.15	19.94	18.23	19.22	128	1.84	0.3058 ± 0.0003	10.0 ± 0.5	-4.1 ± 0.5	3.4 ± 0.2	...
CB-10.650	15:18:05.0	30:37:56.7	18.81	19.86	18.65	19.78	206	2.16	0.0820 ± 0.0003	...	-5.2 ± 1.0	-4.3 ± 0.5	...
CB-10.641	15:18:05.5	30:30:02.0	16.45	18.38	15.72	17.49	945	4.44	0.0660 ± 0.0003	...	...	-2.5 ± 0.3	...
1518+2817	15:18:07.2	28:17:41.0	16.25	18.64	15.97	18.17	737	5.08	0.0459 ± 0.0001	...	...	...	...
CB-10.487	15:18:09.7	30:40:05.6	20.80	21.61	19.46	20.69	81	1.72	0.2462 ± 0.0003	...	...	...	...
CB-10.443	15:18:10.8	30:37:49.9	18.24	19.11	17.36	18.16	202	1.92	star	...	...	...	...
CB-10.368	15:18:12.8	30:44:17.0	18.88	19.55	17.89	18.65	118	1.70	star	...	...	...	...
CB-10.339	15:18:13.4	30:30:03.5	18.21	19.09	17.23	18.16	96	1.67	star	...	...	...	...
CB-10.268	15:18:15.0	30:35:06.4	18.83	20.34	19.19	20.79	218	2.82	0.0803 ± 0.0003	...	...	...	8.3 ± 0.8
CB-10.267	15:18:15.0	30:30:38.0	18.41	19.09	17.22	18.01	194	1.76	star	...	...	...	...
CB-10.163	15:18:17.7	30:34:55.9	19.81	20.40	18.21	18.98	99	1.51	star	...	...	...	...
CB-10.122	15:18:18.9	30:33:07.1	19.39	20.05	18.96	19.78	105	1.59	star	...	...	...	...
CB-10.97	15:18:19.6	30:38:51.5	19.30	20.67	18.84	20.38	178	2.34	0.2464 ± 0.0003	...	...	...	...
1518+3116	15:18:21.0	31:16:44.0	15.90	18.30	15.36	17.58	75	1.79	0.0731 ± 0.0001	...	...	...	...
CB-16.10932	15:18:23.7	30:43:47.7	21.01	21.68	19.93	21.01	71	1.44	star	...	...	...	...
CB-16.10877	15:18:25.2	30:35:23.4	16.32	18.94	15.88	18.21	680	4.87	0.0786 ± 0.0003	...	...	-3.3 ± 0.3	...
CB-16.10796	15:18:27.0	30:29:13.7	17.25	18.94	17.00	18.72	317	3.27	0.0640 ± 0.0003	...	...	...	...
CB-16.10791	15:18:27.0	30:43:06.3	20.04	20.78	18.47	19.20	104	1.65	star	...	...	...	...
CB-16.10752	15:18:27.9	30:41:40.3	18.99	20.29	18.33	19.40	197	2.44	0.1534 ± 0.0003	...	...	...	...
CB-16.10695	15:18:29.2	30:42:18.7	19.28	20.03	17.95	18.71	122	1.75	star	...	...	...	...
CB-16.10647	15:18:30.8	30:31:52.2	19.08	19.70	17.95	18.72	130	1.70	star	...	...	...	...
CB-16.10607	15:18:31.8	30:34:50.7	19.89	20.72	19.34	20.25	69	1.52	star	...	...	...	...
CB-16.10594	15:18:32.2	30:43:02.3	18.38	19.57	17.71	18.90	249	2.43	0.0768 ± 0.0003	...	...	-2.2 ± 0.4	...
CB-15.10208	15:18:32.8	29:42:08.9	19.22	19.95	17.61	18.46	124	1.81	star	...	...	...	...
CB-16.10462	15:18:35.9	30:52:42.4	19.49	20.22	19.50	19.86	62	1.49	0.0728 ± 0.0003	...	...	-4.5 ± 0.6	...
CB-13.11648	15:18:36.2	28:18:45.5	21.44	21.79	21.31	21.69	68	1.24	0.3919 ± 0.0003	28.7 ± 1.2	...	...	...
CB-16.10375	15:18:38.2	30:48:38.2	19.97	20.68	19.30	20.31	101	1.66	0.0770 ± 0.0003	...	...	-3.8 ± 0.7	...
CB-15.9939	15:18:39.5	29:42:54.9	18.42	19.31	17.32	18.18	232	2.35	star	...	...	...	...
CB-16.10317	15:18:39.9	30:52:08.3	16.53	18.46	16.24	18.11	211	2.78	0.0772 ± 0.0003	...	...	1.7 ± 0.3	15.7 ± 0.3
CB-13.11452	15:18:40.4	28:08:15.5	18.00	19.44	17.34	18.59	225	2.64	0.0742 ± 0.0003	...	...	-1.8 ± 0.4	...
CB-13.11433	15:18:40.8	28:17:41.5	19.18	20.10	18.88	20.02	145	2.07	0.0738 ± 0.0003	9.9 ± 1.0	...	...	2.7 ± 0.3
CB-15.9886	15:18:40.9	29:35:27.3	18.35	19.10	16.37	17.53	219	1.87	star	...	...	...	...
CB-15.9875	15:18:41.1	29:41:59.7	19.75	20.76	19.69	20.67	108	1.89	0.2851 ± 0.0003	27.4 ± 1.4	...	...	12.2 ± 1.4
CB-16.10241	15:18:41.5	30:44:09.2	18.05	19.38	17.43	18.68	391	2.87	0.0424 ± 0.0003	...	...	...	...

TABLE 2.5—*Continued*

Object	RA (1950)	Dec. (1950)	g_{tot}	g_{core}	r_{tot}	r_{core}	Area (□″)	irl (″)	z	W_λ([O II]) (Å)	W_λ(Hδ) (Å)	W_λ(Hβ) (Å)	W_λ([O III]5007) (Å)
CB-13.11364	15:18:42.0	28:20:23.1	19.29	20.42	18.98	20.17	98	2.03	0.1510 ± 0.0010	···	···	···	···
CB-16.10208	15:18:42.2	30:39:36.4	17.31	18.87	16.62	18.00	503	3.44	0.0786 ± 0.0003	···	···	-3.6 ± 0.3	···
CB-16.10194	15:18:42.4	30:49:11.0	18.01	19.41	17.28	18.55	290	2.90	0.0799 ± 0.0003	···	···	···	···
CB-13.11340	15:18:42.4	28:13:32.6	19.58	21.02	19.17	20.47	149	2.43	0.3668 ± 0.0003	3.3 ± 0.7	···	···	···
CB-16.10154	15:18:43.4	30:52:07.8	19.40	20.32	18.85	20.06	129	1.93	0.2385 ± 0.0003	···	-5.3 ± 0.8	2.8 ± 0.3	···
CB-15.9768	15:18:43.8	29:36:24.6	19.54	20.30	18.71	19.58	124	1.88	star	···	···	···	···
CB-13.11267	15:18:43.9	28:08:31.2	19.18	20.12	18.60	19.64	141	2.01	0.0765 ± 0.0003	···	···	6.2 ± 0.3	1.7 ± 0.3
CB-16.10124	15:18:44.1	30:38:04.0	16.21	18.44	15.94	18.14	546	4.08	0.0804 ± 0.0003	···	-4.3 ± 0.8	···	···
CB-13.11248	15:18:44.2	28:19:23.3	19.54	20.45	19.38	20.35	114	1.86	0.1166 ± 0.0003	13.5 ± 1.5	···	···	···
CB-16.10108	15:18:44.7	30:43:01.6	20.82	21.40	19.27	19.93	78	1.45	star	···	···	···	···
CB-13.11206	15:18:45.2	28:14:50.0	19.15	20.67	18.61	19.96	93	2.03	0.2359 ± 0.0003	···	···	···	···
CB-13.11195	15:18:45.4	28:16:19.0	18.77	20.09	18.14	19.43	74	1.68	0.1197 ± 0.0003	6.5 ± 0.9	···	···	···
CB-15.9682	15:18:45.8	29:32:58.8	18.17	19.46	17.47	18.47	244	2.75	star	···	···	···	···
CB-16.10062	15:18:45.9	30:43:56.7	18.53	19.68	18.28	19.64	225	2.37	0.0859 ± 0.0003	···	···	-5.6 ± 0.5	···
CB-13.11147	15:18:46.4	28:08:28.6	19.59	20.15	18.44	18.98	100	1.54	star	···	···	···	···
CB-13.11150	15:18:46.4	28:15:52.5	19.95	20.95	19.65	20.59	108	1.91	0.1179 ± 0.0003	···	···	···	···
CB-15.9642	15:18:46.6	29:37:33.0	20.09	21.02	19.14	20.15	98	1.85	0.2356 ± 0.0003	···	···	···	···
CB-16.10028	15:18:46.8	30:53:37.0	18.55	19.73	17.97	19.13	218	2.36	0.0792 ± 0.0003	···	···	-1.2 ± 0.2	···
CB-15.9596	15:18:47.6	29:39:13.2	18.53	20.26	18.27	20.01	262	3.26	0.1172 ± 0.0004	···	···	···	···
CB-16.9983	15:18:47.9	30:47:30.5	17.26	18.73	16.88	18.22	468	2.96	0.0773 ± 0.0003	···	-2.6 ± 0.5	2.3 ± 0.1	···
CB-15.9534	15:18:49.0	29:40:16.9	20.64	21.42	20.49	21.12	91	1.65	0.1144 ± 0.0003	···	···	···	···
CB-13.11032	15:18:49.4	28:15:32.1	17.38	18.99	16.55	18.12	478	3.36	0.1171 ± 0.0003	···	···	-2.3 ± 0.2	···
CB-16.9916	15:18:49.4	30:42:54.4	17.32	18.92	16.71	18.17	422	3.32	0.0773 ± 0.0003	···	···	-2.3 ± 0.3	···
CB-15.9505	15:18:49.8	29:38:04.2	20.46	20.97	19.90	20.75	86	1.63	0.1170 ± 0.0010	···	···	···	···
CB-13.11007	15:18:49.9	28:14:39.7	18.31	19.29	17.39	18.33	232	2.46	star	···	···	···	···
1518+3034	15:18:50.0	30:34:19.0	16.21	18.52	15.77	17.83	1057	5.24	0.0785 ± 0.0001	···	···	···	···
CB-16.9886	15:18:50.3	30:54:49.5	18.13	19.04	17.17	18.09	197	2.26	star	···	···	···	···
CB-16.9877	15:18:50.5	30:52:00.6	19.03	20.46	18.81	20.15	198	2.69	0.0791 ± 0.0003	···	···	-3.4 ± 0.5	···
CB-16.9840	15:18:51.5	30:44:51.7	19.33	20.31	18.75	19.57	95	1.93	0.2021 ± 0.0003	···	···	···	···
CB-15.9414	15:18:51.8	29:48:09.0	19.85	20.90	18.79	19.63	156	3.09	star	···	···	···	···
CB-13.10899	15:18:52.2	28:09:53.4	18.33	19.13	17.09	18.01	141	1.87	star	···	···	···	···
CB-16.9804	15:18:52.3	30:40:47.4	20.21	20.71	18.50	19.33	84	1.46	star	···	···	···	···
CB-14.9875	15:18:52.3	28:48:39.5	17.05	18.73	16.35	17.99	473	3.86	0.0832 ± 0.0003	···	···	-2.2 ± 0.4	···
CB-15.9382	15:18:52.5	29:34:03.1	19.25	20.26	19.31	20.34	172	2.04	0.1212 ± 0.0003	22.8 ± 1.7	···	···	5.4 ± 0.5
CB-13.10879	15:18:52.6	28:23:34.6	18.46	19.81	18.07	19.34	256	2.63	0.1147 ± 0.0003	···	···	···	···
CB-13.10869	15:18:52.8	28:16:55.2	19.49	20.48	18.95	19.81	122	1.92	0.1175 ± 0.0003	···	···	-2.0 ± 0.5	···
CB-13.10847	15:18:53.3	28:14:25.1	20.10	20.66	19.16	19.84	99	1.59	0.1254 ± 0.0003	···	···	···	···
CB-13.10824	15:18:53.9	28:19:23.6	16.85	18.56	16.28	17.86	619	3.92	0.0757 ± 0.0003	2.6 ± 0.6	···	-1.7 ± 0.2	···
CB-15.9321	15:18:54.1	29:38:05.3	19.41	20.50	18.46	19.62	180	2.43	0.2118 ± 0.0003	···	···	···	···
CB-15.9323	15:18:54.2	29:47:10.0	17.93	19.68	17.92	19.47	326	3.17	0.1265 ± 0.0003	11.0 ± 1.6	···	1.9 ± 0.3	6.8 ± 0.3
CB-16.9697	15:18:54.5	30:49:10.7	18.34	19.67	18.61	19.84	253	2.82	0.0842 ± 0.0003	···	···	1.8 ± 0.2	2.8 ± 0.2
2061N-173	15:18:54.5	30:51:44.0	16.87	18.76	16.24	17.98	578	3.54	0.0744 ± 0.0001	···	···	···	···
CB-13.10798	15:18:54.5	28:08:28.3	19.56	20.73	19.97	20.84	136	2.23	0.1265 ± 0.0003	15.6 ± 1.4	···	4.0 ± 0.5	4.0 ± 0.5
CB-16.9686	15:18:54.6	30:48:08.0	18.28	19.55	17.67	18.72	249	2.52	0.0718 ± 0.0003	···	···	-3.0 ± 0.4	···
CB-16.9666	15:18:55.1	30:39:30.6	16.95	18.03	15.49	16.43	358	2.32	star	···	···	···	···

TABLE 2.5—*Continued*

Object	RA	Dec. (1950)	g_{tot}	g_{core}	r_{tot}	r_{core}	Area (□″)	irl (″)	z	W_λ([O II]) (Å)	W_λ(Hδ) (Å)	W_λ(Hβ) (Å)	W_λ([O III]5007) (Å)
CB-15.9263	15:18:55.3	29:36:06.7	19.14	20.43	18.30	19.54	212	2.53	0.2366 ± 0.0003	...	...	...	...
CB-15.9264	15:18:55.3	29:45:02.9	18.28	19.10	17.74	18.56	200	1.84	star	...	...	...	...
CB-16.9640	15:18:55.5	30:45:27.9	18.88	20.21	18.60	19.90	192	2.34	0.0780 ± 0.0003	...	...	...	...
CB-13.10750	15:18:55.7	28:12:57.1	18.76	19.76	18.02	19.28	193	2.12	0.1202 ± 0.0003	6.3 ± 1.1	...	3.4 ± 0.3	...
CB-14.9733	15:18:55.8	28:48:31.6	20.17	20.99	19.44	20.47	106	1.80	0.2770 ± 0.0010	...	...	...	...
CB-16.9609	15:18:56.1	30:45:06.6	19.02	20.05	18.34	19.55	148	2.14	0.0839 ± 0.0003	...	...	-4.3 ± 0.4	...
CB-16.9601	15:18:56.3	30:48:19.3	19.03	20.00	18.16	19.24	185	2.09	0.0808 ± 0.0003	...	...	...	...
CB-13.10702	15:18:56.5	28:15:41.5	19.03	19.70	17.23	18.13	106	1.63	star	...	...	...	...
CB-16.9572	15:18:56.8	30:43:57.0	17.80	19.17	17.05	18.37	439	2.94	0.0772 ± 0.0003	...	...	-2.9 ± 0.4	...
CB-16.9564	15:18:57.0	30:49:25.6	18.81	19.93	18.55	19.59	212	2.24	0.0878 ± 0.0003	...	...	-4.6 ± 0.5	...
CB-13.10666	15:18:57.2	28:08:07.5	18.72	19.48	17.74	18.56	116	1.79	star	...	...	...	...
CB-15.9175	15:18:57.2	29:39:02.6	17.26	19.00	16.42	18.04	565	3.73	0.1323 ± 0.0003	...	...	-3.2 ± 0.4	...
CB-15.9169	15:18:57.3	29:35:23.9	19.05	20.12	18.21	19.23	150	2.24	0.1133 ± 0.0003	...	...	...	...
CB-16.9552	15:18:57.4	30:48:58.9	20.00	20.97	19.59	20.91	106	1.95	0.0781 ± 0.0003	...	...	-6.7 ± 1.3	...
CB-16.9528	15:18:57.8	30:44:35.2	18.22	19.49	17.59	18.81	293	2.81	0.0720 ± 0.0003	...	...	-6.2 ± 0.6	...
CB-16.9511	15:18:58.1	30:56:20.5	18.45	19.94	18.13	19.36	115	2.43	0.0903 ± 0.0003	...	...	...	...
CB-16.9475	15:18:58.8	30:47:24.4	18.41	19.48	17.56	18.54	215	2.20	0.0767 ± 0.0003	...	...	-3.1 ± 0.3	...
CB-13.10583	15:18:58.9	28:22:50.4	19.26	20.45	19.54	20.52	142	2.21	0.1163 ± 0.0003	13.7 ± 1.7	...	2.2 ± 0.5	...
CB-16.9469	15:18:58.9	30:45:05.5	16.14	18.24	15.46	17.40	1061	4.85	0.0768 ± 0.0003	...	...	-2.0 ± 0.3	...
CB-14.9571	15:18:59.0	28:43:34.0	19.08	19.72	18.58	19.18	124	1.68	star	...	...	...	...
CB-13.10577	15:18:59.1	28:14:49.7	18.78	20.08	18.31	19.60	240	2.58	0.0834 ± 0.0003	...	...	-1.8 ± 0.4	...
CB-16.9455	15:18:59.2	30:52:60.0	17.21	18.90	16.45	18.01	618	4.17	0.0757 ± 0.0003	...	...	-3.4 ± 0.3	...
CB-14.9562	15:18:59.5	28:51:28.6	20.31	21.58	19.91	20.74	89	1.92	star	...	...	...	...
CB-15.9076	15:18:59.5	29:44:06.7	19.75	20.79	19.29	20.46	119	1.99	0.1173 ± 0.0003	...	...	...	...
CB-13.10542	15:18:59.7	28:17:07.0	18.67	19.80	17.54	18.77	109	2.12	0.1175 ± 0.0003	...	...	...	...
CB-15.9065	15:18:59.7	29:31:38.9	18.51	19.34	17.29	18.20	203	2.00	star	...	...	...	...
1519+2817A	15:19:00.2	28:17:26.0	15.88	18.22	15.27	17.39	498	4.19	0.0838 ± 0.0005	...	...	...	...
CB-15.9033	15:19:00.2	29:36:09.1	16.07	18.38	15.32	17.54	239	3.19	0.1126 ± 0.0003	...	...	-1.2 ± 0.3	...
CB-16.9420	15:19:00.2	30:51:17.4	18.36	19.49	17.63	18.64	260	2.34	0.0780 ± 0.0003	...	...	-3.5 ± 0.4	...
CB-15.9027	15:19:00.5	29:44:39.8	19.09	20.00	18.09	19.04	172	1.94	0.1166 ± 0.0003	...	...	-2.0 ± 0.3	...
CB-14.9507	15:19:00.7	28:42:41.5	20.48	21.12	20.07	20.91	94	1.64	0.0889 ± 0.0003	...	...	4.2 ± 0.8	...
CB-13.10465	15:19:01.1	28:15:51.2	19.51	19.92	18.56	18.83	21	0.96	star	...	...	...	...
CB-13.10464	15:19:01.1	28:13:26.1	17.96	19.84	18.31	20.09	316	3.49	0.1402 ± 0.0003	25.0 ± 1.4	...	7.1 ± 0.5	8.8 ± 0.5
CB-15.8980	15:19:01.6	29:44:13.8	21.16	21.50	20.26	21.19	69	1.32	0.3516 ± 0.0003	14.7 ± 2.0	...	...	...
CB-16.9356	15:19:01.8	30:46:20.9	19.08	20.06	18.71	19.57	130	2.00	0.0770 ± 0.0003	...	...	...	...
CB-16.9353	15:19:01.8	30:56:08.5	18.72	19.84	18.26	19.44	194	2.23	0.0912 ± 0.0003	...	...	...	...
CB-14.9447	15:19:01.9	28:51:34.1	20.95	21.81	20.24	21.36	36	1.54	0.5397 ± 0.0003	19.9 ± 2.1	...	...	...
CB-15.8955	15:19:02.1	29:35:37.9	18.92	20.31	18.41	19.78	266	2.85	0.1129 ± 0.0003	...	...	...	...
CB-13.10408	15:19:02.3	28:10:54.0	19.13	20.17	18.24	19.49	156	2.24	0.1252 ± 0.0003	6.1 ± 1.1	...	-3.1 ± 0.5	5.2 ± 0.3
2065-356	15:19:02.3	28:06:03.0	15.99	18.76	15.90	18.19	489	4.60	0.0606 ± 0.0002	...	...	...	...
CB-14.9428	15:19:02.4	28:44:06.2	18.20	19.03	17.31	18.19	215	1.89	star	...	...	...	...
CB-14.9396	15:19:03.0	28:39:46.4	19.20	19.78	18.20	18.95	128	1.64	star	...	...	...	...
CB-14.9401	15:19:03.0	28:49:33.3	20.29	21.07	19.07	20.20	106	1.71	0.2127 ± 0.0003	...	...	...	...
CB-15.8920	15:19:03.0	29:40:34.7	19.09	19.99	18.16	19.11	184	1.98	0.1110 ± 0.0003	...	...	...	...
CB-16.9312	15:19:03.0	30:51:21.0	16.52	18.44	16.11	17.91	618	4.00	0.0308 ± 0.0003	...	...	-3.0 ± 0.3	...

TABLE 2.5—*Continued*

Object	RA (1950)	Dec. (1950)	g_{tot}	g_{core}	r_{tot}	r_{core}	Area (□″)	irl (″)	z	W_λ([O II]) (Å)	W_λ(Hδ) (Å)	W_λ(Hβ) (Å)	W_λ([O III]5007) (Å)
CB-16.9310	15:19:03.0	30:47:29.6	18.77	19.80	18.12	19.16	184	2.06	0.0850 ± 0.0003	···	···	-1.7 ± 0.3	···
CB-13.10356	15:19:03.3	28:09:02.7	19.43	20.63	18.40	19.56	148	2.31	0.2283 ± 0.0003	···	···	-1.7 ± 0.4	···
CB-99.5	15:19:03.4	29:35:18.7	···	···	19.77	20.57	102	1.85	0.3699 ± 0.0003	···	-3.2 ± 0.8	···	···
CB-13.10335	15:19:03.8	28:23:52.5	18.61	20.12	18.70	20.25	242	2.73	0.0886 ± 0.0003	15.3 ± 1.4	···	4.4 ± 0.5	···
CB-16.9278	15:19:03.8	30:43:13.8	17.18	18.82	16.62	18.18	611	3.64	0.0806 ± 0.0003	···	···	-3.1 ± 0.3	···
CB-16.9265	15:19:04.2	30:48:02.0	18.94	19.94	18.20	19.26	150	2.11	0.0795 ± 0.0003	···	···	-2.9 ± 0.4	···
CB-14.9343	15:19:04.3	28:48:38.3	18.99	19.81	17.79	18.48	147	2.04	star	···	···	···	···
CB-15.8852	15:19:04.5	29:37:10.2	20.32	21.13	19.70	20.67	97	1.76	0.2404 ± 0.0004	···	···	···	···
CB-16.9234	15:19:05.0	30:45:09.2	16.11	18.08	15.42	17.40	573	4.02	0.0789 ± 0.0003	···	···	-2.4 ± 0.3	···
CB-13.10263	15:19:05.2	28:24:48.9	19.56	20.22	18.62	19.33	114	1.62	star	···	···	···	···
CB-14.9289	15:19:05.5	28:44:07.1	18.21	20.00	18.14	19.88	302	3.32	0.0322 ± 0.0003	···	···	···	4.7 ± 0.2
CB-16.9207	15:19:05.5	30:42:18.4	17.99	19.50	17.55	18.89	369	2.92	0.0761 ± 0.0003	···	···	-3.1 ± 0.5	···
CB-14.9271	15:19:05.8	28:52:30.2	19.91	20.84	19.08	20.17	91	1.86	0.1261 ± 0.0003	···	···	···	···
CB-13.10217	15:19:06.1	28:09:39.0	19.50	20.66	18.61	19.69	173	2.25	0.1999 ± 0.0003	···	···	-1.8 ± 0.3	···
CB-13.10218	15:19:06.1	28:16:40.5	19.07	20.19	18.51	19.51	122	2.10	0.0833 ± 0.0003	···	···	···	···
CB-14.9261	15:19:06.1	28:38:08.0	16.80	18.59	16.04	17.74	650	3.88	0.1091 ± 0.0003	···	···	-2.2 ± 0.3	···
CB-15.8794	15:19:06.2	29:37:28.1	18.37	19.64	17.59	18.79	275	3.00	0.1112 ± 0.0003	···	···	-1.9 ± 0.4	···
CB-13.10171	15:19:07.0	28:19:52.5	19.17	20.27	18.50	19.58	129	2.01	0.1215 ± 0.0003	···	···	-2.5 ± 0.2	···
CB-16.9134	15:19:07.1	30:48:54.5	17.51	18.99	16.70	18.04	296	3.07	0.0795 ± 0.0003	···	···	-2.4 ± 0.3	···
CB-16.9123	15:19:07.2	30:41:27.8	22.09	21.72	19.92	20.58	66	1.17	star	···	···	···	···
CB-13.10128	15:19:07.7	28:13:15.4	18.78	19.94	18.44	19.38	114	2.01	star	···	···	···	···
CB-14.9170	15:19:07.9	28:37:44.9	18.98	20.11	18.29	19.28	196	2.25	0.1082 ± 0.0003	···	···	···	···
1519+3045	15:19:08.0	30:45:47.0	15.34	17.92	14.75	17.42	150	2.74	0.0759 ± 0.0001	···	···	···	···
CB-16.9085	15:19:08.0	30:50:14.8	18.12	19.21	17.19	18.36	101	1.97	0.0767 ± 0.0003	···	···	-2.2 ± 0.3	···
CB-16.9077	15:19:08.1	30:45:13.4	18.58	19.58	17.78	18.93	161	2.11	0.0751 ± 0.0003	···	···	-2.1 ± 0.3	···
CB-15.8706	15:19:08.1	29:35:36.2	18.09	19.57	17.46	18.70	355	3.20	0.1126 ± 0.0003	···	···	-2.2 ± 0.4	···
CB-16.9071	15:19:08.3	30:40:38.4	16.97	19.50	16.83	19.29	697	4.83	0.0825 ± 0.0003	···	···	···	···
CB-13.10072	15:19:08.7	28:20:47.0	18.74	19.80	17.73	18.89	78	1.70	0.1200 ± 0.0003	···	···	-1.9 ± 0.4	···
CB-14.9117	15:19:08.8	28:45:24.9	19.80	20.65	18.58	19.65	19	1.11	0.1724 ± 0.0003	···	···	···	···
CB-15.8675	15:19:08.8	29:31:45.4	19.33	20.47	18.69	19.93	181	2.25	0.1139 ± 0.0003	···	···	···	9.9 ± 0.4
CB-15.8680	15:19:08.8	29:40:23.4	18.47	19.26	17.26	18.14	184	1.89	star	···	···	···	···
CB-13.10051	15:19:08.9	28:06:36.1	20.79	22.04	20.14	21.49	87	2.18	0.3177 ± 0.0003	10.5 ± 1.8	···	···	···
CB-17.8422	15:19:09.1	31:01:08.8	20.12	20.84	18.36	19.48	22	1.01	star	···	···	···	···
CB-16.9018	15:19:09.4	30:44:42.3	20.03	21.05	18.52	19.96	110	1.93	0.3070 ± 0.0003	···	···	···	···
CB-16.9015	15:19:09.5	30:50:11.9	15.46	17.70	14.89	16.72	600	4.65	0.0308 ± 0.0003	···	···	-3.1 ± 0.2	···
CB-13.10021	15:19:09.7	28:22:16.7	18.57	19.61	17.98	19.21	202	2.21	0.0842 ± 0.0003	···	-4.4 ± 1.0	···	···
CB-15.8629	15:19:09.9	29:47:52.1	19.03	19.66	17.91	18.67	159	1.64	star	···	···	···	···
CB-14.9058	15:19:10.0	28:37:55.5	19.35	19.93	17.84	18.57	100	1.53	star	···	···	···	···
CB-16.8981	15:19:10.2	30:45:03.2	18.83	19.98	18.40	19.53	246	2.25	0.0799 ± 0.0003	···	···	···	···
CB-15.8606	15:19:10.3	29:37:53.2	19.46	19.97	17.50	18.26	112	1.57	star	···	···	···	···
CB-13.9981	15:19:10.5	28:09:36.2	20.39	21.46	19.31	20.76	98	2.05	0.2279 ± 0.0003	···	···	···	···
CB-13.9966	15:19:10.8	28:19:28.6	18.41	19.71	18.23	19.54	244	2.52	0.1152 ± 0.0003	17.5 ± 0.9	-3.0 ± 0.7	3.3 ± 0.3	···
CB-16.8945	15:19:10.9	30:47:51.1	17.92	19.10	17.01	18.25	307	2.64	0.0738 ± 0.0003	···	···	-3.3 ± 0.3	···
CB-16.8946	15:19:10.9	30:51:32.0	17.58	19.09	17.07	18.49	298	2.97	0.0814 ± 0.0003	···	···	···	···
CB-15.8571	15:19:11.0	29:41:43.3	18.67	19.69	17.93	19.14	222	2.19	0.0760 ± 0.0003	···	···	-3.4 ± 0.7	···

TABLE 2.5—*Continued*

Object	RA (1950)	Dec. (1950)	g_{tot}	g_{core}	r_{tot}	r_{core}	Area (□″)	irl (″)	z	W_λ([O II]) (Å)	W_λ(Hδ) (Å)	W_λ(Hβ) (Å)	W_λ([O III]5007) (Å)
CB-16.8941	15:19:11.0	30:42:06.1	16.32	18.30	15.75	17.66	481	3.97	0.0771 ± 0.0003	···	···	-4.5 ± 0.4	···
CB-14.9020	15:19:11.0	28:39:06.6	20.51	21.54	20.15	20.99	100	1.79	star	···	···	···	···
CB-16.8933	15:19:11.2	30:47:13.5	19.60	20.95	18.60	20.15	147	2.53	0.3082 ± 0.0003	5.1 ± 1.1	-2.6 ± 0.4	···	···
CB-13.9922	15:19:11.5	28:16:14.3	19.53	20.69	19.31	20.37	144	2.33	0.1153 ± 0.0003	···	···	···	···
CB-13.9916	15:19:11.6	28:07:39.9	20.74	21.72	20.66	21.73	92	1.77	0.1165 ± 0.0003	16.8 ± 2.8	···	···	···
1519+3056	15:19:11.7	30:56:09.0	16.97	19.22	16.27	18.28	553	4.81	0.0899 ± 0.0002	···	···	···	···
CB-14.8997	15:19:11.7	28:45:46.7	18.53	19.75	17.50	18.66	241	2.59	0.1717 ± 0.0003	···	···	-2.1 ± 0.4	···
CB-15.8529	15:19:12.0	29:38:36.3	18.86	19.91	17.93	19.16	239	2.38	0.1138 ± 0.0003	···	···	-2.5 ± 0.4	···
CB-16.8879	15:19:12.0	30:45:20.1	18.55	19.50	17.74	18.84	214	2.09	0.0798 ± 0.0003	···	···	-3.5 ± 0.3	···
CB-14.8976	15:19:12.1	28:49:57.3	19.14	20.15	18.61	19.64	148	2.10	0.1718 ± 0.0003	···	-3.7 ± 0.7	···	···
1519+2817B	15:19:12.2	28:17:18.0	15.64	18.27	15.50	17.76	1336	6.52	0.0707 ± 0.0002	···	···	···	···
CB-16.8869	15:19:12.4	30:49:50.6	19.38	20.03	17.66	18.50	104	1.64	star	···	···	···	···
CB-99.6	15:19:12.8	28:47:59.3	18.73	20.66	20.12	21.00	104	2.35	0.0845 ± 0.0003	···	···	···	17.4 ± 1.4
CB-16.8830	15:19:13.1	30:55:01.1	17.63	19.27	17.24	18.81	347	3.31	0.0745 ± 0.0003	···	···	-2.0 ± 0.3	···
CB-16.8820	15:19:13.4	30:40:31.6	19.15	20.58	19.30	20.51	160	2.69	0.0840 ± 0.0010	···	···	···	···
CB-15.8479	15:19:13.5	29:47:35.7	19.04	19.67	18.10	18.82	122	1.67	star	···	···	···	···
CB-13.9811	15:19:13.6	28:19:01.0	19.29	20.22	18.58	19.45	120	1.94	0.0834 ± 0.0003	···	···	-1.5 ± 0.3	···
CB-16.8814	15:19:13.7	30:49:18.7	15.76	17.39	14.13	15.45	567	3.11	star	···	···	···	···
CB-16.8789	15:19:14.2	30:46:14.5	17.44	18.80	16.55	17.95	254	2.52	0.0777 ± 0.0003	···	···	-3.0 ± 0.4	···
CB-14.8880	15:19:14.3	28:39:25.8	18.95	20.01	18.62	19.53	196	2.22	0.1071 ± 0.0003	···	···	···	···
CB-15.8440	15:19:14.5	29:41:12.5	18.55	19.67	17.81	18.87	234	2.32	0.1145 ± 0.0003	···	···	-1.6 ± 0.3	···
CB-13.9768	15:19:14.7	28:11:47.2	18.67	19.88	18.05	19.33	211	2.37	0.1364 ± 0.0003	8.7 ± 1.1	···	2.3 ± 0.3	···
CB-16.8748	15:19:15.1	30:50:36.2	18.61	19.76	17.73	18.90	135	2.11	0.0779 ± 0.0003	···	···	-2.6 ± 0.3	···
1519+3100	15:19:15.3	31:00:42.0	16.10	18.06	15.67	17.54	1368	4.99	0.0742 ± 0.0001	···	···	···	···
CB-13.9724	15:19:15.7	28:14:03.3	19.27	20.25	18.65	19.59	179	2.16	0.1172 ± 0.0003	···	-2.1 ± 0.5	···	···
CB-14.8827	15:19:15.7	28:43:32.7	18.65	20.28	18.47	20.06	270	2.98	0.0319 ± 0.0003	···	···	···	···
CB-14.8816	15:19:15.8	28:50:21.2	19.84	20.64	19.64	20.78	100	1.69	0.1813 ± 0.0003	15.3 ± 1.1	···	5.7 ± 0.6	7.5 ± 0.6
CB-13.9716	15:19:16.0	28:22:30.0	18.57	19.79	17.86	18.96	241	2.47	0.1179 ± 0.0003	···	···	-2.4 ± 0.3	···
CB-17.8098	15:19:16.1	30:59:23.8	20.47	21.51	19.63	20.48	94	1.81	0.2380 ± 0.0003	···	···	···	···
CB-15.8367	15:19:16.3	29:36:59.0	18.23	19.06	16.89	17.81	204	1.88	star	···	···	···	···
CB-15.8361	15:19:16.4	29:40:18.0	19.23	20.54	19.33	20.59	186	2.51	0.2153 ± 0.0003	···	···	···	5.2 ± 0.8
CB-16.8690	15:19:16.4	30:49:20.3	18.41	19.36	17.42	18.43	176	2.11	0.0787 ± 0.0003	···	···	-2.8 ± 0.3	···
CB-14.8774	15:19:16.5	28:42:33.7	20.76	21.44	19.52	20.77	108	1.99	0.1731 ± 0.0003	···	···	···	···
CB-16.8675	15:19:16.6	30:53:05.5	17.16	18.21	15.18	16.15	264	2.30	star	···	···	···	···
CB-15.8334	15:19:17.0	29:48:10.9	20.55	20.96	19.55	20.64	93	1.44	0.1119 ± 0.0003	···	···	···	···
CB-16.8632	15:19:17.5	30:52:50.5	17.00	18.71	16.32	17.93	226	2.77	0.0800 ± 0.0003	···	···	-3.1 ± 0.3	···
15192+3051	15:19:17.5	30:50:58.0	15.01	17.61	14.31	16.31	1177	5.69	0.0791 ± 0.0001	···	···	···	···
CB-14.8717	15:19:17.6	28:40:07.2	18.71	19.43	17.69	18.44	104	1.66	star	···	···	···	···
CB-15.8295	15:19:17.9	29:41:00.1	17.72	19.52	17.48	19.32	395	3.21	0.1087 ± 0.0003	···	···	1.2 ± 0.3	2.2 ± 0.4
CB-13.9609	15:19:18.0	28:14:27.7	18.88	20.39	18.87	20.31	225	2.97	0.0696 ± 0.0003	10.4 ± 1.9	···	···	···
CB-16.8613	15:19:18.0	30:50:35.8	19.18	20.29	18.62	19.88	118	2.03	0.0704 ± 0.0003	···	···	···	···
CB-13.9605	15:19:18.1	28:15:25.6	19.17	20.11	18.42	19.34	183	2.05	0.1208 ± 0.0003	···	···	···	···
CB-16.8609	15:19:18.2	30:42:08.7	19.19	20.05	18.66	19.54	135	1.94	0.0828 ± 0.0003	···	···	-3.9 ± 0.5	···
CB-16.8609	15:19:18.2	30:42:08.7	19.19	20.05	18.66	19.54	135	1.94	0.0828 ± 0.0003	···	···	-3.9 ± 0.5	···
CB-13.9575	15:19:18.7	28:08:50.4	18.02	19.80	18.10	20.01	301	3.18	0.0759 ± 0.0003	19.2 ± 1.4	···	3.3 ± 0.3	6.5 ± 0.3

TABLE 2.5—*Continued*

Object	RA (1950)	Dec. (1950)	g_{tot}	g_{core}	r_{tot}	r_{core}	Area (□″)	ir1 (″)	z	W_λ([O II]) (Å)	W_λ(Hδ) (Å)	W_λ(Hβ) (Å)	W_λ([O III]5007) (Å)
CB-16.8589	15:19:18.8	30:51:24.8	20.01	20.83	19.02	20.28	101	1.64	0.0795 ± 0.0003	···	···	···	···
CB-13.9570	15:19:18.8	28:17:07.4	18.58	19.76	17.87	18.99	256	2.53	0.1213 ± 0.0003	···	···	···	···
CB-17.7982	15:19:18.9	30:58:29.4	17.75	18.66	16.48	17.53	224	2.03	star	···	···	···	···
CB-15.8242	15:19:19.1	29:37:11.2	17.49	19.61	17.74	19.79	553	4.28	0.0731 ± 0.0003	15.9 ± 1.5	-3.8 ± 0.9	3.4 ± 0.2	2.8 ± 0.2
CB-16.8566	15:19:19.2	30:43:50.1	19.32	20.04	18.18	19.10	135	2.00	star	···	···	···	···
CB-14.8600	15:19:19.8	28:46:30.8	19.00	20.29	18.33	19.38	228	2.59	0.1991 ± 0.0003	···	···	···	···
CB-13.9504	15:19:20.2	28:14:32.7	18.09	19.36	17.25	18.42	433	2.97	0.1177 ± 0.0003	···	···	-3.0 ± 0.3	···
CB-16.8519	15:19:20.4	30:51:41.1	17.69	18.66	16.21	17.29	254	2.30	star	···	···	···	···
CB-15.8160	15:19:20.7	29:35:41.3	17.79	18.72	16.64	17.63	226	2.05	star	···	···	···	···
CB-14.8545	15:19:20.9	28:45:28.2	20.13	20.82	19.16	20.01	94	1.62	0.1719 ± 0.0003	···	···	-3.6 ± 0.6	···
CB-13.9424	15:19:21.5	28:16:19.7	18.76	19.71	17.81	18.95	208	2.13	0.1182 ± 0.0003	···	···	-2.7 ± 0.4	···
CB-13.9412	15:19:21.7	28:14:01.2	18.44	19.86	18.29	19.51	174	2.80	0.1259 ± 0.0003	8.0 ± 1.5	···	···	···
CB-15.8112	15:19:21.8	29:42:26.6	19.34	20.22	18.85	19.99	126	1.95	0.3105 ± 0.0003	12.1 ± 0.8	-5.2 ± 1.0	4.9 ± 0.4	···
CB-17.7850	15:19:21.9	30:59:17.8	19.04	20.16	18.47	19.59	96	1.97	0.0771 ± 0.0003	···	···	···	···
CB-14.8501	15:19:22.0	28:52:21.3	16.55	18.20	16.16	17.77	587	3.26	0.0308 ± 0.0003	···	-3.0 ± 0.5	3.3 ± 0.1	0.5 ± 0.1
CB-16.8403	15:19:22.8	30:51:37.1	19.09	19.80	18.07	19.01	178	1.82	0.0775 ± 0.0003	···	···	-2.3 ± 0.3	···
CB-14.8434	15:19:23.4	28:45:46.5	17.46	19.58	16.91	18.78	212	2.82	0.1719 ± 0.0003	···	···	-1.2 ± 0.3	···
CB-13.9351	15:19:23.5	28:16:37.1	17.06	18.88	16.25	17.92	696	4.18	0.1189 ± 0.0003	6.5 ± 0.5	···	-1.6 ± 0.3	···
CB-13.9352	15:19:23.5	28:25:16.1	19.08	20.14	18.57	19.53	180	2.04	0.1177 ± 0.0003	···	···	···	···
CB-13.9347	15:19:23.6	28:12:39.8	19.14	19.86	17.90	18.60	127	1.76	star	···	···	···	···
CB-16.8362	15:19:23.6	30:41:02.1	18.82	19.87	18.27	19.39	186	2.15	0.0758 ± 0.0003	···	···	-2.9 ± 0.6	···
A1519+2755	15:19:23.8	27:55:11.0	18.72	19.39	18.29	19.00	121	1.72	0.2300 ± 0.0000	···	···	···	···
CB-16.8358	15:19:23.8	30:48:25.3	17.52	19.71	17.79	19.81	447	4.09	0.0737 ± 0.0003	···	···	···	···
CB-15.8011	15:19:24.1	29:35:55.0	18.88	20.60	18.00	19.62	231	2.84	0.2127 ± 0.0003	···	···	···	···
CB-13.9322	15:19:24.3	28:15:34.0	19.53	20.42	18.89	19.96	120	1.96	0.1179 ± 0.0003	···	···	···	···
CB-14.8393	15:19:24.3	28:54:46.8	19.30	20.16	18.32	19.46	130	1.87	0.1137 ± 0.0003	···	···	-2.3 ± 0.5	···
CB-14.8385	15:19:24.5	28:43:34.8	16.53	19.56	16.69	19.64	360	4.39	0.0316 ± 0.0003	···	···	···	1.3 ± 0.2
CB-16.8325	15:19:24.6	30:47:11.4	17.62	19.03	16.86	18.21	247	2.81	0.0770 ± 0.0010	···	···	···	···
CB-13.9294	15:19:24.8	28:12:07.0	17.87	18.75	17.25	18.18	236	2.05	star	···	···	···	···
CB-15.7965	15:19:24.9	29:38:09.8	18.54	19.95	17.90	19.30	248	2.87	0.1149 ± 0.0003	···	···	-2.0 ± 0.4	···
CB-14.8362	15:19:25.0	28:45:32.9	17.84	18.94	16.73	17.87	164	2.07	star	···	···	···	···
CB-16.8305	15:19:25.1	30:49:46.9	17.85	19.21	17.09	18.36	279	2.71	0.0790 ± 0.0003	···	···	···	···
CB-16.8265	15:19:26.0	30:40:14.1	18.52	20.02	17.94	19.39	252	3.10	0.0792 ± 0.0003	···	···	···	···
CB-15.7917	15:19:26.2	29:42:06.0	19.87	21.03	19.52	20.50	119	2.10	0.1124 ± 0.0003	···	···	···	···
CB-14.8290	15:19:26.4	28:49:26.5	19.88	20.80	18.99	20.06	123	1.94	0.1997 ± 0.0003	···	···	···	···
CB-13.9196	15:19:26.9	28:13:08.8	18.17	19.04	17.38	18.21	219	2.03	star	···	···	···	···
CB-16.8217	15:19:27.0	30:52:09.8	19.03	19.73	18.28	18.94	140	1.71	star	···	···	···	···
CB-13.9163	15:19:27.5	28:18:44.8	21.44	21.77	20.41	21.51	63	1.47	0.1200 ± 0.0010	···	···	···	···
CB-13.9148	15:19:27.7	28:07:15.5	18.74	19.98	18.01	19.14	239	2.50	0.1257 ± 0.0003	···	···	-2.4 ± 0.4	···
CB-15.7847	15:19:27.7	29:30:13.8	19.28	20.26	18.37	19.42	109	1.89	0.1127 ± 0.0003	···	···	···	···
CB-16.8183	15:19:27.7	30:48:25.0	18.02	18.85	16.93	17.89	211	1.93	star	···	···	···	···
1519+3053	15:19:27.7	30:53:13.0	16.29	18.52	15.69	17.75	619	4.34	0.0813 ± 0.0001	···	···	···	···
CB-15.7831	15:19:28.1	29:36:03.1	18.79	20.02	18.35	19.62	223	2.50	0.1328 ± 0.0003	6.1 ± 1.4	···	···	···
CB-16.8169	15:19:28.1	30:56:14.7	17.80	19.38	17.47	18.85	88	2.68	0.0849 ± 0.0003	···	···	···	···
2065-313	15:19:28.2	27:48:14.0	16.64	18.41	16.05	17.69	406	3.34	0.0755 ± 0.0001	···	···	···	···

TABLE 2.5—*Continued*

Object	RA (1950)	Dec.	g_{tot}	g_{core}	r_{tot}	r_{core}	Area (□″)	irl (″)	z	W_λ([O II]) (Å)	W_λ(Hδ) (Å)	W_λ(Hβ) (Å)	W_λ([O III]5007) (Å)
CB-14.8209	15:19:28.2	28:41:59.5	17.66	19.35	17.18	18.60	301	3.62	0.1163 ± 0.0003	2.8 ± 0.7	...	-2.3 ± 0.2	...
CB-16.8132	15:19:28.6	30:46:09.0	18.30	20.13	18.55	20.16	253	3.23	0.1160 ± 0.0004	...	...	...	...
CB-13.9100	15:19:28.7	28:12:11.0	20.43	21.42	20.46	21.83	78	1.68	0.1208 ± 0.0003	...	...	...	...
CB-15.7805	15:19:28.9	29:44:01.0	18.21	19.61	18.02	19.72	253	2.63	0.1069 ± 0.0003	20.2 ± 1.4	-2.7 ± 0.6	...	2.7 ± 0.3
CB-14.8174	15:19:29.0	28:47:07.0	19.58	20.87	19.07	20.49	128	2.26	0.2771 ± 0.0003	11.8 ± 1.1	...	...	11.4 ± 0.5
CB-15.7796	15:19:29.0	29:36:51.4	19.09	20.28	18.59	19.74	95	1.94	0.1159 ± 0.0003	...	-2.8 ± 0.6	...	...
CB-16.8115	15:19:29.0	30:46:19.5	18.46	19.43	17.56	18.68	142	2.07	0.0721 ± 0.0003	...	...	-3.5 ± 0.6	...
CB-13.9084	15:19:29.1	28:20:45.0	18.58	19.95	18.43	19.74	224	2.52	0.1177 ± 0.0003	...	-2.8 ± 0.6	...	...
CB-16.8120	15:19:29.1	30:56:59.5	19.18	20.00	18.50	19.42	119	1.90	0.0834 ± 0.0003	...	...	-2.3 ± 0.3	...
CB-16.8088	15:19:29.7	30:51:47.7	18.39	19.62	17.77	19.08	262	2.80	0.0713 ± 0.0003	...	...	-3.1 ± 0.4	...
CB-15.7748	15:19:29.9	29:42:24.2	21.19	21.80	20.06	21.04	71	1.49	star	...	...	...	...
CB-13.9035	15:19:30.1	28:16:50.5	19.50	20.66	18.65	20.06	75	1.71	0.2283 ± 0.0003	7.8 ± 1.1	-3.3 ± 0.7	1.9 ± 0.4	...
CB-14.8125	15:19:30.1	28:45:21.0	20.06	20.68	19.22	20.06	105	1.67	0.1097 ± 0.0003	...	...	-2.7 ± 0.6	...
CB-13.9001	15:19:30.8	28:12:46.3	20.77	21.35	21.16	21.76	85	1.47	star	...	...	...	...
CB-15.7711	15:19:30.8	29:37:50.8	20.36	21.12	19.76	20.81	79	1.57	0.3133 ± 0.0003	13.7 ± 1.2	-2.9 ± 0.6	4.4 ± 0.5	...
CB-16.8020	15:19:30.8	30:53:28.2	17.94	19.37	17.64	19.13	333	3.28	0.0831 ± 0.0003	...	-3.6 ± 0.5	2.7 ± 0.2	...
CB-15.7703	15:19:31.0	29:43:31.1	20.82	21.58	20.20	21.10	78	1.49	0.1139 ± 0.0003	...	...	...	...
CB-16.8007	15:19:31.2	30:53:56.3	15.60	17.94	15.03	17.27	1454	6.04	0.0780 ± 0.0003	...	...	...	...
CB-13.8942	15:19:31.8	28:18:01.7	18.93	20.28	18.20	19.49	211	2.53	0.2289 ± 0.0003	3.5 ± 0.8	-2.5 ± 0.4	...	...
CB-13.8935	15:19:31.9	28:10:16.0	19.67	20.64	19.45	20.31	114	1.93	0.0850 ± 0.0003	30.3 ± 1.7	-4.5 ± 1.0	2.9 ± 0.3	3.7 ± 0.3
CB-15.7659	15:19:31.9	29:38:56.6	19.58	20.34	18.83	19.81	64	1.34	0.1139 ± 0.0003	...	...	...	19.6 ± 0.6
CB-14.8028	15:19:32.0	28:44:29.5	17.54	19.04	16.86	18.22	466	3.32	0.0737 ± 0.0003	...	...	-1.8 ± 0.2	...
CB-16.7962	15:19:32.1	30:51:40.0	18.26	19.39	17.54	18.70	125	2.14	0.0789 ± 0.0003	...	...	-2.3 ± 0.3	...
CB-15.7643	15:19:32.2	29:35:00.5	18.30	19.59	17.59	18.73	250	2.62	0.1126 ± 0.0003	...	...	-1.2 ± 0.3	...
CB-13.8894	15:19:32.7	28:19:39.9	22.81	22.40	21.37	21.42	16	1.00	0.3157 ± 0.0003	...	...	...	...
CB-14.7971	15:19:33.5	28:47:09.8	20.68	21.00	20.04	20.51	79	1.37	star	...	...	...	...
CB-14.7963	15:19:33.5	28:41:42.5	21.00	21.26	20.07	20.74	83	1.51	0.1707 ± 0.0003	...	...	-1.9 ± 0.4	...
CB-13.8837	15:19:33.7	28:17:33.4	17.47	19.05	16.80	18.16	548	3.33	0.1196 ± 0.0003	...	...	-1.6 ± 0.4	...
CB-16.7894	15:19:33.9	30:55:22.1	18.47	19.65	17.76	18.91	129	2.21	0.0802 ± 0.0003	...	...	...	...
CB-15.7559	15:19:34.0	29:44:09.1	20.10	21.14	19.55	20.64	114	2.12	0.1180 ± 0.0010	...	...	...	...
CB-15.7554	15:19:34.1	29:37:52.0	18.89	19.88	17.98	19.01	150	2.09	0.1130 ± 0.0003	...	...	...	...
CB-13.8799	15:19:34.5	28:16:49.5	19.53	20.31	18.50	19.45	87	1.62	0.1184 ± 0.0003	...	...	...	...
CB-14.7918	15:19:34.6	28:44:15.4	21.42	22.16	19.78	20.64	38	1.59	0.4080 ± 0.0003	...	-2.0 ± 0.4	...	...
CB-16.7864	15:19:34.6	30:51:37.1	19.29	20.15	18.63	19.64	116	1.82	0.0800 ± 0.0010	...	...	...	...
CB-14.7914	15:19:34.8	28:54:03.1	18.46	19.83	17.85	19.26	217	2.69	0.1109 ± 0.0003	...	...	...	...
CB-15.7513	15:19:35.2	29:40:04.3	21.16	21.91	19.96	20.96	77	2.17	0.3130 ± 0.0010	...	...	...	...
CB-14.7878	15:19:35.6	28:49:06.6	19.81	20.72	18.75	19.87	107	1.85	0.3003 ± 0.0003	...	-3.1 ± 0.6	-1.7 ± 0.3	...
CB-15.7490	15:19:35.7	29:33:15.2	19.26	20.33	18.50	19.83	180	2.13	0.1148 ± 0.0003	...	...	...	...
CB-16.7818	15:19:35.8	30:42:40.0	17.25	18.91	16.63	18.22	350	3.25	0.0768 ± 0.0003	...	...	-2.4 ± 0.4	...
CB-16.7822	15:19:35.9	30:55:39.4	17.77	19.15	17.07	18.41	277	2.79	0.0811 ± 0.0003	...	...	-3.2 ± 0.4	...
1519+3016	15:19:36.0	30:16:40.0	16.75	18.57	16.27	18.05	523	3.74	0.0740 ± 0.0002	...	...	...	...
CB-15.7470	15:19:36.2	29:42:26.2	18.50	19.79	17.74	19.03	266	2.88	0.0776 ± 0.0003	...	...	...	...
CB-13.8717	15:19:36.3	28:14:40.1	19.01	20.38	18.43	19.71	216	2.63	0.1976 ± 0.0003	15.7 ± 1.3	...	...	...
CB-14.7809	15:19:37.0	28:42:10.1	18.44	19.61	17.71	19.03	247	2.47	0.1287 ± 0.0003	...	...	1.9 ± 0.2	...
CB-14.7812	15:19:37.1	28:54:19.9	19.84	20.38	18.08	18.92	96	1.51	star	...	...	...	...

TABLE 2.5—*Continued*

Object	RA (1950)	Dec.	g_{tot}	g_{core}	r_{tot}	r_{core}	Area (□″)	irl (″)	z	W_λ([O II]) (Å)	W_λ(Hδ) (Å)	W_λ(Hβ) (Å)	W_λ([O III]5007) (Å)
CB-13.8655	15:19:37.4	28:16:27.8	17.97	19.41	17.23	18.49	145	2.37	0.1189 ± 0.0003	···	···	···	···
CB-14.7789	15:19:37.6	28:51:34.3	18.20	19.56	17.34	18.69	309	2.85	0.1103 ± 0.0003	···	···	-2.0 ± 0.3	···
CB-15.7419	15:19:37.7	29:35:38.0	21.26	21.32	19.62	20.69	79	1.30	0.1810 ± 0.0003	···	···	···	···
CB-13.8616	15:19:38.4	28:21:24.8	18.81	19.95	18.26	19.33	198	2.39	0.1177 ± 0.0003	···	···	-1.2 ± 0.3	···
CB-14.7745	15:19:38.4	28:37:32.4	18.55	19.73	18.30	19.42	205	2.35	0.1504 ± 0.0003	7.7 ± 0.6	-2.2 ± 0.4	···	···
CB-14.7746	15:19:38.4	28:50:30.1	20.58	21.73	19.29	20.43	102	1.96	0.3686 ± 0.0003	···	···	···	···
CB-15.7370	15:19:38.7	29:40:40.0	19.24	20.18	18.17	19.23	124	2.01	0.1690 ± 0.0003	···	···	···	···
CB-15.7369	15:19:38.7	29:38:36.8	22.14	22.58	21.11	21.80	32	1.33	0.4493 ± 0.0003	17.4 ± 3.8	···	···	···
CB-13.8582	15:19:39.0	28:11:15.1	19.00	20.68	19.36	20.97	200	2.78	0.1253 ± 0.0003	26.5 ± 2.0	-3.7 ± 0.7	4.3 ± 0.4	7.1 ± 0.5
CB-16.7697	15:19:39.0	30:48:03.3	18.65	19.91	18.71	20.03	239	2.63	0.0748 ± 0.0003	···	···	4.6 ± 0.7	3.7 ± 0.6
CB-15.7336	15:19:39.4	29:32:24.4	17.99	19.66	18.00	19.72	294	3.69	0.0757 ± 0.0003	···	···	16.4 ± 0.9	35.9 ± 0.9
CB-14.7681	15:19:39.6	28:47:21.5	19.36	20.45	18.84	19.85	28	1.25	0.2775 ± 0.0003	32.7 ± 1.2	···	10.9 ± 0.4	7.5 ± 0.4
CB-13.8541	15:19:39.9	28:11:54.8	21.91	22.81	21.71	22.13	25	1.11	0.5189 ± 0.0003	···	···	···	···
CB-16.7658	15:19:40.1	30:46:56.7	17.75	19.17	17.00	18.23	299	2.85	0.0787 ± 0.0003	···	···	···	···
CB-15.7296	15:19:40.2	29:31:37.3	19.22	20.35	19.11	19.99	180	2.20	0.1283 ± 0.0003	15.1 ± 1.9	···	2.4 ± 0.3	···
CB-15.7288	15:19:40.2	29:44:06.8	19.49	20.20	20.27	20.66	69	1.38	star	···	···	···	···
CB-14.7596	15:19:41.2	28:50:40.9	19.55	20.49	19.57	20.42	123	1.96	0.2127 ± 0.0003	21.8 ± 0.8	···	···	5.4 ± 0.3
CB-16.7606	15:19:41.3	30:57:14.5	18.42	19.58	18.28	19.33	228	2.39	0.0693 ± 0.0003	···	···	···	···
CB-13.8464	15:19:41.4	28:09:10.2	20.02	21.02	19.05	20.13	110	1.91	0.1971 ± 0.0003	···	···	-2.3 ± 0.4	···
CB-15.7230	15:19:41.5	29:32:45.4	21.20	22.14	20.05	21.16	69	2.18	0.4479 ± 0.0003	···	···	···	···
CB-13.8454	15:19:41.6	28:23:32.0	17.43	18.95	17.19	18.68	226	2.69	0.1713 ± 0.0003	6.2 ± 0.4	-3.8 ± 0.4	2.9 ± 0.2	0.7 ± 0.2
CB-16.7581	15:19:41.8	30:48:36.1	17.28	19.26	16.85	18.63	262	2.83	0.0759 ± 0.0003	···	···	···	···
CB-16.7552	15:19:42.3	30:53:15.3	16.84	19.43	17.00	19.26	963	5.61	star	···	···	···	···
CB-14.7532	15:19:42.3	28:39:47.2	22.44	22.73	20.60	21.64	21	0.91	0.4856 ± 0.0003	12.4 ± 1.3	···	···	···
CB-13.8397	15:19:42.5	28:10:16.1	18.06	20.35	18.02	19.73	436	4.30	0.1252 ± 0.0003	···	···	-2.2 ± 0.4	···
CB-15.7179	15:19:42.5	29:35:32.2	19.21	20.21	18.39	19.41	143	2.13	0.1133 ± 0.0003	···	···	-2.2 ± 0.4	···
CB-16.7514	15:19:43.1	30:51:06.4	18.54	19.90	18.72	20.14	182	2.56	0.0763 ± 0.0003	···	-7.4 ± 1.2	-2.9 ± 0.6	···
1519+3046	15:19:43.2	30:46:33.0	16.46	18.41	15.90	17.74	978	4.41	0.0785 ± 0.0002	···	···	···	···
CB-15.7131	15:19:43.4	29:40:39.7	18.78	20.36	18.36	19.72	267	3.12	0.1698 ± 0.0003	···	···	···	···
CB-16.7495	15:19:43.6	30:56:36.6	17.69	19.13	16.95	18.29	454	3.04	0.0777 ± 0.0003	···	···	-2.4 ± 0.4	···
CB-14.7469	15:19:43.7	28:44:17.8	17.79	19.23	17.23	18.43	196	2.48	0.0827 ± 0.0003	···	···	-1.6 ± 0.2	···
CB-14.7464	15:19:43.8	28:49:14.3	17.97	19.31	17.41	18.98	267	2.70	0.1098 ± 0.0003	8.8 ± 1.1	···	2.5 ± 0.2	···
2065-292	15:19:44.2	27:39:24.0	15.57	18.79	15.75	18.52	1110	7.06	0.0459 ± 0.0002	···	···	···	···
CB-15.7087	15:19:44.3	29:47:49.1	20.31	20.80	18.57	19.26	93	1.44	star	···	···	···	···
CB-13.8289	15:19:44.4	28:16:59.1	17.80	18.98	17.02	18.11	117	2.03	0.0459 ± 0.0003	···	-1.4 ± 0.4	-2.1 ± 0.2	···
CB-17.6779	15:19:44.5	30:59:51.3	21.10	21.50	19.32	20.20	70	1.48	star	···	···	···	···
CB-16.7452	15:19:44.6	30:45:51.6	17.64	19.46	16.88	18.51	362	3.68	star	···	···	···	···
CB-13.8250	15:19:44.8	28:10:34.5	19.06	20.46	18.79	20.30	221	2.64	0.1189 ± 0.0003	10.7 ± 1.2	···	···	···
CB-13.8251	15:19:44.9	28:22:15.3	18.74	19.91	18.21	19.46	212	2.37	0.0696 ± 0.0003	···	···	-2.8 ± 0.5	···
CB-14.7410	15:19:45.1	28:50:30.9	20.52	21.12	19.88	21.16	88	1.64	0.1711 ± 0.0003	···	···	2.4 ± 0.4	2.1 ± 0.5
CB-15.7045	15:19:45.4	29:41:38.5	19.55	20.42	18.80	19.84	124	1.97	0.1700 ± 0.0003	···	···	···	···
CB-15.7040	15:19:45.5	29:30:47.6	17.51	18.53	15.97	16.82	266	2.21	star	···	···	···	···
CB-13.8205	15:19:45.8	28:13:37.7	20.08	21.15	19.61	21.07	95	1.91	0.1464 ± 0.0003	16.1 ± 1.8	···	···	···
CB-14.7377	15:19:45.8	28:40:32.1	19.48	20.65	19.43	20.69	130	2.16	0.0833 ± 0.0003	···	···	···	1.6 ± 0.4
CB-13.8202	15:19:45.8	28:20:01.2	18.98	20.09	18.41	19.60	189	2.19	0.1187 ± 0.0003	···	···	···	···

TABLE 2.5—*Continued*

Object	RA (1950)	Dec. (1950)	g_{tot}	g_{core}	r_{tot}	r_{core}	Area (□″)	irl (″)	z	W_λ([O II]) (Å)	W_λ(Hδ) (Å)	W_λ(Hβ) (Å)	W_λ([O III]5007) (Å)
CB-99.7	15:19:45.8	30:50:19.0	...	...	18.10	19.26	251	2.39	0.1147 ± 0.0003	...	...	...	...
CB-14.7369	15:19:46.1	28:36:10.4	18.09	18.92	17.01	17.94	221	1.92	star	...	...	...	...
CB-15.7018	15:19:46.4	29:43:14.4	18.89	19.98	18.02	19.31	211	2.23	0.1142 ± 0.0003	...	...	...	...
CB-14.7358	15:19:46.5	28:45:01.9	18.44	19.83	18.72	20.25	238	2.81	0.0773 ± 0.0003	24.0 ± 1.6	...	7.0 ± 0.4	16.8 ± 0.4
CB-14.7338	15:19:47.1	28:54:50.1	18.47	19.24	17.51	18.34	187	1.84	star	...	...	...	...
CB-15.6981	15:19:47.2	29:30:14.0	21.10	21.49	20.01	21.19	68	1.41	0.1110 ± 0.0010	...	...	...	...
CB-13.8136	15:19:47.4	28:19:53.5	18.21	19.40	17.73	18.77	238	2.41	0.1007 ± 0.0003	6.4 ± 0.6	...	...	2.9 ± 0.2
CB-15.6965	15:19:47.7	29:39:23.0	19.88	20.85	19.29	20.47	93	1.76	0.1137 ± 0.0003	...	...	...	...
CB-14.7303	15:19:48.0	28:48:57.6	21.36	21.93	20.37	21.49	57	1.32	0.3674 ± 0.0003	3.4 ± 0.8	...	...	...
CB-14.7297	15:19:48.1	28:42:17.1	19.16	20.29	18.76	20.02	192	2.22	0.1730 ± 0.0003	3.0 ± 0.7	-3.4 ± 0.5	...	...
CB-13.8080	15:19:48.5	28:18:09.2	18.47	19.27	17.42	18.26	188	1.84	star	...	...	...	...
2065-285	15:19:48.6	27:35:32.0	15.58	17.66	14.92	16.65	1255	5.20	0.0778 ± 0.0002	...	...	...	...
CB-15.6909	15:19:48.8	29:31:57.5	19.82	21.06	20.17	21.62	121	2.25	0.1672 ± 0.0003	...	...	5.0 ± 1.0	12.1 ± 1.0
CB-15.6904	15:19:49.0	29:47:41.7	18.87	20.15	18.36	19.58	238	2.49	0.1113 ± 0.0003	...	...	...	...
CB-13.8040	15:19:49.0	28:14:50.3	18.97	20.12	18.48	19.64	203	2.33	0.1227 ± 0.0003	8.4 ± 1.3	...	...	...
CB-15.6886	15:19:49.3	29:38:49.6	19.17	20.10	18.46	19.33	138	1.96	0.1130 ± 0.0003	...	...	-1.9 ± 0.3	...
CB-17.6589	15:19:49.5	31:06:34.1	19.87	20.56	19.37	20.58	98	1.52	star	...	...	...	...
CB-15.6872	15:19:49.5	29:32:43.9	20.83	21.34	22.02	22.14	88	1.73	0.1643 ± 0.0003	44.9 ± 3.7	...	27.8 ± 2.0	71.6 ± 1.9
CB-14.7215	15:19:50.0	28:38:54.7	19.65	20.54	18.96	19.93	106	1.83	0.1705 ± 0.0003	4.1 ± 0.7	...	...	...
CB-17.6555	15:19:50.1	30:59:46.7	17.35	18.89	16.77	18.23	302	2.93	0.0840 ± 0.0003	...	...	-4.7 ± 0.6	...
CB-13.7982	15:19:50.1	28:14:14.0	18.75	20.05	17.95	19.18	245	2.61	0.1478 ± 0.0003	...	...	...	...
CB-17.6550	15:19:50.4	30:59:59.0	18.20	19.06	16.92	17.87	120	1.85	star	...	...	...	...
CB-16.7227	15:19:50.6	30:44:27.5	18.38	19.48	17.66	18.74	230	2.35	0.0916 ± 0.0003	...	...	...	8.3 ± 0.6
CB-14.7162	15:19:51.0	28:48:27.9	19.83	20.67	19.80	20.94	110	1.88	star	...	...	...	...
CB-16.7212	15:19:51.3	30:56:58.1	18.53	19.78	17.90	19.24	237	2.54	0.0789 ± 0.0003	...	...	-3.1 ± 0.4	...
CB-13.7906	15:19:51.3	28:16:57.6	19.57	20.74	19.11	20.25	149	2.39	0.1185 ± 0.0003	...	...	...	...
CB-15.6796	15:19:51.4	29:45:29.9	18.65	20.02	18.41	19.83	227	2.57	0.1805 ± 0.0003	6.5 ± 0.9	...	2.1 ± 0.4	...
CB-14.7134	15:19:51.8	28:38:35.1	18.96	19.99	18.61	19.87	142	2.07	0.0717 ± 0.0003	8.2 ± 1.1	...	3.0 ± 0.3	1.7 ± 0.3
CB-15.6767	15:19:51.8	29:32:54.7	18.62	19.32	17.62	18.38	107	1.62	star	...	...	...	...
CB-16.7181	15:19:52.0	30:53:20.3	17.29	19.09	17.14	18.86	486	3.88	0.0770 ± 0.0003	...	...	...	...
CB-16.7160	15:19:52.4	30:53:52.8	18.96	19.98	18.19	19.23	197	2.20	0.0834 ± 0.0003	...	...	-1.8 ± 0.4	...
CB-14.7104	15:19:52.4	28:52:02.2	17.56	19.19	17.55	19.21	284	2.85	0.0743 ± 0.0003	20.7 ± 1.8	...	2.4 ± 0.3	1.2 ± 0.3
2065-278	15:19:52.8	27:51:19.0	17.00	18.71	16.50	18.07	301	2.96	0.0985 ± 0.0002	...	...	...	...
CB-13.7811	15:19:53.3	28:11:35.9	18.36	19.66	17.76	19.05	254	2.61	0.0764 ± 0.0003	...	...	-3.3 ± 0.5	...
CB-15.6674	15:19:53.8	29:36:35.5	19.50	20.04	19.24	19.93	107	1.56	star	...	...	...	...
CB-13.7758	15:19:54.4	28:15:33.8	19.16	20.38	18.69	19.74	193	2.33	0.1190 ± 0.0003	...	...	...	...
CB-14.7010	15:19:54.5	28:37:49.0	20.61	21.13	19.52	20.46	81	1.48	star	...	...	...	...
CB-14.7015	15:19:54.6	28:46:30.7	20.01	20.78	20.12	20.95	101	1.63	0.2002 ± 0.0003	50.6 ± 0.8	...	10.9 ± 0.3	16.8 ± 0.3
CB-15.6625	15:19:54.7	29:43:08.3	18.86	19.76	17.78	18.59	191	2.04	star	...	...	...	...
CB-16.7055	15:19:55.1	30:53:48.1	18.02	19.21	17.17	18.34	281	2.66	0.0791 ± 0.0003	...	...	-2.6 ± 0.4	...
CB-15.6600	15:19:55.5	29:47:09.7	16.86	18.72	16.18	17.88	746	4.42	0.0741 ± 0.0003	...	...	...	...
CB-17.6355	15:19:55.5	31:03:12.6	22.02	22.64	20.54	21.66	26	1.12	0.4949 ± 0.0003	...	...	...	...
1519+3035	15:19:56.0	30:35:10.0	16.34	18.63	15.86	17.76	865	5.89	0.0774 ± 0.0001	...	...	...	...
CB-13.7657	15:19:56.1	28:08:21.8	21.21	21.71	20.28	21.46	71	1.46	0.4521 ± 0.0003	11.9 ± 0.9	...	...	...
CB-15.6564	15:19:56.1	29:35:55.6	20.11	21.23	19.62	21.21	109	2.18	0.1632 ± 0.0003	...	...	3.1 ± 0.7	...

TABLE 2.5—*Continued*

Object	RA (1950)	Dec. (1950)	g_{tot}	g_{core}	r_{tot}	r_{core}	Area (□″)	irl (″)	z	W_λ([O II]) (Å)	W_λ(Hδ) (Å)	W_λ(Hβ) (Å)	W_λ([O III]5007) (Å)
CB-14.6941	15:19:56.5	28:53:36.9	21.19	21.85	20.82	21.07	68	1.50	star	...	...	...	...
CB-17.6310	15:19:56.5	31:00:01.0	18.66	19.74	18.10	19.25	154	2.17	0.0790 ± 0.0003	...	...	-2.4 ± 0.3	...
CB-14.6912	15:19:56.8	28:38:28.4	19.86	20.73	19.71	20.55	114	1.82	0.1781 ± 0.0003	10.0 ± 0.7	-4.4 ± 0.6	2.4 ± 0.2	...
CB-15.6523	15:19:57.0	29:37:14.2	20.63	21.19	19.93	20.88	92	1.69	0.2139 ± 0.0003	12.2 ± 1.8	...	...	...
CB-15.6519	15:19:57.1	29:41:34.2	17.87	19.36	17.89	19.34	236	2.68	0.0740 ± 0.0003	...	...	2.8 ± 0.4	...
CB-13.7564	15:19:57.6	28:21:34.3	17.99	19.30	18.10	19.62	257	2.57	0.0708 ± 0.0003	20.0 ± 1.1	-2.0 ± 0.5	5.0 ± 0.2	3.1 ± 0.2
CB-16.6959	15:19:57.7	30:54:53.2	18.95	20.05	18.38	19.52	194	2.28	0.0810 ± 0.0003	...	...	-3.8 ± 0.5	...
CB-14.6841	15:19:58.5	28:45:48.0	18.81	19.92	18.34	19.54	207	2.27	0.0852 ± 0.0003	...	...	...	...
CB-13.7490	15:19:58.7	28:09:34.7	18.43	19.71	18.00	19.07	259	2.63	0.0749 ± 0.0003	...	...	-2.1 ± 0.3	...
CB-15.6458	15:19:58.7	29:45:42.7	20.70	21.40	19.40	20.80	82	1.57	0.3312 ± 0.0003	...	-4.7 ± 0.9	...	...
CB-17.6230	15:19:58.7	30:58:22.3	17.72	19.14	17.02	18.33	426	3.03	0.0794 ± 0.0003	...	...	-3.0 ± 0.4	...
CB-16.6916	15:19:58.9	30:50:17.9	17.13	18.73	17.04	18.61	467	3.17	0.0755 ± 0.0003	...	-3.6 ± 0.7	3.5 ± 0.2	1.3 ± 0.2
CB-14.6817	15:19:59.2	28:41:43.7	20.59	21.52	20.55	21.91	82	1.64	0.2270 ± 0.0003	33.2 ± 1.7	...	8.2 ± 0.7	6.7 ± 0.7
CB-13.7450	15:19:59.3	28:20:19.6	18.14	19.67	18.49	20.12	284	2.88	0.0731 ± 0.0003	29.9 ± 2.0	...	...	19.6 ± 0.4
CB-15.6394	15:19:60.0	29:39:03.6	17.84	19.57	17.29	18.82	412	3.30	0.1139 ± 0.0003	...	...	-2.1 ± 0.3	...
1520+3124A	15:19:60.0	31:24:41.0	15.31	17.49	14.52	15.84	941	5.31	0.0316 ± 0.0001	...	...	...	...
CB-14.6762	15:20:00.0	28:43:57.3	18.57	19.97	18.89	20.47	232	2.65	0.0741 ± 0.0003	...	...	5.6 ± 0.2	9.7 ± 0.2
CB-17.6150	15:20:00.6	31:04:31.3	18.07	19.85	17.71	19.60	382	3.20	0.0737 ± 0.0003	...	...	...	...
CB-16.6820	15:20:01.2	30:54:47.0	17.88	19.48	17.09	18.58	394	3.24	0.1441 ± 0.0003	...	...	...	...
CB-14.6704	15:20:01.5	28:36:36.4	17.60	18.96	17.34	18.67	296	2.76	0.0728 ± 0.0003	8.8 ± 0.6	-2.8 ± 0.6	4.9 ± 0.1	1.0 ± 0.2
CB-16.6792	15:20:02.0	30:56:44.8	18.34	19.44	18.04	19.06	230	2.29	0.0776 ± 0.0003	...	...	...	...
CB-14.6670	15:20:02.4	28:51:01.7	19.81	20.63	19.86	20.66	113	1.98	0.3748 ± 0.0003	52.3 ± 0.4	-1.3 ± 0.3	...	...
CB-14.6663	15:20:02.5	28:43:30.7	20.27	21.00	20.42	21.27	83	1.65	0.2295 ± 0.0003	18.2 ± 0.9	...	6.5 ± 0.4	1.8 ± 0.4
CB-17.6067	15:20:02.5	31:02:49.9	19.28	20.27	18.55	19.84	128	2.00	0.0799 ± 0.0003	...	...	-1.5 ± 0.3	...
CB-13.7266	15:20:02.8	28:16:12.9	17.84	19.28	16.99	18.30	206	2.47	0.1186 ± 0.0003	...	...	...	...
CB-16.6732	15:20:03.2	30:48:33.9	18.80	19.92	18.10	19.13	229	2.42	0.0805 ± 0.0003	...	...	...	...
CB-14.6611	15:20:03.7	28:48:12.7	17.41	18.94	16.69	18.28	550	3.38	0.0735 ± 0.0003	...	...	...	...
CB-14.6600	15:20:04.0	28:38:11.6	19.32	19.93	17.56	18.38	34	1.26	star	...	...	...	...
CB-16.6701	15:20:04.2	30:50:22.9	17.34	18.96	16.66	18.22	396	3.14	0.0731 ± 0.0003	...	...	-3.1 ± 0.3	...
CB-16.6671	15:20:05.0	30:54:45.2	18.45	20.10	18.70	20.27	295	3.52	0.0759 ± 0.0003	...	...	...	3.0 ± 0.5
CB-14.6543	15:20:05.2	28:41:51.8	18.99	19.75	18.55	19.48	130	1.80	star	...	...	...	...
CB-14.6541	15:20:05.3	28:47:21.9	19.95	21.20	20.25	21.38	113	2.09	0.1714 ± 0.0003	...	...	...	3.6 ± 0.6
CB-14.6526	15:20:05.8	28:43:22.4	18.83	20.53	19.38	20.82	201	2.77	0.1100 ± 0.0010	...	...	...	...
CB-14.6497	15:20:06.5	28:52:28.3	20.75	21.74	19.57	20.81	74	1.61	0.4334 ± 0.0003	...	...	...	...
2065-240	15:20:06.5	27:52:20.0	17.00	18.86	16.98	18.67	495	3.62	0.0700 ± 0.0003	...	...	...	...
CB-17.5818	15:20:07.5	31:03:44.0	18.80	19.76	18.45	19.43	111	1.98	star	...	...	...	...
CB-14.6412	15:20:08.4	28:53:02.5	17.99	19.83	18.31	19.93	271	3.35	0.1091 ± 0.0003	18.6 ± 1.7	...	7.4 ± 0.7	...
2065-222	15:20:08.9	27:38:02.0	16.33	18.94	16.04	18.29	910	5.76	0.0714 ± 0.0002	...	...	...	...
1520+2752C	15:20:09.0	27:52:37.0	16.41	18.27	15.77	17.65	259	3.08	0.0713 ± 0.0003	...	...	...	...
1520+3124B	15:20:09.0	31:24:15.0	16.59	18.91	15.86	17.99	203	2.77	0.1143 ± 0.0001	...	...	...	...
CB-99.8	15:20:09.2	28:51:01.0	...	...	19.99	21.56	80	2.03	0.4355 ± 0.0004	24.9 ± 6.2	...	...	...
2065-227	15:20:09.8	27:59:04.0	16.49	18.71	15.94	17.96	1125	5.37	0.0740 ± 0.0001	...	...	...	...
CB-14.6329	15:20:09.9	28:38:28.9	18.50	19.94	18.29	19.56	249	2.70	0.2140 ± 0.0003	8.2 ± 0.7	-3.4 ± 0.5	...	...
CB-17.5644	15:20:11.0	31:05:39.0	21.03	21.73	19.95	20.66	56	1.26	star	...	...	...	...
CB-16.6425	15:20:11.1	30:51:18.1	17.79	19.05	17.17	18.35	259	2.52	0.0799 ± 0.0003	...	...	-4.0 ± 0.4	...

TABLE 2.5—*Continued*

Object	RA (1950)	Dec. (1950)	g_{tot}	g_{core}	r_{tot}	r_{core}	Area (□″)	irl (″)	z	W_λ([O II]) (Å)	W_λ(Hδ) (Å)	W_λ(Hβ) (Å)	W_λ([O III]5007) (Å)
2065-218	15:20:11.6	27:52:48.0	16.69	18.34	16.14	17.67	263	3.03	0.0723 ± 0.0002	···	···	···	···
CB-17.5571	15:20:12.2	31:02:47.8	18.88	20.10	18.35	19.47	203	2.31	0.1521 ± 0.0003	···	-2.9 ± 0.6	···	···
1520+3139	15:20:12.5	31:39:11.0	16.37	18.09	16.48	18.18	684	3.62	0.0073 ± 0.0000	···	···	···	···
CB-14.6183	15:20:12.8	28:49:34.8	17.36	18.75	17.01	18.36	371	2.82	0.0693 ± 0.0003	···	···	1.9 ± 0.4	···
CB-16.6363	15:20:13.1	30:54:20.7	18.11	20.18	17.92	20.07	50	2.55	0.0891 ± 0.0003	···	···	3.3 ± 0.4	···
CB-17.5529	15:20:13.3	31:05:17.1	20.53	21.43	19.74	21.36	78	1.75	0.3792 ± 0.0003	16.1 ± 1.0	···	···	···
CB-14.6132	15:20:14.2	28:49:17.8	19.03	20.08	18.53	19.72	206	2.24	0.0735 ± 0.0003	···	···	7.8 ± 0.2	16.9 ± 0.2
CB-17.5469	15:20:14.6	30:58:13.9	18.22	19.56	17.57	18.87	296	2.85	0.0808 ± 0.0003	···	···	-2.8 ± 0.3	···
CB-14.6112	15:20:14.9	28:41:33.0	16.39	18.02	16.12	17.74	815	3.70	0.0491 ± 0.0003	15.4 ± 0.5	-6.7 ± 0.4	···	2.3 ± 0.1
CB-17.5430	15:20:15.6	31:03:13.6	18.17	18.98	17.22	18.09	204	1.90	star	···	···	···	···
CB-16.6263	15:20:15.7	30:50:40.4	18.53	19.57	17.80	18.86	210	2.19	0.0728 ± 0.0003	···	···	-2.3 ± 0.4	···
2065-205	15:20:16.2	27:54:58.0	16.53	18.26	15.89	17.57	739	3.89	0.0794 ± 0.0002	···	···	···	···
CB-17.5391	15:20:16.7	31:01:24.6	18.86	20.14	18.37	19.58	141	2.20	0.0816 ± 0.0003	···	···	-2.3 ± 0.4	···
CB-14.6030	15:20:16.7	28:50:23.2	18.52	19.80	18.24	19.81	228	2.47	0.0846 ± 0.0003	···	-6.0 ± 1.3	···	···
1520+2751	15:20:17.0	27:51:29.0	18.07	19.31	17.30	18.49	249	2.50	0.0662 ± 0.0003	···	···	···	···
2065-198	15:20:17.4	27:53:32.0	15.69	18.06	15.15	17.42	792	4.89	0.0693 ± 0.0002	···	···	···	···
CB-16.6201	15:20:17.4	30:52:14.0	19.84	20.55	18.46	19.24	98	1.61	star	···	···	···	···
CB-17.5353	15:20:17.7	31:05:05.0	19.00	20.11	18.38	19.69	191	2.31	0.0803 ± 0.0003	···	···	-3.7 ± 0.3	···
CB-14.5938	15:20:18.2	28:46:37.5	18.46	19.55	17.78	18.87	235	2.35	0.0861 ± 0.0003	···	···	···	···
1520+2752A	15:20:19.0	27:52:17.0	17.97	19.21	17.18	18.45	273	2.60	0.0706 ± 0.0003	···	···	···	···
CB-14.5842	15:20:20.0	28:49:32.2	17.49	18.64	17.24	18.43	244	2.35	0.0724 ± 0.0003	28.5 ± 1.1	···	9.8 ± 0.1	4.4 ± 0.2
1520+2813B	15:20:20.1	28:13:58.0	16.62	18.84	16.16	18.11	245	2.88	0.0710 ± 0.0002	···	···	···	···
1520+2752B	15:20:21.0	27:52:32.0	17.07	18.75	16.30	17.84	310	3.27	0.0714 ± 0.0003	···	···	···	···
1520+2753B	15:20:21.0	27:53:11.0	17.63	19.01	16.77	18.10	164	2.47	0.0706 ± 0.0003	···	···	···	···
CB-17.5211	15:20:21.0	31:04:14.0	18.94	20.03	18.59	19.62	192	2.24	0.1822 ± 0.0003	4.7 ± 0.7	-4.3 ± 0.6	1.9 ± 0.2	···
CB-16.6057	15:20:21.3	30:54:11.7	17.47	18.95	16.81	18.14	419	3.32	0.0787 ± 0.0003	···	···	-3.3 ± 0.3	···
2065-171	15:20:21.9	27:51:52.0	16.45	18.38	15.88	17.70	470	3.65	0.0695 ± 0.0003	···	···	···	···
1520+2752D	15:20:22.0	27:52:05.0	16.45	18.38	15.88	17.70	470	3.65	0.0749 ± 0.0003	···	···	···	···
CB-17.5149	15:20:22.2	31:02:35.5	19.10	20.23	18.85	19.82	186	2.07	0.0798 ± 0.0003	···	···	-2.6 ± 0.4	···
2065-164	15:20:22.3	27:53:23.0	16.11	18.37	15.48	17.69	141	2.51	0.0728 ± 0.0005	···	···	···	···
CB-16.5935	15:20:24.1	30:49:13.5	20.17	20.89	18.72	19.53	59	1.36	star	···	···	···	···
CB-17.5033	15:20:25.0	31:03:09.3	18.31	19.12	17.29	18.11	184	1.88	star	···	···	···	···
CB-17.4935	15:20:27.6	31:04:05.2	20.38	21.03	20.67	21.57	92	1.69	0.0653 ± 0.0003	···	···	6.5 ± 1.0	14.8 ± 0.8
CB-17.4895	15:20:28.7	31:05:44.8	19.93	20.80	19.91	20.90	102	1.90	0.1851 ± 0.0003	81.7 ± 2.2	···	7.8 ± 0.9	22.4 ± 0.9
2065-119	15:20:32.5	27:51:17.0	16.23	18.17	15.67	17.55	455	3.66	0.0737 ± 0.0003	···	···	···	···
2065-118	15:20:32.7	27:50:59.0	17.22	18.87	16.44	17.98	242	3.13	0.0746 ± 0.0003	···	···	···	···
1520+2750	15:20:37.0	27:50:38.0	16.91	18.49	16.18	17.82	639	3.57	0.0670 ± 0.0003	···	···	···	···
2065-103	15:20:37.4	27:47:41.0	16.59	18.57	15.95	17.79	454	3.82	0.0790 ± 0.0002	···	···	···	···
15207+2957	15:20:42.8	29:56:39.0	14.44	17.03	14.52	16.48	1594	5.85	0.0229 ± 0.0000	···	···	···	···
CB-17.4099	15:20:46.6	31:14:58.1	20.06	21.29	19.46	20.34	106	2.32	star	···	···	···	···
CB-17.4057	15:20:47.6	31:18:42.0	19.70	20.55	18.80	20.05	137	2.09	0.1165 ± 0.0003	···	···	-2.7 ± 0.4	···
CB-17.4006	15:20:48.8	31:18:03.4	18.36	19.61	17.65	18.95	265	2.64	0.1160 ± 0.0003	···	-2.0 ± 0.4	-3.2 ± 0.4	···
CB-17.3934	15:20:50.2	31:18:24.6	19.21	20.39	19.61	20.66	192	2.24	0.1649 ± 0.0003	16.5 ± 2.3	···	···	9.4 ± 1.2
CB-17.3881	15:20:51.2	31:12:21.0	20.40	21.43	19.06	20.23	81	1.69	0.3606 ± 0.0003	···	6.1 ± 0.5	···	···
1520+2817	15:20:51.5	28:17:18.0	17.10	18.54	17.11	18.61	386	2.85	0.0697 ± 0.0001	···	···	···	···

TABLE 2.5—*Continued*

Object	RA (1950)	Dec.	g_{tot}	g_{core}	r_{tot}	r_{core}	Area (□″)	irl (″)	z	W_λ([O II]) (Å)	W_λ(Hδ) (Å)	W_λ(Hβ) (Å)	W_λ([O III]5007) (Å)
CB-17.3860	15:20:51.6	31:09:41.9	19.67	20.56	18.74	19.80	92	1.84	0.2033 ± 0.0003	...	...	...	...
CB-17.3812	15:20:52.5	31:09:43.0	16.37	18.14	15.87	17.55	547	3.80	0.0802 ± 0.0003	...	-2.7 ± 0.6	...	1.6 ± 0.2
CB-17.3727	15:20:54.3	31:07:45.3	21.66	21.80	20.83	21.52	29	1.19	0.3851 ± 0.0003	33.3 ± 1.3	...	...	...
CB-17.3716	15:20:54.6	31:12:51.9	20.09	20.74	20.50	21.50	92	1.58	2.8800 ± 0.0010	...	...	...	...
CB-17.3681	15:20:55.6	31:10:15.8	20.66	21.75	19.97	21.14	81	1.79	0.4232 ± 0.0003	11.3 ± 1.1	...	...	...
CB-17.3663	15:20:55.7	31:02:29.6	15.31	17.16	13.72	15.25	780	3.58	star	...	...	...	...
CB-17.3650	15:20:56.1	31:04:31.8	18.57	19.69	17.91	18.93	227	2.40	0.0737 ± 0.0003	...	...	-3.8 ± 0.5	...
CB-17.3619	15:20:56.7	30:59:05.1	21.24	21.65	21.47	22.06	64	1.35	0.4175 ± 0.0003	65.6 ± 1.3	...	...	...
CB-17.3554	15:20:57.9	30:59:24.1	20.55	22.23	19.95	21.19	105	2.76	star	...	...	...	...
CB-17.3566	15:20:57.9	31:13:39.0	18.82	19.99	19.01	20.18	198	2.22	0.2340 ± 0.0010	16.5 ± 1.0	-6.2 ± 0.9	4.8 ± 0.5	...
CB-17.3506	15:20:59.1	31:00:00.7	17.82	19.20	17.09	18.45	309	2.78	0.0694 ± 0.0003	...	...	...	...
CB-17.3492	15:20:59.7	31:10:28.1	17.58	19.78	17.66	19.55	316	4.31	0.1100 ± 0.0003	10.7 ± 1.9	...	...	...
CB-16.4212	15:21:01.0	30:54:37.1	19.27	20.00	18.68	19.33	129	1.76	star	...	...	...	...
CB-17.3424	15:21:01.2	31:04:40.5	18.97	20.11	18.57	19.79	151	2.20	0.0731 ± 0.0003	...	...	-4.7 ± 0.5	...
CB-17.3396	15:21:01.7	31:03:05.3	17.79	19.13	17.18	18.44	266	2.65	0.0707 ± 0.0003	...	...	...	...
CB-17.3386	15:21:02.1	30:57:41.6	19.46	20.39	18.89	19.84	114	1.90	0.0764 ± 0.0003	...	...	...	...
CB-17.3368	15:21:02.8	31:07:53.3	21.39	21.92	19.65	20.67	30	1.16	star	...	...	...	...
CB-17.3357	15:21:03.2	31:14:55.6	19.15	20.36	18.86	20.09	184	2.28	0.1164 ± 0.0003	...	...	...	9.7 ± 0.2
CB-17.3345	15:21:03.3	31:02:55.2	19.37	20.56	19.04	20.15	120	2.10	0.2366 ± 0.0003	...	...	...	...
CB-17.3300	15:21:04.4	31:04:16.3	18.78	19.62	17.96	18.92	192	1.97	0.0706 ± 0.0003	...	...	...	...
2067-83	15:21:04.7	31:02:18.0	16.80	18.56	16.29	17.87	784	4.01	0.0723 ± 0.0001	...	...	...	...
CB-17.3277	15:21:04.9	30:59:52.1	19.26	20.12	18.34	19.31	130	1.91	0.1515 ± 0.0003	...	...	...	...
2067-78	15:21:05.5	30:59:23.0	16.93	18.77	16.65	18.30	458	3.58	0.0720 ± 0.0002	...	...	...	...
CB-17.3246	15:21:05.5	31:03:14.2	15.71	18.38	15.23	17.67	274	3.37	0.0734 ± 0.0003	...	...	...	...
2067-84	15:21:05.7	31:08:33.0	17.09	18.86	16.30	17.96	493	3.58	0.1130 ± 0.0002	...	...	...	...
CB-17.3260	15:21:05.8	31:18:10.7	17.35	18.85	16.71	18.12	442	3.13	0.0738 ± 0.0003	...	...	-3.5 ± 0.3	...
CB-17.3208	15:21:06.2	30:58:08.3	18.63	19.91	18.10	19.26	243	2.56	0.0732 ± 0.0003	...	...	-1.6 ± 0.3	...
CB-17.3195	15:21:06.6	31:04:52.6	19.13	20.10	18.58	19.69	187	2.09	0.0748 ± 0.0003	...	...	-2.2 ± 0.4	...
2067-81	15:21:07.0	31:06:54.0	16.51	18.52	16.36	18.21	649	3.82	0.0782 ± 0.0002	...	...	...	...
CB-17.3174	15:21:07.2	31:14:15.9	19.29	20.30	18.68	19.71	116	1.96	0.1139 ± 0.0003	...	...	...	11.5 ± 0.3
CB-17.3132	15:21:07.6	30:59:34.9	16.47	17.75	14.92	15.68	393	2.62	star	...	...	...	...
CB-17.3134	15:21:07.8	31:04:14.8	19.44	19.78	18.72	19.17	23	1.14	0.0730 ± 0.0010	...	...	-2.4 ± 0.3	...
CB-17.3075	15:21:09.0	31:06:08.2	19.17	19.90	17.34	18.25	66	1.43	star	...	...	...	...
CB-17.3037	15:21:09.9	31:05:52.9	16.64	18.45	16.18	17.87	870	4.08	0.0769 ± 0.0003	...	...	...	...
CB-17.3044	15:21:10.0	31:11:56.9	19.49	20.34	18.72	19.76	97	1.75	0.1140 ± 0.0003	...	...	-3.2 ± 0.4	...
CB-17.3030	15:21:10.2	31:08:30.5	18.29	19.64	17.78	19.13	295	2.80	0.0741 ± 0.0003	...	...	-3.2 ± 0.3	...
CB-17.2983	15:21:11.3	31:13:34.5	18.68	19.86	18.41	19.66	204	2.25	0.0741 ± 0.0003	...	...	-2.3 ± 0.3	...
CB-16.3728	15:21:11.9	30:56:36.9	18.25	19.73	17.50	19.02	291	3.29	0.0735 ± 0.0003	22.1 ± 2.8	...	...	11.1 ± 0.4
CB-17.2922	15:21:12.2	31:10:55.8	17.22	19.07	16.64	18.35	376	3.24	0.1116 ± 0.0003	...	...	-2.9 ± 0.5	...
CB-17.2899	15:21:12.2	31:03:50.3	18.99	20.20	18.30	19.36	189	2.21	0.1515 ± 0.0003	...	...	...	...
2067-70	15:21:12.3	31:10:10.0	16.95	18.88	16.14	17.96	242	3.20	0.1111 ± 0.0002	...	...	...	...
CB-17.2880	15:21:13.0	31:16:18.4	21.23	21.72	19.93	20.79	69	1.32	star	...	...	...	...
2067-54	15:21:13.1	30:47:37.0	17.36	18.89	16.57	18.19	81	1.82	0.1272 ± 0.0001	...	...	...	...
CB-17.2852	15:21:13.1	30:57:55.2	18.84	19.78	17.89	18.95	182	2.02	0.0745 ± 0.0003	...	...	-1.9 ± 0.3	...
CB-17.2838	15:21:13.8	31:13:36.5	19.09	20.06	18.16	19.30	114	1.94	0.1114 ± 0.0003	...	...	-3.5 ± 0.6	...

TABLE 2.5—*Continued*

Object	RA (1950)	Dec. (1950)	g_{tot}	g_{core}	r_{tot}	r_{core}	Area (□″)	irl (″)	z	W_λ([O II]) (Å)	W_λ(Hδ) (Å)	W_λ(Hβ) (Å)	W_λ([O III]5007) (Å)
CB-16.3583	15:21:14.6	30:55:24.1	19.18	19.81	17.67	18.49	91	1.57	star	...	...	...	...
CB-17.2804	15:21:14.8	31:14:34.0	19.70	20.35	18.75	19.52	110	1.64	star	...	...	...	...
CB-17.2779	15:21:15.2	31:01:51.6	18.64	19.40	17.01	17.95	100	1.67	star	...	...	...	...
CB-17.2748	15:21:15.8	30:59:02.5	18.82	19.56	18.62	19.35	124	1.73	0.2410 ± 0.0010	4.7 ± 0.5	...	20.2 ± 0.8	...
CB-17.2755	15:21:15.9	31:06:58.3	18.37	19.26	17.47	18.48	208	2.05	star	...	...	...	...
CB-17.2740	15:21:16.1	31:02:12.0	17.86	19.33	17.29	18.63	438	3.20	0.1144 ± 0.0003	...	...	-2.6 ± 0.5	...
CB-17.2742	15:21:16.6	31:19:18.9	16.84	19.08	16.71	18.88	525	4.16	0.0760 ± 0.0003	...	...	...	...
CB-17.2682	15:21:17.5	31:01:03.3	18.41	19.84	18.58	20.00	270	2.83	0.0760 ± 0.0003	...	...	...	3.6 ± 0.4
CB-17.2685	15:21:17.9	31:15:48.1	19.59	20.55	19.55	20.66	120	1.92	0.0736 ± 0.0003	...	...	-2.9 ± 0.4	...
CB-17.2663	15:21:18.0	31:05:31.0	20.01	20.96	19.66	21.56	91	1.88	0.1154 ± 0.0003	...	...	19.8 ± 1.5	...
CB-17.2622	15:21:19.1	31:00:28.7	18.97	20.08	18.56	19.86	171	2.26	0.0762 ± 0.0003	...	...	-2.7 ± 0.6	...
CB-17.2627	15:21:19.1	31:08:09.8	18.72	19.68	17.90	18.87	197	2.09	0.0750 ± 0.0003	...	...	-3.4 ± 0.4	...
CB-17.2588	15:21:20.1	31:09:46.8	17.67	19.11	17.22	18.62	128	2.26	0.0776 ± 0.0003	...	...	...	...
CB-17.2589	15:21:20.1	31:12:58.8	17.51	19.05	16.85	18.38	410	3.05	0.0743 ± 0.0003	...	...	-3.5 ± 0.4	...
CB-16.3230	15:21:20.6	30:55:40.6	17.88	19.23	17.16	18.47	372	2.90	0.0739 ± 0.0003	...	...	-1.7 ± 0.3	...
1521+2848	15:21:21.0	28:48:06.0	15.80	18.02	15.26	17.50	183	2.55	0.0821 ± 0.0008	...	...	...	...
CB-17.2530	15:21:21.6	31:17:57.9	18.56	20.28	18.93	20.30	283	3.10	0.1475 ± 0.0003	...	...	...	...
CB-17.2447	15:21:23.2	31:02:45.0	19.33	20.64	19.02	20.69	155	2.51	0.0676 ± 0.0003	...	...	...	7.8 ± 0.8
CB-17.2415	15:21:24.2	31:14:34.8	15.82	17.90	15.18	17.25	719	4.22	0.0749 ± 0.0003	...	...	-3.6 ± 0.3	...
1521+2818	15:21:24.3	28:18:36.0	16.74	18.70	16.36	18.17	729	4.24	0.0545 ± 0.0003	...	...	...	...
CB-17.2396	15:21:24.5	31:04:37.7	20.36	21.63	19.33	20.48	96	2.04	0.2967 ± 0.0003	...	...	...	...
CB-16.2906	15:21:25.4	30:54:13.6	21.38	21.66	19.82	20.63	24	1.10	0.4217 ± 0.0003	...	...	...	...
CB-17.2323	15:21:26.2	31:10:24.4	18.20	19.55	18.21	19.58	293	2.76	0.1163 ± 0.0003	56.9 ± 1.5	...	15.0 ± 0.5	40.9 ± 0.5
CB-17.2319	15:21:26.4	31:10:39.8	19.04	20.05	18.38	19.31	194	2.12	0.1145 ± 0.0003	...	...	...	...
CB-17.2307	15:21:26.6	31:09:23.5	18.46	20.18	18.69	20.47	289	3.26	0.0715 ± 0.0003	...	...	...	8.6 ± 0.8
CB-17.2265	15:21:27.2	30:57:39.1	16.15	17.65	14.19	15.51	577	3.00	star	...	...	...	...
2065-22	15:21:27.5	27:55:45.0	16.34	18.28	15.83	17.62	662	4.05	0.0683 ± 0.0001	...	...	...	...
CB-17.2258	15:21:27.6	31:03:01.0	19.52	20.39	18.74	19.65	122	1.99	star	...	...	...	...
CB-17.2240	15:21:28.2	31:14:44.3	19.37	20.38	18.51	19.76	107	1.99	0.1122 ± 0.0003	...	...	...	3.3 ± 0.3
CB-17.2195	15:21:28.7	30:58:04.1	17.69	19.38	16.88	18.51	551	3.73	0.1261 ± 0.0003	...	...	...	...
CB-17.2196	15:21:29.1	31:12:26.1	19.47	20.51	18.93	20.18	89	1.87	0.0742 ± 0.0003	...	...	-3.1 ± 0.2	...
CB-17.2149	15:21:29.9	31:04:47.8	18.15	19.36	17.30	18.50	264	2.51	0.1114 ± 0.0003	...	...	-2.1 ± 0.4	...
CB-17.2110	15:21:31.1	31:06:13.8	20.10	20.93	19.76	20.75	99	1.80	0.3378 ± 0.0003	34.6 ± 3.0	...	...	...
2067-45	15:21:33.5	31:20:56.0	16.61	18.64	15.93	17.89	943	4.89	0.0800 ± 0.0002	...	...	...	...
2067-37	15:21:39.8	31:13:32.0	16.67	18.64	15.95	17.72	783	5.88	0.0741 ± 0.0002	...	...	...	...
2069-155	15:21:50.6	30:05:02.0	18.37	19.50	17.26	18.54	233	2.33	0.1132 ± 0.0008	...	...	...	...
CB-17.1226	15:21:52.6	31:18:01.1	19.59	20.68	18.83	20.00	98	1.90	0.2068 ± 0.0003	...	...	...	...
CB-17.1173	15:21:54.3	31:22:07.9	18.88	19.95	17.94	19.22	242	2.43	0.1230 ± 0.0003	...	...	...	...
CB-17.1049	15:21:57.5	31:23:14.0	14.92	17.64	14.35	17.04	1030	5.93	0.0739 ± 0.0003	...	...	-3.7 ± 0.3	...
2069-145	15:21:58.9	30:04:55.0	17.47	19.08	16.44	18.20	74	1.66	0.1085 ± 0.0003	...	...	...	...
2069-142	15:21:59.6	30:05:43.0	16.55	19.14	16.28	18.57	497	4.56	0.0756 ± 0.0007	...	...	...	...
CB-17.943	15:21:59.9	31:12:07.1	19.71	20.65	19.76	20.71	112	1.88	star	...	...	...	...
CB-17.928	15:22:00.6	31:21:18.2	18.40	19.87	18.84	20.31	279	2.84	0.0738 ± 0.0003	...	...	9.0 ± 0.7	18.5 ± 1.4
CB-17.886	15:22:01.3	31:13:44.7	18.42	19.14	17.26	18.10	183	1.78	star	...	...	...	...
CB-17.883	15:22:01.9	31:23:30.2	20.03	20.75	18.70	19.58	28	1.17	star	...	...	...	...

TABLE 2.5—*Continued*

Object	RA (1950)	Dec. (1950)	g_{tot}	g_{core}	r_{tot}	r_{core}	Area (□″)	irl (″)	z	W_λ([O II]) (Å)	W_λ(Hδ) (Å)	W_λ(Hβ) (Å)	W_λ([O III]5007) (Å)
CB-17.784	15:22:03.5	31:13:14.0	16.85	18.68	16.63	18.36	727	3.87	0.1259 ± 0.0003	···	-2.5 ± 0.2	···	···
2069-133	15:22:03.8	30:03:50.0	16.29	18.81	15.63	18.07	374	3.67	0.1134 ± 0.0002	···	···	···	···
CB-17.774	15:22:03.9	31:16:22.9	16.34	18.64	15.93	17.93	227	2.97	0.0728 ± 0.0003	···	···	-1.5 ± 0.3	···
CB-17.754	15:22:04.3	31:09:59.4	18.51	19.31	17.41	18.23	183	1.86	star	···	···	···	···
2069-132	15:22:04.8	30:03:27.0	16.66	18.61	15.91	17.75	453	3.63	0.1143 ± 0.0002	···	···	···	···
CB-17.720	15:22:05.6	31:21:31.0	16.13	18.47	16.00	17.89	396	3.84	0.0694 ± 0.0003	···	···	3.4 ± 0.4	16.5 ± 0.6
CB-17.715	15:22:05.8	31:27:53.3	20.63	21.05	19.37	20.29	74	1.31	star	···	···	···	···
CB-17.619	15:22:07.4	31:20:30.2	20.14	21.18	20.12	21.12	104	1.91	0.1125 ± 0.0003	···	···	···	···
CB-17.574	15:22:08.1	31:12:09.0	18.97	20.14	18.43	19.56	199	2.31	0.1253 ± 0.0003	···	···	···	···
CB-17.543	15:22:09.4	31:27:46.4	18.83	19.76	18.15	19.09	187	2.00	0.0729 ± 0.0003	···	···	-3.2 ± 0.4	···
CB-17.480	15:22:10.9	31:16:50.9	16.76	18.75	16.20	18.08	581	4.29	0.0739 ± 0.0003	···	···	···	···
CB-17.482	15:22:11.2	31:26:45.0	19.69	20.58	19.37	20.38	114	1.88	0.0730 ± 0.0003	···	···	-4.1 ± 0.6	···
CB-17.443	15:22:11.9	31:17:28.4	19.41	20.41	18.83	20.02	116	1.90	0.0709 ± 0.0003	···	···	···	···
CB-16.489	15:22:12.1	30:32:57.7	18.23	19.00	17.35	18.19	191	1.84	star	···	···	···	···
CB-17.427	15:22:12.6	31:27:58.4	20.47	21.19	20.40	20.94	91	1.75	star	···	···	···	···
CB-17.393	15:22:12.8	31:07:44.0	17.38	19.00	16.97	18.53	404	3.18	0.0732 ± 0.0003	···	···	···	···
CB-17.407	15:22:13.5	31:33:24.0	18.97	20.14	18.87	20.33	207	2.27	0.1137 ± 0.0003	30.9 ± 5.6	···	···	···
CB-17.345	15:22:14.0	31:09:20.5	19.20	20.14	18.40	19.42	134	1.98	0.1117 ± 0.0003	···	···	-2.7 ± 0.6	···
CB-16.396	15:22:14.1	30:33:17.4	21.00	21.73	20.86	21.76	30	1.34	0.3516 ± 0.0003	33.8 ± 0.8	···	···	···
CB-16.370	15:22:14.4	30:24:59.5	19.03	20.32	18.56	19.85	196	2.42	0.1154 ± 0.0003	···	···	-4.4 ± 0.5	···
CB-16.352	15:22:15.0	30:32:38.4	18.93	19.52	18.17	18.84	178	1.72	star	···	···	···	···
CB-17.320	15:22:15.1	31:22:32.0	18.06	19.43	17.62	18.79	255	2.67	0.0787 ± 0.0003	···	···	-2.7 ± 0.4	···
CB-17.324	15:22:15.1	31:24:29.3	19.55	20.16	19.39	20.23	100	1.52	star	···	···	···	···
CB-17.307	15:22:15.3	31:17:53.5	16.81	18.06	15.17	16.06	381	2.50	star	···	···	···	···
CB-17.275	15:22:16.4	31:27:23.2	17.93	19.47	17.70	19.17	314	3.07	0.1273 ± 0.0003	···	···	···	···
CB-17.257	15:22:16.4	31:16:05.7	17.22	19.57	17.14	19.33	610	5.38	0.0799 ± 0.0003	···	···	···	···
CB-16.286	15:22:16.5	30:34:29.1	19.67	20.65	19.54	20.78	97	1.89	0.1168 ± 0.0003	25.7 ± 1.1	···	4.5 ± 0.5	···
2069-113	15:22:16.6	30:07:52.0	15.71	18.04	15.83	18.04	660	4.52	0.0754 ± 0.0002	···	···	···	···
CB-17.246	15:22:16.6	31:12:43.3	18.44	19.31	17.10	17.98	192	1.95	star	···	···	···	···
15222+3008	15:22:17.0	30:07:60.0	15.71	18.04	15.83	18.04	660	4.52	0.0759 ± 0.0002	···	···	···	···
CB-17.223	15:22:17.4	31:18:15.1	17.28	18.44	···	···	282	2.77	star	···	···	···	···
CB-17.234	15:22:17.4	31:23:41.7	17.56	19.17	16.91	18.27	443	3.57	0.0752 ± 0.0003	···	···	-2.8 ± 0.4	···
CB-16.217	15:22:17.6	30:24:50.8	19.42	20.33	18.43	19.54	168	1.94	0.2074 ± 0.0003	3.2 ± 0.5	-3.1 ± 0.5	···	···
CB-16.203	15:22:18.0	30:29:21.5	18.65	19.78	18.23	19.32	211	2.24	0.1689 ± 0.0003	···	-3.8 ± 0.5	···	···
CB-17.214	15:22:18.0	31:25:28.2	19.19	19.97	17.91	18.69	110	1.67	star	···	···	···	···
15223+3027	15:22:18.0	30:26:60.0	14.95	17.73	14.43	16.58	2015	10.25	0.0312 ± 0.0001	···	···	···	···
CB-16.148	15:22:18.8	30:21:48.9	19.38	20.47	19.18	20.54	131	2.15	0.2104 ± 0.0003	7.4 ± 0.7	-2.8 ± 0.4	···	1.5 ± 0.4
1522+2744	15:22:19.0	27:44:09.0	15.91	18.35	15.60	17.73	530	4.51	0.0681 ± 0.0002	···	···	···	···
CB-17.162	15:22:19.2	31:22:05.4	17.18	19.12	16.98	18.90	462	3.56	0.0744 ± 0.0003	···	···	···	···
CB-16.133	15:22:19.5	30:33:30.5	17.54	19.16	17.03	18.59	468	3.39	0.1116 ± 0.0003	4.4 ± 0.5	-3.3 ± 0.4	···	···
CB-17.127	15:22:19.8	31:13:28.5	20.48	21.26	19.59	20.72	85	1.62	0.2043 ± 0.0003	···	···	···	···
CB-17.129	15:22:20.0	31:19:33.1	15.91	17.48	14.26	15.39	397	2.92	star	···	···	···	···
CB-17.133	15:22:20.5	31:33:55.6	19.93	20.84	19.91	20.59	98	1.82	0.2352 ± 0.0003	···	-7.4 ± 1.1	···	···
2069-104	15:22:20.5	30:10:53.0	15.75	18.37	15.08	17.69	618	5.06	0.1178 ± 0.0002	···	···	···	···
CB-16.73	15:22:20.6	30:28:03.5	19.26	19.97	18.35	19.12	109	1.65	star	···	···	···	···

TABLE 2.5—*Continued*

Object	RA (1950)	Dec. (1950)	g_{tot}	g_{core}	r_{tot}	r_{core}	Area (□″)	irl (″)	z	W_λ([O II]) (Å)	W_λ(Hδ) (Å)	W_λ(Hβ) (Å)	W_λ([O III]5007) (Å)
CB-22.9510	15:22:21.2	30:37:37.9	20.13	20.93	19.46	20.72	98	1.65	0.4453 ± 0.0003	30.1 ± 0.7	...	...	...
2069-102	15:22:21.3	30:10:03.0	17.95	19.34	17.53	18.85	278	2.74	0.1173 ± 0.0003	...	...	...	...
2069-101	15:22:22.1	30:17:40.0	16.15	18.69	15.75	18.11	750	5.22	0.1174 ± 0.0010	...	...	...	...
CB-22.9440	15:22:22.3	30:26:44.4	18.17	20.43	18.16	20.61	448	4.08	0.0773 ± 0.0004	5.9 ± 1.4	...	...	1.8 ± 0.4
CB-17.26	15:22:22.3	31:05:34.3	18.19	18.92	16.67	17.68	193	1.80	star	...	...	...	...
CB-17.42	15:22:22.3	31:19:13.7	21.29	21.68	19.33	20.28	28	1.22	0.3566 ± 0.0003	...	...	...	...
CB-22.9442	15:22:22.7	30:38:05.3	18.47	20.06	18.68	20.25	267	2.92	0.1234 ± 0.0003	13.2 ± 0.7	...	...	4.1 ± 0.4
CB-23.9058	15:22:23.2	31:08:52.2	18.55	19.91	18.09	19.35	262	2.72	0.1129 ± 0.0004	...	...	...	...
CB-22.9384	15:22:23.5	30:24:23.2	18.16	19.55	17.35	18.76	95	1.97	0.1133 ± 0.0003	...	-2.0 ± 0.5	-2.1 ± 0.3	...
CB-23.9014	15:22:24.3	31:10:53.3	18.39	19.89	18.06	19.20	254	2.86	0.1720 ± 0.0003	...	...	...	...
CB-23.8993	15:22:25.0	31:22:11.1	19.18	20.32	18.49	19.83	95	2.03	0.1478 ± 0.0003	...	...	26.1 ± 0.5	...
CB-23.8963	15:22:25.5	31:11:46.1	19.55	20.07	17.74	18.55	107	1.59	star	...	...	...	...
CB-22.9299	15:22:25.5	30:26:11.9	19.78	20.91	19.34	20.23	119	2.12	0.2102 ± 0.0003	...	...	...	...
CB-23.8974	15:22:25.6	31:26:41.6	18.73	19.91	18.58	20.04	200	2.23	0.1704 ± 0.0003	23.0 ± 1.3	...	6.4 ± 0.7	...
1522+2753	15:22:26.0	27:53:43.0	16.35	18.23	15.86	17.59	910	4.46	0.0696 ± 0.0002	...	...	...	...
CB-23.8929	15:22:26.3	31:18:22.6	17.75	19.32	17.25	18.76	337	3.15	0.0782 ± 0.0003	...	...	3.1 ± 0.4	16.2 ± 0.6
CB-22.9259	15:22:26.5	30:29:04.9	19.21	20.23	18.36	19.50	115	1.99	0.1501 ± 0.0003	4.5 ± 0.5	...	...	...
CB-23.8930	15:22:26.7	31:24:53.8	20.42	21.12	19.29	20.24	104	1.72	0.2371 ± 0.0003	...	-3.4 ± 0.7	...	...
CB-22.9231	15:22:27.2	30:30:29.3	20.99	22.15	20.16	21.17	68	1.65	0.4578 ± 0.0003	...	...	...	...
1522+2810	15:22:27.2	28:10:37.0	16.96	19.54	17.33	19.80	226	3.27	0.0316 ± 0.0000	...	...	...	...
CB-23.8887	15:22:27.7	31:20:42.2	18.94	19.65	18.09	18.94	129	1.76	star	...	...	...	...
CB-22.9202	15:22:27.7	30:21:34.8	19.88	20.32	18.00	18.78	102	1.50	star	...	...	...	...
CB-23.8882	15:22:28.0	31:28:17.0	20.42	21.39	19.29	20.43	86	1.75	0.3059 ± 0.0003	...	...	...	...
CB-22.9178	15:22:28.6	30:31:22.1	17.34	19.64	17.64	19.81	659	5.51	0.0303 ± 0.0003	...	-4.8 ± 0.7	3.8 ± 0.2	9.4 ± 0.2
CB-23.8829	15:22:29.0	31:16:27.3	17.88	19.76	18.11	19.67	385	3.53	0.1125 ± 0.0003	...	...	...	...
1522+2748	15:22:29.0	27:48:34.0	15.93	18.17	16.05	18.08	823	4.22	0.0694 ± 0.0003	...	...	...	...
CB-23.8848	15:22:29.0	31:32:28.2	19.83	20.84	20.44	21.42	128	2.01	0.0904 ± 0.0003	...	...	...	19.8 ± 0.6
CB-22.9135	15:22:29.5	30:29:27.0	19.16	19.84	17.29	18.24	118	1.65	star	...	...	...	...
CB-22.9128	15:22:29.5	30:25:12.7	21.07	21.85	20.09	21.08	29	1.35	0.3906 ± 0.0003	...	-2.9 ± 0.6	...	...
CB-23.8802	15:22:29.8	31:11:56.4	16.01	17.54	14.03	15.31	644	2.97	star	...	...	...	...
CB-22.9049	15:22:31.2	30:27:54.7	18.78	19.76	17.77	18.80	184	2.31	0.2343 ± 0.0003	...	-4.5 ± 0.4	-4.4 ± 0.3	...
CB-23.8776	15:22:31.3	31:32:35.0	16.57	17.83	15.30	16.31	304	2.49	star	...	...	...	...
CB-22.9035	15:22:31.6	30:30:19.7	18.92	20.36	18.23	19.63	231	2.66	0.2102 ± 0.0003	...	-1.6 ± 0.3	...	...
2065F-154	15:22:31.9	28:22:15.0	16.75	18.42	16.55	18.18	434	3.17	0.0984 ± 0.0001	...	...	...	...
CB-22.8996	15:22:31.9	30:23:54.8	19.57	20.41	18.66	19.62	125	1.91	0.1513 ± 0.0003	...	...	...	...
CB-23.8724	15:22:32.2	31:13:52.9	16.31	17.74	14.13	15.54	488	2.96	star	...	...	...	...
CB-23.8729	15:22:32.2	31:25:16.9	20.23	20.99	19.11	20.07	96	1.65	0.3047 ± 0.0003	...	...	...	...
2065F-152	15:22:32.9	28:00:38.0	16.86	18.89	16.46	18.34	751	4.30	0.0673 ± 0.0001	...	...	...	...
CB-22.8946	15:22:33.1	30:25:23.3	19.33	20.33	18.91	20.11	181	2.09	0.1108 ± 0.0003	...	-2.6 ± 0.6	...	...
CB-23.8692	15:22:33.5	31:26:39.6	19.10	19.80	17.47	18.29	126	1.73	star	...	...	...	...
CB-22.8908	15:22:34.2	30:34:48.3	18.62	19.75	17.78	19.09	224	2.32	0.1168 ± 0.0003	2.6 ± 0.5	...	-1.9 ± 0.2	...
CB-22.8872	15:22:34.4	30:22:18.5	18.75	19.81	17.92	18.91	196	2.20	0.1501 ± 0.0003	7.8 ± 0.7	...	...	...
CB-23.8626	15:22:34.7	31:18:09.6	18.45	19.21	17.31	18.19	180	1.83	star	...	...	...	...
CB-22.8864	15:22:34.8	30:28:48.3	19.49	20.02	18.81	19.52	109	1.52	star	...	...	...	...
CB-22.8844	15:22:35.3	30:29:25.2	18.51	19.41	17.90	18.87	231	2.30	star	...	...	...	...

TABLE 2.5—*Continued*

Object	RA (1950)	Dec. (1950)	g_{tot}	g_{core}	r_{tot}	r_{core}	Area (□″)	irl (″)	z	W_λ([O II]) (Å)	W_λ(Hδ) (Å)	W_λ(Hβ) (Å)	W_λ([O III]5007) (Å)
CB-23.8611	15:22:35.4	31:25:41.0	19.61	21.23	19.70	21.10	177	3.18	0.2760 ± 0.0010	...	...	...	...
CB-23.8578	15:22:36.5	31:33:16.9	19.52	20.19	18.04	18.80	113	1.71	star	...	...	...	...
CB-22.8764	15:22:37.1	30:33:19.6	18.80	19.55	17.67	18.44	132	1.81	star	...	...	...	...
CB-23.8534	15:22:37.2	31:22:53.0	21.67	22.22	20.53	21.31	26	1.14	0.3140 ± 0.0010	...	...	...	...
CB-00.22	15:22:37.3	30:25:12.9	...	...	21.56	22.01	62	1.57	star	...	...	...	...
CB-23.8514	15:22:38.0	31:29:05.1	21.38	21.97	20.36	21.42	62	1.28	0.3085 ± 0.0003	...	...	...	...
CB-22.8681	15:22:38.4	30:25:59.4	20.12	21.53	19.57	21.06	110	2.34	0.1508 ± 0.0003	6.9 ± 1.5	...	...	...
CB-23.8477	15:22:38.8	31:32:13.0	18.10	18.88	17.11	18.05	204	1.86	star	...	...	...	...
CB-22.8650	15:22:39.2	30:31:09.2	18.87	19.85	18.11	19.10	103	1.81	0.1127 ± 0.0003	...	...	-1.7 ± 0.3	...
CB-22.8599	15:22:40.1	30:24:12.6	19.10	20.45	18.16	19.65	178	2.90	0.1502 ± 0.0003	...	...	...	...
CB-22.8601	15:22:40.4	30:34:05.9	19.47	21.09	19.18	20.61	192	2.66	0.2077 ± 0.0003	3.8 ± 0.9	-1.8 ± 0.4	...	...
CB-22.8544	15:22:41.1	30:23:11.2	18.83	20.01	18.10	19.23	215	2.27	0.1507 ± 0.0003	...	...	...	...
CB-23.8359	15:22:41.9	31:28:38.8	19.48	20.68	19.54	20.99	200	2.49	0.1133 ± 0.0003	...	...	11.8 ± 1.1	...
CB-22.8496	15:22:42.1	30:37:28.9	16.73	19.76	18.21	20.15	211	3.73	0.0498 ± 0.0003	14.4 ± 1.4	-5.1 ± 0.9	...	5.3 ± 0.4
2065F-142	15:22:42.3	28:05:07.0	17.13	18.65	16.50	18.05	447	3.12	0.0728 ± 0.0002	...	...	...	...
CB-23.8327	15:22:42.5	31:19:59.8	22.49	22.94	21.80	22.14	16	0.93	0.0290 ± 0.0010	...	...	...	...
CB-22.8459	15:22:42.7	30:28:17.5	19.33	20.42	18.37	19.49	184	2.15	0.1706 ± 0.0003	...	...	-1.8 ± 0.3	...
CB-23.8278	15:22:43.8	31:26:28.5	19.69	20.58	18.81	20.07	121	1.89	0.1271 ± 0.0003	...	...	...	...
CB-22.8414	15:22:44.1	30:39:00.8	17.56	19.07	16.95	18.31	507	3.34	0.0777 ± 0.0003	...	...	-2.1 ± 0.3	...
CB-23.8248	15:22:44.5	31:19:20.2	18.46	19.25	16.95	17.87	141	1.83	star	...	...	...	...
CB-22.8385	15:22:44.5	30:29:49.8	18.57	20.22	18.50	20.16	173	2.47	0.1274 ± 0.0003	7.6 ± 0.9	...	...	...
CB-22.8364	15:22:44.8	30:26:30.8	17.06	18.65	16.18	17.73	476	3.71	0.0632 ± 0.0003	...	...	-2.0 ± 0.3	...
CB-23.8253	15:22:44.9	31:33:55.7	18.72	19.46	17.48	18.26	196	1.92	star	...	...	...	...
CB-22.8340	15:22:45.2	30:20:20.5	18.98	19.78	18.18	18.93	177	2.17	star	...	...	...	...
CB-22.8326	15:22:46.1	30:36:33.7	20.06	21.24	20.76	21.47	114	2.17	0.2874 ± 0.0003	19.4 ± 0.9	...	5.2 ± 0.7	4.7 ± 0.9
CB-23.8194	15:22:46.3	31:32:37.6	17.82	18.82	15.76	16.90	223	2.11	star	...	...	...	...
CB-22.8279	15:22:46.8	30:24:59.3	19.44	20.34	18.59	19.73	129	1.98	0.1516 ± 0.0003	19.5 ± 0.7	...	1.4 ± 0.3	9.3 ± 0.3
CB-23.8141	15:22:47.1	31:15:23.3	17.73	19.17	16.97	18.17	447	3.15	0.0763 ± 0.0003	...	...	...	...
CB-22.8281	15:22:47.3	30:38:28.5	18.84	19.99	17.69	18.98	221	2.31	0.2082 ± 0.0003	...	...	...	...
CB-22.8236	15:22:47.7	30:21:21.9	18.41	19.14	17.52	18.33	184	1.75	star	...	...	...	...
CB-23.8109	15:22:48.6	31:30:49.4	20.78	21.24	20.41	21.12	78	1.44	0.3809 ± 0.0003	42.4 ± 0.7	...	...	...
CB-22.8210	15:22:48.9	30:33:29.8	19.53	20.50	19.05	20.13	130	2.02	0.1841 ± 0.0003	5.3 ± 0.4	-1.9 ± 0.4	...	2.7 ± 0.2
CB-22.8168	15:22:49.8	30:27:43.5	19.81	20.63	18.89	19.87	98	1.66	0.1721 ± 0.0003	...	...	-3.4 ± 0.4	...
CB-23.8057	15:22:50.1	31:28:37.0	19.09	20.60	19.00	20.29	213	2.56	0.1273 ± 0.0003	...	...	...	...
CB-22.8042	15:22:52.6	30:22:55.6	20.93	21.99	20.84	21.78	83	1.86	0.3445 ± 0.0003	...	...	...	...
CB-22.8047	15:22:52.9	30:30:27.2	22.29	22.80	20.70	21.57	16	1.08	0.5320 ± 0.0010	...	...	...	...
CB-22.8018	15:22:53.6	30:38:17.2	20.83	21.17	20.83	21.31	75	1.31	0.0800 ± 0.0010	...	...	...	...
CB-22.7969	15:22:54.2	30:28:52.6	18.53	19.57	18.17	19.30	226	2.20	0.0306 ± 0.0003	...	-3.0 ± 0.4	...	0.7 ± 0.1
CB-22.7965	15:22:54.3	30:29:30.9	19.80	20.75	19.91	21.08	120	2.07	0.1139 ± 0.0003	41.5 ± 1.2	...	6.6 ± 0.6	...
CB-22.7921	15:22:54.7	30:21:17.6	17.08	18.81	16.75	18.38	498	3.46	0.0816 ± 0.0003	...	-2.2 ± 0.4	...	...
CB-22.7876	15:22:56.4	30:34:38.4	17.61	18.52	16.49	17.55	132	1.91	star	...	...	...	...
CB-22.7803	15:22:57.5	30:25:11.6	19.58	20.61	19.53	20.76	180	2.41	0.1837 ± 0.0003	23.0 ± 0.9	...	...	4.8 ± 0.5
CB-22.7760	15:22:58.3	30:21:25.5	19.98	20.52	18.97	19.89	90	1.53	star	...	...	...	...
CB-22.7781	15:22:58.3	30:33:32.7	19.01	20.54	18.64	19.81	222	2.61	0.3602 ± 0.0003	8.4 ± 0.5	...	...	...
CB-22.7730	15:22:59.1	30:27:18.7	21.31	21.60	19.58	20.63	76	1.54	star	...	...	...	...

TABLE 2.5—*Continued*

Object	RA (1950)	Dec.	g_{tot}	g_{core}	r_{tot}	r_{core}	Area (□″)	irl (″)	z	W_λ([O II]) (Å)	W_λ(Hδ) (Å)	W_λ(Hβ) (Å)	W_λ([O III]5007) (Å)
CB-22.7736	15:22:59.5	30:38:23.7	19.81	21.03	20.52	21.75	120	2.24	0.1506 ± 0.0003	27.4 ± 1.0	···	···	···
CB-22.7667	15:23:00.6	30:23:29.8	21.52	22.34	20.17	21.19	31	1.45	star	···	···	···	···
CB-22.7635	15:23:01.7	30:27:11.2	20.84	21.71	19.80	20.74	82	1.78	0.4533 ± 0.0003	3.3 ± 0.5	-3.4 ± 0.5	···	···
CB-22.7639	15:23:01.7	30:30:05.2	19.23	20.64	18.63	19.99	200	2.60	0.1718 ± 0.0003	···	···	-2.4 ± 0.4	···
CB-22.7589	15:23:02.5	30:23:08.0	22.22	22.60	21.62	22.07	23	1.07	star	···	···	···	···
CB-22.7574	15:23:03.5	30:36:38.1	19.25	19.98	18.15	19.00	115	1.73	star	···	···	···	···
CB-22.7542	15:23:03.6	30:20:56.3	19.73	20.47	19.31	20.42	107	1.72	0.1058 ± 0.0003	34.2 ± 0.7	···	14.5 ± 0.2	7.1 ± 0.2
CB-22.7547	15:23:03.9	30:30:50.7	18.52	20.07	17.84	19.35	278	2.94	0.1719 ± 0.0003	···	···	-2.8 ± 0.4	···
CB-22.7485	15:23:05.0	30:23:17.5	18.45	19.75	17.79	19.13	263	2.72	0.1139 ± 0.0003	···	···	-1.5 ± 0.2	···
CB-22.7447	15:23:06.6	30:37:15.1	20.43	21.54	19.83	21.07	100	2.04	0.3118 ± 0.0003	8.8 ± 1.0	···	3.5 ± 0.8	···
CB-22.7426	15:23:06.7	30:24:47.1	18.71	19.46	17.82	18.66	77	1.51	star	···	···	···	···
CB-20.8940	15:23:06.8	28:41:21.9	18.91	19.71	18.10	18.86	89	1.62	star	···	···	···	···
CB-20.8890	15:23:07.5	28:40:37.6	17.99	19.21	17.40	18.52	278	2.54	0.1598 ± 0.0003	7.7 ± 0.4	-3.3 ± 0.4	3.0 ± 0.2	0.9 ± 0.2
CB-19.8686	15:23:07.5	28:32:03.5	16.22	18.30	15.86	17.72	1039	5.19	0.0636 ± 0.0003	···	···	-1.9 ± 0.3	···
CB-22.7382	15:23:08.1	30:30:08.1	19.94	21.23	19.64	21.14	110	2.12	0.1581 ± 0.0006	···	···	···	···
CB-20.8838	15:23:08.4	28:36:28.0	18.90	19.72	17.92	18.61	187	1.98	star	···	···	···	···
CB-20.8812	15:23:08.9	28:35:47.5	18.62	19.86	18.05	19.35	232	2.48	0.1492 ± 0.0003	···	···	···	···
CB-22.7323	15:23:10.0	30:37:08.7	18.14	19.82	17.58	19.16	289	3.06	0.2095 ± 0.0003	···	-3.1 ± 0.5	···	···
CB-22.7306	15:23:10.1	30:27:13.2	19.70	20.54	19.35	20.40	114	1.86	0.2591 ± 0.0003	17.9 ± 0.6	···	3.6 ± 0.3	11.1 ± 0.4
CB-99.9	15:23:10.6	30:21:16.7	···	···	20.57	21.73	77	1.73	0.3465 ± 0.0003	···	···	···	···
CB-20.8716	15:23:10.8	28:34:13.7	20.44	21.31	19.52	20.51	96	1.85	0.2631 ± 0.0003	···	···	···	···
CB-22.7272	15:23:11.2	30:35:52.0	19.60	20.54	18.78	20.44	108	1.89	0.2592 ± 0.0003	18.7 ± 0.5	-3.3 ± 0.6	6.9 ± 0.3	3.7 ± 0.3
CB-19.8416	15:23:13.3	28:30:37.5	18.57	19.42	17.46	18.33	206	2.07	star	···	···	···	···
CB-22.7182	15:23:13.8	30:38:32.3	20.14	21.25	20.14	21.20	92	1.88	0.3029 ± 0.0003	19.4 ± 0.8	···	8.8 ± 0.4	···
CB-22.7149	15:23:13.9	30:24:23.1	18.49	19.92	18.36	19.74	231	2.61	0.1605 ± 0.0003	13.5 ± 0.5	···	4.0 ± 0.2	1.3 ± 0.2
CB-20.8566	15:23:14.2	28:37:26.6	18.56	19.87	17.59	19.22	241	2.55	0.1497 ± 0.0003	···	···	···	···
CB-22.7119	15:23:14.7	30:30:48.7	17.58	18.98	17.12	18.41	336	2.93	0.0776 ± 0.0003	···	···	···	···
CB-22.7099	15:23:14.9	30:28:45.8	19.91	20.62	18.39	19.24	103	1.65	star	···	···	···	···
CB-20.8499	15:23:15.6	28:34:16.6	19.57	20.51	19.47	20.56	118	1.93	0.1464 ± 0.0003	16.7 ± 0.8	···	···	2.8 ± 0.4
CB-22.7050	15:23:15.6	30:23:02.4	20.39	21.38	20.52	21.40	95	1.88	0.3368 ± 0.0003	32.9 ± 0.6	···	···	···
CB-20.8453	15:23:16.6	28:35:31.8	19.52	20.45	18.68	19.77	91	1.82	0.1580 ± 0.0003	···	···	-2.4 ± 0.5	···
CB-99.10	15:23:17.2	30:36:19.0	···	···	19.79	21.98	157	3.48	0.5771 ± 0.0003	···	···	···	···
CB-22.6980	15:23:17.9	30:26:17.7	21.24	21.77	20.73	21.65	60	1.28	0.1651 ± 0.0003	···	···	3.5 ± 0.5	13.8 ± 0.6
CB-20.8369	15:23:18.7	28:37:01.8	19.47	20.50	18.77	19.96	129	2.06	0.1514 ± 0.0003	···	···	-2.4 ± 0.5	···
CB-22.6963	15:23:18.8	30:30:24.7	18.48	19.78	18.14	19.35	247	2.62	0.1137 ± 0.0003	10.4 ± 0.7	-2.5 ± 0.4	-0.9 ± 0.2	···
CB-22.6969	15:23:19.0	30:38:01.4	17.64	19.15	17.15	18.55	417	3.02	0.0659 ± 0.0003	···	···	-4.5 ± 0.4	···
CB-19.8138	15:23:19.1	28:31:31.9	20.57	21.57	20.15	21.41	82	1.69	0.1583 ± 0.0004	···	···	···	···
CB-20.8319	15:23:20.0	28:41:44.1	18.43	20.04	18.03	19.35	265	3.44	0.1488 ± 0.0003	···	···	···	···
CB-19.8100	15:23:20.1	28:31:04.3	20.77	21.57	20.09	20.65	69	1.45	0.2633 ± 0.0003	···	-2.8 ± 0.6	···	···
CB-22.6919	15:23:20.6	30:33:17.8	19.23	20.25	19.00	20.26	179	2.20	0.2097 ± 0.0003	17.6 ± 0.6	···	···	4.6 ± 0.4
CB-19.8054	15:23:20.9	28:28:03.2	18.84	20.06	17.89	19.25	238	2.56	0.1591 ± 0.0003	···	···	-2.0 ± 0.3	···
CB-22.6868	15:23:22.1	30:35:14.7	21.81	22.49	21.07	21.72	28	1.24	star	···	···	···	···
CB-19.7990	15:23:22.1	28:31:13.6	19.12	20.29	18.60	20.15	202	2.43	0.1590 ± 0.0003	20.2 ± 0.9	···	3.1 ± 0.3	3.2 ± 0.4
CB-22.6852	15:23:22.2	30:28:13.3	20.67	21.29	19.44	20.27	77	1.50	star	···	···	···	···
CB-22.6841	15:23:22.3	30:23:21.7	18.46	19.96	17.73	19.24	264	2.83	0.1671 ± 0.0003	···	···	···	···

TABLE 2.5—*Continued*

Object	RA (1950)	Dec. (1950)	g_{tot}	g_{core}	r_{tot}	r_{core}	Area (□″)	irl (″)	z	W_λ([O II]) (Å)	W_λ(Hδ) (Å)	W_λ(Hβ) (Å)	W_λ([O III]5007) (Å)
CB-22.6831	15:23:22.8	30:30:18.2	20.68	21.55	19.76	20.85	80	1.63	0.3015 ± 0.0003	4.0 ± 0.9	···	···	···
CB-20.8156	15:23:23.2	28:36:34.2	18.07	19.48	17.13	18.43	253	2.71	0.1527 ± 0.0003	···	···	-2.6 ± 0.3	···
CB-22.6803	15:23:23.2	30:20:50.6	20.05	21.22	19.15	20.25	108	2.29	0.2261 ± 0.0003	···	···	-2.5 ± 0.6	···
CB-21.6515	15:23:23.5	29:56:06.3	21.63	22.05	20.23	21.33	29	1.25	0.3031 ± 0.0003	7.3 ± 1.5	···	···	···
CB-22.6796	15:23:24.2	30:34:52.7	19.06	19.94	19.17	20.10	84	1.73	0.1131 ± 0.0003	50.0 ± 0.5	···	17.3 ± 0.2	···
CB-22.6767	15:23:24.5	30:26:36.8	18.11	18.97	16.75	17.76	95	1.67	star	···	···	···	···
CB-20.8101	15:23:24.9	28:39:44.7	21.23	21.94	20.79	21.69	72	1.79	0.1480 ± 0.0010	···	···	···	···
CB-22.6728	15:23:25.5	30:27:37.8	19.53	20.16	19.36	20.18	106	1.60	star	···	···	···	···
CB-20.8052	15:23:26.2	28:37:43.8	19.17	20.48	18.75	20.03	213	2.43	0.1490 ± 0.0003	···	···	···	···
CB-22.6671	15:23:27.0	30:28:53.4	20.42	21.37	19.22	20.57	92	1.82	0.3009 ± 0.0003	···	···	···	···
CB-19.7765	15:23:27.1	28:28:18.7	18.17	19.84	17.45	18.99	352	3.44	0.1615 ± 0.0003	···	···	···	···
CB-22.6654	15:23:27.4	30:30:06.8	20.27	21.12	19.49	20.84	94	1.87	0.1597 ± 0.0003	···	···	···	···
CB-20.7965	15:23:28.0	28:39:06.7	19.17	20.38	18.38	19.51	152	2.52	0.1498 ± 0.0003	···	···	···	···
CB-22.6617	15:23:28.1	30:24:47.8	20.13	20.76	20.21	20.75	89	1.48	star	···	···	···	···
CB-20.7937	15:23:28.3	28:34:09.8	18.71	19.51	17.90	18.64	197	1.94	star	···	···	···	···
CB-21.6335	15:23:28.3	29:58:49.7	18.52	19.62	18.09	19.36	216	2.25	0.1204 ± 0.0003	18.3 ± 3.6	-3.8 ± 0.8	6.1 ± 0.4	2.9 ± 0.5
CB-20.7916	15:23:29.3	28:40:40.6	18.94	20.23	18.64	20.03	158	2.51	0.0667 ± 0.0003	15.0 ± 2.6	···	6.3 ± 0.8	5.8 ± 0.8
CB-22.6584	15:23:29.4	30:30:27.0	18.68	20.68	18.78	20.15	297	3.63	0.1603 ± 0.0003	11.6 ± 1.6	···	···	···
CB-21.6275	15:23:30.0	29:54:10.7	19.05	20.14	18.46	19.63	172	2.07	0.1095 ± 0.0003	···	···	-2.4 ± 0.4	···
CB-19.7638	15:23:30.0	28:32:54.1	20.16	20.84	20.39	21.08	28	1.09	0.1236 ± 0.0003	···	···	-4.3 ± 0.9	···
CB-22.6527	15:23:30.8	30:31:21.5	19.49	20.69	19.50	20.87	105	2.05	0.1141 ± 0.0003	10.8 ± 1.4	···	···	···
CB-20.7823	15:23:30.9	28:37:09.8	19.20	20.22	18.71	19.55	118	1.95	0.1502 ± 0.0003	···	···	···	···
CB-20.7817	15:23:31.0	28:35:10.2	20.25	21.22	19.75	20.70	94	1.82	0.1525 ± 0.0003	···	···	···	···
CB-21.6199	15:23:31.5	29:48:15.7	20.02	20.57	19.01	19.87	34	1.27	0.1160 ± 0.0003	···	···	···	···
CB-20.7796	15:23:31.8	28:39:23.1	18.43	19.73	17.99	19.30	252	2.57	0.0658 ± 0.0003	···	···	-3.2 ± 0.3	···
CB-22.6479	15:23:31.8	30:24:28.6	18.55	20.12	17.43	19.22	248	2.83	0.2092 ± 0.0003	7.9 ± 0.8	···	···	···
CB-22.6492	15:23:31.8	30:30:26.7	21.67	22.12	20.05	20.92	34	1.30	0.3078 ± 0.0003	···	···	-6.4 ± 1.0	···
CB-19.7515	15:23:32.3	28:31:24.3	20.82	21.41	21.19	21.93	70	1.44	0.2286 ± 0.0003	62.6 ± 1.9	···	34.8 ± 1.6	79.3 ± 2.1
CB-21.6181	15:23:32.3	29:56:38.2	16.83	18.43	16.05	17.69	484	3.40	0.0550 ± 0.0003	···	···	-2.3 ± 0.3	···
CB-22.6450	15:23:32.4	30:26:30.9	20.50	21.25	18.91	20.07	96	1.74	0.3028 ± 0.0003	···	···	···	···
CB-20.7763	15:23:32.5	28:37:08.8	19.74	20.57	18.81	19.99	28	1.18	0.1499 ± 0.0003	···	···	···	···
CB-22.6451	15:23:32.8	30:31:15.4	18.63	19.86	17.90	19.06	231	2.36	0.1606 ± 0.0003	···	···	-3.3 ± 0.6	···
CB-21.6147	15:23:33.4	29:58:30.8	19.59	20.46	19.16	20.39	126	1.94	0.0647 ± 0.0003	9.3 ± 1.6	···	···	1.9 ± 0.3
CB-22.6387	15:23:34.2	30:30:31.2	19.43	20.79	18.04	19.68	216	2.59	0.3030 ± 0.0003	···	···	-2.1 ± 0.3	···
CB-19.7425	15:23:34.3	28:33:13.7	19.50	20.59	19.16	20.36	127	2.11	0.1973 ± 0.0003	17.1 ± 1.4	···	1.9 ± 0.4	···
CB-21.6090	15:23:34.5	29:46:16.9	16.84	18.17	15.29	16.14	216	2.36	star	···	···	···	···
CB-20.7646	15:23:34.9	28:38:20.3	19.08	20.18	18.34	19.41	178	2.12	0.1499 ± 0.0003	···	···	···	···
CB-21.6087	15:23:35.3	30:00:45.4	19.65	20.66	19.99	20.90	118	2.05	0.0567 ± 0.0003	···	···	3.9 ± 0.7	8.9 ± 0.7
CB-19.7380	15:23:35.4	28:32:46.1	18.86	20.13	18.36	19.47	212	2.49	0.1491 ± 0.0003	···	···	···	···
CB-21.6042	15:23:35.8	29:48:44.9	19.10	20.02	18.30	19.29	198	2.16	0.1110 ± 0.0003	···	···	-1.6 ± 0.3	···
CB-21.6021	15:23:36.4	29:51:25.4	19.49	20.49	19.09	20.05	114	1.96	0.1167 ± 0.0003	···	···	···	···
CB-21.6029	15:23:36.4	29:53:51.5	18.93	19.96	19.18	20.15	205	2.15	0.1097 ± 0.0003	17.4 ± 1.3	-3.7 ± 0.7	4.3 ± 0.2	5.0 ± 0.3
CB-20.7580	15:23:36.7	28:42:11.6	19.56	20.33	18.13	19.26	23	1.03	star	···	···	···	···
CB-20.7537	15:23:37.3	28:34:49.5	19.72	21.18	19.75	21.18	145	2.63	0.1582 ± 0.0003	···	···	4.6 ± 0.9	···
CB-20.7555	15:23:37.5	28:44:29.2	21.53	22.23	21.25	22.12	33	1.33	0.4493 ± 0.0003	19.1 ± 1.6	···	···	···

TABLE 2.5—*Continued*

Object	RA (1950)	Dec. (1950)	g_{tot}	g_{core}	r_{tot}	r_{core}	Area (□″)	irl (″)	z	W_λ([O II]) (Å)	W_λ(Hδ) (Å)	W_λ(Hβ) (Å)	W_λ([O III]5007) (Å)
CB-21.5985	15:23:37.5	29:58:44.1	18.14	19.80	17.56	19.05	366	3.72	0.1176 ± 0.0003	...	...	-3.0 ± 0.5	...
CB-20.7499	15:23:38.4	28:36:22.8	19.57	20.52	18.76	19.96	77	1.70	0.1463 ± 0.0004	...	...	...	...
CB-21.5934	15:23:38.4	29:54:51.6	19.12	20.19	18.83	19.50	145	2.80	star	...	...	...	...
CB-19.7239	15:23:38.5	28:26:41.3	18.00	19.36	16.66	17.85	262	3.04	star	...	...	...	...
CB-20.7456	15:23:39.3	28:34:36.8	20.62	21.16	20.33	21.22	87	1.65	0.1536 ± 0.0003	26.8 ± 1.1	...	9.4 ± 0.6	4.3 ± 0.6
CB-20.7458	15:23:39.5	28:39:08.5	19.50	20.42	18.59	19.70	82	1.68	0.1592 ± 0.0003	...	...	...	...
CB-21.5849	15:23:40.3	29:47:29.6	16.87	19.09	17.07	19.20	695	4.44	0.0753 ± 0.0003	15.2 ± 1.4	-5.3 ± 1.0	2.3 ± 0.3	3.3 ± 0.3
CB-24.5717	15:23:40.6	32:16:32.0	16.93	19.41	16.82	18.99	805	5.00	0.0789 ± 0.0003	...	...	...	...
CB-20.7388	15:23:40.7	28:35:42.7	18.50	19.92	17.94	19.40	240	2.69	0.1522 ± 0.0003	...	...	...	...
CB-21.5825	15:23:40.9	29:52:19.3	17.14	19.33	16.69	18.69	629	4.36	0.1122 ± 0.0003	...	...	-1.3 ± 0.2	...
CB-20.7368	15:23:41.1	28:37:12.7	20.58	21.26	19.97	20.71	79	1.63	0.2324 ± 0.0003	...	...	...	...
CB-21.5793	15:23:41.2	29:45:36.0	16.22	18.28	15.59	17.55	906	4.86	0.0564 ± 0.0003	...	...	-1.5 ± 0.3	...
CB-20.7332	15:23:41.9	28:38:04.0	18.16	19.66	17.48	18.85	116	2.34	0.1487 ± 0.0003	...	...	...	...
CB-21.5767	15:23:42.0	29:48:07.2	19.29	20.51	18.60	19.79	184	2.37	0.1094 ± 0.0003	...	...	-2.2 ± 0.4	...
CB-20.7275	15:23:42.7	28:33:36.7	18.02	19.37	17.64	18.92	244	2.57	0.0735 ± 0.0003	7.9 ± 1.0	-2.8 ± 0.6	0.8 ± 0.2	1.0 ± 0.2
CB-20.7269	15:23:42.8	28:36:11.7	19.70	20.42	18.75	19.74	111	1.76	0.1467 ± 0.0003	...	...	...	...
CB-21.5695	15:23:43.6	29:55:24.4	17.46	19.60	17.26	19.33	453	3.73	0.1165 ± 0.0003	5.2 ± 1.2	...	...	...
CB-21.5668	15:23:43.7	29:44:41.4	18.29	19.96	17.92	19.62	295	3.06	0.1165 ± 0.0003	...	...	...	...
CB-20.7201	15:23:43.9	28:34:35.7	18.25	19.06	17.14	18.07	116	1.76	star	...	...	...	...
CB-20.7216	15:23:44.1	28:44:02.2	18.16	19.89	18.38	20.00	368	3.31	0.0656 ± 0.0003	15.2 ± 3.4	...	1.4 ± 0.3	3.1 ± 0.4
CB-21.5654	15:23:44.8	30:01:03.9	21.70	22.18	20.92	21.70	26	1.17	0.2859 ± 0.0003	16.9 ± 2.4	...	6.5 ± 0.5	...
CB-24.5574	15:23:44.8	32:17:57.3	20.00	21.22	18.68	20.14	108	2.13	0.2350 ± 0.0003	...	...	...	...
CB-21.5623	15:23:44.8	29:50:49.2	19.13	19.90	17.49	18.29	118	1.73	star	...	...	...	...
CB-19.6953	15:23:45.0	28:33:12.2	16.77	19.13	16.32	18.25	932	6.02	0.0741 ± 0.0003	...	-2.4 ± 0.5	...	...
CB-21.5579	15:23:45.6	29:44:47.7	17.17	18.96	16.44	18.18	546	3.76	0.1167 ± 0.0003	...	...	-3.9 ± 0.4	...
CB-21.5603	15:23:45.7	29:59:36.9	19.85	20.27	18.05	18.85	105	1.51	star	...	...	...	...
CB-20.7140	15:23:45.8	28:44:16.4	18.92	20.10	18.64	19.73	249	2.61	0.2323 ± 0.0003	5.1 ± 0.6	-2.5 ± 0.6	2.1 ± 0.3	...
CB-24.5508	15:23:46.5	32:15:02.2	16.20	18.17	15.63	17.49	801	4.35	0.0791 ± 0.0003	...	...	-2.4 ± 0.3	...
CB-19.6878	15:23:46.7	28:32:51.4	19.36	20.18	17.62	18.60	31	1.27	star	...	...	...	...
CB-20.7092	15:23:46.7	28:37:51.6	19.25	20.30	18.76	19.80	90	1.87	0.1548 ± 0.0003	...	...	...	...
CB-24.5477	15:23:46.9	32:09:20.2	21.87	22.39	21.05	21.79	23	1.07	star	...	...	...	...
CB-21.5548	15:23:47.4	30:00:35.3	17.99	19.92	18.11	19.84	313	3.28	0.1157 ± 0.0003	...	...	2.3 ± 0.4	...
CB-24.5462	15:23:47.5	32:15:46.0	20.03	21.05	19.58	20.66	123	2.10	0.1300 ± 0.0003	...	...	...	...
CB-24.5441	15:23:47.8	32:09:50.7	20.24	21.35	21.01	21.67	89	1.77	star	...	...	...	...
CB-20.7039	15:23:47.9	28:37:09.5	18.11	19.76	17.34	18.90	381	3.22	0.1503 ± 0.0003	...	...	...	...
CB-20.7012	15:23:48.3	28:35:08.7	17.41	19.14	17.22	18.67	453	3.56	0.0642 ± 0.0003	12.0 ± 0.5	-1.8 ± 0.2	6.2 ± 0.1	1.3 ± 0.2
CB-21.5472	15:23:49.1	30:01:21.4	17.22	18.91	16.54	18.11	440	3.27	0.1156 ± 0.0003	...	...	-2.9 ± 0.3	...
CB-20.6976	15:23:49.2	28:38:15.3	16.41	18.45	15.69	17.51	541	4.91	0.0671 ± 0.0003	...	...	-2.8 ± 0.3	...
CB-21.5440	15:23:49.2	29:51:56.7	17.14	19.71	17.33	19.75	701	4.76	0.0572 ± 0.0003	...	...	3.2 ± 0.3	...
CB-21.5413	15:23:50.2	29:59:18.5	18.85	20.05	18.14	19.34	231	2.45	0.1137 ± 0.0003	4.3 ± 1.1	...	...	...
CB-21.5387	15:23:50.6	29:51:12.2	17.83	19.77	17.63	19.36	427	3.57	0.1183 ± 0.0003	...	...	...	...
CB-19.6675	15:23:50.8	28:27:21.4	19.33	20.35	19.58	20.63	121	1.94	0.1749 ± 0.0003	48.3 ± 1.2	...	10.5 ± 0.5	...
CB-21.5385	15:23:51.0	29:58:41.5	18.27	19.54	17.51	18.91	274	2.66	0.1127 ± 0.0003	...	...	-1.8 ± 0.3	...
CB-20.6872	15:23:51.3	28:42:05.6	19.19	20.33	18.38	19.79	169	2.10	0.1507 ± 0.0003	...	...	...	...
CB-21.5324	15:23:51.7	29:44:33.8	18.49	19.91	17.86	19.21	126	2.20	0.0845 ± 0.0003	...	...	...	...

TABLE 2.5—*Continued*

Object	RA (1950)	Dec. (1950)	g_{tot}	g_{core}	r_{tot}	r_{core}	Area (□″)	irl (″)	z	W_λ([O II]) (Å)	W_λ(Hδ) (Å)	W_λ(Hβ) (Å)	W_λ([O III]5007) (Å)
CB-24.5301	15:23:52.0	32:16:45.2	20.26	21.57	20.48	21.27	88	1.90	0.4118 ± 0.0003	9.2 ± 0.7	···	···	···
CB-21.5279	15:23:52.8	29:49:19.8	20.83	21.50	20.42	21.32	82	1.69	0.3573 ± 0.0003	10.3 ± 1.3	···	···	···
CB-20.6768	15:23:52.9	28:33:22.3	18.75	19.50	17.94	18.70	128	1.80	star	···	···	···	···
CB-20.6763	15:23:53.3	28:39:33.9	18.86	19.98	19.21	20.39	195	2.20	0.0993 ± 0.0003	47.4 ± 1.2	···	12.1 ± 0.4	24.0 ± 0.4
CB-24.5255	15:23:53.5	32:19:13.3	20.05	21.49	19.86	21.00	123	2.39	0.3320 ± 0.0010	9.0 ± 0.8	···	···	···
CB-21.5268	15:23:53.7	30:02:02.4	18.43	19.76	17.83	18.94	295	3.11	0.1112 ± 0.0003	···	···	-2.5 ± 0.3	···
CB-20.6734	15:23:53.7	28:34:18.4	21.25	21.92	22.84	21.74	34	1.43	star	···	···	···	···
CB-21.5222	15:23:53.8	29:44:43.4	20.83	21.72	20.46	21.70	77	1.66	0.3575 ± 0.0003	14.7 ± 2.2	···	···	···
CB-24.5229	15:23:53.8	32:14:13.9	18.56	19.60	18.56	19.67	163	2.09	0.1117 ± 0.0003	29.9 ± 0.7	···	7.4 ± 0.2	···
CB-21.5198	15:23:54.5	29:49:57.5	18.06	19.56	17.74	19.06	297	3.09	0.0554 ± 0.0003	···	···	-1.9 ± 0.3	···
CB-24.5215	15:23:54.5	32:17:49.9	18.20	19.48	17.44	18.61	99	1.95	0.1142 ± 0.0003	···	···	-1.8 ± 0.3	···
CB-20.6713	15:23:54.8	28:43:26.4	20.32	21.33	19.50	20.91	100	1.98	0.3368 ± 0.0003	4.1 ± 0.8	···	···	···
CB-24.5183	15:23:55.0	32:10:20.4	19.33	20.53	18.79	19.95	175	2.21	0.0781 ± 0.0003	···	···	-2.4 ± 0.5	···
CB-19.6443	15:23:55.1	28:03:31.9	20.12	21.16	20.79	21.61	103	2.00	0.0322 ± 0.0003	···	···	···	43.5 ± 3.3
CB-21.5179	15:23:55.2	29:55:49.6	19.43	20.41	19.00	20.00	121	1.94	0.1282 ± 0.0003	77.7 ± 1.5	···	17.4 ± 0.4	74.5 ± 0.4
CB-21.5155	15:23:55.5	29:49:12.9	19.08	20.04	18.78	20.01	180	2.04	0.1159 ± 0.0003	28.6 ± 0.8	-4.9 ± 0.5	4.3 ± 0.2	···
1523+2813	15:23:55.6	28:13:24.0	16.90	19.24	17.18	19.40	733	4.81	0.0694 ± 0.0003	···	···	···	···
CB-24.5174	15:23:55.8	32:20:58.7	18.65	19.45	17.44	18.28	211	1.98	star	···	···	···	···
CB-20.6663	15:23:56.2	28:40:06.6	18.42	19.33	17.43	18.40	198	2.01	0.0654 ± 0.0003	···	···	-2.5 ± 0.3	···
CB-19.6397	15:23:56.3	28:05:52.2	15.83	17.53	14.01	15.59	775	3.44	star	···	···	···	···
CB-19.6448	15:23:56.5	28:32:37.4	20.69	22.05	21.22	21.98	93	2.17	0.2642 ± 0.0003	12.9 ± 2.4	···	···	5.4 ± 0.9
CB-24.5119	15:23:56.7	32:08:28.8	21.16	21.93	20.93	22.02	82	1.73	0.4311 ± 0.0003	17.9 ± 1.7	···	···	···
CB-24.5127	15:23:56.9	32:16:16.2	17.63	19.44	17.02	18.66	289	3.06	0.1130 ± 0.0003	16.0 ± 1.2	···	···	···
CB-21.5112	15:23:57.1	29:57:49.7	18.30	19.71	17.66	19.01	269	2.75	0.1139 ± 0.0003	···	···	-1.8 ± 0.3	···
CB-21.5093	15:23:57.2	29:49:52.5	20.94	21.40	19.32	20.26	72	1.39	star	···	···	···	···
CB-20.6626	15:23:57.3	28:39:12.5	19.13	20.17	18.20	19.36	215	2.29	0.1468 ± 0.0003	···	···	···	···
CB-24.5091	15:23:58.1	32:19:03.5	21.69	22.61	21.74	22.09	39	1.49	0.5151 ± 0.0003	26.7 ± 2.0	···	···	···
CB-19.6363	15:23:58.2	28:28:32.5	20.84	21.60	19.82	20.61	91	1.75	0.3157 ± 0.0003	···	···	···	···
CB-21.5048	15:23:58.2	29:53:40.7	16.79	17.94	15.00	15.75	182	2.18	star	···	···	···	···
CB-21.5065	15:23:58.3	30:01:39.5	19.16	19.84	18.15	18.82	168	1.81	star	···	···	···	···
CB-20.6579	15:23:58.7	28:38:24.8	21.45	22.39	21.71	22.08	34	1.37	0.4489 ± 0.0003	36.7 ± 2.1	···	···	···
CB-24.5066	15:23:58.8	32:16:54.5	17.42	19.21	17.05	18.69	302	3.28	0.0786 ± 0.0003	8.7 ± 1.1	-2.1 ± 0.5	···	0.8 ± 0.2
1523+2854	15:23:59.5	28:54:19.0	16.80	18.58	16.21	17.93	551	3.96	0.0674 ± 0.0002	···	···	···	···
CB-24.5038	15:23:59.5	32:11:19.1	19.70	20.43	19.42	20.29	113	1.80	0.1486 ± 0.0003	29.7 ± 0.9	···	···	5.0 ± 0.3
CB-19.6297	15:23:59.7	28:30:11.5	20.72	22.14	20.21	21.86	109	2.21	0.2958 ± 0.0003	54.3 ± 3.6	···	···	···
CB-20.6535	15:23:59.9	28:41:49.4	17.75	19.17	17.03	18.37	303	2.87	0.0982 ± 0.0003	···	-1.3 ± 0.3	-2.9 ± 0.2	···
CB-21.4970	15:24:00.0	29:50:12.4	19.21	20.60	19.18	20.44	228	2.73	0.1149 ± 0.0003	21.4 ± 3.0	-4.7 ± 1.1	···	···
CB-19.6265	15:24:00.6	28:28:34.2	19.99	21.34	18.90	20.32	142	2.47	0.3160 ± 0.0003	···	···	···	···
CB-19.6215	15:24:00.6	28:01:52.9	21.98	22.36	20.55	21.52	30	1.22	0.3805 ± 0.0003	4.6 ± 0.9	···	···	···
CB-24.5000	15:24:01.0	32:16:58.7	20.23	21.01	19.53	20.45	76	1.67	0.2349 ± 0.0003	9.8 ± 0.7	···	···	1.1 ± 0.2
CB-20.6464	15:24:01.4	28:38:04.1	19.85	20.81	19.26	20.47	100	1.90	0.1496 ± 0.0003	···	···	···	···
CB-19.6227	15:24:01.5	28:30:47.7	19.30	20.68	19.06	20.54	197	2.55	0.1561 ± 0.0003	···	···	···	···
CB-24.4953	15:24:01.9	32:11:10.8	18.71	19.69	18.55	19.75	197	2.03	0.0793 ± 0.0003	46.7 ± 1.3	···	15.0 ± 0.2	16.1 ± 0.2
CB-20.6440	15:24:01.9	28:42:10.8	18.60	20.09	18.66	19.95	236	2.69	0.1992 ± 0.0003	11.2 ± 1.0	···	3.4 ± 0.4	1.9 ± 0.4
CB-19.6163	15:24:01.9	28:04:24.8	17.91	19.52	17.25	18.86	319	3.35	0.0742 ± 0.0003	7.1 ± 1.4	···	···	···

TABLE 2.5—*Continued*

Object	RA (1950)	Dec.	g_{tot}	g_{core}	r_{tot}	r_{core}	Area (□″)	irl (″)	z	W_λ([O II]) (Å)	W_λ(Hδ) (Å)	W_λ(Hβ) (Å)	W_λ([O III]5007) (Å)
CB-24.4969	15:24:02.0	32:18:21.4	19.67	20.80	19.81	20.60	121	2.04	0.1543 ± 0.0003	9.0 ± 0.8	-2.9 ± 0.7	3.1 ± 0.3	1.1 ± 0.3
CB-21.4906	15:24:02.1	29:55:30.4	17.45	19.04	16.73	18.18	141	2.36	0.1046 ± 0.0003	3.1 ± 0.7	...	-2.1 ± 0.2	...
CB-19.6194	15:24:02.4	28:28:54.0	18.82	19.94	18.42	19.62	211	2.24	0.1558 ± 0.0003	7.1 ± 0.7	...	1.5 ± 0.2	...
CB-24.4900	15:24:02.8	32:06:30.8	19.39	20.81	19.84	21.09	144	2.50	0.1255 ± 0.0003	...	...	...	6.4 ± 0.8
CB-21.4886	15:24:03.0	30:00:30.0	18.48	20.31	17.76	19.27	290	3.36	0.1822 ± 0.0003	...	...	...	...
CB-24.4921	15:24:03.1	32:19:04.6	20.97	21.89	21.19	22.00	75	1.69	0.3426 ± 0.0003	14.4 ± 1.2	...	...	...
CB-20.6381	15:24:03.3	28:44:31.8	18.44	19.63	17.98	19.16	136	2.24	0.0682 ± 0.0003	...	...	-2.7 ± 0.5	...
CB-21.4841	15:24:03.5	29:50:56.8	17.77	19.09	17.36	18.70	312	2.71	0.0842 ± 0.0003	7.7 ± 0.5	-2.5 ± 0.5	4.0 ± 0.1	...
CB-20.6348	15:24:03.7	28:36:27.2	18.35	19.38	17.87	19.04	218	2.19	0.1555 ± 0.0003	6.8 ± 1.5	...	3.4 ± 0.5	...
CB-21.4835	15:24:04.1	30:00:09.6	19.60	20.43	19.52	20.62	117	1.87	0.0823 ± 0.0003	67.3 ± 4.1	...	7.0 ± 0.5	11.6 ± 0.6
CB-24.4857	15:24:04.2	32:12:19.3	19.39	20.67	19.11	20.01	166	3.12	0.3170 ± 0.0010	...	...	...	...
CB-24.4866	15:24:04.4	32:15:27.5	17.69	19.32	17.45	18.76	352	3.21	0.1167 ± 0.0003	5.7 ± 0.9	-1.9 ± 0.4	...	...
CB-19.6097	15:24:04.9	28:30:18.1	20.22	21.41	20.98	21.93	99	2.07	0.1575 ± 0.0003	...	...	6.6 ± 1.4	9.2 ± 1.6
CB-24.4835	15:24:05.3	32:15:49.6	18.74	20.12	18.51	19.80	242	2.62	0.1163 ± 0.0003	...	...	...	...
CB-19.6029	15:24:05.3	28:06:45.5	20.35	21.56	21.13	21.62	96	2.12	0.2169 ± 0.0003	17.0 ± 1.3	...	...	3.8 ± 0.8
CB-21.4765	15:24:05.7	29:54:00.8	20.03	20.82	19.79	20.70	87	1.71	0.1044 ± 0.0003	12.1 ± 1.8	...	...	1.4 ± 0.3
CB-21.4754	15:24:05.8	29:49:57.2	20.20	20.98	19.51	20.32	100	1.84	0.1158 ± 0.0003	...	...	...	...
CB-20.6269	15:24:06.0	28:43:02.1	19.75	20.64	18.94	20.24	112	1.81	0.1476 ± 0.0003	...	...	...	...
CB-19.5989	15:24:06.2	28:00:52.7	20.38	21.14	20.76	21.65	92	1.81	0.0674 ± 0.0003	...	...	...	22.7 ± 1.2
CB-21.4717	15:24:06.6	29:45:39.1	19.82	20.72	19.39	20.31	87	1.77	0.1133 ± 0.0003	...	...	...	...
CB-21.4735	15:24:06.6	29:57:39.7	18.85	19.57	17.89	18.70	93	1.62	star	...	...	...	...
CB-19.6023	15:24:06.6	28:30:21.0	18.83	19.93	18.32	19.64	81	1.76	0.1566 ± 0.0003	11.0 ± 0.8	-5.8 ± 0.7	1.9 ± 0.2	1.8 ± 0.3
CB-20.6238	15:24:06.9	28:44:00.1	17.15	19.13	16.67	18.45	531	4.70	0.0682 ± 0.0003	...	...	-2.4 ± 0.4	7.7 ± 0.3
CB-19.5930	15:24:07.2	28:00:14.3	20.37	21.51	20.04	21.21	85	1.84	0.3143 ± 0.0004	...	...	...	...
CB-24.4790	15:24:07.3	32:24:12.2	19.02	20.02	18.22	19.34	192	2.22	0.0915 ± 0.0003	...	...	...	...
CB-21.4680	15:24:07.5	29:49:45.2	19.30	20.19	18.46	19.54	82	1.67	0.1112 ± 0.0003	...	...	-1.3 ± 0.3	...
CB-24.4766	15:24:07.5	32:11:44.2	20.50	21.65	19.30	20.48	101	2.02	0.3298 ± 0.0003	...	-2.1 ± 0.5	-2.3 ± 0.6	...
CB-20.6206	15:24:08.0	28:45:23.2	21.68	22.08	21.24	21.53	26	1.10	3.8800 ± 0.0010	...	...	...	...
CB-20.6174	15:24:08.1	28:33:46.5	18.75	20.02	18.26	19.67	33	1.58	0.0990 ± 0.0010	...	...	...	...
CB-24.4717	15:24:08.6	32:10:48.7	20.53	21.61	20.37	21.16	60	1.52	0.2052 ± 0.0003	14.5 ± 1.7	...	...	3.6 ± 0.6
CB-20.6173	15:24:08.7	28:44:22.4	17.68	18.89	17.39	18.73	257	2.41	0.1192 ± 0.0003	5.9 ± 0.5	-3.4 ± 0.6	3.4 ± 0.1	...
CB-21.4635	15:24:08.9	29:49:10.9	19.84	20.91	19.59	20.43	142	2.20	0.1191 ± 0.0003	...	...	-1.9 ± 0.4	...
CB-19.5840	15:24:09.3	27:58:51.1	21.34	22.17	20.20	21.44	34	1.40	0.3673 ± 0.0003	...	...	...	...
CB-21.4629	15:24:09.5	29:58:14.0	20.17	20.92	19.22	20.26	105	1.80	0.1123 ± 0.0003	...	...	...	...
CB-19.5830	15:24:09.8	28:05:19.6	21.83	22.37	21.50	22.11	28	1.26	0.3090 ± 0.0010	...	...	...	...
CB-23.5041	15:24:09.8	31:15:59.0	22.05	22.39	...	...	28	1.37	0.3999 ± 0.0003	...	...	...	...
CB-21.4586	15:24:10.0	29:48:28.9	21.87	22.13	21.26	21.82	30	1.18	0.3775 ± 0.0003	22.7 ± 1.3	...	...	...
CB-24.4635	15:24:10.0	32:05:00.6	20.30	21.51	19.80	20.79	96	2.01	0.5150 ± 0.0003	6.2 ± 0.6	-3.0 ± 0.6	...	...
CB-19.5801	15:24:10.5	28:10:23.1	17.60	18.97	16.84	18.16	386	2.84	0.0782 ± 0.0003	...	...	...	...
1524+2850	15:24:11.0	28:50:41.0	16.01	18.34	15.54	17.78	1368	5.74	0.0673 ± 0.0002	...	...	...	...
CB-19.5823	15:24:11.1	28:27:04.7	19.43	20.29	19.81	20.59	114	1.88	0.1185 ± 0.0003	33.6 ± 1.2	-2.1 ± 0.3	9.3 ± 0.3	8.2 ± 0.3
CB-19.5754	15:24:11.1	28:01:42.7	19.32	20.45	19.31	20.44	134	2.12	0.2051 ± 0.0003	12.9 ± 0.6	...	4.9 ± 0.2	1.4 ± 0.3
CB-20.6032	15:24:11.2	28:37:34.6	20.44	21.36	19.17	20.14	95	1.70	0.2800 ± 0.0003	...	...	...	...
CB-21.4536	15:24:11.2	29:47:30.6	18.94	20.32	18.03	19.60	229	2.82	0.1174 ± 0.0003	...	...	...	...
CB-24.4609	15:24:11.2	32:14:14.3	17.80	19.64	17.86	19.64	392	3.31	0.0789 ± 0.0003	15.2 ± 1.9	...	...	...

TABLE 2.5—*Continued*

Object	RA (1950)	Dec. (1950)	g_{tot}	g_{core}	r_{tot}	r_{core}	Area (□″)	irl (″)	z	W_λ([O II]) (Å)	W_λ(Hδ) (Å)	W_λ(Hβ) (Å)	W_λ([O III]5007) (Å)
CB-24.4602	15:24:11.6	32:18:00.6	20.62	21.66	19.82	21.12	65	1.61	0.2355 ± 0.0003	11.0 ± 1.3	···	···	···
CB-21.4522	15:24:12.1	29:57:31.0	19.07	20.11	18.45	19.62	178	2.06	0.1156 ± 0.0003	···	···	-2.5 ± 0.5	···
CB-20.5984	15:24:12.1	28:41:00.2	19.60	21.26	19.74	20.89	164	3.19	0.2256 ± 0.0003	···	···	···	···
CB-21.4503	15:24:12.2	29:50:05.1	20.05	21.16	19.68	20.94	107	2.13	0.1760 ± 0.0010	···	···	···	···
CB-19.5693	15:24:12.4	28:05:13.0	20.99	21.78	20.39	20.92	71	1.56	star	···	···	···	···
CB-19.5733	15:24:12.9	28:27:40.2	19.59	20.77	19.07	20.22	116	2.08	0.1557 ± 0.0003	···	···	-4.1 ± 0.7	···
CB-23.4920	15:24:13.0	31:21:07.5	18.92	20.04	18.38	19.72	201	2.23	0.2131 ± 0.0003	15.0 ± 0.6	-6.4 ± 0.5	···	2.7 ± 0.2
CB-19.5650	15:24:13.1	27:57:32.2	20.04	21.15	19.11	20.32	121	2.17	0.3103 ± 0.0003	3.0 ± 0.5	-2.0 ± 0.4	···	···
CB-19.5670	15:24:13.3	28:07:55.0	20.62	21.28	20.80	21.61	76	1.60	0.1191 ± 0.0003	43.7 ± 3.1	···	6.1 ± 0.9	12.6 ± 0.9
CB-99.11	15:24:13.4	28:44:40.5	···	···	20.07	21.24	84	1.64	0.5660 ± 0.0010	···	···	···	···
CB-24.4510	15:24:13.5	32:09:15.9	21.30	22.32	21.31	22.35	68	1.61	0.2343 ± 0.0003	46.7 ± 3.2	···	9.2 ± 1.6	25.5 ± 1.7
CB-21.4452	15:24:13.6	29:48:56.4	19.36	20.34	18.74	19.77	138	2.02	0.1115 ± 0.0003	···	···	···	···
CB-23.4879	15:24:14.1	31:25:46.5	17.09	19.42	17.05	19.26	564	5.21	0.0543 ± 0.0003	10.5 ± 1.1	-3.7 ± 0.7	-1.2 ± 0.3	1.0 ± 0.2
CB-20.5863	15:24:14.4	28:34:42.1	17.19	18.85	16.63	18.22	417	3.31	0.0667 ± 0.0003	···	···	-2.2 ± 0.3	···
CB-21.4387	15:24:14.5	29:45:46.2	18.02	19.33	17.68	19.10	238	2.51	0.0839 ± 0.0003	4.6 ± 0.7	···	2.3 ± 0.2	···
CB-23.4840	15:24:14.5	31:15:56.7	19.86	21.11	18.79	20.02	114	2.18	star	···	···	···	···
CB-21.4420	15:24:14.7	30:01:46.1	18.40	20.16	18.71	20.35	270	3.40	0.0582 ± 0.0003	···	···	2.1 ± 0.5	6.4 ± 0.6
CB-24.4477	15:24:14.8	32:17:06.9	21.56	22.65	20.34	21.79	36	1.65	0.3258 ± 0.0003	···	···	···	···
CB-19.5582	15:24:15.0	28:05:12.4	19.46	20.99	19.03	20.34	210	2.84	0.1498 ± 0.0003	11.2 ± 2.6	···	···	3.2 ± 0.8
CB-21.4365	15:24:15.4	29:49:48.8	17.82	19.66	17.12	18.82	442	3.65	0.1146 ± 0.0003	···	···	-4.1 ± 0.4	···
CB-23.4809	15:24:15.5	31:20:04.1	20.54	21.21	20.64	21.27	87	1.65	0.1094 ± 0.0003	33.4 ± 1.4	···	12.2 ± 0.4	···
CB-21.4366	15:24:15.6	29:54:49.2	21.02	21.61	19.81	20.76	68	1.33	star	···	···	···	···
CB-19.5590	15:24:16.0	28:27:12.2	17.88	19.54	17.16	18.64	392	3.40	0.1559 ± 0.0003	···	···	-2.2 ± 0.3	···
CB-24.4446	15:24:16.1	32:24:51.2	18.32	19.80	18.17	19.37	258	2.72	0.1715 ± 0.0003	8.0 ± 1.2	-3.1 ± 0.6	1.3 ± 0.3	2.6 ± 0.3
CB-19.5536	15:24:16.2	28:09:15.3	20.22	21.24	19.60	21.03	102	1.97	0.1514 ± 0.0003	21.8 ± 1.7	-4.6 ± 0.9	···	···
CB-23.4762	15:24:16.6	31:17:36.1	18.89	20.26	18.26	19.58	230	2.57	0.1719 ± 0.0003	2.8 ± 0.5	···	-2.2 ± 0.3	···
CB-20.5769	15:24:16.8	28:34:24.7	21.84	22.69	20.37	21.30	34	1.53	0.4760 ± 0.0010	···	···	···	···
CB-21.4285	15:24:17.0	29:49:21.2	18.99	19.68	17.75	18.54	133	1.71	star	···	···	···	···
CB-19.5472	15:24:17.2	28:07:47.9	16.96	18.56	16.63	18.11	653	3.61	0.0709 ± 0.0003	7.4 ± 0.4	-3.2 ± 0.4	5.8 ± 0.1	1.4 ± 0.1
CB-21.4295	15:24:17.3	29:56:20.2	20.24	20.89	19.01	19.81	66	1.41	star	···	···	···	···
CB-23.4751	15:24:17.4	31:27:16.6	20.10	20.98	20.40	21.23	99	1.87	0.2115 ± 0.0003	38.4 ± 1.3	···	···	8.2 ± 0.5
CB-24.4360	15:24:17.4	32:12:37.0	19.85	20.67	19.35	20.14	108	1.87	0.1716 ± 0.0003	5.2 ± 1.1	-3.5 ± 0.5	-2.2 ± 0.4	···
CB-24.4364	15:24:17.6	32:16:55.3	19.63	21.46	19.66	20.86	180	2.70	0.3319 ± 0.0003	7.5 ± 1.0	···	···	···
CB-19.5511	15:24:17.7	28:28:13.8	19.32	20.53	19.14	20.12	126	2.10	0.1653 ± 0.0003	4.7 ± 1.0	-3.2 ± 0.6	···	···
CB-20.5740	15:24:17.7	28:42:56.9	16.44	18.24	15.86	17.58	832	4.08	0.0643 ± 0.0003	···	···	-2.4 ± 0.3	···
CB-24.4342	15:24:18.5	32:24:36.7	20.77	21.56	21.13	21.99	79	1.70	0.2672 ± 0.0003	21.0 ± 1.9	···	4.5 ± 1.0	9.0 ± 1.0
CB-21.4204	15:24:18.6	29:46:16.6	20.10	20.90	19.78	21.00	96	1.74	0.0823 ± 0.0003	36.2 ± 3.4	···	7.5 ± 0.8	10.2 ± 0.7
CB-19.5360	15:24:19.0	27:53:41.7	18.87	20.51	18.39	20.04	256	2.95	0.2755 ± 0.0003	2.6 ± 0.6	-1.9 ± 0.5	···	···
CB-23.4677	15:24:19.0	31:27:55.2	20.40	21.67	19.86	21.05	104	2.09	0.3752 ± 0.0003	11.4 ± 0.8	···	···	···
CB-21.4194	15:24:19.2	29:54:36.0	19.03	20.13	18.31	19.44	194	2.26	0.1035 ± 0.0003	···	···	-3.0 ± 0.5	···
CB-20.5672	15:24:19.2	28:40:58.2	19.50	20.64	18.85	20.07	135	2.19	0.3065 ± 0.0003	···	···	···	···
CB-24.4313	15:24:19.3	32:19:48.2	19.22	20.21	19.08	20.34	180	2.05	0.1170 ± 0.0003	21.8 ± 1.0	···	4.2 ± 0.3	···
CB-19.5362	15:24:19.6	28:05:06.7	19.09	20.22	18.50	19.88	184	2.14	0.2167 ± 0.0003	6.8 ± 0.4	-2.3 ± 0.4	1.6 ± 0.2	0.8 ± 0.2
CB-21.4145	15:24:19.8	29:44:12.8	21.37	21.85	22.02	21.99	68	1.42	0.0820 ± 0.0010	···	···	···	···
CB-19.5319	15:24:20.0	27:57:14.0	21.11	21.92	20.77	21.61	60	1.43	0.3104 ± 0.0003	···	-4.7 ± 1.0	···	···

TABLE 2.5—*Continued*

Object	RA (1950)	Dec.	g_{tot}	g_{core}	r_{tot}	r_{core}	Area (□″)	irl (″)	z	W_λ([O II]) (Å)	W_λ(Hδ) (Å)	W_λ(Hβ) (Å)	W_λ([O III]5007) (Å)
CB-24.4270	15:24:20.1	32:12:03.1	21.25	22.21	···	···	40	1.48	0.5640 ± 0.0010	···	···	···	···
CB-23.4606	15:24:20.4	31:26:41.9	17.33	19.20	16.71	18.56	95	2.22	0.1012 ± 0.0003	···	-2.1 ± 0.5	-1.3 ± 0.3	···
CB-21.4097	15:24:20.8	29:48:29.6	19.20	20.62	18.65	20.48	206	2.55	0.1156 ± 0.0003	···	···	2.6 ± 0.6	···
CB-23.4572	15:24:20.8	31:17:37.1	21.55	22.35	20.08	21.51	67	1.75	0.3487 ± 0.0003	6.4 ± 0.8	-3.4 ± 0.8	···	···
CB-23.4574	15:24:21.0	31:23:44.8	19.91	20.93	19.16	20.30	138	2.12	0.2124 ± 0.0003	···	-2.0 ± 0.4	···	···
CB-21.4101	15:24:21.0	29:53:41.1	17.96	19.36	17.29	18.65	285	2.91	0.1037 ± 0.0003	···	-2.3 ± 0.4	-2.9 ± 0.3	···
CB-19.5350	15:24:21.4	28:30:45.1	17.77	19.92	17.36	19.35	437	3.73	0.1604 ± 0.0003	4.3 ± 0.9	···	···	7.9 ± 0.4
CB-19.5257	15:24:21.5	27:57:55.3	19.53	20.54	19.39	20.31	119	2.05	0.2677 ± 0.0003	5.5 ± 0.5	-3.6 ± 0.7	1.9 ± 0.2	···
CB-19.5263	15:24:21.7	28:05:40.3	19.57	20.40	18.57	19.50	79	1.61	0.2164 ± 0.0003	···	···	-3.1 ± 0.3	···
CB-24.4190	15:24:21.9	32:06:27.4	21.61	21.93	20.96	21.92	67	1.41	0.4900 ± 0.0003	31.9 ± 1.1	···	···	···
CB-19.5196	15:24:22.5	27:57:05.3	18.89	20.05	18.60	19.66	215	2.32	0.0664 ± 0.0003	44.6 ± 2.3	···	4.7 ± 0.2	30.3 ± 0.3
CB-24.4192	15:24:22.7	32:22:17.3	19.91	20.86	19.44	20.51	108	1.93	0.2318 ± 0.0003	8.1 ± 0.9	-3.2 ± 0.6	2.0 ± 0.3	···
CB-24.4174	15:24:22.8	32:13:41.7	19.52	20.98	18.76	20.44	105	2.11	0.1545 ± 0.0003	···	···	···	···
CB-21.4015	15:24:23.0	29:50:02.5	18.71	19.45	17.44	18.32	187	1.80	star	···	···	···	···
CB-24.4167	15:24:23.2	32:17:15.5	20.40	21.22	19.83	20.87	95	1.76	0.3347 ± 0.0003	6.1 ± 0.7	···	3.3 ± 0.6	···
CB-21.4016	15:24:23.3	29:55:58.1	17.26	18.94	16.49	17.97	475	3.53	0.1152 ± 0.0003	···	···	-2.1 ± 0.2	···
CB-20.5465	15:24:23.3	28:39:25.2	18.80	19.76	18.29	19.32	196	2.07	0.0644 ± 0.0003	···	···	-1.9 ± 0.3	···
CB-23.4490	15:24:23.4	31:28:15.0	19.96	20.75	19.48	20.32	123	2.12	star	···	···	···	···
CB-23.4452	15:24:23.4	31:11:10.8	18.26	19.65	18.00	19.26	283	2.81	0.0975 ± 0.0003	5.7 ± 1.1	-1.8 ± 0.4	-2.4 ± 0.4	···
CB-19.5174	15:24:23.7	28:09:10.2	21.38	22.16	20.16	21.36	38	1.65	0.4862 ± 0.0003	7.3 ± 0.8	···	···	···
CB-19.5126	15:24:23.8	28:00:13.0	20.21	20.98	21.01	21.21	97	1.91	star	···	···	···	···
CB-21.3950	15:24:24.4	29:50:28.0	18.21	19.82	18.03	19.47	317	3.49	0.0836 ± 0.0003	···	···	1.9 ± 0.2	1.6 ± 0.3
CB-19.5104	15:24:24.7	28:07:24.9	17.89	19.57	17.33	18.82	347	3.36	0.1506 ± 0.0003	4.7 ± 0.7	-2.3 ± 0.4	···	···
CB-20.5389	15:24:25.2	28:35:09.3	17.92	19.76	17.51	19.17	351	3.73	0.0983 ± 0.0003	···	···	···	···
CB-24.4095	15:24:25.3	32:18:48.8	18.61	19.79	18.33	19.71	209	2.27	0.1713 ± 0.0003	12.2 ± 0.8	-2.3 ± 0.5	1.9 ± 0.2	···
CB-21.3920	15:24:25.6	29:56:19.9	18.99	19.67	18.48	19.11	123	1.71	star	···	···	···	···
CB-19.5017	15:24:25.8	27:58:03.3	20.46	21.36	21.13	21.40	91	1.74	star	···	···	···	···
CB-20.5365	15:24:25.9	28:39:31.5	18.65	20.20	18.16	19.66	226	2.77	0.1590 ± 0.0003	4.7 ± 1.1	···	···	···
CB-21.3893	15:24:25.9	29:46:22.1	19.27	20.38	19.41	20.42	124	2.04	0.1036 ± 0.0003	66.0 ± 2.2	···	7.1 ± 0.3	9.7 ± 0.3
CB-23.4344	15:24:26.3	31:14:01.9	21.70	22.34	21.07	21.43	32	1.24	star	···	···	···	···
CB-23.4350	15:24:26.9	31:25:32.6	19.04	20.45	18.72	19.75	213	2.60	0.2142 ± 0.0003	5.2 ± 0.6	-2.3 ± 0.3	···	···
CB-23.4306	15:24:27.1	31:11:42.8	20.37	21.56	20.66	21.41	94	1.88	0.2928 ± 0.0003	18.2 ± 0.9	···	···	4.2 ± 0.6
CB-21.3874	15:24:27.2	30:01:38.9	19.49	20.29	19.55	20.36	108	1.78	0.0340 ± 0.0003	···	···	···	3.4 ± 0.4
CB-21.3831	15:24:27.8	29:54:44.8	20.00	21.03	19.63	20.63	109	2.03	0.1142 ± 0.0003	···	···	···	···
CB-19.4933	15:24:28.0	28:02:35.9	19.33	20.13	18.88	19.64	31	1.22	star	···	···	···	···
CB-24.3987	15:24:28.3	32:12:52.4	20.68	21.70	20.33	21.89	81	1.80	0.1045 ± 0.0003	22.7 ± 3.0	···	···	11.1 ± 1.1
CB-24.3993	15:24:28.5	32:20:18.6	19.61	20.61	19.61	20.87	144	2.10	0.1712 ± 0.0003	43.2 ± 1.2	···	5.5 ± 0.3	9.9 ± 0.4
CB-23.4269	15:24:28.6	31:18:59.3	20.79	21.88	20.95	21.70	79	1.90	0.4696 ± 0.0003	25.9 ± 0.5	···	···	···
CB-21.3804	15:24:29.1	30:01:52.7	16.53	18.81	16.27	18.18	965	5.53	0.0667 ± 0.0003	···	-2.4 ± 0.5	···	···
CB-21.3761	15:24:29.4	29:43:53.1	20.60	21.59	20.17	21.37	85	1.81	0.1860 ± 0.0010	···	···	···	···
CB-23.4237	15:24:29.4	31:19:47.0	19.53	20.62	19.42	20.53	133	2.21	0.1041 ± 0.0003	10.7 ± 1.0	···	4.0 ± 0.3	3.0 ± 0.3
CB-19.4851	15:24:29.7	28:07:34.2	20.05	20.89	19.36	20.25	103	1.82	0.2486 ± 0.0003	4.1 ± 0.8	···	···	···
CB-23.4190	15:24:29.8	31:11:34.7	19.32	20.43	19.86	20.54	139	2.13	0.1754 ± 0.0003	18.8 ± 0.8	···	5.0 ± 0.2	6.2 ± 0.4
CB-20.5207	15:24:30.0	28:40:10.6	17.96	19.54	17.87	19.11	313	2.93	0.0724 ± 0.0003	11.8 ± 1.4	···	···	9.6 ± 0.3
CB-20.5177	15:24:30.9	28:38:03.6	19.50	20.39	19.05	20.06	121	1.89	0.1529 ± 0.0003	···	···	5.9 ± 0.4	2.6 ± 0.4

TABLE 2.5—*Continued*

Object	RA (1950)	Dec.	g_{tot}	g_{core}	r_{tot}	r_{core}	Area (□″)	irl (″)	z	W_λ([O II]) (Å)	W_λ(Hδ) (Å)	W_λ(Hβ) (Å)	W_λ([O III]5007) (Å)
CB-23.4193	15:24:30.9	31:28:56.2	17.47	19.30	16.76	18.39	541	3.80	0.1139 ± 0.0003	···	···	-2.2 ± 0.3	···
CB-21.3727	15:24:31.3	29:56:46.0	16.46	18.39	15.77	17.62	653	4.22	0.0829 ± 0.0003	···	···	-2.6 ± 0.6	···
CB-24.3873	15:24:31.7	32:13:35.1	18.73	19.85	18.79	19.99	218	2.40	0.1046 ± 0.0003	36.9 ± 0.6	···	8.7 ± 0.2	23.5 ± 0.2
CB-99.12	15:24:31.7	30:01:19.2	···	···	18.61	19.54	152	2.06	0.1141 ± 0.0003	···	···	-2.6 ± 0.3	13.5 ± 0.2
CB-19.4732	15:24:31.8	28:07:05.8	16.95	18.09	15.34	16.21	348	2.51	star	···	···	···	···
CB-24.3868	15:24:32.3	32:20:40.3	19.64	20.71	18.68	19.78	140	2.25	0.1719 ± 0.0003	···	···	-4.2 ± 0.6	···
CB-21.3677	15:24:32.5	29:58:01.5	19.77	20.26	18.26	18.89	100	1.60	star	···	···	···	···
CB-19.4631	15:24:33.0	27:55:09.9	20.04	21.03	20.35	21.74	98	1.89	0.0675 ± 0.0003	···	···	6.5 ± 0.9	15.7 ± 0.8
CB-19.4649	15:24:33.1	28:03:11.4	19.28	20.59	19.83	20.92	132	2.21	0.0658 ± 0.0003	···	···	2.3 ± 0.4	5.6 ± 0.4
CB-21.3620	15:24:33.4	29:45:02.5	17.27	19.35	17.13	19.16	417	3.45	0.0830 ± 0.0003	6.8 ± 1.4	···	2.3 ± 0.2	···
CB-24.3817	15:24:33.4	32:17:29.8	22.17	22.89	···	···	24	1.24	0.6337 ± 0.0003	···	···	···	···
CB-23.4059	15:24:33.5	31:24:47.8	17.29	19.48	16.77	18.75	681	4.98	0.1029 ± 0.0003	···	···	-2.2 ± 0.3	···
CB-19.4611	15:24:33.6	28:01:22.7	20.47	21.82	20.43	21.47	82	2.04	0.4347 ± 0.0003	39.4 ± 3.1	···	···	···
CB-19.4612	15:24:33.8	28:06:35.0	18.24	19.75	17.86	19.38	302	3.13	0.0937 ± 0.0003	8.8 ± 1.0	-2.6 ± 0.6	1.1 ± 0.2	1.2 ± 0.2
CB-21.3582	15:24:34.7	29:49:17.3	19.26	20.38	18.47	19.64	181	2.21	0.1500 ± 0.0003	6.9 ± 1.2	···	···	3.1 ± 0.3
CB-19.4538	15:24:34.9	28:02:47.3	20.86	21.60	20.34	21.07	72	1.61	star	···	···	···	···
CB-23.3977	15:24:35.2	31:14:36.0	19.76	20.63	19.66	20.82	62	1.43	star	···	···	···	···
CB-99.13	15:24:35.4	29:56:34.6	···	···	18.73	20.02	123	2.17	0.0834 ± 0.0003	···	···	-1.8 ± 0.4	···
CB-23.3966	15:24:36.0	31:20:57.0	20.40	21.27	20.19	21.02	93	1.74	0.1667 ± 0.0003	···	···	-3.2 ± 0.4	···
CB-23.3945	15:24:36.1	31:15:46.7	22.05	22.70	22.25	22.66	30	1.19	0.2926 ± 0.0003	···	···	···	···
CB-21.3522	15:24:36.3	29:50:28.2	18.32	19.67	18.14	19.51	266	2.69	0.0841 ± 0.0003	16.2 ± 0.8	···	5.9 ± 0.2	2.4 ± 0.2
CB-24.3670	15:24:37.0	32:09:51.8	20.28	22.19	21.14	22.24	142	2.87	star	···	···	···	···
CB-23.3907	15:24:37.2	31:19:01.3	22.13	22.54	20.88	22.22	19	1.02	0.4351 ± 0.0003	23.3 ± 0.8	···	···	···
CB-24.3676	15:24:37.3	32:18:13.7	19.87	21.50	19.51	21.04	137	2.98	0.1756 ± 0.0003	···	···	···	···
CB-23.3878	15:24:38.1	31:22:27.2	20.36	21.30	20.13	20.82	81	1.75	0.1723 ± 0.0003	···	···	···	1.8 ± 0.4
CB-21.3477	15:24:38.2	29:59:04.1	16.36	18.42	16.60	18.54	461	3.79	0.0562 ± 0.0003	27.0 ± 0.7	-2.0 ± 0.3	9.8 ± 0.1	6.8 ± 0.2
CB-19.4392	15:24:38.2	28:03:43.0	19.38	20.34	19.47	20.53	128	2.00	0.0655 ± 0.0003	38.5 ± 1.1	···	8.6 ± 0.2	31.1 ± 0.3
CB-24.3653	15:24:38.4	32:22:21.5	19.55	20.60	19.00	20.09	177	2.30	0.1690 ± 0.0003	11.8 ± 0.8	···	0.9 ± 0.2	···
CB-19.4353	15:24:38.7	27:56:18.2	20.17	21.33	19.86	21.30	100	1.97	0.2230 ± 0.0010	···	···	···	···
CB-23.3832	15:24:38.7	31:13:33.6	17.75	19.46	17.05	18.68	332	3.37	0.0799 ± 0.0003	3.3 ± 0.7	-1.9 ± 0.4	-3.4 ± 0.4	···
CB-19.4358	15:24:39.1	28:05:08.2	17.18	19.42	16.82	18.74	550	4.67	0.0679 ± 0.0003	···	···	···	···
CB-21.3418	15:24:39.1	29:50:14.0	18.79	19.36	17.74	18.41	134	1.62	star	···	···	···	···
CB-21.3433	15:24:39.3	30:00:45.7	20.36	21.48	19.89	20.78	106	2.26	star	···	···	···	···
CB-23.3841	15:24:39.3	31:27:37.8	22.23	22.83	···	···	25	1.15	0.3774 ± 0.0003	···	···	···	···
CB-24.3569	15:24:39.4	32:06:57.1	19.45	20.21	17.99	18.70	129	1.94	star	···	···	···	···
CB-24.3596	15:24:39.7	32:21:02.9	20.42	21.49	20.24	21.43	107	2.06	0.3226 ± 0.0003	36.6 ± 1.5	···	8.0 ± 0.7	···
CB-19.4331	15:24:39.9	28:09:48.2	18.44	19.75	18.57	20.03	235	2.50	0.0866 ± 0.0003	31.7 ± 2.1	-2.2 ± 0.5	3.5 ± 0.3	5.7 ± 0.3
1524+2900	15:24:39.9	29:00:23.0	16.69	18.48	16.10	17.87	480	3.44	0.0742 ± 0.0001	···	···	···	···
CB-21.3398	15:24:40.1	29:56:34.0	21.61	22.09	20.80	21.53	69	1.51	0.2097 ± 0.0003	19.3 ± 3.3	···	···	···
CB-19.4290	15:24:40.2	27:59:09.9	19.86	20.71	20.08	20.87	108	1.89	0.1390 ± 0.0003	···	···	3.8 ± 0.5	6.4 ± 0.5
CB-23.3794	15:24:40.3	31:21:15.7	17.89	19.66	17.63	19.20	391	3.41	0.1094 ± 0.0003	···	···	-1.7 ± 0.3	···
CB-24.3526	15:24:40.4	32:07:17.4	19.34	20.20	18.65	19.40	133	2.01	star	···	···	···	···
CB-21.3365	15:24:40.5	29:48:51.0	18.95	20.19	18.36	19.59	210	2.31	0.1153 ± 0.0003	···	···	···	···
CB-23.3759	15:24:40.8	31:16:11.0	19.34	21.01	18.16	19.96	216	2.85	0.2944 ± 0.0003	···	···	···	···
CB-24.3555	15:24:40.8	32:22:35.2	20.34	21.72	19.91	21.01	89	1.94	0.3234 ± 0.0003	···	···	···	···

TABLE 2.5—*Continued*

Object	RA (1950)	Dec. (1950)	g_{tot}	g_{core}	r_{tot}	r_{core}	Area (□″)	irl (″)	z	W_λ([O II]) (Å)	W_λ(Hδ) (Å)	W_λ(Hβ) (Å)	W_λ([O III]5007) (Å)
CB-19.4284	15:24:40.9	28:09:15.1	17.42	18.83	16.72	18.12	325	3.00	0.0740 ± 0.0003	5.0 ± 0.6	-1.9 ± 0.4	-2.0 ± 0.2	...
CB-21.3366	15:24:41.0	29:56:58.9	20.85	21.27	19.13	20.10	80	1.47	star	...	...	...	...
1524 7+2914	15:24:41.0	29:13:52.0	15.41	18.58	15.37	18.24	1596	6.89	0.0667 ± 0.0002	...	...	...	...
CB-24.3482	15:24:41.5	32:06:03.7	20.51	21.59	19.90	20.71	82	1.73	star	...	...	...	...
CB-19.4205	15:24:41.8	27:58:49.8	18.43	19.61	18.13	19.45	226	2.35	0.1406 ± 0.0003	13.4 ± 0.6	...	3.8 ± 0.2	2.0 ± 0.2
CB-23.3717	15:24:41.9	31:17:31.9	22.36	22.88	20.62	21.76	20	1.02	0.3142 ± 0.0003	...	...	...	...
CB-19.4233	15:24:41.9	28:07:08.7	18.53	19.37	17.18	18.12	209	2.00	star	...	...	...	...
CB-23.3722	15:24:42.1	31:22:10.7	15.91	17.49	14.02	15.28	727	3.10	star	...	...	...	...
CB-23.3674	15:24:43.4	31:15:35.7	21.61	22.20	20.12	21.07	30	1.34	0.2960 ± 0.0003	...	...	...	...
CB-23.3684	15:24:43.5	31:21:49.3	20.29	20.99	19.76	20.66	106	1.90	star	...	...	...	...
CB-19.4131	15:24:43.6	27:56:23.0	20.39	21.29	19.19	20.43	103	1.87	0.2783 ± 0.0003	...	-2.3 ± 0.5	-3.3 ± 0.5	...
CB-24.3427	15:24:43.6	32:12:43.4	21.65	22.62	20.85	21.60	34	1.40	star	...	...	...	...
CB-21.3250	15:24:43.9	29:54:40.0	18.83	19.91	19.19	20.23	185	2.10	0.0837 ± 0.0003	28.8 ± 3.0	-7.2 ± 1.6	4.2 ± 0.4	10.0 ± 0.4
CB-21.3247	15:24:43.9	29:51:40.2	18.03	19.81	17.68	19.29	269	3.01	0.1164 ± 0.0003	...	...	-3.2 ± 0.5	...
CB-23.3655	15:24:44.0	31:11:59.2	20.25	20.99	19.35	20.20	121	1.81	star	...	...	...	...
CB-24.3405	15:24:44.5	32:15:55.4	22.22	22.51	20.73	21.76	19	0.90	star	...	...	...	...
CB-24.3400	15:24:44.6	32:14:15.7	17.12	19.50	17.58	19.76	384	4.43	0.0326 ± 0.0003	...	...	5.8 ± 0.3	14.5 ± 0.3
CB-19.4116	15:24:44.8	28:12:31.2	20.25	21.25	19.90	21.03	95	1.84	0.1720 ± 0.0003	...	...	5.9 ± 1.5	...
CB-24.3403	15:24:44.9	32:19:53.2	19.08	20.20	18.37	19.45	203	2.22	star	...	...	...	...
CB-23.3618	15:24:44.9	31:13:01.1	20.24	21.23	21.66	21.66	82	1.86	0.0978 ± 0.0003	...	...	6.7 ± 0.8	15.7 ± 0.9
CB-19.4076	15:24:45.0	27:59:28.1	21.78	22.32	22.11	22.09	34	1.39	0.4861 ± 0.0003	25.6 ± 1.1	-2.9 ± 0.7	...	...
CB-99.14	15:24:45.3	29:45:33.6	...	...	21.39	21.83	40	1.38	0.3652 ± 0.0003	...	...	...	...
CB-19.4073	15:24:45.6	28:10:51.4	17.26	18.88	17.13	18.52	506	3.35	0.0984 ± 0.0003	7.2 ± 0.6	-3.6 ± 0.5	1.9 ± 0.2	...
CB-21.3144	15:24:46.2	29:50:02.5	20.53	21.16	20.12	21.15	67	1.45	0.1731 ± 0.0003	27.8 ± 2.1	...	6.3 ± 0.5	...
CB-19.4015	15:24:46.6	28:04:00.5	18.14	19.03	17.22	18.11	226	2.03	star	...	...	...	...
CB-24.3323	15:24:46.9	32:10:09.1	21.94	22.33	21.09	21.49	24	1.16	star	...	...	...	...
CB-24.3320	15:24:47.4	32:15:50.4	17.96	20.04	18.17	20.00	372	3.83	0.0719 ± 0.0003	8.6 ± 1.6	...	...	...
CB-19.3952	15:24:47.6	27:57:34.5	20.25	21.02	19.52	20.22	100	1.75	0.1276 ± 0.0003	...	...	-1.6 ± 0.2	...
CB-21.3077	15:24:48.1	29:54:45.5	18.51	19.27	17.50	18.34	88	1.61	star	...	...	...	...
CB-23.3524	15:24:48.2	31:27:50.1	17.34	19.71	17.54	19.53	563	4.80	0.1097 ± 0.0008	...	...	...	...
CB-23.3486	15:24:48.8	31:18:30.4	21.60	22.32	...	...	24	1.33	0.2069 ± 0.0003	63.9 ± 2.6	...	6.9 ± 1.1	21.5 ± 1.1
CB-21.3021	15:24:49.0	29:46:24.5	17.28	19.53	17.09	18.95	696	4.86	0.0838 ± 0.0003	...	...	...	...
CB-19.3893	15:24:49.3	28:04:23.4	19.75	20.50	18.16	19.10	119	1.88	star	...	...	...	...
CB-23.3475	15:24:49.6	31:25:47.3	22.21	22.63	20.28	21.35	22	1.01	0.4899 ± 0.0003	...	...	...	...
CB-23.3403	15:24:50.5	31:12:19.9	20.16	21.28	19.53	20.76	78	1.77	0.2354 ± 0.0003	6.6 ± 0.6	...	...	1.6 ± 0.3
CB-21.2980	15:24:50.6	29:56:14.1	19.73	20.59	19.35	20.55	116	1.92	0.1150 ± 0.0010	...	...	...	...
CB-19.3810	15:24:50.9	27:58:52.8	20.09	21.43	19.68	20.64	110	2.34	0.2303 ± 0.0003	...	...	...	...
CB-19.3825	15:24:50.9	28:05:54.4	21.74	22.54	20.43	21.47	25	1.12	star	...	...	...	...
CB-24.3166	15:24:51.2	32:11:16.8	21.69	22.53	21.31	22.24	33	1.30	star	...	...	...	...
CB-21.2950	15:24:51.2	29:52:47.7	20.59	21.81	20.39	21.06	92	1.99	0.3015 ± 0.0003	...	...	...	...
CB-24.3151	15:24:51.4	32:06:45.0	21.40	22.08	...	...	81	1.84	0.2226 ± 0.0003	53.2 ± 1.4	...	19.3 ± 0.9	79.5 ± 0.9
CB-23.3367	15:24:51.4	31:13:59.8	19.99	20.98	20.00	21.09	110	1.92	0.2062 ± 0.0003	29.5 ± 0.6	-1.8 ± 0.3	6.7 ± 0.2	8.5 ± 0.2
CB-23.3384	15:24:51.8	31:23:28.0	20.15	21.06	19.23	20.08	92	1.71	star	...	...	...	...
CB-23.3345	15:24:52.8	31:25:47.5	16.73	18.16	14.99	15.75	425	2.73	star	...	...	...	...
CB-21.2870	15:24:53.0	29:53:02.4	17.84	19.67	17.43	18.94	450	3.69	0.1185 ± 0.0003	...	...	...	...

TABLE 2.5—*Continued*

Object	RA (1950)	Dec. (1950)	g_{tot}	g_{core}	r_{tot}	r_{core}	Area (□″)	irl (″)	z	W_λ([O II]) (Å)	W_λ(Hδ) (Å)	W_λ(Hβ) (Å)	W_λ([O III]5007) (Å)
CB-19.3711	15:24:53.0	27:53:44.3	19.91	20.78	20.09	20.81	121	2.06	0.1070 ± 0.0003	···	···	···	···
CB-23.3315	15:24:53.2	31:17:53.3	16.57	17.95	15.61	16.55	446	2.72	star	···	···	···	···
CB-24.3088	15:24:53.4	32:07:27.4	20.49	21.22	20.75	21.54	87	1.72	0.0654 ± 0.0003	···	···	2.4 ± 0.4	8.5 ± 0.5
CB-19.3715	15:24:53.5	28:03:27.3	20.92	21.77	20.37	20.86	65	1.38	star	···	···	···	···
1524+2901	15:24:53.6	29:01:33.0	15.26	17.99	15.13	17.59	355	4.19	0.0347 ± 0.0002	···	···	···	···
CB-23.3287	15:24:53.9	31:16:35.3	21.98	22.62	···	···	20	1.05	0.6070 ± 0.0010	···	···	···	···
CB-19.3677	15:24:54.5	28:06:50.5	17.34	18.84	17.54	18.97	246	2.75	0.0669 ± 0.0003	28.8 ± 0.6	-5.6 ± 0.6	6.3 ± 0.1	11.0 ± 0.2
CB-23.3256	15:24:55.2	31:19:00.8	20.24	21.05	19.63	20.94	107	1.83	0.2335 ± 0.0003	35.0 ± 0.9	-4.2 ± 0.6	5.8 ± 0.3	6.3 ± 0.3
CB-24.3051	15:24:55.4	32:18:46.9	20.14	21.37	19.80	21.14	109	2.10	0.2314 ± 0.0003	6.5 ± 1.0	···	···	···
CB-19.3638	15:24:55.4	28:03:28.0	19.45	20.36	19.19	20.23	115	1.90	star	···	···	···	···
CB-23.3241	15:24:55.8	31:22:02.1	20.79	21.66	20.96	21.53	75	1.64	0.3613 ± 0.0003	20.8 ± 0.3	···	···	···
CB-23.3215	15:24:56.3	31:17:53.0	17.19	18.33	15.53	16.26	283	2.29	star	···	···	···	···
CB-24.2995	15:24:56.4	32:08:06.1	18.24	19.12	17.04	18.01	225	2.23	star	···	···	···	···
CB-19.3572	15:24:57.0	28:00:18.6	18.55	20.07	18.20	19.67	241	2.75	0.1410 ± 0.0003	5.1 ± 0.8	-2.8 ± 0.5	···	1.1 ± 0.2
CB-23.3182	15:24:57.1	31:15:17.4	21.13	22.01	19.82	20.83	75	1.77	0.3745 ± 0.0003	···	···	···	···
CB-23.3179	15:24:57.6	31:19:44.3	20.52	21.92	19.81	20.84	86	1.91	0.2954 ± 0.0003	7.9 ± 1.7	···	···	···
CB-19.3525	15:24:58.2	27:57:32.5	17.56	19.11	17.05	18.46	494	3.36	0.0681 ± 0.0003	···	···	-1.6 ± 0.3	···
CB-23.3156	15:24:58.2	31:18:13.6	19.80	20.84	19.96	20.80	99	1.84	0.2950 ± 0.0003	7.7 ± 0.5	-5.7 ± 0.7	···	···
CB-24.2939	15:24:58.8	32:14:51.8	21.35	22.32	20.07	20.97	56	1.44	star	···	···	···	···
CB-24.2911	15:24:59.3	32:11:25.6	17.82	19.81	18.21	20.11	317	3.58	0.0714 ± 0.0003	21.5 ± 5.2	···	···	6.7 ± 0.3
CB-19.3446	15:25:00.1	27:55:21.4	17.95	19.61	17.66	19.26	366	3.03	0.1655 ± 0.0003	7.4 ± 0.5	···	2.6 ± 0.2	0.9 ± 0.2
CB-23.3080	15:25:00.3	31:13:24.4	21.37	22.06	21.44	22.37	30	1.27	0.2355 ± 0.0003	19.3 ± 1.2	···	4.1 ± 0.6	10.2 ± 0.6
CB-24.2900	15:25:00.3	32:20:03.0	19.41	20.70	18.87	19.84	157	2.38	0.2107 ± 0.0003	···	···	-3.1 ± 0.2	···
CB-23.3083	15:25:00.7	31:22:22.3	21.59	22.49	21.45	21.98	34	1.39	0.5933 ± 0.0003	4.6 ± 0.4	···	···	···
CB-23.3060	15:25:00.9	31:11:59.6	21.16	21.90	20.36	21.62	77	1.69	0.3682 ± 0.0003	15.2 ± 0.5	···	···	···
CB-19.3442	15:25:00.9	28:10:00.6	15.25	17.11	13.15	15.25	978	3.72	star	···	···	···	···
CB-19.3392	15:25:01.3	27:56:51.5	18.11	19.48	17.57	19.13	218	2.71	0.0749 ± 0.0003	15.8 ± 2.2	-4.1 ± 0.7	···	1.1 ± 0.2
CB-19.3419	15:25:01.5	28:08:08.8	20.38	21.87	20.32	21.63	96	2.21	0.4314 ± 0.0005	···	···	···	···
CB-24.2821	15:25:02.3	32:16:20.2	19.42	20.34	19.10	20.22	124	1.96	0.1258 ± 0.0003	8.5 ± 1.2	···	···	···
CB-24.2794	15:25:02.7	32:10:15.1	19.55	20.71	19.26	20.21	183	2.33	0.2110 ± 0.0003	···	···	···	···
CB-23.2945	15:25:03.4	31:12:28.8	20.42	21.89	20.43	21.13	94	2.05	0.2349 ± 0.0003	7.0 ± 1.4	···	···	···
CB-23.2955	15:25:03.7	31:19:38.4	18.59	19.47	17.69	18.70	222	2.07	star	···	···	···	···
1525+2920	15:25:04.0	29:20:06.0	16.53	18.28	15.92	17.70	619	4.20	0.0666 ± 0.0002	···	···	···	···
CB-23.2938	15:25:04.3	31:24:27.3	20.33	21.58	21.93	22.14	102	2.12	0.1652 ± 0.0003	29.8 ± 1.3	···	4.4 ± 0.5	13.5 ± 0.5
CB-19.3279	15:25:04.3	28:02:30.2	19.03	20.17	19.13	20.33	192	2.22	0.0804 ± 0.0003	22.6 ± 4.5	···	···	4.2 ± 0.5
CB-23.2897	15:25:04.9	31:16:00.7	21.96	22.69	···	···	25	1.22	0.5570 ± 0.0010	···	···	···	···
CB-23.2868	15:25:05.7	31:10:42.9	19.36	20.37	18.95	20.24	85	1.79	0.2905 ± 0.0003	9.5 ± 0.5	···	3.3 ± 0.4	1.7 ± 0.4
CB-19.3209	15:25:05.9	28:03:31.4	21.05	21.87	20.35	21.42	79	1.77	0.3698 ± 0.0003	9.6 ± 0.7	···	···	···
CB-19.3163	15:25:06.7	27:56:10.7	19.89	20.70	19.51	20.19	67	1.62	0.0688 ± 0.0003	···	···	···	···
1525+2847	15:25:07.0	28:47:20.0	15.49	18.39	15.26	17.90	1868	7.05	0.0645 ± 0.0002	···	···	···	···
1525+2853	15:25:07.5	28:53:53.0	16.05	18.05	15.40	17.35	1307	5.00	0.0695 ± 0.0002	···	···	···	···
1525+2746	15:25:08.0	27:46:36.0	15.97	18.11	15.46	17.46	721	4.50	0.0746 ± 0.0001	···	···	···	···
CB-19.3094	15:25:08.1	27:56:41.2	20.22	21.13	20.57	21.18	102	1.89	0.3881 ± 0.0003	47.6 ± 0.8	···	···	···
1525+2856	15:25:08.5	28:56:20.0	16.09	17.96	15.53	17.44	1110	4.94	0.0620 ± 0.0001	···	···	···	···
CB-19.3108	15:25:08.5	28:07:01.8	19.29	20.94	19.58	20.93	210	2.68	0.0798 ± 0.0003	17.0 ± 2.8	···	···	3.6 ± 0.5

TABLE 2.5—*Continued*

Object	RA (1950)	Dec. (1950)	g_{tot}	g_{core}	r_{tot}	r_{core}	Area (□″)	irl (″)	z	W_λ([O II]) (Å)	W_λ(Hδ) (Å)	W_λ(Hβ) (Å)	W_λ([O III]5007) (Å)
CB-23.2795	15:25:09.0	31:23:43.0	20.55	21.59	20.59	21.22	99	2.05	0.2064 ± 0.0003	11.5 ± 1.2	...	...	1.5 ± 0.3
1525+2857	15:25:10.1	28:57:42.0	14.86	17.40	14.52	16.92	1663	6.62	0.0341 ± 0.0001	...	...	...	...
CB-23.2731	15:25:10.2	31:11:43.5	19.16	20.32	18.36	19.45	181	2.20	0.1385 ± 0.0003	...	...	-2.0 ± 0.3	...
CB-23.2712	15:25:11.0	31:16:29.7	19.36	20.16	18.19	18.94	125	2.06	star	...	...	...	...
CB-19.2993	15:25:11.0	28:06:50.7	19.95	20.87	20.27	21.19	114	2.08	0.0785 ± 0.0003	...	...	5.4 ± 0.7	9.1 ± 0.7
I4547	15:25:12.0	28:58:00.0	14.86	17.40	14.52	16.92	1663	6.62	0.0344 ± 0.0001	...	...	...	...
CB-19.2938	15:25:12.0	28:04:29.5	17.64	18.99	16.98	18.21	330	3.02	0.0675 ± 0.0003	...	-2.0 ± 0.3	-3.6 ± 0.3	...
CB-23.2643	15:25:12.3	31:16:04.7	19.70	20.49	19.46	20.68	118	1.94	0.3713 ± 0.0003	2.4 ± 0.4	...	...	...
CB-23.2653	15:25:12.9	31:27:53.2	20.37	21.90	21.33	21.88	110	2.45	0.4509 ± 0.0003	11.0 ± 2.6	...	...	...
CB-19.2898	15:25:13.0	28:01:31.2	21.96	22.60	...	...	23	1.16	0.5030 ± 0.0010	...	...	...	...
CB-23.2605	15:25:13.7	31:23:45.9	22.33	22.72	22.11	22.49	19	1.00	0.4054 ± 0.0003	8.3 ± 0.7	...	...	...
CB-23.2577	15:25:13.9	31:15:42.1	18.17	19.55	18.11	19.80	186	2.40	0.0700 ± 0.0003	29.7 ± 0.7	-3.3 ± 0.5	6.4 ± 0.1	6.7 ± 0.1
CB-19.2876	15:25:13.9	28:04:54.4	17.14	18.79	16.59	18.15	186	2.90	0.0684 ± 0.0003	...	...	-2.8 ± 0.4	...
CB-19.2800	15:25:15.7	28:08:30.8	19.75	20.90	20.44	21.46	111	2.03	star	...	...	...	...
CB-19.2772	15:25:15.7	27:59:05.8	19.49	20.47	18.99	20.17	139	2.08	0.1411 ± 0.0003	19.4 ± 3.4	-1.7 ± 0.4	...	...
CB-23.2510	15:25:15.9	31:19:23.4	20.44	21.34	19.92	20.93	89	1.73	0.3492 ± 0.0003	11.4 ± 0.4	-2.3 ± 0.5	...	...
15252+3108	15:25:16.1	31:09:26.0	15.41	18.90	15.44	18.57	353	5.26	0.0317 ± 0.0000	...	...	...	...
CB-23.2460	15:25:16.8	31:15:52.5	19.40	20.87	19.90	21.15	135	2.59	0.0703 ± 0.0003	19.0 ± 1.5	-3.9 ± 0.8	2.8 ± 0.2	7.0 ± 0.2
CB-23.2422	15:25:17.8	31:16:30.3	19.62	20.82	19.42	20.67	119	2.18	0.1004 ± 0.0003	13.2 ± 1.2	...	...	2.0 ± 0.2
CB-23.2430	15:25:18.2	31:24:21.9	20.89	22.19	20.06	21.50	79	1.78	0.5644 ± 0.0003	16.5 ± 0.7	...	...	...
CB-23.2384	15:25:18.8	31:14:08.9	19.69	21.27	19.11	20.52	166	3.45	0.1879 ± 0.0003	8.2 ± 1.3	...	...	...
CB-19.2631	15:25:18.9	28:04:28.8	19.22	20.62	18.69	20.19	209	2.67	0.2176 ± 0.0003	...	...	...	...
CB-23.2408	15:25:18.9	31:26:41.9	20.41	21.72	20.17	21.57	98	2.14	0.2936 ± 0.0003	8.4 ± 0.9	-5.5 ± 0.9	...	...
1525+2901A	15:25:19.1	29:01:21.0	16.09	18.08	15.35	17.16	238	2.91	0.0651 ± 0.0001	...	...	...	...
CB-23.2349	15:25:19.7	31:19:01.1	21.59	22.45	21.07	22.01	24	1.32	0.3491 ± 0.0003	6.5 ± 0.5	...	...	...
CB-23.2320	15:25:21.1	31:27:35.0	21.50	22.37	21.74	22.44	33	1.31	0.5933 ± 0.0003	28.6 ± 2.6	...	...	...
CB-23.2281	15:25:21.3	31:15:55.6	22.15	22.88	21.72	22.35	25	1.16	0.3390 ± 0.0003	16.4 ± 1.1	...	...	...
CB-23.2258	15:25:22.2	31:17:46.1	21.54	22.27	21.27	22.08	36	1.41	0.1497 ± 0.0003	28.7 ± 3.1	...	...	16.9 ± 1.1
CB-23.2270	15:25:22.4	31:25:06.1	16.98	18.44	16.60	18.13	467	3.11	0.0785 ± 0.0003	8.7 ± 0.4	-3.2 ± 0.5	3.7 ± 0.1	0.9 ± 0.1
1525+2852	15:25:22.9	28:52:23.0	15.69	17.79	15.02	16.90	1487	5.44	0.0645 ± 0.0001	...	...	...	...
CB-23.2232	15:25:23.1	31:19:25.3	20.52	21.31	20.04	21.16	85	1.68	0.2764 ± 0.0003	48.4 ± 3.0	...	9.7 ± 0.9	5.2 ± 0.8
CB-23.2200	15:25:24.0	31:18:15.8	18.82	20.44	18.88	20.54	217	3.09	0.0991 ± 0.0003	...	...	3.1 ± 0.4	2.2 ± 0.5
1525+2903	15:25:26.4	29:03:07.0	16.97	18.48	16.26	17.65	523	3.28	0.0645 ± 0.0002	...	...	...	...
CB-23.2111	15:25:26.7	31:25:55.0	22.01	22.37	21.52	22.34	24	1.08	0.4479 ± 0.0003	46.3 ± 2.2	...	...	...
CB-23.2088	15:25:27.0	31:19:03.3	17.48	19.39	17.29	18.91	528	3.93	0.0702 ± 0.0003	2.9 ± 0.7	...	-3.5 ± 0.4	2.1 ± 0.2
CB-23.2009	15:25:28.7	31:12:47.0	20.04	20.92	20.26	21.16	108	1.99	star	...	...	...	...
1525+2901B	15:25:29.0	29:01:30.0	15.95	18.02	15.75	17.56	1047	4.79	0.0326 ± 0.0001	...	...	...	...
CB-23.1874	15:25:32.3	31:19:36.8	20.79	22.07	20.41	21.53	98	2.14	0.3471 ± 0.0003	18.8 ± 1.1	...	...	...
CB-23.1784	15:25:35.2	31:19:39.9	19.21	20.58	18.41	19.79	232	2.70	0.2054 ± 0.0003	...	...	...	...
1525+2904	15:25:37.4	29:04:54.0	16.56	18.08	15.76	17.46	726	3.67	0.0662 ± 0.0001	...	...	...	...
15257+2905W	15:25:39.7	29:05:28.0	15.39	17.79	14.80	17.16	609	4.47	0.0652 ± 0.0001	...	...	...	...
2079-131	15:25:39.9	29:10:21.0	16.97	18.60	16.35	17.98	504	3.26	0.0631 ± 0.0002	...	...	...	...
1525+2921B	15:25:55.0	29:21:59.0	16.91	17.99	16.59	17.58	123	2.18	0.0664 ± 0.0002	...	...	...	...
1525+2906	15:25:57.8	29:06:58.0	16.18	18.24	15.61	17.59	1189	5.09	0.0674 ± 0.0001	...	...	...	...
1526+2911	15:26:02.0	29:10:60.0	16.12	18.14	15.84	17.70	841	4.56	0.0614 ± 0.0002	...	...	...	...

TABLE 2.5—*Continued*

Object	RA (1950)	Dec. (1950)	g_{tot}	g_{core}	r_{tot}	r_{core}	Area (□″)	irl (″)	z	W_λ([O II]) (Å)	W_λ(Hδ) (Å)	W_λ(Hβ) (Å)	W_λ([O III]5007) (Å)
1526+2900	15:26:05.0	29:00:52.0	15.50	18.30	15.31	17.79	882	5.69	0.0667 ± 0.0001	···	···	···	···
1526+2817	15:26:16.3	28:17:59.0	16.08	18.37	15.90	17.74	304	3.84	0.0729 ± 0.0004	···	···	···	···
1526+2913A	15:26:21.4	29:13:44.0	16.95	18.62	16.15	17.84	390	3.16	0.0855 ± 0.0001	···	···	···	···
1526+2926	15:26:21.8	29:26:22.0	16.90	18.75	16.24	17.97	643	5.02	0.0636 ± 0.0001	···	···	···	···
1526+2908	15:26:27.6	29:08:08.0	16.34	18.25	15.91	17.64	876	4.38	0.0636 ± 0.0002	···	···	···	···
1526+2910	15:26:27.9	29:10:26.0	15.44	17.77	14.85	16.83	1090	5.65	0.0663 ± 0.0002	···	···	···	···
1526+2914	15:26:37.0	29:14:45.0	15.95	18.04	15.54	17.49	950	4.66	0.0648 ± 0.0001	···	···	···	···
1526+2916	15:26:40.0	29:16:20.0	15.78	18.62	15.62	18.03	364	4.13	0.0649 ± 0.0001	···	···	···	···
1526+2913B	15:26:46.0	29:13:43.0	16.34	18.32	15.87	17.75	911	4.54	0.0700 ± 0.0001	···	···	···	···
1527+2912	15:27:06.7	29:12:09.0	16.11	18.13	15.75	17.68	710	4.16	0.0834 ± 0.0001	···	···	···	···
CB-29.8441	15:27:07.0	31:05:10.9	18.92	20.57	19.08	20.64	242	3.07	0.0901 ± 0.0003	11.0 ± 2.6	···	···	···
CB-29.8353	15:27:09.0	31:04:49.3	21.17	21.92	20.70	21.46	58	1.40	0.4657 ± 0.0003	···	···	···	···
CB-29.8316	15:27:09.4	31:00:13.6	17.58	19.51	17.21	19.15	424	3.68	0.1022 ± 0.0003	8.4 ± 2.0	···	···	···
CB-29.8256	15:27:11.1	31:01:29.7	17.80	19.41	17.69	19.18	424	3.23	0.1045 ± 0.0003	7.2 ± 1.1	···	···	···
CB-29.8230	15:27:12.0	31:03:11.0	19.14	20.18	19.01	20.31	141	2.15	0.0541 ± 0.0003	25.7 ± 2.0	···	···	4.8 ± 0.3
CB-29.8243	15:27:12.2	31:10:05.5	20.51	21.17	19.39	20.04	84	1.49	star	···	···	···	···
CB-29.8187	15:27:13.1	31:03:44.7	19.50	20.53	19.60	21.02	128	2.10	0.0537 ± 0.0003	···	···	12.4 ± 0.5	43.8 ± 0.5
CB-29.8162	15:27:13.9	31:05:00.5	19.42	20.19	19.38	20.34	112	1.72	1.2610 ± 0.0010	···	···	···	···
CB-29.8110	15:27:15.2	31:02:40.4	16.81	18.37	16.19	17.58	533	3.43	0.0543 ± 0.0003	···	-2.6 ± 0.3	-2.8 ± 0.3	···
CB-29.8040	15:27:17.4	31:07:02.7	20.37	21.34	19.49	20.53	94	1.77	0.3890 ± 0.0003	19.6 ± 0.7	-3.1 ± 0.4	···	···
CB-29.8003	15:27:17.6	30:59:09.4	20.16	21.09	18.89	19.93	98	1.83	0.1053 ± 0.0003	···	···	-2.3 ± 0.5	···
CB-29.7959	15:27:19.1	31:03:28.6	18.33	20.24	18.56	20.43	301	3.41	0.1044 ± 0.0003	17.0 ± 2.1	-7.0 ± 1.5	4.3 ± 0.4	2.9 ± 0.5
CB-29.7924	15:27:19.9	31:05:08.2	20.74	21.88	19.48	20.54	85	1.89	0.3282 ± 0.0003	6.8 ± 1.1	···	···	···
CB-29.7866	15:27:21.2	31:02:10.8	18.40	19.85	17.89	19.16	241	2.66	0.1049 ± 0.0003	···	···	-3.0 ± 0.5	···
CB-29.7873	15:27:21.6	31:09:07.7	19.57	20.26	17.92	18.67	108	1.65	star	···	···	···	···
CB-29.7842	15:27:22.6	31:13:41.6	18.09	19.50	17.37	18.66	332	2.95	0.1027 ± 0.0003	···	···	···	···
CB-29.7796	15:27:22.6	30:59:27.9	19.97	21.02	19.34	20.51	113	2.06	0.1063 ± 0.0003	···	···	···	···
CB-29.7772	15:27:24.1	31:09:30.0	19.79	21.08	19.70	20.88	130	2.41	0.1154 ± 0.0003	···	···	···	···
CB-29.7743	15:27:25.2	31:12:54.5	19.83	20.79	19.98	21.42	110	1.98	0.1029 ± 0.0003	30.1 ± 2.7	···	···	18.0 ± 1.2
CB-29.7675	15:27:25.5	30:57:43.7	19.47	20.23	17.93	18.79	109	1.65	star	···	···	···	···
CB-29.7693	15:27:26.0	31:05:12.2	19.57	21.02	19.45	21.22	139	2.50	0.1071 ± 0.0003	12.7 ± 2.6	···	···	···
CB-29.7646	15:27:27.1	31:06:21.6	19.28	20.02	18.09	18.80	111	1.68	star	···	···	···	···
CB-29.7622	15:27:27.1	30:57:39.1	18.58	19.55	17.70	18.78	189	2.03	0.1048 ± 0.0003	···	-1.9 ± 0.4	-3.0 ± 0.3	···
CB-29.7623	15:27:28.5	31:13:21.0	19.43	20.68	19.58	20.62	136	2.25	0.2035 ± 0.0003	17.4 ± 1.4	-5.5 ± 1.1	2.7 ± 0.5	···
CB-29.7566	15:27:28.9	31:01:48.2	18.93	20.04	18.39	19.61	210	2.21	0.1646 ± 0.0003	6.9 ± 0.6	···	2.5 ± 0.2	···
CB-29.7534	15:27:29.8	31:00:07.0	21.97	22.26	20.84	21.76	28	1.18	1.1490 ± 0.0010	···	···	···	···
CB-29.7525	15:27:30.4	31:05:19.2	18.13	19.34	17.27	18.52	189	2.33	0.0803 ± 0.0003	···	-1.8 ± 0.4	-1.9 ± 0.2	···
CB-29.7478	15:27:31.9	31:08:37.4	18.86	20.38	18.68	20.34	220	2.65	0.1129 ± 0.0003	9.4 ± 2.2	···	···	···
CB-29.7445	15:27:31.9	30:59:05.9	17.86	18.85	16.84	17.84	218	2.23	star	···	···	···	···
1527+2810	15:27:32.3	28:10:11.0	16.72	18.83	16.41	18.28	642	4.58	0.0738 ± 0.0002	···	···	···	···
CB-28.6783	15:27:33.3	30:56:30.6	19.67	20.39	18.84	19.61	131	2.01	star	···	···	···	···
CB-29.7367	15:27:34.3	31:05:29.8	18.96	20.25	18.53	19.78	208	2.57	0.0913 ± 0.0003	···	···	···	···
CB-29.7332	15:27:34.7	31:00:12.2	20.07	21.08	20.50	21.40	98	1.83	0.2136 ± 0.0003	22.7 ± 0.6	···	6.5 ± 0.3	10.9 ± 0.4
CB-29.7340	15:27:35.7	31:13:60.0	20.42	21.61	20.41	21.47	86	1.91	0.2566 ± 0.0003	34.4 ± 2.8	···	7.8 ± 1.4	8.3 ± 1.1
CB-29.7273	15:27:36.7	31:03:38.0	19.68	20.68	19.12	20.46	116	1.94	0.1378 ± 0.0003	14.3 ± 1.1	···	5.0 ± 0.4	1.4 ± 0.3

TABLE 2.5—*Continued*

Object	RA (1950)	Dec. (1950)	g_{tot}	g_{core}	r_{tot}	r_{core}	Area (□″)	ir1 (″)	z	W_λ([O II]) (Å)	W_λ(Hδ) (Å)	W_λ(Hβ) (Å)	W_λ([O III]5007) (Å)
CB-29.7212	15:27:37.4	30:59:06.7	21.00	21.91	21.24	22.16	57	1.41	0.2800 ± 0.0010	···	···	···	···
CB-29.7239	15:27:37.7	31:06:39.5	19.71	20.39	18.49	19.38	101	1.66	star	···	···	···	···
15277+3039	15:27:37.9	30:39:23.0	15.21	17.54	14.48	15.85	1536	5.79	0.0349 ± 0.0000	···	···	···	···
CB-28.6601	15:27:38.4	30:56:44.7	18.89	19.94	17.99	19.09	206	2.30	0.1149 ± 0.0003	···	···	-1.6 ± 0.3	···
CB-29.7226	15:27:38.5	31:12:58.3	18.09	18.92	16.85	17.78	207	1.90	star	···	···	···	···
CB-29.7176	15:27:39.0	31:04:33.6	22.17	22.54	20.29	21.68	23	1.14	star	···	···	···	···
CB-29.7143	15:27:40.4	31:11:00.7	18.29	19.01	17.06	18.00	193	1.83	star	···	···	···	···
CB-29.7078	15:27:41.3	31:02:27.4	18.24	19.41	17.85	19.14	227	2.39	0.0858 ± 0.0003	24.3 ± 0.9	···	2.3 ± 0.2	4.6 ± 0.2
CB-28.6452	15:27:41.8	30:55:45.4	18.82	19.95	18.03	19.26	217	2.29	0.1111 ± 0.0003	···	···	-1.9 ± 0.3	···
CB-29.7057	15:27:42.1	31:05:21.9	21.44	22.28	19.67	20.95	44	1.55	0.3750 ± 0.0010	···	···	···	···
CB-29.7004	15:27:42.8	31:00:37.8	19.73	20.46	18.47	19.26	99	1.61	star	···	···	···	···
2083-107	15:27:43.1	30:52:49.0	16.22	18.43	15.39	17.56	269	3.17	0.1138 ± 0.0008	···	···	···	···
CB-29.6998	15:27:43.9	31:11:32.6	20.63	21.38	19.89	20.99	78	1.59	0.2901 ± 0.0003	5.7 ± 1.2	···	···	···
CB-29.6958	15:27:44.1	31:04:33.2	19.81	20.82	19.73	21.13	110	1.90	0.1968 ± 0.0003	32.4 ± 1.1	···	5.0 ± 0.4	6.4 ± 0.4
CB-29.6886	15:27:45.8	31:06:34.7	19.91	21.17	19.56	20.78	127	2.34	0.1144 ± 0.0003	···	···	···	···
CB-99.15	15:27:46.7	30:56:32.3	···	···	20.74	21.80	79	2.09	0.5640 ± 0.0010	···	···	···	···
CB-29.6790	15:27:47.4	30:58:29.3	19.27	20.19	18.75	19.71	130	1.95	0.1109 ± 0.0003	···	···	-1.5 ± 0.2	···
CB-29.6751	15:27:48.7	30:59:33.2	22.27	22.77	20.20	21.89	20	0.95	0.3061 ± 0.0003	···	-3.9 ± 1.0	···	···
CB-29.6643	15:27:51.2	30:57:29.5	18.00	18.94	16.49	17.69	232	2.29	star	···	···	···	···
CB-29.6622	15:27:52.4	31:07:38.9	19.66	20.80	19.40	20.53	119	2.15	0.2343 ± 0.0003	13.7 ± 1.0	-3.5 ± 0.6	2.9 ± 0.4	1.9 ± 0.4
CB-27.5650	15:27:52.5	29:40:13.2	18.59	20.17	18.65	20.48	251	2.91	0.1525 ± 0.0003	55.9 ± 3.1	-5.4 ± 1.2	···	5.7 ± 0.5
CB-29.6585	15:27:52.9	31:03:25.9	19.18	20.25	18.72	19.53	133	2.03	0.0932 ± 0.0003	···	···	-4.3 ± 0.6	···
CB-27.5609	15:27:53.8	29:44:26.8	16.08	17.76	14.21	15.53	493	3.03	star	···	···	···	···
CB-29.6525	15:27:54.1	30:58:20.4	17.86	20.03	18.30	20.27	456	4.27	0.0577 ± 0.0003	14.5 ± 1.6	-6.9 ± 1.1	···	4.1 ± 0.3
CB-99.16	15:27:55.0	31:05:31.5	···	···	21.29	21.83	37	1.83	0.5138 ± 0.0008	···	···	···	···
CB-29.6480	15:27:55.4	31:04:14.0	18.85	19.48	18.00	18.76	180	1.75	star	···	···	···	···
CB-27.5484	15:27:56.4	29:40:12.2	19.16	20.05	18.45	19.28	100	1.90	0.1519 ± 0.0003	11.6 ± 0.9	-3.7 ± 0.6	···	···
CB-27.5443	15:27:56.8	29:34:50.5	16.59	17.82	15.25	16.30	413	2.55	star	···	···	···	···
CB-28.5861	15:27:57.0	30:56:38.4	19.68	20.24	19.19	19.95	101	1.52	star	···	···	···	···
CB-27.5420	15:27:58.3	29:44:05.6	19.97	21.20	19.79	20.67	119	2.23	0.2486 ± 0.0003	4.0 ± 0.4	···	···	···
CB-00.28	15:27:58.4	30:58:21.1	···	···	22.07	21.87	19	0.95	star	···	···	···	···
CB-27.5363	15:27:58.5	29:32:11.0	19.41	20.55	18.72	19.85	139	2.26	0.2330 ± 0.0010	6.5 ± 1.0	-3.0 ± 0.5	···	···
CB-27.5377	15:27:59.4	29:44:47.3	19.88	20.98	19.05	20.04	121	2.10	0.2220 ± 0.0003	···	···	-2.1 ± 0.4	···
CB-29.6278	15:27:60.0	31:05:38.4	19.01	20.38	18.94	20.46	231	2.65	0.0861 ± 0.0003	26.0 ± 1.4	···	3.6 ± 0.3	5.1 ± 0.3
CB-29.6290	15:27:60.0	31:09:56.8	21.16	22.06	19.95	21.02	78	1.76	0.3776 ± 0.0003	14.1 ± 1.5	···	···	···
CB-27.5314	15:28:00.1	29:37:30.1	22.35	22.78	21.84	22.18	19	0.90	0.4534 ± 0.0003	30.1 ± 0.9	···	···	···
CB-29.6254	15:28:00.2	31:03:19.8	18.49	19.35	17.60	18.49	127	1.86	star	···	···	···	···
CB-29.6226	15:28:01.2	31:07:18.0	19.08	19.76	18.50	19.35	54	1.54	star	···	···	···	···
CB-29.6190	15:28:01.5	31:00:53.1	21.06	21.46	20.06	21.23	81	1.46	0.2789 ± 0.0003	6.5 ± 0.8	···	···	···
CB-28.5689	15:28:02.4	30:56:30.3	19.32	20.24	18.47	19.58	136	1.99	0.1158 ± 0.0003	···	···	-2.0 ± 0.3	···
CB-27.5196	15:28:02.8	29:35:28.8	20.24	21.25	19.34	20.37	97	1.84	star	···	···	···	···
CB-27.5205	15:28:03.3	29:43:04.9	19.27	20.05	18.79	19.67	181	1.96	star	···	···	···	···
CB-29.6103	15:28:03.8	31:04:06.9	21.35	21.53	19.84	20.52	73	1.39	star	···	···	···	···
CB-27.5119	15:28:04.6	29:33:37.5	22.31	22.46	21.28	21.80	23	1.15	star	···	···	···	···
CB-29.6060	15:28:05.0	31:04:38.9	19.87	20.55	19.52	20.53	99	1.60	star	···	···	···	···

TABLE 2.5—*Continued*

Object	RA (1950)	Dec. (1950)	g_{tot}	g_{core}	r_{tot}	r_{core}	Area (□″)	irl (″)	z	W_λ([O II]) (Å)	W_λ(Hδ) (Å)	W_λ(Hβ) (Å)	W_λ([O III]5007) (Å)
CB-27.5120	15:28:05.2	29:40:13.2	19.98	20.88	19.55	20.72	111	2.01	0.2375 ± 0.0003	15.6 ± 0.7	···	2.9 ± 0.3	2.7 ± 0.4
CB-25.6001	15:28:05.7	28:00:40.0	15.95	17.67	14.30	15.65	699	3.30	star	···	···	···	···
CB-29.6007	15:28:05.8	31:01:29.4	21.57	22.05	20.81	21.67	64	1.49	0.4659 ± 0.0003	10.1 ± 1.1	···	···	···
CB-29.6048	15:28:05.9	31:11:02.0	18.23	19.54	17.84	19.02	212	2.55	star	···	···	···	···
CB-27.5106	15:28:06.0	29:45:10.8	18.68	19.72	17.32	18.48	208	2.17	star	···	···	···	···
CB-25.5953	15:28:07.3	28:05:22.8	18.00	19.58	17.18	18.69	469	3.38	0.1755 ± 0.0003	···	···	-1.8 ± 0.3	···
CB-27.5049	15:28:07.4	29:43:56.6	19.81	20.99	20.00	21.13	116	2.07	0.0649 ± 0.0003	···	···	···	···
CB-27.4986	15:28:07.9	29:31:57.6	19.72	20.21	19.68	20.18	22	1.02	star	···	···	···	···
CB-29.5943	15:28:08.2	31:09:40.8	21.47	21.94	20.22	21.03	59	1.23	0.2136 ± 0.0003	···	···	···	···
CB-27.5012	15:28:08.4	29:45:33.1	19.18	20.50	18.61	19.90	192	2.47	0.2102 ± 0.0003	11.6 ± 0.7	-4.4 ± 0.4	···	1.1 ± 0.2
CB-29.5876	15:28:08.9	31:01:11.9	18.39	19.89	18.49	20.12	283	2.97	0.0663 ± 0.0003	···	···	···	14.2 ± 1.0
CB-25.5872	15:28:09.5	28:05:04.5	18.92	19.91	18.47	19.59	190	2.09	0.1802 ± 0.0003	23.3 ± 0.7	-3.2 ± 0.6	6.2 ± 0.2	3.2 ± 0.2
CB-27.4923	15:28:09.8	29:33:53.9	20.01	21.10	19.49	20.94	113	2.04	0.1136 ± 0.0003	14.9 ± 1.0	···	···	···
CB-28.5372	15:28:10.2	30:56:35.6	19.20	19.85	18.24	19.07	116	1.69	star	···	···	···	···
CB-27.4892	15:28:10.5	29:36:06.5	19.97	20.87	19.66	20.52	93	1.73	0.1858 ± 0.0003	7.5 ± 0.8	-4.3 ± 0.7	2.7 ± 0.2	···
CB-29.5851	15:28:10.6	31:10:30.8	19.42	20.57	19.56	20.79	118	2.19	0.1024 ± 0.0003	16.0 ± 1.7	···	2.5 ± 0.4	3.2 ± 0.4
CB-27.4877	15:28:11.4	29:41:36.1	19.93	20.74	19.40	20.58	106	1.80	0.1125 ± 0.0003	5.6 ± 1.3	-3.6 ± 0.7	-3.3 ± 0.4	···
CB-25.5735	15:28:11.7	28:02:45.9	20.21	21.39	19.86	21.05	94	1.91	0.4499 ± 0.0003	11.9 ± 1.0	···	···	···
CB-29.5737	15:28:11.9	30:58:36.9	20.70	21.52	20.09	21.30	87	1.74	0.2783 ± 0.0003	21.1 ± 1.5	···	6.1 ± 0.9	4.5 ± 0.9
CB-28.5264	15:28:12.8	30:57:06.5	19.61	20.27	19.04	19.88	111	1.66	star	···	···	···	···
CB-29.5695	15:28:13.2	31:04:19.1	21.32	21.78	20.38	20.95	61	1.40	star	···	···	···	···
CB-25.5646	15:28:13.9	28:07:36.2	20.20	21.26	20.06	21.07	94	1.85	0.4528 ± 0.0003	11.0 ± 1.1	···	···	···
CB-27.4799	15:28:14.0	29:43:50.4	21.04	22.10	20.54	21.88	73	1.74	0.3113 ± 0.0009	···	···	···	···
CB-27.4744	15:28:14.4	29:30:43.1	19.99	20.94	18.48	19.77	118	2.39	star	···	···	···	···
CB-29.5570	15:28:14.4	30:57:29.5	19.65	20.23	17.81	18.65	113	1.64	star	···	···	···	···
CB-29.5628	15:28:14.6	31:07:36.1	18.74	19.85	18.16	19.43	199	2.50	0.1013 ± 0.0003	8.6 ± 0.8	···	1.0 ± 0.2	0.9 ± 0.2
CB-25.5570	15:28:15.0	28:02:49.4	20.50	21.35	20.68	21.84	84	1.72	0.1490 ± 0.0003	66.3 ± 3.3	···	···	5.9 ± 0.6
CB-27.4745	15:28:15.2	29:38:41.0	20.54	21.83	20.17	21.46	101	2.18	0.2689 ± 0.0003	11.0 ± 0.8	-4.3 ± 0.9	···	2.6 ± 0.6
CB-25.5562	15:28:15.2	28:03:27.6	19.19	20.43	18.81	20.46	169	2.22	0.2244 ± 0.0003	7.9 ± 0.7	-3.6 ± 0.6	3.1 ± 0.2	1.2 ± 0.3
CB-29.5551	15:28:15.5	31:05:16.5	20.53	21.41	19.51	20.65	83	1.68	0.3426 ± 0.0003	8.3 ± 0.6	···	···	···
CB-25.5525	15:28:16.2	28:09:17.4	17.92	19.46	17.65	19.12	285	3.02	0.0680 ± 0.0003	···	···	···	1.1 ± 0.2
CB-29.5486	15:28:16.4	31:04:38.7	18.69	19.80	18.09	19.30	234	2.47	0.0934 ± 0.0003	32.1 ± 0.5	···	8.3 ± 0.2	7.4 ± 0.2
CB-29.5534	15:28:16.5	31:12:39.9	18.12	19.55	17.40	18.82	180	2.77	0.1016 ± 0.0003	···	···	-1.1 ± 0.2	···
CB-25.5447	15:28:16.9	28:01:44.8	17.27	19.51	17.71	19.59	639	4.41	0.0738 ± 0.0003	14.0 ± 1.7	···	2.2 ± 0.2	1.3 ± 0.2
CB-27.4693	15:28:17.1	29:44:10.4	21.63	22.32	20.45	21.47	34	1.35	0.5623 ± 0.0003	19.3 ± 0.8	···	···	···
CB-27.4691	15:28:17.5	29:47:38.9	19.82	20.93	19.18	20.09	128	2.11	0.2089 ± 0.0003	4.2 ± 0.6	···	···	···
CB-27.4625	15:28:17.6	29:35:17.6	20.21	21.39	19.92	21.47	116	2.15	0.2191 ± 0.0003	17.4 ± 0.9	···	4.3 ± 0.3	2.9 ± 0.4
CB-25.5401	15:28:17.7	27:58:57.4	19.49	20.46	19.34	20.25	132	2.02	0.2598 ± 0.0003	17.3 ± 0.5	···	6.7 ± 0.2	3.3 ± 0.2
CB-29.5412	15:28:18.1	31:07:51.7	18.27	19.88	18.89	20.17	284	3.05	0.1155 ± 0.0003	27.8 ± 1.2	···	7.0 ± 0.4	···
CB-27.4582	15:28:18.4	29:29:16.8	21.84	22.46	···	···	21	1.01	0.5630 ± 0.0010	···	···	···	···
CB-29.5369	15:28:18.5	31:04:17.6	20.64	21.77	20.60	21.79	75	1.70	0.3747 ± 0.0003	···	-5.8 ± 1.0	···	···
CB-28.5018	15:28:18.9	30:57:07.2	20.56	21.87	21.30	21.88	90	1.92	star	···	···	···	···
CB-29.5357	15:28:19.4	31:09:54.7	19.99	20.68	18.72	19.43	89	1.56	star	···	···	···	···
CB-27.4563	15:28:19.5	29:30:02.0	18.68	19.62	18.13	19.13	202	2.08	0.0611 ± 0.0003	16.3 ± 0.9	-3.6 ± 0.6	2.6 ± 0.1	6.9 ± 0.2
CB-27.4583	15:28:19.5	29:40:36.7	20.10	20.95	19.75	20.88	113	1.91	0.2224 ± 0.0003	17.8 ± 0.5	-2.9 ± 0.6	5.2 ± 0.2	3.9 ± 0.3

TABLE 2.5—*Continued*

Object	RA (1950)	Dec.	g_{tot}	g_{core}	r_{tot}	r_{core}	Area (□″)	irl (″)	z	W_λ([O II]) (Å)	W_λ(Hδ) (Å)	W_λ(Hβ) (Å)	W_λ([O III]5007) (Å)
CB-25.5270	15:28:20.1	27:54:41.7	20.61	21.52	20.83	21.86	84	1.82	0.3045 ± 0.0003	40.8 ± 1.1	···	11.2 ± 0.5	···
CB-25.5289	15:28:20.3	28:03:11.4	20.05	21.25	20.87	21.73	99	2.17	0.1804 ± 0.0003	89.7 ± 2.0	10.9 ± 1.1	53.8 ± 1.2	242.1 ± 1.1
CB-29.5242	15:28:20.4	31:03:49.3	21.98	22.41	20.55	21.73	25	1.03	0.4424 ± 0.0003	5.1 ± 1.0	···	···	···
CB-29.5259	15:28:20.9	31:12:16.6	17.88	18.75	15.57	16.25	251	2.03	star	···	···	···	···
CB-25.5233	15:28:21.0	27:58:46.6	20.06	21.05	18.86	20.00	118	2.18	0.3389 ± 0.0003	···	···	···	···
CB-27.4542	15:28:21.1	29:43:42.0	20.22	21.20	20.10	21.23	118	1.95	0.2095 ± 0.0003	40.8 ± 0.8	···	12.0 ± 0.3	17.0 ± 0.4
CB-25.5227	15:28:21.7	28:03:30.6	16.96	18.73	16.31	17.93	270	3.14	0.0765 ± 0.0003	6.1 ± 1.0	-1.6 ± 0.4	-2.0 ± 0.3	···
CB-29.5168	15:28:22.0	31:09:17.3	21.61	22.29	19.84	21.06	59	1.34	0.4622 ± 0.0003	5.9 ± 1.4	···	···	···
CB-27.4515	15:28:22.1	29:46:31.6	21.19	22.03	21.18	22.13	75	1.60	0.4189 ± 0.0003	49.2 ± 3.3	···	···	···
CB-27.4477	15:28:22.2	29:38:03.1	20.30	21.64	20.09	21.44	119	2.23	0.1678 ± 0.0003	···	···	10.5 ± 1.9	18.4 ± 1.3
CB-25.5145	15:28:22.4	27:54:42.4	20.47	21.84	21.46	22.02	87	1.99	0.7300 ± 0.0003	20.5 ± 1.7	···	···	···
CB-25.5204	15:28:22.6	28:09:39.3	19.94	21.32	18.99	20.70	132	2.43	0.1963 ± 0.0003	10.4 ± 1.9	···	···	···
CB-29.5149	15:28:22.7	31:12:45.9	18.23	19.85	18.00	19.56	292	3.26	0.1131 ± 0.0003	17.5 ± 0.8	-4.5 ± 0.8	2.1 ± 0.2	···
CB-27.4432	15:28:23.2	29:38:33.3	19.83	20.62	19.73	21.07	110	1.79	0.0867 ± 0.0003	···	···	10.3 ± 0.4	20.7 ± 0.4
CB-29.5035	15:28:23.6	31:02:45.3	21.30	21.99	20.24	21.42	56	1.34	star	···	···	···	···
CB-27.4383	15:28:23.9	29:35:24.5	20.78	21.64	20.09	21.46	89	1.83	0.1140 ± 0.0010	···	···	···	···
CB-27.4391	15:28:24.4	29:41:25.3	20.28	21.16	19.63	20.73	94	1.86	0.1142 ± 0.0003	8.5 ± 1.4	···	2.1 ± 0.4	···
CB-25.5081	15:28:25.4	28:12:16.1	20.21	21.33	20.29	20.92	95	1.83	0.2385 ± 0.0003	20.8 ± 1.1	···	7.2 ± 0.3	4.3 ± 0.4
CB-29.4898	15:28:25.6	31:00:42.4	20.61	21.54	19.81	20.79	83	1.81	0.2767 ± 0.0003	···	···	-1.8 ± 0.4	···
CB-26.4633	15:28:26.3	29:09:14.0	19.06	19.85	18.98	19.90	132	1.87	0.0624 ± 0.0003	···	···	3.1 ± 0.4	10.4 ± 0.5
CB-25.4973	15:28:26.4	27:55:06.2	21.53	22.32	21.10	21.76	80	2.17	0.6740 ± 0.0010	···	···	···	···
CB-25.5020	15:28:26.6	28:09:49.0	17.00	18.60	16.45	18.03	471	3.14	0.0669 ± 0.0003	8.0 ± 0.7	···	1.8 ± 0.1	0.9 ± 0.2
CB-29.4850	15:28:26.6	31:03:05.1	18.80	19.47	18.07	18.72	165	1.68	star	···	···	···	···
CB-27.4277	15:28:26.7	29:30:29.9	18.74	19.12	18.26	18.35	23	1.04	star	···	···	···	···
CB-27.4287	15:28:27.0	29:36:49.7	20.36	21.16	19.59	20.15	88	1.68	star	···	···	···	···
CB-27.4281	15:28:27.4	29:38:43.4	18.75	20.11	18.87	20.21	233	2.68	0.0659 ± 0.0003	19.3 ± 2.2	-2.1 ± 0.4	3.5 ± 0.2	5.7 ± 0.3
CB-25.4961	15:28:27.5	28:01:08.4	19.57	20.92	20.01	21.28	138	2.65	0.0744 ± 0.0003	18.6 ± 2.4	···	···	4.1 ± 0.5
CB-29.4804	15:28:28.0	31:09:02.6	16.99	19.48	16.65	18.88	676	4.83	0.1050 ± 0.0003	···	···	···	···
CB-25.4891	15:28:28.5	27:55:06.5	19.30	20.16	18.84	19.84	118	1.86	0.0729 ± 0.0003	···	···	···	···
CB-27.4231	15:28:28.7	29:37:20.4	20.25	21.25	19.38	20.23	115	2.07	star	···	···	···	···
CB-25.4946	15:28:28.8	28:11:30.0	22.09	22.72	21.63	22.21	25	1.16	0.4356 ± 0.0004	5.6 ± 1.2	···	···	···
CB-25.4846	15:28:29.4	27:54:40.8	18.99	20.15	18.51	19.73	197	2.21	0.0761 ± 0.0003	···	-4.7 ± 0.7	-4.9 ± 0.6	···
CB-29.4714	15:28:29.4	31:03:12.2	21.61	22.33	20.50	21.61	63	1.47	0.4419 ± 0.0003	11.6 ± 1.8	···	···	···
CB-29.4743	15:28:29.6	31:11:13.3	17.94	19.49	17.39	18.75	395	3.11	0.1350 ± 0.0010	···	···	···	···
CB-25.4888	15:28:29.6	28:06:16.1	18.00	19.11	17.37	18.39	96	1.89	0.0737 ± 0.0003	···	···	-3.2 ± 0.4	···
CB-27.4225	15:28:29.7	29:47:31.4	21.93	22.27	21.09	21.68	25	1.12	0.2768 ± 0.0003	41.1 ± 2.1	···	13.4 ± 0.7	9.7 ± 0.8
CB-25.4806	15:28:30.4	27:54:17.1	20.04	21.26	20.70	21.79	102	2.01	0.1655 ± 0.0003	42.5 ± 1.4	···	8.8 ± 0.6	40.2 ± 0.7
CB-29.4678	15:28:30.6	31:05:24.0	20.26	21.27	19.13	20.36	97	1.82	0.3286 ± 0.0003	···	···	···	···
CB-29.4616	15:28:31.6	31:01:55.3	19.58	20.46	19.55	20.49	80	1.73	0.3427 ± 0.0003	6.7 ± 0.6	···	···	···
CB-27.4102	15:28:31.7	29:30:52.2	15.64	17.36	14.08	15.33	843	3.39	star	···	···	···	···
CB-25.4755	15:28:32.5	28:05:00.2	20.41	21.37	20.37	21.31	86	1.69	0.4792 ± 0.0003	18.0 ± 1.0	···	···	···
CB-29.4596	15:28:32.7	31:10:18.5	19.14	20.33	18.72	19.91	142	2.19	0.1051 ± 0.0003	···	···	-2.1 ± 0.4	···
CB-27.4049	15:28:32.7	29:29:48.8	21.74	22.40	20.44	21.68	23	1.03	0.4174 ± 0.0003	36.8 ± 3.5	···	···	···
CB-25.4746	15:28:33.3	28:10:49.6	22.08	22.62	···	···	21	1.03	0.4360 ± 0.0003	31.0 ± 1.8	···	···	···
CB-26.4310	15:28:34.0	29:11:48.1	19.26	20.05	17.64	18.50	120	1.98	star	···	···	···	···

TABLE 2.5—*Continued*

Object	RA (1950)	Dec. (1950)	g_{tot}	g_{core}	r_{tot}	r_{core}	Area (□″)	irl (″)	z	W_λ([O II]) (Å)	W_λ(Hδ) (Å)	W_λ(Hβ) (Å)	W_λ([O III]5007) (Å)
CB-25.4689	15:28:34.2	28:06:08.1	19.12	20.07	18.25	19.25	133	1.96	0.1483 ± 0.0003	···	···	10.3 ± 0.4	···
CB-25.4667	15:28:34.4	28:01:07.0	18.06	19.68	17.75	19.22	391	3.35	0.1482 ± 0.0003	8.6 ± 0.5	···	···	1.0 ± 0.2
CB-25.4672	15:28:35.0	28:09:34.0	16.27	18.98	16.19	18.52	1055	5.83	0.0682 ± 0.0003	16.0 ± 3.3	···	···	3.1 ± 0.3
CB-27.4021	15:28:35.1	29:47:13.7	21.09	21.93	21.24	21.93	62	1.54	0.1852 ± 0.0003	26.4 ± 4.4	···	···	···
CB-99.17	15:28:35.6	29:10:10.7	···	···	21.23	21.91	29	1.39	0.4245 ± 0.0007	···	···	···	···
CB-25.4635	15:28:35.8	28:05:14.1	18.96	20.08	18.88	19.74	195	2.18	0.0800 ± 0.0003	···	···	-1.6 ± 0.3	···
CB-27.3971	15:28:35.9	29:42:58.1	18.99	21.39	19.51	21.37	301	3.86	0.0580 ± 0.0010	···	-12.5 ± 1.7	···	···
CB-25.4588	15:28:36.4	28:01:24.8	20.45	21.23	19.40	20.82	33	1.38	0.3748 ± 0.0003	20.3 ± 0.8	···	···	···
CB-26.4151	15:28:36.8	29:01:33.7	20.11	21.28	19.87	21.51	111	2.25	0.1117 ± 0.0003	19.7 ± 3.1	···	4.8 ± 1.0	···
CB-27.3897	15:28:37.1	29:35:44.2	21.54	22.12	21.37	21.60	57	1.36	star	···	···	···	···
CB-26.4167	15:28:37.2	29:11:32.3	18.38	19.91	18.61	20.07	247	2.71	0.0863 ± 0.0003	···	-7.0 ± 1.7	···	4.4 ± 0.5
CB-26.4114	15:28:37.8	29:03:37.9	17.82	19.64	17.30	19.10	407	3.30	0.0840 ± 0.0003	···	···	-2.3 ± 0.5	···
CB-25.4516	15:28:38.1	28:00:43.0	20.00	20.79	19.81	20.81	116	1.81	0.2419 ± 0.0003	47.6 ± 0.7	···	14.4 ± 0.3	20.5 ± 0.3
CB-25.4545	15:28:38.1	28:09:01.2	18.78	19.88	18.38	19.56	200	2.15	0.0689 ± 0.0003	···	···	-2.8 ± 0.5	···
CB-27.3869	15:28:38.5	29:40:57.6	21.03	21.60	20.12	21.61	80	1.61	0.1755 ± 0.0003	50.1 ± 1.5	···	9.1 ± 0.6	···
CB-25.4447	15:28:38.9	27:56:35.1	19.54	20.56	18.79	19.88	181	2.02	0.1818 ± 0.0003	···	···	-2.4 ± 0.5	···
CB-26.4078	15:28:39.1	29:06:41.2	18.34	19.11	17.23	18.17	189	1.83	star	···	···	···	···
CB-27.3836	15:28:39.2	29:38:23.4	17.28	18.86	16.69	18.05	531	3.53	0.0607 ± 0.0003	···	···	-2.0 ± 0.2	···
CB-27.3834	15:28:39.3	29:37:58.1	17.89	19.56	17.60	19.31	315	3.07	0.1140 ± 0.0003	4.0 ± 0.9	-3.2 ± 0.6	···	···
CB-25.4437	15:28:40.0	28:06:43.2	18.82	19.91	18.27	19.45	183	2.12	0.0716 ± 0.0003	···	···	-3.0 ± 0.4	···
CB-00.24	15:28:40.0	29:05:51.2	···	···	21.07	21.83	32	1.56	star	···	···	···	···
CB-26.4066	15:28:40.0	29:13:23.6	19.12	19.75	17.31	18.22	120	1.70	star	···	···	···	···
CB-27.3764	15:28:40.7	29:30:36.1	20.11	21.30	19.30	20.53	100	1.96	0.2279 ± 0.0003	···	···	-0.9 ± 0.1	···
CB-26.3998	15:28:41.4	29:05:02.1	18.04	19.43	17.40	18.77	378	2.94	0.0870 ± 0.0003	···	···	-2.5 ± 0.4	···
CB-26.4026	15:28:41.4	29:12:52.7	20.33	20.70	18.38	19.39	94	1.39	star	···	···	···	···
CB-25.4335	15:28:41.6	28:01:14.9	19.03	19.96	18.36	19.56	186	2.12	0.0747 ± 0.0003	···	···	···	···
CB-25.4366	15:28:41.7	28:09:08.3	18.75	19.83	18.49	19.78	196	2.16	0.1474 ± 0.0003	8.2 ± 0.6	···	···	···
CB-27.3765	15:28:42.0	29:44:39.1	20.42	21.45	19.99	21.35	78	1.85	0.2094 ± 0.0003	46.9 ± 1.9	···	···	11.3 ± 0.8
CB-27.3723	15:28:42.1	29:32:21.5	20.24	21.63	21.13	21.64	87	2.02	0.3112 ± 0.0003	7.9 ± 0.9	···	···	···
CB-25.4267	15:28:42.2	27:54:09.0	20.47	21.29	20.38	21.30	87	1.75	0.2994 ± 0.0003	37.2 ± 0.9	···	7.2 ± 0.5	···
CB-25.4314	15:28:42.6	28:06:06.7	18.87	20.55	18.85	20.60	239	2.99	0.1487 ± 0.0003	18.0 ± 1.7	-5.3 ± 1.0	···	2.1 ± 0.4
CB-26.3936	15:28:43.1	29:08:32.4	20.16	20.72	19.67	20.53	97	1.54	0.0829 ± 0.0003	···	···	-2.6 ± 0.5	···
CB-27.3677	15:28:43.5	29:33:43.0	20.36	21.26	19.10	20.53	88	1.74	0.3103 ± 0.0003	4.9 ± 0.5	-2.0 ± 0.4	···	···
CB-26.3893	15:28:43.9	29:07:19.1	18.89	20.04	18.87	20.08	92	1.88	0.0708 ± 0.0003	11.1 ± 1.6	···	···	2.0 ± 0.3
CB-27.3692	15:28:43.9	29:41:24.6	18.77	19.90	18.82	20.10	206	2.23	0.1116 ± 0.0003	21.4 ± 0.6	-4.5 ± 0.6	4.2 ± 0.2	···
CB-27.3658	15:28:44.4	29:35:49.8	21.74	22.14	20.56	21.65	24	1.14	0.3294 ± 0.0003	13.8 ± 0.9	···	2.4 ± 0.4	···
CB-26.3869	15:28:44.4	29:09:30.6	18.20	19.66	17.59	19.02	235	2.74	0.0704 ± 0.0003	···	···	···	4.0 ± 0.4
CB-26.3843	15:28:44.7	29:06:26.2	18.68	19.30	17.56	18.34	186	1.75	star	···	···	···	···
CB-25.4180	15:28:45.1	28:05:55.6	19.83	20.93	20.35	21.34	110	2.03	0.0672 ± 0.0003	···	···	···	3.4 ± 0.5
CB-27.3653	15:28:45.3	29:42:57.9	17.00	18.05	16.14	17.25	348	2.29	star	···	···	···	···
CB-26.3791	15:28:45.5	29:03:52.4	19.93	20.83	19.81	20.89	122	1.96	0.1417 ± 0.0003	···	···	5.6 ± 0.5	5.9 ± 0.6
CB-26.3813	15:28:45.6	29:08:29.6	18.29	19.85	17.65	19.32	304	3.37	0.0804 ± 0.0003	···	···	···	···
CB-25.4150	15:28:45.9	28:07:03.3	19.20	20.35	18.57	20.02	117	2.13	0.2607 ± 0.0003	20.4 ± 0.7	···	6.4 ± 0.3	15.9 ± 0.3
CB-26.3728	15:28:47.1	29:03:54.7	19.07	20.02	18.56	19.77	134	1.97	0.1414 ± 0.0003	11.2 ± 1.3	-2.3 ± 0.6	···	···
CB-26.3738	15:28:47.4	29:10:00.3	19.19	19.84	17.49	18.30	115	1.65	star	···	···	···	···

TABLE 2.5—*Continued*

Object	RA (1950)	Dec. (1950)	g_{tot}	g_{core}	r_{tot}	r_{core}	Area (□″)	irl (″)	z	W_λ([O II]) (Å)	W_λ(Hδ) (Å)	W_λ(Hβ) (Å)	W_λ([O III]5007) (Å)
CB-25.4082	15:28:47.6	28:07:45.6	18.22	19.58	17.98	19.40	236	2.56	0.0730 ± 0.0003	12.0 ± 2.3	···	3.3 ± 0.3	···
CB-25.3990	15:28:48.0	27:54:33.3	22.41	22.87	···	···	20	1.17	0.6020 ± 0.0003	42.5 ± 1.5	···	···	···
CB-26.3684	15:28:48.1	29:02:31.3	20.58	21.71	19.95	20.98	90	1.89	0.3405 ± 0.0003	10.0 ± 1.0	···	···	···
CB-25.3986	15:28:48.7	28:00:22.9	20.52	21.52	19.87	21.14	80	1.81	0.4099 ± 0.0003	22.4 ± 0.8	···	···	···
CB-27.3524	15:28:48.7	29:42:19.6	21.74	22.49	21.43	21.69	30	1.33	star	···	···	···	···
CB-25.4015	15:28:48.8	28:06:17.5	16.58	18.32	15.96	17.69	485	3.93	0.0718 ± 0.0003	9.9 ± 0.7	···	···	1.2 ± 0.2
CB-26.3637	15:28:49.4	29:03:52.5	17.96	19.44	17.55	18.93	384	2.94	0.1323 ± 0.0003	···	···	···	···
CB-27.3442	15:28:49.4	29:32:58.4	15.98	17.52	13.81	15.29	633	3.10	star	···	···	···	···
CB-25.3934	15:28:49.7	27:58:29.9	20.14	21.83	20.53	21.57	113	2.55	0.1994 ± 0.0003	22.5 ± 2.0	···	2.8 ± 0.5	···
CB-27.3487	15:28:49.7	29:43:28.4	20.33	21.15	19.51	20.99	96	1.77	0.2970 ± 0.0003	23.0 ± 0.8	···	4.3 ± 0.3	···
CB-25.3945	15:28:50.5	28:10:18.9	17.98	19.49	17.74	19.01	125	2.14	0.0734 ± 0.0003	···	···	3.2 ± 0.2	42.7 ± 0.2
CB-27.3355	15:28:51.0	29:29:21.6	20.26	20.60	21.09	21.05	32	1.21	star	···	···	···	···
CB-25.3900	15:28:51.0	28:05:12.9	19.68	20.96	19.41	20.64	182	2.36	0.0721 ± 0.0003	···	-5.1 ± 1.2	···	···
CB-25.3844	15:28:51.1	27:54:30.5	18.98	20.21	19.12	20.24	197	2.32	0.1993 ± 0.0003	13.5 ± 0.8	···	3.6 ± 0.3	1.5 ± 0.2
CB-27.3415	15:28:51.5	29:47:26.3	19.59	20.85	18.70	20.14	146	2.63	0.2094 ± 0.0003	···	-4.3 ± 0.5	···	···
CB-26.3540	15:28:52.1	29:03:47.5	20.24	21.06	19.61	20.78	99	1.84	0.0824 ± 0.0003	···	···	-2.4 ± 0.4	···
CB-26.3548	15:28:52.8	29:13:36.8	21.80	22.07	20.74	20.97	34	1.18	star	···	···	···	···
CB-25.3803	15:28:52.9	28:04:23.9	18.73	19.91	17.89	19.15	212	2.32	0.1489 ± 0.0003	···	···	···	···
CB-26.3503	15:28:53.0	29:05:33.1	18.34	19.53	17.52	18.72	312	2.64	0.0827 ± 0.0003	···	···	-1.5 ± 0.3	···
CB-25.3776	15:28:53.1	28:00:22.3	19.18	20.44	18.69	19.84	199	2.28	0.2205 ± 0.0003	4.7 ± 0.6	-2.8 ± 0.4	···	···
CB-27.3322	15:28:53.8	29:48:25.8	19.59	20.60	19.13	20.30	133	2.12	0.0659 ± 0.0003	···	-3.0 ± 0.7	···	···
CB-27.3265	15:28:53.9	29:35:21.7	20.40	21.29	20.42	21.28	96	1.90	0.3385 ± 0.0003	42.9 ± 0.9	···	···	···
CB-26.3438	15:28:54.4	29:00:28.2	18.84	19.99	17.69	18.89	102	1.91	0.2153 ± 0.0003	···	-1.4 ± 0.3	-3.7 ± 0.3	···
CB-27.3267	15:28:54.8	29:44:53.0	20.52	21.97	21.65	22.07	74	1.98	0.0658 ± 0.0003	···	···	13.5 ± 1.9	18.7 ± 2.5
CB-26.3453	15:28:55.2	29:12:44.9	18.06	19.44	17.67	19.18	206	2.39	0.0831 ± 0.0003	8.0 ± 1.8	-5.2 ± 1.0	1.4 ± 0.2	···
CB-27.3221	15:28:55.2	29:36:12.3	20.08	20.88	19.48	20.62	96	1.79	0.3381 ± 0.0003	18.5 ± 0.7	-4.1 ± 0.8	···	···
CB-25.3699	15:28:55.5	28:06:35.2	20.52	21.41	19.39	20.46	85	1.73	0.3230 ± 0.0003	···	···	-2.0 ± 0.3	···
CB-26.3397	15:28:55.6	29:02:57.5	19.11	19.83	18.57	19.47	103	1.69	star	···	···	···	···
CB-27.3216	15:28:55.9	29:42:03.7	18.91	19.90	18.66	19.92	191	2.06	0.1130 ± 0.0003	10.5 ± 0.5	-2.9 ± 0.5	4.3 ± 0.1	···
CB-25.3673	15:28:56.1	28:08:32.5	19.07	20.42	19.01	20.36	161	2.44	0.1490 ± 0.0003	21.9 ± 1.7	-2.4 ± 0.5	···	···
CB-26.3360	15:28:56.5	29:01:56.8	18.39	19.79	17.81	19.22	276	2.77	0.0828 ± 0.0003	···	···	···	···
CB-27.3171	15:28:56.6	29:37:18.8	20.49	21.71	21.17	22.07	103	2.40	0.1137 ± 0.0003	12.9 ± 1.3	-4.9 ± 1.1	2.6 ± 0.6	···
CB-26.3398	15:28:56.7	29:14:17.3	20.82	21.89	19.87	20.67	71	1.77	0.3433 ± 0.0003	···	···	···	···
CB-25.3625	15:28:56.7	28:00:28.0	19.62	20.62	18.88	19.55	126	2.02	star	···	···	···	···
CB-26.3343	15:28:57.3	29:07:18.6	20.67	21.11	19.64	20.35	105	1.62	0.1763 ± 0.0003	···	···	···	···
CB-26.3330	15:28:57.5	29:07:40.6	18.29	19.72	17.11	18.79	78	1.71	0.1760 ± 0.0003	···	···	-1.1 ± 0.2	···
CB-27.3103	15:28:57.7	29:32:25.5	20.97	21.37	20.51	21.15	90	1.57	star	···	···	···	···
CB-26.3277	15:28:58.5	29:06:26.6	21.02	21.60	20.25	20.94	66	1.43	star	···	···	···	···
CB-27.3059	15:28:58.7	29:33:30.7	19.53	20.83	19.61	21.20	138	2.31	0.1136 ± 0.0003	15.5 ± 1.1	···	2.4 ± 0.3	···
CB-25.3579	15:28:59.0	28:11:03.9	18.74	19.94	19.27	20.77	184	2.26	0.0713 ± 0.0003	46.0 ± 1.4	···	23.1 ± 0.3	129.5 ± 0.3
CB-26.3282	15:28:59.2	29:13:58.9	17.21	18.79	16.82	18.30	498	3.25	0.0856 ± 0.0003	···	-4.4 ± 0.5	···	···
CB-27.3061	15:28:59.3	29:40:27.0	18.61	20.04	17.58	18.97	258	2.72	0.2181 ± 0.0003	···	···	···	···
CB-25.3528	15:28:59.5	28:02:17.6	17.24	18.76	16.53	17.98	427	3.51	0.0735 ± 0.0003	···	-1.2 ± 0.3	-2.5 ± 0.3	···
CB-26.3228	15:28:59.6	29:02:57.2	19.78	20.62	19.17	20.24	133	2.00	0.0827 ± 0.0003	···	···	···	···
CB-27.2989	15:29:00.2	29:34:01.5	19.18	20.23	18.50	19.60	187	2.10	0.1132 ± 0.0003	···	···	-1.2 ± 0.3	···

TABLE 2.5—*Continued*

Object	RA (1950)	Dec. (1950)	g_{tot}	g_{core}	r_{tot}	r_{core}	Area (□″)	irl (″)	z	W_λ([O II]) (Å)	W_λ(Hδ) (Å)	W_λ(Hβ) (Å)	W_λ([O III]5007) (Å)
CB-26.3186	15:29:00.7	29:03:59.3	19.95	20.79	19.47	20.46	101	1.89	0.0828 ± 0.0003	···	···	···	···
CB-25.3454	15:29:00.9	27:56:22.7	22.19	22.82	21.55	21.47	18	1.31	star	···	···	···	···
CB-27.2985	15:29:01.0	29:41:23.1	19.33	20.58	18.71	19.87	35	1.41	0.2154 ± 0.0003	6.1 ± 0.6	···	···	1.2 ± 0.3
CB-27.2961	15:29:01.2	29:34:25.4	18.88	20.14	19.10	20.32	209	2.47	0.0666 ± 0.0003	34.5 ± 0.9	-1.9 ± 0.3	8.0 ± 0.2	21.4 ± 0.2
CB-25.3446	15:29:01.6	28:01:26.6	19.48	20.34	18.98	20.13	118	1.89	0.1487 ± 0.0003	11.5 ± 1.8	···	···	···
CB-26.3168	15:29:01.6	29:08:18.6	18.87	20.38	18.73	20.24	256	2.92	0.0821 ± 0.0003	···	···	···	···
CB-25.3480	15:29:01.9	28:12:56.1	18.32	19.83	17.35	18.95	405	3.28	0.2240 ± 0.0003	···	-3.6 ± 0.5	-4.2 ± 0.4	···
CB-26.3170	15:29:01.9	29:12:29.9	16.96	19.41	17.08	19.56	533	4.43	0.0533 ± 0.0003	11.9 ± 1.4	···	3.7 ± 0.4	4.1 ± 0.4
CB-27.2933	15:29:02.1	29:39:00.5	20.21	21.12	19.78	20.70	90	1.73	0.2213 ± 0.0003	19.4 ± 0.5	-4.9 ± 0.7	7.3 ± 0.3	2.8 ± 0.3
CB-27.2881	15:29:02.6	29:30:21.3	19.47	20.77	20.08	21.11	159	2.65	0.0666 ± 0.0003	···	···	···	5.1 ± 0.4
CB-26.3072	15:29:02.9	28:58:21.0	21.30	22.64	20.28	21.48	68	1.83	0.5109 ± 0.0003	47.7 ± 3.2	···	···	···
CB-26.3116	15:29:03.6	29:17:29.9	18.52	19.83	17.87	19.22	265	3.06	0.0664 ± 0.0003	···	···	1.4 ± 0.3	1.3 ± 0.3
CB-27.2882	15:29:03.8	29:41:02.7	19.18	20.86	18.67	20.26	155	2.89	0.3009 ± 0.0003	7.5 ± 0.7	-4.9 ± 0.7	···	···
CB-26.3064	15:29:03.9	29:06:00.9	19.48	20.73	19.67	20.86	181	2.23	0.1320 ± 0.0003	···	-4.2 ± 0.7	2.2 ± 0.4	···
CB-25.3311	15:29:04.4	28:04:24.3	19.42	20.34	19.13	20.22	130	1.91	0.1989 ± 0.0003	5.4 ± 0.5	···	2.1 ± 0.2	1.5 ± 0.3
CB-25.3284	15:29:04.4	27:57:22.1	20.53	21.77	20.47	21.06	72	1.60	star	···	···	···	···
CB-27.2813	15:29:04.7	29:32:45.3	20.36	21.31	19.74	20.42	98	1.83	star	···	···	···	···
CB-26.3015	15:29:05.2	29:05:40.8	18.71	20.01	18.36	19.76	237	2.76	0.0822 ± 0.0003	···	-3.8 ± 0.7	···	···
CB-27.2828	15:29:05.2	29:41:19.1	19.90	20.87	19.55	20.78	95	1.77	0.2167 ± 0.0003	10.9 ± 0.5	-4.4 ± 0.7	4.3 ± 0.2	1.5 ± 0.2
CB-26.3011	15:29:05.6	29:08:42.6	18.81	19.86	18.37	19.38	199	2.13	0.0857 ± 0.0003	···	···	···	···
CB-27.2775	15:29:06.1	29:36:27.2	20.32	21.47	19.75	21.10	98	1.96	0.2199 ± 0.0003	5.4 ± 0.5	···	1.2 ± 0.2	···
CB-25.3208	15:29:06.3	28:02:00.5	20.35	21.56	19.23	20.45	104	2.09	0.3247 ± 0.0003	4.1 ± 0.6	···	···	···
CB-26.2961	15:29:06.5	29:03:31.0	22.37	22.63	21.09	21.81	22	1.02	star	···	···	···	···
CB-27.2762	15:29:06.8	29:39:36.2	18.71	20.70	18.61	20.58	250	3.15	0.0602 ± 0.0003	6.9 ± 1.4	···	···	···
CB-26.2972	15:29:07.0	29:10:13.0	19.49	20.43	19.26	20.04	120	1.95	0.0820 ± 0.0003	···	···	-1.7 ± 0.3	···
CB-26.2958	15:29:07.8	29:14:41.3	19.05	19.87	17.43	18.29	143	1.91	star	···	···	···	···
CB-27.2721	15:29:07.9	29:39:14.4	22.42	22.81	21.36	22.00	19	0.88	0.6710 ± 0.0010	···	···	···	···
CB-25.3151	15:29:08.1	28:07:34.9	20.17	20.91	18.99	19.67	67	1.50	star	···	···	···	···
CB-25.3109	15:29:08.1	27:57:04.3	17.22	18.77	16.59	18.05	256	2.81	0.0675 ± 0.0003	···	···	-2.5 ± 0.3	···
CB-25.3164	15:29:08.3	28:11:41.9	19.27	20.38	18.86	20.25	190	2.21	0.2246 ± 0.0003	12.6 ± 0.6	-2.4 ± 0.5	2.9 ± 0.2	2.4 ± 0.3
CB-26.2880	15:29:09.2	29:08:41.1	19.20	20.19	18.79	19.72	147	2.12	0.0841 ± 0.0003	···	···	-3.2 ± 0.6	···
CB-27.2685	15:29:09.4	29:44:41.3	21.35	22.00	20.19	21.79	31	1.33	0.3084 ± 0.0003	81.4 ± 1.8	···	13.4 ± 0.7	···
CB-26.2858	15:29:09.5	29:04:55.8	18.82	19.85	18.13	19.12	191	2.12	0.1097 ± 0.0003	···	···	-1.8 ± 0.3	···
CB-25.3063	15:29:09.6	28:02:15.7	17.99	19.29	17.18	18.55	280	2.74	0.0735 ± 0.0003	···	-2.4 ± 0.6	···	···
CB-25.3101	15:29:09.8	28:11:59.4	20.33	21.35	19.95	21.01	80	1.65	0.2639 ± 0.0003	11.2 ± 1.9	···	4.5 ± 0.7	···
CB-26.2840	15:29:10.2	29:08:05.8	21.07	22.20	20.23	21.69	80	2.07	0.3770 ± 0.0010	···	···	···	···
CB-26.2809	15:29:10.4	28:59:00.9	17.87	19.49	17.81	19.61	300	2.93	0.0964 ± 0.0003	27.5 ± 0.7	···	7.9 ± 0.2	4.9 ± 0.3
CB-26.2810	15:29:10.9	29:05:46.7	18.04	19.23	17.12	18.37	286	2.60	0.0830 ± 0.0003	···	···	-2.1 ± 0.3	···
CB-25.3005	15:29:11.0	28:00:22.4	21.26	22.11	21.39	22.09	58	1.41	0.3530 ± 0.0003	16.3 ± 1.5	···	···	···
CB-27.2535	15:29:11.4	29:32:41.2	19.41	20.48	19.91	20.94	140	2.19	0.0969 ± 0.0003	25.7 ± 0.8	-2.1 ± 0.4	···	10.7 ± 0.2
CB-25.3001	15:29:11.6	28:06:00.7	16.43	18.24	15.84	17.62	796	4.07	0.0764 ± 0.0003	···	···	···	···
CB-26.2796	15:29:11.7	29:08:35.4	18.72	20.07	18.94	20.58	124	2.36	0.0836 ± 0.0003	···	···	···	23.4 ± 1.7
CB-27.2546	15:29:11.7	29:39:11.6	18.74	20.15	17.88	19.08	286	3.21	0.1127 ± 0.0003	···	···	···	···
CB-25.2921	15:29:12.5	27:57:01.0	17.76	19.60	18.02	19.73	314	3.33	0.0676 ± 0.0003	29.4 ± 1.7	···	2.5 ± 0.2	2.7 ± 0.2
CB-25.2970	15:29:12.5	28:07:07.1	19.19	20.08	18.49	19.54	123	1.89	0.1489 ± 0.0003	11.1 ± 0.7	-2.1 ± 0.4	···	1.1 ± 0.2

TABLE 2.5—*Continued*

Object	RA (1950)	Dec. (1950)	g_{tot}	g_{core}	r_{tot}	r_{core}	Area (□″)	irl (″)	z	W_λ([O II]) (Å)	W_λ(Hδ) (Å)	W_λ(Hβ) (Å)	W_λ([O III]5007) (Å)
CB-26.2764	15:29:12.5	29:09:27.1	17.01	18.61	16.40	17.95	500	3.32	0.0817 ± 0.0003	···	-1.5 ± 0.4	-2.9 ± 0.2	···
CB-26.2739	15:29:12.9	29:06:42.1	19.35	20.61	18.67	19.95	195	2.44	0.1778 ± 0.0003	9.7 ± 2.0	-2.4 ± 0.5	···	···
CB-27.2488	15:29:13.4	29:42:30.4	20.20	21.04	20.33	21.14	95	1.77	0.2174 ± 0.0003	15.4 ± 1.1	···	···	2.9 ± 0.5
CB-26.2741	15:29:13.7	29:15:10.6	19.87	21.06	18.27	19.84	127	2.14	0.3402 ± 0.0003	···	···	···	···
CB-27.2458	15:29:14.4	29:45:37.9	20.26	21.01	20.08	20.99	94	1.71	0.1620 ± 0.0003	26.7 ± 2.8	···	6.4 ± 0.4	1.7 ± 0.4
CB-26.2700	15:29:14.7	29:14:04.1	19.72	20.73	19.63	20.77	181	2.26	0.0831 ± 0.0003	···	···	2.5 ± 0.6	2.8 ± 0.5
CB-26.2668	15:29:14.8	29:05:30.1	19.39	20.81	19.57	21.35	178	2.40	0.1320 ± 0.0003	35.2 ± 1.6	···	10.9 ± 0.9	34.9 ± 0.9
CB-25.2868	15:29:15.0	28:08:03.1	18.75	19.94	18.49	19.63	231	2.40	0.0741 ± 0.0003	···	-3.5 ± 0.8	-2.0 ± 0.3	···
CB-27.2366	15:29:15.8	29:33:49.4	18.93	20.74	18.91	21.00	303	3.54	0.0653 ± 0.0003	42.3 ± 6.7	···	···	5.5 ± 0.5
CB-26.2596	15:29:15.9	28:59:09.6	19.09	19.76	17.27	18.14	123	1.70	star	···	···	···	···
CB-27.2358	15:29:16.8	29:41:15.7	21.05	22.03	21.61	22.31	69	1.60	0.2162 ± 0.0003	···	···	···	25.9 ± 0.7
CB-26.2577	15:29:17.1	29:06:05.9	19.40	20.11	18.49	19.43	117	1.73	0.0858 ± 0.0003	···	-1.9 ± 0.4	-2.9 ± 0.3	···
CB-25.2774	15:29:17.2	28:10:24.4	19.15	19.99	18.43	19.19	171	2.13	star	···	···	···	···
1529+2815	15:29:17.4	28:15:39.0	16.04	18.07	15.48	17.43	850	4.67	0.0741 ± 0.0002	···	···	···	···
CB-26.2570	15:29:17.6	29:08:41.9	17.76	19.04	17.44	18.84	291	2.60	0.0850 ± 0.0003	10.0 ± 0.7	-3.7 ± 0.5	2.2 ± 0.2	0.8 ± 0.2
CB-25.2689	15:29:17.9	28:01:52.5	19.39	21.05	19.34	20.74	207	2.72	0.1752 ± 0.0003	···	-3.6 ± 0.9	···	···
CB-27.2298	15:29:18.0	29:39:17.0	19.22	20.65	19.12	20.39	190	2.52	0.2957 ± 0.0003	14.4 ± 1.1	-5.3 ± 1.0	···	···
CB-26.2535	15:29:18.5	29:07:42.5	20.40	21.14	19.63	20.95	98	1.83	0.1778 ± 0.0003	24.1 ± 4.8	···	···	···
CB-25.2669	15:29:18.6	28:02:53.3	21.87	22.28	20.84	21.76	23	1.02	0.2208 ± 0.0003	20.2 ± 3.3	···	···	3.6 ± 0.8
CB-26.2497	15:29:19.0	29:03:19.2	18.30	19.97	18.23	19.90	308	3.45	0.1148 ± 0.0003	33.4 ± 1.7	-3.6 ± 0.8	2.4 ± 0.3	···
CB-25.2650	15:29:19.4	28:05:26.7	19.94	21.34	20.21	21.80	106	2.18	0.0745 ± 0.0003	···	···	···	15.9 ± 1.0
CB-26.2508	15:29:19.4	29:09:58.4	18.00	19.81	17.45	19.19	448	3.76	0.0869 ± 0.0003	···	···	-1.1 ± 0.3	···
CB-27.2246	15:29:19.6	29:39:17.5	19.76	20.59	19.53	20.68	122	1.92	star	···	···	···	···
CB-26.2455	15:29:20.8	29:09:13.6	17.64	19.31	17.17	18.59	196	2.49	0.0854 ± 0.0003	···	···	-1.9 ± 0.2	···
CB-26.2406	15:29:21.9	29:08:25.9	18.77	19.69	17.91	18.94	204	2.05	0.0862 ± 0.0003	···	···	-2.9 ± 0.3	···
CB-27.2128	15:29:23.5	29:40:54.2	20.04	21.10	20.04	21.37	105	1.96	0.1121 ± 0.0003	41.2 ± 2.2	···	5.8 ± 0.4	···
CB-25.2492	15:29:23.7	28:07:31.7	22.24	22.81	20.93	21.94	25	1.08	star	···	···	···	···
CB-26.2317	15:29:23.9	29:04:27.4	20.60	21.58	20.24	21.37	114	2.79	0.3410 ± 0.0010	···	···	···	···
CB-26.2312	15:29:24.2	29:07:32.7	19.30	20.13	18.46	19.50	124	1.81	0.0858 ± 0.0003	···	···	-1.8 ± 0.4	···
CB-26.2276	15:29:24.4	28:59:05.8	19.82	20.84	19.68	20.91	118	2.17	0.0628 ± 0.0003	···	-6.6 ± 1.0	···	3.5 ± 0.6
CB-26.2254	15:29:25.5	29:06:39.9	20.95	21.49	19.93	20.81	79	1.42	0.1999 ± 0.0003	···	···	···	3.4 ± 0.3
CB-26.2177	15:29:26.7	29:00:50.7	20.57	21.16	21.03	21.77	73	1.52	2.9010 ± 0.0010	···	···	···	···
CB-26.2238	15:29:26.8	29:13:51.3	19.08	19.78	18.24	19.28	68	1.37	star	···	···	···	···
CB-26.2162	15:29:27.5	29:04:17.8	18.62	19.40	17.65	18.51	86	1.58	star	···	···	···	···
CB-26.2167	15:29:28.0	29:11:04.1	17.58	19.16	16.94	18.40	518	3.34	0.0858 ± 0.0003	···	···	-2.7 ± 0.4	···
CB-26.2126	15:29:28.8	29:07:26.5	19.50	20.73	18.72	20.00	146	2.36	0.2000 ± 0.0003	20.0 ± 1.3	···	2.0 ± 0.3	16.7 ± 0.3
CB-25.2253	15:29:29.4	28:06:42.5	19.05	20.66	19.24	20.41	217	2.79	0.2233 ± 0.0003	···	···	···	···
CB-26.2037	15:29:30.2	28:58:57.7	20.11	20.79	19.17	19.95	90	1.56	star	···	···	···	···
CB-26.2038	15:29:31.4	29:10:25.7	19.66	20.56	19.01	20.02	123	2.01	0.0823 ± 0.0003	···	···	-2.1 ± 0.5	···
CB-26.2027	15:29:32.0	29:14:05.4	18.74	19.75	17.91	19.10	218	2.24	0.0840 ± 0.0003	···	···	-2.2 ± 0.3	···
CB-26.1921	15:29:33.0	29:01:46.8	19.52	20.17	17.89	18.72	70	1.47	star	···	···	···	···
CB-26.1860	15:29:34.2	29:03:22.4	17.53	19.14	16.89	18.35	559	3.55	0.0818 ± 0.0003	···	···	-2.4 ± 0.3	···
CB-26.1871	15:29:35.0	29:13:59.3	19.11	19.86	18.18	18.91	119	1.71	star	···	···	···	···
CB-26.1832	15:29:35.7	29:11:24.7	22.46	22.84	21.04	21.85	17	0.86	star	···	···	···	···
CB-26.1816	15:29:35.7	29:07:06.7	21.07	21.95	20.60	21.91	73	1.67	0.2003 ± 0.0003	···	···	7.4 ± 1.2	12.2 ± 1.6

TABLE 2.5—*Continued*

Object	RA (1950)	Dec. (1950)	g_{tot}	g_{core}	r_{tot}	r_{core}	Area (□″)	irl (″)	z	W_λ([O II]) (Å)	W_λ(Hδ) (Å)	W_λ(Hβ) (Å)	W_λ([O III]5007) (Å)
CB-26.1736	15:29:37.0	28:59:20.2	22.20	22.54	21.94	22.40	16	0.89	0.5610 ± 0.0010	···	···	···	···
CB-26.1778	15:29:37.1	29:10:49.3	20.16	21.16	20.16	21.16	103	1.90	0.0844 ± 0.0003	···	···	···	···
CB-26.1716	15:29:37.8	29:02:29.8	19.28	19.95	17.68	18.46	116	1.63	star	···	···	···	···
CB-26.1634	15:29:39.7	29:04:54.4	18.86	19.78	17.98	19.11	36	1.34	star	···	···	···	···
CB-26.1614	15:29:40.4	29:07:34.1	20.06	20.93	19.66	20.74	104	1.85	0.1770 ± 0.0003	14.2 ± 1.8	-3.7 ± 0.8	2.0 ± 0.3	···
CB-26.1647	15:29:40.6	29:14:40.1	19.08	20.37	19.15	20.55	222	2.54	0.0631 ± 0.0003	64.9 ± 6.8	···	···	4.0 ± 0.4
CB-26.1562	15:29:40.7	28:59:01.2	19.98	20.98	19.67	20.60	110	2.09	0.0797 ± 0.0003	···	···	···	···
CB-26.1525	15:29:41.8	29:02:38.1	19.65	20.71	19.58	20.69	120	2.21	0.0940 ± 0.0010	···	···	···	···
CB-26.1540	15:29:42.8	29:15:06.2	19.25	20.76	19.28	20.81	237	3.00	0.0842 ± 0.0003	···	···	···	···
CB-99.18	15:29:42.9	29:06:46.7	···	···	20.96	21.68	63	1.62	0.4515 ± 0.0003	···	···	···	···
CB-26.1468	15:29:43.7	29:04:00.6	20.61	21.11	19.41	19.85	81	1.41	star	···	···	···	···
CB-26.1456	15:29:45.1	29:13:13.1	21.42	21.96	20.36	20.90	34	1.32	star	···	···	···	···
CB-26.1385	15:29:46.0	29:07:15.3	19.80	21.18	20.38	21.62	119	2.32	0.0652 ± 0.0003	···	···	4.5 ± 0.6	10.0 ± 0.8
CB-26.1338	15:29:47.0	29:06:24.8	20.45	20.86	19.59	20.31	85	1.51	star	···	···	···	···
CB-26.1312	15:29:47.8	29:07:36.4	20.39	21.55	21.12	22.01	90	1.81	0.1150 ± 0.0003	···	···	12.9 ± 1.4	···
2092C-62	15:29:48.3	31:17:19.0	17.03	18.86	16.39	18.01	379	3.37	0.1059 ± 0.0001	···	···	···	···
CB-00.23	15:29:48.7	29:04:03.4	···	···	20.54	21.40	69	1.44	star	···	···	···	···
CB-26.1273	15:29:49.2	29:08:10.5	21.85	22.41	19.78	21.11	24	1.05	star	···	···	···	···
CB-26.1233	15:29:50.6	29:12:26.5	18.52	19.23	17.51	18.38	187	1.78	star	···	···	···	···
CB-26.1128	15:29:52.5	29:06:23.1	20.49	21.42	20.39	21.78	95	1.81	0.2143 ± 0.0003	···	···	···	7.4 ± 1.1
CB-26.1079	15:29:53.3	29:02:41.9	18.23	19.40	18.43	19.72	214	2.41	0.0861 ± 0.0003	35.7 ± 0.5	-1.5 ± 0.2	12.2 ± 0.1	46.2 ± 0.1
CB-26.1086	15:29:54.2	29:12:28.2	21.43	22.05	19.96	21.43	63	1.47	0.4604 ± 0.0006	···	···	···	···
CB-26.1012	15:29:55.2	29:08:31.1	18.78	19.43	17.84	18.67	177	1.71	star	···	···	···	···
CB-26.881	15:29:59.0	29:09:55.6	18.16	19.97	18.09	19.55	411	3.51	0.1762 ± 0.0003	4.5 ± 0.7	-2.0 ± 0.5	···	···
2092C-38	15:30:07.6	31:33:59.0	16.83	18.90	16.15	18.12	553	4.00	0.1066 ± 0.0001	···	···	···	···
2089-187	15:30:13.1	28:12:48.0	17.19	18.82	16.57	18.11	432	3.18	0.0700 ± 0.0001	···	···	···	···
1530+2807	15:30:17.7	28:07:22.0	16.23	18.32	15.69	17.60	958	4.91	0.0728 ± 0.0001	···	···	···	···
2089-165	15:30:23.5	28:11:24.0	16.81	18.54	16.04	17.73	242	2.88	0.0710 ± 0.0002	···	···	···	···
2089-168	15:30:23.7	28:09:14.0	17.24	18.82	16.56	18.05	596	3.48	0.0756 ± 0.0001	···	···	···	···
2089-146	15:30:31.5	28:12:13.0	17.32	19.00	16.68	18.20	510	3.54	0.0737 ± 0.0001	···	···	···	···
2092C-15	15:30:32.7	31:37:59.0	16.78	18.68	16.63	18.51	301	3.35	0.0792 ± 0.0003	···	···	···	···
2092C-12	15:30:36.5	31:17:16.0	17.29	18.79	16.60	18.00	470	3.19	0.0532 ± 0.0001	···	···	···	···
2089-132	15:30:38.7	28:05:24.0	16.33	19.18	16.19	18.66	961	7.27	0.0773 ± 0.0002	···	···	···	···
15307+2832	15:30:41.0	28:32:02.0	15.30	18.24	15.09	17.85	1569	6.88	0.0724 ± 0.0002	···	···	···	···
CB-35.8966	15:30:42.4	31:16:27.6	18.16	19.42	17.48	18.66	260	2.60	0.0696 ± 0.0003	···	···	···	···
1530+2812	15:30:44.5	28:12:25.0	15.20	17.58	14.64	17.10	985	5.34	0.0733 ± 0.0001	···	···	···	···
CB-35.8871	15:30:45.2	31:17:00.1	20.83	21.25	19.30	20.16	80	1.41	star	···	···	···	···
CB-35.8581	15:30:51.8	31:10:15.4	19.08	20.29	18.38	19.75	186	2.25	star	···	···	···	···
1530+2803	15:30:53.7	28:03:44.0	16.15	18.10	15.50	17.49	229	2.83	0.0717 ± 0.0001	···	···	···	···
CB-35.8518	15:30:53.9	31:15:14.8	19.70	20.80	18.65	19.93	125	2.13	0.2155 ± 0.0003	···	···	···	···
CB-35.8500	15:30:54.1	31:11:45.5	20.69	21.43	18.98	20.50	22	1.03	star	···	···	···	···
CB-35.8486	15:30:55.7	31:21:16.1	18.38	19.76	18.23	19.75	232	2.72	0.0709 ± 0.0003	7.6 ± 1.5	···	···	6.7 ± 0.5
CB-35.8406	15:30:57.5	31:16:01.7	20.67	21.61	20.04	20.74	82	1.71	0.2785 ± 0.0003	···	···	···	···
CB-35.8356	15:30:59.0	31:16:42.8	18.29	19.00	16.70	17.75	192	1.79	star	···	···	···	···
CB-35.8320	15:30:59.5	31:11:42.7	17.61	18.51	16.50	17.51	246	2.08	star	···	···	···	···

TABLE 2.5—*Continued*

Object	RA (1950)	Dec.	g_{tot}	g_{core}	r_{tot}	r_{core}	Area (□″)	irl (″)	z	W_λ([O II]) (Å)	W_λ(Hδ) (Å)	W_λ(Hβ) (Å)	W_λ([O III]5007) (Å)
CB-35.8348	15:31:00.0	31:21:11.0	19.58	20.69	19.35	20.59	132	2.15	0.0654 ± 0.0003	...	...	...	...
CB-35.8258	15:31:00.6	31:09:42.3	19.32	20.18	18.71	19.74	166	1.93	0.0986 ± 0.0003	...	...	-1.6 ± 0.4	...
CB-35.8192	15:31:03.3	31:19:22.6	17.66	19.02	16.94	18.25	310	2.80	0.0675 ± 0.0003	...	...	-2.4 ± 0.4	...
CB-35.8129	15:31:03.4	31:10:42.8	19.20	19.85	17.68	18.46	118	1.68	star	...	...	...	...
CB-35.8090	15:31:05.2	31:19:24.6	17.82	19.32	17.18	18.56	208	2.50	0.0679 ± 0.0003	...	...	...	...
CB-35.8003	15:31:06.2	31:10:18.5	20.59	21.07	19.39	20.26	86	1.52	star	...	...	...	...
CB-35.8057	15:31:06.5	31:22:46.1	17.46	18.99	16.58	18.17	532	3.30	0.1334 ± 0.0003	...	...	-1.9 ± 0.3	...
CB-35.7890	15:31:08.7	31:07:48.4	18.07	19.38	18.41	19.84	253	2.59	0.0655 ± 0.0003	...	...	8.4 ± 0.6	14.3 ± 0.6
CB-35.7920	15:31:09.3	31:17:44.1	18.98	20.06	18.28	19.45	192	2.24	0.0672 ± 0.0003	...	...	-2.6 ± 0.4	...
CB-35.7853	15:31:09.9	31:10:44.6	20.30	21.02	19.54	20.25	85	1.61	0.0860 ± 0.0010	...	...	...	...
CB-35.7861	15:31:10.2	31:13:57.8	17.83	19.07	16.96	18.17	280	2.64	0.0664 ± 0.0003	...	...	-2.2 ± 0.3	...
2089-71	15:31:10.5	28:14:47.0	17.37	19.34	17.21	18.89	315	3.97	0.0692 ± 0.0002	...	...	...	...
CB-35.7833	15:31:11.4	31:18:58.2	18.49	19.37	17.59	18.56	199	1.99	0.0656 ± 0.0003	...	...	-2.8 ± 0.4	...
CB-35.7731	15:31:12.3	31:09:51.4	19.29	20.02	18.54	19.38	121	1.69	star	...	...	...	...
CB-35.7790	15:31:12.5	31:20:03.1	17.65	18.88	16.79	18.06	158	2.26	0.0667 ± 0.0003	...	...	-3.0 ± 0.3	...
2092-184	15:31:13.3	31:19:52.0	16.76	18.56	16.16	17.85	424	3.55	0.0667 ± 0.0003	...	...	...	...
CB-35.7737	15:31:13.4	31:18:21.6	18.81	20.10	18.16	19.61	131	2.32	0.0650 ± 0.0003	...	...	-3.5 ± 0.5	...
2092-182	15:31:13.7	31:17:54.0	16.49	18.77	15.94	18.09	762	4.80	0.0573 ± 0.0003	...	...	...	...
1531+3118A	15:31:13.8	31:18:43.0	15.76	18.24	15.19	17.57	786	4.84	0.0673 ± 0.0002	...	...	...	...
CB-35.7625	15:31:13.8	31:04:41.9	18.00	19.33	17.18	18.45	342	2.81	0.0991 ± 0.0003	...	...	-2.6 ± 0.4	...
2092-17	15:31:14.0	31:13:56.0	17.32	18.94	16.66	18.16	458	3.28	0.0672 ± 0.0001	...	...	...	...
2089-66	15:31:14.1	28:14:20.0	17.39	19.19	16.79	18.46	486	3.70	0.0732 ± 0.0001	...	...	...	...
2089-65	15:31:14.2	28:14:46.0	17.81	19.30	17.07	18.54	399	3.04	0.0738 ± 0.0002	...	...	...	...
CB-35.7602	15:31:15.2	31:13:12.0	18.75	19.55	17.85	18.64	189	1.86	star	...	...	...	...
CB-35.7629	15:31:15.3	31:17:24.5	19.94	20.67	18.76	19.55	103	1.69	star	...	...	...	...
2089-64	15:31:15.5	28:14:02.0	16.83	18.47	16.20	17.78	787	3.77	0.0737 ± 0.0001	...	...	...	...
2092-179	15:31:15.7	31:26:28.0	17.11	19.16	16.71	18.41	581	4.37	0.1163 ± 0.0002	...	...	...	...
2089-62	15:31:16.0	28:16:59.0	17.50	19.14	16.93	18.51	295	3.39	0.0744 ± 0.0002	...	...	...	...
CB-35.7593	15:31:16.4	31:19:22.3	19.53	20.33	19.21	20.25	126	1.92	0.0684 ± 0.0003	...	...	2.6 ± 0.4	...
CB-35.7504	15:31:17.0	31:12:14.5	21.62	22.24	20.85	21.94	57	1.37	0.2840 ± 0.0010	...	...	...	...
CB-35.7566	15:31:17.1	31:22:10.2	18.73	19.99	18.86	20.12	241	2.48	0.0663 ± 0.0003	9.9 ± 1.3	...	2.9 ± 0.4	4.0 ± 0.4
CB-35.7482	15:31:18.7	31:22:45.2	16.24	18.26	15.70	17.65	791	4.38	0.0672 ± 0.0003	...	...	-2.1 ± 0.3	...
CB-35.7399	15:31:18.7	31:09:02.6	18.20	19.25	17.33	18.46	231	2.23	0.0658 ± 0.0003	...	...	-3.3 ± 0.4	...
CB-35.7428	15:31:19.7	31:19:34.4	17.59	19.09	16.92	18.46	42	1.72	0.0697 ± 0.0003	...	...	-3.8 ± 0.5	...
CB-35.7313	15:31:20.6	31:12:01.7	20.52	21.58	20.08	21.51	93	1.89	0.0616 ± 0.0003	...	...	...	...
CB-35.7350	15:31:20.7	31:16:54.9	17.06	18.92	16.49	18.18	552	3.68	0.0660 ± 0.0003	...	...	...	1.6 ± 0.3
CB-35.7269	15:31:21.5	31:11:14.3	17.23	18.88	16.53	18.11	478	3.61	0.0661 ± 0.0003	...	...	-2.5 ± 0.4	...
CB-35.7292	15:31:22.3	31:20:47.8	16.47	18.27	15.70	17.60	662	4.34	0.0628 ± 0.0003	...	...	-2.2 ± 0.3	...
CB-35.7210	15:31:22.8	31:12:46.9	18.33	19.72	17.84	19.18	280	2.90	0.0679 ± 0.0003	...	...	-1.3 ± 0.3	...
CB-35.7244	15:31:22.9	31:18:06.9	17.65	18.59	16.69	17.78	282	2.39	star	...	...	...	...
CB-35.7088	15:31:24.1	31:05:54.0	19.43	20.76	19.25	20.51	138	2.40	0.1720 ± 0.0003	16.3 ± 2.6	...	...	...
CB-35.7132	15:31:25.0	31:18:40.2	19.57	20.21	18.29	19.03	105	1.57	star	...	...	...	...
CB-35.7015	15:31:26.7	31:10:59.5	20.63	21.67	20.92	21.34	86	1.86	0.1570 ± 0.0010	...	...	...	...
CB-35.6973	15:31:26.8	31:05:39.8	20.52	21.35	20.59	21.36	88	1.76	0.2557 ± 0.0003	...	...	7.0 ± 1.6	13.6 ± 1.1
CB-35.7032	15:31:27.4	31:17:35.0	17.87	19.35	17.27	18.70	318	3.25	0.0680 ± 0.0003	...	...	-2.7 ± 0.4	...

TABLE 2.5—*Continued*

Object	RA (1950)	Dec. (1950)	g_{tot}	g_{core}	r_{tot}	r_{core}	Area (□″)	irl (″)	z	W_λ([O II]) (Å)	W_λ(Hδ) (Å)	W_λ(Hβ) (Å)	W_λ([O III]5007) (Å)
CB-35.6977	15:31:27.7	31:13:30.2	18.13	18.94	17.05	17.97	213	1.96	star	···	···	···	···
CB-35.6974	15:31:28.3	31:17:01.3	18.96	19.72	18.50	19.33	101	1.68	star	···	···	···	···
CB-35.6924	15:31:28.7	31:11:30.3	21.55	22.16	19.63	20.95	70	1.52	0.4212 ± 0.0003	7.1 ± 1.5	···	···	···
CB-35.6900	15:31:29.7	31:14:42.8	17.39	19.14	17.02	18.62	469	3.72	0.0691 ± 0.0003	···	···	-4.6 ± 0.5	···
2089-49	15:31:30.4	28:08:28.0	17.17	19.18	16.80	18.55	582	4.32	0.0729 ± 0.0002	···	···	···	···
CB-35.6810	15:31:30.5	31:06:42.7	19.05	20.26	18.95	20.13	199	2.39	0.0994 ± 0.0003	···	···	···	···
2092-155	15:31:31.9	31:16:06.0	17.79	19.45	17.43	18.83	333	3.32	0.0662 ± 0.0002	···	···	···	···
CB-35.6812	15:31:32.4	31:21:40.2	16.63	18.47	16.04	17.84	956	4.30	0.0694 ± 0.0003	···	···	-2.1 ± 0.3	···
2092-148	15:31:34.0	31:21:49.0	17.33	19.01	16.72	18.33	456	3.44	0.0652 ± 0.0002	···	···	···	···
CB-35.6636	15:31:34.3	31:07:12.3	19.20	19.89	18.08	18.83	117	1.65	star	···	···	···	···
CB-35.6594	15:31:34.9	31:04:19.4	20.22	21.03	19.19	20.02	92	1.64	star	···	···	···	···
CB-35.6670	15:31:35.5	31:21:59.8	19.07	20.22	18.59	19.83	181	2.21	0.1998 ± 0.0003	6.8 ± 0.7	···	2.5 ± 0.3	···
1531+2818	15:31:36.0	28:18:44.0	16.24	18.45	15.84	18.06	679	4.73	0.0187 ± 0.0001	···	···	···	···
CB-35.6545	15:31:36.2	31:07:43.8	20.09	21.35	19.92	21.73	116	2.29	0.4348 ± 0.0003	27.4 ± 4.9	···	···	···
CB-35.6567	15:31:36.7	31:15:02.0	18.05	19.44	17.45	18.80	306	2.89	0.0659 ± 0.0003	···	···	-2.8 ± 0.4	···
CB-35.6521	15:31:37.2	31:11:23.9	21.71	22.79	20.70	21.89	33	1.38	0.3660 ± 0.0010	···	···	···	···
2089-42	15:31:37.7	28:01:49.0	17.21	18.99	16.39	18.22	212	2.75	0.1192 ± 0.0001	···	···	···	···
CB-35.6446	15:31:38.5	31:08:29.6	18.11	18.84	16.83	17.82	194	1.78	star	···	···	···	···
CB-35.6404	15:31:39.5	31:11:11.5	18.65	19.98	18.44	19.78	228	2.48	0.0667 ± 0.0003	···	···	···	···
CB-35.6436	15:31:39.6	31:16:11.3	19.23	20.68	18.64	20.34	213	2.87	0.1160 ± 0.0003	···	···	···	···
CB-35.6365	15:31:40.7	31:13:49.2	19.30	21.04	19.47	21.43	213	2.83	0.0996 ± 0.0003	···	···	···	4.0 ± 1.0
CB-35.6316	15:31:41.6	31:11:48.4	17.13	18.72	17.10	18.70	404	3.04	0.0690 ± 0.0003	9.1 ± 0.7	-1.7 ± 0.3	8.1 ± 0.2	1.8 ± 0.2
CB-35.6323	15:31:42.0	31:15:28.5	19.46	20.31	18.81	19.80	134	1.97	0.0673 ± 0.0003	···	···	-1.9 ± 0.3	···
CB-35.6212	15:31:43.1	31:05:33.7	21.66	21.71	20.63	21.51	68	1.39	0.2704 ± 0.0003	···	···	10.1 ± 1.2	15.6 ± 1.2
CB-35.6230	15:31:43.7	31:13:10.8	20.12	20.76	19.60	20.72	102	1.71	0.0993 ± 0.0003	···	···	10.3 ± 0.6	19.0 ± 0.6
CB-35.6156	15:31:44.9	31:10:32.1	19.86	20.96	20.10	21.14	119	2.20	0.0624 ± 0.0003	···	···	3.4 ± 0.7	···
1531+3150	15:31:45.0	31:50:34.0	16.61	18.54	15.92	17.75	205	2.65	0.0900 ± 0.0001	···	···	···	···
CB-35.6200	15:31:45.5	31:21:44.7	18.48	19.20	17.57	18.43	190	1.79	star	···	···	···	···
CB-35.6097	15:31:46.2	31:10:02.2	19.09	20.24	18.32	19.48	204	2.28	0.1717 ± 0.0003	···	···	-2.3 ± 0.4	···
2092-113	15:31:47.1	31:51:33.0	16.79	18.42	16.05	17.66	532	3.45	0.0894 ± 0.0001	···	···	···	···
2089-33	15:31:48.3	28:08:45.0	16.62	18.97	16.39	18.30	784	4.96	0.0730 ± 0.0001	···	···	···	···
CB-35.5988	15:31:48.5	31:05:31.6	19.70	20.62	19.20	20.24	117	1.85	0.0686 ± 0.0003	···	···	···	···
CB-35.6034	15:31:49.0	31:18:45.5	18.98	20.01	18.45	19.65	193	2.10	0.1047 ± 0.0003	···	···	-4.1 ± 0.6	···
CB-35.5966	15:31:50.6	31:17:59.3	17.45	18.85	16.77	18.10	355	2.85	0.1032 ± 0.0003	···	···	-2.3 ± 0.2	···
CB-35.5919	15:31:51.5	31:15:42.1	18.65	19.37	17.49	18.36	130	1.77	star	···	···	···	···
CB-35.5828	15:31:52.8	31:09:04.8	19.11	19.75	18.03	18.86	128	1.68	star	···	···	···	···
CB-35.5799	15:31:53.4	31:07:11.6	17.60	19.54	17.66	19.56	426	3.56	0.0657 ± 0.0003	14.6 ± 1.5	···	4.8 ± 0.2	2.1 ± 0.2
2092-105	15:31:53.6	31:18:50.0	16.79	18.37	16.20	17.68	389	3.03	0.0654 ± 0.0001	···	···	···	···
15319+2730	15:31:54.0	27:30:00.0	15.13	18.20	15.10	18.02	1512	6.05	0.0341 ± 0.0001	···	···	···	···
CB-35.5805	15:31:54.2	31:13:42.5	18.19	19.50	17.82	19.01	258	2.61	0.1170 ± 0.0003	···	···	1.3 ± 0.2	···
CB-35.5790	15:31:55.4	31:20:08.5	17.12	18.66	16.38	17.85	478	3.39	0.0649 ± 0.0003	···	···	-2.7 ± 0.3	···
CB-35.5762	15:31:55.7	31:16:18.1	21.64	22.22	20.52	21.57	29	1.32	0.6244 ± 0.0003	···	···	···	···
CB-35.5644	15:31:57.4	31:06:58.8	19.00	19.61	18.44	19.13	128	1.67	star	···	···	···	···
CB-35.5600	15:31:59.5	31:13:43.2	19.94	20.89	19.08	20.48	114	2.04	0.3668 ± 0.0003	···	···	···	···
CB-35.5539	15:31:59.9	31:08:10.6	20.06	21.12	20.03	21.49	107	1.98	0.2098 ± 0.0003	···	···	···	···

TABLE 2.5—*Continued*

Object	RA (1950)	Dec. (1950)	g_{tot}	g_{core}	r_{tot}	r_{core}	Area (□″)	irl (″)	z	W_λ([O II]) (Å)	W_λ(Hδ) (Å)	W_λ(Hβ) (Å)	W_λ([O III]5007) (Å)
CB-35.5601	15:32:00.6	31:21:57.3	17.64	18.95	16.73	18.06	237	2.61	star	...	...	...	...
CB-35.5519	15:32:01.2	31:13:28.8	20.55	21.26	19.68	20.77	22	1.05	0.0790 ± 0.0010	...	...	...	...
CB-35.5521	15:32:01.5	31:16:33.3	20.38	21.13	19.75	20.35	77	1.76	0.2268 ± 0.0003	...	...	...	...
CB-35.5466	15:32:02.5	31:11:47.5	21.68	21.91	19.82	21.09	59	1.27	star	...	...	...	...
CB-35.5417	15:32:04.1	31:12:48.2	20.99	21.76	20.85	21.92	72	1.46	0.0694 ± 0.0003	...	...	...	15.4 ± 1.5
CB-35.5311	15:32:06.7	31:12:46.3	20.34	21.40	19.20	20.51	105	1.95	0.2812 ± 0.0003	...	...	...	...
1532+2813	15:32:07.0	28:13:27.0	16.38	18.38	15.85	17.69	947	5.26	0.0744 ± 0.0001	...	...	...	...
CB-35.5279	15:32:07.7	31:15:45.5	20.80	21.43	19.79	20.99	90	1.67	0.3788 ± 0.0003	22.6 ± 1.2	...	...	...
CB-35.5231	15:32:07.9	31:08:47.1	21.03	22.13	19.37	20.76	69	1.89	0.3778 ± 0.0003	16.5 ± 2.1	...	...	...
2092-91	15:32:08.2	31:23:51.0	17.33	18.87	16.70	18.13	326	3.14	0.0679 ± 0.0002	...	...	...	...
CB-35.5272	15:32:08.7	31:20:33.7	17.69	18.57	16.42	17.46	71	1.50	star	...	...	...	...
CB-35.5183	15:32:08.9	31:06:52.4	19.43	20.05	19.10	19.91	103	1.61	star	...	...	...	...
CB-35.5202	15:32:09.5	31:14:05.8	18.87	19.51	17.80	18.61	178	1.66	star	...	...	...	...
CB-35.5049	15:32:13.6	31:16:27.1	18.73	19.48	18.36	19.00	174	1.78	star	...	...	...	...
CB-35.4983	15:32:14.9	31:14:06.2	20.93	21.37	19.90	20.75	77	1.45	star	...	...	...	...
CB-35.4890	15:32:18.1	31:18:18.3	20.47	21.20	19.39	20.26	85	1.56	0.2276 ± 0.0003	...	...	...	...
1532+3152	15:32:37.0	31:52:03.0	16.68	18.62	15.95	17.74	942	4.81	0.1070 ± 0.0002	...	...	...	...
1532+3145	15:32:39.0	31:45:50.0	15.44	18.13	14.98	17.50	1242	6.13	0.0656 ± 0.0001	...	...	...	...
15327+3114	15:32:44.0	31:13:05.0	15.81	19.28	16.38	19.51	98	2.35	0.0062 ± 0.0000	...	...	...	...
N5958	15:32:45.0	28:49:16.0	12.61	16.69	12.86	16.93	3696	11.06	0.0067 ± 0.0001	...	...	...	...
N5961	15:33:14.7	31:01:47.0	13.33	16.71	13.36	16.20	2340	10.07	0.0059 ± 0.0001	...	...	...	...
15333+3058	15:33:15.9	30:58:09.0	14.74	17.78	14.38	17.26	517	7.20	0.0315 ± 0.0000	...	...	...	...
2092-27	15:33:19.2	31:20:02.0	16.85	19.03	16.56	18.32	904	5.34	0.0807 ± 0.0001	...	...	...	...
15335+3142	15:33:32.0	31:41:11.0	15.66	18.46	15.28	17.93	1248	7.87	0.0536 ± 0.0001	...	...	...	...
15343+3051	15:34:17.7	30:50:47.0	14.68	17.11	15.04	17.58	1610	6.04	0.0055 ± 0.0002	...	...	...	...

TABLE 2.6

UNIDENTIFED OBJECTS

Object	RA (1950)	Dec.	g_{tot}	g_{core}	r_{tot}	r_{core}	Area (□″)	irl (″)
CB-1.7719	15:11:03.0	28:04:28.8	20.26	21.29	19.79	20.82	47	2.14
CB-1.7693	15:11:03.7	28:05:35.3	21.50	22.36	20.37	21.64	19	1.56
CB-2.7850	15:11:05.0	28:33:43.4	20.71	21.55	19.99	21.01	31	1.66
CB-1.7629	15:11:06.0	28:06:38.3	20.78	21.18	19.78	20.86	30	1.46
CB-1.7557	15:11:08.6	28:07:58.8	18.67	20.09	18.36	19.59	111	2.84
CB-1.7487	15:11:09.4	28:28:01.6	20.09	21.11	18.97	19.94	48	1.96
CB-2.7647	15:11:09.6	28:43:31.1	21.47	21.76	20.61	22.00	8	1.01
CB-1.7496	15:11:10.4	28:07:16.9	20.64	21.59	19.98	20.99	35	1.71
CB-00.12	15:11:11.2	28:26:12.5	...	...	21.89	22.19	16	1.45
CB-1.7390	15:11:12.2	28:29:34.7	19.08	20.13	18.46	19.57	66	2.15
CB-2.7570	15:11:12.3	28:35:40.8	20.64	21.59	20.12	21.29	40	2.08
CB-1.7429	15:11:12.4	28:05:55.5	19.68	20.80	19.99	21.47	54	2.07
CB-1.7350	15:11:13.5	28:29:18.1	20.44	21.35	20.34	21.45	51	2.05
CB-1.7395	15:11:13.7	28:08:16.0	19.92	20.80	18.94	20.09	50	1.85
CB-00.15	15:11:15.3	28:40:32.1	...	...	21.42	22.16	23	1.74
CB-00.13	15:11:15.3	28:30:27.2	...	...	20.95	22.07	22	2.10
CB-2.7413	15:11:16.4	28:34:24.3	18.02	20.77	18.82	21.00	86	3.43
CB-2.7350	15:11:17.5	28:43:49.5	18.08	20.42	18.17	20.33	135	3.83
CB-00.3	15:11:17.5	28:14:16.3	...	...	21.16	22.01	18	1.40
CB-2.7325	15:11:18.4	28:38:19.4	20.48	21.06	19.98	20.80	16	1.37
CB-2.7276	15:11:19.3	28:41:20.0	22.20	22.77	21.17	22.20	12	1.39
CB-1.7168	15:11:19.5	28:30:20.8	19.51	20.92	19.34	20.49	75	2.51
CB-2.7264	15:11:20.0	28:38:21.4	22.33	22.65	21.09	21.74	7	0.93
CB-1.7191	15:11:20.7	28:04:01.5	19.06	20.40	18.78	19.96	79	2.58
CB-1.7129	15:11:22.4	28:04:22.7	21.02	21.51	20.01	21.25	32	1.55
CB-1.7055	15:11:22.4	28:28:59.8	20.25	21.08	20.12	20.88	38	1.75
CB-1.7077	15:11:23.3	28:10:14.8	20.23	21.18	20.28	21.21	44	1.77
CB-1.7002	15:11:23.7	28:30:35.6	21.31	22.21	20.99	21.83	19	1.47
CB-1.7049	15:11:24.6	28:00:25.2	18.65	19.84	19.20	20.18	82	2.20
CB-1.6843	15:11:27.9	28:26:58.3	18.80	19.67	18.68	19.59	41	1.77
CB-1.6851	15:11:28.7	28:14:03.5	19.67	20.75	19.55	20.76	53	1.99
CB-1.6758	15:11:29.3	28:30:53.7	18.65	20.21	18.17	19.67	120	2.93
CB-2.6883	15:11:29.5	28:35:01.8	19.24	20.58	18.63	19.89	87	2.73
CB-1.6757	15:11:30.3	28:18:43.2	19.78	20.80	19.77	20.83	53	2.20
CB-1.6725	15:11:30.4	28:30:36.8	20.84	21.81	19.41	20.66	31	1.77
CB-1.6784	15:11:30.7	28:05:39.3	21.03	22.18	20.24	21.56	26	1.72
CB-2.6828	15:11:30.8	28:39:16.3	22.16	22.66	20.12	21.38	8	1.05
CB-1.6726	15:11:31.9	28:08:06.1	19.24	20.34	18.80	19.98	55	2.11
CB-00.14	15:11:32.8	28:38:42.9	...	...	21.58	22.05	19	1.37
CB-1.6676	15:11:33.3	28:07:34.4	20.39	21.49	20.53	21.73	44	2.20
CB-1.6599	15:11:33.4	28:32:35.1	20.84	21.60	21.24	21.82	39	1.87
CB-1.6576	15:11:34.1	28:29:51.1	21.28	22.28	21.85	21.89	27	1.65
CB-2.6705	15:11:34.3	28:38:18.5	20.27	21.99	19.78	21.11	46	2.37
CB-1.6598	15:11:34.5	28:17:34.0	21.20	21.52	21.03	21.84	24	1.38
CB-1.6585	15:11:35.0	28:12:39.3	22.65	22.58	20.67	21.60	7	1.21
CB-3.6651	15:11:35.6	29:34:22.5	19.67	20.17	18.15	18.71	18	1.42
CB-1.6572	15:11:36.0	28:01:20.7	22.13	22.79	19.91	21.07	13	1.29
CB-1.6526	15:11:37.1	28:03:55.9	18.58	19.58	17.92	18.89	20	1.39
CB-3.6592	15:11:37.1	29:35:01.5	17.24	18.21	15.88	16.78	108	2.15
CB-2.6591	15:11:37.5	28:39:01.5	18.46	20.20	18.71	20.35	137	3.26
CB-1.6428	15:11:37.9	28:19:00.5	18.35	19.82	17.88	19.27	125	2.95
CB-1.6446	15:11:38.4	28:05:04.6	19.09	20.49	...	...	72	2.23
CB-00.36	15:11:39.1	29:39:44.3	...	...	20.80	21.68	25	2.12
CB-1.6402	15:11:39.6	28:03:48.8	19.99	20.90	20.10	20.91	51	1.95
CB-2.6505	15:11:39.7	28:39:00.1	18.08	19.68	17.92	19.68	103	3.07
CB-1.6301	15:11:40.3	28:26:18.3	21.56	21.61	20.24	20.57	7	0.95
CB-2.6473	15:11:40.3	28:37:16.2	20.23	21.43	19.97	21.25	48	2.17
CB-1.6293	15:11:41.3	28:13:06.1	16.89	19.06	16.28	18.28	394	5.19
CB-3.6427	15:11:41.5	29:31:17.3	18.29	20.14	18.20	19.80	175	3.72
CB-1.6285	15:11:41.7	28:08:31.3	20.08	20.93	19.73	20.97	43	1.84
CB-1.6205	15:11:42.2	28:28:40.6	19.99	21.40	20.31	21.68	59	2.33
CB-3.6406	15:11:42.4	29:25:55.9	20.81	21.24	19.46	20.21	19	1.30

TABLE 2.6—*Continued*

Object	RA (1950)	Dec. (1950)	g_{tot}	g_{core}	r_{tot}	r_{core}	Area (□″)	irl (″)
CB-1.6253	15:11:43.0	28:02:16.3	20.72	21.44	19.77	20.57	28	1.61
CB-3.6366	15:11:43.5	29:29:30.2	21.44	22.43	21.03	21.83	21	1.45
CB-3.6328	15:11:43.8	29:37:55.9	19.29	20.44	18.88	20.13	67	2.25
CB-2.6342	15:11:44.0	28:40:28.8	20.74	21.82	20.22	21.25	37	2.06
CB-1.6059	15:11:45.1	28:32:17.9	21.53	22.22	21.79	21.85	14	1.63
CB-1.6104	15:11:45.1	28:17:17.0	20.76	21.67	19.95	21.17	28	1.63
CB-2.6246	15:11:46.0	28:43:24.3	22.29	22.63	21.04	21.92	12	1.17
CB-1.6028	15:11:46.3	28:27:01.3	21.14	21.98	20.21	21.63	32	1.75
CB-1.6065	15:11:46.7	28:07:23.4	17.90	19.31	17.98	19.26	47	2.10
CB-3.6209	15:11:46.8	29:43:16.9	19.19	20.73	18.38	19.95	108	3.12
CB-00.16	15:11:46.9	28:35:19.2	...	...	21.13	21.89	15	1.57
CB-1.5990	15:11:46.9	28:29:49.5	20.70	21.67	20.56	21.52	20	1.60
CB-3.6229	15:11:47.1	29:29:11.4	19.94	21.32	20.39	21.62	57	2.33
CB-1.6025	15:11:47.7	28:06:24.9	20.84	21.50	20.09	20.81	22	1.36
CB-1.5957	15:11:47.8	28:30:38.9	17.97	19.03	17.22	18.17	110	2.47
CB-1.6008	15:11:48.6	27:59:49.5	20.71	21.40	20.56	21.87	30	1.60
CB-3.6126	15:11:48.9	29:43:37.7	21.43	21.82	20.22	21.00	15	1.16
CB-3.6164	15:11:49.0	29:26:53.2	20.03	21.40	18.50	20.08	52	2.33
CB-1.5952	15:11:49.8	28:00:30.4	17.81	19.58	17.82	19.46	167	3.27
CB-3.6124	15:11:49.8	29:30:57.8	20.65	21.30	19.94	21.04	33	1.58
CB-1.5867	15:11:49.9	28:26:20.3	19.30	20.71	18.51	19.64	88	2.58
CB-3.6081	15:11:51.4	29:27:03.9	20.05	20.76	20.34	21.07	42	1.63
CB-00.11	15:11:51.7	28:29:17.3	...	...	20.83	21.89	25	1.85
CB-3.6031	15:11:52.5	29:27:50.1	20.56	21.28	20.06	21.37	35	1.75
CB-3.5974	15:11:54.5	29:32:25.1	18.97	20.44	18.38	19.64	96	2.70
CB-3.5908	15:11:56.2	29:34:13.6	19.89	20.97	19.70	21.35	59	2.20
CB-3.5865	15:11:56.9	29:37:52.0	20.76	21.48	20.02	21.15	30	1.65
CB-3.5716	15:12:00.9	29:34:13.8	20.98	21.93	20.64	21.66	11	1.38
CB-3.5709	15:12:01.0	29:36:03.3	18.89	20.54	18.32	20.08	72	2.96
CB-00.35	15:12:02.4	29:30:26.5	...	...	21.11	21.94	19	1.61
CB-3.5642	15:12:02.7	29:35:52.5	20.83	21.43	20.58	21.21	9	1.12
CB-00.34	15:12:03.7	29:33:00.4	...	...	20.87	21.56	16	1.45
CB-00.33	15:12:05.3	29:34:26.0	...	...	20.33	21.12	27	1.56
CB-3.5465	15:12:08.4	29:33:55.2	18.63	19.36	17.49	18.46	32	1.58
CB-3.5422	15:12:09.3	29:33:16.0	20.42	20.87	18.80	19.93	6	0.83
CB-3.5346	15:12:10.9	29:39:54.5	21.05	21.73	21.13	21.83	25	1.47
CB-00.32	15:12:11.4	29:30:46.7	...	...	19.49	20.58	18	1.54
CB-3.5270	15:12:14.0	29:31:56.1	20.11	20.54	19.03	20.03	8	0.99
CB-3.5192	15:12:16.0	29:41:54.2	18.96	20.04	18.85	19.98	76	2.11
CB-3.5178	15:12:17.2	29:32:26.1	19.22	20.38	19.04	20.15	65	2.17
CB-3.5115	15:12:18.7	29:32:20.6	18.47	19.32	17.66	18.38	74	1.87
CB-3.5029	15:12:20.7	29:31:12.8	19.06	20.10	18.42	19.57	62	2.14
CB-00.31	15:12:22.7	29:26:49.1	...	...	18.80	20.08	50	2.22
CB-3.4869	15:12:24.2	29:35:13.6	18.90	19.70	18.15	19.25	73	1.93
CB-4.4379	15:12:32.4	30:47:11.9	20.45	21.52	19.76	20.64	46	2.73
CB-4.4346	15:12:33.8	30:42:08.9	19.97	21.53	19.76	20.76	66	2.81
CB-4.4290	15:12:35.0	30:45:38.1	19.41	20.66	18.75	19.99	56	2.30
CB-6.4403	15:12:36.1	32:07:09.0	20.77	21.42	20.40	21.72	31	1.61
CB-4.4234	15:12:37.2	30:34:48.9	19.80	20.96	20.56	20.87	54	2.08
CB-6.4284	15:12:38.6	32:12:01.2	19.60	20.61	18.38	19.54	63	2.05
CB-6.4253	15:12:39.3	32:10:42.0	20.15	20.79	19.70	21.03	49	1.61
CB-6.4279	15:12:39.6	32:00:04.2	19.66	20.61	18.62	19.55	29	1.73
CB-4.4129	15:12:40.0	30:31:32.8	18.59	19.68	18.29	19.40	94	2.25
CB-6.4184	15:12:40.9	32:10:44.7	21.79	22.16	19.88	21.52	16	1.22
CB-4.4090	15:12:41.1	30:31:56.5	19.24	20.07	18.72	19.21	62	1.90
CB-4.4058	15:12:41.8	30:34:02.9	20.01	20.69	19.51	20.45	45	1.68
CB-4.4017	15:12:42.9	30:34:50.4	20.15	21.24	21.02	21.58	40	1.89
CB-6.4015	15:12:44.6	32:10:19.2	21.27	22.56	20.54	21.22	20	2.00
CB-4.3924	15:12:45.1	30:34:00.1	21.55	22.31	20.44	21.63	20	1.57
CB-4.3879	15:12:46.3	30:40:38.0	21.61	22.44	21.18	21.73	16	1.43
CB-4.3885	15:12:46.7	30:28:49.1	19.56	20.82	18.62	19.85	66	2.26
CB-00.47	15:12:46.8	31:33:27.6	...	...	21.33	21.87	15	1.40

TABLE 2.6—*Continued*

Object	RA (1950)	Dec. (1950)	g_{tot}	g_{core}	r_{tot}	r_{core}	Area (□″)	irl (″)
CB-6.3917	15:12:46.8	32:12:17.7	19.86	20.98	19.44	20.31	53	2.05
CB-5.3674	15:12:48.5	31:27:58.4	18.16	18.98	17.67	18.43	67	1.88
CB-5.3591	15:12:50.4	31:30:42.3	20.01	21.20	19.95	21.14	63	2.39
CB-4.3721	15:12:50.8	30:36:45.3	21.78	22.09	21.28	21.75	12	1.26
CB-00.42	15:12:50.8	31:23:54.8	...	...	20.73	21.88	19	1.54
CB-6.3751	15:12:51.1	32:09:17.9	21.99	22.73	21.27	21.87	14	1.30
CB-6.3773	15:12:51.2	31:57:15.3	20.47	22.12	21.36	22.07	42	2.29
CB-5.3539	15:12:51.4	31:31:48.7	20.56	21.68	19.98	21.23	48	2.48
CB-5.3571	15:12:51.8	31:16:04.5	21.02	21.79	19.94	21.20	31	1.70
CB-4.3630	15:12:52.7	30:44:45.1	21.25	22.56	21.23	22.08	16	1.39
CB-6.3662	15:12:53.0	32:12:42.1	21.24	22.05	19.50	20.69	20	1.47
CB-5.3492	15:12:53.5	31:18:37.0	20.75	21.68	19.50	20.78	32	1.71
CB-4.3605	15:12:53.7	30:34:31.9	19.24	20.89	19.78	21.33	70	2.95
CB-6.3631	15:12:54.1	32:05:54.8	20.58	21.39	...	...	47	1.87
CB-5.3459	15:12:54.4	31:15:54.4	18.48	19.24	17.38	18.23	82	1.82
CB-5.3404	15:12:55.0	31:31:06.1	19.63	20.98	19.80	21.09	62	2.26
CB-6.3566	15:12:55.5	32:04:31.7	18.58	20.45	18.07	20.01	120	3.80
CB-5.3393	15:12:56.0	31:19:18.3	21.32	21.70	21.31	21.92	25	1.52
CB-6.3498	15:12:56.5	32:13:33.6	21.22	22.08	20.50	21.70	25	1.62
CB-5.3366	15:12:56.8	31:16:07.4	19.07	19.72	18.22	18.97	56	1.68
CB-5.3339	15:12:57.0	31:26:43.7	22.22	22.60	21.07	21.74	6	0.88
CB-00.50	15:12:57.3	32:05:03.1	...	...	21.11	22.21	27	1.73
CB-6.3494	15:12:57.7	31:56:26.1	19.67	20.57	19.11	20.23	58	1.98
CB-4.3374	15:12:58.0	30:43:49.8	21.43	22.46	21.61	22.13	27	2.42
CB-5.3293	15:12:58.1	31:24:06.1	20.69	21.52	...	...	34	1.74
CB-00.49	15:12:58.8	32:07:36.1	...	...	20.47	21.88	28	1.91
CB-6.3341	15:13:00.3	32:09:02.9	21.73	22.24	19.86	21.06	18	1.39
CB-4.3250	15:13:00.8	30:45:30.4	21.52	22.07	20.12	21.34	22	1.43
CB-00.41	15:13:03.4	30:30:03.3	...	...	22.08	22.54	13	1.24
CB-6.3198	15:13:03.6	32:12:46.6	18.35	19.71	18.27	19.74	110	2.63
CB-5.3045	15:13:04.6	31:24:44.2	19.87	20.93	19.09	20.10	55	2.04
CB-6.3192	15:13:04.9	31:54:29.2	22.62	22.44	21.49	21.85	7	0.92
CB-6.3096	15:13:06.2	32:07:08.3	21.75	22.01	21.36	21.63	18	1.25
CB-5.2955	15:13:06.5	31:26:46.0	21.53	22.26	20.92	22.03	14	1.38
CB-6.3058	15:13:06.8	32:11:04.1	19.99	21.04	19.38	20.24	51	2.05
CB-6.3022	15:13:07.8	32:08:19.5	19.99	21.13	19.63	21.19	48	2.13
CB-00.44	15:13:07.9	31:20:47.8	...	...	21.07	22.04	14	1.68
CB-00.1	15:13:08.4	30:40:03.1	22.16	22.79	20.53	22.17	11	1.33
CB-6.2965	15:13:08.9	32:13:46.0	17.99	18.83	16.77	17.74	89	1.94
CB-5.2821	15:13:10.4	31:24:35.0	21.19	22.09	20.64	21.33	21	1.42
CB-6.2908	15:13:10.6	32:10:50.5	19.67	20.40	19.23	19.92	50	1.69
CB-5.2791	15:13:11.5	31:18:43.6	19.45	20.44	18.81	19.77	63	2.14
CB-00.48	15:13:11.5	32:00:36.6	...	...	20.77	21.92	18	1.44
CB-6.2855	15:13:11.7	32:13:56.8	21.26	22.41	20.07	20.95	23	1.87
CB-4.2824	15:13:11.8	30:44:12.5	21.27	22.11	20.37	21.81	22	1.55
CB-00.51	15:13:12.8	32:09:46.2	...	...	20.95	21.82	27	1.78
CB-6.2827	15:13:13.3	31:56:42.3	20.80	21.59	19.39	20.44	27	1.59
CB-5.2666	15:13:14.6	31:24:08.5	20.92	21.75	20.59	21.63	22	1.71
CB-4.2750	15:13:14.8	30:30:04.5	21.10	22.31	20.91	21.68	23	1.98
CB-00.46	15:13:15.0	31:28:57.4	...	...	21.21	22.00	18	1.71
CB-6.2689	15:13:15.7	32:07:54.9	21.80	22.57	21.33	21.77	13	1.30
CB-5.2582	15:13:16.1	31:27:33.3	20.05	21.09	20.35	21.23	55	2.07
CB-5.2587	15:13:16.6	31:19:11.5	18.85	19.93	18.15	19.20	84	2.25
CB-6.2665	15:13:16.7	31:58:49.5	20.89	21.75	20.22	21.74	29	1.74
CB-4.2642	15:13:17.1	30:31:06.8	21.20	21.68	22.78	21.87	16	1.44
CB-4.2613	15:13:17.1	30:39:09.9	22.24	22.64	21.52	21.99	10	1.09
CB-6.2588	15:13:17.6	32:14:19.3	21.05	21.84	21.00	21.67	34	1.80
CB-00.39	15:13:18.5	30:31:24.5	...	...	21.53	22.13	9	1.41
CB-6.2547	15:13:18.8	32:09:21.9	20.19	20.91	19.70	20.35	51	1.82
CB-00.45	15:13:19.9	31:19:26.0	...	...	21.41	21.90	15	1.41
CB-6.2492	15:13:20.3	32:08:52.5	20.89	22.12	20.11	21.18	37	2.06
CB-6.2517	15:13:20.4	31:56:15.0	18.99	20.05	18.35	19.43	89	2.29

TABLE 2.6—*Continued*

Object	RA (1950)	Dec.	g_{tot}	g_{core}	r_{tot}	r_{core}	Area (□″)	irl (″)
CB-4.2480	15:13:20.5	30:31:48.7	21.25	22.03	19.98	21.17	23	1.68
CB-6.2479	15:13:21.1	32:03:15.1	21.08	22.05	20.50	21.56	27	1.68
CB-4.2421	15:13:21.2	30:38:58.0	22.33	22.94	20.97	22.10	7	0.97
CB-5.2306	15:13:22.6	31:30:04.8	21.88	22.46	20.23	21.02	16	1.29
CB-6.2422	15:13:22.6	32:05:30.5	19.85	20.83	19.94	20.37	17	1.64
CB-5.2314	15:13:22.8	31:22:53.1	21.63	22.02	19.72	20.56	20	1.40
CB-4.2355	15:13:23.2	30:29:40.4	21.36	21.93	20.06	21.31	21	1.47
CB-5.2270	15:13:23.4	31:32:17.6	22.70	22.58	21.36	21.98	15	1.20
CB-4.2308	15:13:23.7	30:45:12.2	19.51	20.53	19.44	20.61	59	2.05
CB-6.2377	15:13:23.8	32:00:30.0	20.42	21.28	19.92	21.11	40	1.82
CB-4.2305	15:13:24.3	30:34:38.6	20.24	21.08	20.40	21.48	47	1.89
CB-6.2294	15:13:25.0	32:13:47.3	20.40	21.46	20.08	21.34	36	1.84
CB-5.2214	15:13:25.3	31:22:41.6	21.70	22.13	20.38	21.23	12	1.07
CB-4.2244	15:13:25.5	30:44:25.5	18.06	19.39	17.27	18.55	106	2.63
CB-6.2292	15:13:25.9	31:57:59.2	18.30	19.58	17.43	18.68	111	2.78
CB-4.2212	15:13:26.6	30:41:25.5	19.38	20.29	18.48	19.53	61	1.92
CB-00.43	15:13:26.7	31:20:51.1	...	...	19.95	21.31	40	2.39
CB-6.2201	15:13:27.8	32:04:54.2	20.38	21.59	20.24	21.13	37	1.85
CB-5.2036	15:13:28.6	31:33:03.9	19.84	21.12	20.07	20.97	58	2.42
CB-6.2104	15:13:29.5	32:10:59.0	20.86	22.11	19.47	20.46	33	1.94
CB-6.2124	15:13:29.5	32:02:55.7	22.19	22.61	20.23	21.51	6	0.92
CB-5.1971	15:13:30.4	31:23:00.8	19.99	21.39	20.26	21.44	64	2.50
CB-5.1926	15:13:30.6	31:34:44.3	20.39	21.81	21.00	21.76	46	2.27
CB-6.2055	15:13:30.8	32:05:03.1	16.56	19.22	16.50	18.90	391	5.24
CB-5.1954	15:13:31.0	31:19:39.9	18.68	19.52	18.06	18.81	27	1.59
CB-6.2008	15:13:31.7	32:04:26.4	17.96	19.48	17.79	19.29	145	3.08
CB-5.1895	15:13:32.4	31:17:51.6	21.00	22.20	21.23	21.52	21	1.72
CB-5.1843	15:13:33.3	31:22:33.1	17.31	19.16	16.85	18.45	276	3.86
CB-5.1797	15:13:34.6	31:24:57.5	19.77	20.80	18.47	20.02	56	2.06
CB-5.1755	15:13:35.3	31:27:23.9	18.97	19.75	17.97	18.84	67	1.86
CB-5.1709	15:13:36.7	31:22:10.1	17.25	18.99	17.07	18.74	192	3.18
CB-5.1667	15:13:38.1	31:21:35.3	20.37	21.08	20.13	20.35	23	1.55
CB-5.1622	15:13:38.8	31:28:14.2	17.83	19.65	17.84	19.75	187	3.26
CB-5.1581	15:13:39.7	31:32:49.2	14.90	16.96	13.42	15.29	220	3.53
CB-5.1543	15:13:41.0	31:28:47.0	20.43	20.84	18.47	19.30	33	1.49
CB-11.7144	15:15:24.0	31:26:15.4	19.98	21.60	19.61	20.91	57	2.70
CB-11.7093	15:15:25.1	31:30:19.3	22.31	22.57	...	...	11	1.28
CB-11.7029	15:15:26.6	31:30:47.7	17.75	19.33	17.12	18.53	181	3.20
CB-11.6955	15:15:28.7	31:31:31.7	17.51	18.51	16.38	17.54	115	2.28
CB-11.6958	15:15:29.1	31:20:49.0	20.53	21.34	20.03	21.42	37	1.81
CB-11.6922	15:15:29.8	31:31:08.7	20.52	21.45	19.49	20.79	43	1.96
CB-11.6889	15:15:30.6	31:34:25.3	22.39	23.15	...	...	8	1.48
CB-11.6800	15:15:32.9	31:30:30.7	22.16	23.13	...	...	8	1.77
CB-11.6798	15:15:33.3	31:23:50.8	21.24	22.05	...	...	26	1.57
CB-11.6746	15:15:34.8	31:16:26.0	20.18	21.43	...	...	45	2.21
CB-11.6635	15:15:37.1	31:33:22.6	19.28	20.30	19.37	20.17	69	2.04
CB-11.6401	15:15:43.0	31:20:38.0	22.34	22.78	...	...	7	0.94
CB-11.6355	15:15:44.3	31:25:48.2	21.67	22.71	...	...	14	1.96
CB-11.6354	15:15:44.6	31:14:55.1	19.57	20.83	20.14	21.08	58	2.36
CB-11.6318	15:15:45.0	31:32:09.9	21.77	22.59	20.91	21.70	13	1.21
CB-11.6097	15:15:50.4	31:33:33.0	21.68	22.35	20.59	21.72	12	1.16
CB-11.6101	15:15:50.5	31:24:28.4	20.63	21.50	20.20	21.17	34	1.70
CB-11.5861	15:15:56.0	31:20:55.8	22.08	22.78	...	...	8	1.32
CB-11.5627	15:16:00.3	31:16:54.1	22.58	22.74	...	...	7	0.83
CB-11.5467	15:16:03.9	31:24:41.8	22.29	22.70	...	...	7	0.94
CB-11.5458	15:16:04.3	31:20:33.3	21.12	22.37	...	...	22	1.70
CB-11.5406	15:16:05.3	31:17:03.4	22.72	22.90	...	...	11	1.22
CB-11.5351	15:16:06.4	31:23:22.1	21.04	21.92	20.59	22.10	31	1.72
CB-11.5036	15:16:14.1	31:25:48.2	18.49	19.80	17.92	19.21	84	2.72
CB-11.4878	15:16:18.0	31:21:56.9	22.12	22.75	20.05	21.89	7	1.18
CB-11.4828	15:16:19.0	31:18:55.4	20.20	21.58	21.03	22.09	55	2.58
CB-11.4703	15:16:22.0	31:32:21.9	20.29	21.03	20.46	21.19	40	1.78

TABLE 2.6—*Continued*

Object	RA (1950)	Dec. (1950)	g_{tot}	g_{core}	r_{tot}	r_{core}	Area (□″)	irl (″)
CB-11.4654	15:16:23.5	31:31:23.6	21.04	22.56	···	···	18	1.90
CB-11.4629	15:16:24.3	31:33:23.9	21.63	22.54	22.41	22.49	18	1.43
CB-11.4641	15:16:24.5	31:15:20.2	22.13	22.63	···	···	13	1.68
CB-11.4459	15:16:29.0	31:20:33.0	16.99	20.25	···	···	22	2.06
CB-11.4359	15:16:31.0	31:22:00.9	21.72	22.87	···	···	12	2.10
CB-11.4259	15:16:33.2	31:26:37.2	22.17	22.81	···	···	8	1.09
CB-7.4877	15:16:35.0	28:30:48.6	19.82	20.84	20.37	21.32	55	2.04
CB-11.4075	15:16:37.7	31:28:18.4	22.21	22.77	···	···	9	1.03
CB-7.4716	15:16:38.0	28:30:46.8	19.27	20.28	19.17	20.10	69	2.19
CB-11.3983	15:16:39.9	31:29:17.3	19.11	21.12	20.22	21.62	107	3.39
CB-7.4571	15:16:40.8	28:23:29.9	20.78	22.02	20.18	21.29	30	1.97
CB-11.3930	15:16:41.3	31:24:27.1	22.45	22.85	···	···	6	0.93
CB-11.3926	15:16:41.5	31:17:33.7	22.32	22.89	···	···	6	0.97
CB-7.4544	15:16:41.9	27:58:57.2	21.96	22.56	21.55	22.07	8	1.11
CB-7.4515	15:16:42.0	28:24:13.1	19.78	20.77	19.09	20.27	48	2.01
CB-7.4501	15:16:42.7	27:58:16.8	19.71	20.32	19.68	20.36	50	1.61
CB-11.3876	15:16:42.9	31:23:25.8	22.26	22.67	···	···	7	0.93
CB-7.4452	15:16:43.1	28:30:32.7	21.52	21.96	21.15	21.95	21	1.33
CB-00.57	15:16:43.7	27:59:49.5	···	···	21.56	21.99	8	1.08
CB-11.3809	15:16:44.5	31:16:04.9	22.23	23.16	···	···	7	1.46
CB-00.60	15:16:44.9	28:33:58.9	···	···	21.37	21.95	13	1.22
CB-11.3769	15:16:45.4	31:19:18.4	22.38	22.97	···	···	8	0.93
CB-7.4360	15:16:45.4	28:23:35.6	20.81	22.15	20.47	21.76	28	1.90
CB-7.4329	15:16:46.8	27:45:18.4	19.48	20.97	19.25	20.74	75	2.92
CB-7.4266	15:16:47.2	28:29:49.6	19.40	20.37	18.99	20.11	64	2.03
CB-7.4293	15:16:47.5	27:42:49.7	21.23	22.12	19.78	21.36	20	1.44
CB-7.4220	15:16:48.1	28:25:46.9	19.18	20.54	19.08	20.60	75	2.40
CB-11.3642	15:16:48.4	31:33:11.9	20.08	21.20	19.57	20.71	46	2.11
CB-7.4250	15:16:48.5	27:44:41.9	19.17	20.32	17.97	19.02	75	2.67
CB-11.3629	15:16:48.9	31:29:13.9	20.57	21.40	19.67	20.54	21	1.56
CB-7.4211	15:16:49.1	27:51:04.1	19.41	20.20	19.16	20.01	54	1.84
CB-11.3622	15:16:49.3	31:16:02.1	16.93	18.59	16.25	17.75	305	3.70
CB-00.56	15:16:50.3	27:59:04.4	···	···	20.71	21.86	26	1.62
CB-11.3559	15:16:50.8	31:22:55.9	22.34	22.97	···	···	7	1.16
CB-7.4084	15:16:51.4	28:29:14.0	20.70	22.02	21.38	21.86	32	1.94
CB-7.4113	15:16:51.6	27:54:16.4	21.72	22.15	20.13	21.05	13	1.21
CB-11.3525	15:16:51.6	31:25:22.8	20.64	21.35	19.47	20.58	37	1.75
CB-8.4144	15:16:51.9	28:38:39.2	18.03	18.95	16.75	17.76	124	2.40
CB-00.58	15:16:52.4	28:22:41.6	···	···	20.48	21.38	20	2.07
CB-7.4026	15:16:53.3	27:46:02.0	21.90	22.54	20.74	21.73	13	1.27
CB-11.3457	15:16:53.4	31:23:59.2	22.03	22.72	21.83	22.20	13	1.36
CB-11.3442	15:16:53.5	31:32:31.5	15.60	17.38	13.87	15.25	374	3.49
CB-7.3972	15:16:54.5	27:45:14.8	20.60	21.47	20.15	21.38	32	1.70
CB-7.3940	15:16:55.1	27:54:28.2	20.98	21.70	20.51	21.61	24	1.49
CB-11.3356	15:16:55.8	31:34:19.4	19.87	20.84	18.84	19.90	59	2.00
CB-7.3889	15:16:55.8	28:01:00.9	21.05	22.37	20.81	21.92	26	1.92
CB-11.3317	15:16:57.3	31:27:38.9	20.39	21.77	···	···	40	2.18
CB-7.3802	15:16:57.9	27:46:20.6	21.00	21.56	19.85	20.78	26	1.53
CB-7.3774	15:16:58.2	28:00:46.3	21.80	22.45	19.94	21.26	15	1.35
CB-7.3716	15:16:59.5	27:47:21.8	20.59	21.26	20.56	21.16	12	1.14
CB-7.3678	15:16:59.6	28:27:55.2	19.46	20.45	18.43	19.55	53	2.02
CB-7.3664	15:17:00.6	27:48:58.9	19.65	20.48	19.48	20.44	53	1.86
CB-11.3168	15:17:01.0	31:26:44.4	21.80	22.72	···	···	11	1.36
CB-7.3498	15:17:03.8	27:44:38.2	20.31	21.33	18.46	20.01	13	1.47
CB-7.3451	15:17:04.8	27:59:01.1	21.27	21.73	20.74	21.26	17	1.35
CB-7.3417	15:17:05.6	27:44:00.8	21.25	22.06	20.66	21.78	12	1.19
CB-7.3389	15:17:06.3	27:49:35.2	21.50	22.52	21.58	21.92	18	1.37
CB-7.3350	15:17:06.5	28:25:59.5	19.10	20.01	18.19	19.49	77	2.08
CB-7.3306	15:17:07.7	28:22:21.3	20.80	21.51	19.44	20.62	31	1.62
CB-7.3294	15:17:08.6	27:48:51.0	19.63	21.00	19.66	20.68	65	2.39
CB-7.3272	15:17:09.2	27:42:54.6	19.94	20.75	19.94	20.64	45	1.83
CB-00.52	15:17:10.0	27:51:53.0	···	···	20.95	21.93	26	2.23

TABLE 2.6—*Continued*

Object	RA (1950)	Dec.	g_{tot}	g_{core}	r_{tot}	r_{core}	Area (□″)	irl (″)
CB-7.3185	15:17:10.4	28:26:53.2	19.33	20.49	18.93	20.07	68	2.26
CB-7.3183	15:17:11.2	27:45:04.6	21.63	22.13	19.96	21.02	14	1.21
CB-00.59	15:17:11.4	28:35:32.1	...	...	21.58	21.87	6	0.93
CB-7.3157	15:17:11.6	27:53:06.6	21.14	21.86	20.51	21.62	18	1.45
CB-7.3107	15:17:11.9	28:28:50.0	19.47	20.49	18.77	19.71	64	2.02
CB-7.3086	15:17:13.0	27:51:33.7	20.92	21.80	19.84	20.95	25	1.64
CB-7.3035	15:17:14.2	27:45:06.1	21.01	21.99	19.94	21.30	19	1.45
CB-7.3009	15:17:14.2	28:23:26.1	18.95	20.34	18.48	19.46	80	2.54
CB-7.3007	15:17:14.7	27:56:57.1	21.44	22.10	21.55	21.39	15	1.31
CB-00.53	15:17:15.2	27:53:26.8	...	...	21.06	21.86	19	1.56
CB-7.2972	15:17:15.3	28:26:18.9	18.70	19.95	18.34	19.55	92	2.48
CB-7.2980	15:17:15.6	27:44:38.5	22.10	22.53	20.37	21.50	10	1.18
CB-7.2841	15:17:18.1	28:26:45.8	20.09	21.13	20.14	20.93	38	1.78
CB-7.2834	15:17:18.7	27:47:43.0	20.59	21.58	20.31	21.65	40	2.13
CB-7.2777	15:17:19.6	27:45:23.3	19.37	21.01	19.70	21.12	77	2.65
CB-8.2789	15:17:19.9	28:36:36.0	18.31	19.96	18.13	19.66	95	3.00
CB-00.54	15:17:20.4	27:57:22.9	...	...	21.35	22.00	13	1.74
CB-7.2650	15:17:21.7	28:25:15.9	21.28	21.70	...	...	11	1.08
CB-7.2655	15:17:22.2	27:50:44.5	19.26	20.32	18.65	19.95	73	2.15
CB-7.2638	15:17:22.5	27:58:37.0	21.97	22.56	21.06	21.81	13	1.28
CB-8.2625	15:17:23.1	28:36:37.7	21.06	22.16	22.05	22.09	25	1.77
CB-7.2536	15:17:24.0	28:26:02.0	18.67	20.11	18.38	19.68	102	2.64
CB-7.2561	15:17:24.1	27:45:42.1	22.01	22.43	21.23	21.79	11	1.09
CB-7.2473	15:17:25.3	28:23:07.8	20.30	21.19	19.21	20.19	16	1.41
CB-00.55	15:17:26.0	27:59:08.9	...	...	21.36	22.06	30	1.73
CB-7.2452	15:17:26.1	27:45:19.7	19.27	20.62	18.76	20.20	51	2.15
CB-8.2463	15:17:26.4	28:34:03.8	20.61	21.20	20.99	21.27	17	1.37
CB-7.2408	15:17:26.5	28:23:40.6	19.44	20.83	18.65	20.05	64	2.59
CB-8.2404	15:17:27.5	28:38:16.1	21.24	21.81	20.12	21.31	26	1.79
CB-7.2343	15:17:28.1	27:43:53.2	19.52	20.69	18.45	19.78	28	1.74
CB-8.2343	15:17:28.9	28:39:21.1	22.34	22.57	21.49	21.86	7	0.90
CB-7.2266	15:17:29.6	27:49:56.0	19.17	20.46	18.42	19.67	84	2.47
CB-7.2186	15:17:31.5	27:54:53.3	18.29	19.40	17.81	18.90	98	2.42
CB-7.2189	15:17:31.5	27:44:36.7	19.57	20.36	18.66	19.70	47	1.70
CB-7.1983	15:17:35.9	27:54:36.8	19.34	20.43	18.58	19.77	70	2.15
CB-10.1333	15:17:46.3	30:43:48.9	19.97	21.75	20.46	21.58	57	2.69
CB-10.1292	15:17:47.4	30:41:08.9	21.14	22.12	19.41	20.97	22	1.65
CB-10.1291	15:17:47.5	30:30:52.0	18.59	20.05	18.63	20.10	104	2.64
CB-10.1258	15:17:48.7	30:27:33.7	19.76	20.46	19.61	20.15	44	1.59
CB-10.1243	15:17:48.8	30:40:50.2	21.67	22.09	20.16	21.22	13	1.15
CB-10.1081	15:17:53.2	30:40:15.7	19.57	20.87	19.07	20.77	61	2.27
CB-10.1076	15:17:53.4	30:25:01.8	19.33	20.56	19.48	21.02	80	2.48
CB-10.860	15:17:58.8	30:26:45.9	21.59	21.93	20.42	21.07	10	1.06
CB-10.724	15:18:02.8	30:32:12.5	20.68	21.78	20.40	21.05	31	1.81
CB-10.676	15:18:04.2	30:35:30.1	21.74	22.27	20.54	21.67	11	1.10
CB-10.659	15:18:04.8	30:30:54.5	20.41	21.16	20.19	21.22	38	1.73
CB-10.602	15:18:06.6	30:34:51.8	20.55	21.39	19.68	21.11	33	1.67
CB-10.585	15:18:06.9	30:33:28.4	21.64	22.49	20.33	21.23	14	1.29
CB-10.557	15:18:07.7	30:26:27.3	19.22	19.87	18.66	19.45	52	1.60
CB-10.524	15:18:08.4	30:36:11.1	20.24	21.87	19.92	21.04	46	3.23
CB-10.521	15:18:08.7	30:30:37.5	21.66	22.30	21.03	22.05	12	1.25
CB-10.379	15:18:12.6	30:33:36.5	19.56	20.15	18.95	19.91	33	1.48
CB-00.69	15:18:16.4	30:27:45.6	...	...	21.51	22.38	19	1.62
CB-10.175	15:18:17.4	30:27:05.8	19.47	20.58	19.27	20.29	73	2.18
CB-10.60	15:18:20.6	30:26:18.3	19.92	20.77	19.55	20.60	45	1.82
CB-00.68	15:18:21.1	30:43:28.6	...	...	20.35	21.77	31	1.82
CB-16.10942	15:18:23.5	30:32:24.0	20.43	20.94	19.89	20.68	31	1.46
CB-16.10907	15:18:24.4	30:39:15.4	19.60	20.64	18.68	19.94	66	2.34
CB-15.10592	15:18:24.8	29:42:37.0	18.86	19.58	18.29	19.06	60	1.78
CB-00.70	15:18:25.8	30:33:18.6	...	...	20.74	21.50	19	1.77
CB-13.11937	15:18:29.6	28:18:01.5	18.99	20.40	19.33	20.70	91	2.68
CB-15.10357	15:18:29.7	29:46:09.3	20.71	21.86	...	...	50	2.36

TABLE 2.6—*Continued*

Object	RA (1950)	Dec.	g_{tot}	g_{core}	r_{tot}	r_{core}	Area (□″)	irl (″)
CB-16.10681	15:18:29.7	30:27:59.5	18.03	19.43	18.04	19.39	131	2.73
CB-15.10321	15:18:30.2	29:36:17.4	21.72	22.35	21.28	21.72	15	1.18
CB-15.10271	15:18:31.1	29:36:57.9	18.49	19.31	17.54	18.38	53	1.79
CB-15.10249	15:18:31.4	29:43:28.2	18.17	18.91	16.28	17.29	84	1.84
CB-13.11822	15:18:32.0	28:17:32.7	19.72	20.88	19.45	20.57	55	2.19
CB-15.10207	15:18:32.8	29:34:20.9	19.94	20.99	18.97	20.47	66	2.55
CB-13.11765	15:18:33.4	28:21:12.3	19.06	20.15	18.45	19.68	81	2.22
CB-15.10152	15:18:34.0	29:44:34.9	20.25	21.12	20.45	21.17	40	1.74
CB-15.10144	15:18:34.1	29:32:59.7	20.21	20.87	19.71	20.60	41	1.70
CB-16.10521	15:18:34.2	30:39:27.6	18.24	19.45	18.23	19.38	103	2.38
CB-15.10139	15:18:34.3	29:36:11.1	19.64	20.79	19.64	20.74	61	2.18
CB-15.10123	15:18:34.9	29:47:07.2	22.01	22.29	20.42	20.98	8	1.06
CB-16.10500	15:18:35.0	30:42:14.9	19.03	19.79	17.73	18.59	61	1.85
CB-16.10486	15:18:35.2	30:44:57.3	18.92	19.78	17.91	18.82	78	1.98
CB-13.11678	15:18:35.2	28:18:15.8	20.98	21.70	20.12	20.91	28	1.68
CB-15.10089	15:18:35.8	29:42:51.7	22.15	22.64	20.29	21.60	13	1.22
CB-15.10082	15:18:36.0	29:34:04.6	20.26	20.78	20.26	21.10	34	1.41
CB-13.11647	15:18:36.2	28:10:44.6	19.47	20.62	18.94	19.99	81	2.69
CB-13.11629	15:18:36.7	28:13:41.3	19.24	20.36	18.13	19.33	74	2.30
CB-16.10422	15:18:36.8	30:42:41.9	17.46	18.89	16.75	18.14	177	3.05
CB-15.10045	15:18:36.9	29:48:10.9	21.69	21.99	20.23	20.82	19	1.27
CB-13.11590	15:18:37.5	28:16:14.4	22.04	22.60	20.62	21.73	10	1.09
CB-16.10397	15:18:37.7	30:34:28.5	17.93	18.74	16.64	17.66	71	1.85
CB-15.10000	15:18:38.0	29:33:28.0	20.59	21.16	19.55	20.50	18	1.37
CB-15.10001	15:18:38.0	29:39:45.7	20.30	21.33	18.99	20.78	45	1.98
CB-13.11547	15:18:38.5	28:23:44.3	19.06	19.67	18.06	18.80	57	1.60
CB-16.10344	15:18:39.1	30:38:26.2	17.40	19.52	17.54	19.45	207	3.78
CB-15.9943	15:18:39.5	29:37:23.4	21.35	21.82	20.65	21.20	20	1.38
CB-13.11475	15:18:39.9	28:13:52.9	19.87	21.10	19.83	21.12	47	1.99
CB-16.10266	15:18:40.9	30:53:48.0	20.43	21.17	21.16	21.88	38	1.79
CB-15.9848	15:18:41.7	29:30:23.2	19.89	20.89	19.38	20.49	57	2.15
CB-00.5	15:18:43.3	28:22:34.4	...	...	21.06	21.78	19	1.42
CB-14.10094	15:18:47.0	28:48:58.9	19.71	20.80	19.36	20.91	63	2.17
CB-16.10009	15:18:47.3	30:41:32.8	20.39	21.49	20.31	21.55	30	1.95
CB-13.11111	15:18:47.4	28:06:49.3	19.36	20.58	18.72	19.78	69	2.33
CB-16.9958	15:18:48.3	30:45:09.8	20.58	21.37	20.46	21.40	30	1.70
CB-14.10021	15:18:48.6	28:51:53.6	20.14	20.63	19.22	19.90	39	1.43
CB-13.11049	15:18:48.8	28:14:11.3	20.98	21.29	21.31	22.04	23	1.28
CB-16.9930	15:18:49.0	30:49:06.4	20.85	21.92	20.99	21.75	26	1.61
CB-15.9510	15:18:49.7	29:46:58.1	20.74	21.56	20.77	21.77	34	2.06
CB-14.9937	15:18:50.7	28:54:03.6	19.30	19.99	18.28	19.06	59	1.70
CB-15.9452	15:18:50.9	29:42:27.1	22.29	22.65	21.51	22.00	9	1.01
CB-15.9435	15:18:51.2	29:38:39.6	19.30	20.59	18.74	20.18	83	2.56
CB-13.10933	15:18:51.4	28:12:38.5	20.92	21.63	20.97	21.54	32	1.76
CB-14.9914	15:18:51.4	28:54:25.1	21.14	21.84	20.83	21.81	24	1.54
CB-16.9835	15:18:51.5	30:50:50.3	19.34	20.57	19.77	20.61	71	2.74
CB-16.9784	15:18:52.8	30:46:02.4	19.30	20.18	18.62	19.68	68	2.00
CB-15.9348	15:18:53.5	29:29:54.6	20.19	20.94	19.68	20.57	44	1.74
CB-16.9748	15:18:53.5	30:47:43.0	20.27	20.74	20.05	20.86	35	1.43
CB-14.9824	15:18:53.6	28:49:26.7	21.01	21.84	20.96	21.88	25	1.60
CB-14.9814	15:18:53.8	28:37:11.3	20.79	21.47	20.97	21.64	38	1.83
CB-14.9777	15:18:54.8	28:51:46.7	21.55	22.15	20.82	21.79	15	1.21
CB-14.9745	15:18:55.5	28:37:20.2	18.90	20.05	18.76	19.72	84	2.26
CB-00.66	15:18:55.9	30:50:54.8	...	...	21.37	22.06	23	1.90
CB-14.9655	15:18:57.3	28:46:24.4	20.62	21.18	20.44	21.53	30	1.53
CB-14.9649	15:18:57.6	28:41:48.8	18.32	20.73	18.96	21.06	205	4.48
CB-00.10	15:18:58.1	29:33:04.4	...	...	20.32	21.59	28	1.77
CB-13.10503	15:19:00.4	28:14:14.4	21.07	21.77	20.31	21.39	30	1.78
CB-16.9396	15:19:00.4	30:39:25.8	18.58	20.77	18.64	20.84	162	4.69
CB-14.9351	15:19:04.0	28:38:08.1	20.64	21.35	20.34	21.08	28	1.54
CB-15.8857	15:19:04.4	29:39:48.5	19.69	20.84	19.47	20.83	66	2.41
CB-13.10283	15:19:04.7	28:14:09.1	19.95	21.07	19.67	20.87	48	2.01

TABLE 2.6—*Continued*

Object	RA (1950)	Dec. (1950)	g_{tot}	g_{core}	r_{tot}	r_{core}	Area (□″)	irl (″)
CB-15.8799	15:19:06.2	29:40:12.7	21.74	22.28	21.50	21.77	10	1.14
CB-14.9252	15:19:06.3	28:49:01.1	19.05	19.78	18.47	19.34	65	1.79
CB-16.9171	15:19:06.4	30:45:34.9	21.30	21.83	20.59	21.01	13	1.97
CB-16.9084	15:19:08.0	30:45:45.5	15.34	17.92	14.75	17.42	73	2.74
CB-16.9089	15:19:08.0	30:52:09.5	19.06	20.82	18.71	20.46	111	3.60
CB-16.9069	15:19:08.3	30:51:46.5	20.32	21.13	20.03	20.98	36	1.80
CB-15.8577	15:19:10.9	29:32:30.5	21.21	21.75	20.56	21.84	26	1.53
CB-14.8959	15:19:12.5	28:39:51.4	19.66	20.26	19.07	19.98	45	1.56
CB-14.8914	15:19:13.4	28:42:56.3	21.95	22.90	21.23	22.22	12	1.31
CB-15.8460	15:19:13.7	29:34:25.3	20.93	21.54	20.98	21.26	9	1.05
CB-16.8747	15:19:15.1	30:50:23.2	18.97	20.06	18.27	19.50	55	2.05
CB-15.8401	15:19:15.3	29:35:53.0	20.91	21.60	20.41	21.38	37	1.78
CB-14.8776	15:19:16.5	28:45:47.4	21.50	22.60	21.41	22.28	20	1.95
CB-16.8685	15:19:16.5	30:41:55.6	22.70	23.11	20.49	21.96	6	1.02
CB-15.8300	15:19:17.7	29:35:58.7	20.26	21.25	20.21	20.95	37	1.84
CB-17.8020	15:19:17.8	30:57:22.5	19.18	20.36	19.66	20.64	71	2.23
CB-14.8696	15:19:18.0	28:49:25.1	21.81	22.36	21.54	22.09	8	1.01
CB-14.8633	15:19:19.1	28:41:44.9	19.43	20.61	19.67	20.79	65	2.15
CB-16.8533	15:19:20.0	30:46:53.5	18.55	19.54	18.17	19.14	44	1.88
CB-13.9518	15:19:20.1	28:25:29.7	20.79	22.21	21.03	21.92	27	1.88
CB-16.8458	15:19:21.6	30:40:42.2	19.05	20.49	18.77	20.17	91	2.90
CB-00.67	15:19:21.6	30:51:14.2	...	...	21.92	22.08	8	1.18
CB-15.8115	15:19:21.7	29:29:47.0	19.56	20.96	19.31	20.88	66	2.58
CB-14.8463	15:19:22.8	28:40:49.7	21.69	22.12	21.32	22.18	16	1.26
CB-15.8057	15:19:23.0	29:47:34.7	19.53	20.86	19.00	20.37	74	2.42
CB-16.8370	15:19:23.5	30:53:03.2	17.50	18.97	16.78	18.20	180	3.02
CB-16.8371	15:19:23.6	30:55:36.6	18.44	20.01	18.13	19.79	99	2.70
CB-15.7991	15:19:24.5	29:41:25.0	20.83	21.93	20.12	21.00	27	1.89
CB-13.9265	15:19:25.4	28:06:37.3	21.97	22.96	20.89	21.54	9	1.31
CB-16.8283	15:19:25.6	30:45:20.7	21.52	21.77	20.44	21.60	21	1.31
CB-16.8232	15:19:26.7	30:52:23.9	19.55	20.41	19.10	20.12	28	1.61
CB-16.8213	15:19:27.0	30:46:42.5	21.03	21.68	20.49	21.47	6	0.94
CB-15.7876	15:19:27.2	29:46:25.1	20.70	21.36	20.35	21.66	10	1.10
CB-15.7754	15:19:29.5	29:29:34.4	21.72	22.79	21.18	22.06	15	1.78
CB-00.4	15:19:29.7	28:08:06.9	...	...	20.20	21.66	26	1.77
CB-14.8129	15:19:30.0	28:41:05.5	19.67	20.64	19.34	20.48	53	1.96
CB-16.8018	15:19:30.9	30:43:10.2	19.53	20.78	19.38	20.61	63	2.19
CB-16.7924	15:19:33.1	30:43:53.6	20.47	21.46	20.04	21.23	41	1.94
CB-13.8809	15:19:34.2	28:12:33.7	21.44	22.06	20.27	21.41	20	1.49
CB-16.7860	15:19:34.8	30:43:30.6	21.07	22.11	20.26	21.47	28	1.77
CB-16.7772	15:19:36.9	30:47:39.1	18.31	19.84	17.87	19.51	124	2.78
CB-13.8603	15:19:38.5	28:14:58.6	20.92	21.71	19.99	21.23	34	1.78
CB-14.7718	15:19:38.7	28:42:45.5	19.25	20.65	18.94	20.64	73	2.72
CB-13.8577	15:19:39.1	28:18:31.8	19.20	20.23	18.23	19.43	55	2.05
CB-00.6	15:19:40.4	28:41:33.6	...	...	21.67	22.11	15	1.35
CB-15.7225	15:19:41.6	29:41:44.6	19.21	20.12	18.48	19.53	61	1.90
CB-15.7099	15:19:44.1	29:37:12.2	21.86	22.73	20.89	21.52	13	1.58
CB-17.6733	15:19:45.7	31:05:09.3	21.41	22.18	19.55	21.08	15	1.53
CB-16.7387	15:19:46.7	30:47:42.9	22.58	22.56	20.14	20.98	11	1.07
CB-13.8116	15:19:47.7	28:13:35.3	19.23	21.25	20.83	21.39	74	3.80
CB-13.8072	15:19:48.4	28:06:11.7	19.01	20.45	18.99	20.26	95	2.63
CB-17.6607	15:19:49.1	30:59:02.8	18.90	19.56	16.96	17.90	64	1.68
CB-14.7245	15:19:49.3	28:45:40.3	19.40	20.21	19.31	20.12	61	1.89
CB-16.7284	15:19:49.3	30:49:22.6	19.06	20.00	18.68	19.53	67	2.01
CB-13.7997	15:19:49.8	28:22:43.4	20.17	21.11	19.86	20.96	44	1.94
CB-13.7943	15:19:50.9	28:23:24.4	20.43	21.33	19.79	20.75	34	1.68
CB-13.7890	15:19:51.6	28:13:22.9	21.43	22.07	20.67	21.80	24	1.59
CB-16.7175	15:19:52.1	30:48:20.0	18.66	19.74	18.58	19.88	84	2.17
CB-17.6473	15:19:52.4	30:58:11.8	19.17	20.17	18.21	19.52	23	1.54
CB-15.6726	15:19:52.7	29:35:28.8	19.62	20.98	19.66	21.04	65	2.35
CB-14.7071	15:19:53.1	28:42:08.0	19.83	20.41	18.33	19.13	45	1.62
CB-17.6445	15:19:53.3	31:01:33.7	22.29	23.01	20.80	21.85	8	1.03

TABLE 2.6—*Continued*

Object	RA (1950)	Dec. (1950)	g_{tot}	g_{core}	r_{tot}	r_{core}	Area (□″)	irl (″)
CB-16.7111	15:19:53.5	30:54:20.8	21.64	22.44	20.31	21.86	16	1.37
CB-15.6667	15:19:53.9	29:40:07.5	22.30	22.89	20.45	21.71	12	1.20
CB-00.64	15:19:54.6	31:00:06.6	...	...	21.73	22.25	19	1.45
CB-13.7735	15:19:54.8	28:06:19.1	20.18	21.32	18.95	20.20	46	2.35
CB-14.6982	15:19:55.5	28:49:15.0	21.48	21.72	20.03	20.35	11	1.11
CB-13.7691	15:19:55.8	28:24:57.5	18.54	19.88	18.03	19.43	87	2.46
CB-13.7658	15:19:56.3	28:16:02.6	18.20	19.56	17.48	18.65	84	2.45
CB-15.6487	15:19:57.7	29:31:03.7	21.58	22.17	21.15	21.69	17	1.35
CB-17.6220	15:19:59.0	31:00:59.0	18.87	19.93	18.59	19.70	83	2.18
CB-13.7416	15:19:59.7	28:10:22.0	20.36	21.39	19.37	20.44	39	1.88
CB-15.6387	15:20:00.1	29:29:55.9	19.35	20.31	19.29	20.50	65	1.93
CB-16.6870	15:20:00.1	30:48:56.1	20.44	21.30	19.74	21.11	38	1.79
CB-17.6163	15:20:00.2	30:59:47.1	18.89	19.94	17.69	18.63	80	2.29
CB-13.7347	15:20:01.1	28:22:09.9	16.81	18.43	16.10	17.65	269	3.57
CB-14.6685	15:20:01.9	28:44:54.4	20.20	20.90	20.06	20.73	35	1.56
CB-15.6300	15:20:02.0	29:46:52.7	19.94	21.44	18.70	20.22	55	2.35
CB-00.9	15:20:02.9	29:33:00.3	...	...	20.88	21.62	24	1.75
CB-15.6259	15:20:02.9	29:46:18.9	16.39	17.74	14.60	15.67	147	2.60
CB-15.6198	15:20:04.1	29:43:35.1	19.69	21.14	19.75	21.39	73	2.58
CB-15.6165	15:20:04.5	29:31:10.5	21.14	22.02	20.08	21.06	25	1.76
CB-13.7175	15:20:04.5	28:19:02.8	18.90	20.08	18.18	19.36	95	2.42
CB-17.5963	15:20:04.6	31:04:23.4	20.12	20.94	19.86	20.77	40	1.72
CB-15.6151	15:20:04.9	29:44:35.8	20.77	21.67	19.67	20.70	33	1.76
CB-00.8	15:20:05.8	29:33:54.6	...	...	21.29	21.83	15	1.34
CB-17.5901	15:20:05.9	31:02:06.0	21.69	22.45	21.26	21.94	14	1.28
CB-15.6092	15:20:06.0	29:46:50.2	19.01	19.63	18.33	19.01	63	1.67
CB-15.6037	15:20:07.1	29:37:24.4	19.21	19.87	17.50	18.36	54	1.66
CB-14.6450	15:20:07.5	28:51:04.7	20.47	21.66	20.80	21.70	35	1.83
CB-15.6007	15:20:07.7	29:44:50.2	17.62	19.78	17.41	19.31	247	3.95
CB-16.6552	15:20:08.2	30:49:53.0	19.97	21.67	20.23	21.83	60	2.68
CB-00.7	15:20:08.6	29:33:07.3	...	...	21.65	21.92	16	1.39
CB-15.5943	15:20:08.8	29:46:35.8	19.13	19.85	18.56	19.44	39	1.62
CB-15.5896	15:20:09.5	29:33:55.3	18.93	20.11	18.26	19.37	81	2.25
CB-16.6479	15:20:09.8	30:48:53.6	20.68	21.99	19.33	21.29	42	2.49
CB-14.6316	15:20:10.3	28:53:09.6	18.62	19.33	17.26	18.17	74	1.79
CB-14.6278	15:20:10.8	28:36:44.3	19.66	20.30	18.17	19.08	22	1.39
CB-14.6271	15:20:10.9	28:44:18.2	21.44	21.81	20.47	20.88	8	0.97
CB-16.6387	15:20:12.2	30:50:09.9	20.09	20.71	19.26	20.43	41	1.64
CB-15.5781	15:20:12.3	29:36:00.4	17.98	19.64	18.11	19.74	148	3.10
CB-16.6330	15:20:13.9	30:48:25.2	21.18	21.51	19.82	20.64	24	1.33
CB-14.6053	15:20:16.2	28:47:01.6	21.16	21.84	20.19	21.74	23	1.44
CB-14.5987	15:20:17.4	28:44:17.6	18.21	19.58	17.83	19.13	45	2.10
CB-16.6137	15:20:19.1	30:49:15.0	21.72	22.68	20.52	21.55	16	1.61
CB-14.5787	15:20:21.3	28:47:47.4	20.54	22.13	20.93	22.10	36	2.10
CB-17.5122	15:20:23.1	31:07:18.8	19.91	21.03	19.50	21.12	59	2.21
CB-16.5896	15:20:25.2	30:48:13.7	18.70	20.08	18.44	20.04	105	2.63
CB-17.4988	15:20:26.4	31:02:39.7	20.21	21.01	19.26	20.69	48	2.06
CB-16.5819	15:20:27.4	30:48:49.4	21.34	22.07	20.73	21.88	19	1.40
CB-17.4872	15:20:29.1	31:00:29.4	22.76	22.69	20.90	21.51	9	1.20
CB-17.4773	15:20:31.2	31:03:02.7	21.83	22.52	20.80	21.72	12	1.24
CB-17.4655	15:20:33.4	31:03:18.1	20.51	21.38	20.77	21.53	34	1.80
CB-17.4618	15:20:34.3	31:02:52.0	18.55	20.05	18.15	19.52	109	2.91
CB-17.4545	15:20:35.8	31:00:00.9	18.34	19.56	17.58	18.79	41	2.06
CB-17.4452	15:20:38.0	31:10:50.5	21.10	21.93	20.21	20.69	29	1.86
CB-00.63	15:20:38.1	30:59:55.1	...	...	21.84	22.23	6	1.07
CB-17.4347	15:20:40.4	31:12:18.8	17.25	18.87	16.75	18.10	269	3.56
CB-17.4312	15:20:41.2	31:16:43.4	18.62	19.72	17.69	18.86	102	2.43
CB-17.4229	15:20:43.3	31:14:08.1	18.70	19.88	18.41	19.72	88	2.35
CB-17.4204	15:20:43.8	31:08:13.2	17.07	18.24	...	...	158	2.76
CB-17.4168	15:20:44.9	31:10:47.2	17.93	19.69	17.64	19.54	139	3.06
CB-17.4117	15:20:46.1	31:06:37.6	18.34	19.17	16.59	17.65	75	1.90
CB-17.4081	15:20:46.9	31:07:19.4	20.27	21.04	19.60	20.85	36	1.62

TABLE 2.6—*Continued*

Object	RA (1950)	Dec. (1950)	g_{tot}	g_{core}	r_{tot}	r_{core}	Area (□″)	irl (″)
CB-17.4009	15:20:48.5	31:09:17.6	19.45	20.85	19.19	20.54	49	2.28
CB-17.3918	15:20:50.1	31:08:13.7	21.62	22.52	21.13	21.73	14	1.46
CB-17.3813	15:20:52.6	31:11:27.2	18.84	20.63	19.10	20.87	123	3.13
CB-17.3749	15:20:53.7	31:09:38.7	21.88	22.70	20.91	21.68	14	1.40
CB-17.3589	15:20:57.3	31:04:47.1	19.17	20.25	18.70	19.98	72	2.13
CB-17.3556	15:20:58.0	31:05:27.8	20.25	21.27	20.16	21.42	39	1.86
CB-17.3487	15:20:59.7	31:09:34.3	19.89	21.06	20.36	21.65	45	2.18
CB-17.3459	15:21:00.0	30:59:15.7	20.66	21.63	20.13	21.25	30	1.69
CB-17.3446	15:21:00.8	31:16:15.6	21.68	22.25	...	...	8	1.18
CB-17.3412	15:21:01.5	31:15:29.4	20.81	21.58	19.88	21.00	33	1.74
CB-17.3341	15:21:03.4	31:00:12.6	20.69	21.05	20.68	21.63	30	1.36
CB-16.3968	15:21:07.1	30:53:55.5	20.83	22.11	19.77	20.88	29	1.85
CB-17.3096	15:21:08.7	31:11:39.0	17.47	19.28	16.63	18.41	63	3.07
CB-17.3011	15:21:10.6	31:10:26.9	20.70	21.33	19.95	21.26	30	1.63
CB-17.2858	15:21:13.1	31:01:20.2	19.09	20.37	19.19	20.54	51	2.16
CB-17.2834	15:21:13.7	31:04:54.9	20.70	21.87	20.89	21.83	31	1.76
CB-17.2564	15:21:20.6	31:06:02.7	21.04	21.75	21.74	21.74	26	1.52
CB-17.2480	15:21:22.1	30:57:38.6	20.23	21.02	20.98	22.02	32	1.58
CB-17.2487	15:21:22.3	31:08:00.8	19.95	20.84	19.96	20.98	51	1.91
CB-17.2489	15:21:22.4	31:10:30.4	19.18	20.13	18.88	20.16	71	2.01
CB-17.2364	15:21:25.5	31:14:14.5	18.17	19.64	17.59	18.98	111	2.89
CB-17.2211	15:21:28.5	31:03:44.0	19.75	20.98	19.86	20.88	58	2.20
CB-17.2114	15:21:31.3	31:16:03.2	18.58	19.91	17.69	18.92	114	2.65
CB-17.2054	15:21:32.5	31:11:44.5	17.32	19.31	17.30	19.09	255	4.15
CB-17.1988	15:21:34.2	31:10:21.4	19.40	20.43	19.67	20.74	59	2.13
CB-17.1911	15:21:36.1	31:07:52.8	20.24	21.53	20.66	21.22	52	2.77
CB-17.1868	15:21:37.0	31:02:36.6	17.89	19.73	17.68	19.57	161	3.34
CB-17.1880	15:21:37.1	31:14:52.0	18.06	19.27	17.98	19.27	89	2.37
CB-17.1823	15:21:37.9	31:07:11.0	19.22	20.28	18.47	19.72	19	1.48
CB-17.1559	15:21:44.2	31:21:52.5	18.73	19.78	18.11	19.08	77	2.08
CB-17.1525	15:21:45.1	31:15:52.2	20.61	21.28	21.10	21.39	32	1.64
CB-17.1479	15:21:46.5	31:24:28.4	20.25	20.71	19.95	20.77	37	1.41
CB-17.1436	15:21:47.3	31:18:55.7	17.45	18.53	16.06	17.30	143	2.64
CB-17.1392	15:21:48.4	31:19:21.4	18.98	20.15	18.70	19.47	41	2.14
CB-17.1344	15:21:50.0	31:23:44.8	18.27	19.50	17.69	18.97	120	2.56
CB-00.61	15:21:55.7	31:23:35.2	...	...	22.16	22.15	6	1.58
CB-17.946	15:22:00.5	31:34:06.4	18.98	19.69	18.21	18.90	61	1.69
CB-17.836	15:22:02.8	31:17:42.4	21.11	21.56	20.18	21.29	22	1.38
CB-17.802	15:22:03.6	31:24:23.8	18.17	19.69	17.91	19.18	141	3.00
CB-16.844	15:22:04.8	30:32:59.2	19.78	20.78	18.86	19.97	64	2.33
CB-17.752	15:22:05.0	31:32:43.5	20.98	21.77	19.98	20.96	26	1.59
CB-17.701	15:22:05.3	31:08:01.6	19.95	20.78	...	...	10	1.16
CB-17.646	15:22:06.3	31:06:59.8	21.96	22.16	20.04	21.27	12	1.06
CB-16.728	15:22:07.1	30:35:40.9	20.62	21.86	19.67	20.89	40	2.49
CB-17.649	15:22:07.1	31:32:06.5	20.57	21.61	19.71	20.95	37	2.08
CB-17.584	15:22:08.4	31:25:33.3	20.25	21.61	20.09	21.16	41	2.00
CB-16.628	15:22:09.0	30:31:40.4	20.67	21.53	19.92	21.15	33	1.77
CB-00.62	15:22:09.2	31:13:17.6	...	...	21.30	22.10	21	1.81
CB-16.594	15:22:10.0	30:36:27.3	19.49	20.20	19.55	20.32	51	1.72
CB-16.456	15:22:12.5	30:26:16.6	18.17	19.40	17.82	19.08	27	1.67
CB-16.447	15:22:13.2	30:38:36.3	22.18	22.35	19.94	21.13	11	0.98
CB-16.414	15:22:13.3	30:21:51.5	20.00	20.76	19.40	20.45	42	1.77
CB-17.368	15:22:13.6	31:16:48.4	17.57	18.98	16.96	18.35	182	2.91
CB-17.356	15:22:13.9	31:17:04.4	20.28	21.15	19.73	20.77	41	1.93
CB-16.294	15:22:15.7	30:21:40.0	19.15	19.98	19.06	19.94	62	1.87
CB-17.194	15:22:17.8	31:08:15.4	21.82	22.16	20.22	21.10	14	1.23
CB-17.93	15:22:20.7	31:11:14.3	19.73	21.40	19.21	20.93	76	2.82
CB-17.84	15:22:21.3	31:15:33.8	21.26	21.89	19.97	21.14	21	1.45
CB-17.69	15:22:21.4	31:07:45.2	18.21	19.90	17.56	19.23	63	3.13
CB-23.9060	15:22:23.4	31:14:41.8	20.19	21.29	20.07	21.28	44	1.99
CB-22.9376	15:22:23.8	30:30:11.3	20.60	21.45	19.56	21.20	36	1.75
CB-23.9032	15:22:24.2	31:18:30.0	20.94	21.31	20.34	21.28	30	1.48

TABLE 2.6—*Continued*

Object	RA (1950)	Dec. (1950)	g_{tot}	g_{core}	r_{tot}	r_{core}	Area ($\square''$)	irl ($''$)
CB-23.9037	15:22:24.3	31:30:22.4	21.08	22.03	20.80	22.01	23	1.50
CB-22.9342	15:22:24.8	30:34:24.5	21.23	22.15	21.09	21.67	22	1.55
CB-23.8871	15:22:27.6	31:09:14.0	21.79	22.37	23.35	22.29	9	1.01
CB-23.8796	15:22:30.2	31:18:37.6	21.48	22.17	20.42	21.39	17	1.42
CB-23.8742	15:22:31.5	31:16:21.4	21.32	21.83	20.74	21.89	20	1.39
CB-23.8698	15:22:32.9	31:17:04.9	21.13	22.01	20.86	21.47	21	1.47
CB-22.8966	15:22:33.0	30:33:53.5	21.24	22.22	21.85	22.09	23	1.71
CB-23.8674	15:22:33.7	31:23:01.2	21.00	21.71	20.41	21.20	27	1.50
CB-23.8601	15:22:35.5	31:18:58.2	21.43	21.86	20.57	21.48	20	1.40
CB-23.8574	15:22:36.2	31:23:43.6	20.06	21.26	19.95	21.27	52	2.18
CB-22.8722	15:22:38.0	30:37:17.9	20.67	21.55	20.44	21.39	30	1.69
CB-23.8495	15:22:38.0	31:19:45.9	21.26	22.29	19.72	21.38	20	1.51
CB-23.8439	15:22:39.3	31:17:46.6	19.00	19.52	17.89	18.71	58	1.56
CB-23.8408	15:22:40.4	31:22:21.9	20.77	21.30	19.77	20.58	29	1.43
CB-23.8399	15:22:40.8	31:24:42.3	21.11	21.85	20.66	21.76	28	1.64
CB-23.8364	15:22:41.3	31:17:40.5	21.58	22.16	20.62	21.50	13	1.17
CB-22.8429	15:22:43.5	30:33:17.6	21.34	21.67	19.96	20.68	28	1.46
CB-23.8201	15:22:45.7	31:18:55.8	19.85	21.12	19.42	20.77	63	2.35
CB-22.8100	15:22:51.5	30:26:14.4	20.82	21.56	21.65	22.04	23	1.48
CB-23.7916	15:22:53.7	31:28:22.7	17.71	19.50	17.72	19.57	183	3.42
CB-23.7869	15:22:55.1	31:31:18.9	19.01	20.02	18.05	19.17	28	1.62
CB-23.7790	15:22:56.5	31:24:11.9	16.24	18.62	15.92	17.89	188	3.87
CB-23.7722	15:22:58.5	31:27:52.2	17.30	18.34	15.18	16.02	137	2.34
CB-22.7678	15:23:00.7	30:33:39.7	20.96	21.59	20.87	21.73	21	1.22
CB-20.9245	15:23:00.8	28:39:42.1	19.41	20.55	18.71	19.82	57	2.02
CB-20.9123	15:23:03.2	28:42:12.3	18.22	19.99	18.64	20.32	59	2.81
CB-20.9024	15:23:05.2	28:41:39.5	20.81	21.97	20.75	21.78	34	1.91
CB-19.8716	15:23:06.8	28:27:01.0	17.95	18.87	16.77	17.85	114	2.18
CB-00.18	15:23:10.8	28:45:20.4	...	...	20.45	21.72	23	1.82
CB-19.8480	15:23:12.1	28:27:17.9	19.75	20.68	19.46	20.44	58	1.96
CB-20.8661	15:23:12.4	28:42:56.0	20.22	21.26	20.35	21.31	39	1.95
CB-20.8643	15:23:12.9	28:45:16.2	19.24	20.35	19.64	20.51	65	2.16
CB-22.7181	15:23:13.3	30:28:58.8	19.41	20.64	19.33	20.79	37	1.97
CB-20.8522	15:23:15.4	28:40:05.0	21.45	21.70	20.82	21.47	22	1.38
CB-20.8484	15:23:16.3	28:45:08.8	19.83	20.70	19.19	20.23	55	2.03
CB-20.8424	15:23:17.4	28:38:48.3	20.53	21.48	21.55	21.99	37	1.83
CB-19.8182	15:23:17.9	28:29:00.5	18.61	19.68	17.62	18.84	8	0.97
CB-20.8289	15:23:20.4	28:36:12.1	20.01	20.91	19.15	20.20	48	2.01
CB-21.6583	15:23:22.2	30:00:59.8	17.22	18.89	16.43	18.05	282	3.88
CB-21.6488	15:23:24.4	29:58:27.6	18.73	20.00	18.07	19.38	101	2.59
CB-21.6439	15:23:25.1	29:50:08.0	20.68	21.25	19.43	20.22	34	1.61
CB-20.8067	15:23:25.7	28:35:01.1	20.73	21.77	20.05	21.23	31	1.72
CB-22.6754	15:23:25.7	30:38:23.9	21.32	21.87	20.25	21.01	22	1.53
CB-21.6418	15:23:26.0	29:58:56.8	18.98	20.47	18.47	20.02	92	2.97
CB-00.21	15:23:27.1	29:59:28.9	...	...	21.36	21.78	9	1.20
CB-21.6348	15:23:27.4	29:48:37.7	17.69	19.37	...	...	165	4.23
CB-22.6628	15:23:28.3	30:38:23.3	18.87	19.57	17.56	18.34	66	1.73
CB-00.19	15:23:30.7	29:44:13.6	...	...	21.55	22.02	12	1.44
CB-21.6156	15:23:32.6	29:42:55.6	21.03	21.79	20.13	21.11	27	1.49
CB-22.6391	15:23:33.8	30:23:34.4	18.48	20.22	18.26	19.79	116	3.33
CB-24.5970	15:23:33.9	32:21:21.1	17.12	19.14	17.09	19.10	193	3.47
CB-22.6369	15:23:34.8	30:36:10.4	19.78	20.62	19.49	20.68	48	1.78
CB-24.5902	15:23:35.7	32:21:15.9	18.32	19.88	18.54	19.90	129	2.79
CB-22.6322	15:23:35.9	30:31:50.1	19.92	20.68	19.94	20.82	21	1.39
CB-24.5865	15:23:37.0	32:20:56.1	18.44	19.22	17.62	18.41	76	1.86
CB-24.5825	15:23:38.2	32:21:47.4	19.63	20.55	18.80	19.99	57	1.94
CB-22.6248	15:23:38.5	30:36:47.9	19.98	21.44	19.58	21.38	62	2.52
CB-24.5778	15:23:39.5	32:19:44.9	20.52	21.71	21.04	21.75	47	2.49
CB-24.5752	15:23:39.6	32:08:19.8	18.36	19.59	17.47	18.69	80	2.31
CB-22.6194	15:23:39.8	30:37:59.9	21.34	22.10	20.47	21.75	14	1.28
CB-24.5701	15:23:40.6	32:12:01.3	21.92	22.40	...	...	6	1.03
CB-21.5790	15:23:41.8	29:58:17.3	19.74	20.30	19.30	20.36	47	1.54

TABLE 2.6—*Continued*

Object	RA (1950)	Dec. (1950)	g_{tot}	g_{core}	r_{tot}	r_{core}	Area (□″)	irl (″)
CB-24.5662	15:23:41.9	32:13:33.6	21.13	22.52	...	...	19	1.93
CB-24.5673	15:23:42.0	32:19:49.4	19.73	20.70	19.30	20.37	52	1.92
CB-24.5627	15:23:43.0	32:14:07.9	22.28	22.61	...	...	8	0.94
CB-24.5623	15:23:43.4	32:18:36.8	21.48	22.30	21.58	22.17	18	1.41
CB-24.5590	15:23:44.2	32:12:11.6	21.99	22.52	...	...	8	1.07
CB-24.5542	15:23:45.8	32:19:48.8	20.51	21.78	21.29	22.26	48	2.30
CB-24.5519	15:23:46.0	32:11:37.2	22.21	22.88	20.04	21.50	12	1.52
CB-21.5476	15:23:48.3	29:46:39.3	20.61	21.82	21.10	21.70	35	2.00
CB-24.5387	15:23:49.2	32:07:37.9	21.98	22.51	20.73	21.61	10	1.12
CB-24.5393	15:23:49.7	32:19:41.6	22.12	22.64	...	...	9	1.07
CB-20.6924	15:23:50.0	28:37:37.3	20.05	21.00	21.18	21.83	40	1.82
CB-19.6608	15:23:51.5	28:08:06.1	20.44	21.39	20.01	20.89	36	1.78
CB-20.6836	15:23:51.7	28:37:13.6	22.36	22.65	21.75	22.06	6	0.88
CB-19.6562	15:23:52.5	28:08:29.0	21.63	22.53	...	...	17	1.78
CB-24.5271	15:23:52.7	32:13:49.5	22.29	22.77	21.72	22.24	9	1.03
CB-21.5310	15:23:52.8	30:00:11.4	21.17	22.11	21.41	21.87	20	1.38
CB-24.5254	15:23:52.9	32:08:04.3	21.16	22.08	20.81	21.96	22	1.54
CB-24.5239	15:23:53.1	32:04:59.4	18.76	20.10	18.72	20.15	99	2.54
CB-19.6479	15:23:54.1	28:03:53.5	21.86	22.87	...	...	11	1.63
CB-19.6396	15:23:55.8	27:53:57.3	20.09	20.99	19.39	20.24	48	1.89
CB-19.6392	15:23:56.3	28:01:37.0	17.10	19.37	17.33	19.34	254	4.65
CB-19.6377	15:23:56.9	28:10:11.4	22.19	22.49	...	...	7	0.94
CB-19.6323	15:23:57.7	28:03:50.7	21.90	22.69	22.27	22.88	12	1.26
CB-21.5041	15:23:58.2	29:48:48.2	20.14	21.16	20.26	21.18	45	1.93
CB-19.6268	15:23:59.1	28:01:43.1	22.27	22.74	...	...	7	0.90
CB-19.6245	15:23:59.3	27:54:33.2	20.33	21.08	20.16	20.86	26	1.55
CB-19.6273	15:23:59.4	28:09:26.0	21.61	22.50	...	...	14	1.50
CB-21.4972	15:24:00.2	29:58:14.1	21.07	21.54	20.02	21.00	13	1.20
CB-24.4993	15:24:01.0	32:14:25.0	22.08	22.42	22.44	22.42	8	1.12
CB-21.4896	15:24:01.8	29:43:38.9	22.92	23.42	20.70	21.95	7	1.00
CB-19.6141	15:24:02.1	27:56:51.8	22.46	23.10	...	...	6	1.37
CB-19.6151	15:24:02.6	28:11:18.2	19.26	20.05	17.72	18.52	69	2.13
CB-23.5335	15:24:02.8	31:25:58.3	21.48	22.27	...	...	17	1.46
CB-19.6086	15:24:03.3	27:54:08.1	20.18	20.93	19.13	20.02	44	1.81
CB-19.6094	15:24:03.5	28:02:00.3	22.15	23.03	...	...	10	1.45
CB-23.5300	15:24:03.7	31:26:22.7	22.08	22.47	...	...	8	0.93
CB-19.6127	15:24:04.0	28:26:60.0	20.93	21.95	21.45	21.90	20	1.52
CB-19.6083	15:24:04.2	28:12:05.9	18.55	20.66	18.79	20.95	143	3.50
CB-23.5267	15:24:04.6	31:25:19.3	19.45	20.79	20.13	21.62	62	2.34
CB-23.5207	15:24:06.1	31:20:58.8	20.34	21.38	19.50	20.72	43	2.02
CB-24.4798	15:24:06.4	32:14:07.8	21.86	22.48	...	...	11	1.19
CB-24.4802	15:24:06.5	32:16:23.0	21.72	22.60	...	...	15	1.43
CB-23.5170	15:24:07.0	31:24:33.9	19.59	21.23	20.31	21.41	76	2.85
CB-23.5137	15:24:07.1	31:09:57.1	19.73	20.74	18.76	19.93	56	2.13
CB-19.5921	15:24:07.6	28:04:31.2	22.45	22.85	21.44	21.84	6	0.84
CB-23.5113	15:24:08.2	31:19:07.8	21.89	21.79	21.02	21.46	25	1.43
CB-23.5114	15:24:08.6	31:27:19.7	21.98	22.79	...	...	10	1.21
CB-19.5895	15:24:08.6	28:10:51.7	19.53	20.94	19.86	21.47	64	2.29
CB-21.4645	15:24:08.7	29:54:24.7	23.00	23.43	21.73	21.53	13	1.54
CB-24.4712	15:24:09.2	32:21:05.0	20.50	22.00	21.71	22.10	38	2.14
CB-19.5794	15:24:10.3	28:00:31.9	22.01	22.69	...	...	9	1.11
CB-23.4995	15:24:10.5	31:10:25.9	20.67	22.27	19.88	20.88	33	2.32
CB-21.4592	15:24:10.7	30:01:12.1	21.17	21.79	21.28	21.63	16	1.33
CB-23.5009	15:24:11.0	31:29:08.4	20.34	21.22	19.61	21.15	42	1.82
CB-23.4996	15:24:11.1	31:20:44.7	21.48	22.34	21.28	21.79	16	1.60
CB-20.6027	15:24:11.1	28:35:22.3	20.59	21.83	19.77	21.41	47	2.30
CB-23.4966	15:24:11.4	31:15:07.1	21.94	22.38	...	...	6	0.83
CB-19.5710	15:24:11.9	28:00:00.8	21.96	22.71	...	...	12	1.27
CB-23.4951	15:24:12.1	31:19:53.9	21.94	22.50	...	...	10	1.09
CB-24.4562	15:24:12.1	32:12:02.4	21.02	22.19	21.04	21.84	28	1.96
CB-23.4940	15:24:12.5	31:18:51.5	21.69	22.25	...	...	14	1.21
CB-24.4530	15:24:13.5	32:20:11.4	22.40	22.84	...	...	7	1.07

TABLE 2.6—*Continued*

Object	RA (1950)	Dec. (1950)	g_{tot}	g_{core}	r_{tot}	r_{core}	Area ($\square''$)	irl ($''$)
CB-19.5612	15:24:14.0	27:57:07.7	22.30	22.82	20.82	21.94	6	1.01
CB-23.4788	15:24:15.7	31:13:18.3	21.69	22.49	...	...	10	1.30
CB-19.5503	15:24:16.1	27:55:49.5	22.07	22.55	21.21	22.30	8	1.01
CB-23.4778	15:24:16.4	31:21:52.5	22.18	22.44	21.72	21.96	8	0.99
CB-19.5442	15:24:17.2	27:55:00.8	21.74	22.53	...	...	12	1.44
CB-23.4686	15:24:17.8	31:10:15.1	21.96	22.94	...	...	9	1.67
CB-24.4320	15:24:18.7	32:13:44.8	22.33	22.70	...	...	6	0.86
CB-19.5437	15:24:19.0	28:26:45.7	19.62	20.45	18.74	19.68	54	1.89
CB-23.4639	15:24:19.0	31:13:43.3	22.02	22.68	...	...	7	1.54
CB-23.4628	15:24:19.4	31:18:57.4	21.16	22.22	20.68	21.88	23	1.82
CB-19.5332	15:24:20.4	28:06:47.2	20.44	21.71	19.98	21.32	47	2.14
CB-20.5612	15:24:20.9	28:45:39.5	17.49	19.36	17.39	19.09	196	4.03
CB-24.4222	15:24:21.2	32:12:31.0	22.61	23.14	...	...	6	1.04
CB-23.4547	15:24:21.8	31:22:31.8	19.39	20.04	17.91	18.67	47	1.63
CB-20.5550	15:24:21.9	28:38:04.4	21.24	22.28	21.06	21.86	25	2.04
CB-19.5198	15:24:23.0	28:07:34.6	22.08	22.64	...	...	8	1.16
CB-19.5250	15:24:23.1	28:27:52.3	19.40	20.26	19.48	20.44	63	1.90
CB-24.4178	15:24:23.3	32:24:41.5	21.94	22.75	...	...	12	1.31
CB-19.5219	15:24:23.8	28:27:18.8	21.27	21.91	20.96	21.54	26	1.71
CB-00.17	15:24:24.5	28:36:15.2	...	...	21.44	22.07	14	1.22
CB-21.3938	15:24:24.8	29:52:54.9	21.13	21.72	20.49	21.80	22	1.37
CB-19.5056	15:24:25.1	27:59:25.0	22.01	22.52	...	...	7	1.05
CB-23.4392	15:24:25.3	31:17:22.9	21.92	22.41	...	...	10	1.04
CB-19.5064	15:24:25.4	28:05:06.5	21.67	22.40	...	...	13	1.29
CB-23.4384	15:24:26.1	31:28:59.2	21.62	22.39	22.06	22.59	15	1.39
CB-24.4030	15:24:26.6	32:05:02.9	22.62	23.08	...	...	7	1.07
CB-24.4027	15:24:27.3	32:16:39.8	20.98	22.01	20.39	21.50	27	1.75
CB-21.3837	15:24:27.5	29:50:23.9	19.09	20.05	18.45	19.79	77	2.15
CB-24.4002	15:24:27.5	32:07:53.4	21.19	22.21	20.83	21.74	29	1.94
CB-20.5300	15:24:27.8	28:40:07.4	19.68	20.60	19.26	20.34	48	1.86
CB-19.4924	15:24:28.0	27:59:05.3	22.00	22.79	...	...	8	1.24
CB-23.4285	15:24:28.2	31:20:54.7	22.13	22.76	...	...	7	1.03
CB-19.4892	15:24:28.3	27:54:22.6	22.63	23.07	...	...	6	1.01
CB-19.4969	15:24:28.4	28:27:20.5	17.84	19.31	17.21	18.75	164	2.96
CB-20.5275	15:24:28.6	28:43:46.2	17.64	18.51	16.26	17.42	102	2.00
CB-24.3948	15:24:28.9	32:05:03.7	22.23	22.91	...	...	7	1.04
CB-20.5245	15:24:29.0	28:35:54.3	18.60	19.39	17.40	18.22	73	1.83
CB-24.3970	15:24:29.3	32:23:32.5	22.35	22.91	...	...	6	0.88
CB-23.4191	15:24:30.2	31:17:24.1	22.29	22.79	...	...	8	0.97
CB-19.4794	15:24:30.3	27:59:52.9	21.65	22.77	...	...	15	1.81
CB-19.4786	15:24:30.7	28:08:21.5	22.03	22.81	21.63	22.25	10	1.26
CB-23.4157	15:24:31.4	31:23:20.2	22.46	22.73	...	...	6	0.91
CB-21.3686	15:24:31.9	29:51:03.9	21.48	22.26	20.66	21.40	16	1.36
CB-19.4683	15:24:32.2	27:59:29.5	22.37	22.62	...	...	14	1.22
CB-20.5127	15:24:32.3	28:45:57.8	20.01	20.58	18.61	19.29	39	1.56
CB-24.3798	15:24:33.3	32:09:23.2	21.84	22.40	22.06	22.24	17	1.64
CB-20.5076	15:24:33.4	28:45:36.5	20.93	22.08	19.96	21.16	24	1.77
CB-20.5031	15:24:34.1	28:38:30.2	18.13	19.72	18.38	19.82	156	3.12
CB-00.20	15:24:34.4	29:57:35.8	...	...	20.02	21.20	43	2.05
CB-24.3768	15:24:34.4	32:11:09.9	21.81	22.51	...	...	10	1.17
CB-23.4012	15:24:34.9	31:26:28.5	20.48	21.67	20.57	21.59	18	1.55
CB-24.3760	15:24:35.0	32:15:44.6	22.47	22.93	...	...	6	1.01
CB-24.3719	15:24:36.0	32:14:29.7	21.98	22.52	...	...	11	1.11
CB-21.3527	15:24:36.3	29:52:19.6	18.70	20.18	18.33	19.72	84	2.93
CB-24.3705	15:24:36.6	32:16:36.5	22.10	22.67	...	...	6	1.35
CB-21.3474	15:24:37.3	29:43:44.1	22.01	22.54	21.07	21.97	15	1.35
CB-23.3920	15:24:37.4	31:24:54.5	21.86	22.91	21.65	21.98	11	2.13
CB-21.3256	15:24:43.0	29:44:20.8	19.14	20.92	18.81	20.60	101	3.49
CB-24.3443	15:24:44.1	32:24:48.3	21.52	21.97	21.18	22.09	17	1.27
CB-21.3248	15:24:44.3	30:00:16.8	20.95	21.52	21.42	21.73	18	1.32
CB-24.3361	15:24:45.6	32:10:45.4	22.55	23.01	...	...	6	1.06
CB-23.3596	15:24:46.1	31:22:22.6	21.74	22.68	...	...	15	1.39

TABLE 2.6—*Continued*

Object	RA (1950)	Dec.	g_{tot}	g_{core}	r_{tot}	r_{core}	Area (□″)	irl (″)
CB-23.3523	15:24:48.0	31:23:46.3	19.91	21.30	21.35	22.08	52	2.35
CB-21.3050	15:24:48.2	29:42:57.1	19.73	20.67	19.08	20.62	65	2.22
CB-24.3297	15:24:48.3	32:21:33.0	21.72	22.68	···	···	13	1.39
CB-19.3873	15:24:49.2	27:57:16.6	20.62	22.21	21.90	22.11	33	2.22
CB-21.3031	15:24:49.5	29:58:58.7	22.22	22.51	20.99	22.04	13	1.21
CB-24.3232	15:24:49.7	32:18:25.6	20.19	21.59	20.28	21.54	54	2.23
CB-19.3824	15:24:50.3	27:54:01.7	22.38	22.88	···	···	6	0.94
CB-21.2958	15:24:50.9	29:51:50.9	17.41	18.37	16.36	17.45	83	2.06
CB-24.3145	15:24:52.7	32:24:12.4	21.54	22.38	···	···	16	1.46
CB-24.3107	15:24:53.2	32:12:31.5	22.05	22.63	···	···	8	1.02
CB-24.3115	15:24:53.6	32:22:25.7	21.21	22.06	···	···	24	1.64
CB-24.3070	15:24:54.4	32:15:50.0	21.99	22.74	···	···	9	1.07
CB-21.2814	15:24:54.4	29:57:36.4	18.92	20.28	18.39	19.89	91	2.63
CB-24.3037	15:24:55.0	32:06:17.0	17.29	19.76	17.63	19.96	295	4.53
CB-23.3266	15:24:55.1	31:27:06.8	22.16	22.54	···	···	14	1.32
CB-21.2774	15:24:55.4	30:00:47.2	21.10	21.47	18.52	20.22	6	0.85
CB-19.3617	15:24:55.7	27:57:14.7	18.39	19.77	18.18	19.56	113	2.65
CB-24.2955	15:24:57.7	32:09:19.1	22.09	22.92	21.96	22.48	9	1.30
CB-19.3535	15:24:58.5	28:06:07.9	20.33	21.42	20.73	21.81	37	1.81
CB-24.2961	15:24:58.6	32:24:54.1	22.10	22.72	···	···	12	1.21
CB-19.3469	15:24:59.5	27:53:18.6	21.29	22.60	···	···	21	2.54
CB-19.3482	15:24:59.9	28:05:43.1	20.43	21.38	21.81	22.17	38	2.02
CB-24.2872	15:25:00.4	32:10:48.0	19.92	21.11	20.13	21.26	40	1.92
CB-24.2866	15:25:01.2	32:22:20.7	18.81	20.47	19.05	20.56	116	3.11
CB-24.2820	15:25:01.6	32:06:07.1	21.84	22.36	···	···	8	1.23
CB-19.3322	15:25:02.8	27:57:37.8	22.26	22.79	···	···	6	0.86
CB-24.2795	15:25:03.2	32:18:20.0	20.98	21.85	20.60	21.85	34	1.88
CB-19.3244	15:25:04.8	28:00:14.4	21.63	22.57	···	···	15	1.40
CB-24.2708	15:25:04.9	32:08:34.3	21.61	22.22	20.35	21.24	13	1.21
CB-24.2723	15:25:05.0	32:15:00.1	20.43	21.38	20.78	21.47	40	1.77
CB-19.3201	15:25:05.7	27:58:42.6	22.98	22.74	···	···	6	0.87
CB-24.2661	15:25:05.7	32:06:15.4	19.08	19.90	17.50	18.38	89	2.10
CB-24.2687	15:25:06.2	32:21:15.0	20.07	21.33	18.45	20.09	48	2.16
CB-23.2873	15:25:06.2	31:23:35.6	20.84	21.84	19.85	21.11	33	1.82
CB-23.2848	15:25:06.5	31:12:56.4	20.92	22.24	21.27	21.94	29	2.15
CB-19.3169	15:25:07.3	28:11:35.9	20.46	21.88	20.41	21.43	38	1.98
CB-24.2639	15:25:07.4	32:22:41.1	19.83	20.64	18.97	20.18	15	1.26
CB-23.2826	15:25:07.6	31:19:59.6	20.43	21.59	20.61	21.09	46	2.21
CB-24.2584	15:25:08.7	32:22:17.9	20.30	21.45	20.30	21.32	44	2.18
CB-19.3012	15:25:09.9	27:56:45.6	21.63	22.40	20.48	21.70	14	1.37
CB-19.3047	15:25:10.1	28:11:45.1	21.88	22.49	21.84	22.28	14	1.23
CB-19.2992	15:25:10.2	27:53:53.3	22.57	22.99	20.96	21.72	6	0.84
CB-24.2498	15:25:10.9	32:23:38.0	19.89	21.25	19.59	21.21	55	2.29
CB-19.2945	15:25:11.2	27:53:05.7	20.97	21.68	20.50	20.82	22	1.55
CB-23.2691	15:25:11.9	31:24:46.7	21.96	22.95	···	···	10	1.26
CB-19.2924	15:25:12.0	27:57:11.9	21.36	22.16	22.08	22.65	21	1.43
CB-19.2857	15:25:14.7	28:11:36.8	22.05	22.79	···	···	7	1.07
CB-19.2820	15:25:14.8	28:00:13.6	21.11	21.89	21.09	21.71	24	1.55
CB-19.2758	15:25:16.8	28:11:44.3	21.85	22.59	20.28	21.04	12	1.19
CB-19.2734	15:25:16.9	28:06:32.5	22.26	22.91	···	···	7	1.09
CB-19.2704	15:25:17.2	28:01:06.8	22.94	22.74	···	···	7	1.55
CB-19.2635	15:25:18.5	28:00:42.5	20.46	21.91	20.06	21.30	42	2.58
CB-23.2356	15:25:20.1	31:26:02.6	21.69	22.45	21.98	22.28	15	1.35
CB-19.2541	15:25:20.7	28:03:52.7	20.86	22.38	···	···	27	2.99
CB-19.2513	15:25:21.8	28:09:38.5	21.40	22.22	21.57	21.82	16	1.41
CB-19.2462	15:25:23.0	28:08:02.4	19.54	20.74	18.82	19.46	65	2.33
CB-23.2158	15:25:24.8	31:14:09.6	22.05	22.63	···	···	6	1.19
CB-23.2174	15:25:25.3	31:27:55.7	19.87	21.27	19.45	20.82	57	2.38
CB-23.2126	15:25:25.8	31:16:02.9	21.93	22.73	21.62	22.03	10	1.40
CB-23.2129	15:25:26.3	31:28:53.3	19.98	20.35	19.72	20.32	43	1.44
CB-23.2037	15:25:28.6	31:23:49.8	21.33	22.45	···	···	16	2.00
CB-23.2001	15:25:29.7	31:24:44.7	20.88	21.87	21.75	22.29	38	2.01

TABLE 2.6—*Continued*

Object	RA (1950)	Dec.	g_{tot}	g_{core}	r_{tot}	r_{core}	Area (□″)	irl (″)
CB-23.1979	15:25:29.8	31:17:24.0	20.14	21.44	19.31	20.50	45	2.07
CB-23.1932	15:25:31.4	31:26:29.3	21.13	22.40	22.05	22.80	30	2.54
CB-23.1821	15:25:33.9	31:21:54.7	22.61	23.28	...	...	18	1.50
CB-23.1724	15:25:36.9	31:19:41.4	17.22	18.47	16.36	17.52	149	3.08
CB-29.8651	15:27:02.1	31:14:23.0	21.34	22.88	19.68	21.21	20	1.98
CB-29.8574	15:27:04.0	31:10:48.4	20.35	21.52	19.37	20.70	29	1.82
CB-29.8501	15:27:06.5	31:14:35.8	21.86	22.29	20.52	21.17	8	0.93
CB-28.7712	15:27:08.0	30:55:42.6	18.35	20.10	18.93	20.51	135	3.14
CB-29.8295	15:27:10.3	31:05:45.7	18.78	20.60	18.80	20.63	101	2.94
CB-29.8269	15:27:11.1	31:05:24.5	21.68	22.42	21.05	21.77	14	1.28
CB-29.8142	15:27:14.7	31:07:10.9	22.24	22.39	20.84	21.84	10	1.04
CB-29.8100	15:27:15.7	31:05:50.0	20.39	20.85	19.79	20.95	35	1.52
CB-28.7359	15:27:18.1	30:55:54.4	18.03	19.93	18.03	19.76	72	2.81
CB-29.7989	15:27:19.0	31:12:24.1	21.18	21.62	20.15	21.00	28	1.48
CB-29.7435	15:27:33.3	31:12:23.7	19.78	20.50	19.63	20.41	46	1.69
CB-00.29	15:27:42.9	31:12:27.8	...	...	21.53	22.03	15	1.27
CB-27.5750	15:27:49.5	29:42:37.1	21.35	21.87	20.32	21.72	23	1.57
CB-27.5702	15:27:51.3	29:43:42.6	22.11	22.46	21.59	22.39	7	0.92
CB-29.6572	15:27:54.0	31:07:20.6	22.43	22.93	21.40	22.12	6	1.01
CB-27.5526	15:27:55.0	29:36:51.8	19.13	20.66	19.16	20.78	60	2.64
CB-27.5549	15:27:55.0	29:41:45.6	21.82	22.27	...	...	9	1.07
CB-00.30	15:27:55.3	31:14:01.4	...	...	20.69	21.70	25	1.93
CB-27.5438	15:27:57.4	29:39:49.5	19.54	20.48	19.03	20.37	56	1.90
CB-25.6435	15:27:58.1	28:08:52.7	20.42	21.26	20.59	21.44	11	1.18
CB-25.6379	15:27:59.5	28:12:45.6	20.17	21.45	19.45	20.49	43	1.97
CB-25.6299	15:28:00.4	28:05:15.8	20.14	21.63	21.02	21.80	50	2.35
CB-27.5316	15:28:00.9	29:47:46.0	22.35	22.78	...	...	8	1.02
CB-27.5264	15:28:01.8	29:44:53.2	21.36	22.43	20.18	21.66	19	1.96
CB-27.5208	15:28:02.0	29:29:41.9	22.61	23.01	...	...	6	0.90
CB-25.6198	15:28:02.5	28:03:52.8	20.15	21.13	20.21	21.07	32	1.76
CB-25.6135	15:28:02.9	27:56:22.6	19.27	20.96	19.31	21.07	82	2.72
CB-25.6175	15:28:03.1	28:07:16.4	21.08	21.94	21.15	22.05	26	1.58
CB-29.6104	15:28:03.9	31:05:43.7	22.81	22.98	21.01	21.74	7	0.90
CB-25.6105	15:28:04.0	28:02:33.0	21.00	22.02	21.27	22.13	26	1.64
CB-25.6107	15:28:04.5	28:08:23.8	18.80	20.22	18.36	19.75	109	2.88
CB-25.6034	15:28:05.6	28:04:08.5	20.51	21.35	20.74	21.74	32	1.74
CB-29.6067	15:28:05.7	31:14:08.6	19.53	20.85	18.61	19.93	77	2.52
CB-27.5037	15:28:06.3	29:29:15.9	19.93	20.81	19.80	20.36	43	1.85
CB-25.6029	15:28:06.4	28:13:11.3	21.94	22.06	...	...	9	1.24
CB-25.5939	15:28:06.8	27:55:27.4	22.39	22.78	...	...	7	0.90
CB-25.5917	15:28:08.2	28:07:47.7	21.63	22.55	21.86	22.22	16	1.45
CB-25.5898	15:28:08.4	28:02:08.0	21.86	22.45	...	...	11	1.17
CB-25.5866	15:28:08.7	27:54:30.6	19.74	20.98	19.56	21.29	66	2.28
CB-27.4947	15:28:08.8	29:30:53.5	22.83	23.46	...	...	7	1.16
CB-27.4974	15:28:08.9	29:40:40.9	21.65	22.45	...	...	16	1.40
CB-25.5815	15:28:10.1	27:59:53.4	20.51	21.48	20.39	21.66	26	1.78
CB-25.5849	15:28:10.7	28:12:24.1	20.11	21.38	20.65	21.74	52	2.17
CB-27.4846	15:28:11.9	29:36:53.6	22.93	23.20	...	...	6	0.91
CB-29.5750	15:28:12.3	31:06:09.6	18.98	20.80	18.57	20.74	113	3.01
CB-25.5727	15:28:12.5	28:09:24.7	21.30	22.32	22.26	22.85	17	1.42
CB-27.4807	15:28:13.3	29:39:06.8	21.81	22.73	...	...	8	1.28
CB-25.5644	15:28:13.5	28:02:28.0	20.30	21.19	20.41	21.41	53	2.07
CB-25.5471	15:28:15.8	27:53:28.7	19.76	20.84	19.22	20.39	51	2.09
CB-25.5473	15:28:17.0	28:06:35.2	22.43	22.89	21.08	22.07	8	0.98
CB-27.4525	15:28:20.3	29:29:30.4	21.61	22.25	21.09	21.92	16	2.06
CB-29.5082	15:28:22.4	30:58:54.2	21.73	22.25	21.44	22.02	12	1.19
CB-28.4859	15:28:23.4	30:55:15.2	18.94	19.86	18.34	19.48	74	2.01
CB-26.4747	15:28:23.9	29:14:05.1	19.37	20.06	18.78	19.60	52	1.73
CB-25.5090	15:28:24.0	28:00:06.9	19.26	20.34	18.97	19.96	71	2.26
CB-27.4348	15:28:24.2	29:29:25.5	20.25	21.59	...	...	29	2.75
CB-29.5045	15:28:24.2	31:10:34.1	20.40	21.50	20.71	21.25	37	2.24
CB-27.4321	15:28:25.6	29:33:16.7	21.52	22.78	...	...	21	1.83

TABLE 2.6—*Continued*

Object	RA (1950)	Dec. (1950)	g_{tot}	g_{core}	r_{tot}	r_{core}	Area (□″)	irl (″)
CB-26.4667	15:28:25.7	29:11:34.0	19.79	20.71	19.15	20.45	59	2.00
CB-29.4927	15:28:26.5	31:13:42.4	20.38	21.01	19.92	20.55	34	1.56
CB-25.4977	15:28:27.9	28:11:57.1	19.06	20.57	18.89	20.37	102	3.14
CB-27.4248	15:28:28.5	29:39:27.2	22.40	22.94	...	...	9	1.05
CB-26.4519	15:28:29.1	29:12:47.1	22.34	22.84	20.67	21.76	9	1.03
CB-00.27	15:28:30.3	29:13:50.8	...	...	21.68	22.15	14	1.40
CB-26.4431	15:28:30.4	29:07:14.5	21.78	22.83	21.08	22.07	14	1.72
CB-25.4847	15:28:30.6	28:06:46.6	19.47	20.90	19.63	20.80	68	2.63
CB-25.4767	15:28:32.0	28:01:41.2	22.15	22.64	...	...	6	0.91
CB-00.26	15:28:32.1	29:12:51.7	...	...	20.48	21.69	19	1.51
CB-26.4372	15:28:32.2	29:06:21.2	20.04	20.60	18.65	19.35	42	1.55
CB-27.4109	15:28:32.7	29:42:55.8	20.60	22.00	21.13	21.69	37	2.41
CB-26.4334	15:28:33.0	29:04:08.2	19.22	20.81	20.34	21.35	83	2.70
CB-29.4532	15:28:33.0	30:58:57.2	18.98	20.15	18.19	19.59	82	2.35
CB-27.4036	15:28:33.6	29:36:42.8	21.69	22.70	...	...	14	1.38
CB-26.4269	15:28:34.0	29:00:07.8	21.14	21.61	21.30	22.01	28	1.52
CB-27.4043	15:28:34.2	29:43:28.9	20.35	22.27	20.81	21.80	52	2.67
CB-26.4231	15:28:34.8	29:00:57.4	20.79	22.18	20.51	21.76	34	2.09
CB-25.4618	15:28:35.3	27:56:19.8	22.52	23.25	...	...	7	1.10
CB-27.3929	15:28:35.7	29:29:31.4	21.77	22.53	...	...	10	1.41
CB-29.4461	15:28:35.8	31:14:26.2	21.75	22.42	19.97	21.78	11	1.25
CB-29.4362	15:28:37.6	31:11:25.9	21.34	21.60	20.95	21.46	22	1.35
CB-25.4386	15:28:40.5	27:58:08.5	21.81	22.55	21.70	22.24	12	1.36
CB-25.4288	15:28:42.6	28:02:16.4	22.41	22.89	...	...	6	0.92
CB-27.3647	15:28:44.1	29:28:43.2	21.94	22.73	...	...	10	1.30
CB-26.3797	15:28:46.2	29:12:22.1	19.24	20.69	18.70	20.39	60	2.50
CB-27.3585	15:28:47.1	29:37:58.6	22.17	22.64	...	...	7	0.91
CB-25.4065	15:28:47.1	27:57:38.9	22.24	22.91	...	...	9	1.32
CB-27.3577	15:28:47.9	29:44:12.4	22.38	23.09	...	...	9	1.18
CB-26.3697	15:28:48.8	29:13:01.9	20.90	21.48	20.03	21.04	23	1.45
CB-26.3691	15:28:49.4	29:16:28.6	20.55	21.45	20.86	22.00	31	1.59
CB-26.3655	15:28:50.1	29:14:12.6	22.27	21.97	20.75	21.77	20	1.22
CB-27.3315	15:28:53.3	29:42:22.5	21.60	22.18	19.57	20.97	20	1.65
CB-25.3667	15:28:55.5	28:01:22.2	21.33	22.44	...	...	18	1.67
CB-27.3179	15:28:56.8	29:40:19.6	19.76	21.52	20.42	21.20	85	3.79
CB-27.3133	15:28:57.9	29:41:37.6	19.21	20.78	18.95	20.27	77	2.58
CB-25.3490	15:29:00.7	28:03:28.5	20.27	21.80	19.96	21.19	47	2.65
CB-25.3507	15:29:01.0	28:10:56.8	19.76	20.80	19.87	20.82	60	2.18
CB-27.2862	15:29:03.6	29:33:45.2	22.23	22.55	...	...	6	0.88
CB-25.3322	15:29:04.0	28:02:06.8	21.67	22.67	21.78	22.36	12	1.50
CB-25.3248	15:29:05.5	27:59:23.5	20.26	21.25	19.69	20.68	45	2.23
CB-25.3251	15:29:06.0	28:06:52.5	19.51	20.40	19.26	20.47	62	2.03
CB-27.2677	15:29:08.6	29:34:46.3	22.18	22.64	...	...	7	0.98
CB-27.2598	15:29:09.7	29:29:14.7	21.49	22.55	21.73	22.54	24	1.75
CB-27.2624	15:29:10.4	29:39:43.3	21.80	22.40	21.46	21.93	12	1.24
CB-27.2547	15:29:12.4	29:45:36.6	21.89	22.67	...	...	11	1.22
CB-27.2477	15:29:12.5	29:31:24.3	21.17	22.43	21.95	22.19	19	1.74
CB-25.2905	15:29:13.2	28:00:04.4	22.87	22.90	21.15	21.82	7	1.15
CB-27.2442	15:29:13.2	29:29:20.5	16.96	18.08	15.57	16.55	144	2.33
CB-27.2398	15:29:14.6	29:31:39.1	21.22	22.41	21.61	22.03	22	1.67
CB-25.2801	15:29:15.0	27:54:07.1	20.31	21.40	19.72	20.89	39	1.95
CB-27.2400	15:29:15.8	29:43:59.7	19.19	20.55	19.18	20.49	80	2.46
CB-25.2773	15:29:16.7	28:05:46.6	22.14	22.64	...	...	6	0.92
CB-27.2306	15:29:17.0	29:31:24.2	19.63	20.77	19.98	21.03	60	2.20
CB-25.2694	15:29:18.5	28:08:49.7	21.99	22.52	...	...	9	1.10
CB-27.2223	15:29:19.8	29:34:57.0	21.09	21.92	21.93	22.08	18	1.32
CB-25.2599	15:29:20.4	28:03:43.1	20.13	21.05	20.39	21.30	37	1.71
CB-27.2219	15:29:20.5	29:40:46.0	21.73	22.77	20.65	21.86	18	1.89
CB-25.2563	15:29:21.9	28:10:20.3	22.21	22.87	...	...	10	1.32
CB-25.2521	15:29:22.1	27:59:28.7	21.19	22.73	...	...	21	1.87
CB-25.2534	15:29:22.6	28:08:48.1	19.64	20.19	19.40	20.15	46	1.52
CB-26.2383	15:29:23.1	29:11:58.6	20.57	21.46	21.12	21.65	36	1.82

TABLE 2.6—*Continued*

Object	RA (1950)	Dec.	g_{tot}	g_{core}	r_{tot}	r_{core}	Area (□″)	irl (″)
CB-25.2483	15:29:23.4	28:01:02.0	19.07	20.24	18.77	19.80	76	2.22
CB-27.2082	15:29:24.5	29:40:27.1	19.74	20.68	18.82	19.92	52	1.90
CB-25.2438	15:29:25.8	28:12:05.3	20.19	21.87	20.58	21.81	54	2.48
CB-25.2348	15:29:27.1	28:04:54.2	22.51	22.25	21.26	21.78	6	1.14
CB-25.2232	15:29:30.3	28:09:38.9	20.33	21.53	19.65	21.25	42	2.06
CB-26.2008	15:29:31.2	29:02:44.0	21.42	22.83	20.09	21.41	19	1.56
CB-26.1925	15:29:33.5	29:07:59.3	19.00	20.19	18.28	19.35	90	2.27
CB-00.25	15:29:33.6	28:58:02.0	...	...	21.09	21.84	20	1.47
CB-26.1389	15:29:46.8	29:16:10.8	19.69	20.17	18.73	19.71	46	1.49
CB-26.1157	15:29:52.3	29:11:00.3	22.19	22.67	21.28	22.10	7	0.97
CB-26.966	15:29:56.9	29:12:32.2	20.95	22.32	20.43	21.88	29	2.20
CB-35.8818	15:30:46.1	31:15:26.1	17.29	19.31	17.32	19.26	206	3.50
CB-35.8757	15:30:48.0	31:16:22.4	20.61	21.96	20.93	21.59	34	1.92
CB-35.8747	15:30:49.0	31:22:03.2	19.55	20.37	19.46	20.63	26	1.52
CB-35.8649	15:30:50.1	31:07:37.2	17.65	19.25	16.79	18.24	176	3.37
CB-35.8526	15:30:53.0	31:09:11.5	20.51	20.88	20.05	20.83	35	1.50
CB-35.8432	15:30:55.4	31:05:29.0	18.79	20.12	18.16	19.38	83	2.72
CB-35.8443	15:30:56.4	31:17:11.5	21.96	22.78	21.83	22.08	11	1.13
CB-35.8206	15:31:01.6	31:10:46.4	22.23	22.56	20.57	21.66	6	0.95
CB-35.8174	15:31:04.1	31:23:02.0	22.39	22.12	...	...	6	0.95
CB-35.8023	15:31:07.5	31:23:27.4	20.05	21.18	19.31	20.67	28	1.86
CB-35.7940	15:31:08.0	31:11:03.3	20.33	20.85	20.17	21.00	32	1.46
CB-35.7771	15:31:11.1	31:05:10.9	19.75	20.43	19.27	20.23	49	1.69
CB-35.6752	15:31:32.0	31:08:24.4	19.87	21.20	19.58	21.20	64	2.44
CB-35.6701	15:31:34.3	31:17:15.9	17.70	20.18	18.30	20.40	273	4.69
CB-35.6538	15:31:38.2	31:21:45.3	20.17	21.31	19.90	21.11	48	2.12
CB-00.37	15:31:44.5	31:20:24.3	...	...	21.95	22.30	16	1.52
CB-35.6135	15:31:46.6	31:19:26.3	18.46	19.69	18.40	19.72	96	2.33
CB-35.5923	15:31:50.5	31:08:35.0	19.16	20.80	18.79	20.23	88	2.82
CB-35.5861	15:31:53.0	31:16:26.6	17.94	19.29	17.42	18.68	120	2.66
CB-35.5625	15:31:58.5	31:11:48.5	21.10	21.75	21.15	21.77	27	1.54
CB-35.5499	15:32:02.7	31:21:26.0	22.13	22.74	20.70	21.91	6	1.08
CB-00.38	15:32:04.1	31:17:18.3	...	...	21.82	22.19	15	1.29
CB-35.5407	15:32:05.6	31:21:08.7	20.44	21.60	20.16	21.39	34	1.86
CB-35.5343	15:32:05.8	31:12:11.8	21.26	22.72	21.50	22.25	21	1.70
CB-35.5299	15:32:05.9	31:04:36.0	18.84	19.96	18.97	20.18	74	2.18
CB-35.5164	15:32:10.6	31:15:40.2	20.22	21.09	19.55	20.76	14	1.42
CB-35.5116	15:32:10.9	31:07:14.6	20.59	21.31	20.71	21.47	33	1.70
CB-35.5067	15:32:11.8	31:06:13.6	19.61	20.66	19.18	20.49	50	2.03
CB-35.5086	15:32:12.2	31:12:22.7	19.25	19.94	17.81	18.62	59	1.74
CB-35.5136	15:32:12.4	31:22:23.3	18.94	19.97	18.24	19.48	28	1.63
CB-35.4951	15:32:16.2	31:15:54.8	21.26	22.38	21.56	22.23	18	2.02

TABLE 2.7

Quasars Found Serendipitously

Objects	RA (1950.0)	Dec. (1950.0)	$g_{\rm tot}$	$r_{\rm tot}$	z
CB-1.6913	15:11:27.9	28:04:41.1	20.53	19.83	1.040
CB-17.3716	15:20:54.6	31:12:51.9	20.09	20.50	2.887
CB-20.6206	15:24:08.0	28:25:23.2	21.68	21.24	3.880
CB-29.8162	15:27:13.9	31:05:00.5	19.42	19.38	1.264
CB-29.7534	15:27:29.8	31:00:07.0	21.97	20.84	1.147
CB-26.2177	15:29:26.4	29:00:50.7	20.57	21.03	2.886

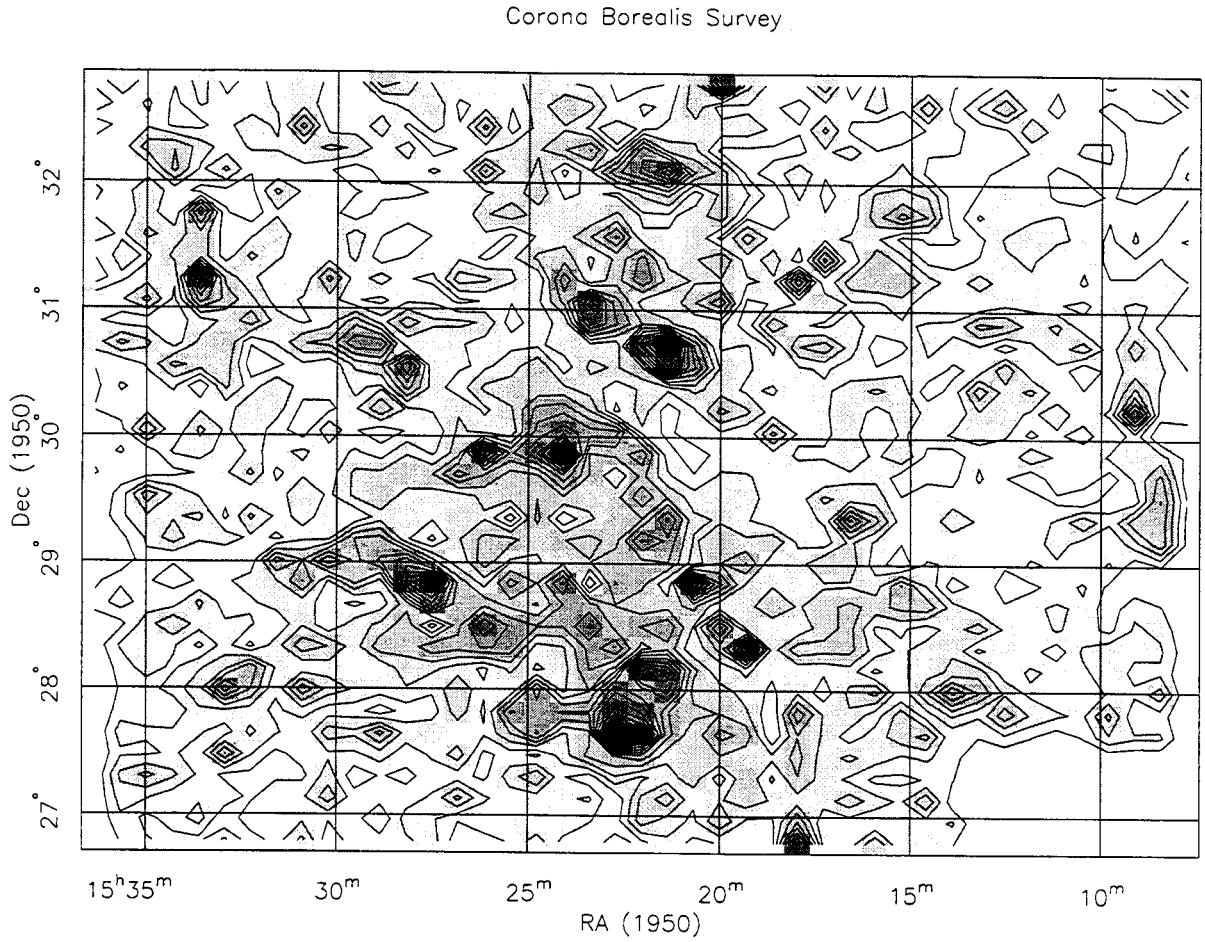

Fig. 2.1.— A combined contour/grayscale plot of the galaxy density on the sky in the Corona Borealis supercluster for all galaxies brighter than $g = 19^m$. The contour levels run from 100 galaxies per square degree to 1200 galaxies per square degree. The ridge of galaxies between Abell 2061 and Abell 2067 connects the two strikingly dense regions at $\alpha = 15^h22^m$, $\delta = +30°36^m$ and $\alpha = 15^h24^m$, $\delta = +31°0^m$. The blank region in the southwest corner is where the plate sensitometer spots are located.

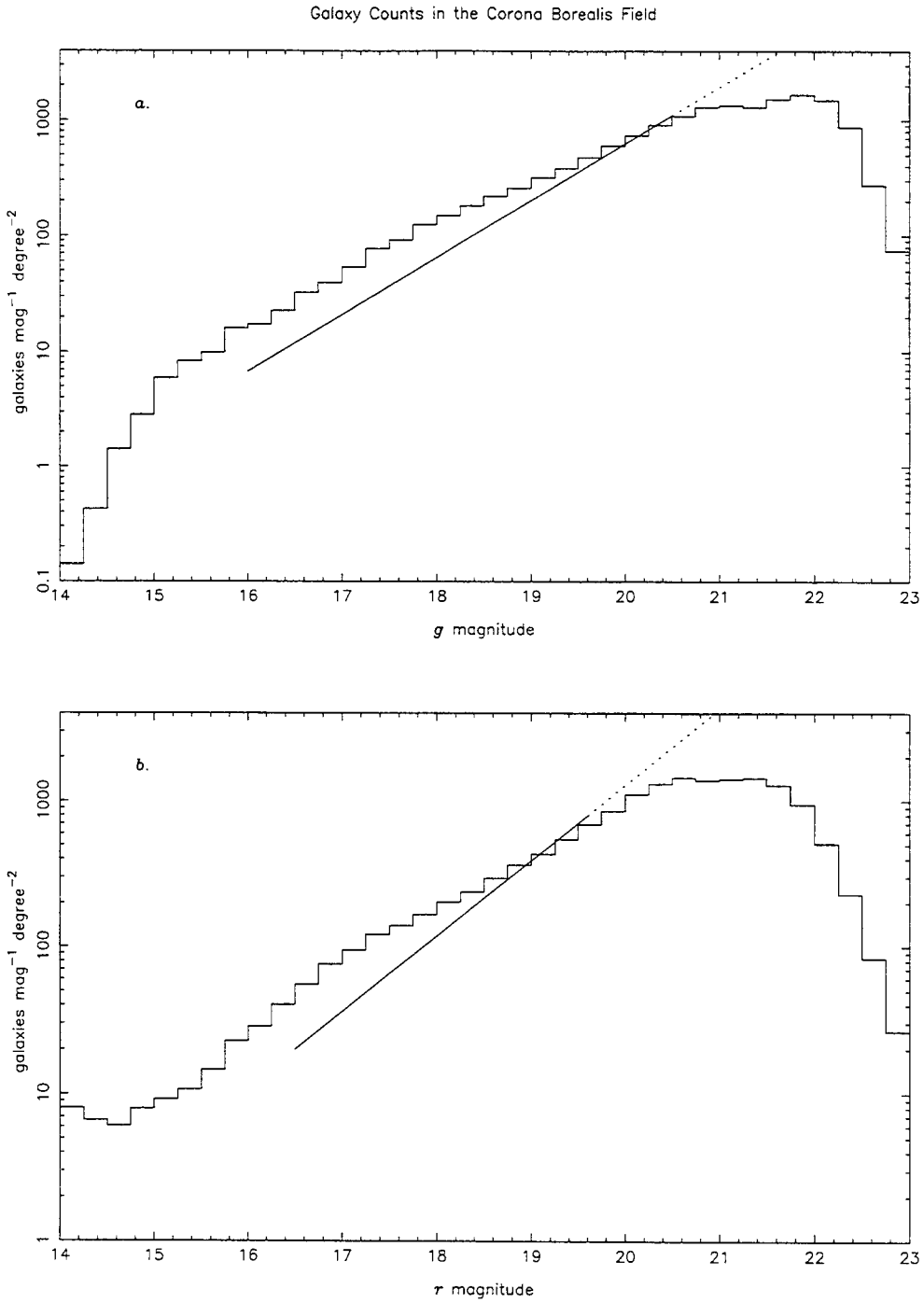

Fig. 2.2.— Galaxy counts in the (a) g and (b) r bands in the Corona Borealis field. The straight line is a fit to the counts of Weir, Djorgovski, and Fayyad (1995) from a high-Galactic latitude field. The solid line marks the region in which the counts are reliable; the dotted line is an extrapolation to fainter magnitudes. The counts in the Corona Borealis field are a $\sim$3 higher than the counts in the comparison field.

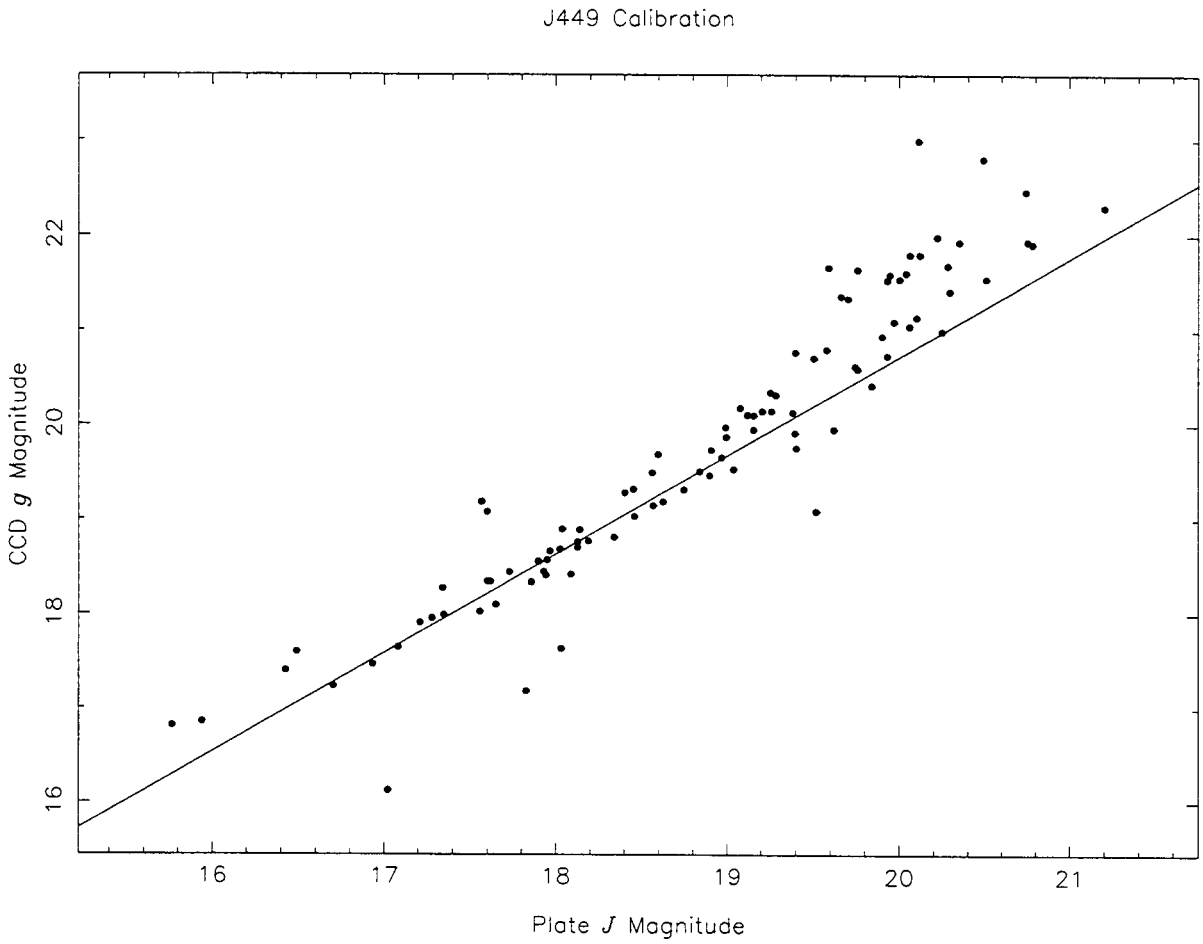

Fig. 2.3.— CCD g magnitudes for galaxies in Abell 2069 plotted against the plate instrumental magnitudes. The straight line is the best fit to the data in the region $16^m < g < 20.5^m$. The RMS error is $\sim 0.3^m$ in this range and is considerably worse for $g > 20.5^m$.

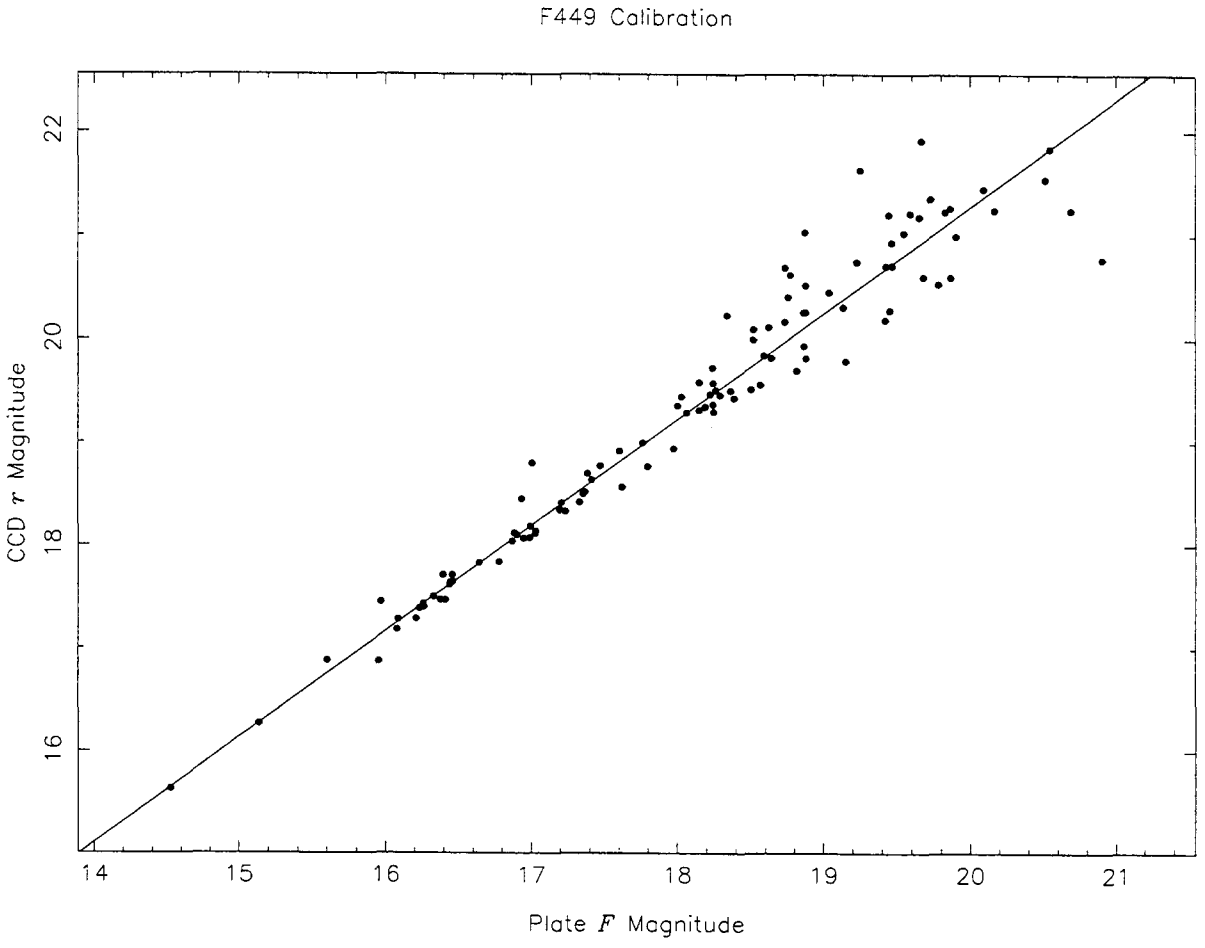

Fig. 2.4.— CCD r magnitudes for galaxies in Abell 2069 plotted against the plate instrumental magnitudes. The straight line is the best fit to the data in the region $16.5^m < r < 19.6^m$. The RMS error is $\sim 0.2^m$ in this range and is considerably worse for $r > 19.6^m$.

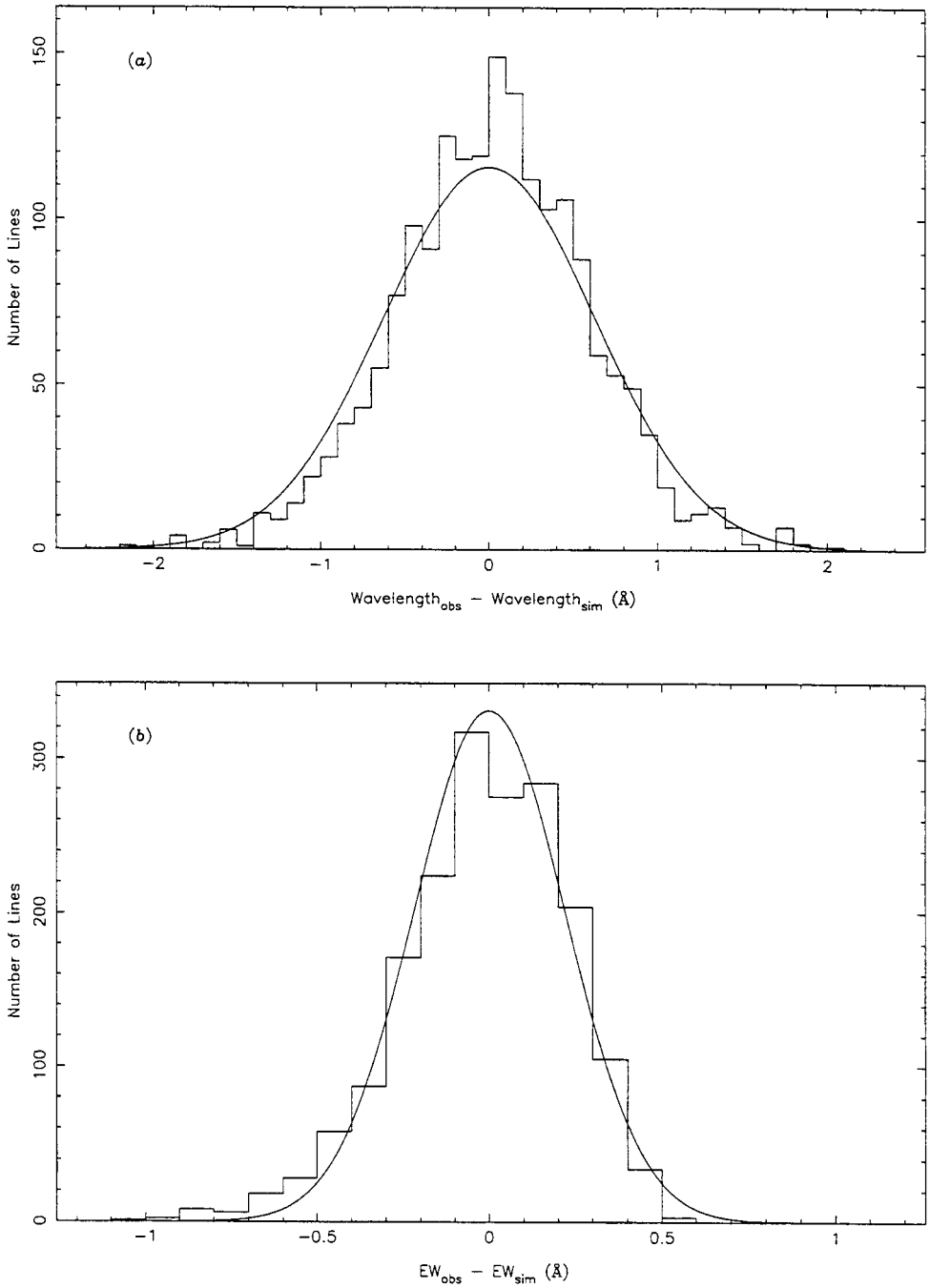

Fig. 2.5.— Histograms of errors (a) in line centroids and (b) in equivalent widths for 1825 simulated spectra. Each spectrum has a signal-to-noise ratio of 17.3 and contains one absorption with an equivalent width of 1.28Å and FWHM of 6Å — a line which is only barely detectable. The smooth lines show the Gaussian error distribution estimated by the program itself. The close agreement between the two distributions indicates that the program is accurately estimating the errors in the line centroids and equivalent widths.

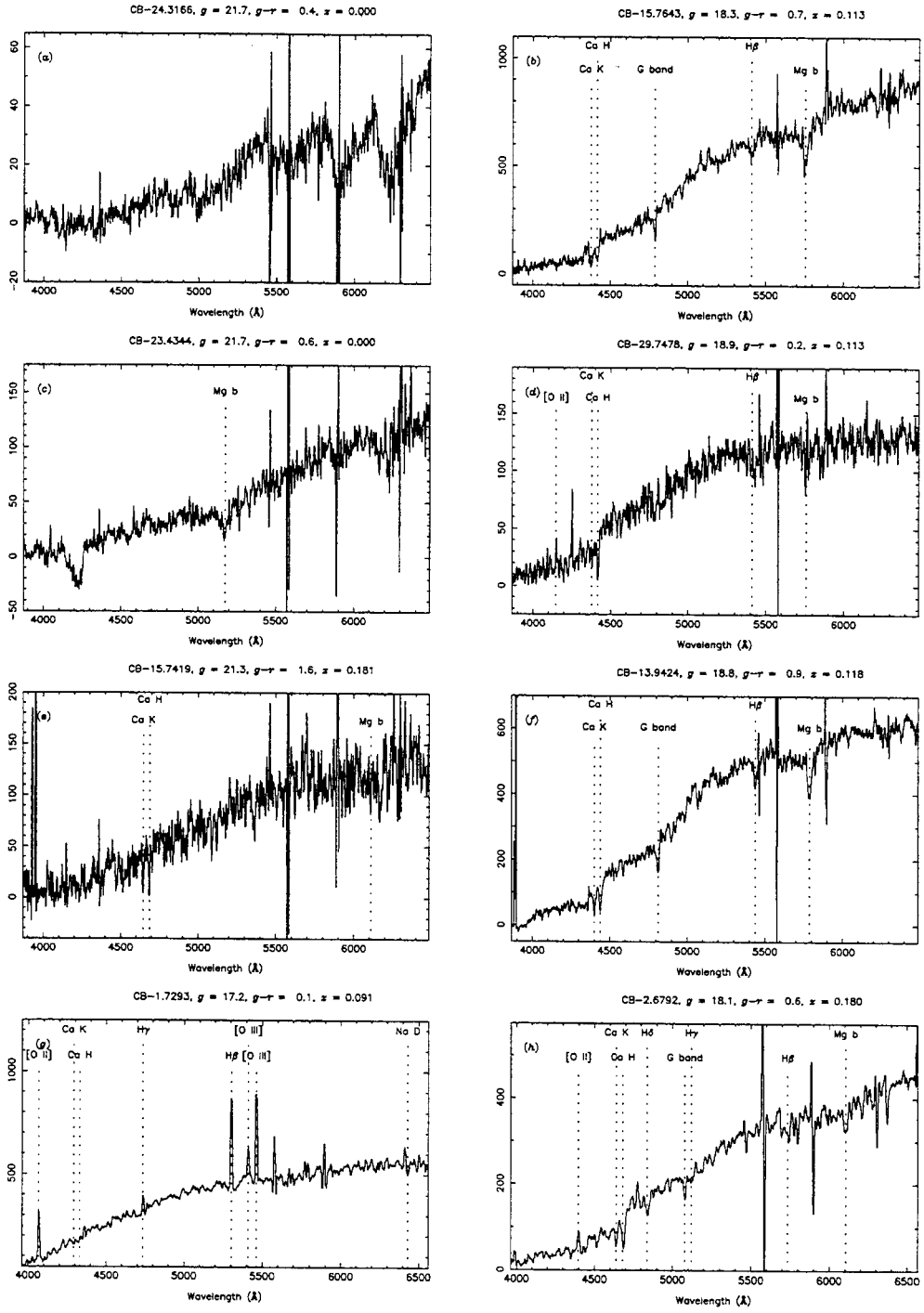

Fig. 2.6.— Spectra of 24 randomly-selected objects from our survey. Spectral features are identified by the vertical dotted lines. The redshift, g magnitude, and $g-r$ color are recorded in the title above each spectrum. See the text for notes about particular objects.

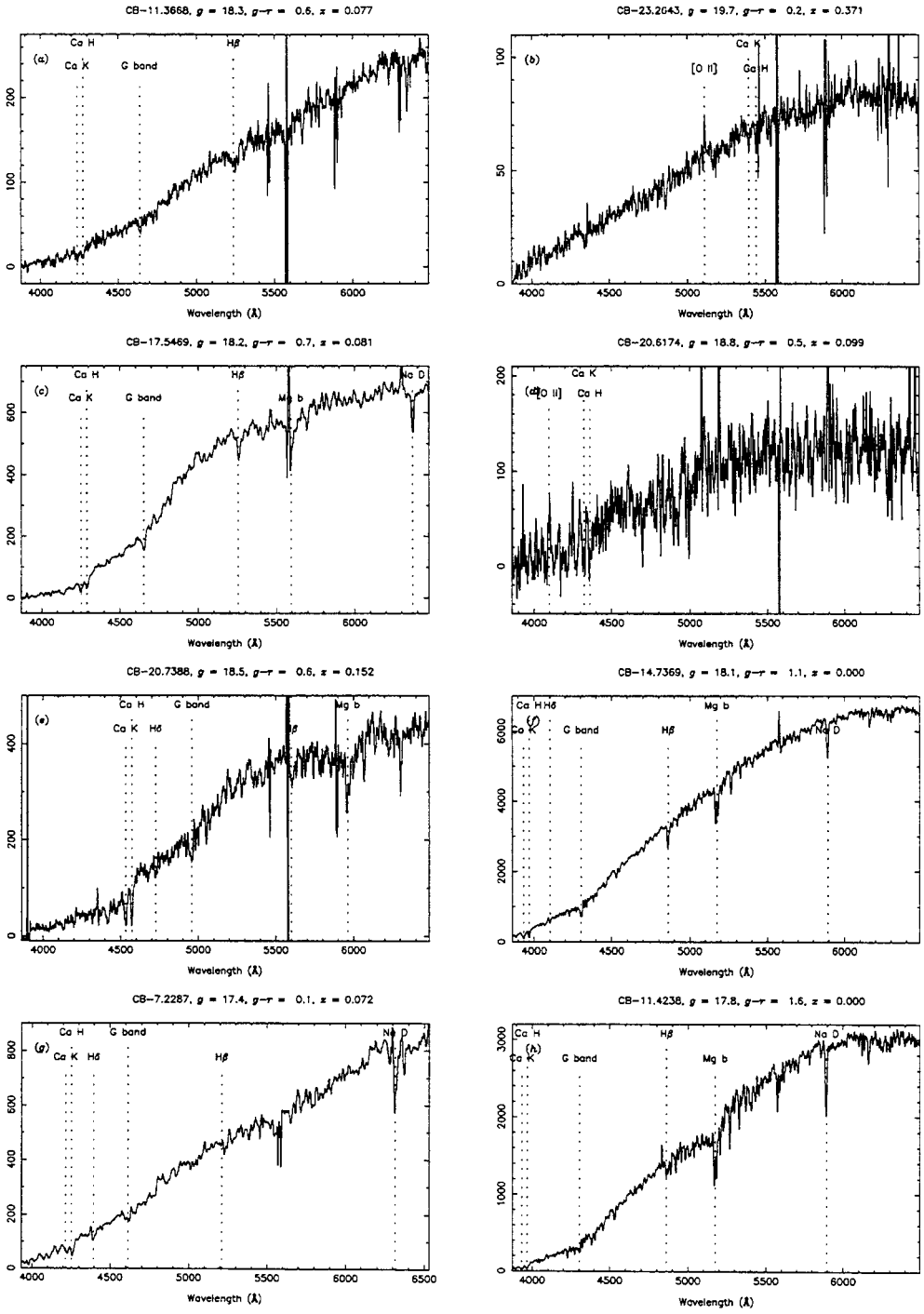

Fig. 2.7.— Same as Figure 2.6.

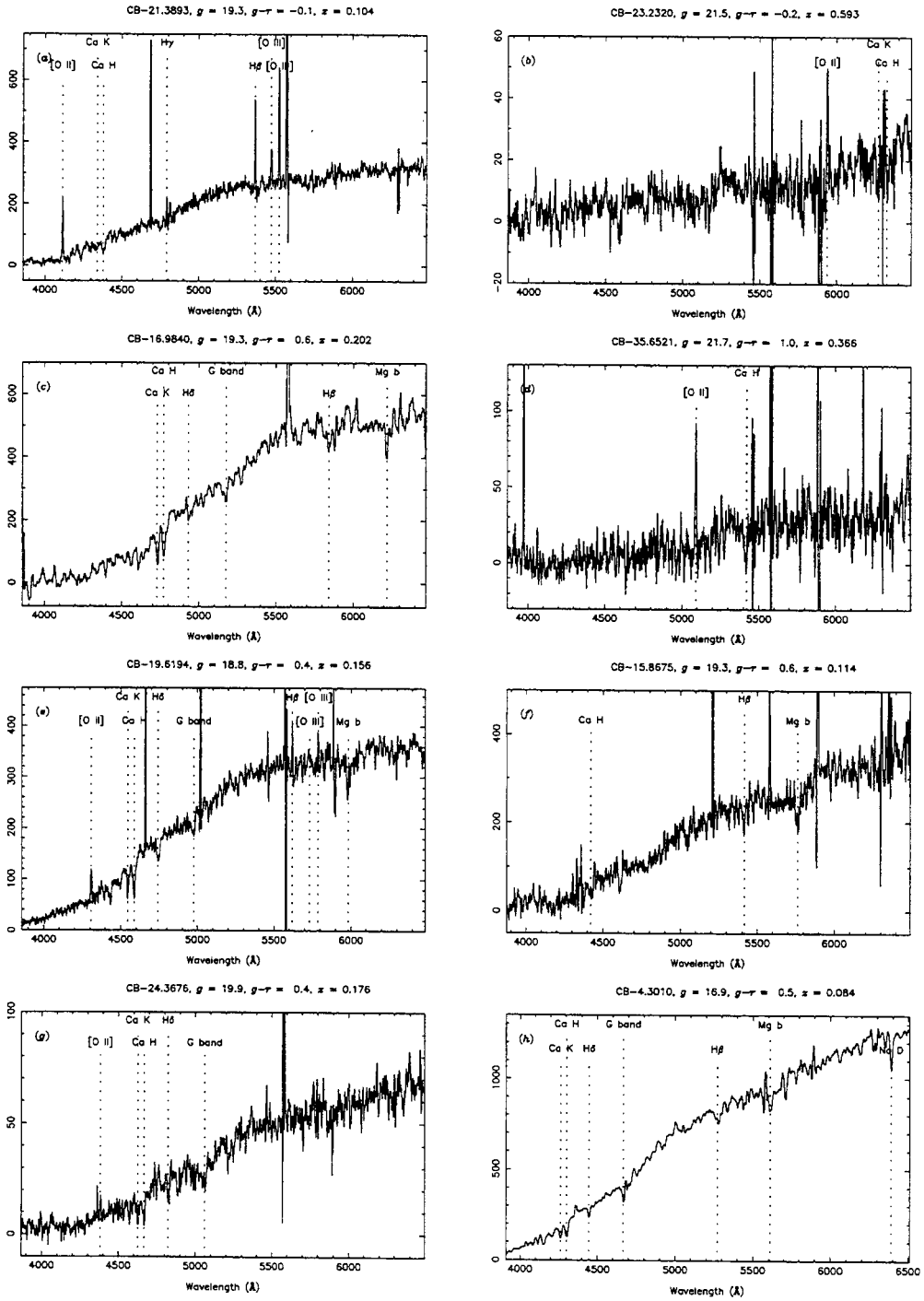

Fig. 2.8.— Same as Figure 2.6.

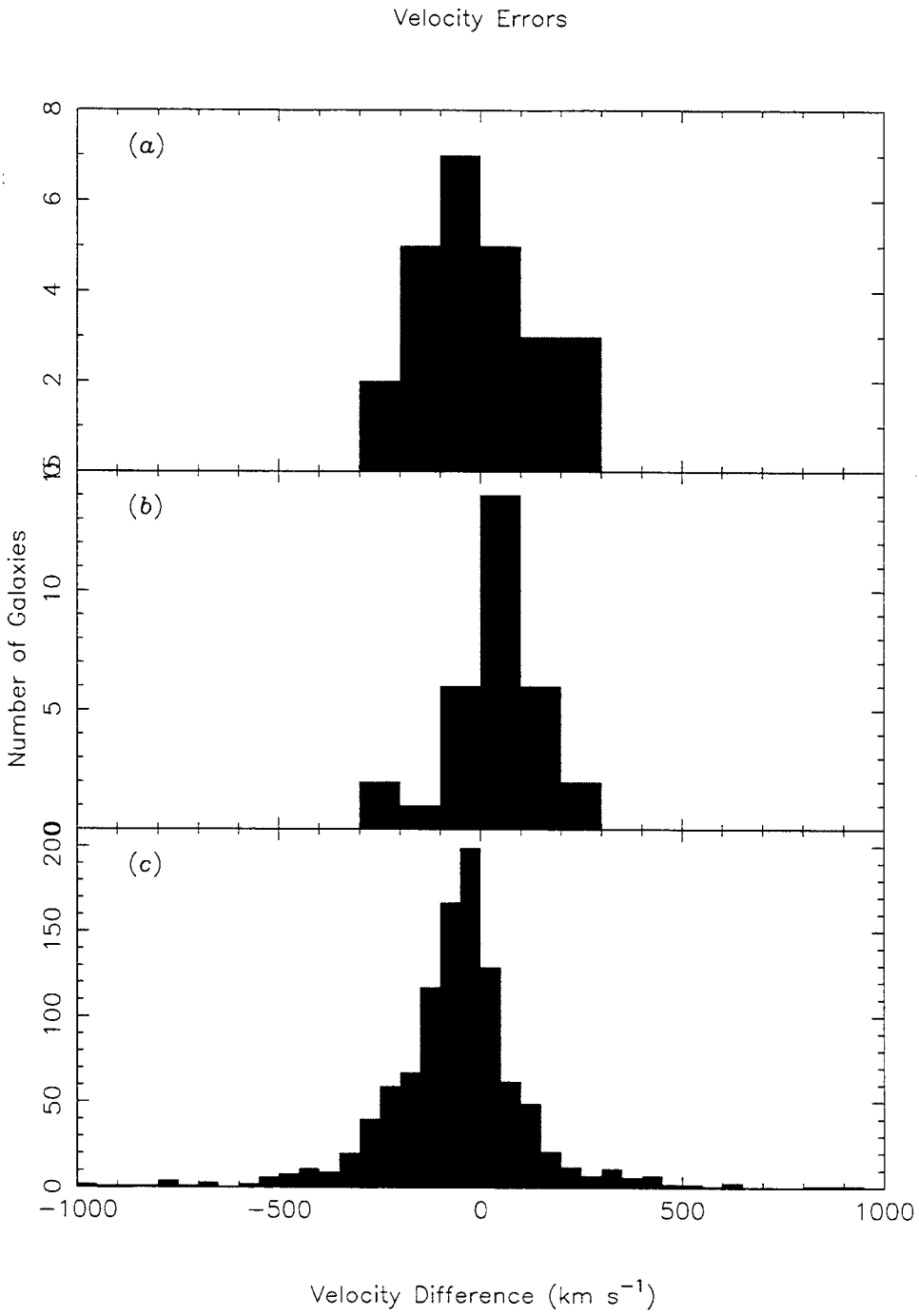

Fig. 2.9.— Histogram of velocity errors for (a) objects which were successfully observed twice, (b) objects which were matched to objects in the literature, and (c) objects for which velocities were determined with both the line measurement program and the cross-correlation program. The three distributions are roughly Gaussian with no significant bias. The standard deviations of the distributions are all consistent with typical velocity errors of 100 km s^{-1}.

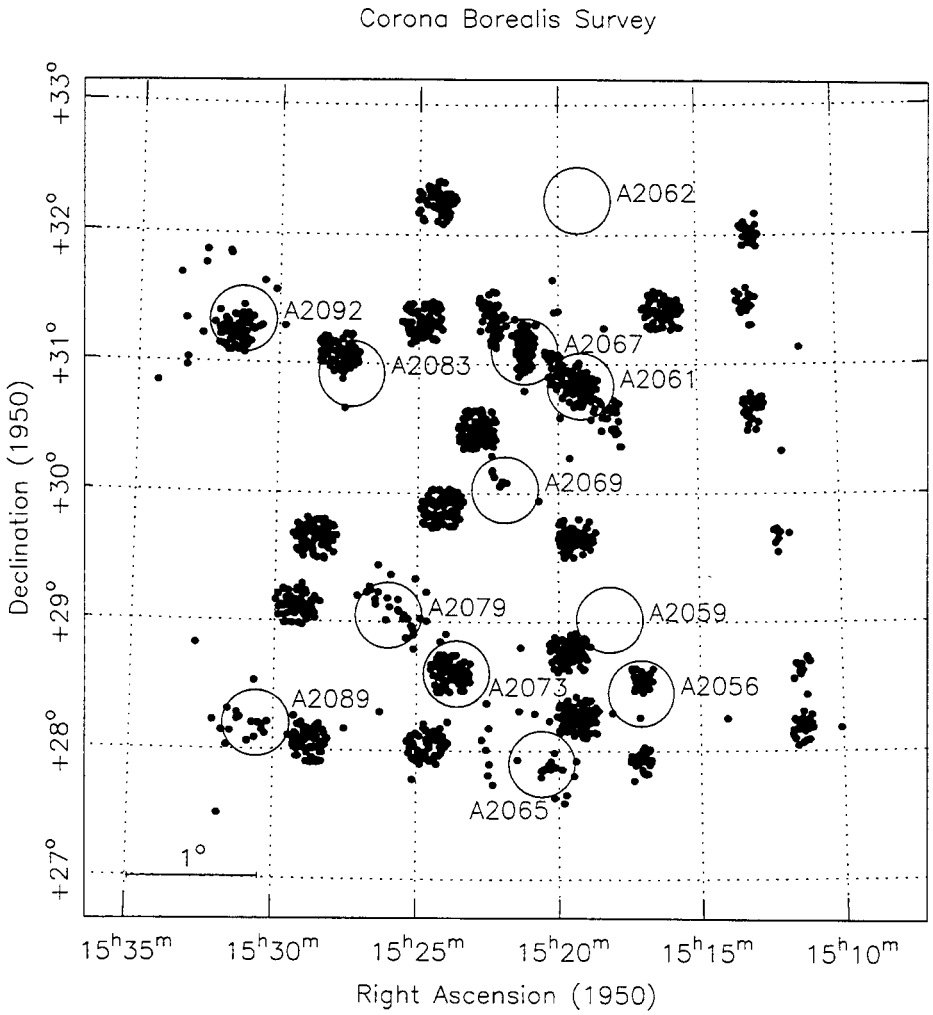

Fig. 2.10.— Celestial location of objects identified in our survey. The Abell clusters in Corona Borealis are marked with circles and identified by their Abell numbers. The bar in the southeast corner of the plot indicates one degree of arc.

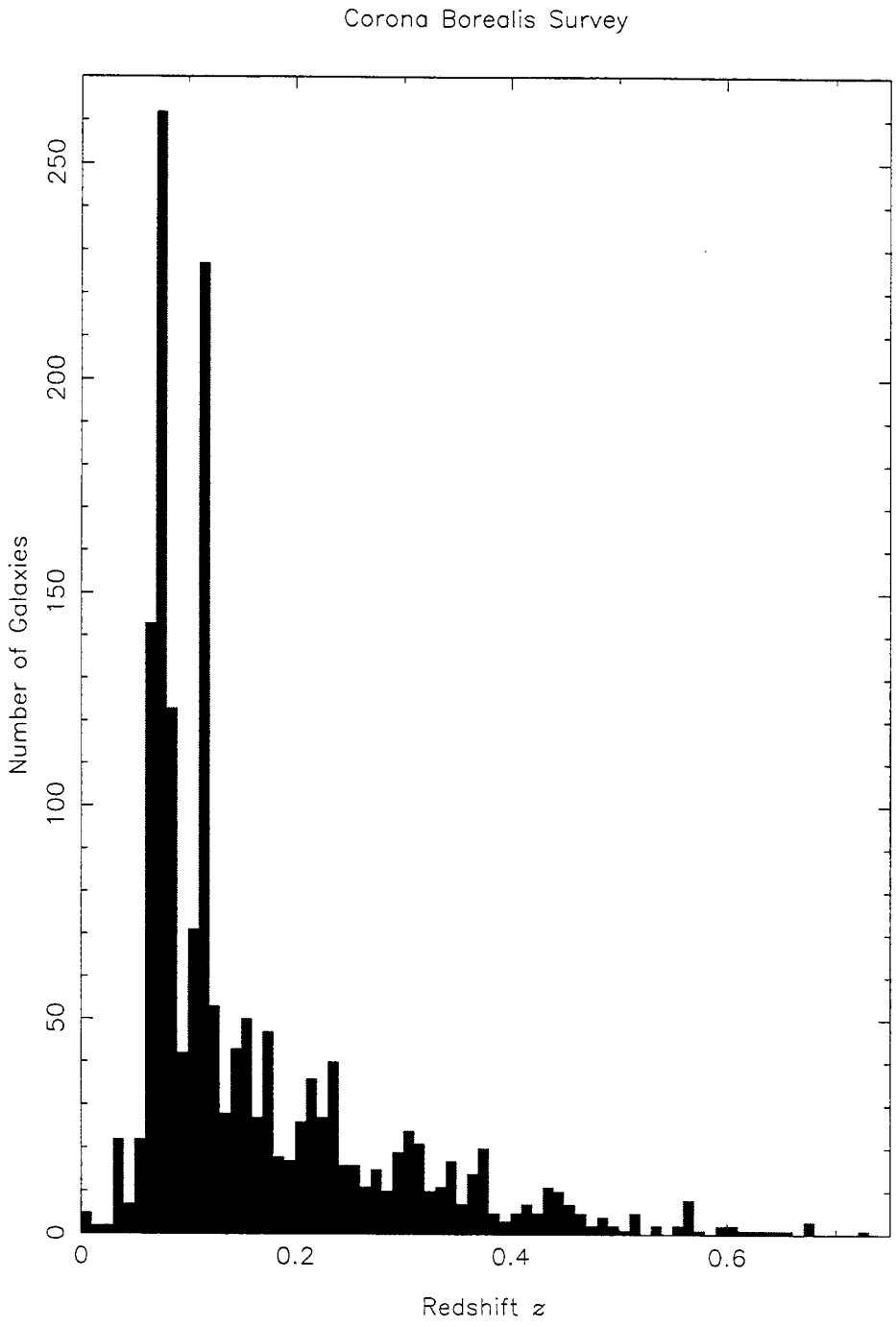

Fig. 2.11.— Redshift histogram of all galaxies in our survey. The Corona Borealis supercluster is the largest peak ($z \approx 0.07$). The background supercluster is at $z \approx 0.11$. These superclusters are each overdense relative to the field by a factor of a few.

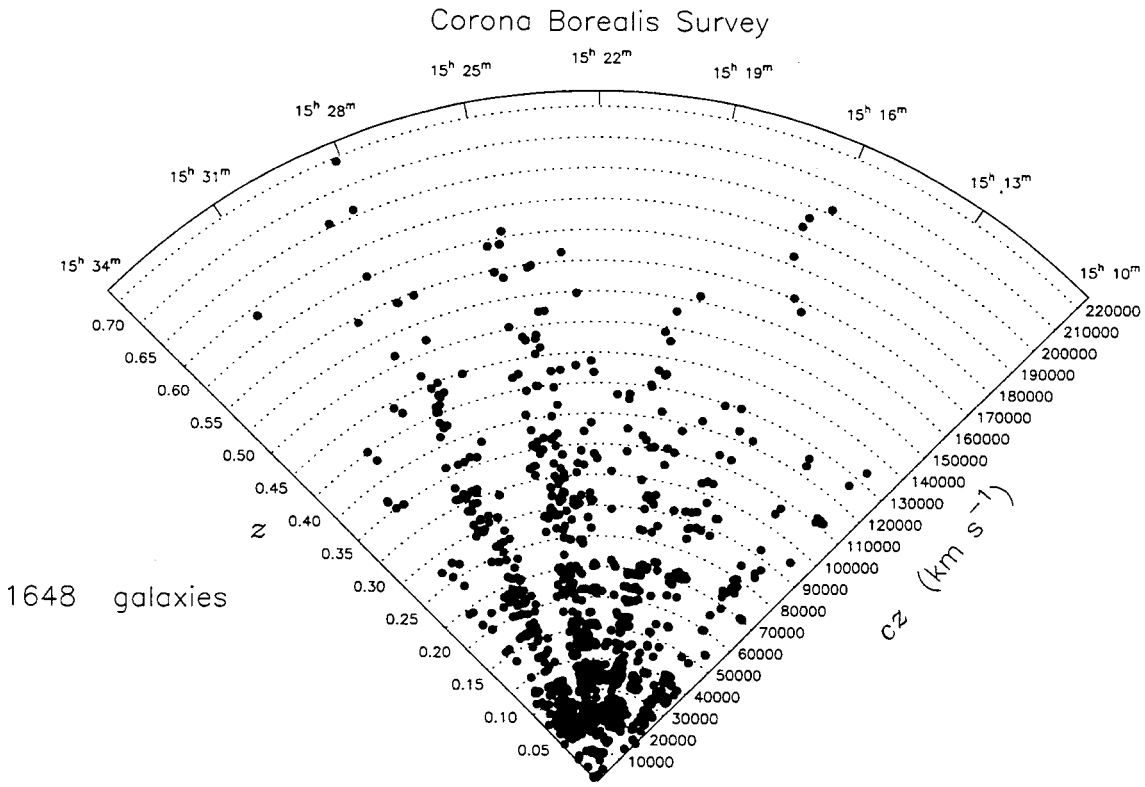

Fig. 2.12.— Redshift-right-ascension pie diagram for all 1649 galaxies in our survey. Note that the opening angle of the plot is 90°whereas the opening angle of the survey is only 6°.

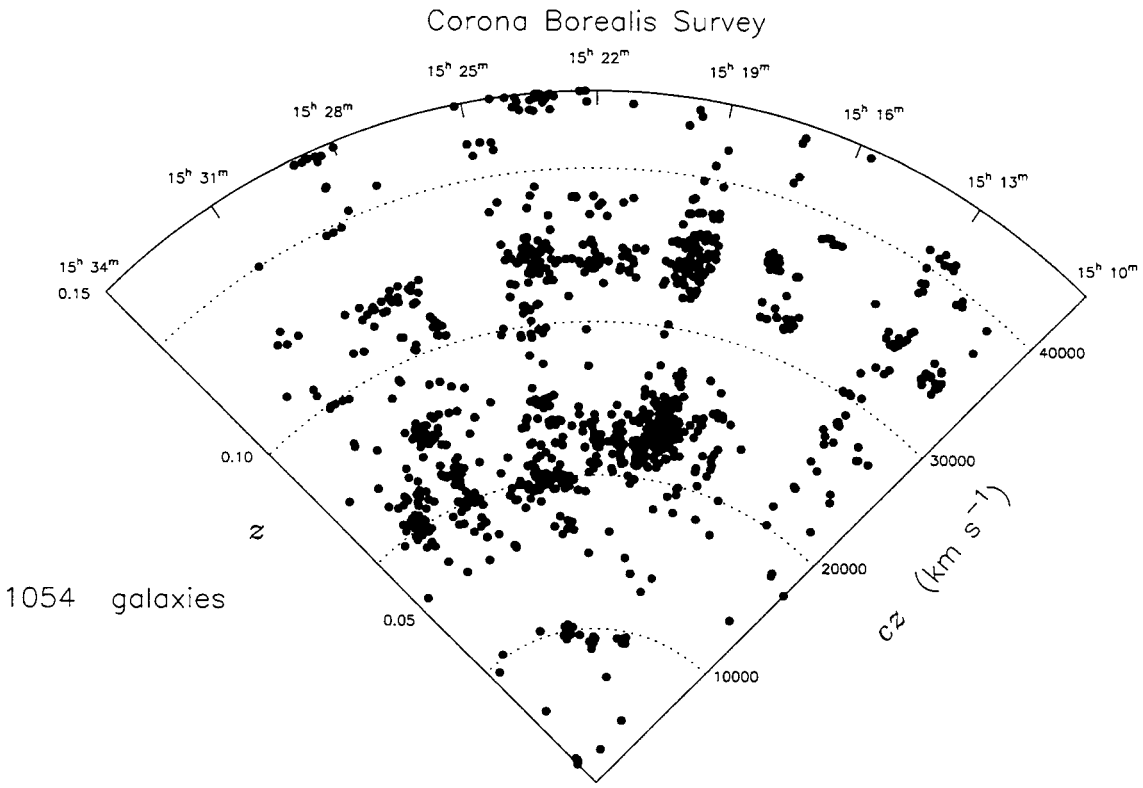

Fig. 2.13.— Redshift-right-ascension pie diagram for the 1054 galaxies in our survey with $z \leq 0.15$. Note that the opening angle of the plot is 90°whereas the opening angle of the survey is only 6°. The two superclusters are the conspicuous chains of galaxies at $z \approx 0.07$ and $z \approx 0.12$. There is a void of $\sim 75h^{-1}$ Mpc between the densest regions of the two superclusters.

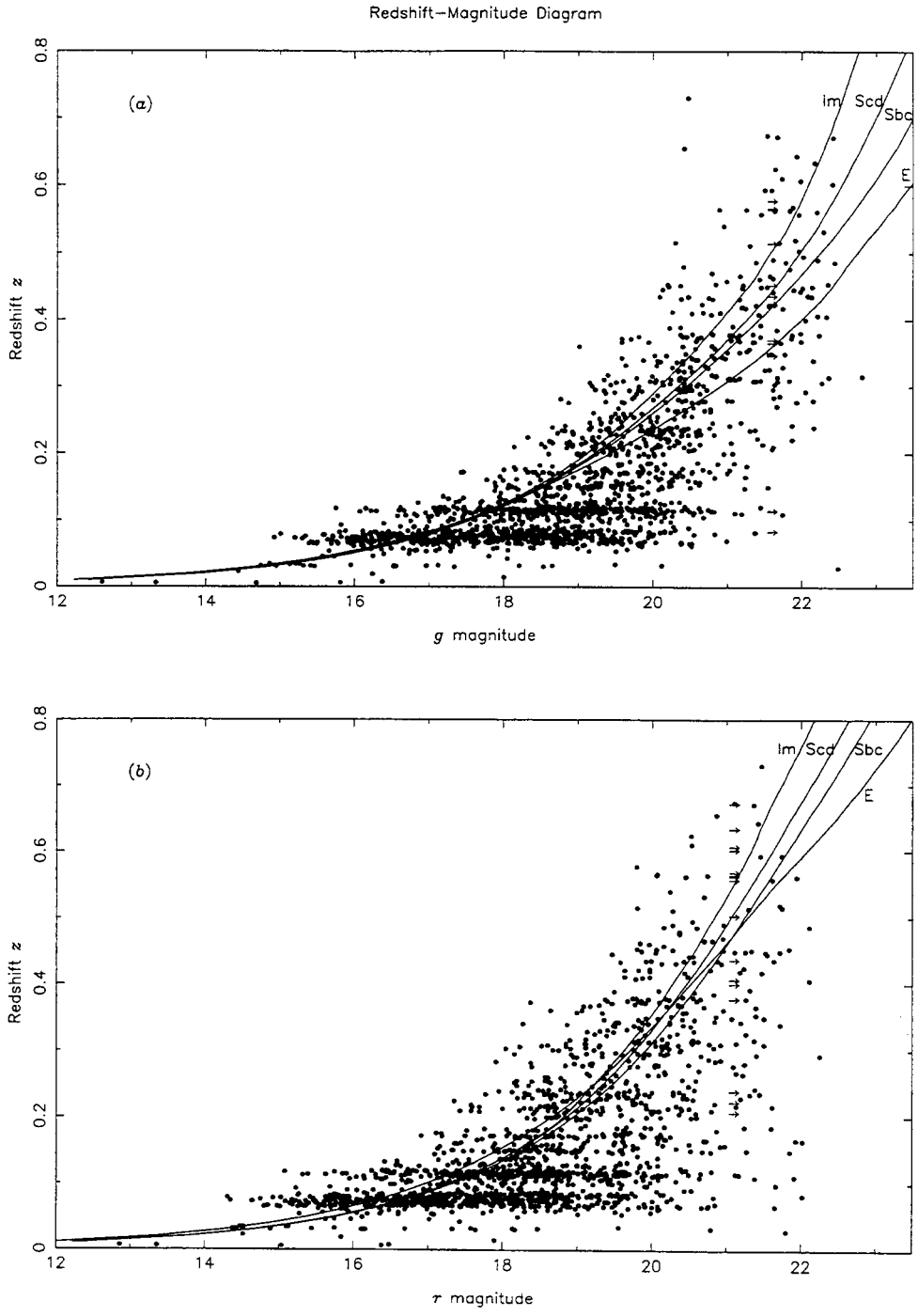

Fig. 2.14.— Magnitude-redshift diagrams in (a) g and (b) r bands. The lines mark the tracks of non-evolving, k-corrected L^* galaxies with spectral energy distributions typical of Hubble types E, Sbc, Scd, and Im. The two superclusters are the prominent strips of galaxies at $z \approx 0.07$ and $z \approx 0.12$. The brightest galaxies observed are ~ 2.5 times (1^m) brighter than L^*.

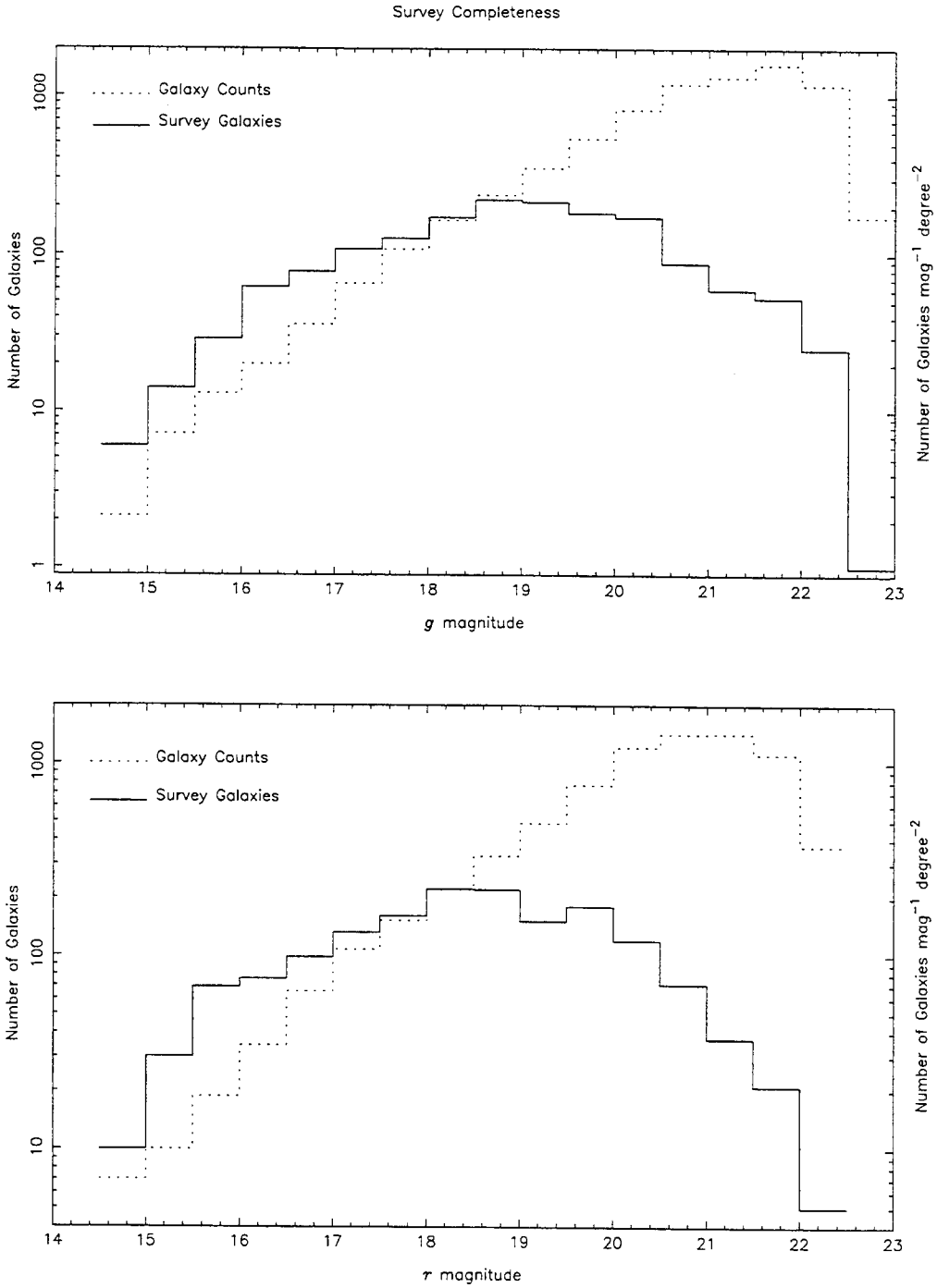

Fig. 2.15.— Completeness in g and r bands for the survey. The solid histogram gives the number of galaxies in each magnitude bin for which we have measured a redshift. The dotted histogram, drawn relative to the scale on the right-hand ordinate, gives the number of galaxies per magnitude per square degree in our survey field. By comparing the *shapes* of the two curves, we determine that the survey is only strictly magnitude-limited to $g = 19^m$ and $r = 18.5^m$.

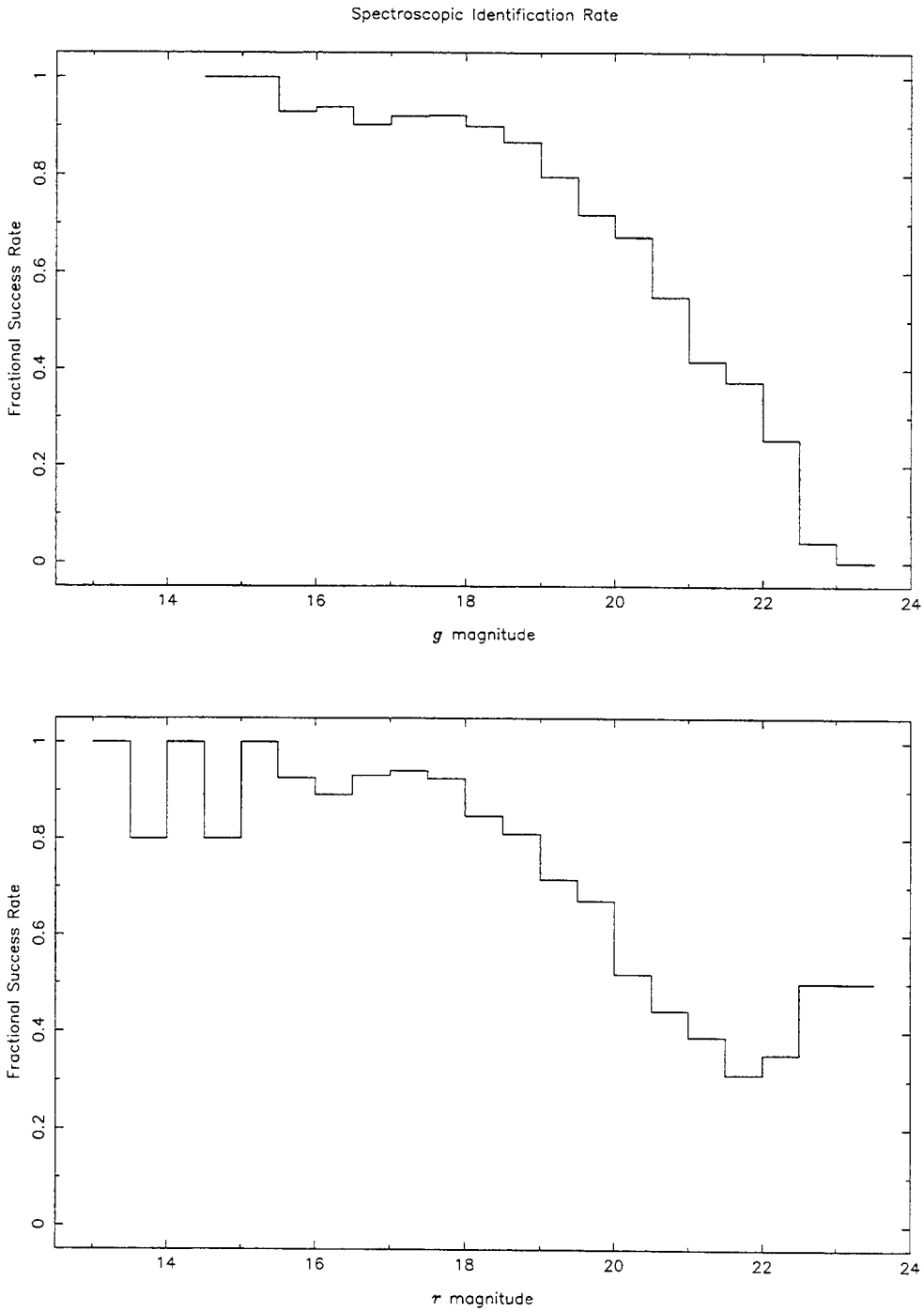

Fig. 2.16.— Spectroscopic identification rate, the ratio of objects identified to the number of fibers placed on objects, in g and r band for the survey.

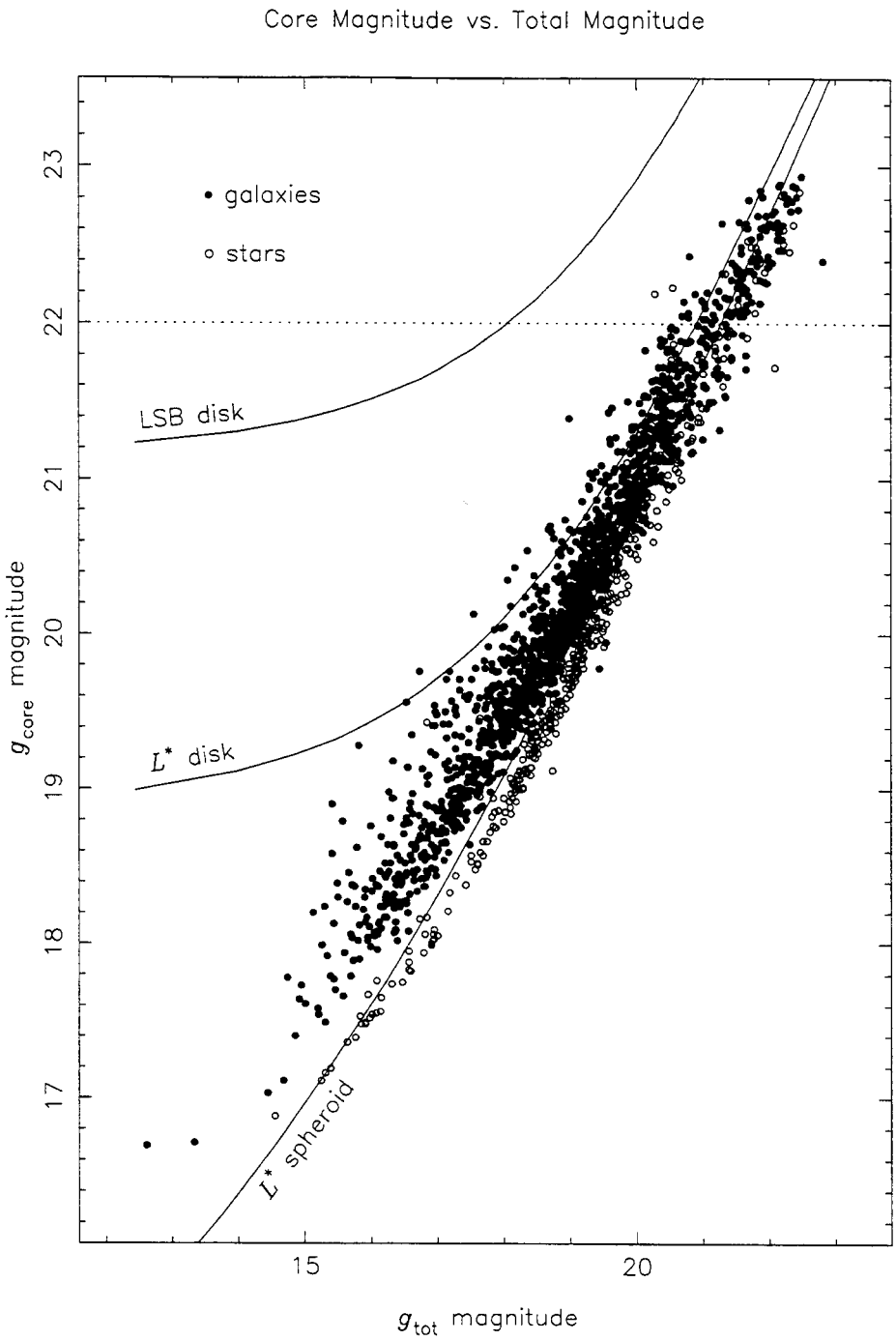

Fig. 2.17.— Core magnitude $g_{\rm core}$ versus total magnitude $g_{\rm total}$ for the stars and galaxies in our sample which were detected on the J plate. The dotted line at $g_{\rm core} = 22.0^m$ is our surface brightness completeness limit. The three solid lines labelled "LSB," "L^* disk," and "L^* spheroid" mark the tracks (as function of redshift) of our simple models of those galaxies, as observed in $2''$ seeing. For a sample magnitude limited at $g_{\rm total} = 21^m$, the L^* disk and L^* spheroid leave the sample through the faintness of their total magnitude rather than through the faintness of their core magnitude, as desired for a sample limited by total magnitude.

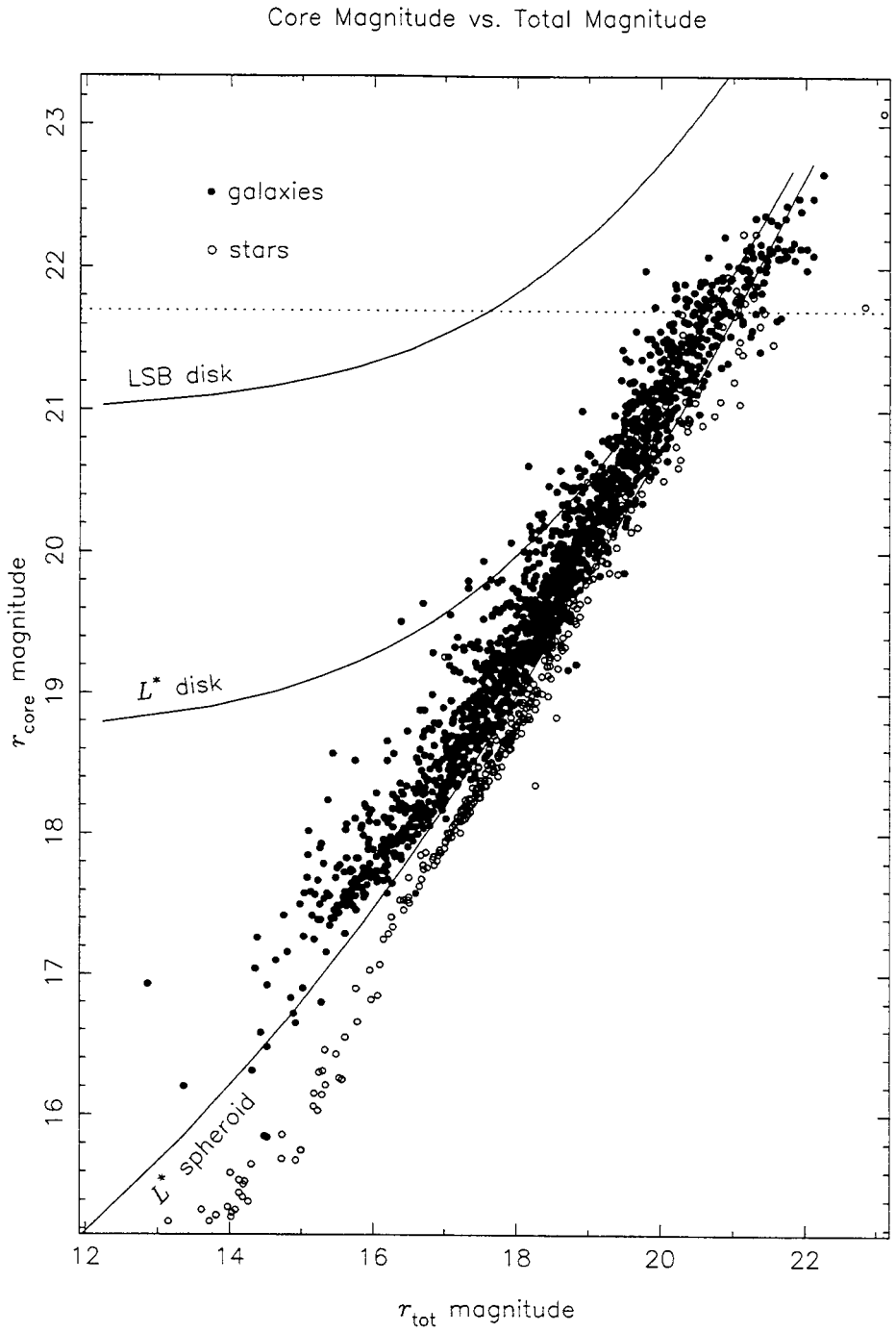

Fig. 2.18.— Core magnitude $r_{\rm core}$ versus total magnitude $r_{\rm total}$ for the stars and galaxies in our sample which were detected on the F plate. The dotted line at $r_{\rm core} = 21.7^m$ is our surface brightness completeness limit. The three solid lines labelled "LSB," "L^* disk," and "L^* spheroid" mark the tracks (as a function of redshift) of our simple models of those galaxies, as observed in $2''$ seeing. For a sample magnitude limited at $r_{\rm total} = 20.5^m$, the L^* disk and L^* spheroid leave the sample through the faintness of their total magnitude rather than through the faintness of their core magnitude, as desired for a sample limited by total magnitude.

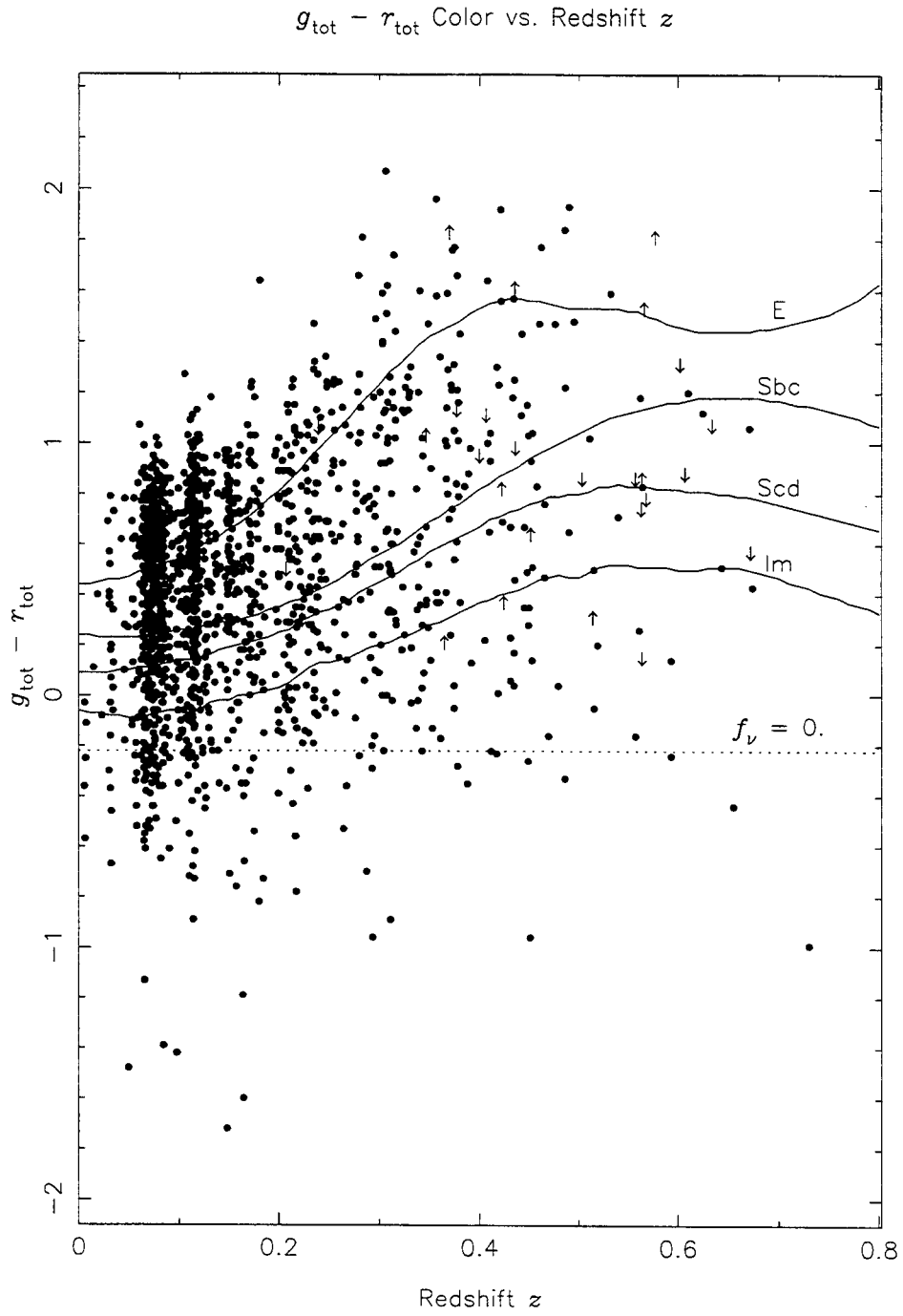

Fig. 2.19.— $g - r$ colors of the galaxies in our sample as a function of redshift. The arrows represent upper and lower limits for galaxies that were only detected on one plate. The tracks of non-evolving, k-corrected spectra of Hubble types E, Sbc, Scd, and Im (Coleman, Wu, and Weedman 1980) are also shown. The dotted line represents the color of an object with a flat spectrum ($f_\nu = 0.$). Despite the scatter created by our substantial magnitude errors ($\sigma(g - r) \approx 0.4^m$), it is clear that there is an excess of blue galaxies at all redshifts.

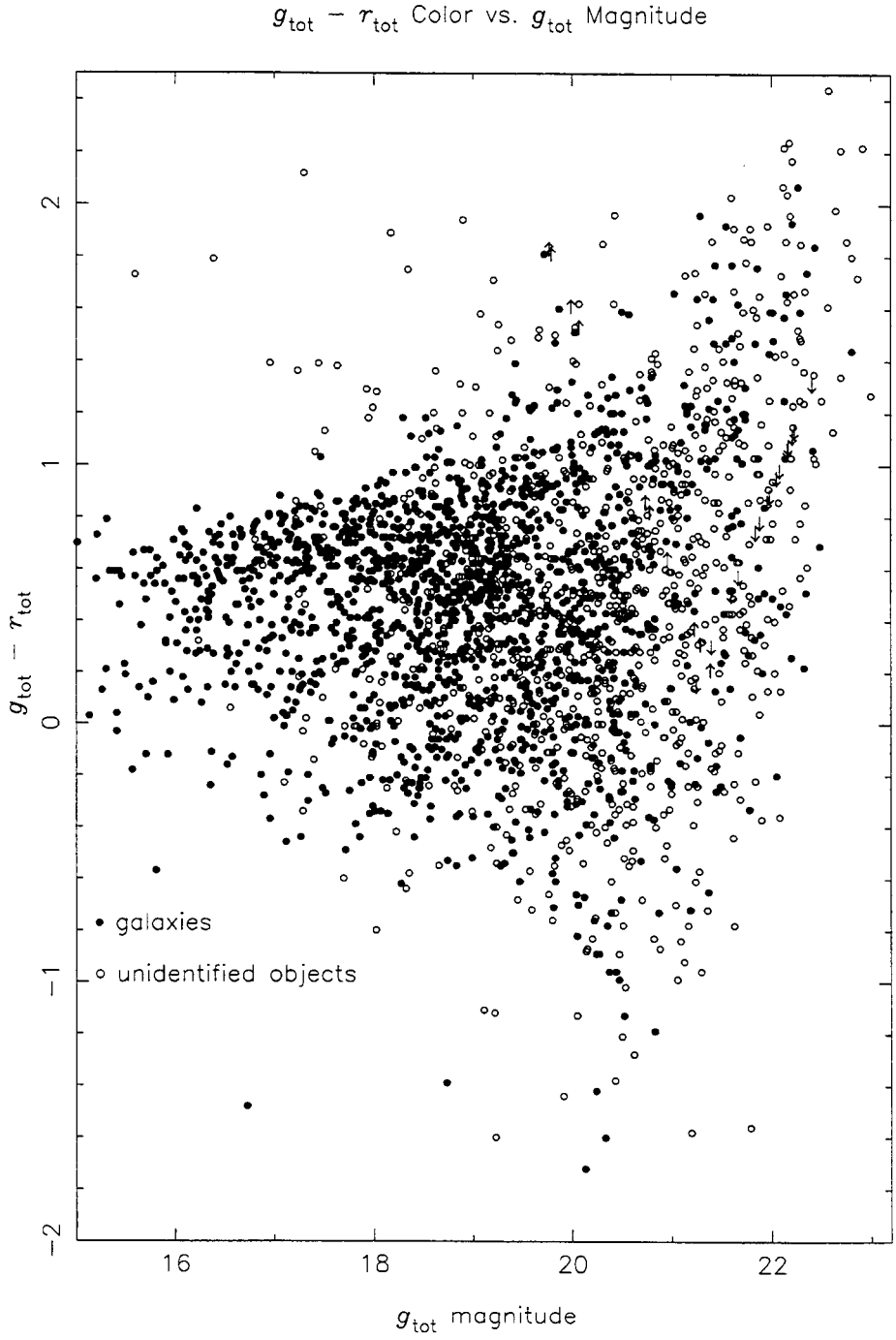

Fig. 2.20.— $g - r$ color distributions as a function of g magnitude of the galaxies and unidentified objects. The fact that the galaxies and unidentified objects cover the same range in color, except for the region with $g - r \gtrsim 1^m$ and $g \lesssim 20^m$ which is occupied by stars (see Figure 2.21), suggests that the survey suffers from no significant color biases.

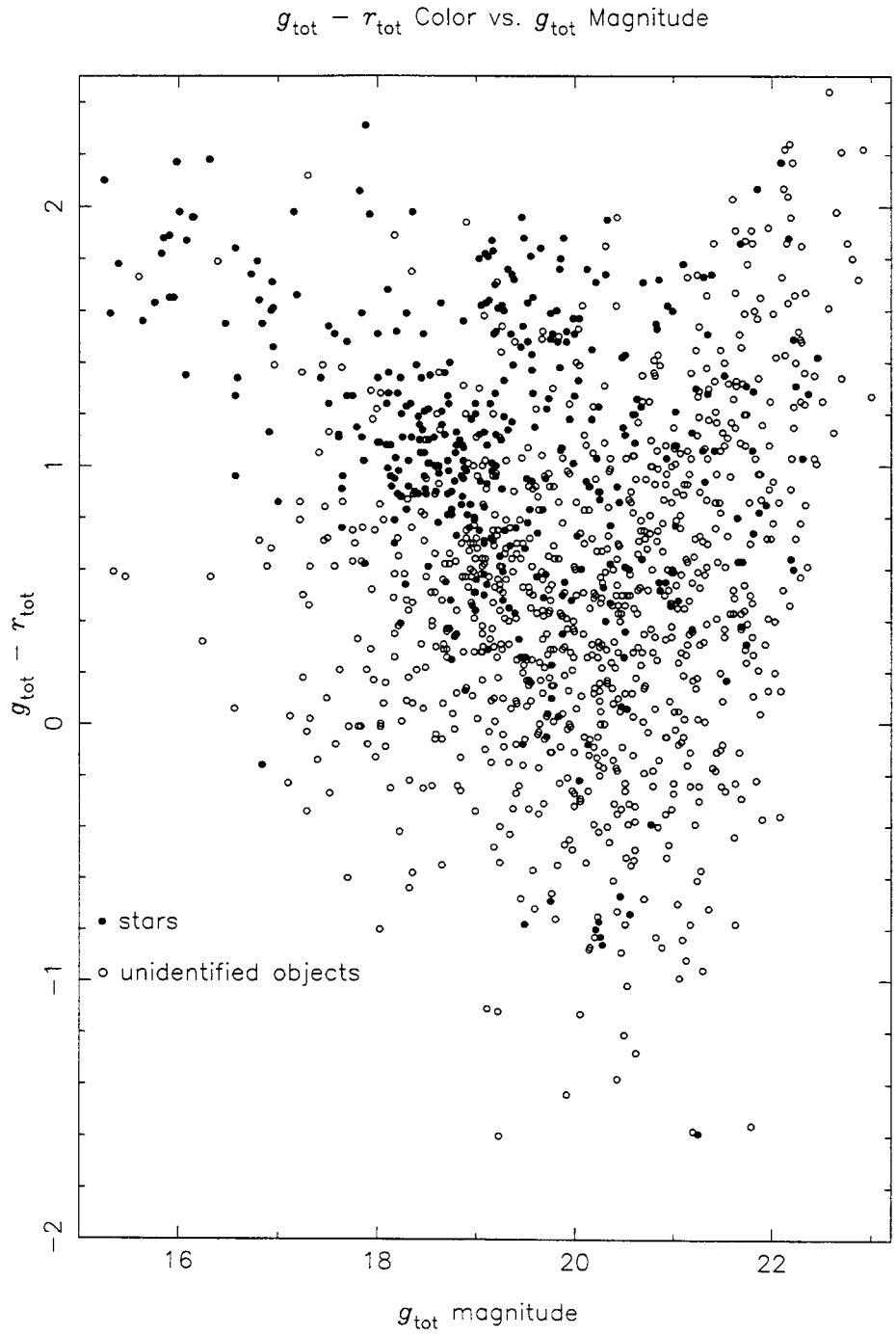

Fig. 2.21.— $g - r$ color distributions as a function of g magnitude of the stars and unidentified objects. This plot is complementary to Figure 2.20 and illustrates that the region with $g - r \gtrsim 1^m$ and $g \lesssim 20^m$ is occupied by stars.

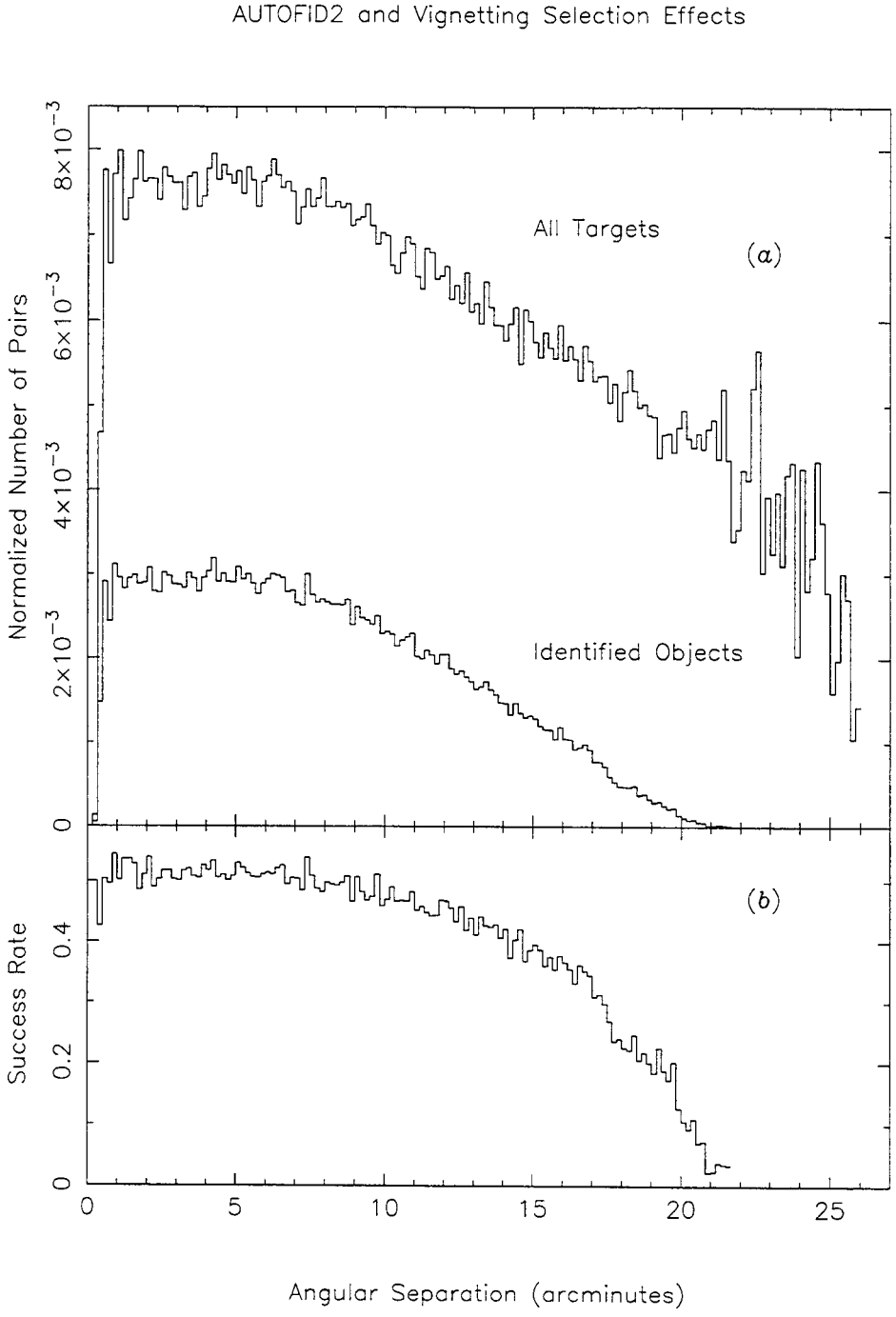

Fig. 2.22.— (a) ratios of number of pairs attempted and identified to the number of pairs in the input catalog as a function of angular separation on the sky, and (b) ratio of number of pairs identified to the number of pairs targeted. The upper panel (a) illustrates the spatial selection effects induced by the program AUTOFID2. The lower panel (b) illustrates the effect of the vignetting at the edges of the field.

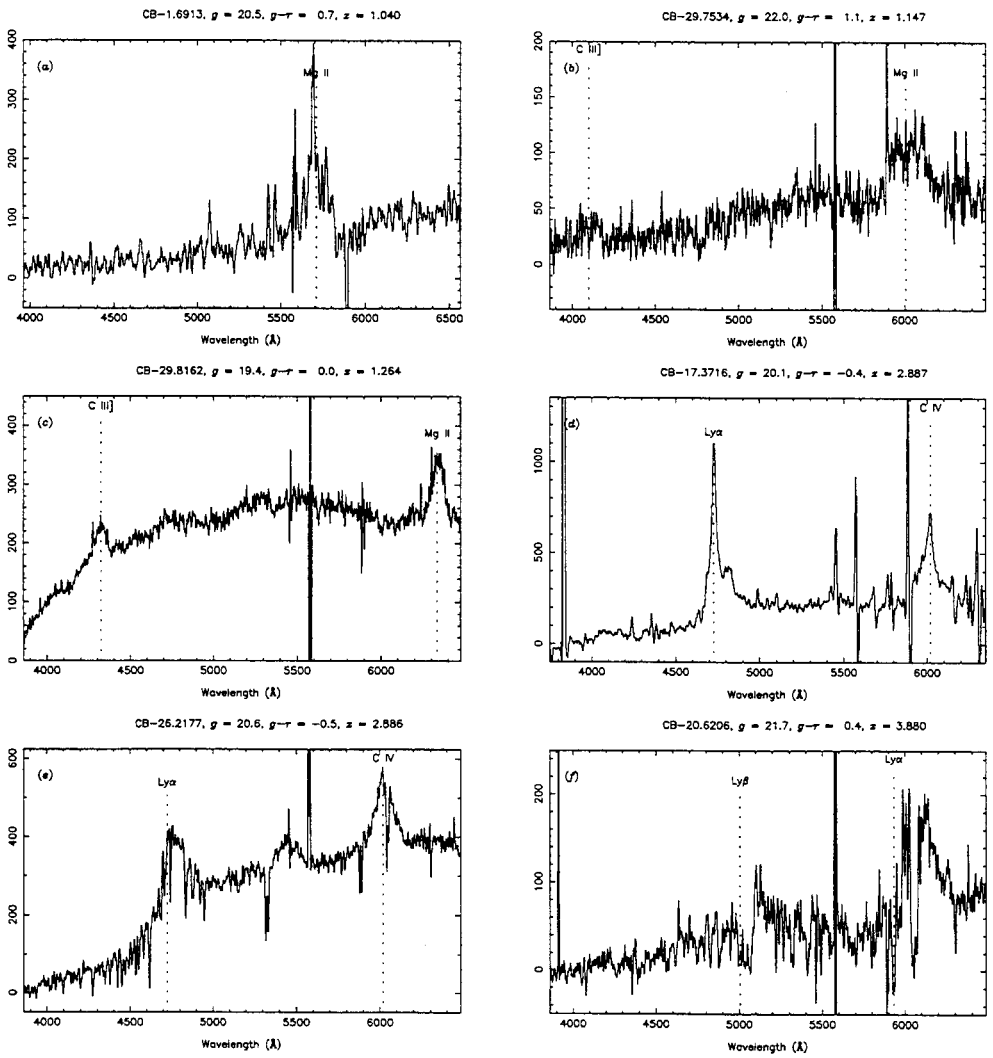

Fig. 2.23.— Spectra of the six quasars discovered in our survey. The prominent emission lines are labelled with dotted lines. The g magnitude, $g - r$ color, and redshift are given at the top of each panel.

Chapter 3 The Structure and Dynamics of the Corona Borealis Supercluster

3.1 Introduction

Superclusters are the largest known structures in the universe. With densities $\lesssim 10$ times the density of the field, superclusters have either very recently begun to collapse under their own gravity or are still expanding with the Hubble flow, although at a decelerated rate. The dynamical times of superclusters are comparable to the age of the universe, and so signatures of the dominant physical processes when the supercluster was formed have not yet been erased by dynamical evolution. One can therefore imagine that studies of superclusters will ultimately yield clues about the formation of galaxies and large-scale structure. In addition, studies of the peculiar velocities of galaxies generated on the outskirts of superclusters offer a means of estimating the mean density of the universe Ω_0.

The Corona Borealis supercluster is the most prominent example of superclustering in the northern sky. Using the "Lick Counts," Shane and Wirtanen (1954) were the first to remark on the extraordinary cloud of galaxies that constitute the supercluster. Abell also noted the Corona Borealis supercluster and included it in his catalog of "second-order clusters," or clusters of clusters of galaxies. In fact, the Corona Borealis supercluster includes 7 Abell clusters at $z \approx 0.07$ in a 36 deg^2 region on the sky and contributes significant power to the two-point correlation function of nearby Abell clusters. In the same region, there are five background Abell clusters, three of which are at $z \approx 0.11$. Counts of galaxies in the field of the supercluster, which include the background clusters, show a factor of 3 excess over counts in similarly high galactic fields. Picard (1991a) speculated that the supercluster may be responsible for the excess counts, although he realized that if the supercluster were

entirely responsible for the excess, it would generate fluctuations in the microwave background of the order $\delta T/T \approx 2 \times 10^{-4}$, far in excess of what is observed (Smoot *et al.* 1992).

The true extent of the Corona Borealis supercluster on the sky is unknown. Bahcall (1992) has marshalled circumstantial evidence to argue that while the region containing the 7 Abell clusters is only $\sim 20h^{-1}$ Mpc (h is the Hubble constant H_0 divided by 100 km s^{-1} Mpc^{-1}) on a side, the entire supercluster extends for at least $\sim 100h^{-1}$ Mpc on the sky. First, one of the peaks in the redshift distibution of the Broadhurst *et al.* (1990) pencil-beam survey is at the redshift of Corona Borealis, even though the survey was aimed 45° away from the core of the supercluster. Second, the far side of the Boötes void, at right ascension 14^h30^m, declination +50°, is also at a redshift of $z \approx 0.07$ (Kirshner *et al.* 1987). As our data show, the depth of Corona Borealis on the sky is only $\sim 40h^{-1}$ Mpc. Corona Borealis thus appears to be a flattened pancake similar to the structures originally envisioned by Zeldovich (1970). Although it is certainly not practical to survey the whole $100h^{-1}$ Mpc $\times$ $100h^{-1}$ Mpc region (which corresponds to 730 square degrees), our aim is to delineate accurately the structure of the core of Corona Borealis out to a radius of $\sim 20h^{-1}$ Mpc.

The only previous observational investigation of the dynamics of a supercluster was the study by Postman, Geller, and Huchra (1988) of the Corona Borealis supercluster. They collected 182 redshifts for galaxies mainly near the cores of the Abell clusters contained within supercluster. By adding up the virial masses of the Abell clusters, they concluded that the lower limit to the mass of the supercluster is $2.4 \times 10^{15} h^{-1}$ M$_\odot$. They also computed that if the mass-to-light ratio on supercluster scales is comparable to that on cluster scales, then the supercluster mass is $8.2 \times 10^{15} h^{-1}$ M$_\odot$, or about the mass required to bind the system (assuming a supercluster radius of $10 - 15h^{-1}$ Mpc). Their analysis was limited by the fact that they had to make assumptions about the shape of the supercluster. In order to overcome this limitation, a new study of the dynamics of the supercluster would require several thousand redshifts, a number sufficient to measure the mean density of the supercluster to 5%. We thus decided to undertake a large redshift survey of the Corona Borealis Supercluster

using the 176-fiber Norris Spectrograph on the Palomar 5-m telescope. In addition to creating an accurate map of the structure of the supercluster, we hoped to be able to answer two fundamental questions about the dynamics of the supercluster: is the supercluster bound, and are there substantial departures from the Hubble flow in the supercluster?

The paper, the second in the series of papers presenting the results from the Norris Survey of the Corona Borealis supercluster, is organized as follows. In §2, we review the technical details of the survey. In §3, we describe our visual impressions of the Corona Borealis Supercluster from our data. In §4, we apply the virial theorem in order to estimate the mass of the supercluster, and we compute the mass-to-light ratio of the supercluster using the luminosity function computed in Small, Sargent, and Hamilton (1996a), Paper IV in the series. In §5, we present an analysis of the velocity field of the supercluster based on fitting a simple model to the observed two-point correlation function. In §6, we briefly summarize our results.

3.2 The Norris Survey of the Corona Borealis Supercluster

The Norris Survey of the Corona Borealis Supercluser has been described in detail in Small *et al.* (1996), Paper I of the current series, and will be only briefly reviewed here. The core of the supercluster covers a $6° \times 6°$ region of the sky centered at right ascension 15^h20^m, declination $+30°$ and consists of 7 rich Abell clusters at $z \approx 0.07$. Since the field-of-view of the 176-fiber Norris Spectrograph is only 400 arcmin^2, we planned to observe 36 fields arranged in a rectangular grid with a grid spacing of $1°$. We mainly tried to avoid the cores of the Abell clusters since redshifts for many galaxies in the cores are available from the literature. As it turned out, we successfully observed 23 of the fields and 9 additional fields along the ridge of galaxies between Abell 2061 and Abell 2067, yielding redshifts for 1491 extragalactic objects. We have extended our survey with 163 redshifts from the literature, resulting in 1654 redshifts

in the entire survey. Only 528 objects lie in the redshift range of the supercluster, $0.06 < z < 0.09$. (We describe how we chose this redshift range in §3 below.) Of these, 489 (93%) are more than one Abell radius ($1.5h^{-1}$ Mpc) from the core of an Abell cluster.

The survey is only complete in apparent magnitude to Gunn $r = 18.5^m$. However, we have substantial numbers of galaxies out to $r = 22.0^m$. The lack of a magnitude-limited sample does not cause difficulties for the analysis in this paper since the redshift range we are studying is so narrow, $\Delta z = 0.03$. We do not expect significant changes in the selection function of the survey over such a small redshift range. The velocities errors in our sample are typically ~ 100 km s^{-1}, a factor of at least 3 smaller than the pairwise velocity dispersion of galaxies. The use of a fiber-fed spectrograph imposes spatial sampling biases on the survey. The fibers cannot be placed within $16''$ of each other, and their motion is further restricted by limits on the bending angles of the fibers. These two effects combine to eliminate pairs of objects with angular separations of $\lesssim 30''$, or with separations on the plane of the sky $\lesssim 0.1h^{-1}$ Mpc at $z \approx 0.07$. Since we are concerned mainly with separations of $\gtrsim 1h^{-1}$ Mpc, the bias against pairs with small angular separations can be ignored. The number of pairs with angular separations on scales of $10'$ to $20'$ is diminished by the fiber assignment program and by vignetting in the spectrograph. The affected spatial scales are $\lesssim 2h^{-1}$ Mpc at the redshift of the supercluster.

3.3 The Structure of the Corona Borealis Supercluster

Even projected on the sky, the Corona Borealis supercluster has an irregular shape. In Figure 3.1, we plot the surface density of galaxies across the field. The Abell clusters in the field, including the ones that are more distant than the supercluster, stand out prominently against the field galaxies. Four of the Abell clusters (A2056, A2065, A2079, and A2089) are together in the southern part of the supercluster, A2061 and

A2067 are right next to each other in the northern part, and A2092 is isolated in the northeastern part. Only in the diamond-shaped region described by A2056, A2065, A2079, and A2089 can an extended area with excess galaxy counts be discerned.

In Figure 3.2, we plot redshift-right-ascension diagrams for all galaxies in our survey with $z < 0.10$. The diagrams are split by declination as indicated in the figure. An inspection of the figure reinforces the impression that the density distribution of the supercluster is far from smooth. The supercluster is sharply delimited along the line-of-sight by foreground and background underdense regions. The well defined boundaries of the supercluster lead us to restrict our analyses of the supercluster to galaxies with $0.06 < z < 0.09$. The group of galaxies at $cz \approx 10000$ km s^{-1} are part of the "Great Wall" of galaxies described by Geller and Huchra (1989).

The location on the sky of all Corona Borealis supercluster galaxies in our survey is plotted in Figure 3.3. The seven large circles mark the positions of the Abell clusters in the supercluster, and the squares mark the locations of the fields which we have observed. The 17 small squares, 6 at right ascension 15^h13^m, 2 at right ascension 15^h17^m, and 9 along the A2061-A2067 ridge, represent fields which were observed when only a 1024^2 CCD was available at Palomar, thus reducing the number of usable fibers by a factor of 2. The galaxies in the plot that do not lie within one of the rectangles have been taken from the literature. The number of galaxies successfully identified at all redshifts ranges from 10 to 42 for the small squares and from 59 to 87 for the large squares. Thus, the Norris fields which contain only a few supercluster galaxies are sparsely populated because the supercluster is truly not dense in those regions. Once again, one has the impression that the supercluster is lumpy and irregular. While there are certainly supercluster galaxies in the space between the Abell clusters, the surface density of galaxies falls rapidly with increasing distance from the cluster cores. The comparatively small number of supercluster galaxies in the central part of the region defined by the seven Abell clusters is particularly striking. Also impressive is the rapid decline in density to the northwest of the A2061-A2067 ridge.

In Figure 3.4, we plot the recession velocity cz of all galaxies versus their angular

distance from the center of the supercluster. To determine the center on the sky of the supercluster, we have simply computed the mean right ascension and declination of a sample of supercluster galaxies magnitude-limited at $r \leq 18.5^m$. The celestial coordinates (1950 equinox) of the center are right ascension 15^h23^m, declination $+29°48^m$. We have distinguished in the plot between galaxies with absorption-line spectra (solid circles), emission-line spectra (unfilled circles), and unknown spectra (crosses; these galaxies are taken from the literature). The Corona Borealis Supercluster is the broad swath of galaxies with velocities between $\sim$ 18000 km s^{-1} and $\sim$ 27000 km s^{-1}. The structure centered at $\sim$ 33000 km s^{-1} is a background supercluster which we have dubbed the "Abell 2069 Supercluster." It is striking that the velocity dispersion of the Corona Borealis supercluster does not decline strongly with angular distance from the center, as is seen for isolated Abell clusters (*e.g.,* Coma, Kent and Gunn 1982; Abell 2670, Sharples, Ellis, and Gray 1988). It is also notable that absorption-line galaxies appear to be more strongly clustered than the emission-line galaxies.

3.4 The Mass of the Corona Borealis Supercluster

Since the supercluster is apparently unrelaxed and contains obvious substructure (*e.g.,* the Abell clusters themselves), there is no completely satisfactory way to estimate the mass of the supercluster. Although it is certainly questionable to apply the virial theorem to estimate the mass of the supercluster, we choose to do so since N-body simulations demonstrate that virial mass estimates are generally within a factor of 2 the correct value, even when the system is not virialized (Carlberg 1994). According to Carlberg's simulations, the virial theorem yields a consistently low estimate of the mass because galaxies lose orbital energy during infall into large structures, resulting in a slight reduction of the galaxies' velocity dispersion with respect to that

of the dark matter. The virial mass may be estimated from observables using

$$M_V = \frac{3\pi}{G}\sigma^2\left\langle\frac{1}{r_p}\right\rangle^{-1}, \tag{3.1}$$

where σ is the line-of-sight velocity dispersion and $\langle 1/r_p\rangle^{-1}$ is the mean harmonic projected separation,

$$\left\langle\frac{1}{r_p}\right\rangle^{-1} = \frac{D}{2}N(N-1)\left(\sum_i\sum_{j<i}\frac{1}{\theta_{ij}}\right)^{-1}, \tag{3.2}$$

where θ_{ij} is the angular separation of galaxies i and j, D is the radial distance to the cluster, and N is the total number of galaxies. We use the statistically robust techniques of Beers, Flynn, and Gebhardt (1990) to estimate the mean redshift $\bar{z}$ and velocity dispersion σ of the supercluster. We find $\bar{z} = 0.0747 \pm 0.0003$ and $\sigma = 1792 \pm 91$ km s^{-1} (corrected by $(1+\bar{z})^{-1}$ for cosmological effects). With these values, we find the virial mass of the Corona Borealis supercluster to be $(1.7 \pm 0.2) \times 10^{16} h^{-1}$ $M_\odot$, in good agreement with the estimate of Postman, Geller, and Huchra (1988).

By integrating the supercluster luminosity function, we can compute the mean luminosity density of the supercluster and thereby measure the mass-to-light ratio of the supercluster on scales of $10 - 20h^{-1}$ Mpc. In Paper IV, we fit the supercluster luminosity function with a Schechter function with $\phi^* = 0.01 \pm 0.04h^3$ Mpc^{-3}, $M(B)^* = (-19.85 \pm 0.32) + 5\log_{10} h$, and $\alpha = -1.33 \pm 0.13$. The mean luminosity density of the supercluster is

$$\langle L_B\rangle = \phi^* L^* \Gamma(\alpha+2) = (1.9 \pm 1.0) \times 10^9 h L_\odot \mathrm{Mpc}^{-3}, \tag{3.3}$$

where Γ is the usual gamma function. Taking the solid angle of the survey to be 0.11 sr and the limits of the supercluster to be at $z = 0.06$ and $z = 0.09$, the volume of the supercluster is $4 \times 10^4 h^{-3}$ Mpc^3. The mass-to-light ratio of the supercluster in the B band is thus $(224 \pm 121)h\left(\frac{M}{L}\right)_\odot$, similar to that of rich clusters of galaxies (Faber and Gallagher 1979). Allowing for a factor of 2 underestimate of the mass of the supercluster, our result taken at face value implies that $\Omega_0 \lesssim 0.3$ on supercluster

scales. The mass of the supercluster appears to be sufficient ($> \frac{1}{2}M_V$) to bind the system.

A structure with a mass of $2 \times 10^{16} M_\odot$ is very rare in a flat cold dark matter universe. Out to $z = 1$ and over the entire sky, one would expect to observe $\lesssim 1$ object with such an enormous mass (C.-P. Ma, private communication). Unfortunately, the cumulative mass distribution function is falling extremely rapidly at $\sim 10^{16}$ $M_\odot$. In a cold dark matter universe, one would expect to observe ~ 100 objects with half the mass of the Corona Borealis Supercluster in the volume out to $z = 1$. Therefore, the existence of an object as massive as the Corona Borealis supercluster comparatively close to our Galaxy cannot yet be used to constrain the cold dark matter theory.

3.5 The Peculiar Velocity Field of the Supercluster

3.5.1 The Two-Point Correlation Function $\xi(r_p, \pi)$

Redshift-space maps of the spatial distribution of galaxies are distorted by the peculiar motions of galaxies. The measured redshift of a galaxy is the sum of the Hubble motion of the galaxy plus the line-of-sight peculiar velocity. The "fingers of God" seen in redshift surveys of rich clusters of galaxies, in which the large velocity dispersion of a cluster spreads out the cluster galaxies along the line-of-sight in redshift space, are the most prominent signatures of redshift space distortions. On large scales, coherent infall into overdense regions and outflow from underdense regions enhance the correlation function. Since the velocities on large scales can be simply related to the mean mass density of the universe Ω_0 with linear theory, an analysis of redshift space distortion can in principle yield an estimate of Ω_0 (Sargent and Turner 1977, Fisher *et al.* 1994a). The distribution of galaxies on the plane of the sky is not, however, distorted by peculiar velocities. Thus, correlation functions, which one assumes are isotropic in real space, are anisotropic in redshift space. It is, therefore, useful to compute correlation functions as functions of separations along the line-of-

sight (π) and perpendicular to the line-of-sight (r_p).

The two-point correlation function $\xi(r_p, \pi)$ is the joint probability δP of finding a galaxy in each of two volume elements dV_1, dV_2 separated by r_p and π,

$$\delta P = \bar{n}^2(1 + \xi(r_p, \pi))dV_1 dV_2, \tag{3.4}$$

where $\bar{n}$ is the mean galaxy density. In order to compute $\xi(r_p, \pi)$, we construct a catalog of randomly distributed points with same selection function as the real data. We estimate $\xi(r_p, \pi)$ using the estimator derived by Hamilton (1993):

$$1 + \xi(r_p, \pi) = \frac{DD(r_p, \pi)RR(r_p, \pi)}{DR(r_p, \pi)^2}, \tag{3.5}$$

where $\mathrm{DD}(r_p, \pi)$, $\mathrm{RR}(r_p, \pi)$, and $\mathrm{DR}(r_p, \pi)$ are the number of data-data, random-random, and data-random pairs, respectively, with separations r_p and π. The virtue of Hamilton's estimator is that it is affected only in second order by density fluctuations on the scale of the survey. In addition, Hamilton's estimator does not require an independent measurement of the mean galaxy density of the survey.

We calculate the error in $\xi(r_p, \pi)$ using simple Poisson statistics, $\sigma(\xi) = (1 + \xi)/\sqrt{DD}$. Traditionally, bootstrap resampling of the data has been employed to estimate the errors (Ling, Frenk, and Barrow 1986). However, bootstrap errors are not expected to yield accurate estimates of the errors for correlation statistics (Press *et al.* 1992, Fisher *et al.* 1994b). This is illustrated by considering an attempt to estimate the significance of a void in an observed galaxy distribution using bootstrap errors. The void will always remain empty in the bootstrap samples, causing an underestimate of the error in the mean density. Similarly, the bootstrap method will overestimate the error in the estimate of the mean density of an overdense region. Since ξ is pair-weighted, it is heavily weighted by the densest regions. Using N-body simulations, Fisher *et al.* (1994b) have found that the simple Poisson error estimate is, in fact, slightly more accurate than bootstrap error estimates for $3 \lesssim r \lesssim 15h^{-1}$ Mpc. For $r \lesssim 3h^{-1}$ Mpc, we double the Poisson errors to match crudely the error

estimated by Fisher *et al.* (1994b) for an ensemble of N-body simulations.

The random catalog has 50 times the number of galaxies as the real catalog so that errors in the counts for the random catalog will be negligible. Since the supercluster covers a narrow range of redshift, $\Delta z = 0.03$, we chose the redshifts of the galaxies in the random catalog uniformly in the interval $0.06 < z < 0.09$. We have also drawn redshifts for the galaxies in the random catalog from the distribution $P(z|m)$ that a galaxy with an apparent magnitude m has redshift z, a technique described in detail in Small (1996), Paper III in the series. The results with two methods were indistinguishable within the errors.

Since the survey was sparsely sampled, some care must be taken in assigning the celestial coordinates to the galaxies in the random catalog. For each galaxy in the real catalog, we choose 50 celestial coordinates at the same time that we choose the 50 redshifts. The celestial coordinates are selected randomly from the survey field to which the real galaxy belongs. This method correctly accounts for the varying number of galaxies successfully identified per survey field. If a galaxy in the real catalog was taken from the literature, then we chose the 50 celestial coordinates in the random catalog to be uniformly distributed throughout the whole $6° \times 6°$ survey area. We compared the results using this method with those obtained using a scheme in which, for every galaxy in the real catalog, 50 celestial coordinates were chosen at random from a circle with radius $1'$ centered on the real object. There were no significant differences between the results using the two schemes.

3.5.2 A Model for $\xi(r_p, \pi)$

The distortions of $\xi(r_p, \pi)$ contain information on the velocity distribution function of galaxy pairs, $F(\mathbf{w}|\mathbf{r})$, where $\mathbf{w}$ is the velocity difference of a pair with vector separation $\mathbf{v}$. Peebles (1980) has modeled $\xi(r_p, \pi)$ as a convolution of the real space correlation function $\xi(r)$ with $F(\mathbf{w}|\mathbf{r})$,

$$1 + \xi(r_p, \pi) = \int [1 + \xi(r)] F(\mathbf{w}|\mathbf{r}) d^3\mathbf{w} \tag{3.6}$$

This expression can be simplified if we assume that the velocity dispersion of pairs varies slowly with pair separation and that there is no preferred direction in the velocity field. With those assumptions, $\xi(r_p, \pi)$ depends only on the distribution of line-of-sight velocities, and we have

$$1 + \xi(r_p, \pi) = \int [1 + \xi(r)] F(v_{los}|r) dv_{los}. \tag{3.7}$$

If we separate $\mathbf{r}$ into components (r_p, y) perpendicular to and along the line-of-sight, then $r^2 = r_p^2 + y^2$, $v_{los} = H_0(\pi - y)$, and

$$1 + \xi(r_p, \pi) = \int [1 + \xi(\sqrt{r_p^2 + y^2})] F(H_0(\pi - y)|r) dy \tag{3.8}$$

It has been found in the analyses of previous surveys (Davis and Peebles 1983, Fisher *et al.* 1994a) that an exponential distribution of pairwise line-of-sight velocities,

$$F(v_{los}) = \frac{1}{\sqrt{2}\sigma_{12}} e^{-\sqrt{2}v_{los}/\sigma_{12}}, \tag{3.9}$$

where σ_{12} is the line-of-sight velocity dispersion, fits the data well. In general, one should also include the mean streaming of galaxies due to coherent motions generated by large-scale structure. However, as discussed below, we find adequate fits without incorporating mean streaming into the model. Also, we are neglecting the scale dependence of σ_{12}. The Cosmic Virial Theorem (Peebles 1980) predicts that the dispersion of bound objects scales as $\sigma_{12} \propto r^{1-\gamma/2}$, which is only weakly dependent on r for γ in the observed range 1.6 to 1.8.

We estimate σ_{12} by fitting Equation 3.8 to the observed $\xi(r_p, \pi)$. A traditional χ^2 analysis is not appropriate, however. The points of ξ are correlated, and the distribution of ξ is not gaussian over portions of the (r_p, π) plane. Since we are more interested in just whether or not the model (Equation 3.8) can fit the data in a region with as complex structure as the supercluster, rather than in the precise value of σ_{12}, we have merely done the fitting by eye. In any case, a measurement of σ_{12} for the supercluster would be of little value for comparisons with other surveys or with

models of structure formation since the value we measure would not be representative of a fair sample of the universe.

3.5.3 Fits to $\xi(r_p, \pi)$ for the Supercluster

In Figure 3.5, we plot $\xi(r_p, \pi)$ for all galaxies in the Corona Borealis supercluster. Contours above $\xi(r_p, \pi) = 1$ are spaced logarithmically (0.1 dex), while contours below $\xi(r_p, \pi) = 1$ are drawn every $\Delta\xi(r_p, \pi) = 0.2$. The dark dashed line is at $\xi(r_p, \pi) = 0$. Levels below $\xi(r_p, \pi) = 0$ are given by the light dashed lines. The prominent elongation of the contours along the π axis for $r_p \lesssim 5h^{-1}$ Mpc is caused by the velocity dispersion of bound clusters of galaxies and is the equivalent of the "fingers of God" seen in redshift space. The clustering is surprisingly weak in the supercluster, with $\xi(r_p, \pi)$ rising above 1 only within $\lesssim 3h^{-1}$ Mpc of the origin of the plot.

$\xi(r_p, \pi)$ is plotted against separation along the line-of-sight (π) for $0 < r_p < 2h^{-1}$ Mpc in Figure 3.6. We also show fits to Equation 3.8 with $\sigma_{12} = 600$, 700, and 800 km s^{-1}, assuming that the real space correlation function is $\xi(r) = (r/r_0)^{-\gamma}$, $r_0 = 2.75h^{-1}$ Mpc, $\gamma = 1.7$. The estimated value of the pairwise velocity dispersion $\sigma_{12} \sim 700 \pm 100$ km s^{-1} is much larger than the canonical value $\sigma_{12} = 340 \pm 40$ km s^{-1} computed by Davis and Peebles (1983) for the CfA1 survey, but it is roughly consistent with the recent results of Marzke *et al.* (1995) and Guzzo *et al.* (1995), both of whom have found $\sigma \sim 600$ km s^{-1}.

In Figure 3.7, we plot $\xi(r_p, \pi)$ against line-of-sight separation π for $2 < r_p < 4h^{-1}$ Mpc. The data are adequately fit with $\sigma_{12} = 375 \pm 100$ km s^{-1}. The fact that the model successfully represents the observations while *not* incorporating mean streaming suggests that the Corona Borealis Supercluster has not yet generated streaming motions with velocities $\gtrsim 100$ km s^{-1}.

3.6 Summary

We have not been able to achieve our original goal of accurately delineating the structure of the supercluster because the supercluster is considerably less dense than we believed at the beginning of this project. In particular, the background ($z \approx 0.11$) Abell 2069 supercluster contributes substantially to the projected galaxy counts. Nevertheless, our data illustrate that the galaxy distribution within the supercluster is irregular, clumpy, and unrelaxed overall. The mass of the supercluster is enormous, $(1.7 \pm 0.2) \times 10^{16} M_{\odot}$, which is more than sufficient to bind the system. The mass-to-light ratio of the supercluster is, however, comparable to that of rich clusters of galaxies. The clustering of galaxies within the supercluster is quite weak and can be fit adequately by assuming that there are no streaming motions. These last two facts imply that the supercluster has only recently begun to separate from the Hubble flow.

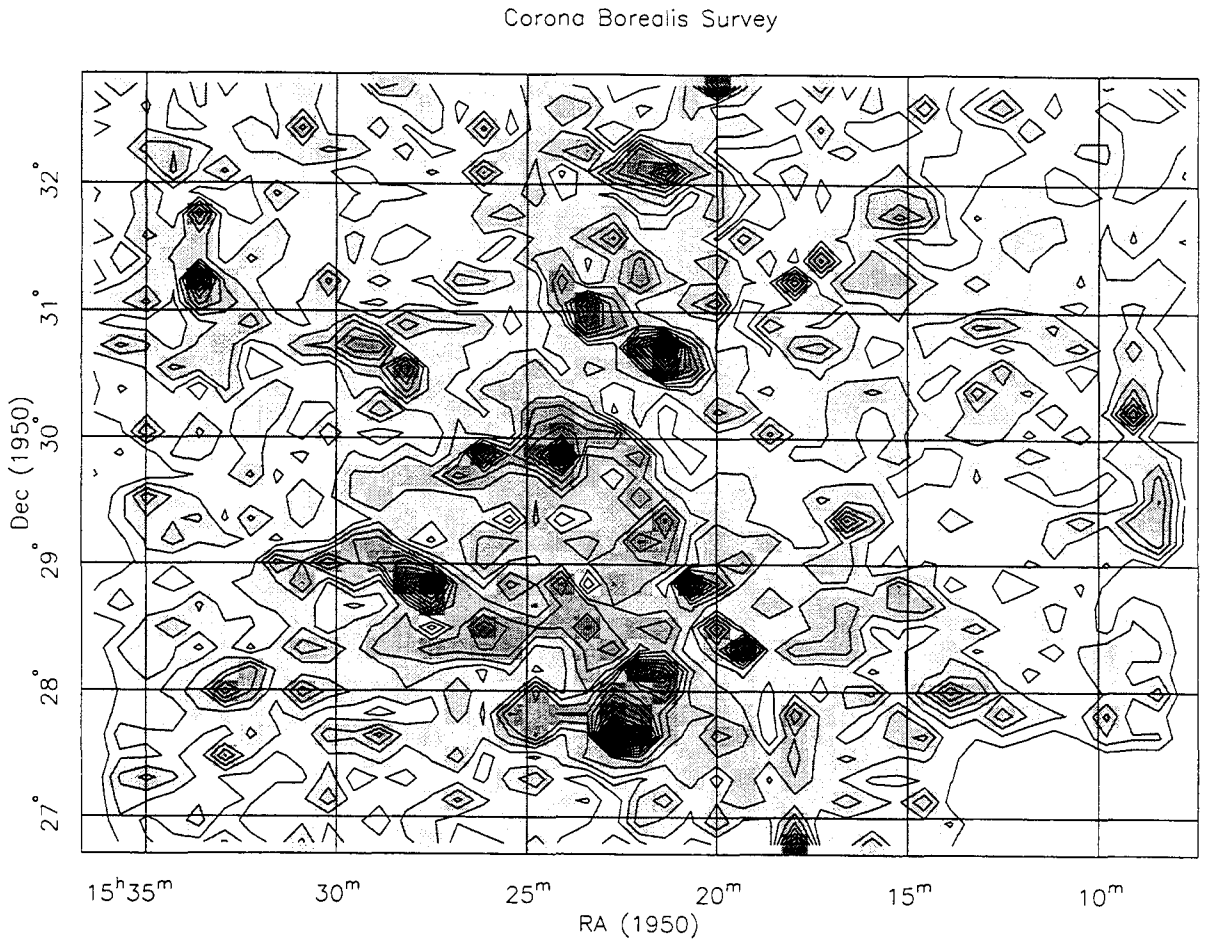

Fig. 3.1.— A combined contour/grayscale plot of the galaxy density on the sky in the Corona Borealis supercluster for all galaxies brighter than $g = 19^m$. The contour levels run from 100 galaxies per square degree to 1200 galaxies per square degree. The ridge of galaxies between Abell 2061 and Abell 2067 connects the two strikingly dense regions at $\alpha = 15^h22^m$, $\delta = +30°36^m$ and $\alpha = 15^h24^m$, $\delta = +31°0^m$. The blank region in the southwest corner is where the plate sensitometer spots are located.

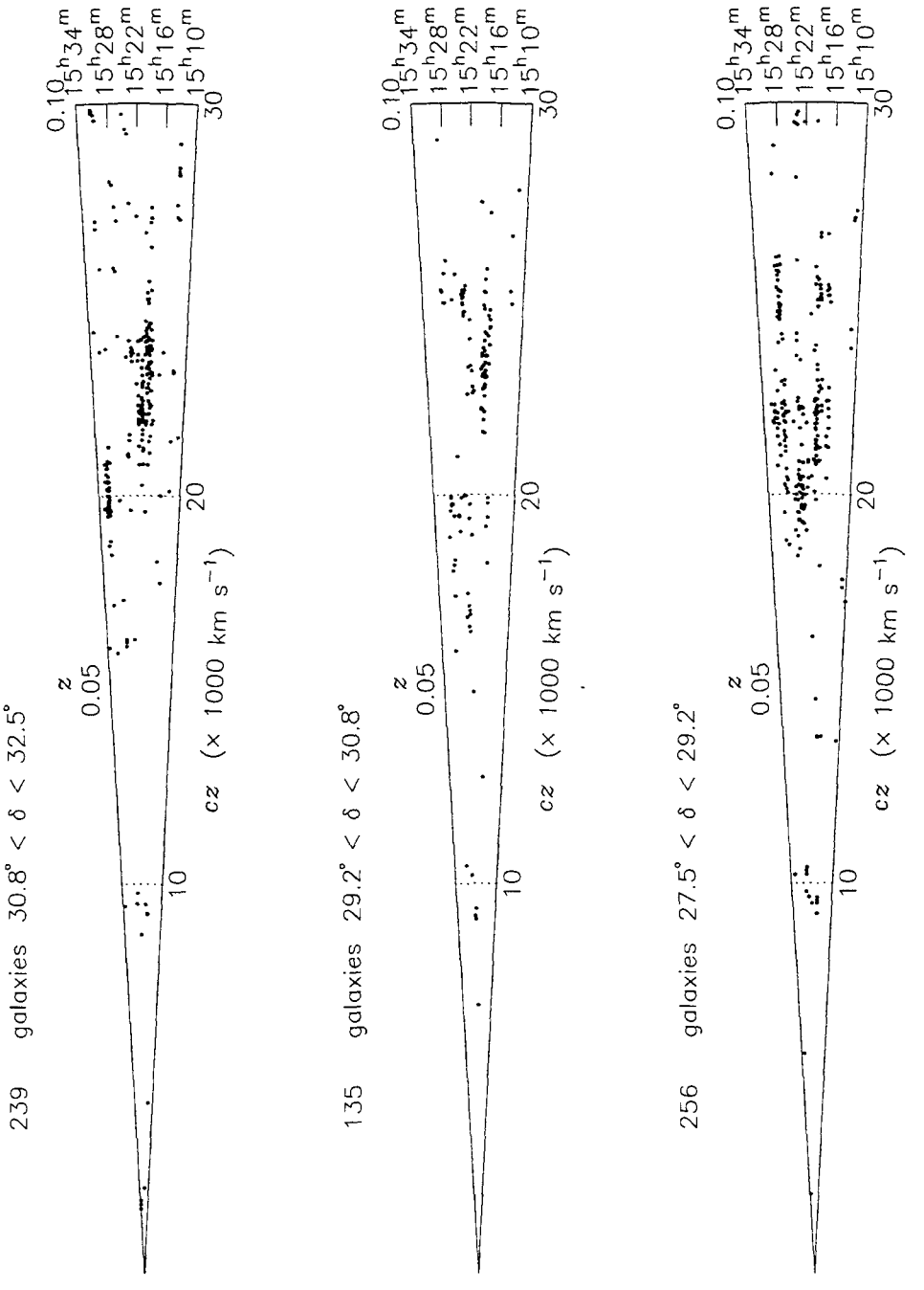

Fig. 3.2.— Redshift-right-ascension cone diagrams for galaxies in our survey with $cz < 30000$ km s^{-1}, divided into 3 declination slices. The Corona Borealis supercluster is the prominent overdense region between $cz \approx 18000$ km s^{-1} and $cz \approx 27000$ km s^{-1}. The smaller structure at $cz \approx 10000$ km s^{-1} is part of the "Great Wall" of galaxies. The galaxy distribution in the supercluster is quite clumpy, suggesting that the supercluster is not yet relaxed.

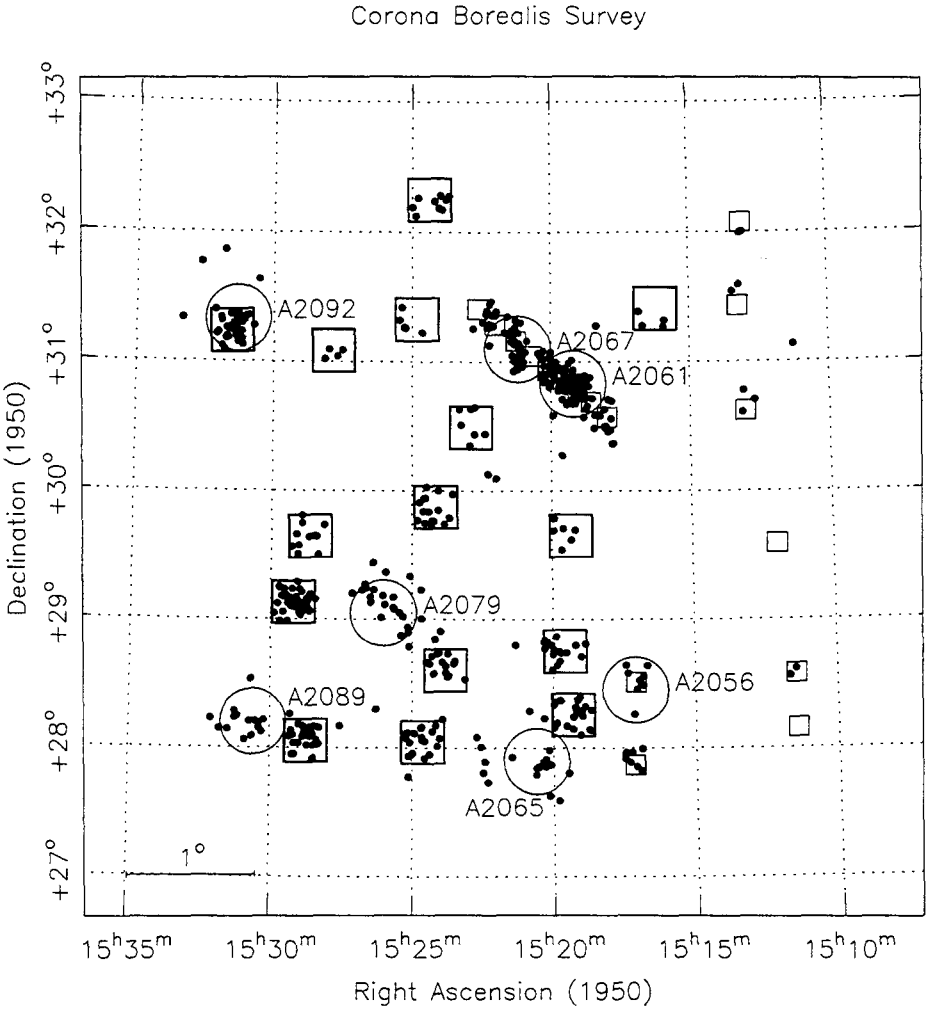

Fig. 3.3.— Location on the sky of galaxies in the Corona Borealis Supercluster. The seven large circles mark the positions of the 7 Abell clusters contained within the supercluster. The 32 survey fields are represented by squares. The data in the small squares were obtained when only half of the Norris Spectrograph's fibers were useable because a large format 2048^2 CCD was not yet available at Palomar. The data in the large squares were obtained using the full complement of 176 fibers. The number of galaxies successfully identified at all redshifts ranges from 10 to 42 for the small squares and from 59 to 87 for the large squares. Galaxies not in one of the squares were obtained from the literature.

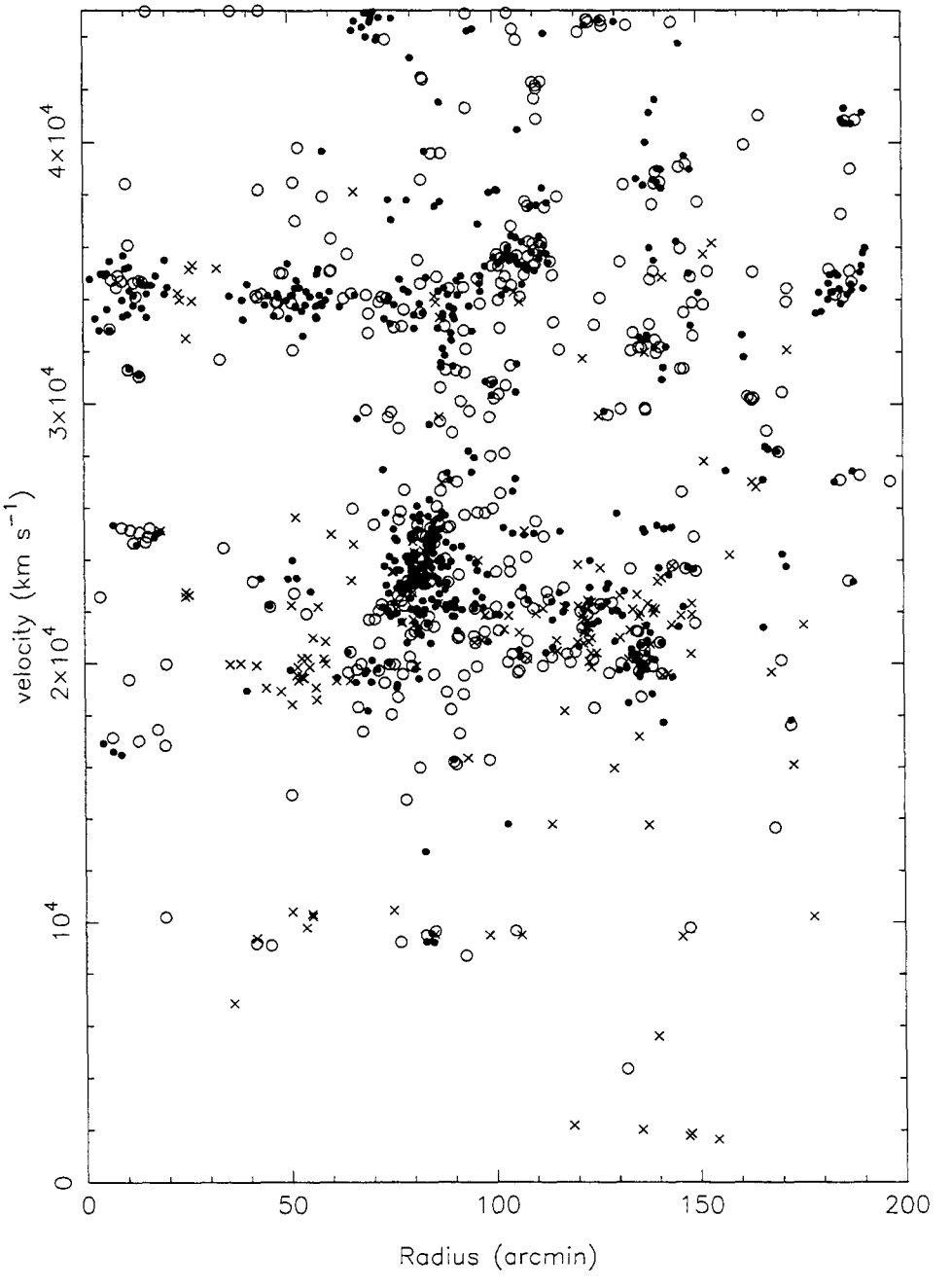

Fig. 3.4.— Recession velocity cz versus angular separation from the supercluster centers. The solid circles are absorption-lines galaxies, the unfilled circles are emission-line galaxies, and the crosses are galaxies taken from the literature whose spectral properties are not known. In order of increasing redshift, the prominent structures are the "Great Wall" at $cz \approx 10000$ km s^{-1}, the Corona Borealis Supercluster at $cz \approx 21000$ km s^{-1}, and the Abell 2069 Supercluster at $cz \approx 33000$ km s^{-1}.

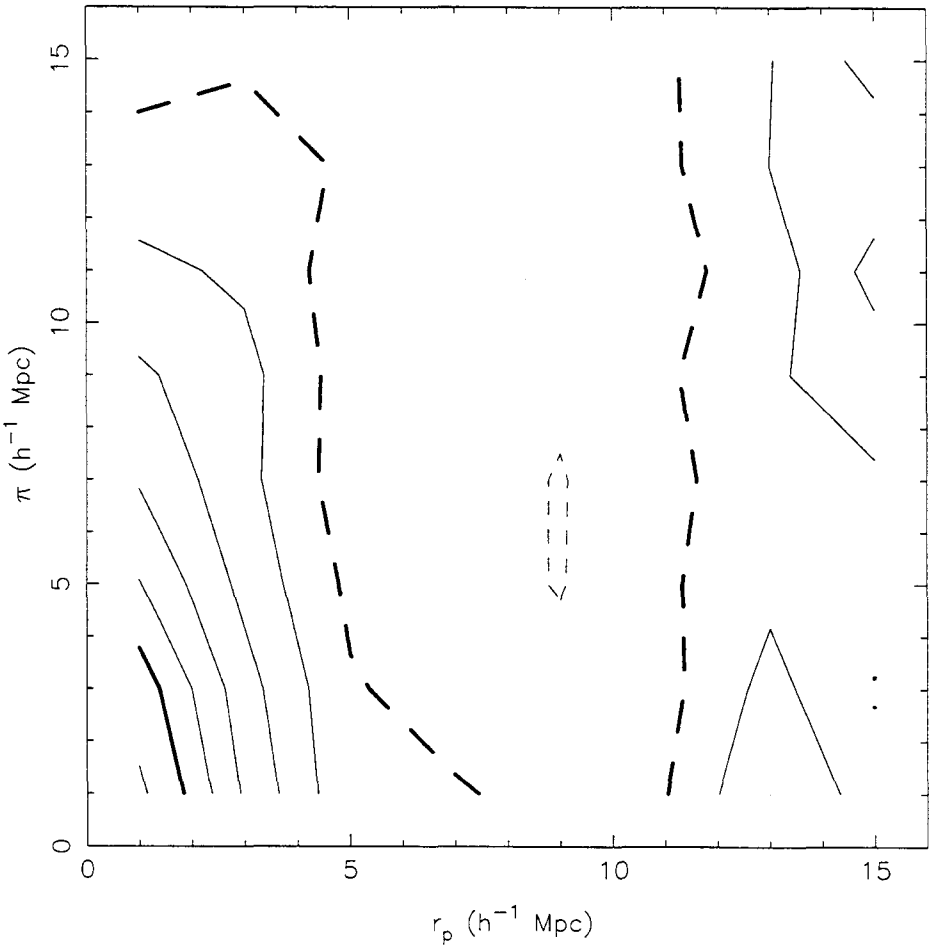

Fig. 3.5.— Contour plot of $\xi(r_p, \pi)$ for the Corona Borealis Supercluster.The contours are in steps of $\Delta\xi(r_p, \pi) = 0.2$ for $\xi(r_p, \pi) < 1$ and logarithmic (0.1 dex) for $\xi(r_p, \pi) > 1$. $\xi(r_p, \pi) = 1$ is marked by the heavy solid contour while $\xi(r_p, \pi) = 0$ is marked by the heavy dashed contour. The dashed contours represent $\xi(r_p, \pi) < 0$. The prominent elongation of the contours along the π axis for $r_p \lesssim 5h^{-1}$ Mpc is due to high velocity dispersion of virialized clusters of galaxies. The clustering in the supercluster is quite weak.

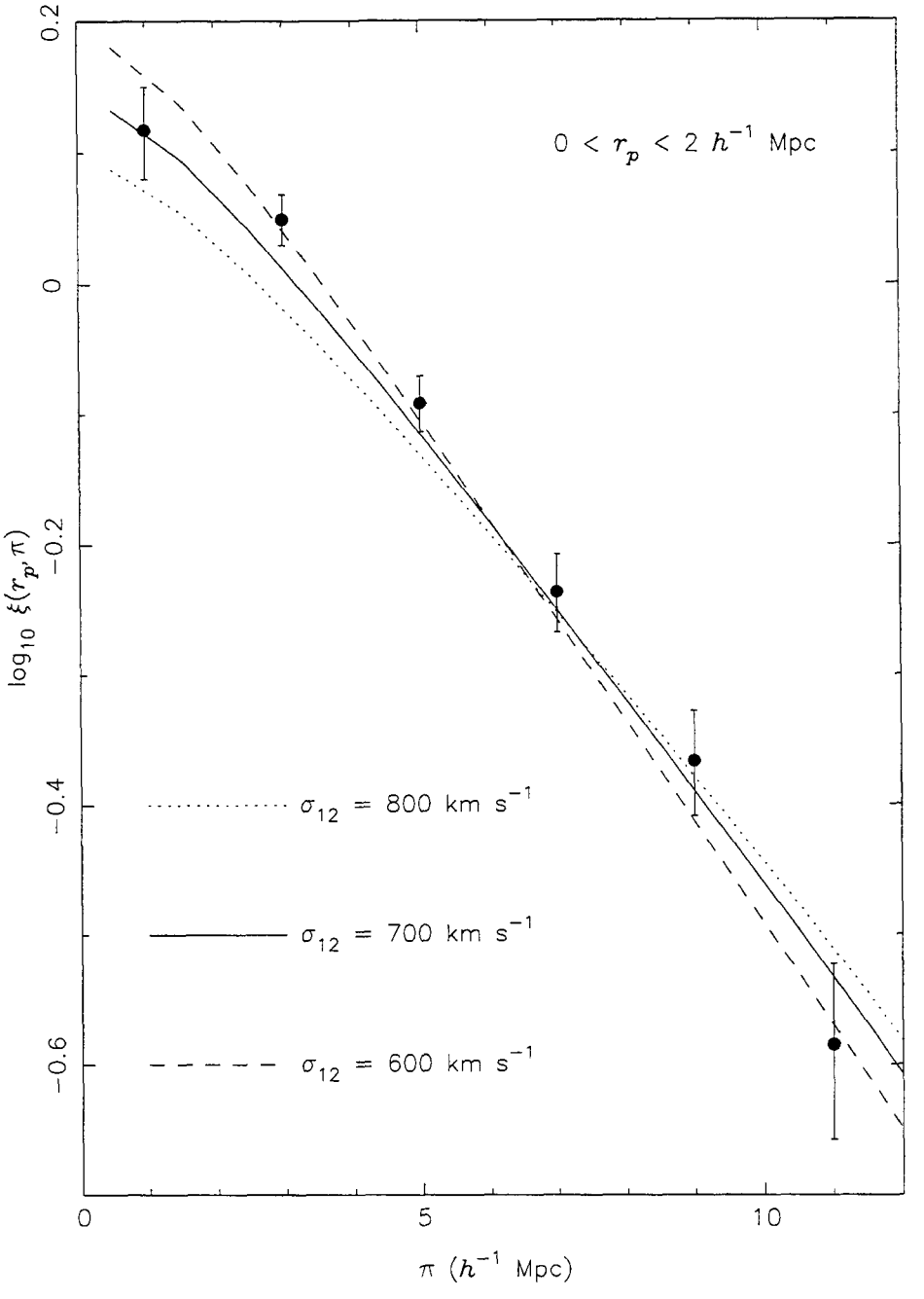

Fig. 3.6.— $\xi(r_p, \pi)$ as a function of π for $0 < r_p < 2h^{-1}$ Mpc for the Corona Borealis Supercluster. The data are adequately fit by Equation 4.9 with $\sigma_{12} = 700 \pm 100$ km s^{-1} and no mean streaming.

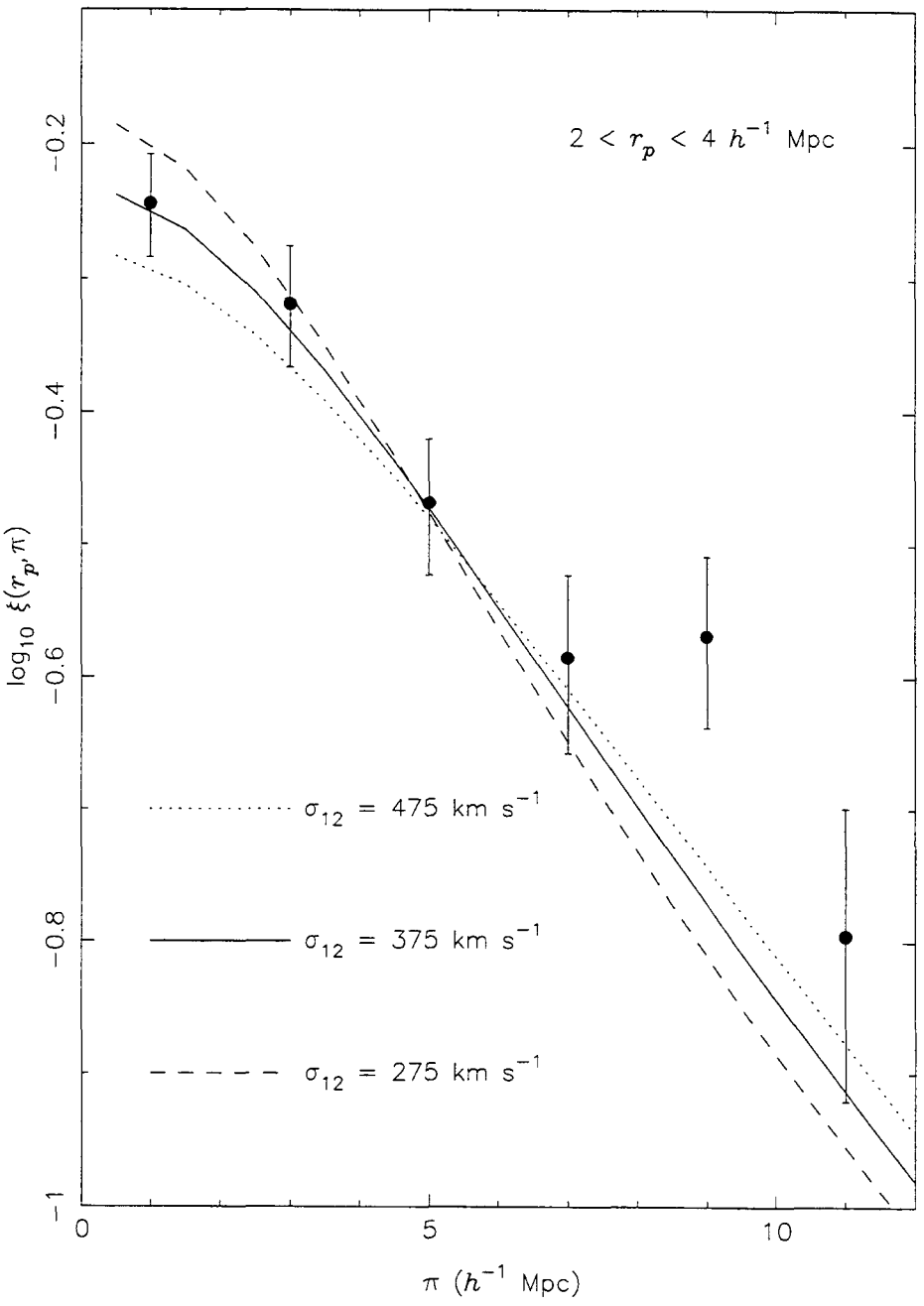

Fig. 3.7.— $\xi(r_p, \pi)$ as a function of π for $2 < r_p < 4h^{-1}$ Mpc for the Corona Borealis Supercluster. The data are adequately fit by Equation 4.9 with $\sigma_{12} = 375 \pm 100$ km s^{-1} and no mean streaming.

Chapter 4 Evolution of Galaxy Clustering and Large-Scale Structure to $z \sim 0.5$

4.1 Introduction

One of the most cherished postulates of the standard model of cosmology is that gravitational instability shaped the large-scale structure of the universe: tiny fluctuations in the early universe have grown through the action of gravity to become the galaxies, clusters of galaxies, and superclusters of galaxies which we observe today (Peebles 1994). In order to observe the evolution of structure, one needs to construct a sample of galaxies with cosmologically significant redshifts, a task which has only recently become possible with use of efficient multiplexing spectrographs on 4m class telescopes. In this paper, we investigate large-scale structure and the evolution of galaxy clustering out to $z = 0.5$ using galaxies from our redshift survey of the Corona Borealis Supercluster.

A simple way to characterize clustering is to measure a hierarchy of n-point correlation functions (Peebles 1980). In practice, only the two-point correlation function $\xi(r)$ can be accurately measured from redshift surveys. $\xi(r)$ has been measured locally for optical samples of galaxies and has been found to have a power-law form $\xi(r) = (r/r_0)^{-\gamma}$ with the correlation length $r_0 \sim 5 - 6h^{-1}$ Mpc (h is the present value of the Hubble constant measured in units of 100 km s^{-1} Mpc^{-1}) and $\gamma \sim 1.7 - 1.8$ for $r \lesssim 20h^{-1}$ Mpc (Loveday *et al.* 1995, Marzke *et al.* 1995). Cole *et al.* (1994) have measured $\xi(r)$ for $z \lesssim 0.3$ and find no evidence for evolution in the comoving correlation length. However, Le Fèvre *et al.* (1995) have observed evolution of the correlation length in a large sample of galaxies with $0 < z < 1.3$. In addition, studies

of the two-point angular correlation function of galaxies find that faint galaxies are significantly less correlated than what would be predicted from the local correlation function with only modest growth of clustering (Brainerd, Smail, and Mould 1995). Unfortunately, interpretations of the evolution of clustering are complicated by the fact that one may not be observing the same types of galaxies at high redshift as at low redshift. In local samples, early-type galaxies are clustered more strongly than late-type galaxies (Loveday *et al.* 1995). Indeed, Brainerd, Smail, and Mould (1995) suggest that, by accounting for the change in the observed morphological mix with redshift, rapid clustering evolution need not be required.

The two-point correlation function is distorted in redshift space by peculiar velocities. On small scales, the velocity dispersion of bound clusters of galaxies suppresses the apparent correlation function, whereas on large scales, coherent motions of galaxies towards overdense regions and away from underdense regions enhance the correlation function. An analysis of the distortions allows one in principle to measure the mean velocity dispersion of pairs of galaxies, σ_{12}, and to estimate the mean density of the universe, Ω_0 (modulo the bias parameter). The canonical value of σ_{12} is 340 ± 40 km s^{-1}, which was obtained by Davis and Peebles (1983) using data from the CfA1 redshift survey. This measurement of σ_{12} has become one of the strongest constraints on models of structure formation because the standard cold dark matter model, with the power spectrum normalized to match the quadrupole anisotropy measured in the cosmic microwave background, predicts $\sigma_{12} \approx 1000$ km s^{-1} for a flat universe (Davis *et al.* 1985). The value of σ_{12} predicted by the CDM model can be reduced either by assuming an open universe or by assuming that the galaxies are a biased tracer of the underlying mass distribution, but it is very difficult to reduce σ_{12} to the value measured by Davis and Peebles (1983). Recently, however, Guzzo *et al.* (1995) and Marzke *et al.* (1995), using the Perseus-Pisces redshift survey and the combined CfA2/SSRS redshift survey, respectively, have obtained values of σ_{12} which are roughly twice as high as the canonical 340 ± 40 km s^{-1} and have emphasized the sensitivity of σ_{12} to the volume in which it is measured and to the treatment of the richest clusters in the sample. Our survey allows us to measure σ_{12} in the largest

volume yet probed, $\sim 5 \times 10^6 h^{-1}$ Mpc^3. This volume is sufficiently large that the value of σ_{12} measured in our survey should be within $\sim 10\%$ of the cosmic mean (Marzke *et al.* 1995).

A measurement of the mean streaming motion of galaxy pairs can be used to estimate Ω_0. Unfortunately, our data set is not large enough to usefully constrain Ω_0, especially since it is very difficult to disentangle the effects on the two point correlation function of large structures perpendicular to the line-of-sight from those of large-scale streaming (Fisher *et al.* 1994a).

There have been recent reports of clustering of galaxies on scales far larger than those on which $\xi(r)$ is measured. Most famously, Broadhurst *et al.* (1990) found that peaks in their narrow pencil-beam survey of the North and South galactic poles occurred at regular intervals of $\sim 128h^{-1}$ Mpc. Landy *et al.* (1995) have detected excess power on $100h^{-1}$ scales in the two-dimensional power spectrum of galaxies in the Las Campanas Redshift Survey (Shectman *et al.* 1995). Estimating the significance of the result of Broadhurst *et al.* (1990) is complicated by the fact that small-scale power in the three-dimensional power spectrum projects to large scales in the one-dimensional power spectrum (Kaiser and Peacock 1991). The amount of power projected varies roughly as the inverse of the angular size of the survey. The Broadhurst *et al.* (1990) pencil-beam was $10'$ wide. In contrast, our survey is 6° wide, thus greatly reducing the power projected to large scales.

The paper, the third in the series of papers presenting results from the Norris Survey of the Corona Borealis Survey, is organized as follows. In §2, we briefly describe the survey, emphasizing those points which are relevant to the current analysis. We review the techniques for measuring $\xi(r_p, \pi)$ and discuss how to measure the real space correlation function and the pairwise velocity dispersion in §3. The evolution of the real space correlation function is investigated in §4. The results for the pairwise velocity dispersion are presented in §5. The presence of structure on $\sim 100h^{-1}$ Mpc scales is analyzed in §6. We summarize our conclusions in §7.

Unless otherwise noted, we use $q_0 = 0.5$ throughout the paper.

4.2 The Norris Survey of the Corona Borealis Supercluster

The Norris Survey of the Corona Borealis Supercluser has been described in detail in Small *et al.* (1996), Paper I of the current series, and will be only briefly reviewed here. The core of the supercluster covers a $6° \times 6°$ region of the sky centered at right ascension 15^h20^m, declination $+30°$ and consists of 7 rich Abell clusters at $z \approx 0.07$. Since the field-of-view of the 176-fiber Norris Spectrograph is only 400 arcmin^2, we planned to observe 36 fields arranged in a rectangular grid with a grid spacing of 1°. As it turned out, we successfully observed 23 of the fields and 9 additional fields along the ridge of galaxies between Abell 2061 and Abell 2067, yielding redshifts for 1491 extragalactic objects. We have extended our survey with 163 redshifts from the literature, resulting in 1654 redshifts in the entire survey. 1022 of these galaxies lie beyond the Corona Borealis Supercluster, although of these 1022, 298 galaxies are in a background supercluster ($z \approx 0.11$) which we have dubbed the "Abell 2069 Supercluster."

The survey is only complete in apparent magnitude to Gunn $r = 18.5^m$. However, we have substantial numbers of galaxies out to $r = 22.0^m$. In order to compute the two-point correlation function one must create a random sample of galaxies with the same selection effects as the real data. We chose random redshifts not from the probability distribution $P(M|z)$ that an object at redshift z has an absolute magnitude M, which would be appropriate for a magnitude limited sample, but rather from the probability distribution $P(z|m)$ that an object with apparent magnitude m has a redshift z. We describe the creation of the random sample in more detail below (§3.1).

The velocity errors in our sample are typically ~ 100 km s^{-1}. In order to compute the real space two-point correlation function, we integrate the redshift space two-point correlation function along the line-of-sight, thus accounting for the effects of velocity errors (and real peculiar velocities). The sampling of galaxies on the sky is not uniform in our survey. The Norris Spectrograph fibers cannot be placed within

16″ of each other, and their motion is further restricted by limits on the bending angles of the fibers. These two effects combine to eliminate pairs of objects with angular separations of $\lesssim 30''$. However, as illustrated in Figure 4.1, this bias is insignificant since a pair of galaxies at $z = 0.5$, the highest redshift we consider in this paper, must have a separation of less than $0.3h^{-1}$ Mpc to be affected. The fiber assignment program introduces a bias against pairs with separations $\gtrsim 10'$. Vignetting at the edges of the spectrograph field of view further limits the number of pairs at large separations. Since the survey fields do not overlap, the bias against pairs with separations between 10′ and 20′ causes the correlation function on comoving scales that subtend 10′-20′ to be severely underestimated and very noisy. The affected range is shown in Figure 4.2 as a function of redshift.

We do not believe that the survey is biased against particular galaxy types to $z = 0.5$. The 4000Å break and Ca H, Ca K lines of old stellar populations and the [O II] line of star-forming galaxies are within our spectral range to $z = 0.5$. The color distribution of the objects that we observed but failed to identify is similar to the color distribution of the objects that we successfully observed (Paper I). (Note that this does not imply that the morphological mix at $z = 0.5$ is identical to the morphological mix at $z = 0$.)

4.3 The Two-Point Correlation Function $\xi(r_p, \pi)$

4.3.1 Definition and Computation of $\xi(r_p, \pi)$

Redshift-space maps of the spatial distribution of galaxies are distorted by the peculiar motions of galaxies. The measured redshift of a galaxy is the sum of the Hubble motion of the galaxy plus the line-of-sight peculiar velocity. The "fingers of God" seen in redshift surveys of rich clusters of galaxies, in which the large velocity dispersion of a cluster spreads out the cluster galaxies along the line-of-sight in redshift space, are the most prominent signatures of redshift space distortions. On large scales, coherent infall into overdense regions and outflow from underdense regions enhance

the correlation function. Since the velocities on large scales can be simply related to the mean mass density of the universe Ω_0 with linear theory, an analysis of redshift space distortion can in principle yield an estimate of Ω_0 (Sargent and Turner 1977, Fisher *et al.* 1994a). The distribution of galaxies on the plane of the sky is not, however, distorted by peculiar velocities. Thus, correlation functions, which one assumes are isotropic in real space, are anisotropic in redshift space. It is, therefore, useful to compute correlation functions as functions of separations along the line-of-sight (π) and perpendicular to the line-of-sight (r_p).

The two-point correlation function $\xi(r_p, \pi)$ is the joint probability δP of finding a galaxy in each of two volume elements dV_1, dV_2 separated by r_p and π,

$$\delta P = \bar{n}^2(1 + \xi(r_p, \pi))dV_1 dV_2, \tag{4.1}$$

where $\bar{n}$ is the mean galaxy density. In order to compute $\xi(r_p, \pi)$, we construct a catalog of randomly distributed points with same selection function as the real data. We estimate $\xi(r_p, \pi)$ using the estimator derived by Hamilton (1993):

$$1 + \xi(r_p, \pi) = \frac{DD(r_p, \pi)RR(r_p, \pi)}{DR(r_p, \pi)^2}, \tag{4.2}$$

where $\mathrm{DD}(r_p, \pi)$, $\mathrm{RR}(r_p, \pi)$, and $\mathrm{DR}(r_p, \pi)$ are the number of data-data, random-random, and data-random pairs, respectively, with separations r_p and π. The virtue of Hamilton's estimator is that it is affected only in second order by density fluctuations on the scale of the survey. In addition, Hamilton's estimator does not require an independent measurement of the mean galaxy density of the survey.

We calculate the error in $\xi(r_p, \pi)$ using simple Poisson statistics, $\sigma(\xi) = (1 + \xi)/\sqrt{DD}$. Traditionally, bootstrap resampling of the data has been employed to estimate the errors (Ling, Frenk, and Barrow 1986). However, bootstrap errors are not expected to yield accurate estimates of the errors for correlation statistics (Press *et al.* 1992, Fisher *et al.* 1994b). This is illustrated by considering an attempt to estimate the significance of a void in an observed galaxy distribution using bootstrap

errors. The void will always remain empty in the bootstrap samples, causing an underestimate of the error in the mean density. Similarly, the bootstrap method will overestimate the error in the estimate of the mean density of an overdense region. Since ξ is pair-weighted, it is heavily weighted by the densest regions. Using N-body simulations, Fisher *et al.* (1994b) have found that the simple Poisson error estimate is, in fact, slightly more accurate than bootstrap error estimates for $3 \lesssim r \lesssim 15h^{-1}$ Mpc. For $r \lesssim 3h^{-1}$ Mpc, we double the Poisson errors to match crudely the error estimated by Fisher *et al.* (1994b) for an ensemble of N-body simulations.

The random catalog has 50 times the number of galaxies as the real catalog so that the errors in the counts for the random catalog will be negligible. As noted above, our sample of galaxies is not magnitude-limited. In order to generate the redshifts of the galaxies in the random catalog, we have selected the redshifts from the distribution $P(z|m)$ that a galaxy with an apparent magnitude m has a redshift z:

$$P(z|m) = \frac{\phi[M(z,m)]\frac{dV}{dz}}{\int_0^\infty \phi[M(z',m)]\frac{dV}{dz'}dz'} \tag{4.3}$$

Here, $\phi(M)$ is the luminosity function, $M(z,m)$ is the absolute magnitude of a galaxy such that it would have apparent magnitude m at redshift z, and dV/dz is the relativistic volume element. For each galaxy in the real catalog, we choose 50 redshifts from $P(z|m)$. We have also drawn the redshifts from the observed redshift distribution, heavily smoothed with a gaussian with a dispersion of 9000 km s^{-1}. Our results for the two methods of choosing redshifts agree well.

Since the survey was sparsely sampled, some care must be taken in assigning the celestial coordinates to the galaxies in the random catalog. For each galaxy in the real catalog, we choose 50 celestial coordinates at the same time that we choose the 50 redshifts. The celestial coordinates are selected randomly from the survey field to which the real galaxy belongs. This method correctly accounts for the varying number of galaxies successfully identified per survey field. If a galaxy in the real catalog was taken from the literature, then we chose the 50 celestial coordinates in the random catalog to be uniformly distributed throughout the whole $6^\circ \times 6^\circ$ survey

area. We compared the results using this method with those using a scheme in which, for every galaxy in the real catalog, 50 celestial coordinates were chosen at random from a circle with radius $1'$ centered on the real object. There were no significant differences between the results using the two schemes.

4.3.2 The Spatial Correlation Function $\xi(r)$

In order to compute the real space correlation function $\xi(r)$, we project $\xi(r_p, \pi)$ onto the r_p axis. The projection depends only on the real space correlation function:

$$w_p(r_p) = 2\int_0^\infty \xi(r_p, \pi) d\pi \tag{4.4}$$

$$= 2\int_0^\infty \xi[(r_p^2 + y^2)^{1/2}] dy, \tag{4.5}$$

where y is the line-of-sight separation in real space. The integrand in the second expression for $w_p(r_p)$ is the correlation function in real space. If we assume that $\xi(r) = (r/r_0)^{-\gamma}$, the integral for $w_p(r_p)$ can be evaluated analytically to give:

$$w_p(r_p) = r_p \left(\frac{r_0}{r_p}\right)^\gamma \frac{\Gamma\left(\frac{1}{2}\right)\Gamma\left(\frac{\gamma-1}{2}\right)}{\Gamma\left(\frac{\gamma}{2}\right)} \tag{4.6}$$

By fitting a power law to $w_p(r_p)$, we can measure the correlation length and power law index of the real space correlation function.

4.3.3 A Model for $\xi(r_p, \pi)$

The distortions of $\xi(r_p, \pi)$ contain information on the velocity distribution function of galaxy pairs, $F(\mathbf{w}|\mathbf{r})$, where $\mathbf{w}$ is the velocity difference of a pair with vector separation $\mathbf{v}$. Peebles (1980) has modeled $\xi(r_p, \pi)$ as a convolution of the real space correlation function $\xi(r)$ with $F(\mathbf{w}|\mathbf{r})$,

$$1 + \xi(r_p, \pi) = \int [1 + \xi(r)] F(\mathbf{w}|\mathbf{r}) d^3\mathbf{w} \tag{4.7}$$

This expression can be simplified if we assume that the velocity dispersion of pairs varies slowly with pair separation and that there is no preferred direction in the velocity field. With those assumptions, $\xi(r_p, \pi)$ depends only on the distribution of line-of-sight velocities, and we have

$$1 + \xi(r_p, \pi) = \int [1 + \xi(r)] F(v_{los}|r) dv_{los} \tag{4.8}$$

If we separate $\mathbf{r}$ into components (r_p, y) perpendicular to and along the line-of-sight, then $r^2 = r_p^2 + y^2$, $v_{los} = H_0(\pi - y)$, and

$$1 + \xi(r_p, \pi) = \int [1 + \xi(\sqrt{r_p^2 + y^2})] F(H_0(\pi - y)|r) dy \tag{4.9}$$

It has been found in the analyses of previous surveys (Davis and Peebles 1983, Fisher *et al.* 1994a) that an exponential distribution of pairwise line-of-sight velocities,

$$F(v_{los}) = \frac{1}{\sqrt{2}\sigma_{12}} e^{-\sqrt{2}v_{los}/\sigma_{12}}, \tag{4.10}$$

where σ_{12} is the line-of-sight velocity dispersion, fits the data well. We have assumed that the mean of the distribution of pairwise line-of-sight velocities is 0. In general, one would expect coherent infall on large scales to generate streaming motions and thus that the mean would not be zero. However, on the small scales for which have sufficient data, the dispersion σ_{12} is much larger than the expected streaming motions. Also, we are neglecting the scale dependence of σ_{12}. The Cosmic Virial Theorem (Peebles 1980) predicts that the dispersion of bound objects scales as $\sigma_{12} \propto r^{1-\gamma/2}$, which is only weakly dependent on r for γ in the observed range 1.6 to 1.8.

We estimate σ_{12} by fitting Equation 4.9 to the observed $\xi(r_p, \pi)$. A traditional χ^2 analysis is not appropriate, however. The points of ξ are correlated, and the distribution of ξ is not gaussian over portions of the (r_p, π) plane. Since the differences associated with the treatment of the richest structures in the survey (*e.g.*, whether or not to exclude the superclusters or merely to remove galaxies near the Abell cluster cores are much larger than the statistical errors, we have merely done the fitting by

eye. This is sufficient for answering the main question we wish to address in this analysis, namely, is σ_{12} larger than the canonical value of 340 ± 40 km s^{-1} (Davis and Peebles 1983)?

4.4 The Evolution of $\xi(r, z)$

Assuming that $\xi(r, z)$ is well fit by a power-law $(r/r_0)^{-\gamma}$, where r and r_0 are comoving coordinates, we can describe the evolution of $\xi(r, z)$ using (Groth and Peebles 1977)

$$\xi(r, z) = \xi(r, 0)(1 + z)^{-(3+\epsilon-\gamma)/\gamma} \tag{4.11}$$

For clustering which is fixed in comoving coordinates, the evolutionary parameter $\epsilon = \gamma - 3$. For clustering which is fixed in physical coordinates, $\epsilon = 0$. Linear theory predicts $\epsilon = \gamma - 1$ (Peebles 1980).

We have computed $\xi(r)$ in the redshift intervals $0.2 < z < 0.3$ and $0.3 < z < 0.5$ by fitting to the projected correlation function $w_p(r_p)$. In Figure 4.3, we plot $w_p(r_p)$ for our two redshift intervals, along with fits to the local $w_p(r_p)$ computed from the CfA+SSRS (Marzke *et al.* 1995) and Stromlo/APM surveys (Loveday *et al.* 1995). $w_p(r_p)$ declines dramatically with redshift between $z = 0.$ and $z \approx 0.4$. In order to compute the evolutionary parameter ϵ, we have included measurements of $r_0(z)$ from the CfA+SSRS survey, the Stromlo/APM survey, and the CFRS survey (Le Fèvre *et al.* 1995). The data from these surveys and our own are shown in Figure 4.4 along with the best fit to Equation 4.11. We assume $\gamma = 1.65$ and that γ does not change with redshift. We measure $\epsilon = 2.25 \pm 0.1$, although the value of χ^2 per degree of freedom ν is quite poor, $\chi^2/\nu = 21.5/5$. Despite the uncertainties in the fit, it is clear that the measured value of ϵ is significantly larger than the value predicted by linear theory ($\epsilon = 0.7$ for $\gamma = 1.7$).

The interpretation of the decline is not straightforward, however, since we may not be observing similar galaxy populations at the various epochs. In local samples, it is found that intrinsically bright galaxies are more strongly clustered than intrin-

sically faint galaxies and that early-type galaxies are more strongly clustered than late-type galaxies (Loveday *et al.* 1995). Galaxies with faint absolute magnitudes are progessively excluded from our survey with increasing redshift. Galaxies in the range $0.2 < z < 0.3$ are almost all brighter than $M(B) = -18.5 + 5\log_{10} h$, and galaxies in the range $0.3 < z < 0.5$ are almost all brighter than $M(B) = -19.0 + 5\log_{10} h$. Since the intrinsically faint galaxies are less clustered than the intrinsically bright galaxies, a survey with a fainter magnitude limit than ours would presumeably measure smaller correlation lengths than we have, thereby further increasing the value of the evolutionary parameter ϵ over the linear theory prediction.

We have shown in Small, Sargent, and Hamilton (1996a), Paper IV in the current series, that the median color of the galaxies becomes bluer with increasing redshift. In the redshift interval $0.2 < z < 0.3$, 64% (137/215) of the galaxies in our survey have emission lines, whereas 77% (146/190) of the galaxies have emission lines in the redshift interval $0.3 < z < 0.5$. The increasing blue fraction with redshift could dilute the measured correlation function and artificially inflate the measured value of ϵ. In order to investigate this effect, we have computed $w_p(r_p)$ separately for the absorption-line objects and the emission-line objects. We divided the data according to spectral type rather than photometric color because we know the spectral type of every galaxy in the survey while there are a handful of galaxies which were detected on only one of the original POSS-II plates. (Estimates of $w_p(r_p)$ with smaller samples separated by color into galaxies redder than a Coleman, Wu, and Weedman (1980) Sbc galaxy and those as blue or bluer than their Sbc galaxy were consistent with those computed for the samples divided by spectral properties.) In Figures 4.5 and 4.6 we plot $w_p(r_p)$ as a function of redshift for the emission-line and absorption-line objects, respectively. We also include in the figures fits to $w_p(r_p)$ for the appropriate galaxy types from Loveday *et al.* (1995) and from Le Fèvre *et al.* (1995). We do not see any signs of evolution of the clustering strength of the emission-line galaxies, contrary to the results of Le Fèvre *et al.* (1995). The emission-line galaxies do evolve, however. The emission-line galaxies are less strongly correlated than the absorption-line galaxies, as seen in local samples. Unfortunately, we do not have a sufficient

number of galaxies with $0.3 < z < 0.5$ to confirm the observation of Le Fèvre *et al.* (1995) that the blue and red populations become similarly clustered for $z \gtrsim 0.5$.

The lack of evidence for a reduction in the strength of the clustering of red galaxies with redshift suggests that large value of the evolutionary parameter ϵ that we have measured is partly due to the change in the observed morphological mix with redshift, in accord with the conclusions of Brainerd, Smail, and Mould (1995). The evolution of the clustering of the blue galaxies is still, however, dramatic. Loveday *et al.* (1995) measured $r_0 = 4.4 \pm 0.1h^{-1}$ Mpc (in *proper units*) for spiral and irregular galaxies with $z_{med} = 0.05$. Combining this result with our estimate of the correlation length (converted to proper units) for blue galaxies with $0.2 < z < 0.5$ ($z_{med} = 0.3$), $r_0 = 2.1 \pm 0.2h^{-1}$ Mpc, we find roughly that $\epsilon \approx 2$ for the blue population alone.

4.5 The Pairwise Velocity Dispersion σ_{12}

We have computed σ_{12} for three samples from our survey: all galaxies with $0 < z < 0.5$, all galaxies with $0 < z < 0.5$ that are not within $5h^{-1}$ Mpc of the center of an Abell cluster, and all galaxies with $0.13 < z < 0.5$. We have chosen these three samples to illustrate the sensitivity of σ_{12} to presence of rich clusters in the survey volume. The volume of our survey to $z = 0.5$ is $5 \times 10^6 h^{-3}$ Mpc^3, which is roughly 3 times larger than the volume of the combined CfA+SSRS redshift survey.

In Figure 4.7, we plot $\xi(r_p, \pi)$ for all galaxies with $0 < z < 0.5$. The dark solid line marks $\xi(r_p, \pi) = 1$. Contours above $\xi(r_p, \pi) = 1$ are spaced logarithmically (0.1 dex), while contours below $\xi(r_p, \pi) = 1$ are drawn every $\Delta\xi(r_p, \pi) = 0.2$. The dark dashed line is at $\xi(r_p, \pi) = 0$. Levels below $\xi(r_p, \pi) = 0.$ are given by the light dashed lines. The prominent elongation of the contours along the π axis for $r_p \lesssim 5h^{-1}$ Mpc is caused by the velocity dispersion of bound clusters of galaxies and is the equivalent of the "fingers of God" seen in redshift space. The rise in $\xi(r_p, \pi)$ at $r_p \approx 12h^{-1}$ Mpc is due to the correlation of the Abell clusters in the survey. In Figure 4.8, we plot $\xi(r_p, \pi)$ versus π for $0 < r_p < 1h^{-1}$ Mpc along with curves computed using Equation 4.9 for σ_{12} =800, 900, and 1000 km s^{-1}, where σ_{12} has been corrected for a redshift

of $z_{med} = 0.11$. The curve with $\sigma_{12} = 900$ km s^{-1} fits the data well. The curves with $\sigma_{12} = 800$ and 1000 km s^{-1} bracket the range of acceptable fits.

$\xi(r_p, \pi)$ for all galaxies with $0 < z < 0.5$ and not within $5h^{-1}$ Mpc of an Abell cluster is shown in Figure 4.9. The contour levels are the same as for Figure 4.7. The elongation of the contours along the π axis for small r_p are not as pronounced as for the sample which included galaxies in the cores of the Abell clusters. The weak compression of the contours along the π axis for $r_p \approx 5h^{-1}$ Mpc is the signature of coherent galaxy motions generated by large-scale structure. This compression was not visible in Figure 4.7 because of the large velocity dispersion of the Abell clusters in the complete sample of galaxies with $0 < z < 0.5$. As shown in Figure 4.10, the pairwise velocity dispersion drops by nearly 300 km s^{-1} with the removal from the sample of the galaxies in the Abell clusters. $\xi(r_p, \pi)$ is well fit using Equation 4.9 with $\sigma_{12} = 625 \pm 100$ km s^{-1} (corrected for $z_{med} = 0.23$).

Lastly, we plot $\xi(r_p, \pi)$ for all galaxies with $0.13 < z < 0.5$ in Figure 4.11. By restricting the galaxies to have $z > 0.13$, we remove the two superclusters. The contour levels are the same as for Figure 4.7. The elongation of the contours along the π axis for small r_p is still apparent, but it is substantially reduced from the two samples which included the superclusters. The presence of coherent large-scale motions is evident in the compression of the contours along the π axis for $r_p \approx 5h^{-1}$ Mpc. $\xi(r_p, \pi)$ is plotted versus π for $0 < r_p < 2h^{-1}$ Mpc in Figure 4.12. We find using Equation 4.9 that $\sigma_{12} = 325 \pm 100$ km s^{-1}, which agrees within the errors with the original result of Davis and Peebles (1983) and with the results of Marzke *et al.* (1995) for the combined CfA+SSRS survey with the Abell clusters of richness class one or greater removed.

We confirm, for the largest volume yet studied, the results of Guzzo *et al.* (1995) and Marzke *et al.* (1995) that the value of σ_{12} averaged over all galaxies is substantially larger than the canonical value of 340 ± 40 km s^{-1} and that σ_{12} could be as large as 600 km s^{-1}. Such a large value is consistent with the value of σ_{12} predicted by low density ($\Omega h \approx 0.2$) and biased cold dark matter models (Davis *et al.* 1985).

4.6 Structure on Scales of $\sim 100h^{-1}$ Mpc

In Figure 4.13, we plot the redshift-right-ascension diagram for all the objects in our survey with $cz < 80000$ km s^{-1}. The Corona Borealis and Abell 2069 superclusters are the two prominent structures at $z \approx 0.07$ and $z \approx 0.11$, respectively. The structure at $cz \approx 10000$ km s^{-1} is part of the "Great Wall" of galaxies identified in the CfA redshift survey (Geller and Huchra 1989). Between the structures, there are large underdense regions with scales of $\sim 100h^{-1}$ Mpc.

The presence of structure on scales of $\sim 100h^{-1}$ Mpc is confirmed by computing the one-dimensional power spectrum in our survey. Following Kaiser and Peacock (1991), we compute

$$\delta_k = \frac{1}{N}\sum_{i=1}^{N} e^{ikx_i} \tag{4.12}$$

where N is total number of objects and x_i is the comoving distance to object i. We plot the power spectrum $|\delta_k|^2$, the contribution to the fractional density variance from a single mode, in Figure 4.14. The prominent peak in the power spectrum at $k \approx 0.06h$ radians Mpc^{-1} corresponds to structures on the scale of $\sim 100h^{-1}$ Mpc. Computing the significance of a peak in the one-dimensional power spectrum is complicated by that fact that small scale power in the three-dimensional power spectrum is projected onto large scales (small k) in the one-dimensional power spectrum. Kaiser and Peacock (1991) estimate that for a cylindrical survey with depth L and radius R, the mean power for one mode is

$$|\delta_k|^2 = 1.79\left(\frac{\pi}{L}\right)R\left(\frac{r_0}{R}\right)^{1.7} \tag{4.13}$$

where r_0 is the correlation length of small scale clustering and we have assumed that the power-law index of the correlation function is $\gamma = 1.7$. Taking $L \sim 1000h^{-1}$ Mpc (which corresponds to the survey extending to $z \sim 0.5$), $R \sim 30h^{-1}$ Mpc, and $r_0 \sim 5h^{-1}$ Mpc, we find that the expected mean power at large-scales is $|\delta_k|^2 \sim 0.01$. The probability that such a peak with height ~ 0.08 would occur at random is only $\exp(-0.08/0.01) = 3\times10^{-4}$. Our results, in agreement with those of Broadhurst *et al.*

(1990) and Landy *et al.* (1995), strongly suggest that $\sim 100h^{-1}$ Mpc is a preferred scale in the galaxy distribution.

4.7 Summary

We have presented an analysis of large-scale structure and the evolution of clustering for galaxies selected from the Norris Survey of the Corona Borealis Supercluster. We have found compelling evidence for a decline in the strength of galaxy clustering with redshift. The observed decline is quite dramatic and, if we assume that the variation of the observed morphological mix with redshift is minor, implies a value of the evolutionary parameter $\epsilon = 2.25 \pm 0.1$ which is considerably larger than the linear theory prediction ($\epsilon = 0.7$ for correlation function power-law index $\gamma = 0.7$). The variation of the observed morphological mix does, however, appear to play an important role. When our samples are divided into absorption-line (red) galaxies and emission-line (blue) galaxies, we find that there is no sign of evolution of the clustering of the red galaxies while the clustering of the blue galaxies is changing rapidly with redshift. These observations are consistent with the notion that red galaxies have been in place in the dense regions of the universe, and thus highly clustered, for a long time while the blue galaxies have only started falling into the clusters at late times.

We have measured the pairwise velocity dispersion σ_{12} for 3 samples of galaxies taken from our survey. Our estimates suggest, like those of Guzzo *et al.* (1995) and Marzke *et al.* (1995), that σ_{12} is approximately twice the canonical value measured by Davis and Peebles (1983), $\sigma_{12} = 340 \pm 40$ km s^{-1}. The estimates are, however, very sensitive to the removal or inclusion of the richest clusters of galaxies. By removing the superclusters, we can reduce σ_{12} by a factor of 2. The low value of σ_{12} measured by Davis and Peebles (1983) had been one of the most stringent constraints on models of structure formation. The models gain considerable room for maneuver if σ_{12} really is in the neighborhood of 600 km s^{-1}.

The large-scale structure in our survey is striking. For $z \lesssim 0.2$, where we have

sampled the galaxy distribution well, we see structures of $\sim 100h^{-1}$ Mpc. Large superclusters are bordered by vast underdense regions. The visual impression is confirmed by the power spectrum of our survey, which exhibits a highly significant peak at wavenumbers that correspond to $\sim 100h^{-1}$ Mpc scales. If there is indeed a preferred scale in the galaxy distribution, this will present a great challenge to hierarchical structure formation models, which are based on the assumption that the power spectrum is scale free.

TABLE 4.1

POWER-LAW FITS TO $w_p(r_p)$

sample	$z_{\rm med}$	$N_{\rm obj}$	r_0 (h^{-1} Mpc)	γ
$0 < z < 0.5$	0.11	1610	6.14 ± 0.01	1.65 ± 0.01
$0 < z < 0.5$, cluster galaxies removed	0.12	1327	4.77 ± 0.02	1.71 ± 0.01
$0.13 < z < 0.5$	0.23	628	4.61 ± 0.05	1.70 ± 1.70
$0.2 < z < 0.5$	0.29	399	4.26 ± 0.15	1.63 ± 0.10
	0.29	399	4.43 ± 0.08	1.7 (fixed)
$0.2 < z < 0.5$, red	0.26	122	5.33 ± 0.29	1.42 ± 0.17
	0.26	122	6.62 ± 0.14	1.7 (fixed)
$0.2 < z < 0.5$, blue	0.30	276	2.73 ± 0.29	1.40 ± 0.17
	0.30	276	3.78 ± 0.14	1.7 (fixed)
$0.2 < z < 0.3$	0.24	213	3.96 ± 0.18	1.50 ± 0.11
	0.24	213	2.91 ± 0.29	1.7 (fixed)
$0.3 < z < 0.5$	0.36	186	2.63 ± 0.46	1.51 ± 0.30
	0.36	186	3.13 ± 0.26	1.7 (fixed)

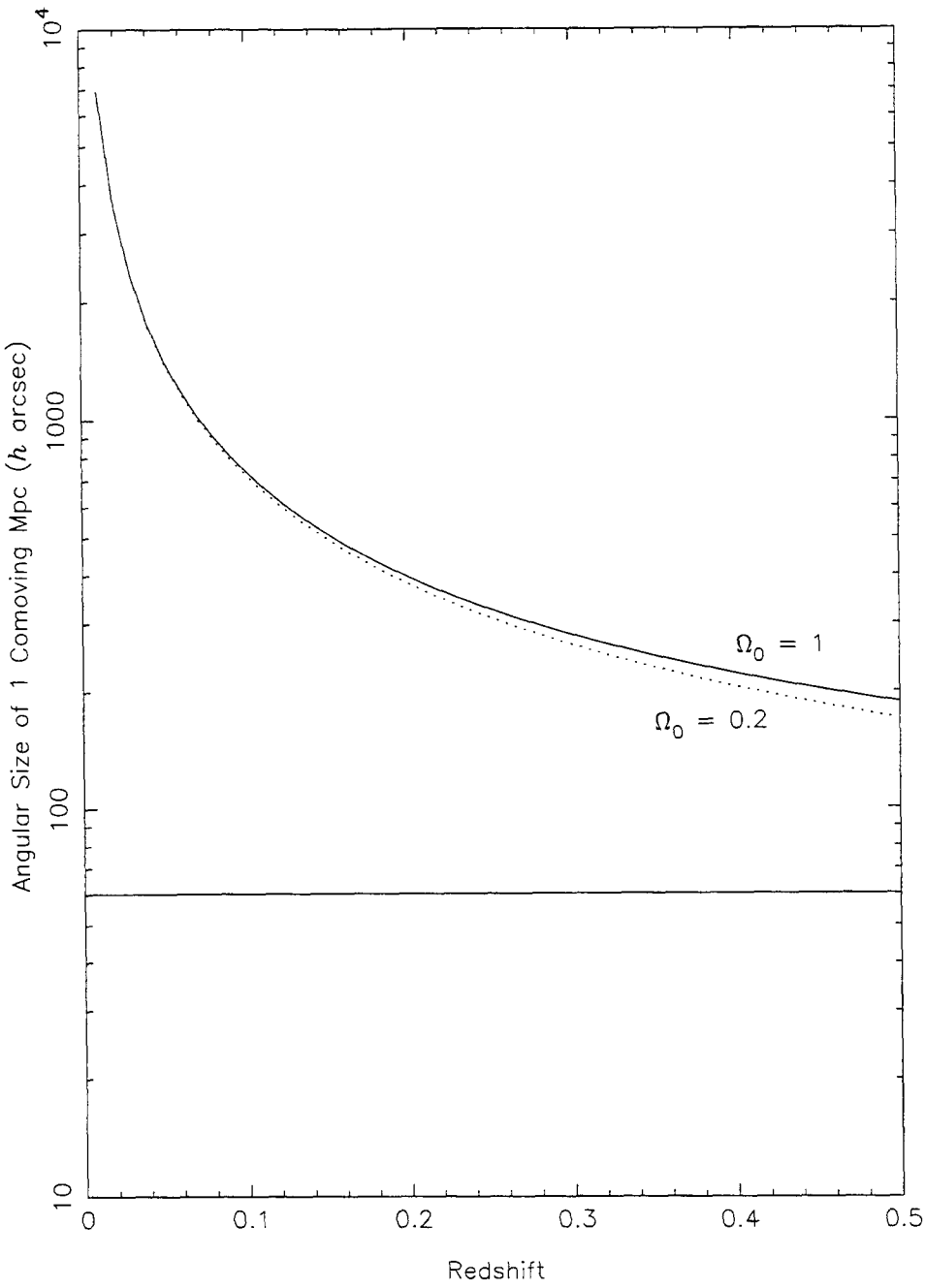

Fig. 4.1.— Angular size of 1 comoving Mpc as a function of redshift for $\Omega_0 = 1$ and $\Omega_0 = 0.2$. The fiber placement algorithm (AUTOFID2) introduces a strong bias against pairs with separations less than 60″. The horizontal line marks this scale. Since our estimates of $\xi(r)$ are limited to $r \gtrsim 0.5h^{-1}$ Mpc, the bias against small separation pairs does not have a significant effect on our analysis.

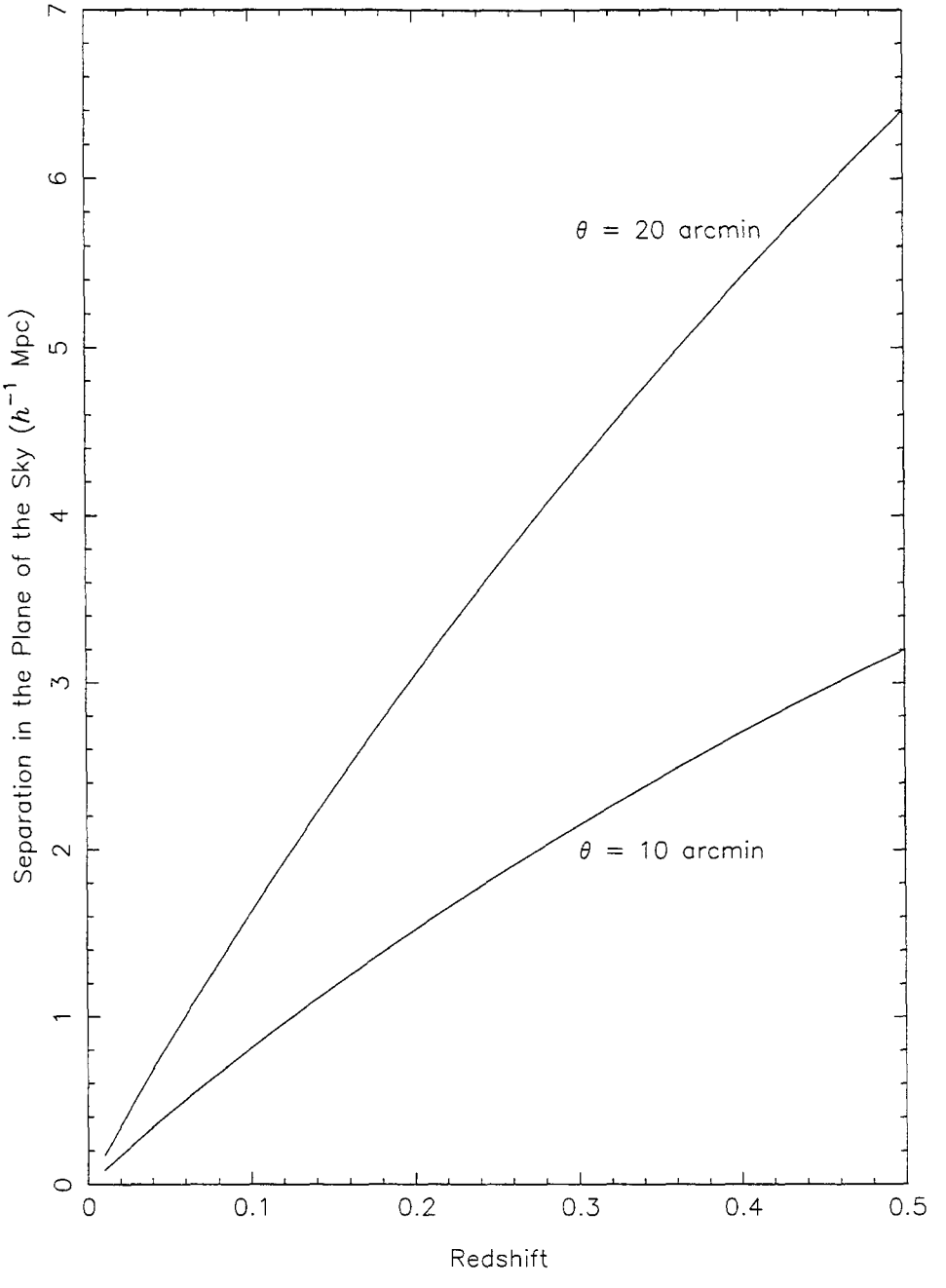

Fig. 4.2.— Comoving scales affected by the bias against large angular separation pairs as a function of redshift. There is a substantial bias against pairs of galaxies with angular separations between 10′ and 20′ due to the fiber assignment algorithm and to vignetting of the edge of the spectrograph field. The number of pairs with comoving separations on the plane of the sky that correspond to these angular scales is greatly reduced.

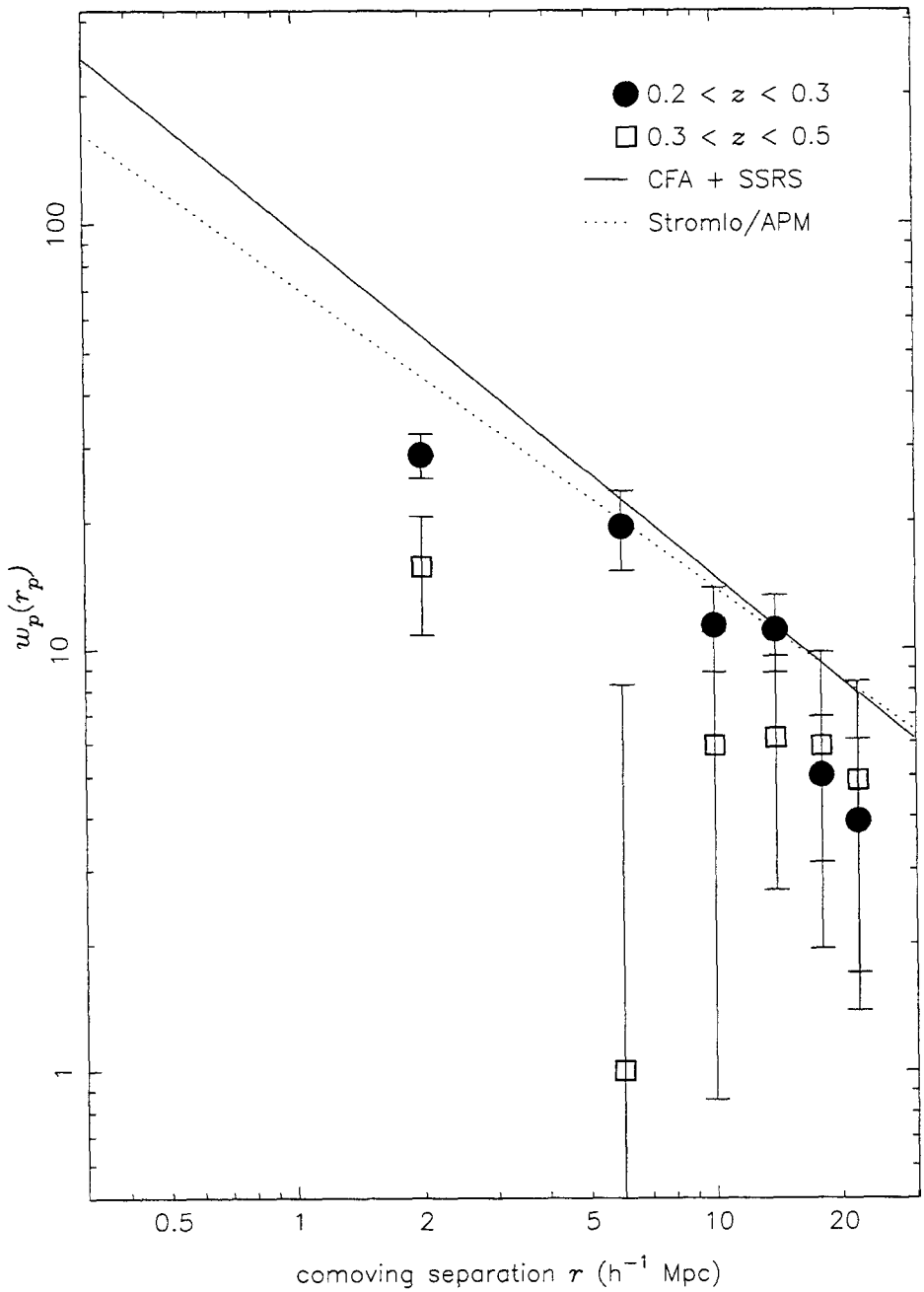

Fig. 4.3.— Projected correlation function $w_p(r_p)$ as a function of redshift. We plot $w_p(r_p)$ for the redshift intervals $0.2 < z < 0.3$ and $0.3 < z < 0.5$. We also plot fits to $w_p(r_p)$ measured in the CfA+SSRS (solid line) and Stromlo/APM (dotted line) local redshift surveys. It is evident that the clustering strength declines with redshift. The unfilled square at $r = 6h^{-1}$ Mpc which is unusually low is affected by the large angle bias discussed in §2.

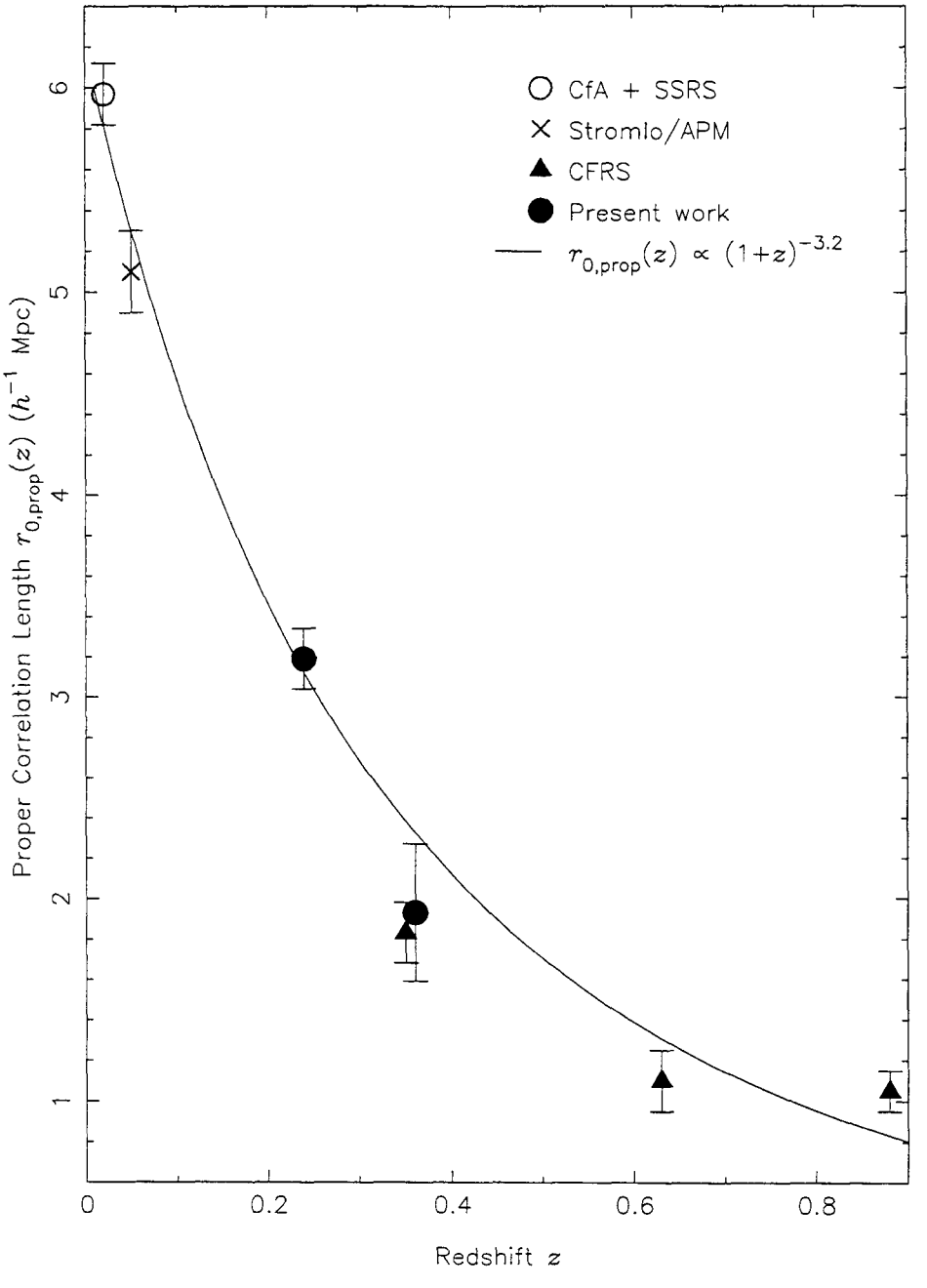

Fig. 4.4.— Evolution of the proper correlation length with redshift. The solid line shows the fit to $r_{0,\mathrm{prop}}(z) = r_{0,\mathrm{prop}}(0)(1+z)^{-(3+\epsilon)/\gamma}$ with $r_{0,\mathrm{prop}}(0) = 6.2h^{-1}$ Mpc, $\epsilon = 2.25$, and $\gamma = 1.65$.

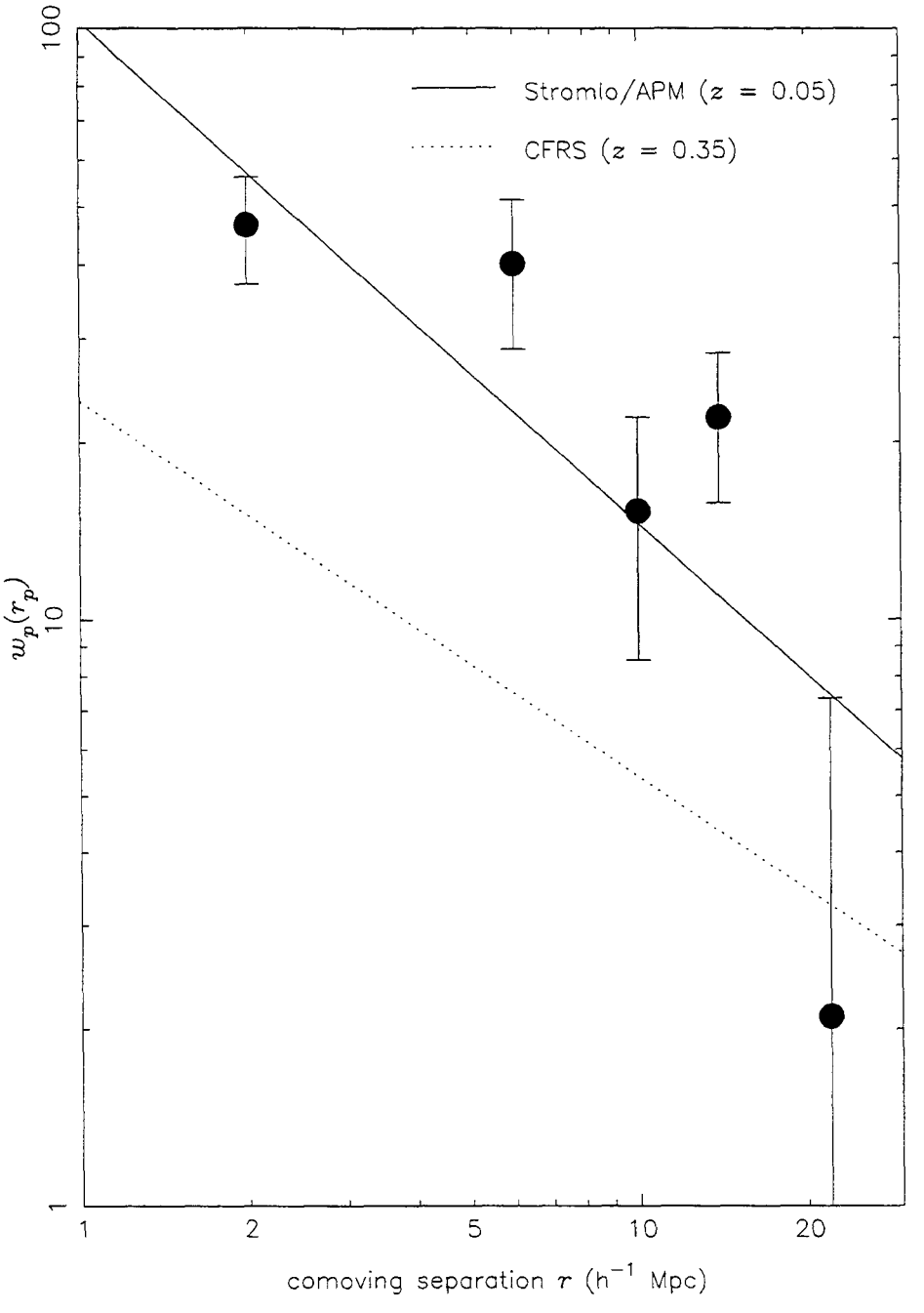

Fig. 4.5.— Projected correlation function $w_p(r_p)$ of absorption-line galaxies. The filled circles are $w_p(r_p)$ for absorption-line galaxies in our sample with $0.2 < z < 0.5$ ($z_{med} = 0.26$). The solid line shows the fit to $w_p(r_p)$ as measured by Loveday *et al.* (1995) for early-type galaxies with $z_{med} = 0.05$. The dotted line shows the fit to $w_p(r_p)$ as measured by Le Fèvre *et al.* (1995) for red galaxies with $0.2 < z < 0.5$. Our results suggest that the clustering strength of red galaxies has not changed markedly since $z \sim 0.3$, in disagreement with the conclusion of Le Fèvre *et al.* (1995).

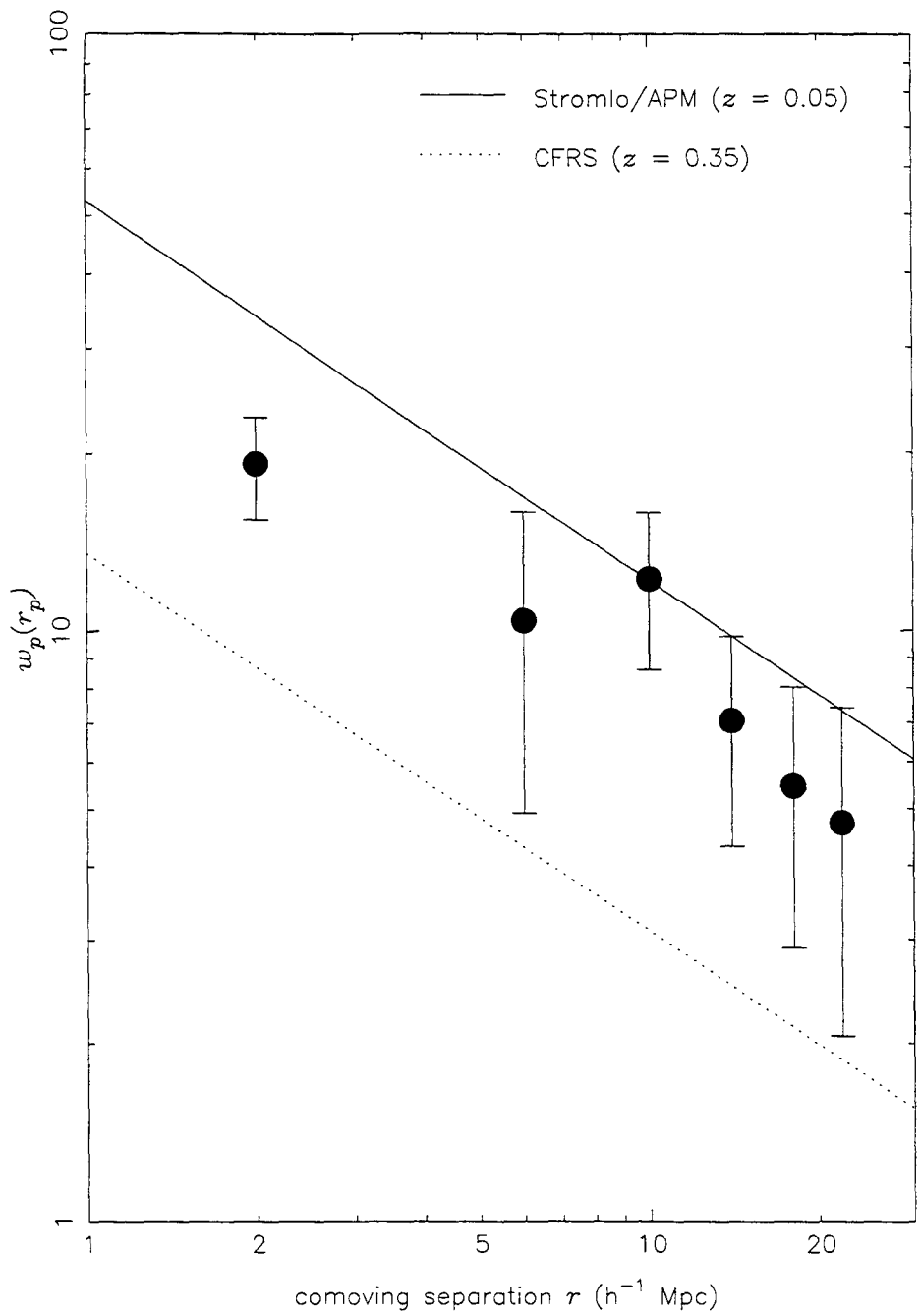

Fig. 4.6.— Projected correlation function $w_p(r_p)$ of emission-line galaxies. The filled circles are $w_p(r_p)$ for emission-line galaxies in our sample with $0.2 < z < 0.5$ ($z_{med} = 0.30$). The solid line shows the fit to $w_p(r_p)$ as measured by Loveday *et al.* (1995) for late-type galaxies with $z_{med} = 0.05$. The dotted line shows the fit to $w_p(r_p)$ as measured by Le Fèvre *et al.* (1995) for blue galaxies with $0.2 < z < 0.5$. We find that blue galaxies are significantly less clustered at $0.2 < z < 0.5$ than locally. However, we do not observe as dramatic a decline as that observed by Le Fèvre *et al.* (1995).

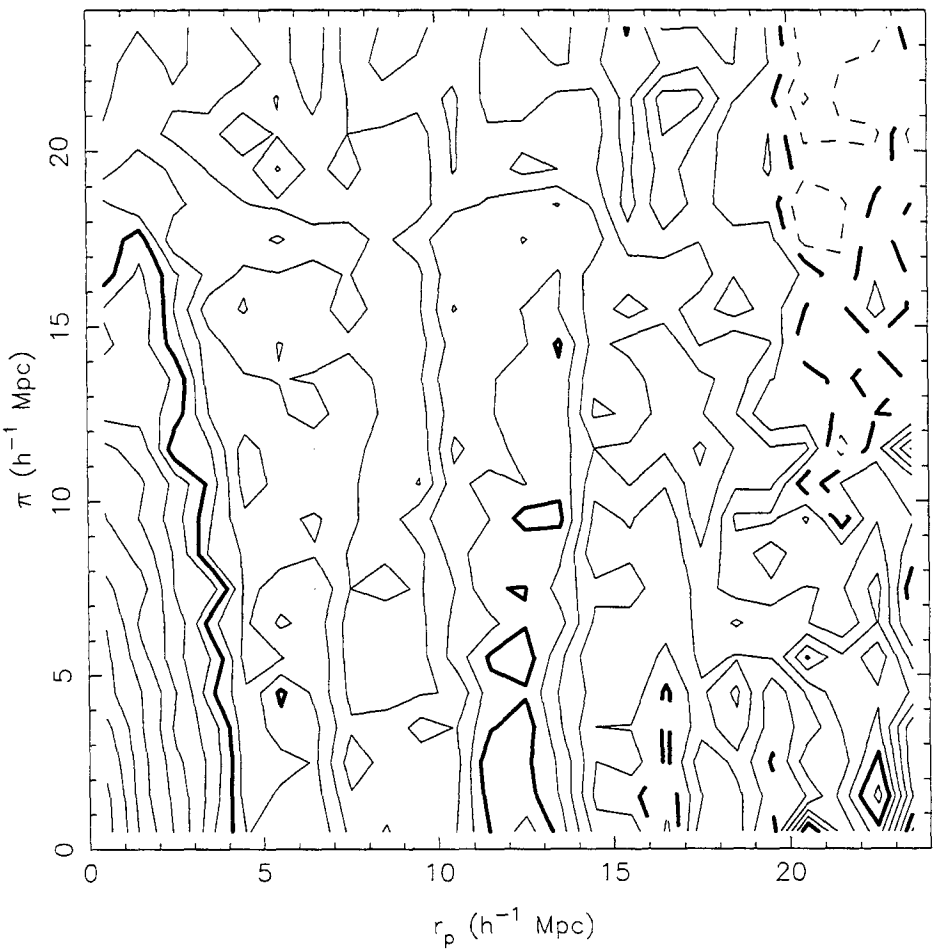

Fig. 4.7.— Contour plot of $\xi(r_p, \pi)$ for all galaxies with $0 < z < 0.5$. The contours are in steps of $\Delta\xi(r_p, \pi) = 0.2$ for $\xi(r_p, \pi) < 1$ and logarithmic (0.1 dex) for $\xi(r_p, \pi) > 1$. $\xi(r_p, \pi) = 1$ is marked by the heavy solid contour while $\xi(r_p, \pi) = 0$ is marked by the heavy dashed contour. The dashed contours represent $\xi(r_p, \pi) < 0$. The prominent elongation of the contours along the π axis for $r_p \lesssim 5h^{-1}$ Mpc is due to high velocity dispersion of virialized clusters of galaxies.

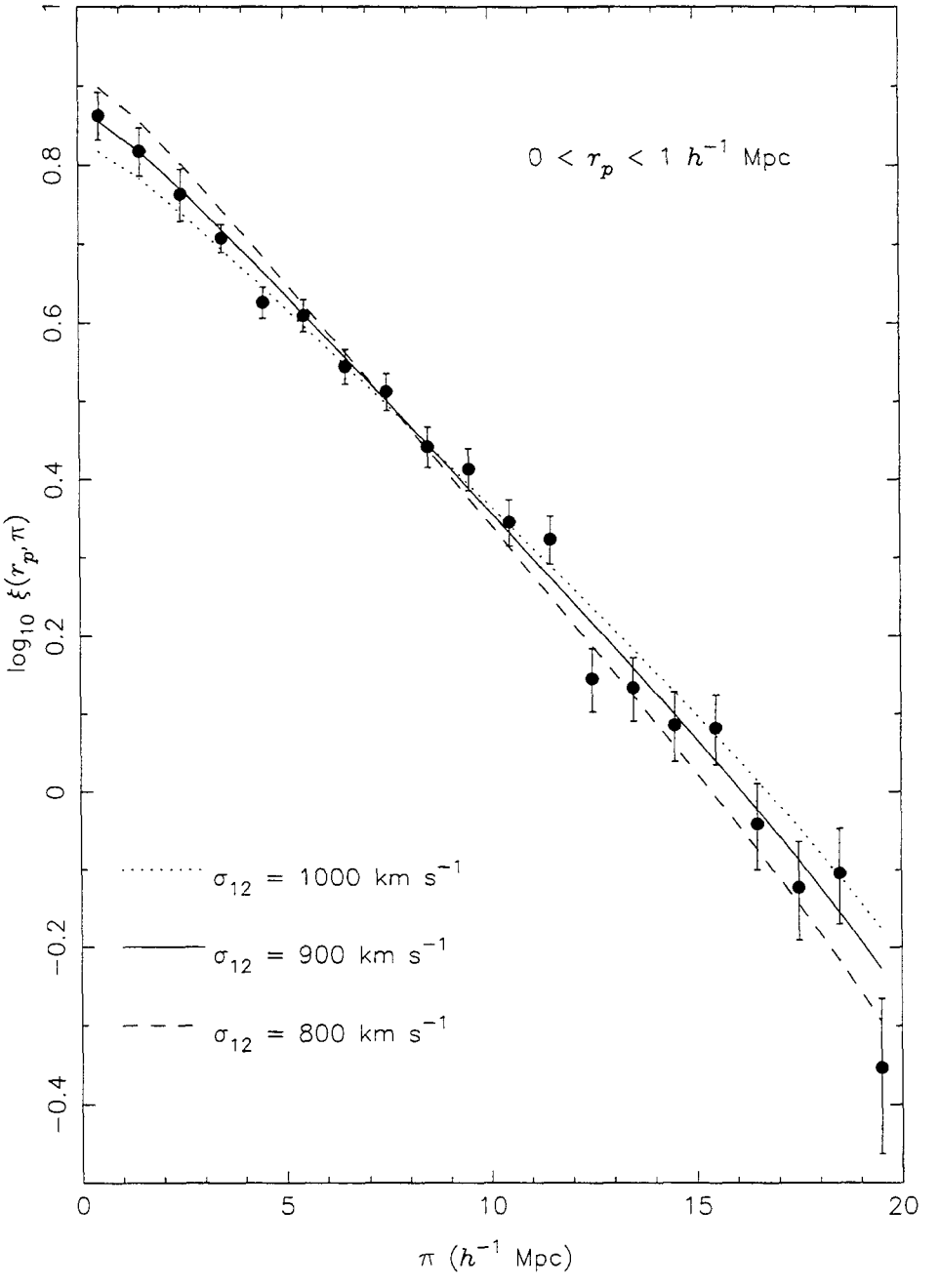

Fig. 4.8.— $\xi(r_p, \pi)$ as a function of π for $0 < r_p < 1h^{-1}$ Mpc for all galaxies with $0 < z < 0.5$. The data are well fit by Equation 4.9 with $\sigma_{12} = 900 \pm 100$ km s^{-1}.

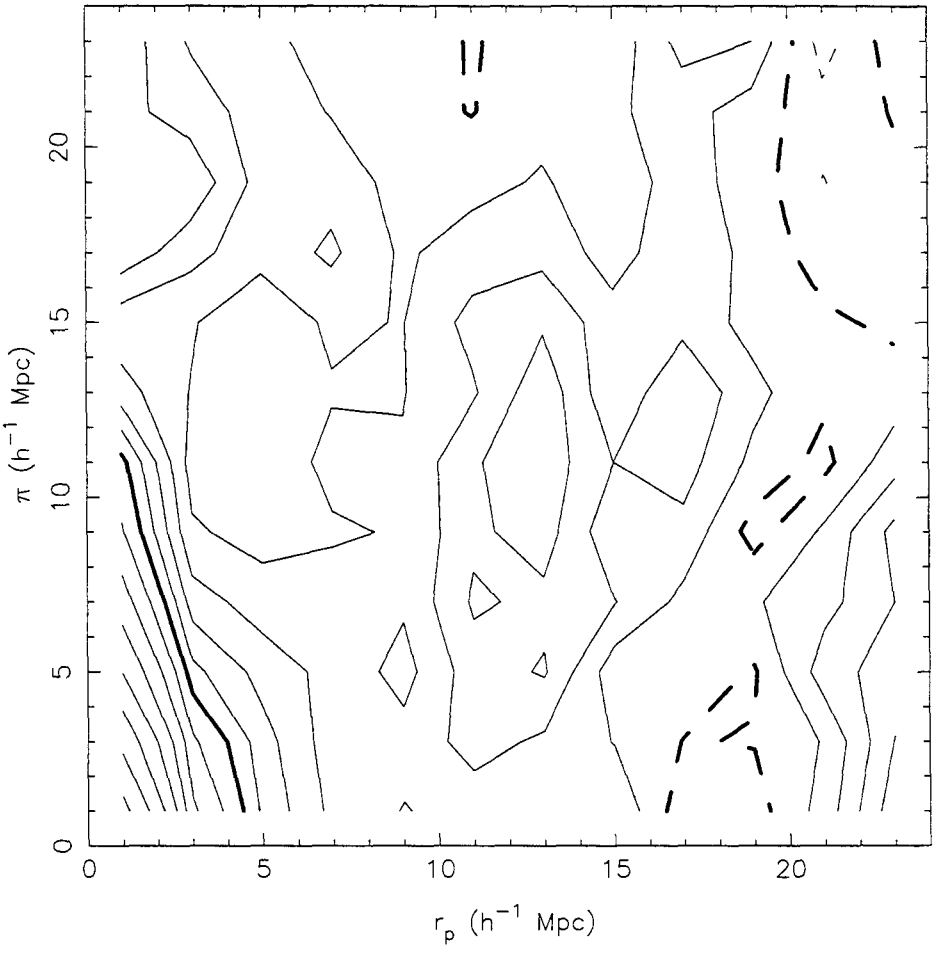

Fig. 4.9.— $\xi(r_p, \pi)$ for galaxies with $0 < z < 0.5$ and more than $5h^{-1}$ Mpc from the center of an Abell cluster. The contours are identical to those in Figure 4.7. The elongation of the contours along the π axis at small r_p is visible as well as the weak compression of the contours at $r_p \approx 5h^{-1}$ due to coherent galaxy motions generated by large scale structure.

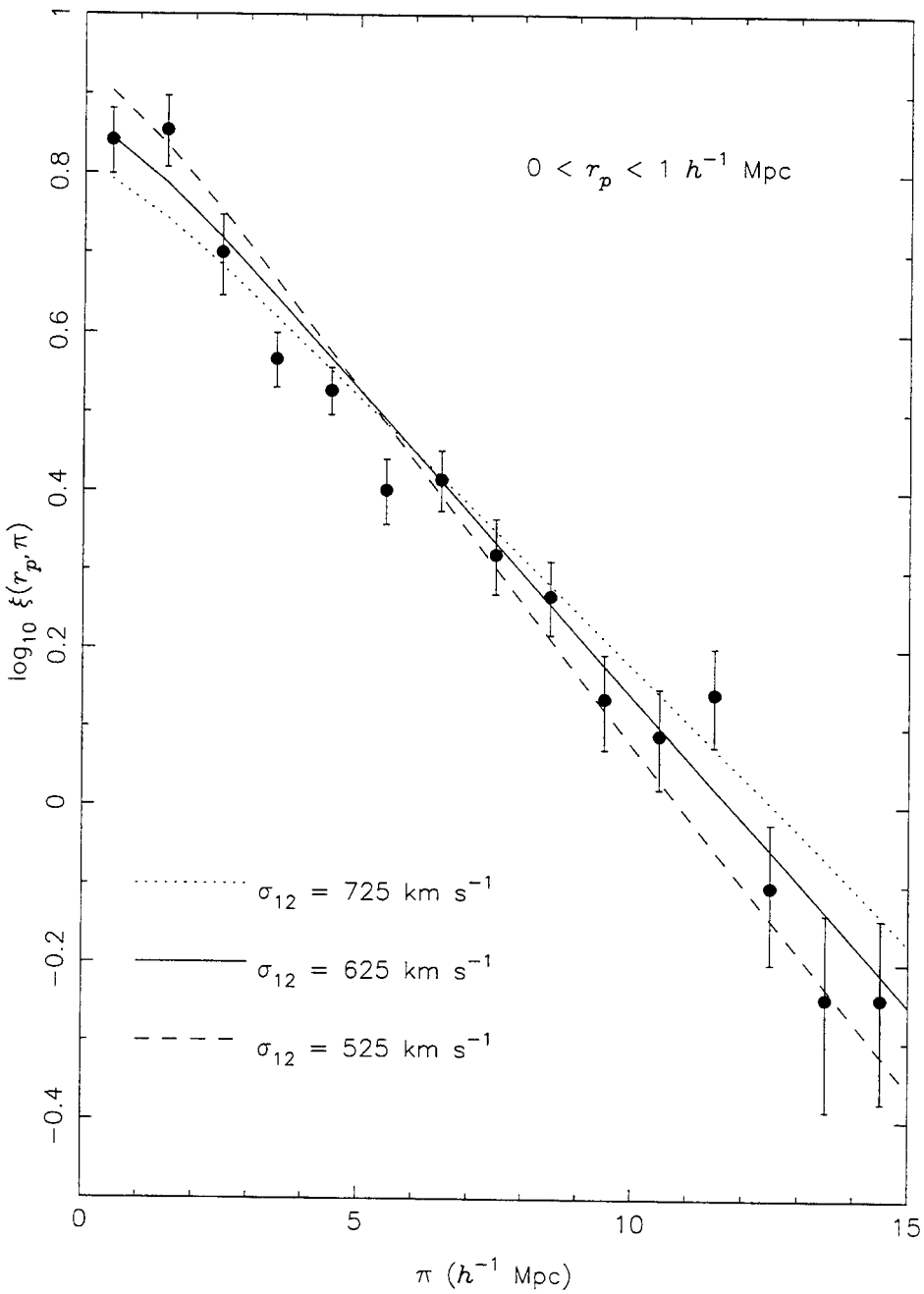

Fig. 4.10.— $\xi(r_p, \pi)$ as a function of π for $0 < r_p < 1h^{-1}$ Mpc for galaxies in the range $0 < z < 0.5$ and more than $5h^{-1}$ Mpc from the center of an Abell cluster. The data are well fit by Equation 4.9 with $\sigma_{12} = 625 \pm 100$ km s^{-1}.

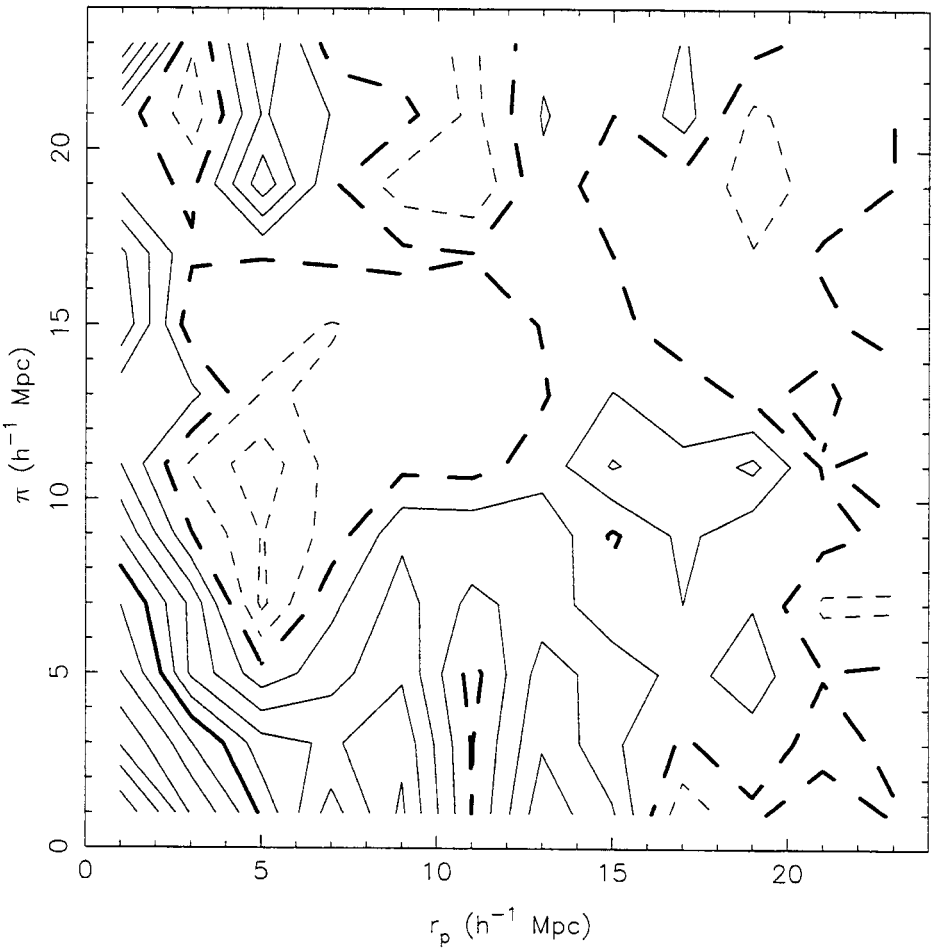

Fig. 4.11.— $\xi(r_p, \pi)$ for all galaxies with $0.13 < z < 0.5$. The contours are identical to those in Figure 4.7. The two superclusters are not included in this sample. The elongation of the contours along the π axis at small r_p is visible as well as the weak compression of the contours at $r_p \approx 5h^{-1}$ due to coherent galaxy motions generated by large scale structure.

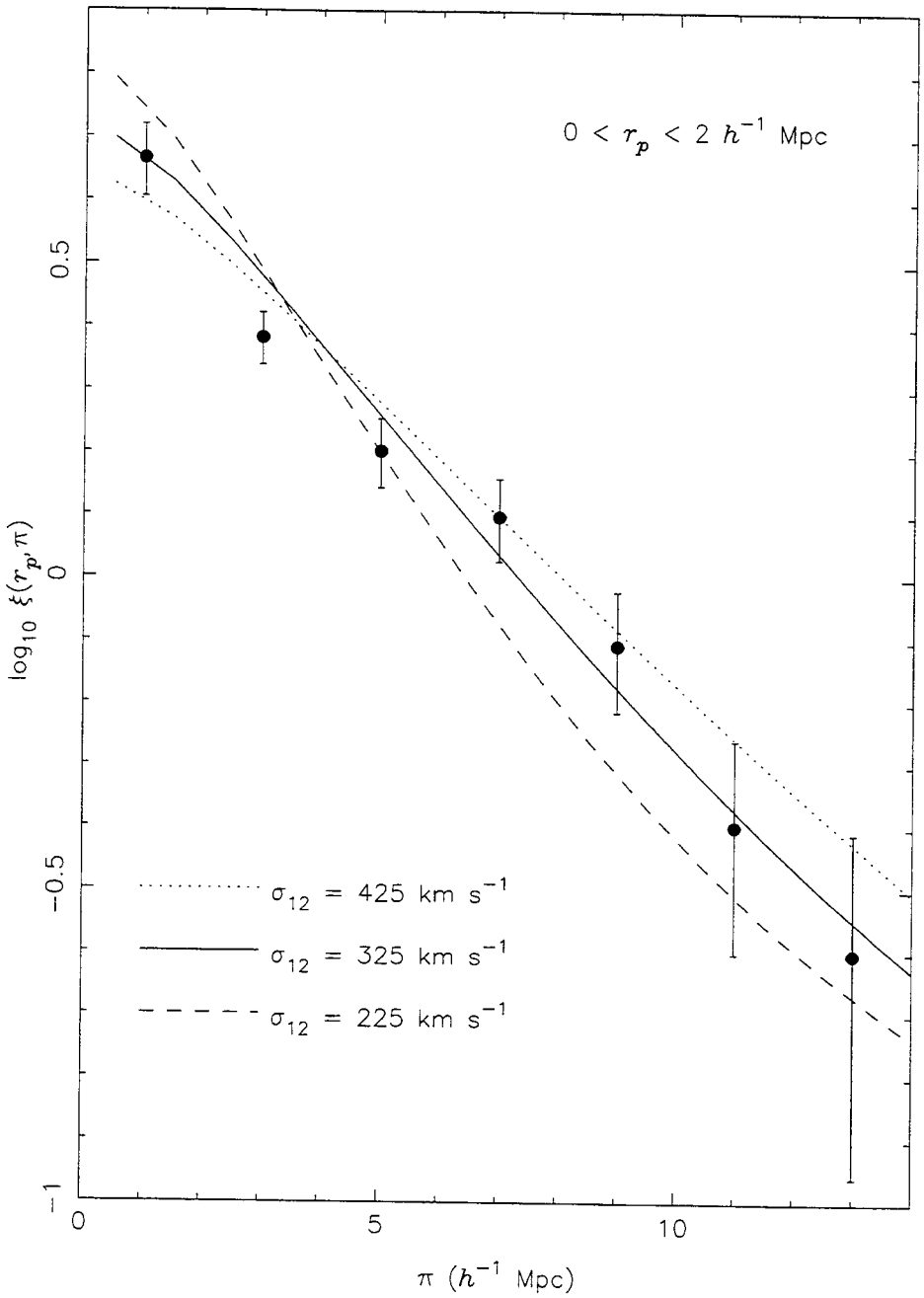

Fig. 4.12.— $\xi(r_p, \pi)$ as a function of π for $0 < r_p < 2h^{-1}$ Mpc for galaxies in the range $0.13 < z < 0.5$, thereby excluding the superclusters. The data are well fit by Equation 4.9 with $\sigma_{12} = 325 \pm 100$ km s^{-1}.

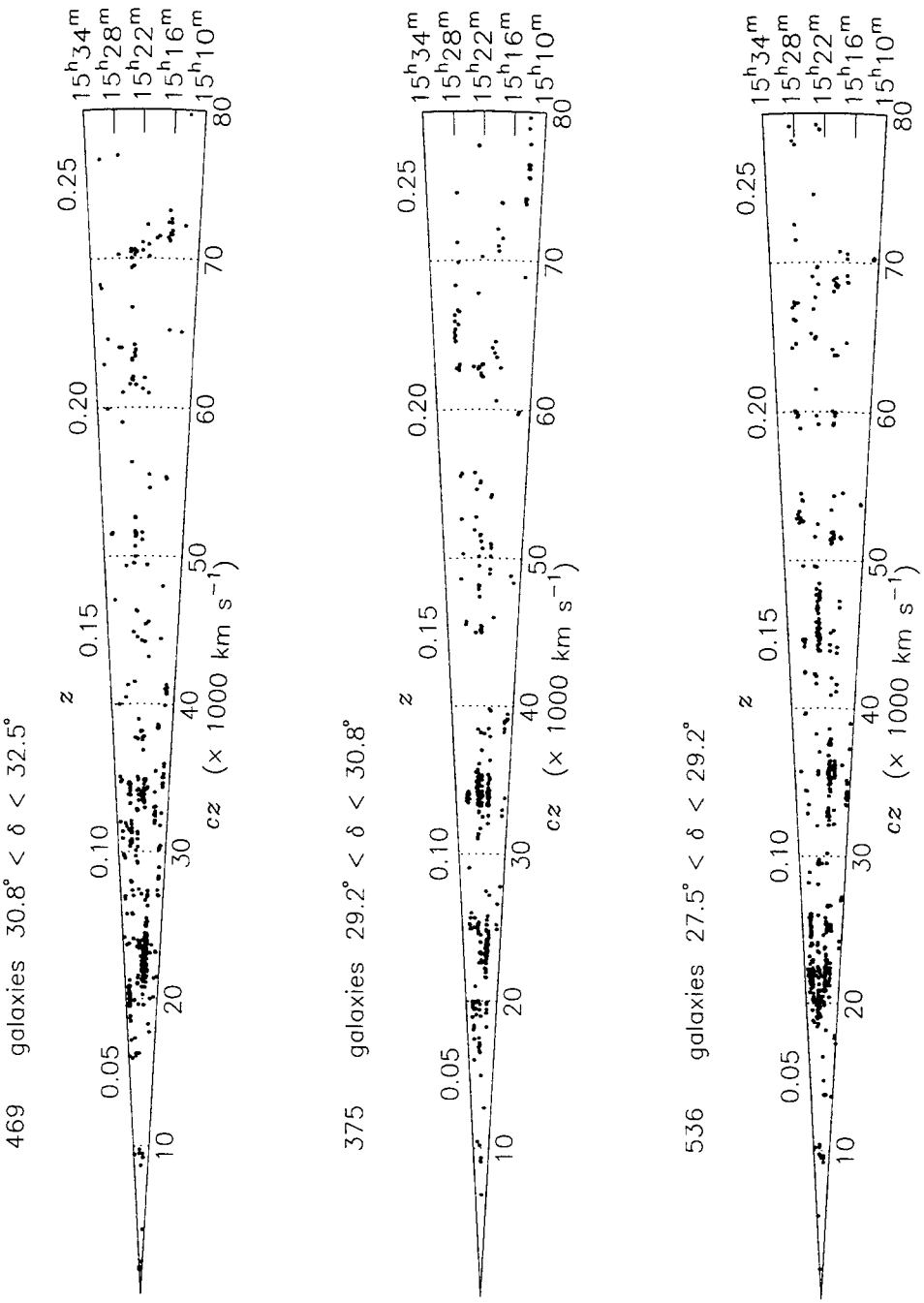

Fig. 4.13.— Redshift-right-ascension cone diagrams for galaxies in our survey with $cz < 80000$ km s^{-1}, divided into 3 declination slices. The Corona Borealis Supercluster is the prominent clump of galaxies at $z \approx 0.07$. The Abell 2069 Supercluster is at $z \approx 0.11$. The galaxies at $cz \approx 10000$ km s^{-1} are part of the "Great Wall" of galaxies identified by Geller and Huchra (1989).

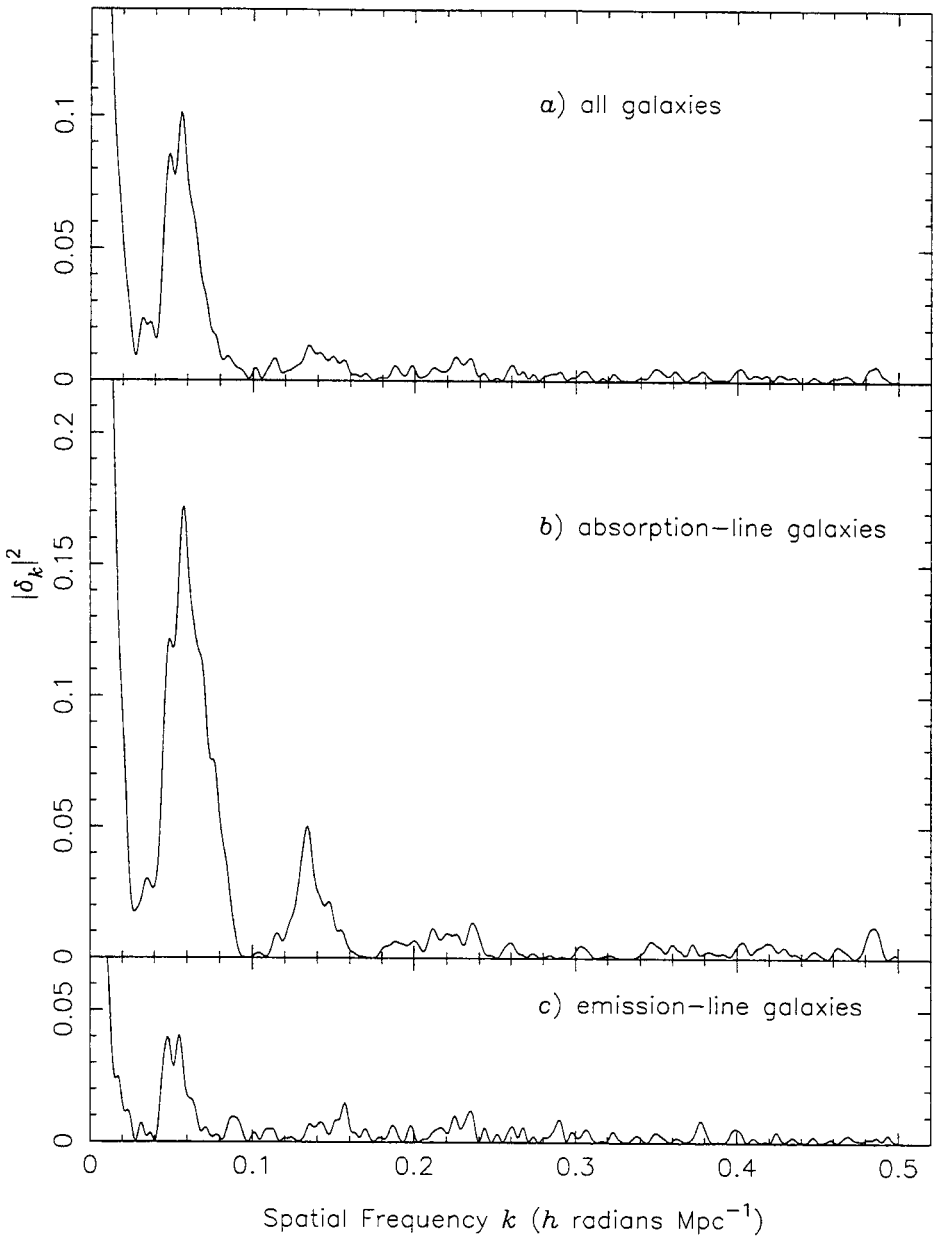

Fig. 4.14.— One-dimensional power spectra of (a) all the galaxies in our survey, (b) the absorption-line galaxies alone, and (c) the emission-line galaxies alone. The peaks in each panel at $k \approx 0.06h^{-1}$ radians Mpc^{-1} correspond to a spatial scale of $\sim 100h^{-1}$ Mpc. There is substantially more power in the absorption-line galaxies on this scale than in the emission-line galaxies.

Chapter 5 Galaxy Evolution to $z \sim 0.5$

5.1 Introduction

Only with recent introduction of efficient multi-object spectrographs on 4-m class telescopes has it become possible to construct large samples of faint galaxies with measured redshifts. With such a sample, one can compute the luminosity function of galaxies as a function of redshift and thereby directly observe the evolution (or lack thereof) of the galaxy population. Previously, however, clues that some sort of galaxy evolution must be occurring have been gleaned from both deep photometric surveys (*e.g.*, Peterson *et al.* 1979, Koo 1981, and, more recently, Tyson 1988 and Metcalfe *et al.* 1995) and from small surveys of faint galaxies (*e.g.*, Broadhurst, Ellis, and Shanks 1988, Cowie, Songaila, and Hu 1991, and Glazebrook *et al.* 1995a). The photometric surveys have found that the local galaxy luminosity function, normalized to the galaxy counts at the bright end ($B \sim 16^m$), underestimates the number of galaxies counted at magnitudes fainter than $B \gtrsim 21^m$. The early faint galaxy redshift surveys, while insufficient to compute the luminosity function at higher redshifts, do provide a constraint on galaxy evolution through the redshift distribution observed at faint magnitudes. These redshift surveys have shown that while the range of redshifts observed at faint magnitudes is consistent with the range expected from assuming that galaxies have not evolved, the number of galaxies at intermediate redshifts ($z \sim 0.5$) is underestimated.

The evidence for evolution is, of course, dependent upon having the correct model for the local luminosity function. While redshift surveys of local galaxies (Loveday *et al.* 1992, Marzke, Huchra, and Geller 1994) have precisely estimated the characteristic magnitude M^* of the luminosity function, there remains considerable uncertainty about both the normalization and the slope at low luminosities. The normalization could conceivably be biased by the properties of the local galaxy distribution or by

photometric errors in calibrating the measured intensities on the photographic plates used for the large-angle, local surveys. Increasing the normalization by a factor of 2 would significantly reduce the evolution required for galaxies brighter than $B \sim 22^m$. A steeper faint-end slope would also reduce the required evolution. The photographic surveys on which the local galaxy luminosity function is based all have quite bright surface brightness limits ($B \lesssim 25^m$ arcsec^{-2}) and low luminosity, low surface brightness objects could be missed entirely.

In this paper, we investigate the evolution of the galaxian luminosity function from $z = 0$ to $z = 0.5$ based on data obtained during the course of our redshift survey of the Corona Borealis supercluster. The primary motivation for the survey was to study the dynamics of the supercluster. However, the majority of galaxies for which we measured redshifts actually lie behind the Corona Borealis supercluster, thus providing a sample suitable for study of the evolution of the luminosity function. The galaxies were originally selected from plates taken as part of the Second Palomar Observatory Sky Survey (POSS-II; Reid *et al.* 1991) and have therefore been calibrated in the Gunn g and r bands, which correspond to the photographic J and F bands. Previous redshift surveys have been either selected in bluer bands (B), for sensitivity to changes in star-formation rates, or redder bands (I and K), for sensitivity to old stellar populations which more reliably trace mass. Although we had no option but to use the g and r bands, the two bands have the virtue that corrections to the rest B-band, where luminosity functions are traditionally computed, are small since the g band matches the rest B-band at $z \approx 0.2$ and the r band matches the rest B-band at $z \approx 0.5$.

The paper, the fourth in the series presenting results from the Norris Survey of the Corona Borealis Supercluster, is organized as follows. In §2, we summarize our survey, particularly emphasizing those features that are directly relevant to the computation of the luminosity function. We discuss the details of the computation of the luminosity function in §3. The results are given in §4 for both field galaxies and for the two superclusters individually and are discussed in §5. Finally, we draw conclusions in §6.

We use a Hubble constant $H_0 = 100h$ km s^{-1} Mpc^{-3} and a deceleration parameter $q_0 = 0.5$.

5.2 The Norris Survey of the Corona Borealis Supercluster

The Norris Survey of the Corona Borealis Supercluser has been described in detail in Small *et al.* (1996), Paper I of the current series, and will be only briefly reviewed here. The core of the supercluster covers a $6° \times 6°$ region of the sky centered at right ascension 15^h20^m, declination $+30°$ and consists of 7 rich Abell clusters at $z \approx 0.07$. Since the field-of-view of the 176-fiber Norris Spectrograph is only 400 arcmin^2, we planned to observe 36 fields arranged in a rectangular grid with a grid spacing of 1°. As it turned out, we successfully observed 23 of the fields and 9 additional fields along the ridge of galaxies between Abell 2061 and Abell 2067, yielding redshifts for 1491 extragalactic objects. We have extended our survey with 163 redshifts from the literature, resulting in 1654 redshifts in the entire survey. 1022 of these galaxies lie beyond the Corona Borealis Supercluster, although of these 1022, 298 galaxies are in a background supercluster ($z \approx 0.11$) which we have dubbed the "Abell 2069 Supercluster."

Since the Norris Spectrograph has a high density of fibers (1 fiber for every 2.3 arcmin^2), we covered a broad range in apparent magnitude: $13.0^m \lesssim r \lesssim 21.6^m$. With this broad range, we are able to compute the local luminosity function down to $M(B) \sim -15^m + 5\log_{10} h$ and the luminosity function for $0.2 < z \leq 0.5$ to $M(B) \sim -18.5^m + 5\log_{10} h$. As our original motivation for the survey was to study the dynamics of the Corona Borealis supercluster, we chose a comparatively high spectral resolution for a faint galaxy redshift survey. A third of the objects were observed with ~ 8Å spectral resolution when the largest CCD available at Palomar was a 1024^2 device with 24μm pixels, and the rest were observed with ~ 4Å resolution with a very efficient 2048^2 CCD (also with 24μm pixels). The high quality spectra

in our survey will enable us to correlate the spectral properties of individual galaxies with evolution of the luminosity function of the population of galaxies.

As noted above and described in detail in Paper I, the objects have been selected from POSS-II photographic plates of POSS-II field 449, which neatly covers the entire core of the supercluster. We have both a J (Kodak III-aJ emulsion with a GG395 filter) and an F (Kodak III-aF emulsion with a RG610 filter) plate. The plates were digitized with 1 arcsec^2 pixels at the Space Telescope Science Institute and then processed using the Sky Image Cataloging and Analysis Tool (SKICAT, Weir 1995). The instrumental intensities recorded by SKICAT were calibrated with CCD sequences in g, r, and i of galaxies in Abell 2069. The random magnitude errors are $g \sim 0.3^m$ and $r \sim 0.2^m$ for $g < 20.5^m$ and $r < 19.6^m$ and become substantially worse at fainter magnitudes.

The survey is only complete in magnitude to $r = 18.5^m$. However, we have substantial numbers of galaxies out to $r = 22.0^m$. In order to use these galaxies in our analysis, we define small samples of the data that are complete to fainter limits. By repeatedly constructing and then averaging over the samples, we can compute accurate estimates of the luminosity functions as long as we do not suffer from redshift or galaxy type selection biases. Since we limit the computation of the luminosity function to $z < 0.5$, we are unlikely to be affected by a bias in redshift. The 4000Å break and Ca H, Ca K lines of old stellar populations and the [O II] line of star-forming galaxies are within our spectral range to $z = 0.5$. The color distribution of the objects that we observed but failed to identify is similar to the color distribution of the objects that we successfully observed, which leads us to conclude that we do not suffer any biases against certain types of galaxies.

In Paper I, we carefully studied the surface brightness selection effects present in our sample. We found that by restricting our sample to objects with core magnitudes $r_{\rm core} \leq 21.7^m$, where the core magnitude is the integrated magnitude within the central 9 arcsec^2, we are free from surface brightness selection effects. For comparison, $r_{\rm core} = 21.7^m$ corresponds to a central surface brightness of $\mu \leq 24.1$ r mag arcsec^{-2} for a galaxy with an L^* ($\approx -20.2 + 5 \log_{10} h$ mag in the r band) disk.

5.3 Calculation of the Luminosity Function

5.3.1 k-Corrections

Galaxy luminosity functions are generally compared in the rest-frame B band. Since our photometric data were obtained in the observed g and r bands, we need to convert, using k-corrections and rest-frame colors, to the rest-frame B band. This task is greatly eased by the fact that the observed g and r bands match the rest-frame B band at $z \sim 0.2$ and $z \sim 0.5$, respectively. We identify each galaxy in the survey with one of the four spectral energy distributions (corresponding to the Hubble types E, Sbc, Scd, and Im) from Coleman, Wu, and Weedman (1980) on the basis of the galaxy's observed $g - r$ color and redshift. Once a galaxy is associated with a particular Hubble type, we can then compute the k-correction and assign the galaxy rest-frame $B - g$ and $B - r$ colors from the Coleman, Wu, and Weedman (1980) spectral energy distributions. We compute the absolute rest-frame B-band magnitude as follows:

$$\begin{aligned} M(B)_{\rm rest} &= M(r)_{\rm rest} + (B-r)_{\rm rest} \\ &= r_{\rm obs} - 5\log_{10} D_L(z) - 25. - k_r(z) + (B-r)_{\rm rest} \\ &= r_{\rm obs} - 5\log_{10} D_L(z) - 25. + 2.5\log_{10}(1+z) - k_{eff}, \end{aligned} \tag{5.1}$$

where k_{eff} incorporates the corrections based on the spectral energy distribution and D_L is the luminosity distance in Mpc. The $2.5\log_{10}(1+z)$ term represents the change in the bandwidth with redshift and is included in the traditional k-correction. Following Lilly *et al.* (1995), we have separated the bandwidth stretching term, which has negligible error since it depends only on the accurately measured redshift, from the terms which depend on the spectral energy distribution and are therefore much more uncertain. We plot k_{eff} for the g and r bands in Figure 5.1. By converting from $g_{\rm obs}$ for objects with $z \lesssim 0.3$ and from $r_{\rm obs}$ for objects with $z \gtrsim 0.3$, k_{eff} may be kept less than 1^m for $z < 0.7$ for all spectral types.

5.3.2 Method

We have used the step-wise maximum-likelihood (SWML) method of Efstathiou, Ellis, and Peterson (1988) to estimate the luminosity function. The probability of observing a galaxy of absolute magnitude M_i at redshift z_i in a flux-limited catalog is given by,

$$p_i \propto \frac{\phi(M_i)}{\int_{-\infty}^{M_{max}(z_i)} \phi(M) dM}, \tag{5.2}$$

where ϕ is the luminosity function and $M_{max}(z_i)$ is the instrinsically faintest galaxy observable at z_i in the flux-limited catalog. The luminosity function is parameterized as a set of numbers ϕ_k, and then the likelihood,

$$\mathcal{L} = \prod_{i=1}^{N} p_i, \tag{5.3}$$

where N is the number of galaxies in the sample, is maximized with respect to the ϕ_k. The virtue of the SWML method is that it is not biased by the presence of clustering since the normalization of the luminosity function cancels out of the expression for the probability p_i. One must then estimate the mean galaxy density separately. We use a standard technique, which we describe below. We did not use the traditional $1/V_{max}$ method (Schmidt 1968) employed by Ellis *et al.* (1995) and Lilly *et al.* (1995) since the method is sensitive to clustering. We have, however, compared the results of the two techniques for samples with $z > 0.2$, where the clustering in our survey is not pronounced, and found that they agree satisfactorily. For $z < 0.2$, we can construct volume-limited sub-samples with $r \leq 20.5$ in which any galaxy with $M(B) \leq -18.5^m + 5\log_{10} h$ is visible in the entire volume. Of course, the value of the luminosity function in a given magnitude bin for a volume-limited sample is estimated by counting the number galaxies with absolute magnitudes in the bin and then dividing by the volume of the sample and the width of the bin. The SWML luminosity functions for $z < 0.2$ agree well with the luminosity functions estimated from the volume-limited samples.

We compute the mean density $\bar{n}$ of a magnitude-limited sub-sample using the

following estimator:

$$\bar{n} = \frac{1}{V}\sum_{i=1}^{N}\frac{1}{s(z_i)}, \tag{5.4}$$

where V is the volume of the sample, N is the number of objects in the sample, and s is the selection function. The selection function,

$$s(z_i) = \frac{\int_{-\infty}^{M_{lim}(z)}\phi(M)dM}{\int_{-\infty}^{M_{max}}\phi(M)dM}, \tag{5.5}$$

gives the fraction of the luminosity function visible at a given redshift. Here, ϕ is the luminosity function, $M_{lim}(z)$ is the maximum absolute magnitude that an object can have at redshift z and still be included in the sample, and M_{max} is the absolute magnitude of the most instrinsically faint galaxy in the sample. In practice, one does not begin evaluating the integrals at $-\infty$, but rather at the absolute magnitude of the most instrinsically bright galaxy in the sample. The estimator in Equation 5.5 is almost identical to the minimum variance estimator derived by Davis and Huchra (1982) for $s \gtrsim 0.1$ and is unbiased by density inhomogeneities.

We have adjusted the widths of the absolute magnitude bins in order to ensure that there are equal numbers of objects per bin. We never use fewer than 10 objects per bin. An additional complication of computing a luminosity function in the B band where the objects have been selected in the r band is that one must ensure that any object, regardless of its color, is detectable in both bands. If one ignores this complication, then the faintest objects at a given redshift will be biased in color. In our survey, since the r band is centered at a longer wavelength than the B-band, the faintest objects would be biased to the red. In order to avoid such a bias, we adjust our absolute B magnitude limits as a function of redshift so that the bluest galaxy at any B magnitude limit would be observable in the r band.

If there are a sufficient number of points, we have fit a Schechter (1976) function,

$$\phi(M)dM = \phi^* e^{-e^{.92(M^*-M)}+.92(M^*-M)\alpha}, \tag{5.6}$$

where ϕ^* is the normalization, M^* determines the location of the bright-end exponen-

tial cutoff, and α is the faint-end slope, using a standard χ^2 minimization algorithm with the Schechter function integrated over the width of the magnitude bin. We intend these fits to be useful for comparisons with other work. Usually, there are too few points for the fits to be well defined.

5.3.3 Sub-Samples

Since the SWML method can only be applied to a magnitude-limited sample, we must generate magnitude-limited sub-samples from our survey. This is a straightforward task since we have the galaxy counts in the field from our two POSS-II plates (see Figure 5 of Paper I). Once a magnitude limit is chosen, we compute the effective area on the sky of the sub-sample by dividing the galaxy counts per square degree at the magnitude limit by the number of objects with measured redshifts at the magnitude limit. We then randomly reject objects in the brighter magnitude bins until the magnitude distribution of the objects in the sub-sample has the same shape as the galaxy counts. In order to estimate the luminosity function, we average together the results of 100 sub-samples and use the standard deviation of the 100 sub-samples as the standard deviation of the estimated luminosity function.

5.4 Results

In the following subsections, we report our results for the local luminosity function, the evolution of the luminosity function, and the luminosity functions of the Corona Borealis and Abell 2069 superclusters. The parameters of the best fitting Schechter functions are summarized in Table 5.1. We wish to emphasize that the fitted Schechter functions are intended only to guide the eye and that comparisons of the various luminosity functions in this paper are best done by comparing the individual data points.

5.4.1 The Local Luminosity Function

The local galaxy luminosity function is plotted in Figure 5.2. The unfilled circles show the luminosity function for $r \leq 18.5^m$, $z \leq 0.2$, with the superclusters removed. The filled circles show the luminosity function for $z \leq 0.2$, with the superclusters included. The points brighter than $\lesssim -18^m + 5\log_{10} h$ come from a sample with $r \leq 18.5^m$, and the fainter points come from a sample with $r \leq 20.5^m$. In order to remove the superclusters, we simply delete all objects with $0.06 \leq z \leq 0.13$. The solid curve shows the luminosity function computed by Loveday *et al.* (1992) for 1658 galaxies with $0.002 \leq z \leq 0.13$ and $15^m < b_J < 17.15^m$ selected from the APM Galaxy Survey (Maddox *et al.* 1990a). The median redshift of the Loveday *et al.* (1992) survey is $z = 0.051$. Both of our local luminosity functions have shapes similar to that of Loveday *et al.* (1992), but they have significantly higher normalizations. If we conservatively compare the Loveday *et al.* (1992) to our luminosity function with the superclusters removed, then we find that the normalization of the local luminosity function must be increased by a factor of 2. We do verify, however, that the slope at the low luminosity end is flat, at least for galaxies which do not have unusually low surface brightnesses which would not be detectable on photographic plates.

5.4.2 The Luminosity Function to $z = 0.5$

We have computed the field galaxy luminosity function in two redshift intervals: $0 < z < 0.2$ and $0.2 < z < 0.5$. The results are plotted in Figure 5.3. The luminosity functions for the low redshift interval are identical to those shown in Figure 5.2. The unfilled squares are the luminosity function of the high redshift interval. Since we chose to observe the Corona Borealis field because it contains one of the most prominent examples of galaxy clustering in the northern sky, it is not fair to include the Corona Borealis supercluster and the Abell 2069 supercluster (which is also responsible for the great projected overdensity) in the local field luminosity function. On the other hand, it is also unreasonable to completely remove the two superclusters since we may be observing superclusters in the higher redshift sample and we

have not removed them. The true local luminosity function should be bracketed by the luminosity function with the superclusters removed and the luminosity function with the superclusters included. Assuming that the normalization of the true local luminosity function is indeed lower than the normalization of the luminosity function with the superclusters included, then we do see evidence for evolution in the luminosity function, which in this case appears to be an increase in the comoving number density.

5.4.3 The Luminosity Function to $z = 0.5$ Divided by Color

We have divided our sample of galaxies into those which are redder than the Coleman, Wu, and Weedman (1980) Sbc galaxy (rest-frame $g - r = 0.24^m$) and those which are as blue or bluer than the Coleman, Wu, and Weedman (1980) Sbc galaxy. The luminosity functions of the red galaxies are shown in Figure 5.4, and the luminosity functions of the blue galaxies are shown in Figure 5.5.

There is no sign of evolution of the red galaxies. The $0.2 < z \leq 0.5$ luminosity function (the two unfilled squares) match within the errors both the local luminosity function with the superclusters removed and the local luminosity function with the superclusters included. This is in accord with results of Lilly *et al.* (1995), who divided galaxies into red and blue classes just as we have, and with those of Ellis *et al.* (1995), who divided galaxies into [O II]-strong and [O II]-weak classes. The lack of evolution is not surprising given that the light of red galaxies is dominated by long-lived stellar populations.

In contrast to the red galaxies, the luminosity function of blue galaxies shows striking evidence for evolution. The high redshift points are consistently above the low redshift points, with the difference becoming larger at fainter intrinsic magnitudes. The luminosity function at $0.2 < z \leq 0.5$ appears to have a higher normalization than the local luminosity function and to have a steeper faint-end slope. Since blue galaxies do not cluster as strongly as red galaxies, the differences between the local luminosity functions with and without the superclusters removed are minor, thus

making conclusions about evolution more robust. Again, these results agree with those recently presented by Lilly *et al.* (1995) and Ellis *et al.* (1995).

5.4.4 The Supercluster Luminosity Functions

The luminosity functions of the Corona Borealis supercluster and the Abell 2069 supercluster are given in Figure 5.6. We take the redshift range of the Corona Borealis supercluster to be $0.06 \leq z \leq 0.09$ and that of the Abell 2069 supercluster to be $0.10 \leq z \leq 0.13$. The faintest four points of the Corona Borealis luminosity function come from a sample with $r \leq 20.0^m$, whereas the brighter points come from a sample with $r \leq 18.5^m$. Similarly, the faintest two points of the Abell 2069 supercluster luminosity function come from a sample with $r \leq 20.0^m$, whereas the brighter points come from a sample with $r \leq 18.5^m$. We also plot the Loveday *et al.* (1992) luminosity function for comparison. The normalization of the Corona Borealis supercluster function is a factor of 2 greater than that of the Abell 2069 supercluster. The shapes of the luminosity functions of the two superclusters are similar. The Schechter function fits to the two supercluster luminosity functions both suggest that the supercluster luminosity functions rise more steeply ($\alpha \sim$ -1.3 to -1.5) to faint absolute magnitudes than the local field galaxy luminosity function ($\alpha \sim$ -0.7 to -1.0). In addition, M^*, the characteristic luminosity of the Schechter function, is nearly a magnitude brighter in the superclusters than in the local field.

5.5 Discussion

5.5.1 The Local Luminosity Function

Evidence for rapid evolution of the galaxy luminosity function to $z \sim 0.1$ from galaxy counts was based crucially on normalizing the local luminosity function to the bright ($B \sim 16^m$) galaxy counts from Schmidt-telescope photographic surveys (*e.g.,* Maddox *et al.* 1990b). It now appears that normalizing at $B \sim 16^m$ is incorrect since the normalizations of the local luminosity functions of our survey and that of Ellis *et al.*

(1995) are at least a factor of 2 higher than that of Loveday *et al.* (1992). It unlikely that systematic errors in the conversion of plate instrumental intensities to calibrated magnitudes could be entirely responsible for the differences (Metcalfe, Fong, and Shanks 1995). The difference could be explained by the presence of a local underdensity extending to the median depth of the APM survey, $\sim 150h^{-1}$ Mpc ($z \sim 0.05$). Glazebrook *et al.* (1994) discounted this explanation using an argument based on extrapolations of measured galaxy clustering. If one assumes that galaxy clustering can be described on all scales by a power law correlation function $\xi(r) = (r_0/r)^\gamma$ with $r_0 \sim 5h^{-1}$ Mpc and $\gamma \sim 1.8$ (Marzke *et al.* 1995), then one would predict that by reaching a depth of $\sim 150h^{-1}$ Mpc, the APM survey contained a fair sample of the local universe. The presence of a $\sim 100h^{-1}$ Mpc diameter void in between the two superclusters in our survey and the detection of excess power on $\sim 100h^{-1}$ Mpc scales in the Las Campanas redshift survey by Landy *et al.* (1995) suggest, however, that it is incorrect to assume that galaxy clustering can be accurately described on large scales by an extrapolation of the clustering on small scales. Thus, the explanation for the low normalization of the local counts from photographic surveys may indeed be that we live in a local underdensity.

It has also been proposed that the faint-end of the luminosity function may be steeper than the canonical slope $\alpha \approx -1.0$, where α is Schechter parameter describing the faint-end slope (Equation 5.6). A steep faint-end slope would remove the need for rapid evolution of the luminosity function at small redshifts. Loveday *et al.* (1992) measured the luminosity function to $M(B) = -15 + 5\log h$ and found no evidence for an upturn in the luminosity function. However, McGaugh (1994) has noted that field galaxy surveys based on photographic plates with high surface brightness detection thresholds may completely miss low surface brightness galaxies. If low surface brightness galaxies exist in great numbers and if they have low luminosities, then they could make up a steep and undetected tail to the luminosity function. Unfortunately, as our survey is also constructed from plate material, we too are not sensitive to low surface brightness galaxies. We measure $\alpha \lesssim -1$ for our local luminosity function, in agreement with Loveday *et al.* (1992). Ellis *et al.* (1995), part of whose survey was

selected from images with a low surface brightness limit of $\mu_{b_J} = 26.5$ mag arcsec^{-2}, also measure $\alpha \approx -1.$, which suggests that there may not be a large population of low surface brightness galaxies.

5.5.2 The Evolution of the Luminosity Function to $z = 0.5$

We asserted in §4.2 that the luminosity function of blue galaxies (as blue or bluer than Sbc) evolved from $0 < z \leq 0.2$ to $0.2 < z \leq 0.5$ and that the luminosity function of red galaxies (redder than Sbc) did not. A powerful way to verify this result is to compute $\langle V/V_{max} \rangle$ for appropriate samples (Schmidt 1968). If there is no evolution in the number density of objects, $\langle V/V_{max} \rangle = 0.5$; if the number density declines, $\langle V/V_{max} \rangle < 0.5$; and if the number density increases, $\langle V/V_{max} \rangle > 0.5$. As with the luminosity function computation, we estimate $\langle V/V_{max} \rangle$ for a given redshift range and magnitude limit from the average of $\langle V/V_{max} \rangle$ calculated for 100 magnitude-limited sub-samples drawn from the parent catalog. The quoted error is the standard deviation of the 100 realizations. The values of $\langle V/V_{max} \rangle$ for various samples, all with the two superclusters removed, are given in Table 5.2. For blue galaxies as a whole (Hubble types Sbc, Scd, and Im), we have evidence at the 2.5σ level for an increase in the number density with redshift. The evolution is most evident in the bluest galaxies. A sample with only galaxies with colors typical of types Sbc and Scd is consistent with no evolution, whereas a sample with only the bluest galaxies (Hubble type Im) is clearly evolving. According to the $\langle V/V_{max} \rangle$ test, the red galaxies do not evolve, in agreement with the luminosity function analysis.

Now that we have established that the blue galaxies are evolving with redshift, we wish to investigate whether we can detect differences in the spectral properties of the evolving population with redshift. First, we remark that the color distribution of objects with measured redshifts is similar to the color distribution of unidentified objects, leading us to believe that the type distribution of the identified objects is not strongly biased (Paper I). Although emission lines are generally easier to detect than absorption lines, the difficulty of identifying emission lines at observed wavelengths

longer than 5577Å, where there are many strong night sky features, combined with the strength of Ca H, Ca K, and the 4000Å break in absorption line objects at $0.4 \lesssim z \lesssim 0.6$ mitigate the bias in favor of emission line objects. A sample of the spectra of 8 absorption line objects in this redshift range is shown in Figure 5.7 to illustrate the strength of their characteristic features.

In Figure 5.8, we plot the observed $g-r$ color of all the objects in our survey along with the tracks of five representative model spectra. The bluest spectrum is simply a flat-spectrum object, $f_\nu = 0$. The four other spectra are typical of the Hubble types E, Sbc, Scd, and Im and are taken from Coleman, Wu, and Weedman (1980). The large, solid diamonds mark the median color in the redshift ranges $0.13 < z < 0.2$ (arranged to exclude the superclusters), $0.2 < z < 0.3$, $0.3 < z < 0.4$, $0.4 < z < 0.5$, and $0.5 < z < 0.6$. One can see that the median color becomes progressively bluer with respect to the model spectra with increasing redshift. From the luminosity function analysis, we expect the number of red galaxies not to change with redshift while the number of blue galaxies should increase, thus shifting the median color of the galaxy population to the blue, in accord with the observations.

The shift of the median color to the blue is presumeably associated with increased star formation activity at earlier times. In our spectra, there are two convenient star formation indicators, [O II] λ3727 and Hδ λ4101. [O II] emission is found in galaxies with ongoing star formation, and its strength is proportional to the strength of Hα (Kennicutt 1992). Strong Hδ absorption is a signature of the presence of a population of A-stars, which are visible $\sim$1 Gyr after a burst of star formation. Both of these lines are reliably measured by automated programs (see Paper I) since both occur in regions of the spectrum where the continuum is featureless and there is little crowding from other lines. An important virtue of the Hδ line is that, since it appears in absorption, a galaxy with detectable Hδ would have been identified no matter what its spectral characteristics, which implies that there is no bias towards detecting objects with Hδ absorption. A galaxy with [O II] emission is, of course, easier to identify than if it had had only absorption lines. However, as we discussed above, the combination of the difficulty of identifying weak emission lines in the face

of strong sky subtraction residuals and of the ease of identifying the strong features characteristic of absorption line galaxies at moderate redshifts suggests to us our survey is not strongly biased towards detecting objects with [O II]. In Figures 5.9 and 5.10, we plot as a function of redshift the fraction of galaxies with [O II] emission and the fraction of galaxies with Hδ absorption, respectively. The vertical dotted line in Figure 5.10 marks the redshift beyond which Hδ is shifted into the region of the spectrum in which sky subtraction becomes increasingly difficult. Both figures show an increase in star formation activity with redshift, a result which is consistent with the results from the analyses of the luminosity function and the median colors.

The increase in star formation activity with redshift could either be due to an increase in the number of galaxies forming stars or to stronger bursts in the same galaxies that are currently forming stars now. In other words, we wish to decide whether we are observing evolution in the number of star forming galaxies or in the luminosity of star forming galaxies. In Figure 5.11, we plot the rest equivalent width of [O II] versus redshift for the galaxies in our sample. As the range of rest equivalent widths does not vary significantly with redshift, which implies that individual galaxies were not forming stars more rapidly at $z \sim 0.5$ than at $z \sim 0$, we conclude that observed increase in star formation activity with redshift must be due to an increase in the number of star forming galaxies.

5.5.3 The Supercluster Luminosity Functions

The luminosity functions of the two superclusters have quite similar shapes, although their normalizations differ by a factor of 2. Both superclusters are substantially more dense than the field, by a factor of 10 for the Corona Borealis supercluster and a factor of 5 for the Abell 2069 supercluster, on scales of several $\times 10^4$ Mpc^3. It is important to know whether we are fairly sampling the superclusters in the sense that we are not biased towards either the Abell clusters within the superclusters or to the "field" of the superclusters. The mean density of the Corona Borealis supercluster, computed by simply integrating the fitted luminosity function from $M(B) = -23^m$ to $M(B) =$

-15^m, is $\bar{n} \approx 0.9h^3$ Mpc^{-3}. For each galaxy in our survey, we can define a local galaxy density $\bar{n}_{local}$ around the given galaxy by measuring the distance to, say, the fifth nearest neighbor, d_5, and computing $\bar{n}_{local} = d_5^{-3}$. The median local galaxy density for the galaxies with measured redshifts in the Corona Borealis supercluster is $\bar{n}_{local} \approx 0.9h^3$ Mpc^{-3}, which is identical to the mean density of the supercluster and implies that we have fairly sampled the supercluster. For the Abell 2069 supercluster, $\bar{n} \approx 0.9h^3$ Mpc^{-3} also, but the median local galaxy density is only $\bar{n}_{local} = 0.4h^3$ Mpc^{-3}. Thus, we are somewhat biased towards the "field" of the Abell 2069 supercluster. The overall resemblance between the supercluster luminosity functions and the field galaxy luminosity function suggests that galaxy formation and evolution must not depend strongly in environment. There are, however, two important differences between the luminosity functions in the field and in the superclusters that must ultimately be due to environmental effects.

First, the characteristic absolute magnitude M^* of the supercluster luminosity functions is nearly a magnitude brighter than that measured in our survey for local field galaxies. The high density environments of the superclusters are clearly conducive to the formation of luminous galaxies.

The second difference is that the faint-end slopes of the two supercluster luminosity functions are steeper ($\alpha \sim$ -1.3 to -1.5) than the faint-end slope of the field galaxy luminosity function ($\alpha \sim$ -0.7 to -1.0). Our results are consistent, however, with those of previous studies of the luminosity function in rich clusters (*e.g.,* Sandage, Binggeli, and Tammann 1985, Bernstein *et al.* 1995, and De Propris *et al.* 1995) which have found that the faint-end slope is steep, ranging from $\alpha \approx -1.3$ to $\alpha \approx -2.2$. This agreement would be unexpected if there are large numbers of low surface brightness galaxies in the superclusters since our original object detection used a high surface brightness threshold on Schmidt photographic plates. In fact, Bernstein *et al.* (1995), who recently measured the luminosity function of the core of the Coma cluster using a deep CCD image and found $\alpha = -1.42 \pm 0.05$ for $-19.4 < M_R < -11.4$, did not find a large population of low surface brightness galaxies, despite having a very faint detection threshold of $27.6R$ mag arcsec^2.

5.6 Summary

We have presented an analysis of the luminosity function of galaxies in the Norris Survey of the Corona Borealis Supercluster. We have found compelling evidence for evolution of the field galaxy luminosity function within our sample. The evolution is, however, limited to the galaxies that are as blue or bluer than Hubble type Sbc and is strongest for samples restricted to the bluest (Im) galaxies. The median color of the field galaxy population becomes increasingly bluer with redshift, and a larger fraction of galaxies at higher redshift exhibit spectral signatures of ongoing or recently completed star formation. We are unable to detect any evolution of galaxies redder than Sbc. Since the blue galaxies at $0.2 < z < 0.5$ are evidently not evolving into the red population observed at low redshifts, one is naturally led to ask, what has happened to the blue galaxies? Since the low and high redshift luminosity functions do not have the same shape, pure luminosity evolution cannot be solely responsible for the observed changes. A crucial clue is provided by galaxy counts as a function of morphological type obtained with the *Hubble Space Telescope (HST)* (Glazebrook *et al.* 1995b, Driver *et al.* 1995). The counts of faint elliptical and early-type spiral galaxies match predictions based on counts in the local universe, provided that the local luminosity function is normalized a factor of 2 higher than found by Loveday *et al.* (1992). In contrast, the *HST* number counts of late-type and irregular galaxies are far in excess of the counts expected from observations of nearby galaxies, even with a high normalization of the local luminosity function. It is perhaps the case that the excess galaxies at $z \sim 0.5$ merge and thereby reduce their number by $z = 0$. Moreover, mergers would naturally create the irregular morphologies commonly seen in the *HST* images.

The galaxy evolution that we have observed is consistent with the results derived from the quasar absorption-selected sample of Steidel, Dickinson, and Persson (1994). The authors found that the galaxies responsible for quasar absorption lines in the range $0.2 \leq z \leq 1.0$, which typically have luminosities near L^*, do not evolve. The faint blue galaxies—the ones which we have seen to be evolving strongly— do not

appear in the Steidel, Dickinson, and Persson (1994) sample. Since the luminosity function of the absorbing galaxies computed by Steidel, Dickinson, and Persson (1994) has a normalization approximately equal to that of our local luminosity function for red galaxies and is well fit by a Schechter function, we are tempted to identify our non-evolving population of red luminous galaxies with the similarly non-evolving population of quasar absorbers.

The luminosity function of local field galaxies, while having a shape which is well described by a Schechter function with bright-end cutoff $M(B) + 5\log_{10} h \approx -19.5^m$ and faint-end slope $\alpha \approx -1.0$ in agreement with the results of wide-angle shallow surveys, has a normalization that is a factor of $\sim$2 higher. Since it seems doubtful that errors in the calibration of photographic plate magnitudes could conspire to reduce the normalization of the luminosity function without also changing the shape, we conclude, albeit reluctantly, that the local samples must be underestimating the normalization because we live in a low density region with a scale of $\sim 100h^{-1}$ Mpc.

The luminosity functions of the two superclusters show significant differences from the field galaxy luminosity function, despite considerable overall similarity. The characteristic luminosity is brighter, by nearly a magnitude, and the faint-end slope is steeper ($\alpha \sim -1.4$ instead of $\alpha \sim -1.0$). Since the superclusters are 5-10 $\times$ denser than the field, we are likely observing the influence of the environment on galaxy formation and evolution.

TABLE 5.1

SCHECHTER FUNCTION FITS

sample[a]	ϕ^* (h^3 Mpc^{-3})	$M(B)^* - 5\log_{10} h$	α	χ^2/ν[b]
$z \leq 0.2$, SC's removed	0.06 ± 0.02	-19.05 ± 0.26	-0.67 ± 0.23	1.86/2
$z \leq 0.2$, SC's included	0.05 ± 0.01	-19.51 ± 0.18	-1.19 ± 0.11	7.28/8
$0.2 < z \leq 0.5$	0.01 ± 0.03	-20.66 ± 2.73	-2.10 ± 0.93	0.8/2
$z \leq 0.2$, red, SC's removed	0.02 ± 0.01	-18.95 ± 0.52	-0.65 ± 0.45	2.76/3
$z \leq 0.2$, red, SC's included	0.04 ± 0.01	-19.05 ± 0.16	-0.80 ± 0.11	4.08/2
$0.2 < z \leq 0.5$, red	..... too few data points			
$z \leq 0.2$, blue, SC's removed	0.04 ± 0.02	-18.92 ± 0.32	-0.70 ± 0.29	2.00/2
$z \leq 0.2$, blue, SC's included	0.05 ± 0.01	-19.01 ± 0.17	-0.72 ± 0.13	3.44/2
$0.2 < z \leq 0.5$, blue	0.01 ± 0.05	-20.31 ± 2.29	-2.07 ± 1.17	0.38/2
Corona Borealis SC	0.10 ± 0.04	-19.85 ± 0.32	-1.33 ± 0.13	15.12/9
Abell 2069 SC	0.05 ± 0.04	-19.91 ± 0.59	-1.53 ± 0.24	3.36/4

[a]SC stands for "supercluster."
[b]ν is the number of degrees of freedom of the fit.

TABLE 5.2

$\langle V/V_{max} \rangle$ FOR $0 < z \leq 0.5$

sample	$\langle V/V_{max} \rangle$
$r \leq 20.5$, all red galaxies	0.47 ± 0.04
$r \leq 20.5$, all blue galaxies	0.55 ± 0.02
$r \leq 20.5$, Sbc, Scd galaxies	0.53 ± 0.04
$r \leq 20.5$, Im galaxies	0.58 ± 0.03

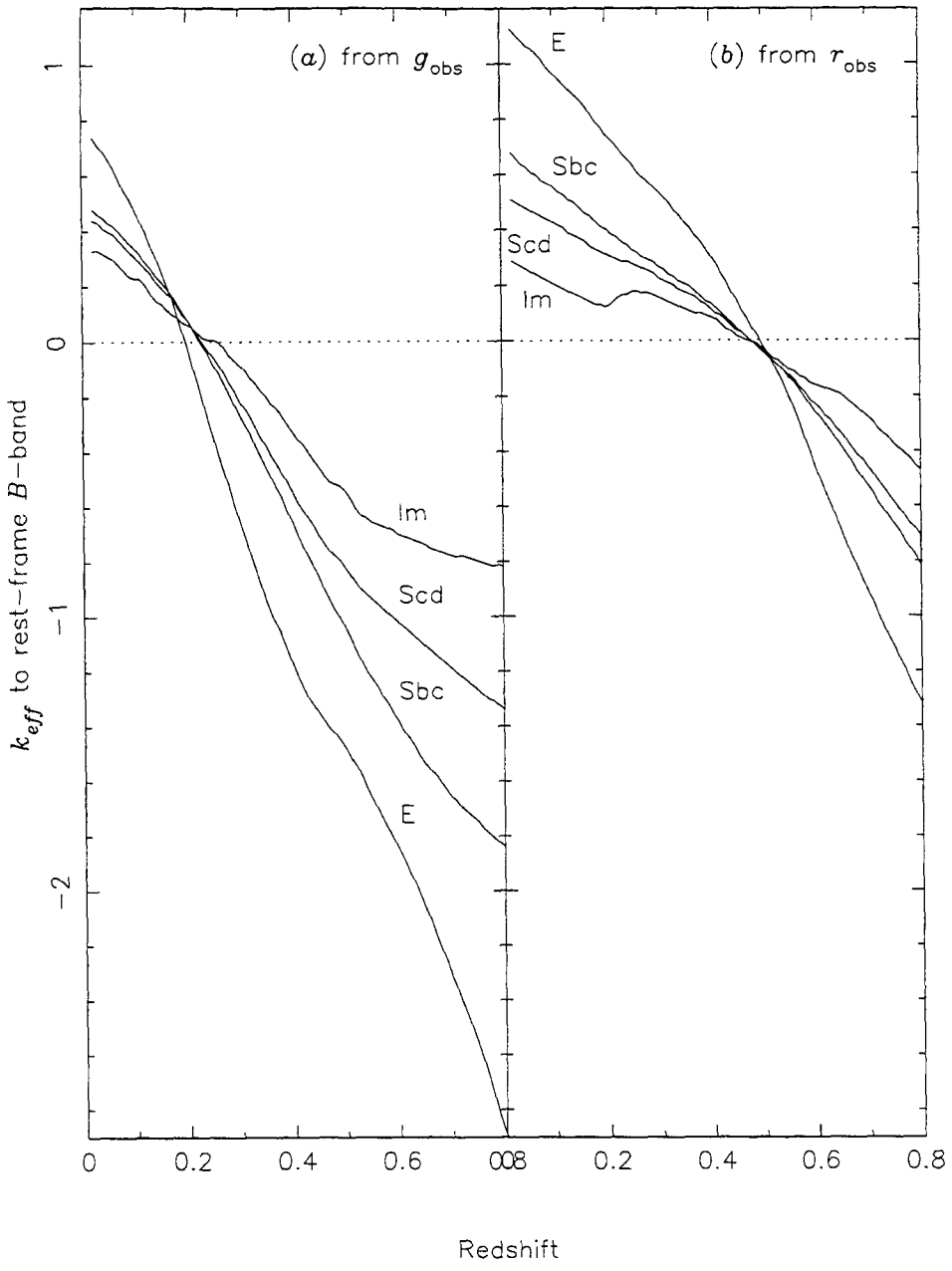

Fig. 5.1.— Effective k-corrections from the observed (a) g and (b) r bands to the rest-frame B band. The effective k-correction, k_{eff}, is the traditional k-correction with the bandwidth stretching term removed and the rest-frame color correction to the B band added. It thus incorporates all of the spectrum-dependent corrections required to transform from the observed band to the rest-frame B band. The four curves in each panel labeled E, Sbc, Scd, and Im are the four spectral types from Coleman, Wu, and Weedman (1980). By transforming from the observed g band for $z \lesssim 0.3$ and from the observed r band for $z \gtrsim 0.3$, k_{eff} is always less than 1^m.

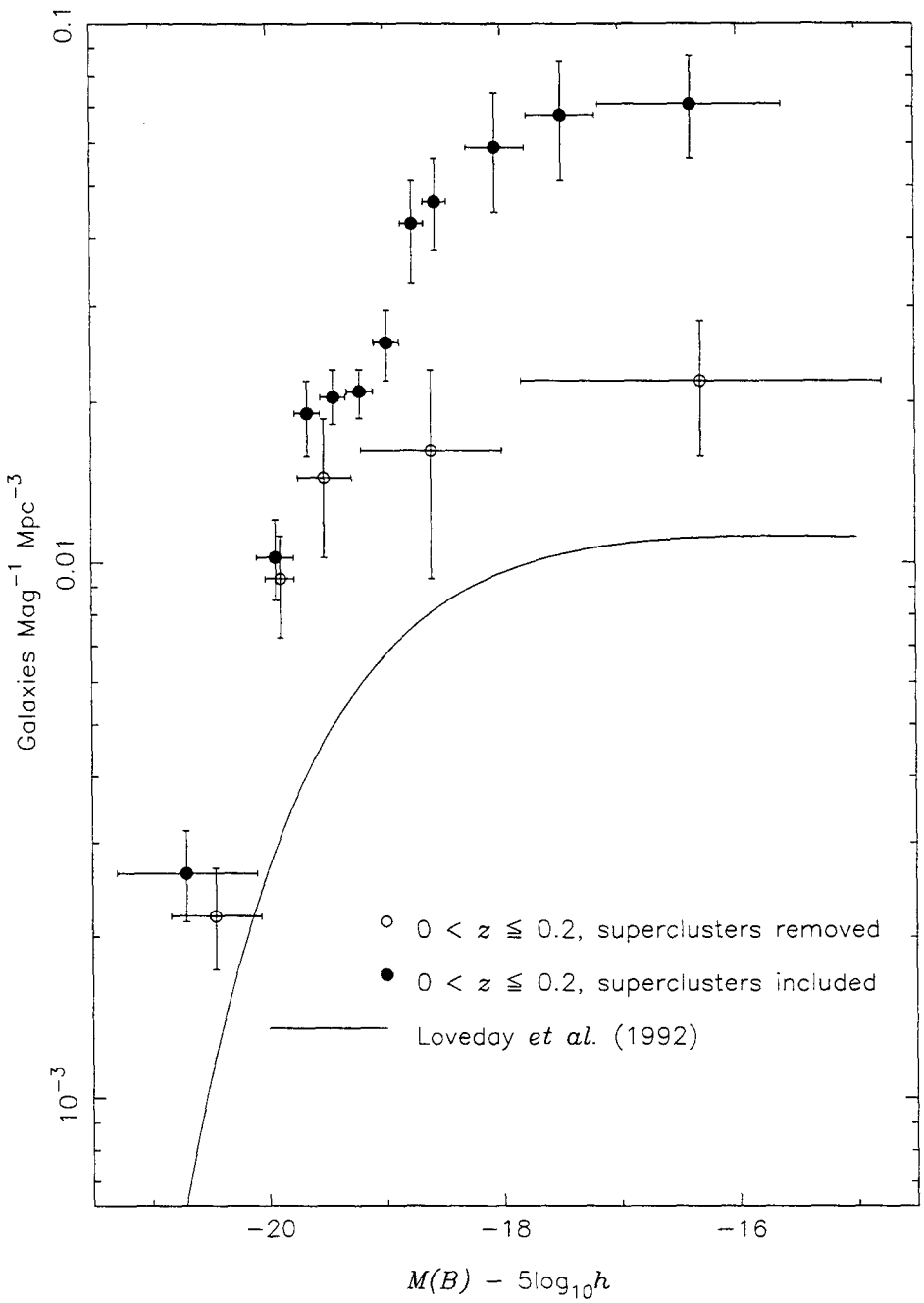

Fig. 5.2.— Luminosity function for galaxies with $r \leq 18.5$ and $0 < z \leq 0.2$. The unfilled circles show the luminosity function with the two superclusters at $z \approx 0.07$ and $z \approx 0.11$ removed. The filled circles show the luminosity function with the superclusters included. The solid curve is the Schechter function fit to the local luminosity function of Loveday *et al.* (1992). Although the shapes of the luminosity functions are similar, the normalization of the Loveday *et al.* (1992) luminosity function is low by at least a factor of 2.

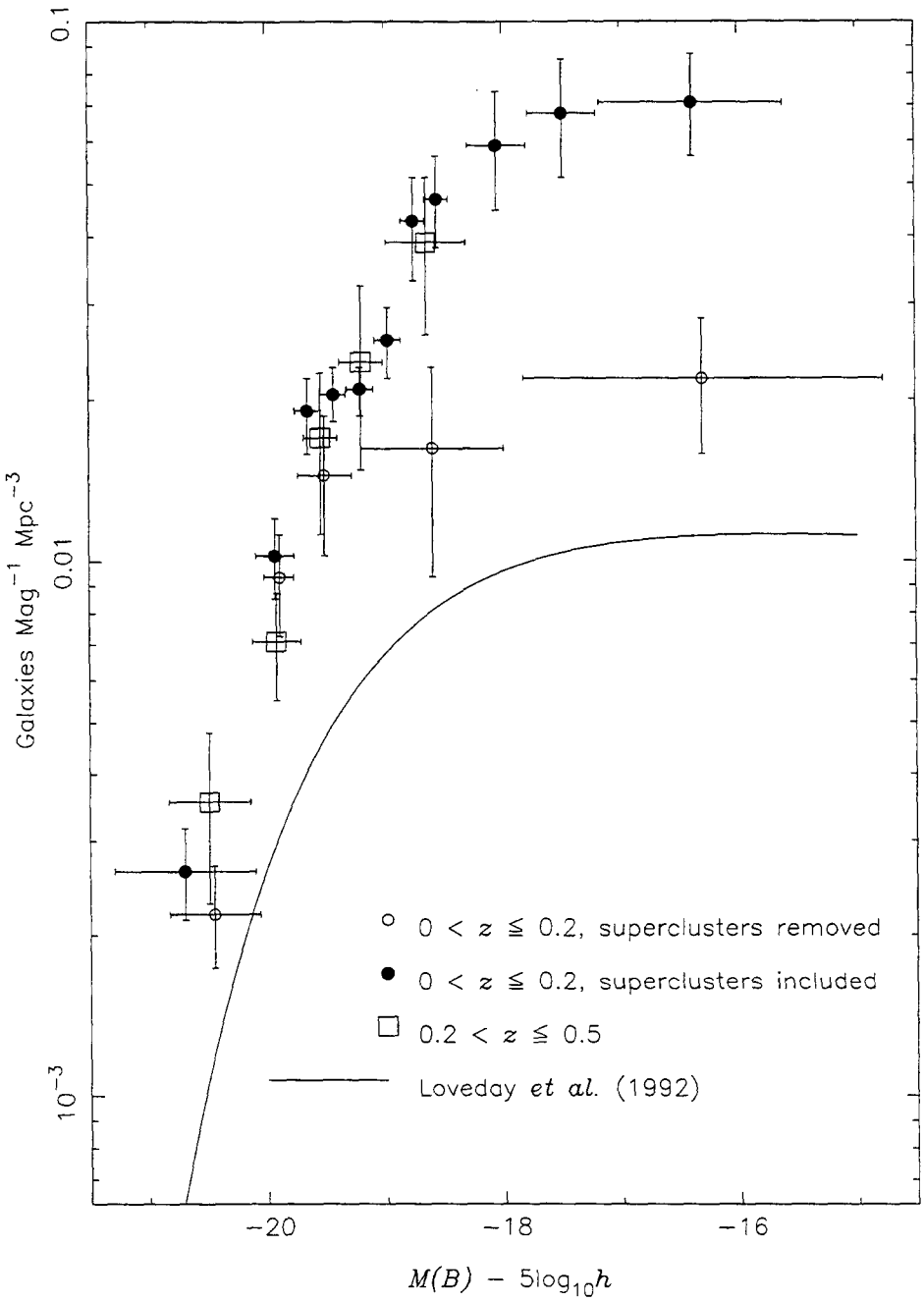

Fig. 5.3.— Luminosity function for galaxies between $z = 0$ and $z = 0.5$. As in Figure 5.2, the unfilled circles, filled circles, and solid curve show the local luminosity function with superclusters removed, the local luminosity function with the supercluster included, and the Loveday *et al.* (1992) luminosity function, respectively. The unfilled squares show the luminosity function for galaxies with $0.2 < z \leq 0.5$. Since the true local luminosity function is unlikely to be as high as the luminosity function which includes the two superclusters, it appears that the number density of galaxies has increased to higher redshift.

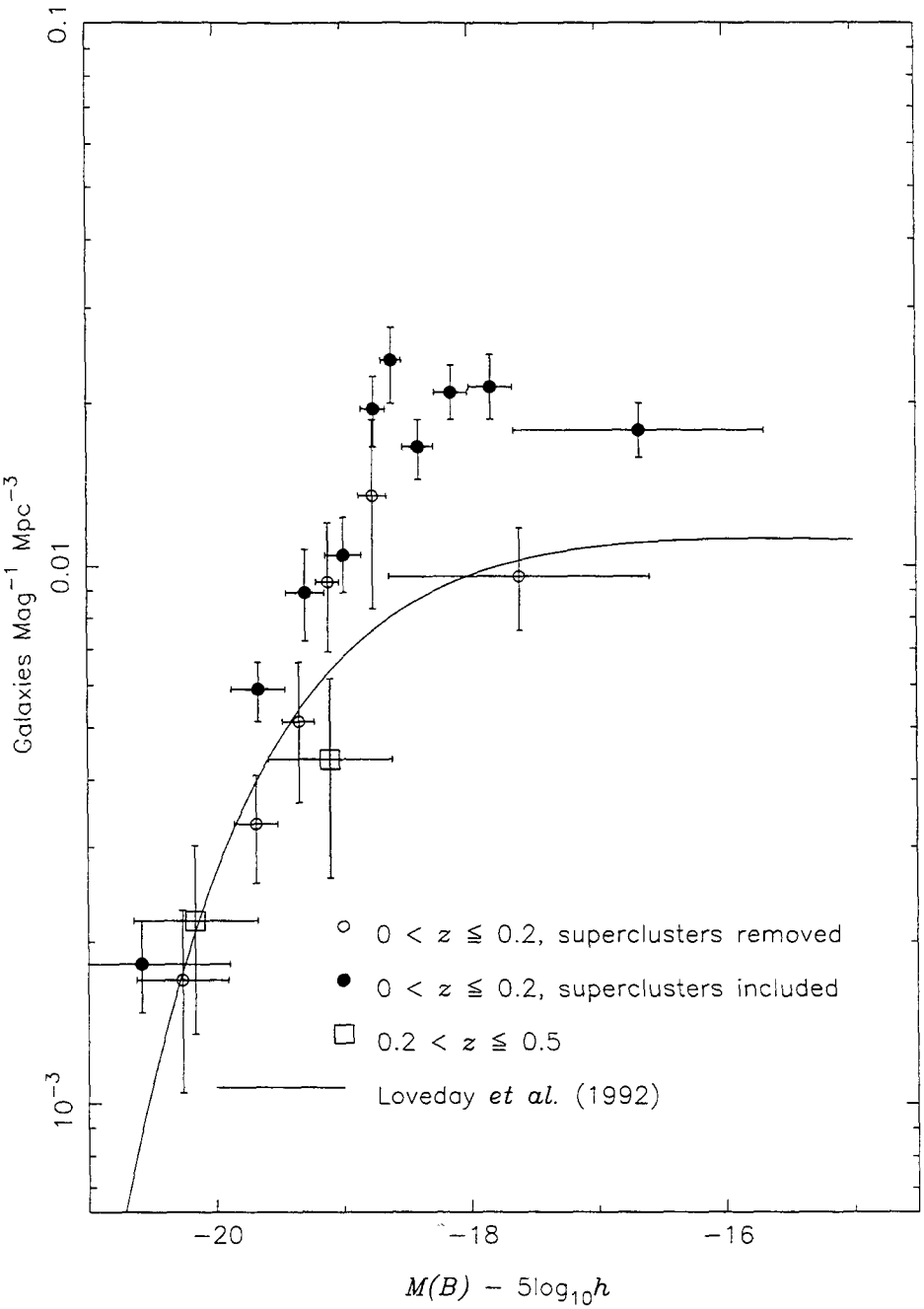

Fig. 5.4.— Luminosity function for red galaxies between $z = 0$ and $z = 0.5$. We define red galaxies as galaxies redder than Coleman, Wu, and Weedman (1980) Sbc galaxies. The open circles show the local luminosity function of red galaxies with the superclusters removed. The solid circles show the local luminosity function of red galaxies with the superclusters included. The (two) open squares show the luminosity function of red galaxies with $0.2 < z \leq 0.5$. The solid curve is the Schechter function fit to the local luminosity function of Loveday *et al.* (1992). These data suggest that the luminosity function of red galaxies does not evolve to $z = 0.5$.

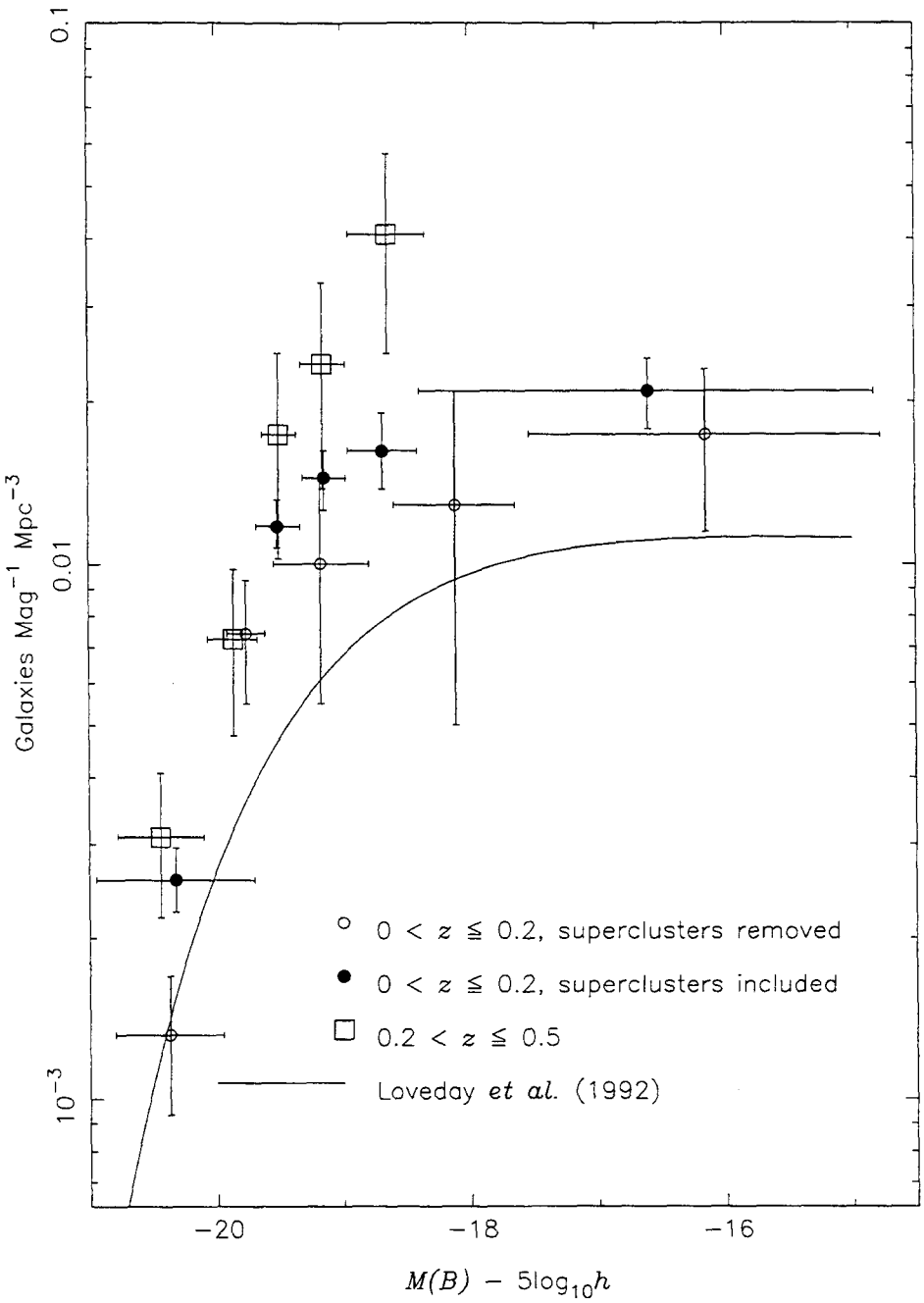

Fig. 5.5.— Luminosity function for blue galaxies between $z = 0$ and $z = 0.5$. We define blue galaxies as galaxies as blue or bluer than the Coleman, Wu, and Weedman (1980) Sbc galaxy. The open circles show the local luminosity function of blue galaxies with the superclusters removed. The solid circles show the local luminosity function of blue galaxies with the superclusters included. The open squares show the luminosity function of blue galaxies with $0.2 < z \leq 0.5$. The solid curve is the Schechter function fit to the local luminosity function of Loveday *et al.* (1992). These data suggest that the luminosity function of blue galaxies has evolved significantly from $0 < z \leq 0.2$ to $0.2 < z \leq 0.5$.

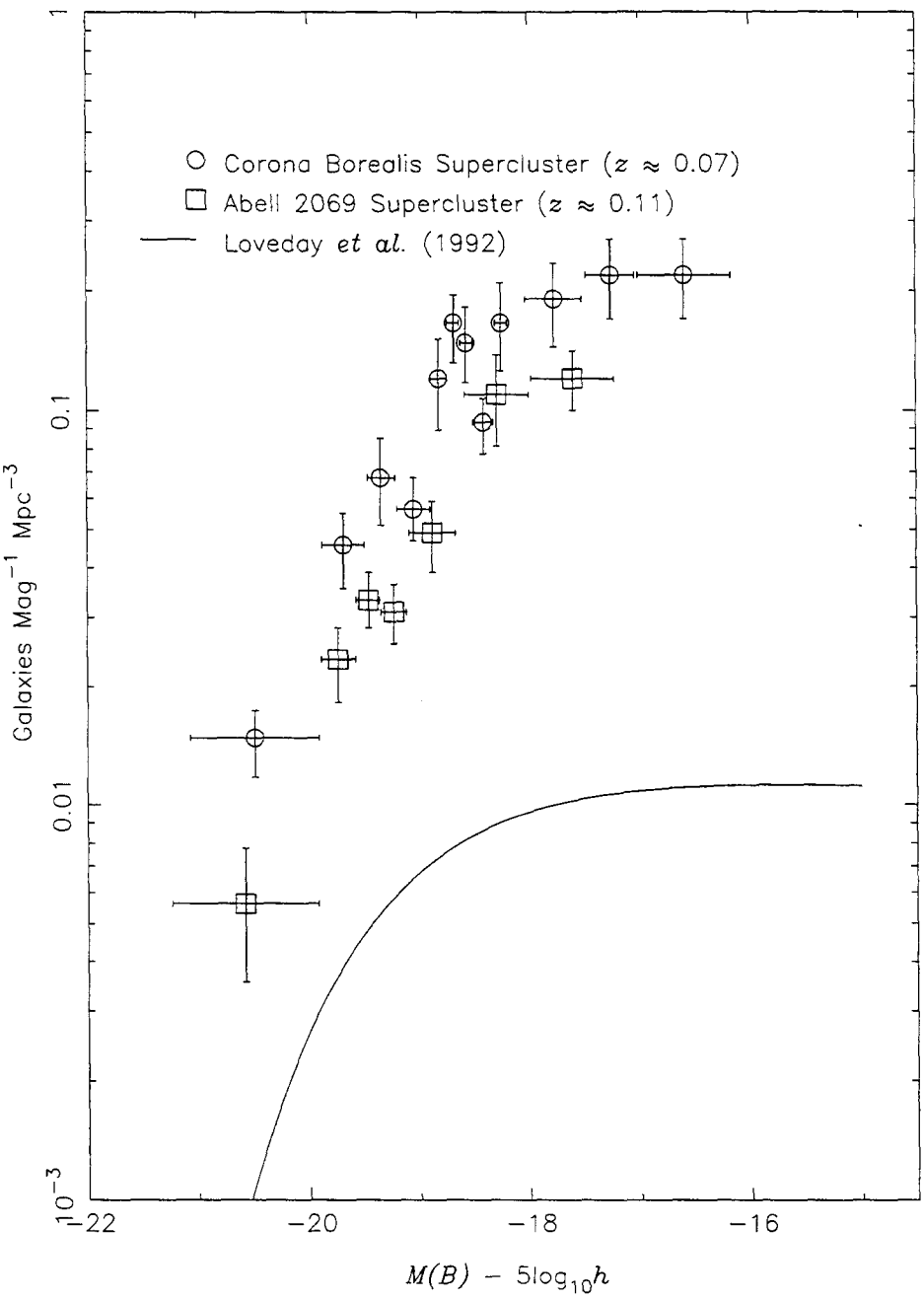

Fig. 5.6.— Luminosity functions of the Corona Borealis supercluster (circles) and the background supercluster (squares). The Schechter function fit to the local luminosity function of Loveday *et al.* (1992) is shown by the solid line. The luminosity functions of the two superclusters have similar shapes, but the normalizations differ by a factor of 2.

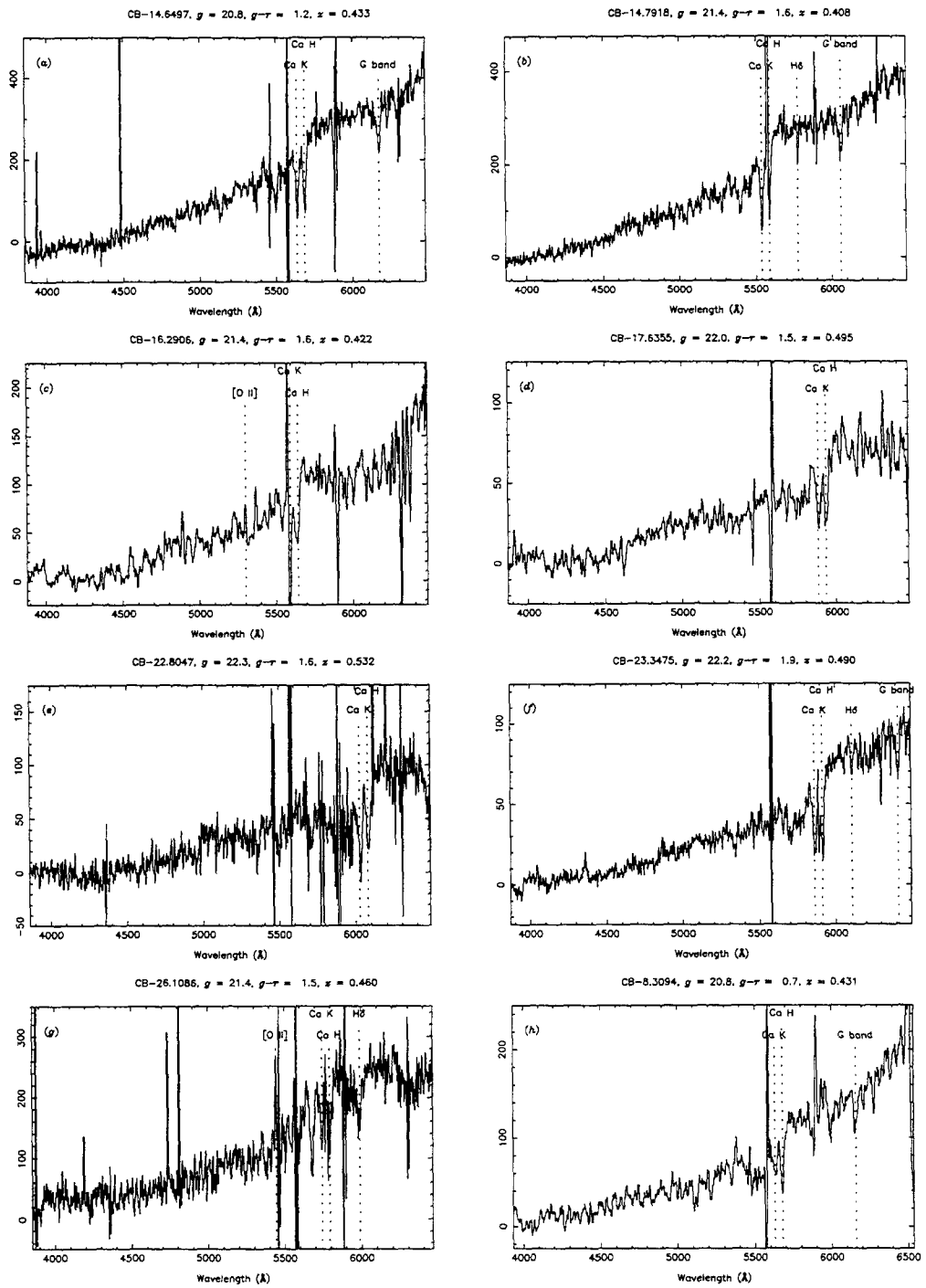

Fig. 5.7.— A representative sample of absorption-line galaxies at $0.4 < z < 0.6$ illustrating the strength of Ca H, Ca K, and the 4000Å break.

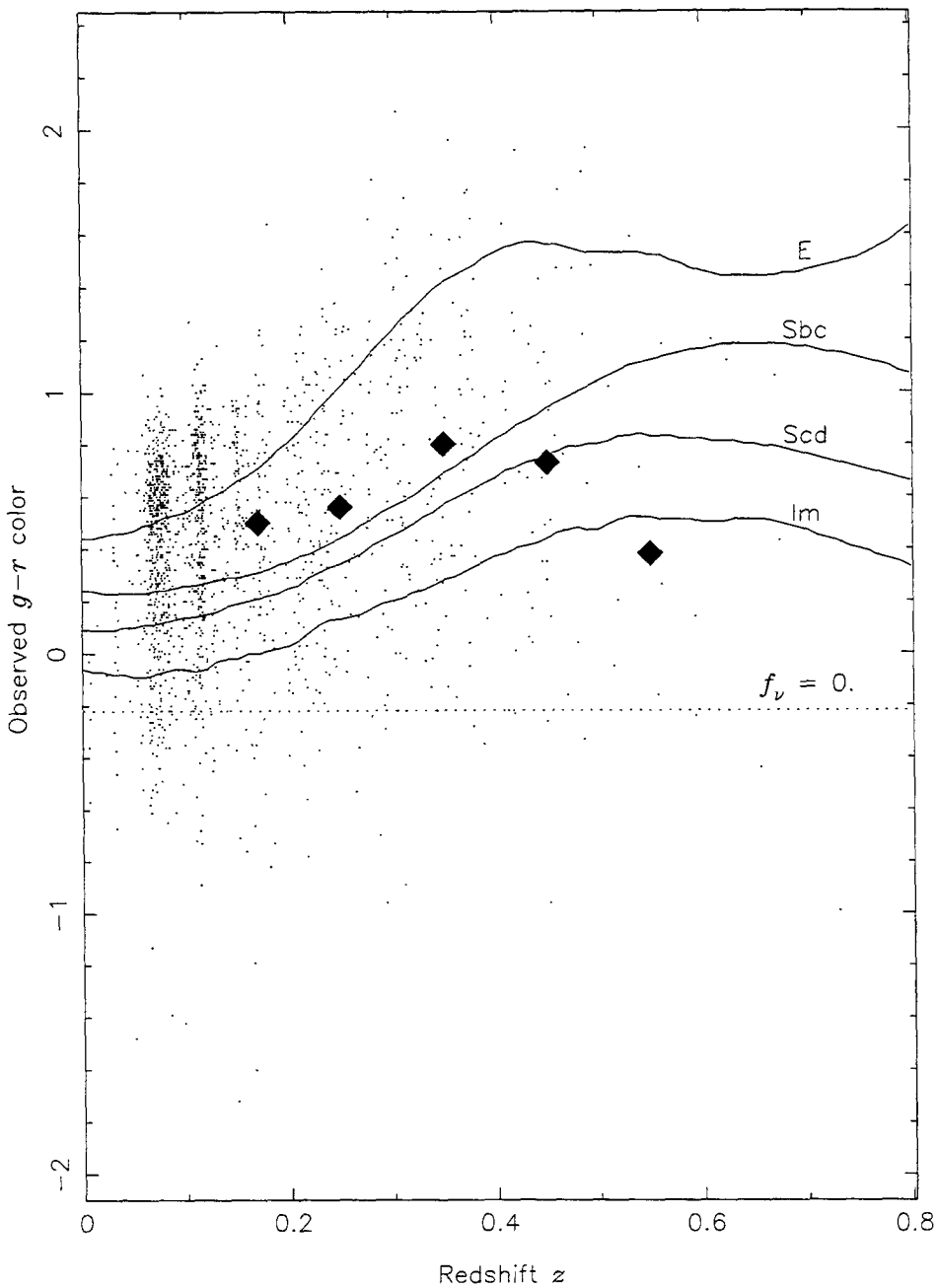

Fig. 5.8.— Median observed $g-r$ color as a function of redshift. We plot the observed $g-r$ color as a function of redshift along with the tracks of five representative model spectra. The bluest track is that of flat-spectrum galaxy, $f_\nu = 0$. The other four tracks are those typical of the Hubble types E, Sbc, Scd, and Im. The large, filled triangles mark the median $g-r$ color in the redshift intervals $0.13 < z < 0.2$, $0.2 < z < 0.3$, $0.3 < z < 0.4$, $0.4 < z < 0.5$, and $0.5 < z < 0.6$. The median color of the galaxy population becomes bluer with increasing redshift.

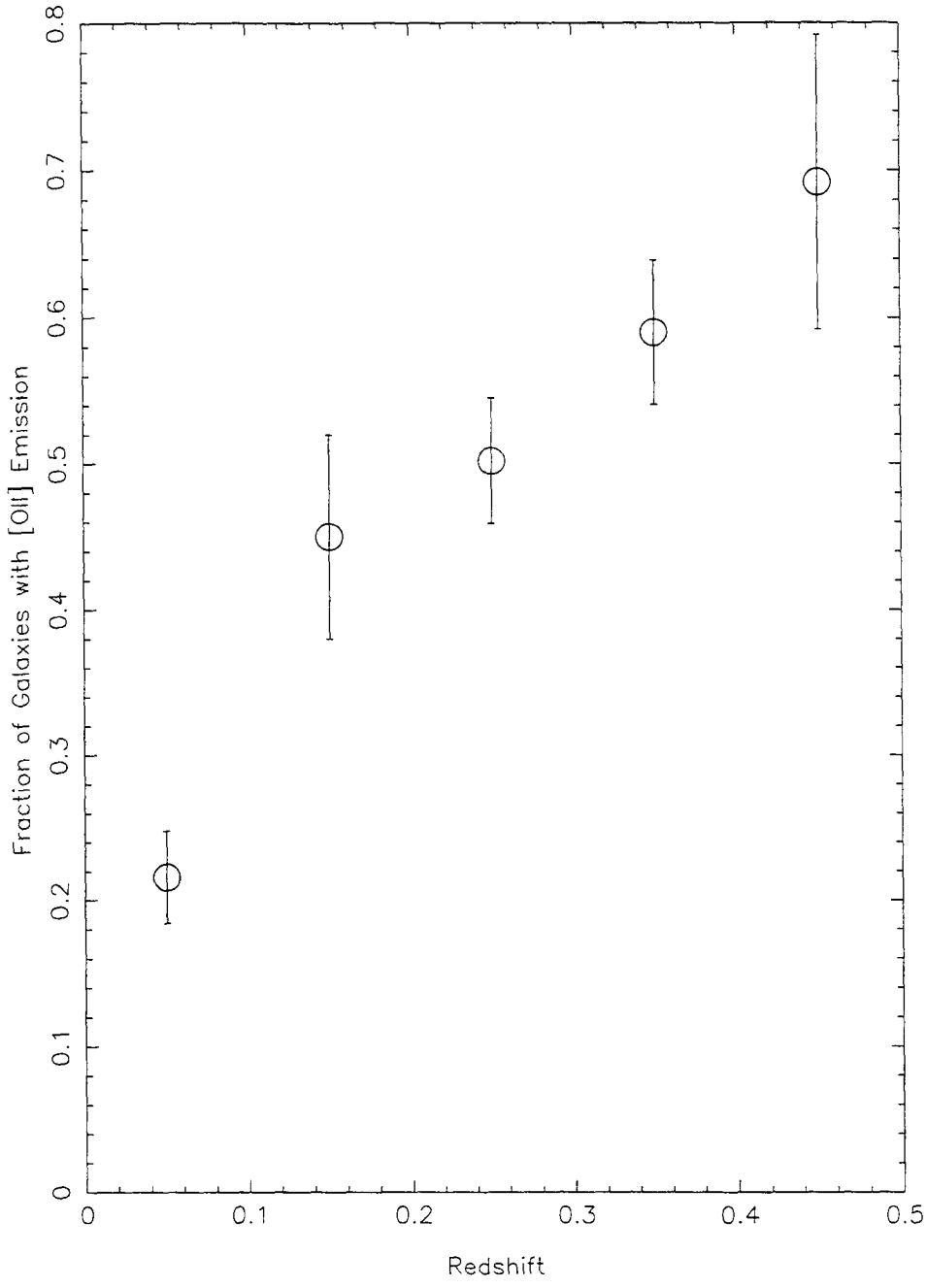

Fig. 5.9.— Fraction of galaxies with [O II] λ3727 emission as a function of redshift. The redshift intervals are $0 < z < 0.06$, $0.13 < z < 0.2$, and every tenth thereafter. The superclusters are excluded from the analysis. As [O II] is an indicator of ongoing star formation, the increasing fraction of galaxies exhibiting [O II] with redshift is evidence for an increase in the rate of star formation with redshift.

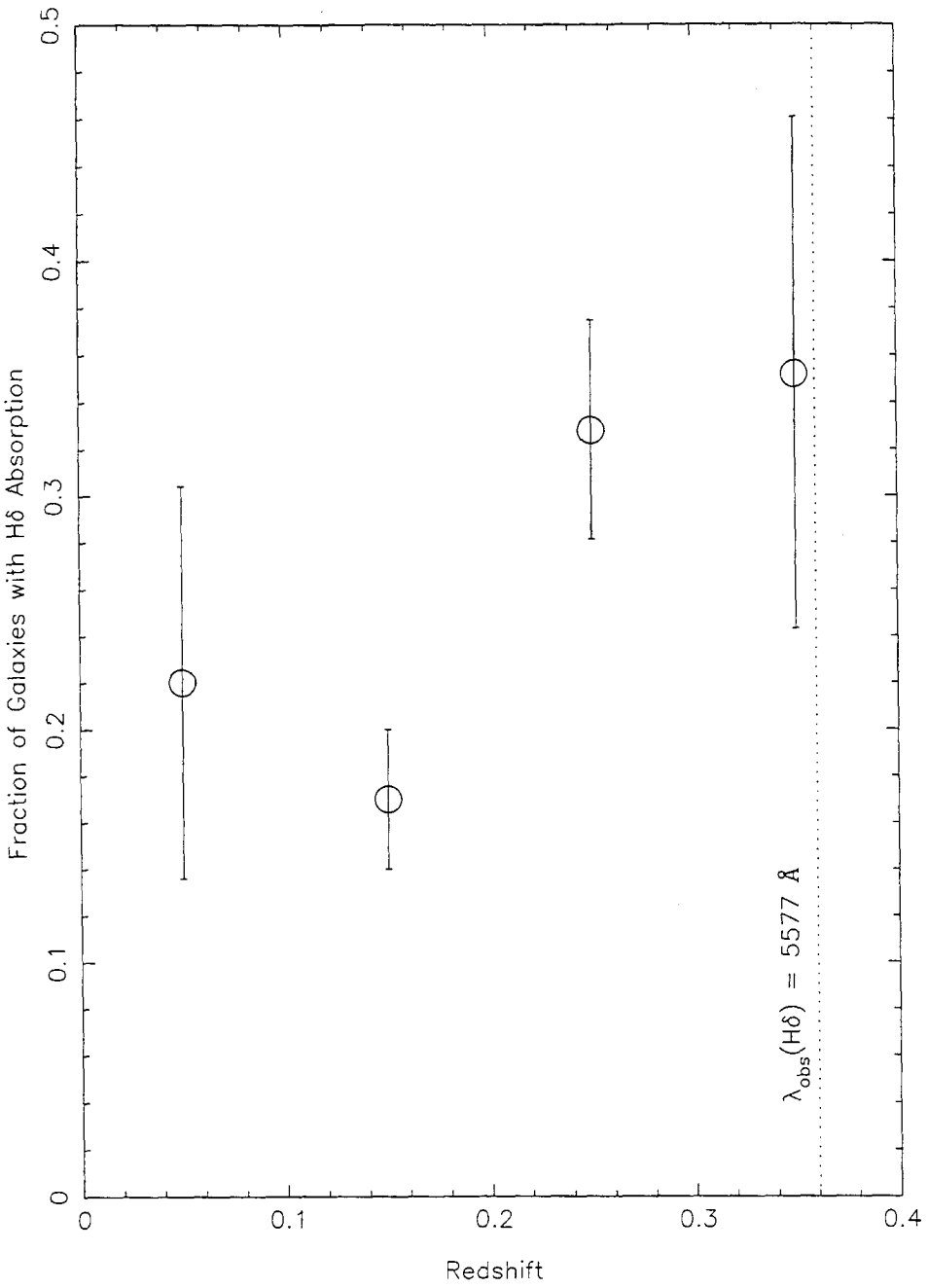

Fig. 5.10.— Fraction of galaxies with Hδ λ4101 absorption as a function of redshift. The redshift intervals are $0 < z < 0.06$, $0.13 < z < 0.2$, $0.2 < z < 0.3$, and $0.3 < z < 0.4$. The vertical dotted lines marks the redshift beyond which Hδ is shifted into the region of the spectrum that is heavily contaminated by night sky emission. Hδ absorption is a signature of the presence of a $\sim$1 Gyr old A-star population. The increase in the fraction of galaxies with Hδ absorption with redshift indicates that the rate of star formation was higher in the past.

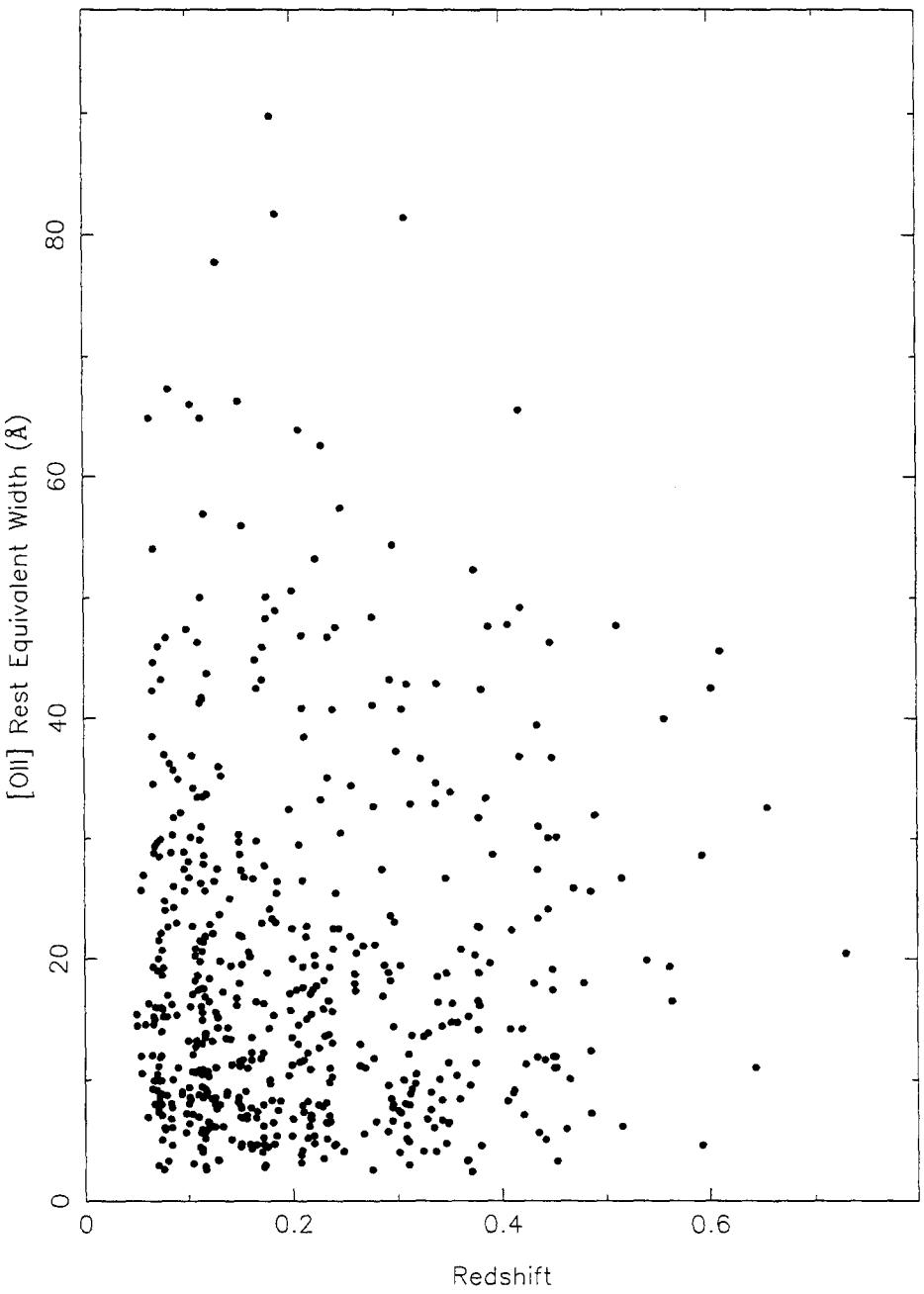

Fig. 5.11.— Rest equivalent width of [O II] as a function of redshift for the galaxies in our survey. The range of equivalent widths does not vary significantly with redshift, which suggests that individual galaxies were not forming stars more rapidly in the past.

Bibliography

Abell, G. 1958, *ApJS*, **3**, 211.

Bahcall, N. 1992, in *Clusters and Superclusters of Galaxies*, ed. A.C. Fabian (Dordrecht: Kluwer Academic Publishers), 275.

Beers, T., Flynn, K., and Gebhardt, K. 1990, *AJ*, **100**, 32.

Bernstein, G., Nichol, R., Tyson, J., Ulmer, M., and Wittman, D. 1995, *AJ*, **110**, 1507.

Brainerd, T., Smail, I., and Mould, J. 1995, *MNRAS*, **275**, 781.

Broadhurst, T., Ellis, R., Koo, D., and Szalay, A. 1990, *Nature*, **343**, 726.

Broadhurst, T., Ellis, R., and Shanks, T. 1988, *MNRAS*, **235**, 827.

Carlberg, R. 1994, *ApJ*, **433**, 468.

Cole, S., Ellis, R., Broadhurst, T., and Colless, M. 1994, *MNRAS*, **267**, 541.

Coleman, G., Wu, C.-C., and Weedman, D. 1980, *ApJS*, **43**, 393.

Cowie, L., Songaila, A., and Hu, E. 1991, *Nature*, **354**, 460.

Davis, M., Efstathiou, G., Frenk, C., and White, S. 1985, *ApJ*, **292**, 371.

Davis, M. and Huchra, J. 1982, *ApJ*, **254**, 437.

Davis, M. and Peebles, P. 1983, *ApJ*, **267**, 465.

De Propris, R., Pritchet, C., Harris, W., and McClure, R. 1995, *ApJ*, **450**, 534.

Driver, S., Windhorst, R., Ostrander, E., Keel, W., Griffiths, R., and Ratnatunga, K. 1995, *ApJ*, **449**, L23.

Efstathiou, G., Ellis, R., and Peterson, B. 1988, *MNRAS*, **232**, 431.

Ellis, R., Colless, M., Broadhurst, T., Heyl, J., and Glazebrook, K. 1995, *MNRAS submitted.*

Faber, S. and Gallagher, J. 1979, *ARAA*, **17**, 135.

Fisher, K., Davis, M., Strauss, M., Yahil, A., and Huchra, J. 1994a, *MNRAS*, **267**, 927.

Fisher, K., Davis, M., Strauss, M., Yahil, A., and Huchra, J. 1994b, *MNRAS*, **266**, 50.

Geller, M. and Huchra, J. 1989, *Science*, **246**, 897.

Glazebrook, K., Ellis, R., Colless, M., Broadhurst, T., Allington-Smith, J., and Tanvir, N. 1995a, *MNRAS*, **273**, 257.

Glazebrook, K., Ellis, R., Santiago, B., and Griffiths, R. 1995b, *MNRAS*, **275**, L19.

Glazebrook, K., Peacock, J., Collins, C., and Miller, L. 1994, *MNRAS*, **266**, 65.

Groth, E. and Peebles, P. 1977, *ApJ*, **217**, 385.

Guzzo, L., Fisher, K., Strauss, M., Giovanelli, R., and Haynes, M. 1995, *preprint.*

Hamilton, A. 1993, *ApJ*, **417**, 19.

Hamilton, D., Oke, J., Carr, M., Cromer, J., Harris, F., Cohen, J., Emery, E., and Blakeée, L. 1993, *PASP*, **105**, 1308.

Huchra, J., Geller, M., Clemens, C., Tokarz, S., and Michel, A. 1992, *Bull. C.D.S.*, **41**, 31.

Jarvis, J. and Tyson, J. 1979, *SPIE Proc. on Instrumentation in Astronomy*, **172**, 422.

Kaiser, N. and Peacock, J. 1991, *ApJ*, **379**, 482.

Kennicutt, R. 1992, *ApJ*, **388**, 310.

Kent, S. and Gunn, J. 1982, *AJ*, **87**, 945.

Kirshner, R., Oemler, A., Schechter, P., and Shectman, S. 1987, *ApJ*, **314**, 493.

Koo, D. 1981. Ph.D. thesis, University of California, Berkeley.

Landy, S., Shectman, S., Lin, H., Kirshner, R., Oemler, A., and Tucker, D. 1995, *ApJ in press.*

Le Fèvre, O., Hudon, D., Lilly, S., Crampton, D., Hammer, F., and Tresse, L. 1995, *ApJ in press.*

Lilly, S., Tresse, L., Hammer, F., Crampton, D., and Le Fèvre, O. 1995, *ApJ in press.*

Ling, E., Frenk, C., and Barrow, J. 1986, *MNRAS*, **223**, 21P.

Loveday, J., Maddox, S., Efstathiou, G., and Peterson, B. 1995, *ApJ*, **442**, 457.

Loveday, J., Peterson, B., Efstathiou, G., and Maddox, S. 1992, *ApJ*, **390**, 338.

Maddox, S., Sutherland, W., Efstathiou, G., and Loveday, J. 1990a, *MNRAS*, **243**, 692.

Maddox, S., Sutherland, W., Efstathiou, G., Loveday, J., and Peterson, B. 1990b, *MNRAS*, **247**, 1P.

Marzke, R., Geller, M., Da Costa, L., and Huchra, J. 1995, *AJ*, **110**, 477.

Marzke, R., Huchra, J., and Geller, M. 1994, *ApJ*, **428**, 43.

McGaugh, S. 1994, *Nature*, **367**, 538.

Metcalfe, N., Fong, R., and Shanks, T. 1995, *MNRAS*, **274**, 769.

Metcalfe, N., Shanks, T., Fong, R., and Roche, N. 1995, *MNRAS*, **273**, 257.

Peebles, P. 1980, *The Large-Scale Structure of the Universe* (Princeton: Princeton University Press).

Peebles, P. 1994, *Principles of Physical Cosmology* (Princeton: Princeton University Press).

Peterson, B., Ellis, R., Kibblewhite, F., Bridgeland, M., Hooley, T., and Horne, D. 1979, *ApJ*, **233**, L109.

Picard, A. 1991a, *AJ*, **102**, 445.

Picard, A. 1991b. Ph.D. thesis, California Institute of Technology.

Postman, M., Geller, M., and Huchra, J. 1988, *AJ*, **95**, 267.

Press, W., Teukolsky, S., Vetterling, W., and Flannery, B. 1992, *Numerical Recipes 2nd. edn.* (Cambridge: Cambridge University Press).

Reid, I. *et al.* 1991, *PASP*, **331**, 465.

Sandage, A., Binggeli, B., and Tammann, G. 1985, *AJ*, **90**, 1759.

Sargent, W. and Turner, E. 1977, *ApJ*, **212**, L3.

Schechter, P. 1976, *ApJ*, **203**, 297.

Schmidt, M. 1968, *ApJ*, **151**, 393.

Schneider, D. *et al.* 1993, *ApJS*, **87**, 45.

Shane, C. and Wirtanen, C. 1954, *AJ*, **59**, 285.

Shane, C. and Wirtanen, C. 1967, *Pub. Lick Obs.*, **22**, 1.

Sharples, R., Ellis, R., and Gray, P. 1988, *MNRAS*, **231**, 479.

Shectman, S., Landy, S., Oemler, A., Tucker, D., Kirshner, R., Lin, H., and Schechter, P. 1995, in *Wide-Field Spectroscopy and the Distant Universe*, ed. S. Maddox and A. Aragón-Salamanca (Singapore: World Scientific), 98.

Small, T. 1996, *ApJ submitted* (Paper III).

Small, T., Sargent, W., and Hamilton, D. 1996a, *ApJ submitted* (Paper IV).

Small, T., Sargent, W., and Hamilton, D. 1996b, *ApJS submitted* (Paper I).

Smoot, G. *et al.* 1992, *ApJ*, **396**, L1.

Sprayberry, D., Impey, C., Bothun, G., and Irwin, M. 1995, *AJ*, **109**, 558.

Steidel, C., Dickinson, M., and Persson, S. 1994, *ApJ*, **437**, L75.

Thuan, T. and Gunn, J. 1976, *PASP*, **88**, 543.

Tonry, J. and Davis, M. 1979, *AJ*, **84**, 1511.

Tyson, J. 1988, *AJ*, **96**, 1.

Valdes, F. 1982, *SPIE Proc. on Instrumentation in Astronomy*, **331**, 465.

Weir, N. 1995. Ph.D. thesis, California Institute of Technology.

Weir, N., Djorgovski, S., and Fayyad, U. 1995, *AJ*, **110**, 1.

Weir, N., Fayyad, U., and Djorgovski, S. 1995, *AJ*, **109**, 2401.

Wyse, R. and Gilmore, G. 1992, *MNRAS*, **257**, 1.

Young, P., Sargent, W., Boksenberg, A., Carswell, R., and Whelan, J. 1979, *ApJ*, **229**, 891.

Zeldovich, Y. 1970, *A&A*, **5**, 84.